Lecture Notes on

Stellar Oscillations

Jørgen Christensen-Dalsgaard

Institut for Fysik og Astronomi, Aarhus Universitet
Teoretisk Astrofysik Center, Danmarks Grundforskningsfond

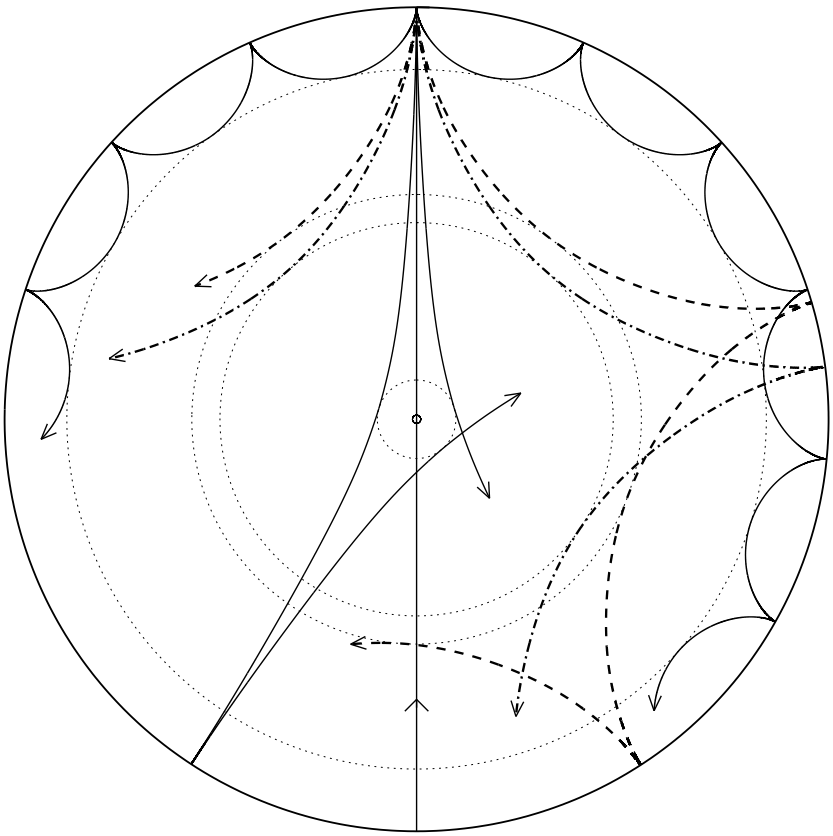

Fifth Edition

January 2014

Cover: Propagation of rays of sound waves through a cross section of a solar model (see also Section 5.2.3). The ray paths are bent by the increase with depth in sound speed until they reach the *inner turning point* (indicated by the dotted circles), where the waves undergo total internal refraction. At the surface the waves are reflected by the rapid decrease in density. The rays correspond to modes with frequency of 3000 μHz; in order of decreasing depth of penetration their degrees l are: 0 (the straight ray passing through the centre), 2, 20, 25 and 75.

Preface

The purpose of the present set of notes is to provide the technical background for the study of stellar pulsation, particularly as far as the oscillation frequencies are concerned. Thus the notes are heavily biased towards the use of oscillation data to study the interior of stars; also, given the importance of the study of solar oscillations, a great deal of emphasis is given to the understanding of their properties. In order to provide this background, the notes go into considerably more detail on derivations and properties of equations than is common, *e.g.*, in review papers on this topic. However, in a course on stellar pulsations they must be supplemented with other texts that consider the application of these techniques to, for example, helioseismology. More general background information about stellar pulsation can be found in the books by Unno *et al.* (1989) and Cox (1980). An excellent description of the theory of stellar pulsation, which in many ways has yet to be superseded, was given by Ledoux & Walraven (1958). Cox (1967) (reprinted in Cox & Giuli 1968) gave a very clear physical description of the instability of Cepheids, and the reason for the location of the instability strip.

The notes were originally written for a course in helioseismology given in 1985, and they were substantially revised in the Spring of 1989 for use in a course on pulsating stars.

I am grateful to the students who attended these courses for their comments. This has led to the elimination of some, although surely not all, errors in the text. Further comments and corrections are most welcome.

Preface to 3rd edition

The notes have been very substantially revised and extended in this edition, relative to the previous two editions. Thus Chapters 6 and 9 are essentially new, as are sections 2.4, the present section 5.1, section 5.3.2, section 5.5 and section 7.6. Some of this material has been adopted from various reviews, particularly Christensen-Dalsgaard & Berthomieu (1991). Also, the equation numbering has been revised. It is quite plausible that additional errors have crept in during this revision; as always, I should be most grateful to be told about them.

Preface to 4th edition

In this edition three appendices have been added, including a fairly extensive set of student problems in Appendix C. Furthermore, Chapter 10, on the excitation of oscillations, is new. The remaining revisions are relatively minor, although new material and updated results have been added throughout.

Preface to 5th edition

The present edition has been extensively revised. New material includes a presentation of the recent data on solar-like oscillations in distant stars, which mark the beginning of a new era of asteroseismology. Also, the discussion of asymptotic eigenfunctions of stellar oscillations, and of stochastic excitation of solar-like oscillations, has been substantially extended.

Unlike previous editions, the present one has been typeset using LaTeX, leading to substantial changes in appearance and changes to the equation numbering.

I am grateful to Ross Rosenwald for his careful reading of the 4th edition, which uncovered a substantial number of misprints, and to Frank Pijpers for comments on a draft of the present edition. I thank Sarbani Basu, Francois Bouchy, Bill Chaplin, Yvonne Elsworth, Hans Kjeldsen, Jesper Schou, and Steve Tomczyk for help with figures or other material.

The present edition has been made available on the World Wide Web, at URL `http://astro.phys.au.dk/~jcd/oscilnotes/`.

Aarhus, 29 January, 2014

Jørgen Christensen-Dalsgaard

Contents

Chapter 1

Introduction

There are two reasons for studying stellar pulsations: to understand why, and how, certain types of stars pulsate; and to use the pulsations to learn about the more general properties of these, and hence perhaps other, types of stars.

Stars whose luminosity varies periodically have been known for centuries. However, only within the last hundred years has it been definitely established that in many cases these variations are due to *intrinsic* pulsations of the stars themselves. For obvious reasons studies of pulsating stars initially concentrated on stars with large amplitudes, such as the Cepheids and the long period variables. The variations of these stars could be understood in terms of pulsations in the fundamental radial mode, where the star expands and contracts, while preserving spherical symmetry. It was realized very early (Shapley 1914) that the period of such motion is approximately given by the dynamical time scale of the star:

$$t_{\rm dyn} \simeq \left(\frac{R^3}{GM}\right)^{1/2} \simeq (G\bar{\rho})^{-1/2} \,, \tag{1.1}$$

where R is the radius of the star, M is its mass, $\bar{\rho}$ is its mean density, and G is the gravitational constant. Thus observation of the period immediately gives an estimate of one intrinsic property of the star, *viz.* its mean density.

It is a characteristic property of the Cepheids that they lie in a narrow, almost vertical strip in the HR diagram, the so-called *instability strip*. As a result, there is a direct relation between the luminosities of these stars and their radii; assuming also a mass-luminosity relation one obtains a relation between the luminosities and the periods, provided that the latter scale as $t_{\rm dyn}$. This argument motivates the existence of a *period-luminosity relation* for the Cepheids: thus the periods, which are easy to determine observationally, may be used to infer the intrinsic luminosities; since the apparent luminosities can be measured, one can determine the distance to the stars. This provides one of the most important distance indicators in astrophysics.

The main emphasis in the early studies was on understanding the causes of the pulsations, particularly the concentration of pulsating stars in the instability strip. As in many other branches of astrophysics major contributions to the understanding of stellar pulsation were made by Eddington (*e.g.* Eddington 1926). However, the identification of the actual cause of the pulsations, and of the reason for the instability strip, was first arrived at independently by Zhevakin (1953) and by Cox & Whitney (1958).

In parallel with these developments, it has come to be realized that some, and probably very many, stars pulsate in more complicated manners than the Cepheids. In many instances more than one mode of oscillation is excited simultaneously in a star; these modes may include both radial overtones, in addition to the fundamental, and *nonradial* modes, where the motion does not preserve spherical symmetry. (It is interesting that Emden [1907], who laid the foundation for the study of polytropic stellar models, also considered a rudimentary description of such nonradial oscillations.) This development is extremely important for attempts to use pulsations to learn about the properties of stars: each observed period is in principle (and often in practice) an independent measure of the structure of the star, and hence the amount of information about the star grows with the number of modes that can be detected. A very simple example are the *double mode Cepheids*, which have been studied extensively by, among others, J. Otzen Petersen, Copenhagen (*e.g.* Petersen 1973, 1974, 1978). These are apparently normal Cepheids which pulsate simultaneously in two modes, in most cases identified as the fundamental and the first overtone of radial pulsation. While measurement of a single mode, as discussed above, provides a measure of the mean density of the star, two periods roughly speaking allow determination of its mass and radius. It is striking that, as discussed by Petersen, even this limited information about the stars led to a conflict with the results of stellar evolution theory which has only been resolved very recently with the computation of new, improved opacity tables.

In other stars, the number of modes is larger. An extreme case is the Sun, where currently several thousand individual modes have been identified. It is expected that with more careful observation, frequencies for as many as 10^6 modes can be determined accurately. Even given likely advances in observations of other pulsating stars, this would mean that more than half the total number of known oscillation frequencies for *all* stars would belong to the Sun. This vast amount of information about the solar interior forms the basis for *helioseismology*, the science of learning about the Sun from the observed frequencies. This has already led to a considerable amount of information about the structure and rotation of the solar interior; much more is expected from observations, including some from space, now being prepared.

The observed solar oscillations mostly have periods in the vicinity of five minutes, considerably shorter than the fundamental radial period for the Sun, which is approximately 1 hour. Both the solar five-minute oscillations and the fundamental radial oscillation are acoustic modes, or *p modes*, driven predominantly by pressure fluctuations; but whereas the fundamental radial mode has no nodes, the five-minute modes are of high radial order, with 20 – 30 nodes in the radial direction.

The observational basis for helioseismology, and the applications of the theory developed in these notes, are described in a number of reviews. General background information was provided by, for example, Deubner & Gough (1984), Leibacher *et al.* (1985), Christensen-Dalsgaard, Gough & Toomre (1985), Libbrecht (1988), Gough & Toomre (1991) and Christensen-Dalsgaard & Berthomieu (1991). Examples of more specialized applications of helioseismology to the study of the solar interior were given by Christensen-Dalsgaard (1988a, 1996a).

Since we believe the Sun to be a normal star, similarly rich spectra of oscillations would be expected in other similar stars. An immediate problem in observations of stars, however, is that they have no, or very limited, spatial resolution. Most of the observed solar modes have relatively short horizontal wavelength on the solar surface, and hence would not be detected in stellar observations. A second problem in trying to detect the expected solar-

like oscillations in other stars is their very small amplitudes. On the Sun the *maximum* velocity amplitude in a single mode is about $15\,\mathrm{cm\,s^{-1}}$, whereas the luminosity amplitudes are of the order of 1 micromagnitude or less. Clearly extreme care is required in observing such oscillations in other stars, where the total light-level is low. In fact, despite several attempts and some tentative results, no definite detection of oscillations in a solar-like star has been made. Nevertheless, to obtain information, although less detailed than available for the Sun, for other stars would be extremely valuable; hence a great deal of effort is being spent on developing new instrumentation with the required sensitivity.

Although oscillations in solar-like stars have not been definitely detected, other types of stars display rich spectra of oscillations. A particularly interesting case are the white dwarfs; pulsations are observed in several groups of white dwarfs, at different effective temperatures. Here the periods are considerably *longer* than the period of the fundamental radial oscillation, indicating that a radically different type of pulsation is responsible for the variations. In fact it now seems certain that the oscillations are driven by buoyancy, as are internal gravity waves; such modes are called *g modes*. An excellent review of the properties of pulsating white dwarfs was given by Winget (1988). Another group of stars of considerable interest are the δ Scuti stars, which fall in the instability strip near the main sequence.

The present notes are mainly concerned with the basic theory of stellar pulsation, particularly with regards to the oscillation periods and their use to probe stellar interiors. However, as a background to the theoretical developments, Chapter 2 gives a brief introduction to the problems encountered in analyses of observations of pulsating stars, and summarizes the existing data on the Sun, as well as on δ Scuti stars and white dwarfs. A main theme in the theoretical analysis is the interplay between numerical calculations and simpler analytical considerations. It is a characteristic feature of many of the observed modes of oscillation that their overall properties can be understood quite simply in terms of asymptotic theory, which therefore gives an excellent insight into the relation between the structure of a star, say, and its oscillation frequencies. Asymptotic results also form the basis for some of the techniques for *inverse analysis* used to infer properties of the solar interior from observed oscillation frequencies. However, to make full use of the observations accurate numerical techniques are evidently required. This demand for accuracy motivates including a short chapter on some of the numerical techniques that are used to compute frequencies of stellar models. Departures from spherical symmetry, in particular rotation, induces fine structure in the frequencies. This provides a way of probing the internal rotation of stars, including the Sun, in substantial detail. A chapter on inverse analyses discusses the techniques that are used to analyse the observed solar frequencies and gives brief summaries of some of the results. The notes end with an outline of some aspects of the theory of the excitation of stellar pulsations, and how they may be used to understand the location of the Cepheid instability strip.

Chapter 2

Analysis of oscillation data

Observation of a variable star results in a determination of the variation of the properties of the star, such as the luminosity or the radial velocity, with time. To interpret the data, we need to isolate the properties of the underlying oscillations. When only a single mode is present, its period can normally be determined simply, and often very accurately. The analysis is much more complicated in the case of several modes, particularly when their amplitudes are small or their frequencies closely spaced. Here one has to use some form of Fourier analysis in time to isolate the frequencies that are present in the data.

For lack of better information, it was often assumed in the past that stellar oscillations have the simplest possible geometry, namely radial symmetry. This assumption is successful in many cases; however, radial oscillations are only a few among the many possible oscillations of a star, and the possible presence of nonradial modes must be kept in mind in analyses of oscillation observations (evidence for such modes in stars other than the Sun was summarized by Unno *et al.* 1989). A nonradial mode is characterized by three wavenumbers: the degree l and azimuthal order m which determine the behaviour of the mode over the surface of the star (see below) and the radial order n which reflects the properties in the radial direction (see Section 5.3). In general the frequencies ω_{nlm} of stellar oscillations depend on all three wave numbers. It is convenient, however, to separate the frequency into the *multiplet* frequency ω_{nl}, obtained as a suitable average over azimuthal order m and corresponding to the spherically symmetric structure of the star, and the *frequency splitting* $\delta\omega_{nlm} = \omega_{nlm} - \omega_{nl}$.

Analyses of oscillation data must attempt to separate these different frequency components. In the case of the Sun the oscillations can be observed directly as functions of position on the solar disk as well as time. Thus here it is possible to analyze their spatial properties. This is done by means of a generalized 2-dimensional Fourier transform in position on the solar surface, to isolate particular values of l and m. This is followed by a Fourier transform in time which isolates the frequencies of the modes of that type. In fact, the average over the stellar surface implicit in observations of stellar oscillations can be thought of as one example of such a spatial Fourier transform.

In this chapter I give a brief description of how the observable properties of the oscillations may be analyzed. The problems discussed here were treated in considerable detail by Christensen-Dalsgaard & Gough (1982). There are several books specifically on time-series analysis (*e.g.* Blackman & Tukey 1959; Bracewell 1978); an essentially "nuts-and-bolts"

description, with computer algorithms and examples, was given by Press *et al.* (1986). In addition, I summarize some observations of solar and stellar oscillations.

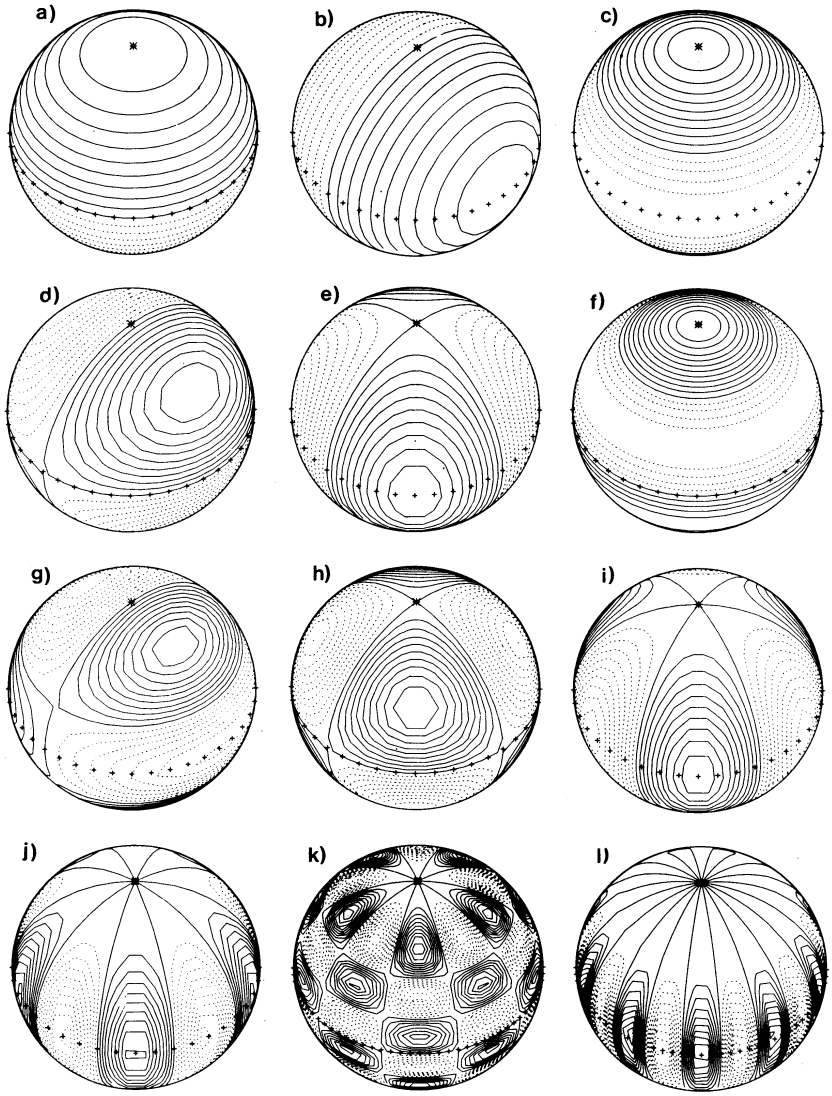

Figure 2.1: Contour plots of the real part of spherical harmonics Y_l^m [*cf.* equation (2.1); for simplicity the phase factor $(-1)^m$ has been suppressed]. Positive contours are indicated by continuous lines and negative contours by dashed lines. The $\theta = 0$ axis has been inclined by 45° towards the viewer, and is indicated by the star. The equator is shown by "++++". The following cases are illustrated: a) $l = 1$, $m = 0$; b) $l = 1$, $m = 1$; c) $l = 2$, $m = 0$; d) $l = 2$, $m = 1$; e) $l = 2$, $m = 2$; f) $l = 3$, $m = 0$; g) $l = 3$, $m = 1$; h) $l = 3$, $m = 2$; i) $l = 3$, $m = 3$; j) $l = 5$, $m = 5$; k) $l = 10$, $m = 5$; l) $l = 10$, $m = 10$.

2.1 Spatial filtering

As shown in Chapter 4, small-amplitude oscillations of a spherical object like a star can be described in terms of spherical harmonics $Y_l^m(\theta, \phi)$ of co-latitude θ (*i.e.*, angular distance from the polar axis) and longitude ϕ. Here

$$Y_l^m(\theta, \phi) = (-1)^m c_{lm} \; P_l^m \; (\cos\theta) \exp(i\, m\, \phi) \; , \tag{2.1}$$

where P_l^m is a Legendre function, and the normalization constant c_{lm} is determined by

$$c_{lm}^2 = \frac{(2l+1)(l-m)!}{4\pi(l+m)!} \; , \tag{2.2}$$

such that the integral of $|Y_l^m|^2$ over the unit sphere is 1. The degree l measures the total horizontal wave number k_h on the surface by

$$k_\mathrm{h} = \frac{L}{R} \; , \tag{2.3}$$

where $L = \sqrt{l(l+1)}$, and R is the radius of the Sun. Equivalently the wavelength is

$$\lambda = \frac{2\pi}{k_\mathrm{h}} = \frac{2\pi R}{L} \; . \tag{2.4}$$

Thus L is, roughly speaking, the number of wavelengths along the solar circumference. The azimuthal order m measures the number of nodes (*i.e.*, zeros) along the equator. The appearance of a few spherical harmonics is illustrated in Figure 2.1. Explicit expressions for selected Legendre functions, and a large number of useful results on their general properties, are given in Abramowitz & Stegun (1964). A summary is provided in Appendix A.

In writing down the spherical harmonics, I have left open the choice of polar axis. In fact, it is intuitively obvious that for a spherically symmetric star the choice of orientation of the coordinate system is irrelevant. If, on the other hand, the star is not spherically symmetric but possesses an axis of symmetry, this should be chosen as polar axis. The most important example of this is rotation, which is discussed in Chapter 8. In the present section I neglect departures from symmetry, and hence I am free to choose any direction of the polar axis.

Observations show that the solar oscillations consist of a superposition of a large number of modes, with degrees ranging from 0 to more than 1500. Thus here the observations and the data analysis must be organized so as to be sensitive to only a few degrees, to get time strings with contributions from sufficiently few individual oscillations that their frequencies can subsequently be resolved by Fourier analysis in time. The simplest form of mode isolation is obtained in whole-disk (or integrated-light) observations, where the intensity variations or velocity in light from the entire solar disk are observed. This corresponds to observing the Sun as a star, and, roughly speaking, averages out modes of high degree, where regions of positive and negative fluctuations approximately cancel.

To get a quantitative measure of the sensitivity of such observations to various modes, we consider first observations of intensity oscillations. The analysis in Chapter 4 shows that the oscillation in any scalar quantity, in particular the intensity, may be written on the form

$$\begin{aligned} I(\theta, \phi\,;\, t) \; &= \; \sqrt{4\pi}\Re\left\{I_0\, Y_l^m(\theta, \phi) \;\; \exp[-i(\omega_0 t - \delta_0)]\right\} \\ &= \; I_0\sqrt{4\pi}(-1)^m c_{lm} P_l^m(\cos\theta)\cos(m\phi - \omega_0 t + \delta_0) \; , \end{aligned} \tag{2.5}$$

where $\Re(z)$ is the real part of a complex quantity z. With the normalization chosen for the spherical harmonic, the *rms* of the intensity perturbation over the solar surface and time is $I_0/\sqrt{2}$. The response in whole-disk observations is obtained as the average over the disk of the Sun. Neglecting limb darkening, the result is

$$I(t) = \frac{1}{A}\int_A I(\theta,\phi;t)\mathrm{d}A \ , \tag{2.6}$$

where A is area on the disk. To evaluate the integral, a definite choice of coordinate system is needed. As mentioned above, we are free to choose the computationally most convenient orientation, which is to have the polar axis point towards the observer. Then the integral is zero unless $m = 0$, and for $m = 0$

$$I(t) = S_l^{(\mathrm{I})} I_0 \cos(\omega_0 t - \delta_0) \ , \tag{2.7}$$

where the spatial response function $S_l^{(\mathrm{I})}$ is

$$\begin{aligned} S_l^{(\mathrm{I})} &= \frac{1}{\pi}\int_0^{2\pi}\mathrm{d}\phi\int_0^{\pi/2}\sqrt{2l+1}P_l(\cos\theta)\cos\theta\sin\theta\mathrm{d}\theta \\ &= 2\sqrt{2l+1}\int_0^{\pi/2}P_l(\cos\theta)\ \cos\theta\sin\theta\,\mathrm{d}\theta \ . \end{aligned} \tag{2.8}$$

This may be calculated directly for low l, or by recursion. Some results are shown in Figure 2.2.

Observations of the velocity oscillations are carried out by measuring the Doppler shift of spectral lines; hence such observations are only sensitive to the line-of-sight component of velocity. For low-degree modes with periods shorter than about an hour, the velocity field is predominantly in the radial direction [*cf.* equation (4.67)], and may be written as

$$V(\theta,\phi;t) = \sqrt{4\pi}\Re\left\{V_0\, Y_l^m(\theta,\phi)\exp[-i(\omega_0 t - \delta_0)]\mathbf{a}_r\right\} \ , \tag{2.9}$$

where $\mathbf{a}_r$ is the unit vector in the radial direction. Here the *rms* over the solar surface and time of the radial component of velocity is $V_0/\sqrt{2}$. The result of whole-disk Doppler velocity observations may consequently be written, choosing again the polar axis to point towards the observer, as

$$v(t) = S_l^{(\mathrm{V})} V_0 \cos(\omega_0 t - \delta_0) \ , \tag{2.10}$$

where

$$S_l^{(\mathrm{V})} = 2\sqrt{2l+1}\int_0^{\pi/2}P_l(\cos\theta)\cos^2\theta\sin\theta\mathrm{d}\theta \tag{2.11}$$

is the velocity response function. This differs from $S_l^{(\mathrm{I})}$ only by the factor $\cos\theta$ in the integrand, which is due to the projection of the velocity onto the line of sight. As a result the response is slightly larger at $l = 3$ than for intensity observations (see Figure 2.2).

The response corresponding to a different choice of polar axis can be obtained by direct integration of the spherical harmonics, with a different orientation, over the stellar disk. A simpler approach, however, is to note that there are transformation formulae connecting spherical harmonics corresponding to different orientations of the coordinate system (Edmonds 1960). An important special case is when the polar axis is in the plane of the

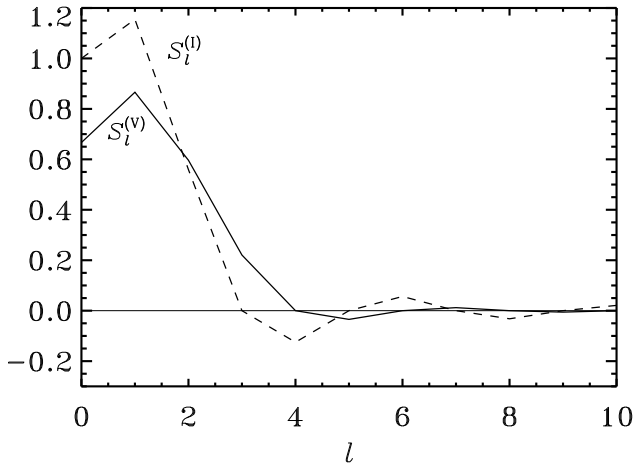

Figure 2.2: Spatial response functions $S_l^{(\mathrm{I})}$ and $S_l^{(\mathrm{V})}$ for observations of intensity and line-of-sight velocity, respectively, in light integrated over a stellar disk.

sky; this is approximately satisfied for the Sun, where the inclination of the rotation axis, relative to the sky, is at most about 7°. One then obtains the response as

$$S'_{lm} = \Gamma_{lm} S_l \ , \tag{2.12}$$

where S_l is the response as determined in equation (2.8) or (2.11), and the coefficients Γ_{lm} can be evaluated as described by Christensen-Dalsgaard & Gough (1982). In particular it is easy to see that Γ_{lm} is zero when $l - m$ is odd, for in this case the Legendre function $P_l^m(\cos\theta)$ is antisymmetric around the equator. Also $\Gamma_{l\,-m} = \Gamma_{lm}$. The non-trivial values of Γ_{lm} for the lowest degrees are:

$$\begin{aligned} \Gamma_{00} &= 1 \\ \Gamma_{11} &= \tfrac{1}{\sqrt{2}} \\ \Gamma_{20} &= \tfrac{1}{2} \qquad\qquad \Gamma_{22} = \tfrac{\sqrt{6}}{4} \\ \Gamma_{31} &= \tfrac{\sqrt{3}}{4} \qquad\qquad \Gamma_{33} = \tfrac{\sqrt{5}}{4} \end{aligned} \tag{2.13}$$

To isolate modes of higher degrees, one must analyse observations made as functions of θ and ϕ. Had data been available that covered the entire Sun, modes corresponding to a single pair (l_0, m_0) could in principle have been isolated by multiplying the data, after suitable scaling, with a spherical harmonic $Y_{l_0}^{m_0}(\theta, \phi)$ and integrating over the solar surface; it follows from the orthogonality of the spherical harmonics that the result would contain only oscillations corresponding to the degree and azimuthal order selected. In practice the observations are restricted to the visible disk of the Sun, and the sensitivity to velocity oscillations is further limited close to the limb due to the projection onto the line of sight.

To illustrate the principles in the mode separation in a little more detail, I note that, according to equations (2.1) and (2.9), the combined observed Doppler velocity on the solar surface is of the form

$$V_D(\theta,\phi,t) = \sin\theta\cos\phi \sum_{n,l,m} A_{nlm}(t) c_{lm} P_l^m(\cos\theta)\cos[m\phi - \omega_{nlm}t - \delta_{nlm}(t)] \ . \qquad (2.14)$$

Now the axis of the coordinate system has been taken to be in the plane of the sky; longitude ϕ is measured from the central meridian. [Also, to simplify the notation the factor $(-1)^m\sqrt{4\pi}$ has been included in A_{nlm}.] For simplicity, I still assume that the velocity is predominantly in the radial direction, as is the case for five-minute oscillations of low or moderate degree; the factor $\sin\theta\cos\phi$ results from the projection of the velocity vector onto the line of sight. The amplitudes A_{nlm} and phases δ_{nlm} may vary with time, as a result of the excitation and damping of the modes.

As discussed above, it may be assumed that V_D has been observed as a function of position (θ,ϕ) on the solar surface. The spatial transform may be thought of as an integration of the observations multiplied by a weight function $W_{l_0m_0}(\theta,\phi)$ designed to give greatest response to modes in the vicinity of $l = l_0, m = m_0$. The result is the filtered time string

$$\begin{aligned} V_{l_0m_0}(t) &= \int_A V_D(\theta,\phi,t) W_{l_0m_0}(\theta,\phi)\mathrm{d}A \\ &= \sum_{n,l,m} S_{l_0m_0lm} A_{nlm}\cos[\omega_{nlm}t + \hat{\delta}_{nlm,l_0m_0}] \ . \end{aligned} \qquad (2.15)$$

Here, the integral is over area on the solar disk, and $\mathrm{d}A = \sin^2\theta\cos\phi\,\mathrm{d}\theta\mathrm{d}\phi$; also, I introduced the *spatial response function* $S_{l_0m_0lm}$, defined by

$$(S_{l_0m_0lm})^2 = \left(S^{(+)}_{l_0m_0lm}\right)^2 + \left(S^{(-)}_{l_0m_0lm}\right)^2 \ , \qquad (2.16)$$

where

$$S^{(+)}_{l_0m_0lm} = c_{lm}\int_A W_{l_0m_0}(\theta,\phi) P_l^m(\cos\theta)\cos(m\phi)\sin\theta\cos\phi\,\mathrm{d}A \ , \qquad (2.17)$$

and

$$S^{(-)}_{l_0m_0lm} = c_{lm}\int_A W_{l_0m_0}(\theta,\phi) P_l^m(\cos\theta)\sin(m\phi)\sin\theta\cos\phi\,\mathrm{d}A \ . \qquad (2.18)$$

The new phases $\hat{\delta}_{nlm,l_0m_0}$ in equation (2.15) depend on the original phases δ_{nlm} and on $S^{(+)}_{l_0m_0lm}$ and $S^{(-)}_{l_0m_0lm}$.

It is evident that to simplify the subsequent analysis of the time string $V_{l_0m_0}(t)$, it is desirable that it contain contributions from a limited number of spherical harmonics (l,m). This is to be accomplished through a suitable choice of the weight function $W_{l_0m_0}(\theta,\phi)$ such that $S_{l_0m_0lm}$ is large for $l = l_0$, $m = m_0$ and "small" otherwise. Indeed, it follows from the orthogonality of the spherical harmonics that, if $W_{l_0m_0}$ is taken to be the spherical harmonic $Y_{l_0}^{m_0}$, if the integrals in equations (2.17) and (2.18) are extended to the full sphere, and if, in the integrals, $\sin\theta\cos\phi\,\mathrm{d}A$ is replaced by $\sin\theta\,\mathrm{d}\theta\mathrm{d}\phi$, then essentially $S_{l_0m_0lm} \propto \delta_{l_0l}\delta_{m_0m}$. It is obvious that, with realistic observations restricted to one hemisphere of the Sun, this optimal level of concentration cannot be achieved. However, the result suggests that suitable weights can be obtained from spherical harmonics. Weights of this nature are almost always used in the analysis. The resulting response functions are typically of order

unity for $|l-l_0| \lesssim 2$, $|m-m_0| \lesssim 2$ and relatively small elsewhere (*e.g.* Duvall & Harvey 1983; Christensen-Dalsgaard 1984a); this is roughly comparable to the mode isolation achieved in whole disk observations. That the response extends over a range in l and m is analogous to the quantum-mechanical uncertainty principle between localization in space and momentum (here represented by wavenumber). If the area being analyzed is reduced, the spread in l and m is increased; conversely, intensity observations, which do not include the projection factor $\sin\theta\cos\phi$, effectively sample a larger area of the Sun and therefore, in general, lead to somewhat greater concentration in l and m (see also Fig. 2.2).

2.2 Fourier analysis of time strings

The preceding section considered the spatial analysis of oscillation observations, either implicitly through observation in integrated light or explicitly through a spatial transform. Following this analysis we are left with timestrings containing a relatively limited number of modes. These modes may then be separated through Fourier analysis in time. Here I mainly consider simple harmonic oscillations. These are typical of small-amplitude pulsating stars, such as the Sun. Some remarks on periodic oscillations with more complex behaviour are given in Section 2.2.5.

A simple harmonic oscillating signal can be written as

$$v(t) = a_0 \cos(\omega_0 t - \delta_0) \; . \tag{2.19}$$

Here ω_0 is the angular frequency, and the period of oscillation is $\Pi = 2\pi/\omega_0$. Oscillations are often also discussed in terms of their cyclic frequency $\nu = 1/\Pi = \omega/2\pi$, measured in mHz or μHz. A period of 5 minutes (typical of the most important class of solar oscillations) corresponds to $\nu = 3.3$ mHz $= 3300$ μHz, and $\omega = 0.021\,\mathrm{s}^{-1}$. In studies of classical pulsating stars it is common to measure the period in units of the dynamical time scale $t_{\rm dyn}$ [*cf.* equation (1.1)] by representing it in terms of the *pulsation constant*

$$Q = \Pi \left(\frac{M}{M_\odot}\right)^{1/2} \left(\frac{R}{R_\odot}\right)^{-3/2} \; , \tag{2.20}$$

where $M_\odot$ and $R_\odot$ are the solar mass and radius. Thus Q provides information about the more intricate properties of stellar interior structure, beyond the simple scaling of the period with the dynamical time scale.

2.2.1 Analysis of a single oscillation

The signal in equation (2.19) is assumed to be observed from $t = 0$ to $t = T$. Then the Fourier transform is

$$\begin{aligned}
\tilde{v}(\omega) &= \int_0^T v(t) \mathrm{e}^{i\omega t} \mathrm{d}t = \frac{1}{2} a_0 \int_0^T \left[\mathrm{e}^{i(\omega_0 t - \delta_0)} + \mathrm{e}^{-i(\omega_0 t - \delta_0)}\right] \mathrm{e}^{i\omega t} \mathrm{d}t \\
&= \frac{1}{2} a_0 \left\{ \frac{\mathrm{e}^{-i\delta_0}}{i(\omega+\omega_0)} [\mathrm{e}^{i(\omega+\omega_0)T} - 1] + \frac{\mathrm{e}^{i\delta_0}}{i(\omega-\omega_0)} [\mathrm{e}^{i(\omega-\omega_0)T} - 1] \right\} \\
&= a_0 \left\{ \mathrm{e}^{i[T/2(\omega+\omega_0)-\delta_0]} \frac{\sin[T/2(\omega+\omega_0)]}{\omega+\omega_0} + \mathrm{e}^{i[T/2(\omega-\omega_0)+\delta_0]} \frac{\sin[T/2(\omega-\omega_0)]}{\omega-\omega_0} \right\} \\
&= \frac{T}{2} a_0 \left\{ \mathrm{e}^{i[T/2(\omega+\omega_0)-\delta_0]} \mathrm{sinc}\,[\frac{T}{2}(\omega+\omega_0)] + \mathrm{e}^{i[T/2(\omega-\omega_0)+\delta_0]} \mathrm{sinc}\,[\frac{T}{2}(\omega-\omega_0)] \right\} \; ,
\end{aligned} \tag{2.21}$$

where

$$\mathrm{sinc}\,(x) = \frac{\sin x}{x}\ . \tag{2.22}$$

Plots of $\mathrm{sinc}\,(x)$ and $\mathrm{sinc}^{\,2}(x)$ are shown in Figure 2.3. The power spectrum is

$$P(\omega) = |\tilde{v}(\omega)|^2 \tag{2.23}$$

and has the appearance shown schematically in Figure 2.4.

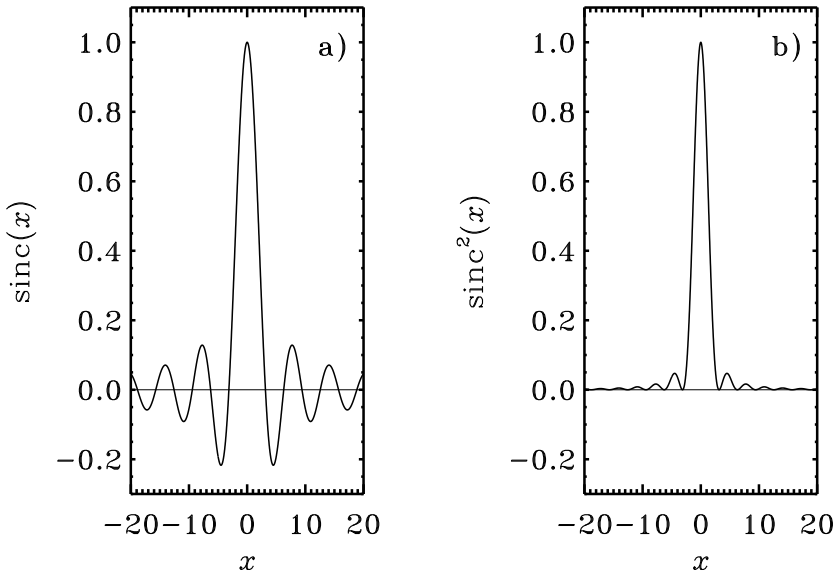

Figure 2.3: The sinc function (a) and $\mathrm{sinc}^{\,2}$ function (b) [*cf.* equation (2.22)].

If $T\omega_0 \gg 1$ the two components of the spectrum at $\omega = -\omega_0$ and $\omega = \omega_0$ are well separated, and we need only consider, say, the positive ω-axis; then, approximately

$$P(\omega) \simeq \frac{1}{4}\,T^2 a_0^2 \mathrm{sinc}^{\,2}\left[\frac{T}{2}(\omega - \omega_0)\right]\ . \tag{2.24}$$

I use this approximation in the following. Then both the maximum and the centre of gravity of P is at $\omega = \omega_0$. Thus in principle both quantities can be used to determine the frequencies from observations of oscillation. In practice the observed peak often has a more complex structure, due to observational noise and fluctuations in the oscillation amplitude. In such cases the centre of gravity is often better defined than the location of the maximum of the peak. As a measure of the accuracy of the frequency determination, and of the ability to separate closely spaced peaks, we may use the width $\delta\omega$ of the peak, which may be estimated by, say

$$\frac{T}{2}\,\frac{\delta\omega}{2} \simeq \frac{\pi}{2}\ , \qquad \delta\omega \simeq \frac{2\pi}{T}\ , \qquad \delta\nu \simeq \frac{1}{T}\ . \tag{2.25}$$

(More precisely, the half width at half maximum of $\mathrm{sinc}^2(x)$ is 0.443π.) Hence to determine the frequency accurately, we need extended observations (T must be large.) In fact, the relative resolution

$$\frac{\delta\omega}{\omega_0} \simeq \frac{2\pi}{\omega_0 T} = \frac{\Pi}{T} \tag{2.26}$$

is 1 divided by the number of oscillation periods during the observing time T. Note also that for 8 hours of observations (a typical value for observations from a single site) the width in cyclic frequency is $\delta\nu = 34\,\mu$Hz.

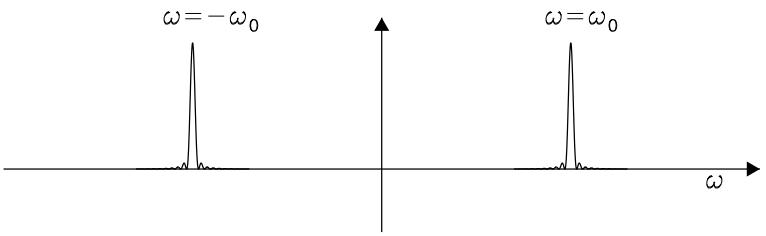

Figure 2.4: Schematic appearance of the power spectrum of a single harmonic oscillation. Note that the oscillation gives rise to a peak on both the positive and the negative ω-axis.

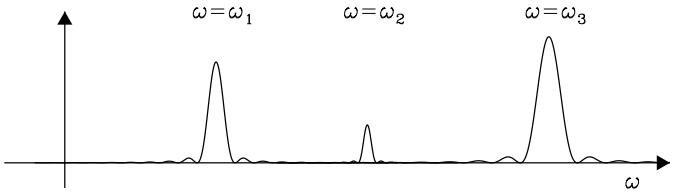

Figure 2.5: Schematic representation of spectrum containing 3 well-separated modes.

2.2.2 Several simultaneous oscillations

Here the time string is

$$v(t) = a_1 \cos(\omega_1 t - \delta_1) + a_2 \cos(\omega_2 t - \delta_2) + a_3 \cos(\omega_3 t - \delta_3) + \cdots . \tag{2.27}$$

The spectrum might be expected to be, roughly, the sum of the spectra of the individual oscillations, as shown schematically in Figure 2.5. This would allow the individual frequencies to be determined. This is the case if the modes are well separated, with $|\omega_i - \omega_j|T \gg 1$ for all pairs $i \neq j$. However, in the Sun and other types of pulsating stars the oscillation

frequencies are densely packed, and the situation may be a great deal more complicated. I consider the case of just two oscillations in more detail:

$$v(t) = a_1 \cos(\omega_1 t - \delta_1) + a_2 \cos(\omega_2 t - \delta_2) \; . \tag{2.28}$$

Then on the positive ω-axis we get the Fourier transform

$$\begin{aligned} &\tilde{v}(\omega) \simeq \\ &\frac{T}{2} \left\{ a_1 \mathrm{e}^{i[T/2(\omega-\omega_1)+\delta_1]} \mathrm{sinc} \left[\frac{T}{2}(\omega - \omega_1) \right] + a_2 \mathrm{e}^{i[T/2(\omega-\omega_2)+\delta_2]} \mathrm{sinc} \left[\frac{T}{2}(\omega - \omega_2) \right] \right\} \; , \end{aligned} \tag{2.29}$$

and the power

$$\begin{aligned} P(\omega) \; = \; & \frac{T^2}{4} \left\{ a_1^2 \mathrm{sinc}^{\,2} \left[\frac{T}{2}(\omega - \omega_1) \right] + a_2^2 \mathrm{sinc}^{\,2} \left[\frac{T}{2}(\omega - \omega_2) \right] \right. \\ & \left. + 2 a_1 a_2 \mathrm{sinc} \left[\frac{T}{2}(\omega - \omega_1) \right] \mathrm{sinc} \left[\frac{T}{2}(\omega - \omega_2) \right] \cos \left[\frac{T}{2}(\omega_2 - \omega_1) - (\delta_2 - \delta_1) \right] \right\} \; . \end{aligned} \tag{2.30}$$

Note that a naive summation of the two individual spectra would result in the first two terms; the last term is caused by *interference* between the modes, which is very important for closely spaced frequencies. The outcome depends critically on the relative phases, and to some extent the relative amplitudes, of the oscillations.

In Figure 2.6 are shown some examples of spectra containing two oscillations. Here, to limit the parameter space, $a_1 = a_2$. $\Delta\omega = \omega_2 - \omega_1$ is the frequency difference (which is non-negative in all cases), and $\Delta\delta = \delta_2 - \delta_1$ is the phase difference at $t = 0$. The vertical lines show the locations of the frequencies ω_1 and ω_2. Note in particular that when $\Delta\delta = 3\pi/2$, the splitting is artificially exaggerated when $\Delta\omega$ is small; the peaks in power are shifted by considerable amounts relative to the actual frequencies. This might easily cause confusion in the interpretation of observed spectra. These effects were discussed by Loumos & Deeming (1978) and analyzed in more detail by Christensen-Dalsgaard & Gough (1982). From the results in Figure 2.6 we obtain the rough estimate of the frequency separation that can be resolved in observations of duration T regardless of the relative phase:

$$\delta\omega \simeq \frac{12}{T} \; . \tag{2.31}$$

Note that this is about twice as large as the width of the individual peaks estimated in equation (2.25).

To demonstrate in more detail the effect on the observed spectrum of the duration of the time series, I consider the analysis of an artificial data set with varying resolution, for the important case of low-degree, high-order p modes of a rotating star. I use a simplified approximation to the asymptotic theory presented in Chapter 7 [*cf.* equations (7.55) and (7.58)], and the discussion of the effects of rotation in Chapter 8 [*cf.* equation (8.45)], and hence approximate the frequencies of such modes as

$$\nu_{nlm} \simeq \Delta\nu_0 (n + \frac{l}{2} + \epsilon_0) - l(l+1) D_0 + m \Delta\nu_{\mathrm{rot}} \; , \tag{2.32}$$

where n is the radial order (*i.e.*, the number of nodes in the radial direction), and l and m were defined in Section 2.1. Here the last term is caused by rotation, with $\Delta\nu_{\mathrm{rot}} = 1/\Pi_{\mathrm{rot}}$, where Π_{rot} is an average over the star of the rotation period. The remaining

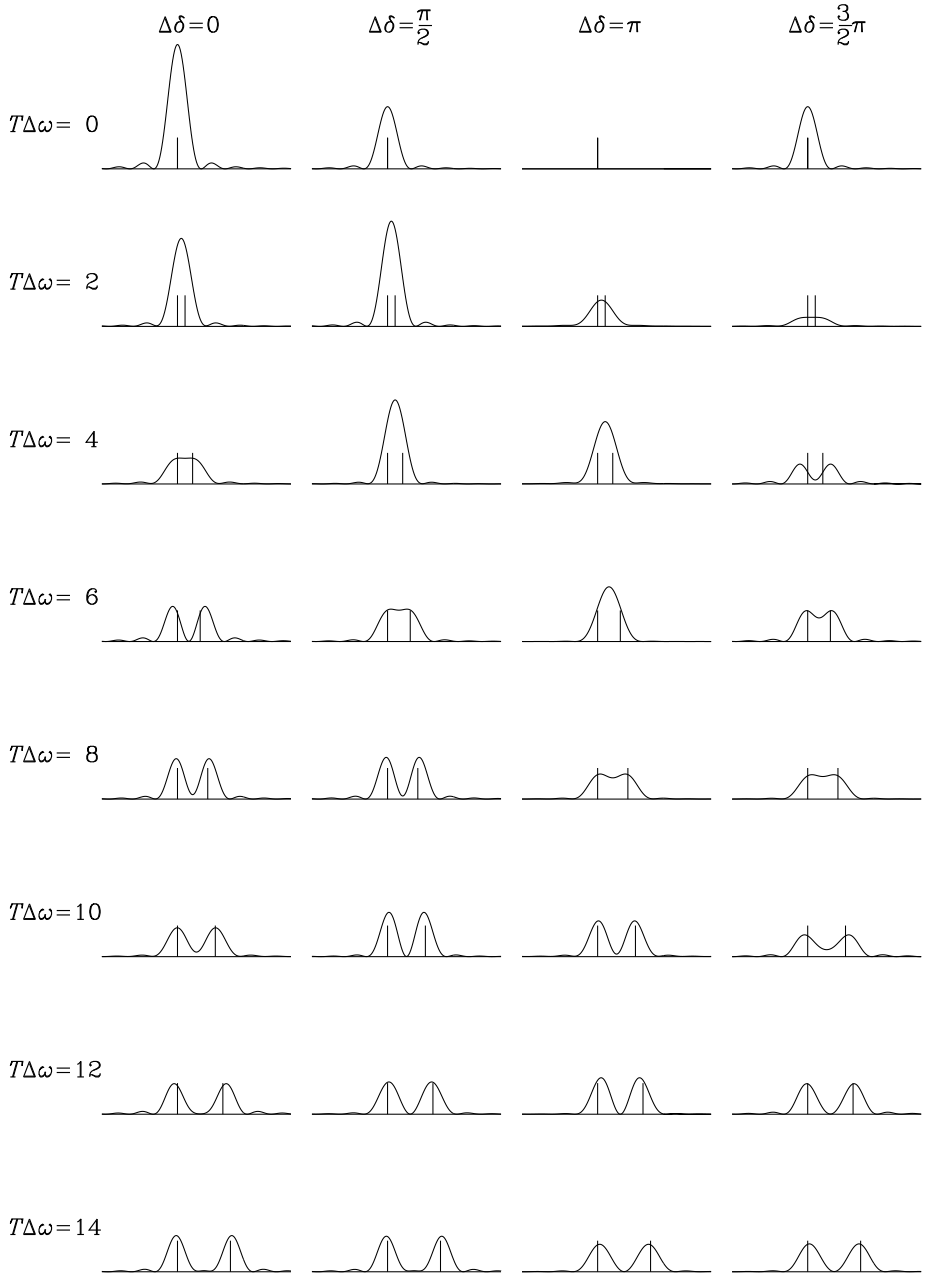

Figure 2.6: Spectra of two modes closely spaced in frequency, with the same amplitude [*cf.* equation (2.30)]. The vertical lines the frequency and amplitude of the two modes. $\Delta\omega = \omega_2 - \omega_1$ is the frequency difference between the modes, and $\Delta\delta = \delta_2 - \delta_1$ is the phase difference at $t = 0$.

terms approximate the frequencies of the nonrotating star. The dominant term is the first, according to which the frequencies depend predominantly on n and l in the combination $n + l/2$. Thus to this level of precision the modes are organized in groups according to the

parity of l. The term in $l(l+1)$ causes a separation of the frequencies according to l, and finally the last term causes a separation, which is normally considerably smaller, according to m. There is an evident interest in being able to resolve these frequency separations observationally.

The frequencies were calculated from equation (2.32), with $\Delta\nu_0 = 120\,\mu$Hz, $\epsilon_0 = 1.2$, $D_0 = 1.5\,\mu$Hz and a rotational splitting $\Delta\nu_{\rm rot} = 1\,\mu$Hz (corresponding to about twice the solar surface rotation rate). These values are fairly typical for solar-like stars. The response of the observations to the modes was calculated as described in Section 2.1; for simplicity the rotation axis was assumed to be in the plane of the sky, so that only modes with even $l - m$ can be observed. For clarity the responses for $l = 3$ were increased by a factor 2.5. The amplitudes and phases of the modes were chosen randomly, but were the same for all time strings. The data were assumed to be noise-free.

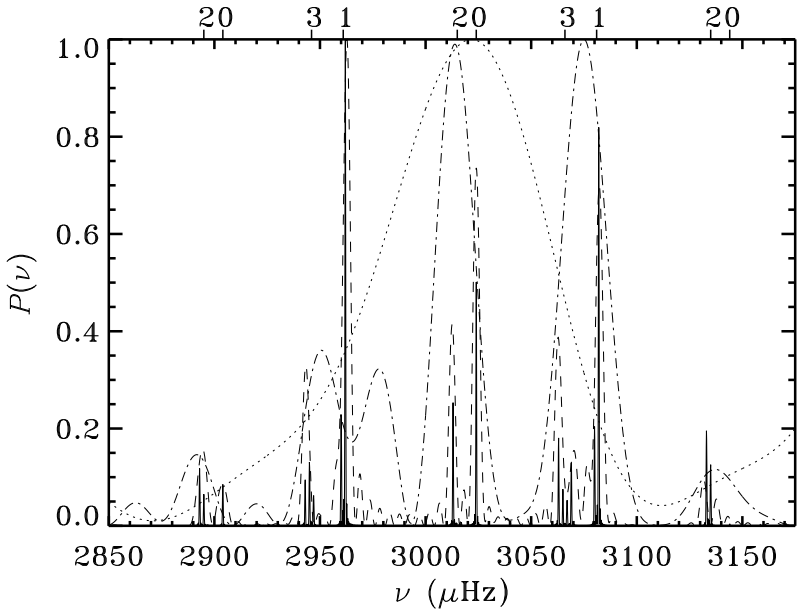

Figure 2.7: Power spectra of simulated time series of duration 600 h (————), 60 h (– – – – – – –), 10 h (—·—·—·—) and 3 h (·····). The power is on an arbitrary scale and has been normalized to a maximum value of 1. The location of the central frequency for each group of rotationally split modes, as well as the value of the degree, are indicated on the top of the diagram. (From Christensen-Dalsgaard 1984b.)

Short segments of the resulting power spectra, for $T = 3\,\text{h}, 10\,\text{h}, 60\,\text{h}$ and 600 h, are shown in Figure 2.7. The power is on an arbitrary scale, normalized so that the maximum is unity in each case. For $T = 600\,$h the modes are completely resolved. At $T = 60\,$h the rotational splitting is unresolved, but the modes at individual n and l can to a large extent be distinguished; however, a spurious peak appears next to the dominant peak with $l = 1$ at $2960\,\mu$Hz. For $T = 10\,$h modes having degrees of the same parity merge; here

the odd-l group at $\nu \simeq 2960\,\mu$Hz gives rise to two clearly resolved, but fictitious, peaks of which one is displaced by about $20\,\mu$Hz relative to the centre of the group. These effects are qualitatively similar to those seen in Figure 2.6. Finally, the spectrum for $T = 3\,$h is dominated by interference and bears little immediate relation to the underlying frequencies.

The case shown in Figure 2.7 was chosen as typical among a fairly large sample with different random phases and amplitudes. The results clearly emphasize the care that is required when interpreting inadequately resolved data. Furthermore, in general all values of m are expected to be observed for stellar oscillations, adding to the complexity.

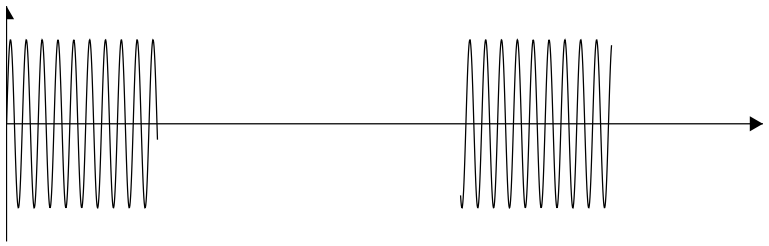

Figure 2.8: Sketch of interrupted time series. This corresponds to two 8 hour data segments, separated by a 16 hour gap.

2.2.3 Data with gaps

From a single site (except very near one of the poles) the Sun or a star can typically be observed for no more than 10–12 hours out of each 24 hours. As discussed in connection with Figure 2.7, this is far from enough to give the required frequency resolution. Thus one is faced with combining data from several days. This adds confusion to the spectra. I consider again the signal in equation (2.19), but now observe it for $t = 0$ to T and τ to $\tau + T$. The signal is unknown between T and τ, and it is common to set it to zero here, as sketched in Figure 2.8. Then the Fourier transform is, on the positive ω-axis,

$$\begin{aligned}
\tilde{v}(\omega) &= \int_0^T v\,(t)\,\mathrm{e}^{i\omega t}\mathrm{d}t + \int_\tau^{\tau+T} v(t)\mathrm{e}^{i\omega t}\mathrm{d}t \\
&\simeq \frac{T}{2}\,a_0\left\{\mathrm{e}^{i[\frac{T}{2}(\omega-\omega_0)+\delta_0]} + \mathrm{e}^{i[(\tau+\frac{T}{2})(\omega-\omega_0)+\delta_0]}\right\}\mathrm{sinc}\,[\frac{T}{2}(\omega-\omega_0)] \\
&= Ta_0 e^{i[1/2(\tau+T)(\omega-\omega_0)+\delta_0]}\cos[\frac{\tau}{2}(\omega-\omega_0)]\mathrm{sinc}\,[\frac{T}{2}(\omega-\omega_0)]\;, \qquad (2.33)
\end{aligned}$$

and the power is

$$P(\omega) = T^2 a_0^2 \cos^2[\frac{\tau}{2}(\omega-\omega_0)]\mathrm{sinc}^{\,2}[\frac{T}{2}(\omega-\omega_0)]\;. \qquad (2.34)$$

Thus one gets the spectrum from the single-day case, modulated by the $\cos^2[\frac{1}{2}\tau(\omega-\omega_0)]$ factor. As $\tau > T$ this introduces apparent fine structure in the spectrum. An example with $\tau = 3\,T$ is shown in Figure 2.9.

When more days are combined this so-called side-band structure can be somewhat suppressed, but never entirely removed. In particular, there generally remain two additional

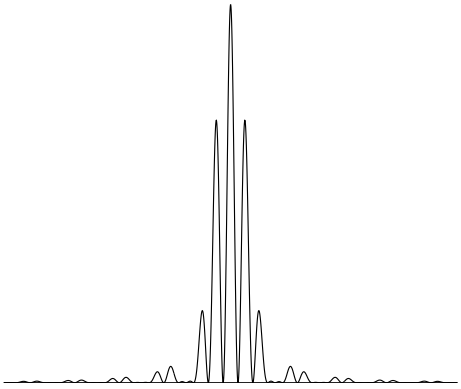

Figure 2.9: Power spectrum of the time series shown in Figure 2.8 [*cf.* equation (2.34)].

peaks separated from the main peak by $\delta\omega = 2\pi/\tau$ or $\delta\nu = 1/\tau$. For $\tau = 24$ hours, $\delta\nu = 11.57$ μHz.

Exercise 2.1:

Evaluate the power spectrum for the signal in equation (2.19), observed between 0 and T, τ and $\tau + T$, ... $N\tau$, $N\tau + T$, and verify the statement made above.

If several closely spaced modes are present as well, the resulting interference may get quite complicated, and the interpretation correspondingly difficult. An example of this is shown in Figure 2.10, together with the corresponding spectrum resulting from a single day's observations.

The effects of gaps can conveniently be represented in terms of the so-called *window function* $w(t)$, defined such that $w(t) = 1$ during the periods with data and $w(t) = 0$ during the gaps. Thus the observed data can be written as

$$v(t) = w(t)v_0(t) \; , \tag{2.35}$$

where $v_0(t)$ is the underlying signal (which, we assume, is there whether it is observed or not). It follows from the convolution theorem of Fourier analysis that the Fourier transform of $v(t)$ is the convolution of the transforms of $v_0(t)$ and $w(t)$:

$$\tilde{v}(\omega) = (\tilde{w} * \tilde{v}_0)(\omega) = \int \tilde{w}(\omega - \omega')\tilde{v}_0(\omega')\mathrm{d}\omega' \; ; \tag{2.36}$$

here '$*$' denotes convolution, and $\tilde{w}(\omega)$ is the transform of a timestring consisting of 0 and 1, which is centred at zero frequency. It follows from equation (2.36) that if the peaks in the original power spectrum $P_0(\omega) = |\tilde{v}_0(\omega)|^2$ are well separated compared with the spread

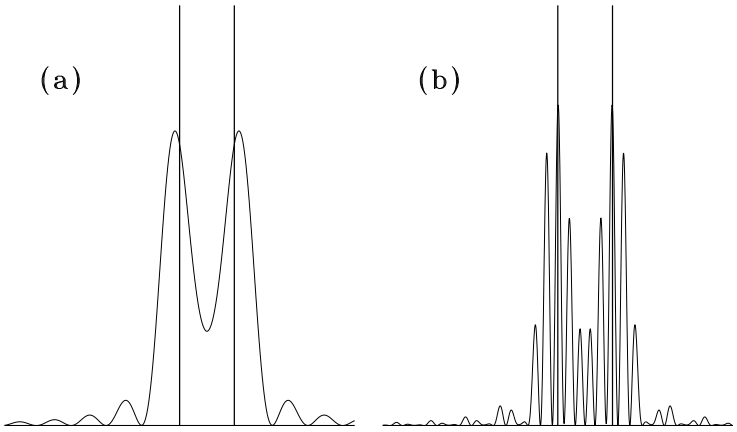

Figure 2.10: In (a) is shown the spectrum for two closely spaced modes with $T\Delta\omega = 10$, $\Delta\delta = 3\pi/2$, observed during a single day, from Figure 2.6. In (b) is shown the corresponding case, but observed for two 8 hour segments separated by 24 hours.

of the window function transform $P_w(\omega) = |\tilde{w}(\omega)|^2$, the observed spectrum $P(\omega) = |\tilde{v}(\omega)|^2$ consists of copies of $P_w(\omega)$, shifted to be centred on the 'true' frequencies. Needless to say, the situation becomes far more complex when the window function transforms overlap, resulting in interference.

There are techniques that to some extent may compensate for the effects of gaps in the data, even in the presence of noise (*e.g.* Brown & Christensen-Dalsgaard 1990). However, these are relatively inefficient when the data segments are shorter than the gaps. To overcome these problems, several independent projects are under way to construct networks of observatories with a suitable distribution of sites around the Earth, to study solar oscillations with minimal interruptions. Campaigns to coordinate observations of stellar oscillations from different observatories have also been organized. Furthermore, the SOHO spacecraft has carried helioseismic instruments to the L_1 point between the Earth and the Sun, where the observations can be carried out without interruptions. This has the added advantage of avoiding the effects of the Earth's atmosphere.

2.2.4 Further complications

The analysis in the preceding sections is somewhat unrealistic, in that it is assumed that the oscillation amplitudes are strictly constant. If the oscillation is damped, one has, instead of equation (2.19)

$$v(t) = a_0 \cos(\omega_0 t - \delta_0) \mathrm{e}^{-\eta t} \,, \tag{2.37}$$

where η is the *damping rate*. If this signal is observed for an infinitely long time, one obtains the power spectrum

$$P(\omega) = \frac{1}{4} \frac{a_0^2}{(\omega - \omega_0)^2 + \eta^2} \,. \tag{2.38}$$

A peak of this form is called a *Lorentzian profile*. It has a half width at half maximum of η.

Exercise 2.2:

Verify equation (2.38).

If the signal in equation (2.37) is observed for a finite time T, the resulting peak is intermediate between the sinc^2 function and the Lorentzian, tending to the former for $\eta T \ll 1$, and towards the latter for $\eta T \gg 1$. This transition is illustrated in Figure 2.11.

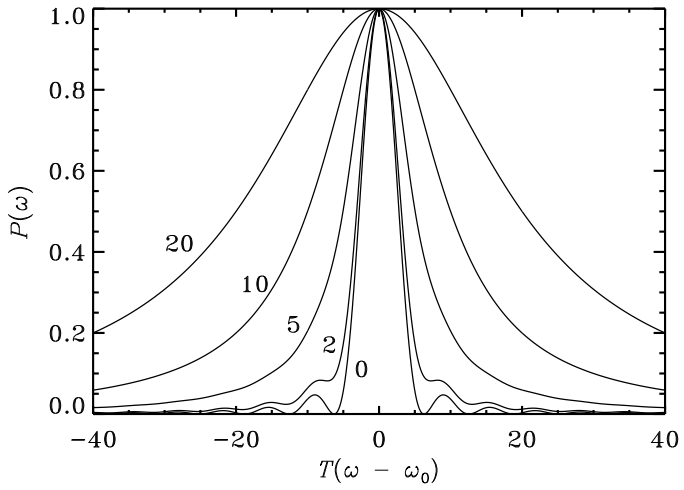

Figure 2.11: Power spectrum for the damped oscillator in equation (2.37), observed for a finite time T. The abscissa is frequency separation, in units of T^{-1}. The ordinate has been normalized to have maximum value 1. The curves are labelled by the value of ηT, where η is the damping rate.

Equation (2.37) is evidently also an idealization, in that it (implicitly) assumes a sudden excitation of the mode, followed by an exponential decay. In the Sun, at least, it appears that the oscillations are excited stochastically, by essentially random fluctuations due to the turbulent motion in the outer parts of the solar convection zone. It may be shown that this process, combined with exponential decay, gives rise to a spectrum that on average has a Lorentzian profile. The statistics of the determination of frequencies, amplitudes and line widths from such a spectrum was studied by Sørensen (1988), Kumar, Franklin & Goldreich (1988) and Schou (1993). These issues are discussed in more detail in Section 10.3. It should be noted (see also Figure 10.4) that the stochastic nature of the excitation gives rise to a number of sharp peaks, with a distribution around the the general Lorentzian envelope; thus, in particular, it cannot be assumed that the maximum power corresponds to the true frequency of the mode. Substantial care is therefore required in analyzing data of this nature.

So far I have considered only noise-free data. Actual observations of oscillations contain noise from the observing process, from the Earth's atmosphere and from the random velocity

(or intensity) fields in the solar or stellar atmosphere. At each frequency in the power spectrum the noise may be considered as an oscillation with a random amplitude and phase; this interferes with the actual, regular oscillations, and may suppress or artificially enhance some of the oscillations. However, because the noise is random, it may be shown to decrease in importance with increasingly long time series.

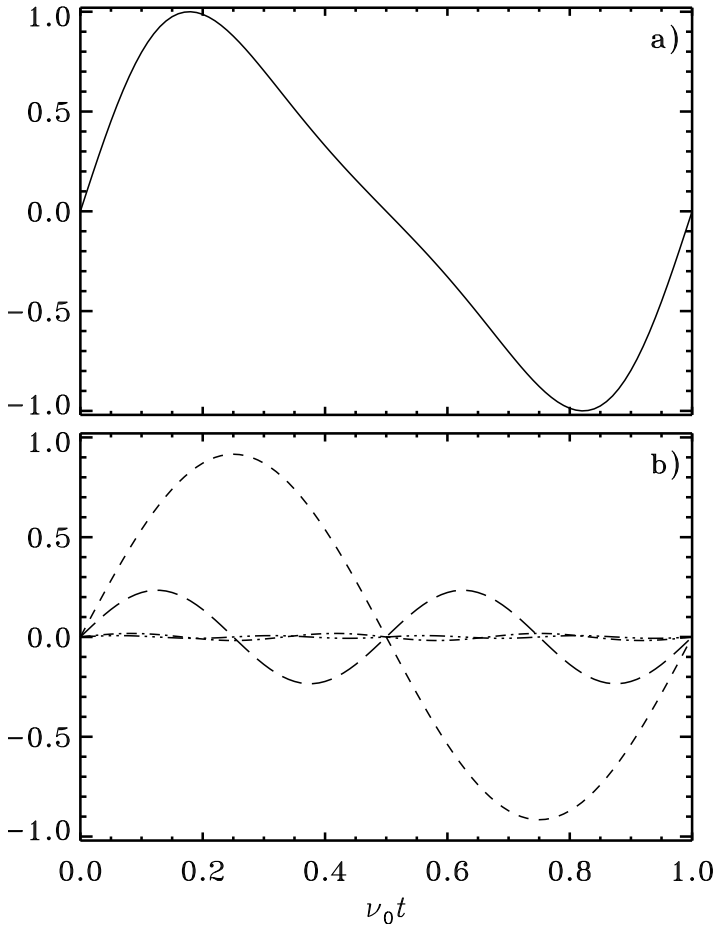

Figure 2.12: (a) Example of non-sinusoidal oscillation, plotted against relative phase $\nu_0 t = \omega_0 t/2\pi$. This is roughly similar to observed light curves of large-amplitude Cepheids. (b) The first 3 Fourier components of the oscillation shown in panel (a). The remaining components have so small amplitudes that they do not contribute significantly to the total signal.

2.2.5 Large-amplitude oscillations

For large-amplitude pulsating stars, such as Cepheids, the oscillation typically no longer behaves like the simple sine function in equation (2.19). Very often the oscillation is still strictly periodic, however, with a well-defined frequency ω_0. Also the light curve, for example, in many cases has a shape similar to the one shown in Figure 2.12, with a rapid rise

and a more gradual decrease.

It is still possible to carry out a Fourier analysis of the oscillation. Now, however, peaks appear at the harmonics $k\omega_0$ of the basic oscillation frequency, where $k = 1, 2, \ldots$. This corresponds to representing the observed signal as a Fourier series

$$v(t) = \sum_k a_k \sin(k\,\omega_0 t - \phi_k) \; . \tag{2.39}$$

Figure 2.12b shows the first few Fourier components of the oscillation in Figure 2.12. More generally the shape of the oscillation is determined, say, by the amplitude ratios a_k/a_1 and the phase differences $\phi_k - k\,\phi_1$. These quantities have proved very convenient for the characterization of observed light curves (*e.g.* Andreasen & Petersen 1987), as well as for the analysis of numerical results. One may hope that further work in this direction will allow an understanding of the physical reasons underlying the observed behaviour.

In a double-mode, large-amplitude pulsating star, with basic frequencies ω_1 and ω_2, Fourier analysis in general produces peaks at the combination frequencies $k\omega_1 + j\omega_2$, for integral k and j. Thus the spectrum may become quite complex. In particular, the detection of additional basic frequencies is difficult, since these might easily be confused with the combination frequencies, given the finite observational resolution.

2.3 Results on solar oscillations

By far the richest spectrum of oscillations has been observed for the Sun; this allows detailed investigations of the properties of the solar interior. Thus it is reasonable to summarize the observational situation for the Sun. Figure 2.13 shows schematically the modes that have been definitely observed, as well as modes for which detection has been claimed in the past. Only the modes in the five-minute region have definitely been observed and identified. As mentioned in Chapter 1, they are standing acoustic waves, generally of high radial order. It is interesting that they are observed at all values of the degree, from purely radial modes at $l = 0$ to modes of very short horizontal wavelength at $l = 1500$. Furthermore, there is relatively little change in the amplitude per mode between these two extremes. The p and f modes have now been detected to frequencies as low as $500\,\mu$Hz (*e.g.* Schou 1998; Bertello *et al.* 2000). The apparent existence of oscillations at even lower frequency has caused very substantial interest; if real and of solar origin, they would correspond to standing gravity waves, or g modes, whose frequencies are very sensitive to conditions in the deep solar interior. However, it should be noted that recent analyses have provided stringent upper limits to the amplitudes of such modes, which makes highly questionable earlier claims of detections (*e.g.* Appourchaux *et al.* 2000).

Figure 2.14 shows an example of an observed power spectrum of solar oscillations. This was obtained by means of Doppler velocity measurements in light integrated over the solar disk, and hence, according to the analysis in Section 2.1, is dominated by modes of degrees 0 – 3. The data were obtained from the BiSON network of six stations globally distributed in longitude, to suppress the daily side-bands, and span roughly four months. Thus the intrinsic frequency resolution, as determined by equation (2.25), is smaller than the thickness of the lines. There is a visible increase in the line-width when going from low to high frequency. The broadening of the peaks at high frequency is probably caused by the damping and excitation processes, as discussed in Section 2.2.4; thus the observations indicate that the damping rate increases with increasing frequency. Finally, there is clearly

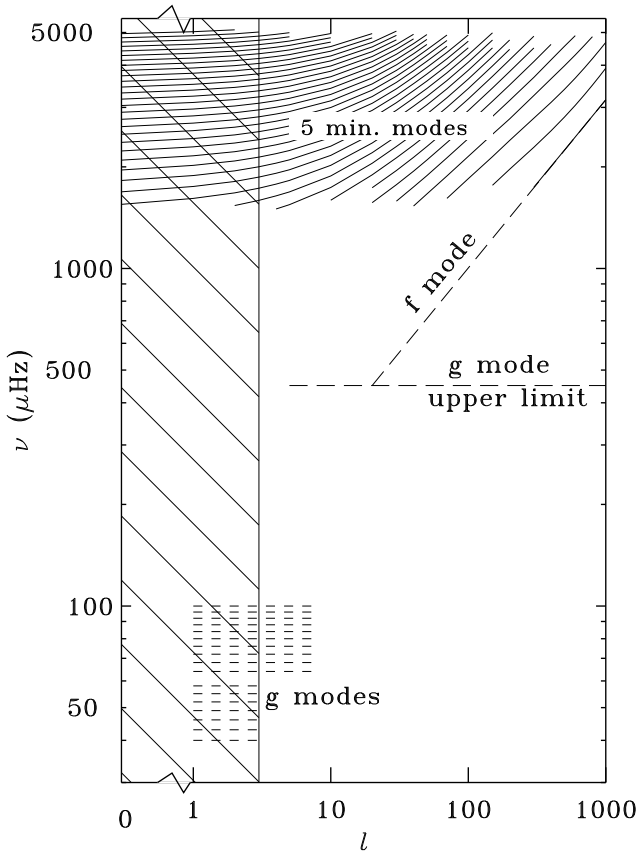

Figure 2.13: Schematic illustration of the oscillations observed in the Sun. The 5 minute oscillations are standing acoustic waves. They have been completely identified. Each of the lines in this part of the diagram corresponds to a given value of the radial order n. The f mode, which is essentially a surface gravity wave, has been observed at high degree; acoustic modes have frequencies exceeding that of the f mode. The presence of the long-period oscillations was suggested by early observations, but the reality, let alone solar origin, of these oscillations has not been established; had they corresponded to oscillations of the Sun, they would likely have been g modes of low degree. Note that g modes are restricted to lie underneath the frequency indicated as "g mode upper limit". The hatching indicates the region in l that can be observed in light integrated over the disk, as is generally the case for stars.

a well-defined distribution of amplitudes, with a maximum around 3000 μHz and very small values below 2000, and above 4500, μHz. The maximum power corresponds to a velocity amplitude of around $15\,\mathrm{cm\,s^{-1}}$; observations in broad-band intensity show amplitudes up to around 4 ppm. The power distribution is essentially the same at all degrees where the five-minute oscillations are observed. An interesting analysis of the observed dependence of

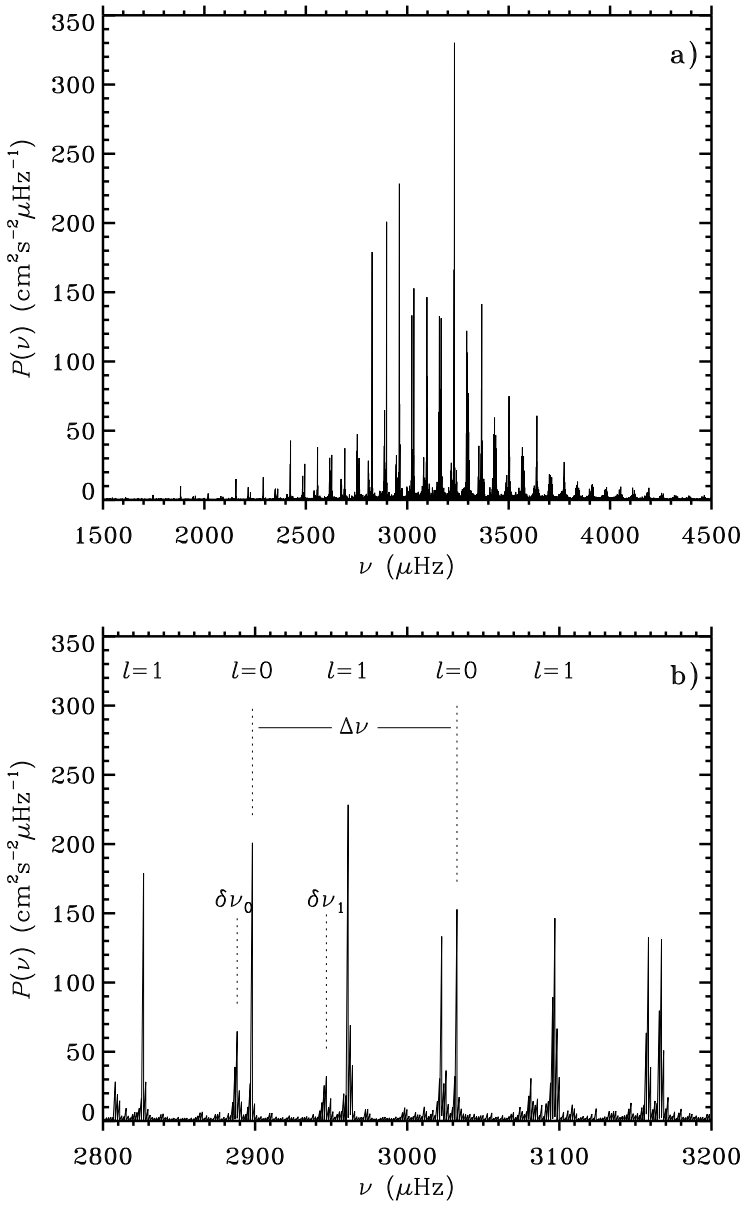

Figure 2.14: Power spectrum of solar oscillations, obtained from Doppler observations in light integrated over the disk of the Sun. The ordinate is normalized to show velocity power per frequency bin. The data were obtained from six observing stations and span approximately four months. Panel (b) provides an expanded view of the central part of the frequency range. Here some modes have been labelled by their degree l, and the large and small frequency separations $\Delta\nu$ and $\delta\nu_l$ [*cf.* equations (2.40) and (2.41)] have been indicated. (See Elsworth *et al.* 1995.)

mode amplitudes on degree, azimuthal order and frequency was presented by Libbrecht *et al.* (1986). Woodard *et al.* (2001) recently made a careful investigation of the dependence of the mode energy on degree and frequency of oscillation, based on observations from the SOHO spacecraft.

The spectrum illustrated in Figure 2.14 evidently has a highly regular frequency structure, most clearly visible in the expanded view in panel (b). This reflects the asymptotic expression in equation (2.32), apart from the rotational effects which are invisible at this frequency resolution. According to the leading term in equation (2.32), the peaks should occur in groups corresponding to even and odd degree, such that $n + l/2$ are the same, the groups being uniformly spaced with a separation $\Delta\nu/2$; this apparent degeneracy is lifted by the second term in equation (2.32). Thus the spectrum is characterized by the *large frequency separation*

$$\Delta\nu = \nu_{n+1\,l} - \nu_{nl} \ , \tag{2.40}$$

and the *small frequency separation*

$$\delta\nu_l = \nu_{nl} - \nu_{n-1\,l+2} \simeq (4l+6)D_0 \ . \tag{2.41}$$

These separations are indicated in Figure 2.14b, where also selected peaks corresponding to $l = 0$ and 1 have been labelled, in each case with a neighbouring peak with $l = 2$ or 3, respectively. It should be noticed that the observed amplitudes of the $l = 3$ peaks are much reduced relative to the $l = 1$ peaks, as predicted by the spatial response function $S_l^{(\mathrm{V})}$ shown in Figure 2.2; on the other hand, the observed amplitudes for $l = 0$ and 2 are roughly similar, as expected.

To illustrate in more detail the properties of the frequency spectrum, it is convenient to use an *echelle diagram* (*e.g.* Grec, Fossat & Pomerantz 1983). Here the frequencies are reduced modulo $\Delta\nu$ by expressing them as

$$\nu_{nl} = \nu_0 + k\Delta\nu + \tilde{\nu}_{nl} \ , \tag{2.42}$$

where ν_0 is a suitably chosen reference, and k is an integer such that $\tilde{\nu}_{nl}$ is between 0 and $\Delta\nu$; the diagram is produced by plotting $\tilde{\nu}_{nl}$ on the abscissa and $\nu_0 + k\Delta\nu$ on the ordinate. Graphically, this may be thought of as cutting the frequency axis into pieces of length $\Delta\nu$ and stacking them above each other. If the asymptotic relation (2.32) had been precisely satisfied, the result would be points arranged on a set of vertical lines corresponding to the different values of l, the lines being separated by the appropriate $\delta\nu_l$. The actual behaviour is shown in Figure 2.15, based on frequencies from BiSON observations. The general behaviour is clearly as expected, although with significant departures. The curvature of the lines indicate that the frequency for each l are not precisely uniformly spaced; as discussed in Section 7.7.3 this results from variations in structure near the solar surface. Also, it is fairly evident that the small separation varies with mode order.

To illustrate the quality of current frequency determinations, Figure 2.16 shows observed frequencies at low and moderate degree from one year's observations with the High Altitude Observatory's LOWL instrument (see Tomczyk *et al.* 1995). The error bars have been magnified by a factor 1000 over the usual 1σ error bars. For the most accurate measurements, the relative standard deviation is well below 10^{-5}, thus substantially exceeding the precision with which the solar mass is known. Precise measurements of frequencies, frequency separations and rotational splittings for low-degree modes were published by Elsworth *et al.* (1990), Toutain & Fröhlich (1992), Fröhlich *et al.* (1997), Lazrek *et al.* (1997), Chaplin

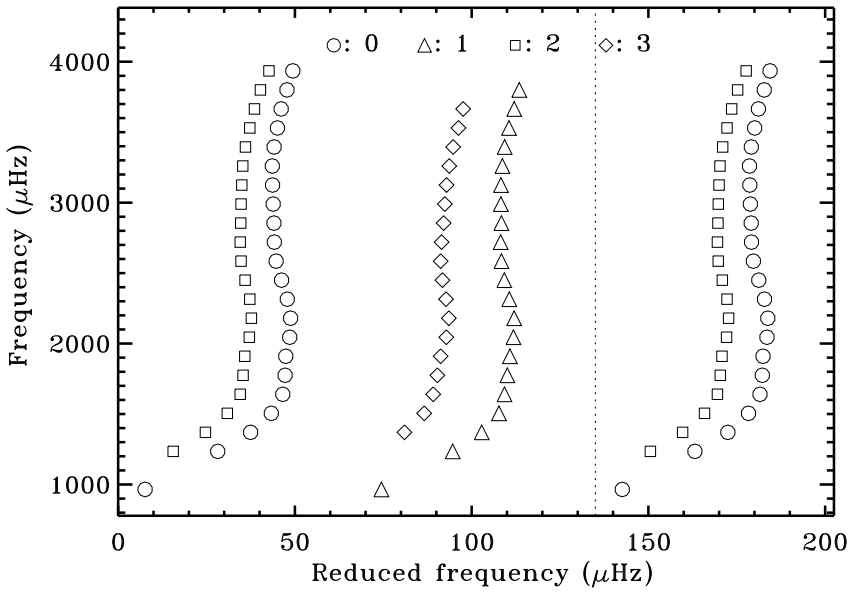

Figure 2.15: Echelle diagram for observed solar frequencies obtained with the BiSON network (Chaplin *et al.* 2002), plotted with $\nu_0 = 830\,\mu$Hz and $\Delta\nu = 135\,\mu$Hz (*cf.* eq. 2.42). Circles, triangles, squares and diamonds are used for modes of degree $l = 0, 1, 2$ and 3, respectively. For clarity the points for $l = 0$ and 2 have been repeated in the right-hand part of the diagram; the dotted vertical line indicates $\Delta\nu$.

et al. (1998, 1999, 2001ab); such measurements are of great diagnostic importance for the properties of the solar core (*cf.* Section 7.3). An extensive set of high-degree frequencies was obtained by Bachmann *et al.* (1995).

From spatially resolved observations, individual frequencies ω_{nlm} can in principle be determined. Because of observational errors and the large amount of data resulting from such determination, it has been common to present the results in terms of coefficients in fits to the m-dependence of the frequencies, either averaged over n at given l (Brown & Morrow 1987) or for individual n and l (*e.g.*, Libbrecht 1989). A convenient form of the expansion was established by Ritzwoller & Lavely (1991); this can be expressed as

$$\omega_{nlm} = \omega_{nl0} + 2\pi \sum_{j=1}^{j_{\max}} a_j(n,l) \mathcal{P}_j^{(l)}(m) \;, \tag{2.43}$$

in terms of the so-called a coefficients $a_j(n,l)$. Here the $\mathcal{P}_j^{(l)}$ are polynomials of degree j which satisfy the orthogonality relation $\sum_m \mathcal{P}_i^{(l)}(m)\mathcal{P}_j^{(l)}(m) = 0$ for $i \neq j$ (see also Schou *et al.*, 1994). Explicit expressions for these polynomials were given by Pijpers (1997). As discussed in Chapters 8 and 9 [*cf.* Section 8.2 and equation (9.25)] the coefficients a_j with odd j arise from rotational splitting; the coefficients with even j are caused by departures

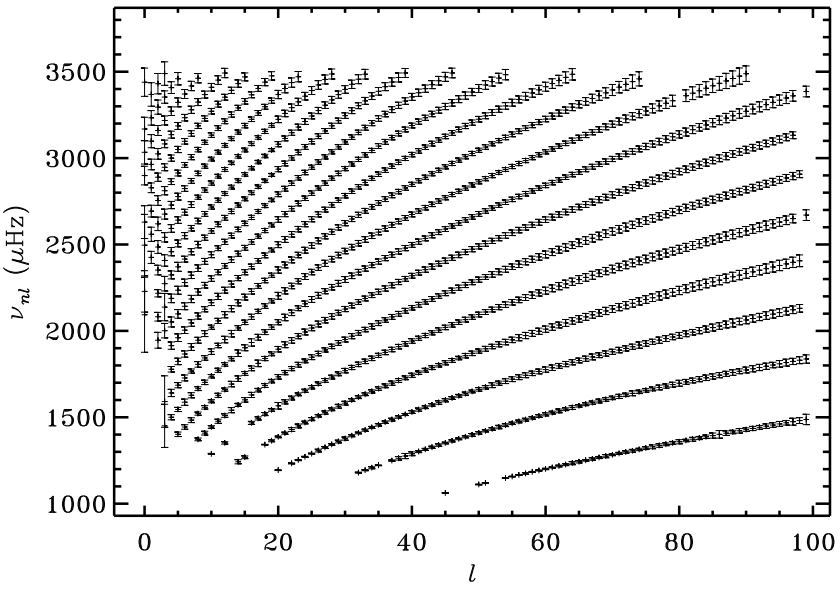

Figure 2.16: Plot of observed solar p-mode multiplet frequencies, as a function of the degree l, from one year of observations. The vertical lines show the 1000σ error bars. Each ridge corresponds to a given value of the radial order n, the lowest ridge having $n = 1$. (See Tomczyk, Schou & Thompson 1996).

from spherical symmetry in solar structure, or from effects of magnetic fields.

It is probably a fair assessment that the major developments in helioseismology in recent years have resulted from improvements in the observations. The principal problems in early data was the presence of gaps, leading to sidebands in the power spectra, and the effects of atmospheric noise. The problems with gaps have been overcome through observations from global networks; nearly continuous observations, which are furthermore free of effects of the Earth's atmosphere, have been obtained from space. The result has been greatly sets of frequencies, extending to high degree, which has very substantially improved our knowledge about the solar interior.

As shown in Figure 2.9, gaps in the timeseries introduce sidebands in the spectrum; these add confusion to the mode identification and contribute to the background of noise in the spectra. Largely uninterrupted timeseries of several days', and up to a few weeks', duration have been obtained from the South Pole (*e.g.* Grec *et al.* 1980; Duvall *et al.* 1991); however, to utilize fully the phase stability of the modes at relatively low frequency requires continuous observations over far longer periods, and these cannot be obtained from a single terrestrial site.

Nearly continuous observations can be achieved from a network of observing stations, suitably placed around the Earth (*e.g.* Hill & Newkirk 1985). An overview of network projects was given by Hill (1990). A group from the University of Birmingham has operated

the BiSON[1] network for many years, to perform whole-disk observations using the resonant scattering technique (*e.g.* Chaplin *et al.* 1996). A similar network (the IRIS[2] network) has been set up by a group at the University of Nice (Fossat 1991).

An even more ambitious network has been established in the GONG[3] project, organized by the National Solar Observatory of the United States (for introductions to the project, see Harvey, Kennedy & Leibacher 1987; Harvey *et al.* 1996). This project has involved the setting up at carefully selected locations of six identical observing stations. They use an interferometric technique to observe solar oscillations of degrees up to around 250. In addition to the design and construction of the observing equipment, a great deal of effort is going into preparing for the merging and analysis of the very large amounts of data expected, and into establishing the necessary theoretical tools. The network became operational in October 1995 when the last station, in Udaipur (India) started observing. The GONG network, and early results obtained with it, was described by Gough *et al.* (1996) and in accompanying papers.

Major efforts have gone into the development of helioseismic instruments for the *SOHO*[4] spacecraft, which was launched in December 1995 (*e.g.* Domingo, Fleck & Poland 1995), as a joint project between ESA and NASA. *SOHO* is located near the L_1 point between the Earth and the Sun, and hence is in continuous sunlight. This permits nearly unbroken observations of solar oscillations. A further advantage is the absence of effects from the Earth's atmosphere. These are particularly troublesome for observations of high-degree modes, where seeing is a serious limitation (*e.g.* Hill *et al.* 1991), and for intensity observations of low-degree modes, which suffer from transparency fluctuations.

SOHO carries three instrument packages for helioseismic observations:

- The GOLF instrument (for **G**lobal **O**scillations at **L**ow **F**requency; see Gabriel *et al.* 1995, 1997). This uses the resonant scattering technique in integrated light. Because of the great stability of this technique, it is hoped to measure oscillations at comparatively low frequency, possibly even g modes. Unlike the p modes, which have formed the basis for helioseismology so far, the g modes have their largest amplitude near the solar centre; hence, detection of these modes would greatly aid the study of the structure and rotation of the core. Also, since the lifetime of p modes increases rapidly with decreasing frequency, very great precision is possible for low-frequency p modes.

- The SOI-MDI experiment (for **S**olar **O**scillations **I**nvestigation – **M**ichelson **D**oppler **I**mager; see Scherrer *et al.* 1995; Rhodes *et al.* 1997) uses the Michelson interferometer technique. By observing the entire solar disk with a resolution of 4 arcseconds, and parts of the disk with a resolution of 1.2 arcseconds, it is possible to measure oscillations of degree as high as a few thousand; furthermore, very precise data have been obtained on modes of degree up to about 1000, including those modes for which ground-based observation is severely limited by seeing. As a result, it has been possible to study the structure and dynamics of the solar convection zone, and of the radiative interior, in great detail.

[1] **Bi**rmingham **S**olar **O**scillation **N**etwork
[2] **I**nternational **R**esearch on the **I**nterior of the **S**un
[3] **G**lobal **O**scillation **N**etwork **G**roup
[4] **SO**lar and **H**eliospheric **O**bservatory

- The VIRGO experiment (for **V**ariability of solar **IR**radiance and **G**ravity **O**scillations; see Fröhlich *et al.* 1995, 1997). This contains radiometers and Sun photometers to measure oscillations in solar irradiance and broad-band intensity. It is hoped that this will allow the detection of g modes; furthermore, the observations supplement those obtained in Doppler velocity, particularly with regards to investigating the phase relations for the oscillations in the solar atmosphere.

Several very extensive tables of five-minute oscillation frequencies have become available in recent years. As examples, tables of multiplet frequencies are provided at `http://astro.phys.au.dk/~jcd/oscilnotes/data/`. One set, described in more detail by Basu *et al.* (1997), consists of a combination of BiSON low-degree data and data for modes of low and intermediate degree from the LOWL instrument. The second set was obtained from around 4 months of observations with the GONG network (see Schou *et al.* 2002). Links to further data are also given; these in particular include very extensive results obtained with the MDI instrument on SOHO, covering both multiplet frequencies and a coefficients (*cf.* eq. 2.43) (see Schou 1999; Schou *et al.* 2002).

2.4 Other types of multi-periodic stars

Observations of stellar oscillations provide constraints on the properties of the star and, as mentioned in Chapter 1, the information content increases with the number of observable modes. Fortunately, pulsating stars are found throughout the Hertzsprung-Russell diagram. This is illustrated schematically in Fig. 2.17, which summarizes the known classes of stars, in relation to selected evolution tracks; some of these classes will be discussed in more detail in the following,

An important region in the diagram is the *Cepheid instability strip*, populated by the Cepheids ('Ceph') and RR Lyrae stars ('RR Lyr') as well as, close to the main sequence, the δ Scuti stars ('δ Sct'). These are believed to be excited by an opacity mechanism associated with the second helium ionization zone; as discussed in detail in Chapter 10 this provides an explanation for the localized nature of these stars in the HR diagram. In the Cepheids and RR Lyrae stars typically only a single period is observed, in most cases assumed to correspond to the fundamental radial mode. The stars near the main sequence, on the other hand, generally show several periods, making them potentially more interesting for investigations of the stellar interiors. This is also true for the more massive slowly pulsating B stars ('SPB') and β Cephei stars ('β Cep'); the former have periods of around a day or more whereas the latter have periods of the order of hours. These oscillations are also excited by opacity mechanisms, although related to opacity features dominated by iron-group elements.

The rapidly oscillating Ap stars ('roAp') are also located in the instability strip, but with fairly peculiar characteristics. They oscillate in high-order acoustic modes, rather like the Sun, but the oscillations are closely tied to the large-scale magnetic field found in these stars; this is probably related to the abundance inhomogeneities set up across the stellar surface as a result of the suppression of convection by the magnetic field.

Red giants show oscillations of very long periods, corresponding to the large dynamic timescale resulting from their huge radii (*cf.* eq. 1.1). The Mira variables have very large amplitudes in the visible band, up to eight magnitudes, although the amplitude in the luminosity oscillations are more modest; much of the effect in the visible arises from the

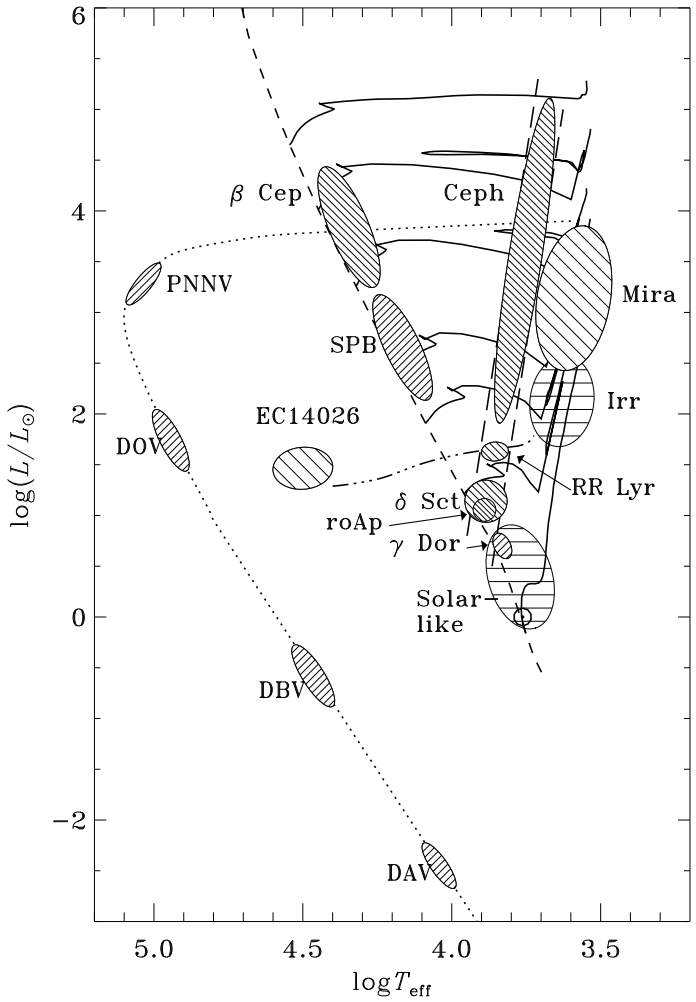

Figure 2.17: Schematic Hertzsprung-Russell diagram illustrating the location of several classes of pulsating stars. The dashed line shows the zero-age main sequence, the continuous curves are selected evolution tracks, at masses 1, 2, 3, 4, 7, 12 and 20 $M_\odot$, the dot-dashed line is the horizontal branch and the dotted curve is the white-dwarf cooling curve.

temperature-sensitivity of the formation of molecules in the stellar atmospheres. They are typically single periodic. The irregular variables ('Irr') have lower amplitudes and show variations in the amplitudes and possibly periods.

The final stages of stellar evolution are represented by the subdwarf B variable stars (also known as 'EC 14026' stars, after the first member of the group to be discovered), discussed in more detail in Section 2.4.3 below. Their pulsations are also, as for the main-sequence B stars, caused by an opacity mechanism related to iron-group elements. Several groups of white dwarfs, discussed in Section 2.4.4, also pulsate.

Finally, oscillations corresponding to those observed in the Sun are expected in a broad group of stars. The solar oscillations are believed to be excited stochastically by the near-surface convection (see also Section 10.6). Thus oscillations of a similar nature are expected in all stars with effective temperature $T_{\rm eff} \lesssim 7000\,{\rm K}$, which have vigorous outer convection. As discussed in Section 2.4.1, this expectation has recently been dramatically confirmed.

2.4.1 Solar-like oscillations in other stars

The archetypal example is obviously the spectrum shown in Figure 2.14, obtained for the Sun observed as a star, in disk-averaged light. This is characterized by a broad spectrum of almost uniformly spaced peaks, approximately satisfying the asymptotic relation (2.32) and hence characterized by the large frequency separation $\Delta\nu$ and the small frequency separation $\delta\nu$ [*cf.* equations (2.40) and (2.41)]. The power distribution results from the broad-band nature of the excitation (see also Section 10.6) which causes all modes in a fairly extensive frequency range to be excited. This greatly simplifies the identification of the modes and hence the comparison with stellar models. In the search for solar-like oscillations the nearly uniformly spaced frequency pattern, and the distribution of mode power, are typically the characteristics to look for.

The main difficulty in observing solar-like oscillations are the extremely small amplitudes, either in Doppler or intensity observations, judging from the maximal solar amplitudes of around $15\,{\rm cm\,s^{-1}}$ and 4 ppm, respectively. Christensen-Dalsgaard & Frandsen (1983a) made rough estimates of the expected amplitudes from which Kjeldsen & Bedding (1995) concluded that the amplitudes approximately scaled proportional to

$$\frac{L}{M} \propto \frac{T_{\rm eff}^4}{g_{\rm s}} \,, \tag{2.44}$$

where L and M are the luminosity and mass of the star, and $g_{\rm s}$ is the surface gravity. More detailed calculations by Houdek *et al.* (1999) largely confirmed these results (see also Section 10.3). Accordingly, main-sequence stars more massive than the Sun are expected to have substantially higher amplitudes, and relatively large amplitude are predicted for red giants.

A major improvement in the observational techniques has recently resulted from the development of very stable radial-velocity measurements to search for extra-solar planets as reflected in the motion of their central stars. As discussed below, these have led to striking detections of solar-like oscillations in a few cases, and more detections and detailed investigations are expected in the near future from such observations.

Very substantial observational efforts have been made to detect solar-like oscillations in stars near the main sequence. For example, Gilliland *et al.* (1993) carried out an extensive coordinated campaign on the open cluster M67, with most of the world's largest telescopes; this failed to detect any oscillations, in some cases with upper limits well below the theoretical predictions. Perhaps the first plausible detection was made by Kjeldsen *et al.* (1995), who observed the subgiant η Bootis using a technique based on measurements of equivalent widths of spectral lines. The resulting power spectrum, shown in Figure 2.18, does display the enhancement of power expected for solar-like oscillations; the determination of the oscillation frequencies was complicated by the fact that only observations from a single site were observable, leading to the window function (*cf.* Section 2.2.3) illustrated in the inset. However, Kjeldsen *et al.* were able to determine both the frequency separations $\Delta\nu$

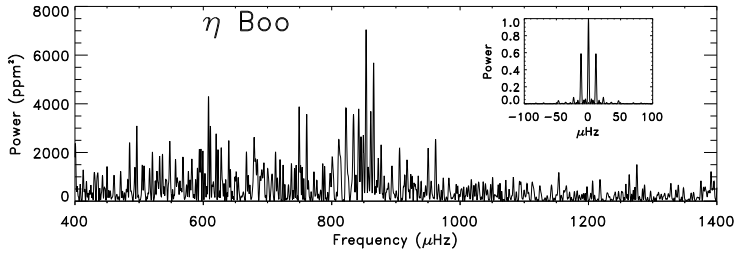

Figure 2.18: Observed power spectrum of η Bootis, based on equivalent-width observations by Kjeldsen *et al.* (1995). The inset shows the window function of these single-site observations. (From Bedding & Kjeldsen 1995.)

and $\delta\nu_0$, which were in reasonable agreement with expectations based on evolution models of the star. It should be noted, however, that Brown *et al.* (1997) failed to find oscillations in this star in Doppler velocity, with an upper limit which they estimated to be well below the amplitudes claimed by Kjeldsen *et al.*; thus the reality of these oscillations remains somewhat questionable.

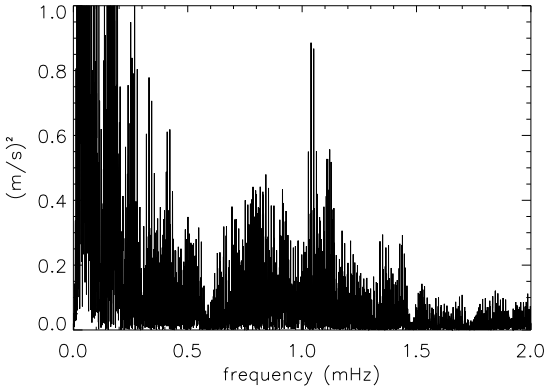

Figure 2.19: Observed power spectrum of Procyon, based on radial-velocity observations. (From Barban *et al.* 1999.)

A promising case is Procyon (α CMi) where Brown *et al.* (1991) reported oscillations in radial velocity with approximately the expected dependence on frequency. This early detection has recently been confirmed by Martić *et al.* (1999), again using radial-velocity observations; a power spectrum of these observations is shown in Figure 2.19. A careful analysis by Barban *et al.* (1999), comparing the observed spectra with simulated data for models of Procyon, led to a determination of the large separation $\Delta\nu \simeq 56\,\mu$Hz, in good agreement with model predictions. Interestingly, the observed amplitude was only about

1/3 of the predictions, confirming the inference from M67 that the theoretical estimates provide an overestimate; it should be noted that both Procyon and the stars observed in M67 are somewhat hotter than the Sun.

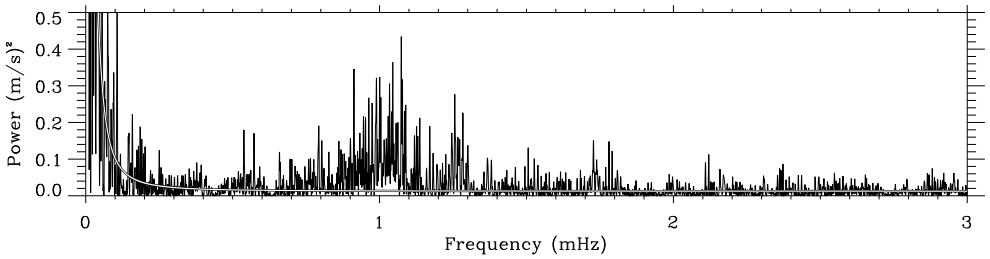

Figure 2.20: Power spectrum of β Hydri, from radial-velocity observations by Bedding *et al.* (2001). The white line marks the noise level.

Detection of a power enhancement at the expected frequency was recently reported by Bedding *et al.* (2001) from radial-velocity observations of the star β Hyi. This is a subgiant with approximately the same effective temperature as the Sun, while the luminosity is higher by a factor of around 3.5. The resulting power spectrum is shown in Figure 2.20; there is a very clearly defined enhancement of power around 1 mHz, far exceeding the noise level. This is perhaps the first incontrovertible detection of solar-like oscillations in another star; the amplitude is approximately consistent with theoretical expectations.

A star of particularly great interest is α Cen A: it is quite similar to the Sun and, being member of a nearby well-studied binary system, its parameters are known quite precisely. Detailed modelling of the α Cen system has been carried out by Guenther & Demarque (2000) and Morel *et al.* (2000). Kjeldsen *et al.* (1999) carried out extensive observations of line-intensity variations in α Cen A; although hints of oscillations were found, they were only able definitely to determine an upper limit to the oscillations, consistent with expectations. Very encouraging results have been obtained using the star tracker on the otherwise failed WIRE satellite (see Buzasi 2000). Schou & Buzasi (2001) obtained a convincing detection of oscillations in continuum intensity, with a maximum amplitude of around 6 ppm, roughly consistent with theoretical expectations and a large separation of 106 μHz, again largely consistent with model predictions. Definite Doppler-velocity observations, with a remarkable signal-to-noise ratio, were obtained by Bouchy & Carrier (2001) with the Swiss CORALIE instrument[5] on La Silla. The resulting power spectrum, shown in Figure 2.21, has a power distribution similar to what is observed in the Sun, although shifted to slightly lower frequency. A substantial number of modes have been identified in the spectrum, although at the time of writing these have not yet been definitely identified. As in the other cases a serious difficulty with the analysis is the fact that the observations shown in Figure 2.21 are from a single site; however, simultaneous observations from the Anglo-Australian Telescope in Australia are currently being analyzed and will likely help substantially in reducing the sidebands in the spectrum. These results show the power of modern carefully stabilized spectrographs for this type of observations. Even more dramatic results can be

[5]developed to search for extra-solar planets by measuring the resulting radial velocity of the central stars

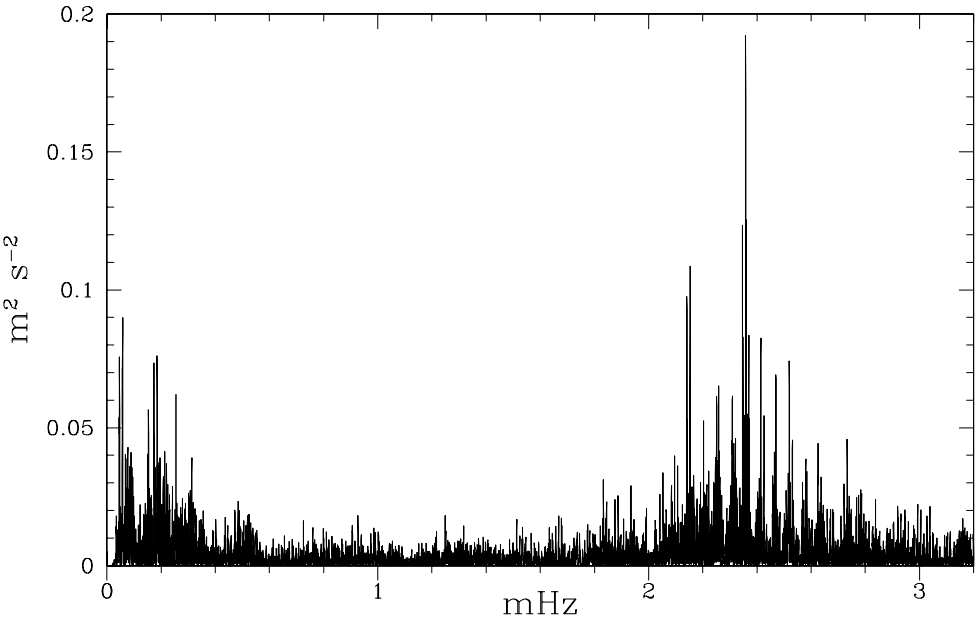

Figure 2.21: Power spectrum of oscillations of α Cen A, from radial-velocity observations with the CORALIE spectrograph. (From Bouchy & Carrier 2001.)

expected when the HARPS instrument starts operations on the ESO 3.6-m telescope on La Silla.

As mentioned above, solar-like oscillations of relatively large amplitude may be expected in red giants. Strong evidence has been found for solar-like oscillations in the star Arcturus (*e.g.* Smith, McMillan & Merline 1987; Innis *et al.* 1988; Merline 1998), including indications of a frequency pattern in accordance with the dominant behaviour of equation (2.32). Also, Edmonds & Gilliland (1996) found variations in K giants in the globular cluster 47 Tuc which were apparently consistent with solar-like pulsations. Based on observations with the WIRE star tracker Buzasi *et al.* (2000) claimed detection of solar-like oscillations in α Ursa Majoris A, a giant of spectral type K0 III, with an estimated mass, from membership of a binary system, of around $5M_\odot$. Guenther *et al.* (2000) analyzed the evolution and oscillation frequencies of this star. They noted that, as a result of the late evolutionary state of the star, the spectra for $l > 0$ were completely dominated by modes behaving like g modes, leading to very dense frequency spectra; thus the only modes that could realistically be identified were the radial modes, which are purely acoustic. Comparing with the observed frequencies, they obtained a tentative identification of some of the modes, although they noted that this was not yet unique. Dziembowski *et al.* (2001) carried out a more careful analysis of the possible causes of oscillations of α UMa A and concluded that the observed properties of the amplitudes were unlikely to be consistent with solar-like, stochastic excitation. Thus the current results on α UMa should perhaps be regarded with some caution.

Even so, red giants remain promising targets for asteroseismology. Frandsen *et al.*

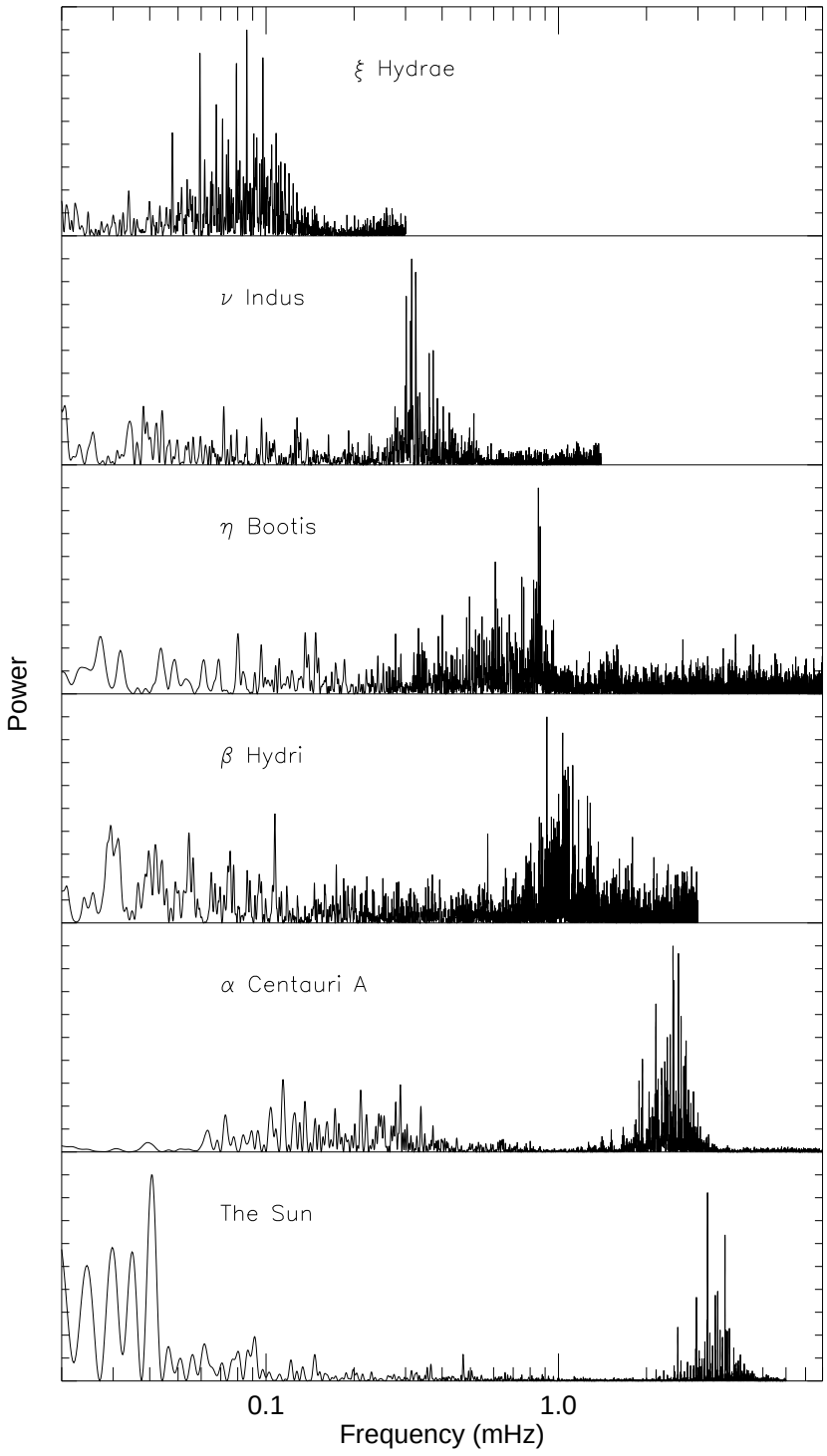

Figure 2.22: Power spectra of 5 stars showing solar-like oscillations, compared with solar data from the GOLF instrument. The power scale is arbitrary. (Figure kindly provided by Hans Kjeldsen.)

(2002) obtained clear evidence for solar-like oscillations in ξ Hydrae, using the CORALIE instrument. This star is in the shell hydrogen-burning, or perhaps more likely in the core helium-burning, stage (see also Teixeira *et al.* 2003). With a radius of $10R_\odot$ and a mass of $3M_\odot$, the maximum power is at periods of around 3 – 4 hours; but the power distribution is otherwise quite similar to the solar case.

An overview of some of the stars for which solar-like oscillations have been observed is provided by Figure 2.22, based largely on data obtained by the Aarhus and Sydney groups. Here solar data from the GOLF instrument are included, analyzed over a period of 55 hours, to provide a frequency resolution corresponding approximately to the data for α Cen A. The similarity of the power distributions, over a large range in stellar parameters and hence frequencies, is obvious.

For red supergiants the relevant periods are of order weeks or months, and hence decades of observations are required to resolve the oscillations and study their properties. Fortunately, very extensive sets of data are available from amateur observations, spanning in some cases a century. Although the precision of these mostly visual estimates is not as high as for professional observations, the large amplitudes of the variability allow reliable analysis of the oscillations; also the very extensive base of observations makes it possible to study the statistical properties of the variability. In a very interesting analysis, Mattei *et al.* (1997) related the *variability* in the oscillation amplitudes to the amplitudes. This isolated the semi-regular variables as a clearly defined class, with a strong correlation between variability and amplitude. Christensen-Dalsgaard, Kjeldsen & Mattei (2001) argued that this relation corresponded closely to what would result from stochastically excited oscillations where the amplitudes have an exponential distribution, as has indeed been verified for the Sun (*e.g.* Kumar, Franklin & Goldreich 1988; Chaplin *et al.* 1997; Chang & Gough 1998; see also Section 10.3). Also, Bedding (2003) analyzed several examples of long-period variables, obtaining oscillation spectra reminiscent of solar-like oscillations. If confirmed by more detailed analyses, such studies would provide extensive data on the excitation of solar-like oscillations over a very broad range of stellar parameters.

The increasing observational basis for the study of solar-like oscillations in other stars evidently promises extremely valuable information about the interior properties of these stars and hence tests of the theory of stellar structure and evolution. In addition, the results provide information about the excitation mechanisms responsible for the oscillations. From the unexpectedly low amplitude found in Procyon, and the low upper limit to detections in M67, it is already clear that the scaling in equation (2.44) predicts too high amplitudes for stars hotter than the Sun. Interestingly, the amplitudes observed so far appear rather to be consistent with a scaling with $g_{\rm s}^{-1}$ (evidently, for stars with effective temperature close to the that of Sun such as η Boo, α Cen A or β Hyi, the two scalings are equivalent). The physical reason for this behaviour is so far not understood.

2.4.2 Observations of δ Scuti oscillations

The δ Scuti stars fall in an extension of the Cepheid instability strip, close to the main sequence. They typically have masses around $2 - 2.5M_\odot$ and are either near or just after the end of core hydrogen burning. Although they have been recognized as a separate class of pulsating stars since the work of Eggen (1957ab), only within the last decade have the details of their spectra of pulsations become clear. The fact that these stars typically have periods of the order of one hour presents a considerable difficulty: observations from

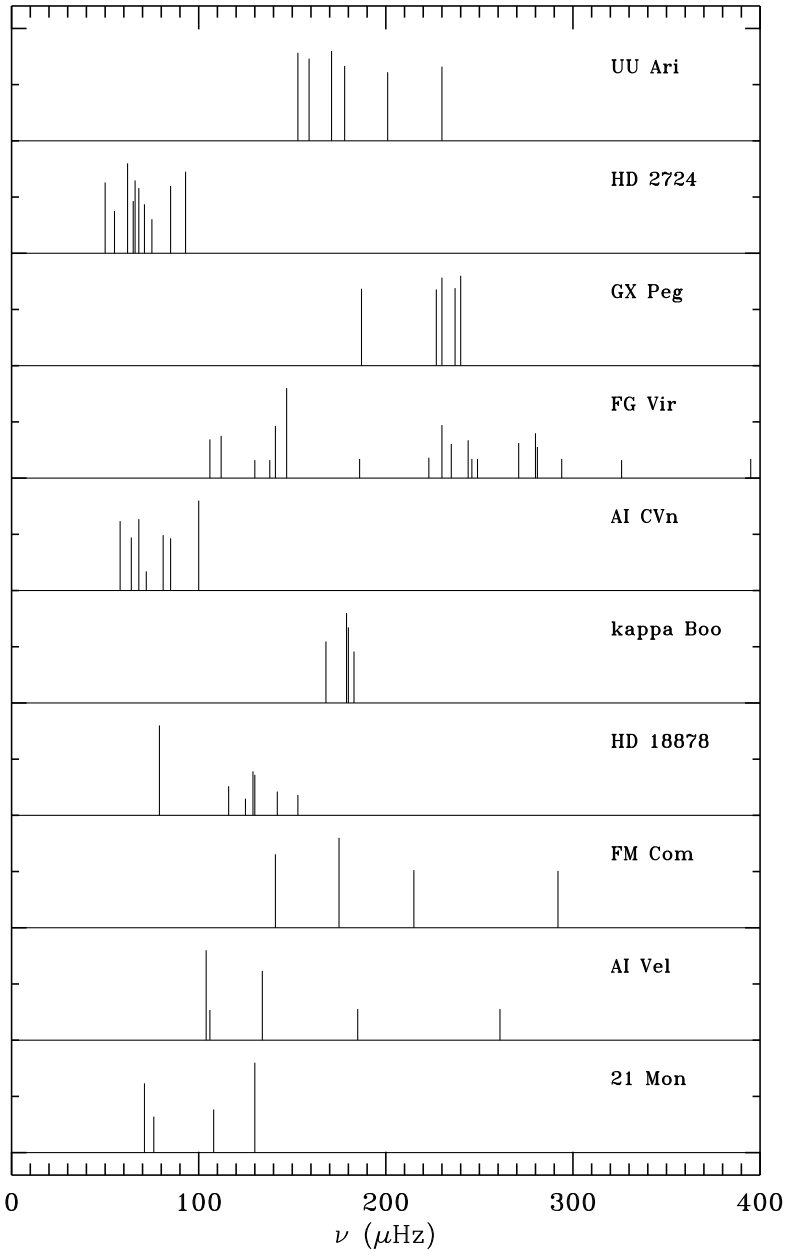

Figure 2.23: Schematic oscillation spectra of a number of δ Scuti stars.

a single site will lead to a great deal of confusion from the side-bands (*cf.* Section 2.2.3), complicating the determination of the oscillation frequencies. However, thanks to a number of observing campaigns involving two or more observatories extensive data for a number of stars have become available (*e.g.* Michel & Baglin 1991; Michel *et al.* 1992; for reviews, see Breger 1995ab). A detailed discussion of many aspects of the study of δ Scuti stars was

provided in the volume edited by Breger & Montgomery (2000).

The most extensive observations of δ Scuti stars have been photometric, although the oscillations have also been observed spectroscopically. Recent multi-site campaigns have resulted in the determination of very substantial sets of frequencies in some cases (*e.g.* Breger *et al.* 1998, 1999; Handler *et al.* 2000). Schematic spectra of several stars are shown in Figure 2.23. The observed frequency range corresponds to low-order acoustic modes. However, the distributions of modes excited to observable frequencies are evidently strikingly different: in some cases only modes in a narrow frequency band are found, whereas in other cases the observed modes extend quite widely in frequency. So far, no obvious correlation between the frequency distribution and other parameters of the stars has been found.

From a comparison with computed oscillation spectra (see Section 5.3.2) it is clear that only a subset of the possible modes of oscillation are excited to observable amplitudes in these stars. However, the reasons for the mode selection is currently unclear. This greatly complicates the mode identification. A further complication comes from the fact that the basic parameters of these stars, such as their mass and radius, are in most cases known with poor accuracy. On the other hand, the δ Scuti stars have the potential for providing very valuable information about stellar evolution: unlike the Sun, these stars have convective cores, and hence the frequency observations may give information about the properties of such cores, including the otherwise highly uncertain degree of overshoot from the cores. Therefore, a great deal of effort is going into further observations of δ Scuti stars as well as in calculations to elucidate the diagnostic potential of the observations and analyze the existing data. Particularly promising are observations of δ Scuti stars in open clusters. With CCD photometry it is possible to study several variable stars in such a cluster at once, and furthermore "classical" observations of the cluster can be used to constrain the parameters of the stars, such as their distance, age and chemical composition (*e.g.* Breger *et al.* 1993ab; Hernández *et al.* 1998).

2.4.3 Subdwarf B variables

This group of stars[6] was identified as pulsating in parallel theoretical (Charpinet *et al.* 1996) and observational (Kilkenny *et al.* 1997; Billères *et al.* 1997) investigations. It consists of hot so-called *horizontal-branch* stars, in the phase of core helium burning, following ignition in a helium flash at the tip of the red-giant branch. Their location at the blue end of the horizontal branch, with effective temperature around 35 000 K, is a result of their having lost most of the original hydrogen envelope. For a recent review, see O'Donoghue *et al.* (1999).

Since their discovery, around 20 members of this group have been detected. The oscillations are excited through the opacity mechanism operating in the opacity bump coming from iron-group elements, likely enhanced by radiatively driven levitation and settling (Charpinet *et al.* 1997). They are characterized by rich spectra of oscillation frequencies, potentially allowing detailed investigations in this late and relatively poorly understood phase of evolution.

Most observations of these stars have been carried out in broad-band photometry. However, recently two groups have succeeded in measuring oscillations in radial velocity. Such

[6] Also known as *EC 14026 stars*, after the first member of the class to be discovered.

observations are potentially very important in providing information about the identification (*i.e.*, the degree and possibly azimuthal order) of the modes. O'Toole *et al.* (2000) observed the star PG 1605+072 and found clear evidence of oscillations in three modes (or groups of modes) in the Balmer lines of hydrogen. The frequencies agreed with those obtained through photometry, with substantially higher frequency resolution, from a multi-site campaign by Kilkenny *et al.* (1999). Interestingly, O'Toole *et al.* found that for a given mode the radial-velocity amplitudes decreased with increasing order in the Balmer series (*i.e.*, decreasing wavelength). This presumably reflects aspects, so far not understood, of the behaviour of the oscillations in the stellar atmosphere. Jeffery & Pollacco (2000) observed the stars KPD 2109+4401 and PB 8783; in the latter case, five or six modes were identified, again agreeing in frequency with modes observed in photometry; the photometric observations show strong evidence for rotational splitting of most of these modes, indicating that they are nonradial. Further spectroscopic observations, with longer time basis, are required to resolve the modes and obtain more precise information about the amplitude and phase relations, for use in the mode identification. Additional information can also be expected from other properties of the spectral lines; an important example is observation of oscillations in equivalent widths.

The rich spectra of oscillation frequencies potentially strongly constrain the properties of the stars, provided the observed frequencies can be identified with modes of stellar models. Even without further observational information about the degrees of the modes, this may be possible through fits of the frequencies to those of models of varying parameters. A very interesting example was provided by the analysis by Brassard *et al.* (2001) of observations of PG 0014+067. Identification of the modes led to stringent constraints on the parameters of the star, including the mass $M_{\rm env}$ of the outer hydrogen-rich layer, which was determined as $\log M_{\rm env}/M = -4.31 \pm 0.22$. Also, the surface gravity was obtained with a precision of around 2 per cent. Interestingly, the remaining residuals between the observed and fitted frequencies were substantially larger than the observational errors, indicating errors in the model calculations; one might hope that further analysis of these residuals may indicate how the models should be improved, beyond the assumptions of the original calculation.

2.4.4 Pulsating white dwarfs

The first observations of oscillations in white dwarfs were made in 1970 – 1975 (McGraw & Robinson 1976). The initial results were obtained for so-called DA white dwarfs, characterized by the presence of hydrogen in their spectra, with effective temperatures around 10 000 K. Since then, additional groups of pulsating white dwarfs have been detected, each characterized by a fairly sharply defined instability region. These regions are indicated schematically in the HR diagram in Figure 2.17; they include planetary-nebula nuclei variables ('PNNV') which are in a stage of rapid evolution.

The typical periods of pulsating white dwarfs are in the range 3 – 10 mins. This is far longer than the dynamical timescales $t_{\rm dyn}$ for these stars [*cf.* equation (1.1)] which are of the order of seconds. In fact, the observed modes are identified with the so-called g modes, *i.e.*, standing gravity waves. As discussed in Chapter 5, such modes may have arbitrarily long periods. As for the δ Scuti stars, it is characteristic that not all the possible modes in a given frequency range are observed; the mode selection is apparently related to the possibility of trapping of modes in regions of chemical inhomogeneity, although the precise mechanism is so far not understood.

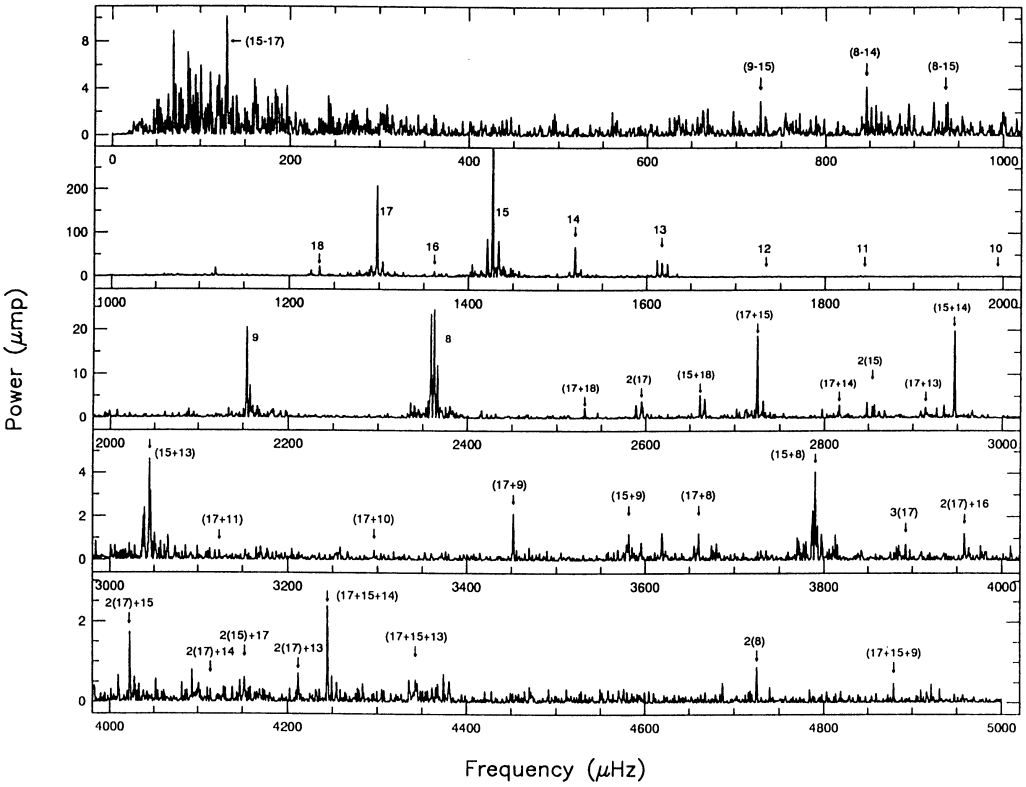

Figure 2.24: Power spectrum of the DB variable GD358, obtained with the Whole Earth Telescope. Numbers with arrows represent multiplet identifications. As discussed in Section 2.2.5, nonlinear effects give rise to linear combinations of the basic frequencies (see also Appendix C, Problem 1.4); these are indicated in the figure as, *e.g.*, '(15+18)' or '2(17)'. (From Winget *et al.* 1994.)

The oscillations have been observed photometrically. As in other cases the complications associated with gaps in the data from a single site have led to collaborative efforts to obtain continuous data through the combined efforts of several observatories. This has been organized in the very ambitious Whole Earth Telescope (WET) project, where more than ten observatories have been involved in campaigns to observe a single star over 1 – 2 weeks (for overviews, see Winget 1993; Kawaler 1995). This has led to some of the the most detailed pulsation spectra for stars other than the Sun. As an example, Figure 2.24 shows the spectrum obtained for a DB variable.

The analysis of the observed frequencies is providing a great deal of information about the white dwarfs, such as accurate determination of white-dwarf masses and rotation rates (*e.g.* Bradley & Winget 1994). Metcalfe, Winget & Charbonneau (2001) made a detailed analysis of the frequencies of GD358, resulting amongst other parameters in a determination of the mass fraction of oxygen in the core of the white dwarf; they noted that, when combined with evolution models of the preceding phases of evolution, this constrains the

rate of alpha-particle capture in carbon twelve. Perhaps the most interesting result is the measurement of period changes in white dwarfs, caused by the evolution of the stars along the white-dwarf cooling sequence (*e.g.* Winget *et al.* 1985; Kepler *et al.* 1991). In early stages of the evolution towards the white-dwarf phase the cooling is dominated by neutrino emission from the core of the stars; thus the observations promises to yield information about physical processes involving electrons and neutrinos which cannot be studied experimentally (*e.g.* O'Brien *et al.* 1998; Costa, Kepler & Winget 1999; O'Brien & Kawaler 2000). Measurements of period changes of cooler white dwars, in particular the DA variables, may provide a test of the crystallization of matter in the stellar interiors and yield constraints on the overall cooling timescale of white dwarfs (*e.g.* Winget *et al.* 1997). This is crucial for estimates of the age of the Galaxy from the observed distribution in luminosity of white dwarfs (*e.g.* Wood 1992).

Chapter 3

A little hydrodynamics

To provide a background for the presentation of the theory of stellar oscillations, this chapter briefly discusses some basic principles of hydrodynamics. A slightly more detailed description, but still essentially without derivations, was given by Cox (1980). In addition, any of the many detailed books on hydrodynamics (*e.g.* Batchelor 1967; Landau & Lifshitz 1959) can be consulted. Ledoux & Walraven (1958) give a very comprehensive introduction to hydrodynamics, with special emphasis on the application to stellar oscillations.

3.1 Basic equations of hydrodynamics

It is assumed that the gas can be treated as a continuum, so that its properties can be specified as functions of position $\mathbf{r}$ and time t. These properties include the local density $\rho(\mathbf{r}, t)$, the local pressure $p(\mathbf{r}, t)$ (and any other thermodynamic quantities that may be needed), as well as the local instantaneous velocity $\mathbf{v}(\mathbf{r}, t)$. Here $\mathbf{r}$ denotes the position vector to a given point in space, and the description therefore corresponds to what is seen by a stationary observer. This is known as the *Eulerian* description. In addition, it is often convenient to use the *Lagrangian* description, which is that of an observer who follows the motion of the gas. Here a given element of gas can be labelled, *e.g.* by its initial position $\mathbf{r}_0$, and its motion is specified by giving its position $\mathbf{r}(t, \mathbf{r}_0)$ as a function of time. Its velocity

$$\mathbf{v}(\mathbf{r}, t) = \frac{\mathrm{d}\mathbf{r}}{\mathrm{d}t} \qquad \text{at fixed } \mathbf{r}_0 \tag{3.1}$$

is equivalent to the Eulerian velocity mentioned above.

The time derivative of a quantity ϕ, observed when following the motion is

$$\frac{\mathrm{d}\phi}{\mathrm{d}t} = \left(\frac{\partial\phi}{\partial t}\right)_{\mathbf{r}} + \nabla\phi \cdot \frac{\mathrm{d}\mathbf{r}}{\mathrm{d}t} = \frac{\partial\phi}{\partial t} + \mathbf{v} \cdot \nabla\phi \,. \tag{3.2}$$

The time derivative $\mathrm{d}/\mathrm{d}t$ following the motion is also known as the material time derivative; in contrast $\partial/\partial t$ is the local time derivative (*i.e.*, the time derivative at a fixed point).

The properties of the gas are expressed as scalar and vector fields. Thus we need a little vector algebra; convenient summaries can be found, *e.g.* in books on electromagnetism (such

as Jackson 1975; Reitz, Milford & Christy 1979). I shall assume the rules for manipulating gradients and divergences to be known. In addition, we need Gauss's theorem:

$$\int_{\partial V} \mathbf{a} \cdot \mathbf{n} \, \mathrm{d}A = \int_V \operatorname{div} \mathbf{a} \, \mathrm{d}V \ , \tag{3.3}$$

where V is a volume, with surface ∂V, $\mathbf{n}$ is the outward directed normal to ∂V, and $\mathbf{a}$ is any vector field. From this one also obtains

$$\int_{\partial V} \phi \mathbf{n} \, \mathrm{d}A = \int_V \nabla \phi \, \mathrm{d}V \tag{3.4}$$

for any scalar field ϕ.

3.1.1 The equation of continuity

The fact that mass is conserved can be expressed as

$$\frac{\partial \rho}{\partial t} + \operatorname{div} (\rho \mathbf{v}) = 0 \ , \tag{3.5}$$

where ρ is density. This is a typical conservation equation, balancing the rate of change of a quantity in a volume with the flux of the quantity into the volume. Had there been any sources of mass, they would have appeared on the right-hand side. By using the relation (3.2), equation (3.5) may also be written

$$\frac{\mathrm{d}\rho}{\mathrm{d}t} + \rho \operatorname{div} \mathbf{v} = 0 \ , \tag{3.6}$$

giving the rate of change of density following the motion. Note that $\rho = 1/V$, where V is the volume of unit mass; thus an alternative formulation is

$$\frac{1}{V} \frac{\mathrm{d}V}{\mathrm{d}t} = \operatorname{div} \mathbf{v} \ . \tag{3.7}$$

Hence $\operatorname{div} \mathbf{v}$ is the rate of expansion of a given volume of gas, when following the motion.

3.1.2 Equations of motion

Under solar or stellar conditions one can generally ignore the internal friction (or *viscosity*) in the gas. The forces on a volume of gas therefore consist of

i) Surface forces, *i.e.*, the pressure on the surface of the volume

ii) Body forces.

Thus the equations of motion can be written

$$\rho \frac{\mathrm{d}\mathbf{v}}{\mathrm{d}t} = -\nabla p + \rho \mathbf{f} \ , \tag{3.8}$$

where $\mathbf{f}$ is the body force per unit mass which has yet to be specified. The pressure p is defined such that the force on a surface element $\mathrm{d}A$ with outward normal $\mathbf{n}$ is $-p \, \mathbf{n} \, \mathrm{d}A$. This may be identified with the ordinary thermodynamic pressure.

By using equation (3.2), we may also write equation (3.8) as

$$\rho \frac{\partial \mathbf{v}}{\partial t} + \rho \mathbf{v} \cdot \nabla \mathbf{v} = -\nabla p + \rho \mathbf{f} \ . \tag{3.9}$$

Among the possible body forces I consider only gravity. Thus in particular I neglect effects of magnetic fields, which might otherwise provide a body force on the gas. The force per unit mass from gravity is the gravitational acceleration $\mathbf{g}$, which can be written as the gradient of the gravitational potential Φ:

$$\mathbf{g} = -\nabla \Phi \ , \tag{3.10}$$

where Φ satisfies Poisson's equation

$$\nabla^2 \Phi = 4\pi G \rho \ . \tag{3.11}$$

It is often convenient to use also the integral solution to Poisson's equation

$$\Phi \left(\mathbf{r}, t \right) = -G \int_V \frac{\rho(\mathbf{r}', t) \mathrm{d}V}{|\mathbf{r} - \mathbf{r}'|} \ . \tag{3.12}$$

3.1.3 Energy equation

To complete the equations we need a relation between p and ρ. This must take the form of a thermodynamic relation. Specifically the first law of thermodynamics,

$$\frac{\mathrm{d}q}{\mathrm{d}t} = \frac{\mathrm{d}E}{\mathrm{d}t} + p \frac{\mathrm{d}V}{\mathrm{d}t} \ , \tag{3.13}$$

must be satisfied; here $\mathrm{d}q/\mathrm{d}t$ is the rate of heat loss or gain, and E the internal energy, per unit mass. As before $V = 1/\rho$ is specific volume. Thus equation (3.13) expresses the fact that the heat gain goes partly to change the internal energy, partly into work expanding or compressing the gas. Alternative formulations of equation (3.13), using the equation of continuity, are

$$\frac{\mathrm{d}q}{\mathrm{d}t} = \frac{\mathrm{d}E}{\mathrm{d}t} - \frac{p}{\rho^2} \frac{\mathrm{d}\rho}{\mathrm{d}t} = \frac{\mathrm{d}E}{\mathrm{d}t} + \frac{p}{\rho} \operatorname{div} \mathbf{v} \ . \tag{3.14}$$

By using thermodynamic identities the energy equation can be expressed in terms of other, and more convenient, variables.

$$\frac{\mathrm{d}q}{\mathrm{d}t} = \frac{1}{\rho(\Gamma_3 - 1)} \left(\frac{\mathrm{d}p}{\mathrm{d}t} - \frac{\Gamma_1 p}{\rho} \frac{\mathrm{d}\rho}{\mathrm{d}t} \right) \tag{3.15}$$

$$= c_p \left(\frac{\mathrm{d}T}{\mathrm{d}t} - \frac{\Gamma_2 - 1}{\Gamma_2} \frac{T}{p} \frac{\mathrm{d}p}{\mathrm{d}t} \right) \tag{3.16}$$

$$= c_V \left[\frac{\mathrm{d}T}{\mathrm{d}t} - (\Gamma_3 - 1) \frac{T}{\rho} \frac{\mathrm{d}\rho}{\mathrm{d}t} \right] \ . \tag{3.17}$$

Here c_p and c_V are the specific heat per unit mass at constant pressure and volume, and the adiabatic exponents are defined by

$$\Gamma_1 = \left(\frac{\partial \ln p}{\partial \ln \rho} \right)_{\mathrm{ad}}, \quad \frac{\Gamma_2 - 1}{\Gamma_2} = \left(\frac{\partial \ln T}{\partial \ln p} \right)_{\mathrm{ad}}, \quad \Gamma_3 - 1 = \left(\frac{\partial \ln T}{\partial \ln \rho} \right)_{\mathrm{ad}} . \tag{3.18}$$

These relations are discussed in more detail in, *e.g.*, Cox & Giuli (1968).

It is evident that the relation between p, ρ and T, as well as the Γ_i's, depend on the thermodynamic state and composition of the gas. Indeed, as will be discussed below, the dependence of Γ_1 on the properties of the gas forms the basis for using observed solar oscillation frequencies to probe the details of the statistical mechanics of partially ionized gases and to infer the helium abundance of the solar convective envelope. However, in many cases one may as a first approximation regard the gas as fully ionized and neglect effects of degeneracy and radiation pressure. Then the equation of state is simply

$$p = \frac{k_{\rm B}\rho T}{\mu m_{\rm u}} \, , \tag{3.19}$$

where $k_{\rm B}$ is Boltzmann's constant, $m_{\rm u}$ is the atomic mass unit and μ is the mean molecular weight. Also

$$\Gamma_1 = \Gamma_2 = \Gamma_3 = 5/3 \, . \tag{3.20}$$

I note that radiation pressure decreases Γ_1 below this value; this effect becomes noticeable in stars whose mass exceeds a few solar masses. Thus Otzen Petersen (1975) showed that radiation pressure caused a systematic increase of the pulsation constant (*cf.* eq. 2.20) with increasing luminosity along the Cepheid instability strip.

We need to consider the heat gain in more detail. Specifically, it can be written as

$$\rho \frac{{\rm d}q}{{\rm d}t} = \rho\,\epsilon - {\rm div}\,\mathbf{F} \, ; \tag{3.21}$$

here ϵ is the rate of energy generation per unit mass (*e.g.* from nuclear reactions), and $\mathbf{F}$ is the flux of energy. In general, radiation is the only significant contributor to the energy flux; in particular, molecular conduction is almost always negligible.

In convection zones turbulent gas motion provides a very efficient transport of energy. Ideally the entire hydrodynamical system, including convection, must be described as a whole. In this case only the radiative flux would be included in equation (3.21). However, under most circumstances the resulting equations are too complex to be handled analytically or numerically. Thus it is customary to separate out the convective motion, by performing averages of the equations over length scales that are large compared with the convective motion, but small compared with other scales of interest. In this case the convective flux appears as an additional contribution in equation (3.21). The convective flux must then be determined, from the other quantities characterizing the system, by considering the equations for the turbulent motion. A familiar example of this (which is also characteristic of the lack of sophistication in current treatments of convection) is the mixing-length theory.

The incorporation of convection in the hydrodynamical equations was discussed in some detail by Unno *et al.* (1989). However, it is fair to say that this is currently one of the principal uncertainties in stellar hydrodynamics.

The general calculation of the radiative flux is also non-trivial. In stellar atmospheres the full radiative transfer problem, as known from the theory of the structure of stellar atmospheres, must be solved in combination with the hydrodynamic equations. This is another active area of research, and the subject of a major monograph (Mihalas & Mihalas 1984). In stellar interiors the diffusion approximation is adequate, and the radiative flux is given by

$$\mathbf{F} = -\frac{4\pi}{3\kappa\rho}\,\nabla B = -\frac{4a\tilde{c}T^3}{3\kappa\rho}\,\nabla T \, , \tag{3.22}$$

where $B = (a\tilde{c}/4\pi)T^4$ is the integrated Planck function, κ is the opacity, $\tilde{c}$ is the speed of light and a is the radiation density constant; this provides a relation between the state of the gas and the radiative flux, which is analogous to a simple conduction equation.

When the mean free path of a photon is very large, one can neglect the contribution from absorption to the heating of the gas. Then we have that

$$\operatorname{div} \mathbf{F} = 4\pi\rho\kappa_{\rm a} B \ , \tag{3.23}$$

where $\kappa_{\rm a}$ is the opacity arising from absorption; this is the so-called *Newton's law of cooling*. Finally, one can generalize the Eddington approximation, which may be known from the theory of static stellar atmospheres, to the three-dimensional case (see Unno & Spiegel 1966), to obtain

$$\operatorname{div} \mathbf{F} = -4\pi\rho\kappa_{\rm a}(J - B) \ , \tag{3.24}$$

$$\mathbf{F} = -\frac{4\pi}{3(\kappa_{\rm a} + \kappa_{\rm s})\rho}\nabla J \ , \tag{3.25}$$

where $\kappa_{\rm s}$ is the scattering opacity and J is the mean intensity. As shown by Unno & Spiegel the Eddington approximation tends to the diffusion approximation when $\kappa_{\rm a}\rho \to \infty$. Furthermore, it has the correct limit in the optically thin case.

Here I have implicitly assumed that the scattering and absorption coefficients are independent of the frequency of radiation. In the diffusion approximation, the generalization to frequency-dependence leads to the introduction of the Rosseland mean opacity. In the optically thin case, one must in general take into account the details of the distribution of intensity with frequency; thus, in equations (3.23) – (3.25) the absorption and scattering coefficients must be thought of as suitable averages, whereas $\mathbf{F}$ and J are frequency-integrated quantities.

3.1.4 The adiabatic approximation

For the purpose of calculating stellar oscillation frequencies, the complications of the energy equation can be avoided to a high degree of precision, by neglecting the heating term in the energy equation. To see that this is justified, consider the energy equation on the form, using equation (3.22)

$$\frac{{\rm d}T}{{\rm d}t} - \frac{\Gamma_2 - 1}{\Gamma_2}\frac{T}{p}\frac{{\rm d}p}{{\rm d}t} = \frac{1}{c_p}\left[\epsilon + \frac{1}{\rho}\operatorname{div}\left(\frac{4a\tilde{c}T^3}{3\kappa\rho}\nabla T\right)\right] \ . \tag{3.26}$$

Here the term in the temperature gradient can be estimated as

$$\frac{1}{\rho c_p}\operatorname{div}\left(\frac{4a\tilde{c}T^3}{3\kappa\rho}\nabla T\right) \sim \frac{4a\tilde{c}T^4}{3\kappa\rho^2 c_p \mathcal{L}^2} = \frac{T}{\tau_F} \ , \tag{3.27}$$

where $\mathcal{L}$ is a characteristic length scale, and τ_F is a characteristic time scale for radiation,

$$\tau_F = \frac{3\kappa\rho^2 c_p \mathcal{L}^2}{4a\tilde{c}T^3} \simeq 10^{12}\frac{\kappa\rho^2\mathcal{L}^2}{T^3} \ , \qquad \text{in cgs units} \ . \tag{3.28}$$

Typical values for the entire Sun are $\kappa = 1$, $\rho = 1$, $T = 10^6$, $\mathcal{L} = 10^{10}$, and hence $\tau_F \sim 10^7$ years. This corresponds to the Kelvin-Helmholtz time for the star. For the solar convection zone the corresponding values are $\kappa = 100$, $\rho = 10^{-5}$, $T = 10^4$, $\mathcal{L} = 10^9$, and hence

$\tau_F \sim 10^3$ years. In the outer parts of the star the term in ϵ vanishes, whereas in the core it corresponds to a characteristic time $\tau_\epsilon \sim c_p T/\epsilon$ which is again of the order of the Kelvin-Helmholtz time. T/τ_F or T/τ_ϵ must be compared with the time derivative of T in equation (3.26), which can be estimated as $T/$(period of oscillation). Typical periods are of the order of minutes to hours, and hence the heating term in equation (3.26) is generally very small compared with the time-derivative terms. Near the surface, on the other hand, the density, and hence the radiative time scale, is low, and the full energy equation must be taken into account.

Where the heating can be neglected, the motion occurs *adiabatically*. Then p and ρ are related by

$$\frac{\mathrm{d}p}{\mathrm{d}t} = \frac{\Gamma_1 p}{\rho} \frac{\mathrm{d}\rho}{\mathrm{d}t} \; . \tag{3.29}$$

This equation, together with the continuity equation (3.5), the equations of motion (3.9) and Poisson's equation (3.11), form the complete set of equations for adiabatic motion. Most of our subsequent work is based on these equations.

3.2 Equilibrium states and perturbation analysis

A general hydrodynamical description of a star, using the equations presented in the preceding section, is far too complex to handle, even numerically on the largest existing computers. To put this in perspective, it may be mentioned that Å. Nordlund and R. Stein (*e.g.* Nordlund & Stein 1989; Stein, Nordlund & Kuhn 1989), by stretching the capabilities of existing computers to the limits, have been able to follow numerically the development of a very small region near the solar surface for a few hours. Even though this is a tremendous achievement, which will be of great value to our understanding of solar convection and solar oscillations, it clearly demonstrates the impracticality of a direct numerical solution for, say, general oscillations involving the entire Sun. Furthermore, even to the extent that such a solution were possible, the results would in general be so complicated that a simplified analysis is needed to understand them. Fortunately, in the case of stellar oscillations, considerable simplifications are possible. The observed solar oscillations have very small amplitudes compared with the characteristic scales of the Sun, and so it can be treated as a small perturbation around a static equilibrium state. Even in "classical" pulsating stars, where the surface amplitudes are large, most of the energy in the motion is in regions where the amplitudes are relatively small; thus many of the properties of these oscillations, including their periods, can be understood in terms of small-perturbation theory. In this section I discuss the general equations for such small perturbations.

3.2.1 The equilibrium structure

The equilibrium structure is assumed to be static, so that all time derivatives can be neglected. In addition, I assume that there are no velocities. Then the continuity equation, (3.5), is trivially satisfied. The equations of motion (3.9) reduce to the equation of hydrostatic support,

$$\nabla p_0 = \rho_0 \mathbf{g}_0 = -\rho_0 \nabla \Phi_0 \; , \tag{3.30}$$

where I have denoted equilibrium quantities with the subscript "0". Poisson's equation (3.11) is unchanged,

$$\nabla^2 \Phi_0 = 4\pi G \rho_0 \; . \tag{3.31}$$

Finally the energy equation (3.21) is

$$0 = \frac{\mathrm{d}q}{\mathrm{d}t} = \epsilon_0 - \frac{1}{\rho_0}\mathrm{div}\,\mathbf{F}_0 \ . \tag{3.32}$$

It might be noted that one often considers equilibrium structures that change on long time scales. Here hydrostatic equilibrium is enforced (departures from hydrostatic equilibrium result in motion on essentially the free-fall time scale for the star, of the order of hours). However, it is not assumed that there is no heating, so that the general energy equation (3.21) is used. Such a star is said to be in hydrostatic, but not in thermal, equilibrium. Typical examples are stars where nuclear burning does not supply the main source of energy, as during the pre-main-sequence contraction, or after hydrogen exhaustion in the core. Even during normal main sequence evolution the heating term provides a small contribution to the energy, which is normally taken into account in calculations of stellar evolution. However, we need not consider this further here.

For the present purpose the most important example of equilibrium is clearly a spherically symmetric state, where the structure depends only on the distance r to the centre. Here $\mathbf{g}_0 = -g_0\mathbf{a}_r$, where $\mathbf{a}_r$ is a unit vector directed radially outward, and equation (3.30) becomes

$$\frac{\mathrm{d}p_0}{\mathrm{d}r} = -g_0\rho_0 \ . \tag{3.33}$$

Also, Poisson's equation may be integrated once, to yield

$$g_0 = \frac{G}{r^2}\int_0^r 4\pi\rho_0 r'^2\,\mathrm{d}r' = \frac{G\,m_0}{r^2} \ , \tag{3.34}$$

where $m_0(r)$ is the mass in the sphere interior to r. The flux is directed radially outward, $\mathbf{F} = F_{r,0}\mathbf{a}_r$, so that the energy equation gives

$$\rho_0\epsilon_0 = \frac{1}{r^2}\frac{\mathrm{d}}{\mathrm{d}r}\left(r^2\,F_{r,0}\right) = \frac{1}{4\pi r^2}\,\frac{\mathrm{d}L_0}{\mathrm{d}r} \ ,$$

where $L_0 = 4\pi r^2\,F_{r,0}$ is the total flow of energy through the sphere with radius r; hence

$$\frac{\mathrm{d}L_0}{\mathrm{d}r} = 4\pi r^2\rho_0\epsilon_0 \ . \tag{3.35}$$

Finally the diffusion expression (3.22) for the flux may be written

$$\frac{\mathrm{d}T_0}{\mathrm{d}r} = -\frac{3\kappa_0\rho_0}{16\pi r^2 a\tilde{c}T_0^3}L_0 \ . \tag{3.36}$$

Equations (3.33) – (3.36) are clearly the familiar equations for stellar structure.

3.2.2 Perturbation analysis

We consider small perturbations around the equilibrium state. Thus, *e.g.*, the pressure is written as

$$p(\mathbf{r},t) = p_0(\mathbf{r}) + p'(\mathbf{r},t) \ , \tag{3.37}$$

where p' is a small perturbation; this is the so-called *Eulerian* perturbation, *i.e.*, the perturbation at a given point. The equations are then linearized in the perturbations, by

expanding them in the perturbations retaining only terms that do not contain products of the perturbations.

Just as in the general case it is convenient to use also a description involving a reference frame following the motion; the perturbation in this frame is called the *Lagrangian* perturbation. If an element of gas is moved from $\mathbf{r}_0$ to $\mathbf{r}_0 + \boldsymbol{\delta}\mathbf{r}$ due to the perturbation, the Lagrangian perturbation to pressure may be calculated as

$$\begin{aligned} \delta p(\mathbf{r}) &= p(\mathbf{r}_0 + \boldsymbol{\delta}\mathbf{r}) - p_0(\mathbf{r}_0) = p(\mathbf{r}_0) + \boldsymbol{\delta}\mathbf{r} \cdot \nabla p_0 - p_0(\mathbf{r}_0) \\ &= p'(\mathbf{r}_0) + \boldsymbol{\delta}\mathbf{r} \cdot \nabla p_0 \ . \end{aligned} \tag{3.38}$$

Equation (3.38) is of course completely equivalent to the relation (3.2) between the local and the material time derivative. Note also that the velocity is given by the time derivative of the displacement $\boldsymbol{\delta}\mathbf{r}$,

$$\mathbf{v} = \frac{\partial \boldsymbol{\delta}\mathbf{r}}{\partial t} \ . \tag{3.39}$$

Equations for the perturbations are obtained by inserting expressions like (3.37) in the full equations, subtracting equilibrium equations and neglecting quantities of order higher than one in p', ρ', $\mathbf{v}$, *etc.* For the continuity equation the result is

$$\frac{\partial \rho'}{\partial t} + \mathrm{div}\,(\rho_0 \mathbf{v}) = 0 \ , \tag{3.40}$$

or, by using equation (3.39) and integrating with respect to time

$$\rho' + \mathrm{div}\,(\rho_0 \boldsymbol{\delta}\mathbf{r}) = 0 \ . \tag{3.41}$$

Note that this equation may also, by using the analogue to equation (3.38), be written as

$$\delta\rho + \rho_0 \mathrm{div}\,(\boldsymbol{\delta}\mathbf{r}) = 0 \ , \tag{3.42}$$

which corresponds to equation (3.6).

The equations of motion become

$$\rho_0 \frac{\partial^2 \boldsymbol{\delta}\mathbf{r}}{\partial t^2} = \rho_0 \frac{\partial \mathbf{v}}{\partial t} = -\nabla p' + \rho_0 \mathbf{g}' + \rho' \mathbf{g}_0 \ , \tag{3.43}$$

where, obviously, $\mathbf{g}' = -\nabla\Phi'$. Also, the perturbation Φ' in the gravitational potential satisfies the perturbed Poisson's equation

$$\nabla^2 \Phi' = 4\pi G \rho' \ , \tag{3.44}$$

with the solution, equivalent to equation (3.12)

$$\Phi' = -G \int_V \frac{\rho'(\mathbf{r}', t)}{|\mathbf{r} - \mathbf{r}'|} \, \mathrm{d}V \ . \tag{3.45}$$

The energy equation requires a little thought. We need to calculate, *e.g.*,

$$\frac{\mathrm{d}p}{\mathrm{d}t} = \frac{\partial p}{\partial t} + \mathbf{v} \cdot \nabla p = \frac{\partial p'}{\partial t} + \mathbf{v} \cdot \nabla p_0 = \frac{\partial p'}{\partial t} + \frac{\partial \boldsymbol{\delta}\mathbf{r}}{\partial t} \cdot \nabla p_0 = \frac{\partial}{\partial t}(\delta p) \ , \tag{3.46}$$

to first order in the perturbations. Note that to this order there is no difference between the local and the material time derivative of the *perturbations*. Thus we have for the energy equation, from *e.g.* equation (3.15),

$$\frac{\partial \delta q}{\partial t} = \frac{1}{\rho_0(\Gamma_{3,0}-1)} \left(\frac{\partial \delta p}{\partial t} - \frac{\Gamma_{1,0} p_0}{\rho_0} \frac{\partial \delta \rho}{\partial t} \right) . \tag{3.47}$$

This equation is most simply expressed in Lagrangian perturbations, but it may be transformed into Eulerian perturbations by using equation (3.38). From equation (3.21) the perturbation to the heating rate is given by

$$\rho_0 \frac{\partial \delta q}{\partial t} = \delta(\rho\epsilon - \operatorname{div} \mathbf{F}) = (\rho\epsilon - \operatorname{div} \mathbf{F})' , \tag{3.48}$$

if equation (3.32) is used. Finally it is straightforward to obtain the perturbation to the radiative flux, in the diffusion approximation, from equation (3.22).

For adiabatic motion we neglect the heating term and obtain

$$\frac{\partial \delta p}{\partial t} - \frac{\Gamma_{1,0} p_0}{\rho_0} \frac{\partial \delta \rho}{\partial t} = 0 ,$$

or, by integrating over time

$$\delta p = \frac{\Gamma_{1,0} p_0}{\rho_0} \delta\rho , \tag{3.49}$$

or, on Eulerian form

$$p' + \boldsymbol{\delta r} \cdot \nabla p_0 = \frac{\Gamma_{1,0} p_0}{\rho_0} (\rho' + \boldsymbol{\delta r} \cdot \nabla \rho_0) . \tag{3.50}$$

3.3 Simple waves

It is instructive to consider simple examples of wave motion. This provides an introduction to the techniques needed to handle the perturbations. In addition, general stellar oscillations can in many cases be approximated by simple waves, which therefore give physical insight into the behaviour of the oscillations.

3.3.1 Acoustic waves

As the simplest possible equilibrium situation, we may consider the spatially homogeneous case. Here all derivatives of equilibrium quantities vanish. According to equation (3.30) gravity must then be negligible. Such a situation clearly cannot be realized exactly. However, if the equilibrium structure varies slowly compared with the oscillations, this may be a reasonable approximation. I also neglect the perturbation to the gravitational potential; for rapidly varying perturbations regions with positive and negative ρ' nearly cancel in equation (3.45), and hence Φ' is small. Finally, I assume the adiabatic approximation (3.49).

The equations of motion (3.43) give

$$\rho_0 \frac{\partial^2 \boldsymbol{\delta r}}{\partial t^2} = -\nabla p' ,$$

or, by taking the divergence

$$\rho_0 \frac{\partial^2}{\partial t^2}(\mathrm{div}\,\boldsymbol{\delta}\mathbf{r}) = -\nabla^2 p' \ .$$

However, $\mathrm{div}\,\boldsymbol{\delta}\mathbf{r}$ can be eliminated by using the continuity equation (3.41), and p' can be expressed in terms of ρ' from the adiabatic relation. The result is

$$\frac{\partial^2 \rho'}{\partial t^2} = \frac{\Gamma_{1,0} p_0}{\rho_0} \nabla^2 \rho' = c_0^2 \nabla^2 \rho' \ , \tag{3.51}$$

where

$$c_0^2 \equiv \frac{\Gamma_{1,0} p_0}{\rho_0} \tag{3.52}$$

has the dimension of a squared velocity. This equation has the form of the wave equation. Thus it has solutions in the form of plane waves

$$\rho' = a \exp[i(\mathbf{k}\cdot\mathbf{r} - \omega\, t)] \ . \tag{3.53}$$

(As discussed in more detail in Chapter 4 it is convenient to write the solution in complex form; the physically realistic solution is obtained by taking the real part of the complex solution.) By substituting equation (3.53) into (3.51) we obtain

$$-\omega^2 \rho' = c_0^2\, \mathrm{div}\,(i\mathbf{k}\rho') = -c_0^2 |\mathbf{k}|^2 \rho' \ . \tag{3.54}$$

Thus this is a solution, provided ω satisfies the *dispersion relation*

$$\omega^2 = c_0^2\, |\mathbf{k}|^2 \ . \tag{3.55}$$

The waves are plane sound waves, and equation (3.55) is the dispersion relation for such waves. The adiabatic sound speed c_0 is the speed of propagation of the waves. I note that when the ideal gas law, equation (3.19), is satisfied, the sound speed is given by

$$c_0^2 = \frac{\Gamma_{1,0} k_\mathrm{B} T_0}{\mu m_\mathrm{u}} \ . \tag{3.56}$$

Thus c_0 is essentially determined by T_0/μ.

With a suitable choice of phases the real solution can be written as

$$\rho' = a \cos(\mathbf{k}\cdot\mathbf{r} - \omega t) \ , \tag{3.57}$$

$$p' = c_0^2 a \cos(\mathbf{k}\cdot\mathbf{r} - \omega t) \ , \tag{3.58}$$

$$\boldsymbol{\delta}\mathbf{r} = \frac{c_0^2}{\rho_0 \omega^2} a\, \cos(\mathbf{k}\cdot\mathbf{r} - \omega t + \frac{\pi}{2})\, \mathbf{k} \ . \tag{3.59}$$

Thus the displacement $\boldsymbol{\delta}\mathbf{r}$, and hence the velocity $\mathbf{v}$, is in the direction of the wave vector $\mathbf{k}$.

3.3.2 Internal gravity waves

As a slightly more complicated case, we consider a layer of gas stratified under gravity. Thus here there is a pressure gradient, determined by equation (3.33). However, I assume that the equilibrium quantities vary so slowly that their gradients can be neglected compared

with gradients of perturbations. Also, as before, I neglect the perturbation to the gravitational potential. Clearly one solution must be the adiabatic sound waves considered above. However, here we seek other solutions in the form of waves with much lower frequencies.

It is possible to derive an approximate wave equation under these circumstances (*cf.* Section 7.5). However, to simplify the analysis I assume a solution in the form of a plane wave from the outset. Thus I take all perturbation variables to vary as

$$\exp[i(\mathbf{k}\cdot\mathbf{r}-\omega t)] \; . \tag{3.60}$$

Because of the presence of gravity there is a preferred direction in the problem. I choose a vertical coordinate r directed upward, so that $\mathbf{g}_0 = -g_0\mathbf{a}_r$, and

$$\nabla p_0 = \frac{\mathrm{d}p_0}{\mathrm{d}r}\mathbf{a}_r \; , \qquad \nabla\rho_0 = \frac{\mathrm{d}\rho_0}{\mathrm{d}r}\mathbf{a}_r \; . \tag{3.61}$$

Also, I separate the displacement $\boldsymbol{\delta}\mathbf{r}$ and the wave vector $\mathbf{k}$ into radial and horizontal components,

$$\boldsymbol{\delta}\mathbf{r} = \xi_r\mathbf{a}_r + \boldsymbol{\xi}_\mathrm{h} \; , \tag{3.62}$$

$$\mathbf{k} = k_r\mathbf{a}_r + \mathbf{k}_\mathrm{h} \; . \tag{3.63}$$

The radial and horizontal components of the equations (3.43) are

$$-\rho_0\omega^2\xi_r = -ik_rp' - \rho'g_0 \; , \tag{3.64}$$

$$-\rho_0\omega^2\boldsymbol{\xi}_\mathrm{h} = -i\,\mathbf{k}_\mathrm{h}p' \; , \tag{3.65}$$

and the continuity equation, (3.41), can be written

$$\rho' + \rho_0 ik_r\xi_r + \rho_0 i\,\mathbf{k}_\mathrm{h}\cdot\boldsymbol{\xi}_\mathrm{h} = 0 \; . \tag{3.66}$$

From equations (3.65) and (3.66) we find the pressure perturbation

$$p' = \frac{\omega^2}{k_\mathrm{h}^2}(\rho' + ik_r\rho_0\xi_r) \; . \tag{3.67}$$

This may be used in equation (3.64), to obtain

$$-\rho_0\omega^2\xi_r = -i\frac{k_r}{k_\mathrm{h}^2}\omega^2\rho' + \omega^2\rho_0\frac{k_r^2}{k_\mathrm{h}^2}\xi_r - \rho'g_0 \; . \tag{3.68}$$

For very small frequency the first term in ρ' can be neglected compared with the second, yielding

$$\rho_0\omega^2\left(1+\frac{k_r^2}{k_\mathrm{h}^2}\right)\xi_r = \rho'g_0 \; . \tag{3.69}$$

Notice that this equation has a fairly simple physical meaning. Buoyancy acting on the density perturbation provides a vertical force $\rho'g_0$ per unit volume that drives the motion. The left-hand side gives the vertical acceleration times the mass ρ_0 per unit volume; however, it is modified by the term in the wave numbers. This arises from the pressure perturbation; in order to move vertically, a blob of gas must displace matter horizontally, and this increases its effective inertia. This effect is stronger the longer the horizontal wavelength of the perturbation, and hence the smaller its horizontal wave number.

The adiabatic relation (3.50) gives

$$\rho' = c_0^{-2} p' + \rho_0 \boldsymbol{\delta r} \cdot \left(\frac{1}{p_0 \Gamma_{1,0}} \nabla p_0 - \frac{1}{\rho_0} \nabla \rho_0 \right) . \tag{3.70}$$

However, we may estimate the importance of the term in p' by noting that, according to equation (3.67),

$$\frac{c_0^{-2} p'}{\rho'} \simeq \frac{\omega^2}{c_0^2 k_{\rm h}^2} . \tag{3.71}$$

Here the denominator on the right-hand side is the sound-wave frequency corresponding to the horizontal wave number $k_{\rm h}$ (*cf.* eq. 3.55); since we are specifically interested in oscillations with frequencies far smaller than the frequencies of sound waves, this term can be neglected. Physically, the neglect of the pressure perturbation essentially corresponds to assuming that the perturbation is always in hydrostatic equilibrium; this might be compared with the conventional discussion of convective stability in terms of displaced blobs of fluid, where pressure balance is also assumed. Inserting the expression for ρ' resulting from equation (3.70), when p' is neglected, in equation (3.69) finally yields

$$\omega^2 \left(1 + \frac{k_r^2}{k_{\rm h}^2} \right) \xi_r = N^2 \xi_r , \tag{3.72}$$

where

$$N^2 = g_0 \left(\frac{1}{\Gamma_{1,0}} \frac{{\rm d} \ln p_0}{{\rm d}r} - \frac{{\rm d} \ln \rho_0}{{\rm d}r} \right) \tag{3.73}$$

is the square of the *buoyancy or Brunt-Väisälä frequency* N.

The physical significance of N follows from the 'blob' argument for convective stability (*e.g.* Christensen-Dalsgaard 1993a; see also Cox 1980, Section 17.2): if a fluid element is displaced upwards adiabatically, its behaviour depends on whether the density of the element is higher or smaller than its new surroundings. When $N^2 > 0$ the element is heavier than the displaced fluid, and buoyancy forces it back towards the original position; thus in this case the element executes an oscillation around the equilibrium position. On the other hand, if $N^2 < 0$ the element is lighter than the displaced fluid and buoyancy acts to enhance the motion, forcing the element away from equilibrium; this corresponds to convective instability.

From equation (3.72) we obtain the dispersion relation

$$\omega^2 = \frac{N^2}{1 + k_r^2/k_{\rm h}^2} . \tag{3.74}$$

When $N^2 > 0$ the motion is oscillatory. Then N is the frequency in the limit of infinite $k_{\rm h}$, *i.e.*, for infinitely small horizontal wavelength. This corresponds to oscillations of fluid elements in the form of slender "needles". For greater horizontal wavelength the horizontal motion increases the inertia, as discussed above, and hence decreases the frequency. These waves are known as internal *gravity waves* (not to be confused with the gravitational waves in general relativity).

The condition that $N^2 > 0$ can also be written as

$$\frac{{\rm d} \ln \rho_0}{{\rm d} \ln p_0} > \frac{1}{\Gamma_{1,0}} ; \tag{3.75}$$

when it is not satisfied, ω is imaginary, and the motion grows exponentially with time. This is the linear case of convective instability. In general the motion grows until it breaks down into turbulence due to nonlinear effects. Thus gravity waves cannot propagate in convective regions. I return to this when discussing the asymptotic theory of stellar oscillations.

The condition (3.75) is the proper criterion for convective stability; it is normally known as *the Ledoux condition*. The more usual condition, in terms of p and T, *viz*

$$\frac{\mathrm{d}\ln T_0}{\mathrm{d}\ln p_0} < \nabla_{\rm ad} = \frac{\Gamma_{2,0}-1}{\Gamma_{2,0}} \; , \tag{3.76}$$

can be obtained from equation (3.74) by using thermodynamic identities, when the chemical composition is homogeneous. Equation (3.76) is known as the *Schwarzschild criterion*. When there are gradients in the chemical composition, the two conditions are *not* equivalent. Nonetheless, the Schwarzschild criterion is most often used in calculations of stellar evolution, due to computational convenience.

3.3.3 Surface gravity waves

In addition to the internal gravity waves described above, there is a distinct, and more familiar, type of gravity waves, known, *e.g.* from the Bay of Aarhus. These are waves at a discontinuity in density.

We consider a liquid at constant density ρ_0, with a free surface. Thus the pressure on the surface is assumed to be constant. The layer is infinitely deep. I assume that the liquid is incompressible, so that ρ_0 is constant and the density perturbation $\rho' = 0$. From the equation of continuity we therefore get

$$\mathrm{div}\,\mathbf{v} = 0 \; . \tag{3.77}$$

Gravity $\mathbf{g}$ is assumed to be uniform, and directed vertically downwards. Since the density perturbation is zero, so is the perturbation to the gravitational potential.

In the interior of the liquid the equations of motion reduce to

$$\rho_0 \frac{\partial \mathbf{v}}{\partial t} = -\nabla p' \; . \tag{3.78}$$

The divergence of this equation gives

$$\nabla^2 p' = 0 \; . \tag{3.79}$$

We introduce a horizontal coordinate x, and a vertical coordinate z increasing downward, with $z = 0$ at the free surface. We now seek a solution in the form of a wave propagating along the surface, in the x-direction. Here p' has the form

$$p'(x,z,t) = f(z)\,\cos(k_{\rm h}x - \omega t) \; , \tag{3.80}$$

where f is a function yet to be determined. By substituting equation (3.80) into equation (3.79) we obtain

$$\frac{\mathrm{d}^2 f}{\mathrm{d}z^2} = k_{\rm h}^2 f \; ,$$

or

$$f(z) = a\exp(-k_{\rm h}z) + b\exp(k_{\rm h}z) \; . \tag{3.81}$$

As the layer is assumed to be infinitely deep, b must be zero.

We must now consider the boundary condition at the free surface. Here the pressure is constant, and therefore the Lagrangian pressure perturbation vanishes (the pressure is constant on the perturbed surface), *i.e.*,

$$0 = \delta p = p' + \boldsymbol{\delta \mathbf{r}} \cdot \nabla p_0 = p' + \xi_z \rho_0 g_0 \qquad \text{at } z = 0 \,, \tag{3.82}$$

where ξ_z is the z-component of the displacement. This is obtained from the vertical component of equation (3.78), for the solution in equation (3.81) with $b = 0$, as

$$\xi_z = -\frac{k_\mathrm{h}}{\rho_0 \omega^2}\, p' \,. \tag{3.83}$$

Thus equation (3.82) reduces to

$$0 = \left(1 - \frac{g_0 k_\mathrm{h}}{\omega^2}\right) p' \,,$$

and hence the dispersion relation for the surface waves is

$$\omega^2 = g_0 k_\mathrm{h} \,. \tag{3.84}$$

The frequencies of the surface gravity waves depend only on their wavelength and on gravity, but not on the internal structure of the layer, in particular the density. In this they resemble a pendulum, whose frequency is also independent of its constitution. Indeed, the frequency of a wave with wave number k_h, and wavelength λ, is the same as the frequency of a mathematical pendulum with length

$$\mathcal{L} = \frac{1}{k_\mathrm{h}} = \frac{\lambda}{2\pi} \,. \tag{3.85}$$

Chapter 4

Equations of linear stellar oscillations

In the present chapter the equations governing small oscillations around a spherical equilibrium state are derived. The general equations were presented in Section 3.2. However, here we make explicit use of the spherical symmetry. These equations describe the general, so-called *nonradial* oscillations, where spherical symmetry of the perturbations is not assumed. The more familiar case of *radial*, or spherically symmetric, oscillations, is contained as a special case.

4.1 Mathematical preliminaries

It is convenient to write the solution to the perturbation equations on complex form, with the physically realistic solution being obtained as the real part of the complex solution. To see that this is possible, notice that the general equations can be written as

$$\mathbf{A}\frac{\partial \mathbf{y}}{\partial t} = \mathcal{B}(\mathbf{y}) \ , \tag{4.1}$$

where the vector $\mathbf{y}$ consists of the perturbation variables $(\boldsymbol{\delta}\mathbf{r}, p', \rho', \cdots)$, $\mathbf{A}$ is a matrix with real coefficients, and $\mathcal{B}$ is a linear matrix operator involving spatial gradients, *etc.*, with real coefficients. Neither $\mathbf{A}$ nor $\mathcal{B}$ depend on time. If $\mathbf{y}$ is a complex solution to equation (4.1) then the complex conjugate $\mathbf{y}^*$ is also a solution, since

$$\mathbf{A}\frac{\partial \mathbf{y}^*}{\partial t} = \left(\mathbf{A}\frac{\partial \mathbf{y}}{\partial t}\right)^* = [\mathcal{B}(\mathbf{y})]^* = \mathcal{B}(\mathbf{y}^*) \ , \tag{4.2}$$

and hence, as the system is linear and homogeneous, the real part $\Re(\mathbf{y}) = 1/2(\mathbf{y} + \mathbf{y}^*)$ is a solution.

Because of the independence of time of the coefficients in equation (4.1), solutions can be found of the form

$$\mathbf{y}(\mathbf{r}, t) = \hat{\mathbf{y}}(\mathbf{r}) \exp(-\,i\,\omega\,t) \ . \tag{4.3}$$

This is a solution if the *amplitude function* $\hat{\mathbf{y}}$ satisfies the eigenvalue equation

$$-i\omega\mathbf{A}\cdot\hat{\mathbf{y}} = \mathcal{B}(\hat{\mathbf{y}}) \ . \tag{4.4}$$

Equations of this form were also considered in Section 3.3 for simple waves. Note that in equations (4.3) and (4.4) the frequency ω must in general be assumed to be complex.

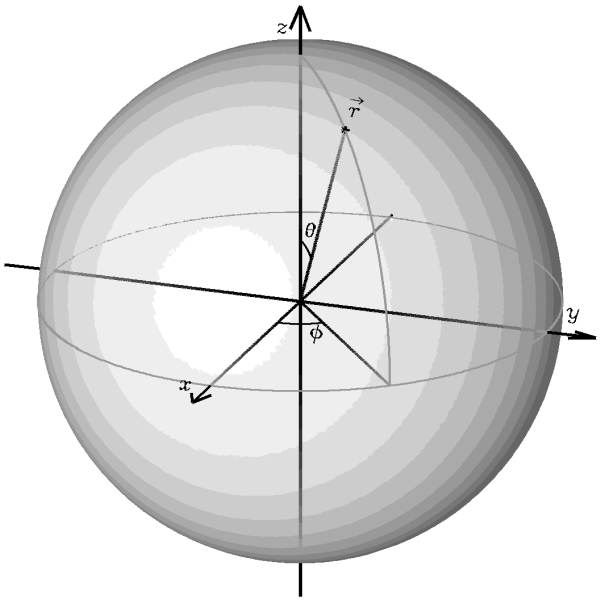

Figure 4.1: The spherical polar coordinate system.

Equation (4.3) is an example of the *separability* of the solution to a system of linear partial differential equations, when the equations do not depend of one of the coordinates. As the equilibrium state is spherically symmetric, we may expect a similar separability in spatial coordinates. Specifically I use spherical polar coordinates (r, θ, ϕ) (*cf.* Figure 4.1), where r is the distance to the centre, θ is colatitude (*i.e.*, the angle from the polar axis), and ϕ is longitude. Here the equilibrium is independent of θ and ϕ, and the solution must be separable. However, the form of the separated solution depends on the physical nature of the problem, and so must be discussed in the context of the reduction of the equations. This is done in the next section.

Here I present some relations in spherical polar coordinates that will be needed in the following [see also Appendix 2 of Batchelor (1967)]. Let $\mathbf{a}_r$, $\mathbf{a}_\theta$ and $\mathbf{a}_\phi$ be unit vectors in the r, θ and ϕ directions, let V be a general scalar field, and let

$$\mathbf{F} = F_r \mathbf{a}_r + F_\theta \mathbf{a}_\theta + F_\phi \mathbf{a}_\phi \tag{4.5}$$

be a vector field. Then the gradient of V is

$$\nabla V = \frac{\partial V}{\partial r}\mathbf{a}_r + \frac{1}{r}\frac{\partial V}{\partial \theta}\mathbf{a}_\theta + \frac{1}{r\sin\theta}\frac{\partial V}{\partial \phi}\mathbf{a}_\phi \,, \tag{4.6}$$

the divergence of $\mathbf{F}$ is

$$\operatorname{div}\mathbf{F} = \frac{1}{r^2}\frac{\partial}{\partial r}(r^2 F_r) + \frac{1}{r\sin\theta}\frac{\partial}{\partial \theta}(\sin\theta F_\theta) + \frac{1}{r\sin\theta}\frac{\partial F_\phi}{\partial \phi} \,, \tag{4.7}$$

and consequently the Laplacian of V is

$$\begin{aligned} \nabla^2 V &= \operatorname{div}(\nabla V) \\ &= \frac{1}{r^2}\frac{\partial}{\partial r}\left(r^2\frac{\partial V}{\partial r}\right) + \frac{1}{r^2\sin\theta}\frac{\partial}{\partial \theta}\left(\sin\theta\frac{\partial V}{\partial \theta}\right) + \frac{1}{r^2\sin^2\theta}\frac{\partial^2 V}{\partial \phi^2} \,. \end{aligned} \tag{4.8}$$

Finally, we need the directional derivatives, in the direction, say, of the vector

$$\mathbf{n} = n_r\mathbf{a}_r + n_\theta\mathbf{a}_\theta + n_\phi\mathbf{a}_\phi. \tag{4.9}$$

The directional derivative $\mathbf{n}\cdot\nabla V$ of a scalar is obtained, as would be naively expected, as the scalar product of $\mathbf{n}$ with the gradient in equation (4.6). However, in the directional derivatives $\mathbf{n}\cdot\nabla\mathbf{F}$ of a vector field, the change in the unit vectors $\mathbf{a}_r$, $\mathbf{a}_\theta$ and $\mathbf{a}_\phi$ must be taken into account. The result is

$$\begin{aligned} \mathbf{n}\cdot\nabla\mathbf{F} &= \left(\mathbf{n}\cdot\nabla F_r - \frac{n_\theta F_\theta}{r} - \frac{n_\phi F_\phi}{r}\right)\mathbf{a}_r \\ &\quad + \left(\mathbf{n}\cdot\nabla F_\theta - \frac{n_\phi F_\phi}{r}\cot\theta + \frac{n_\theta F_r}{r}\right)\mathbf{a}_\theta \\ &\quad + \left(\mathbf{n}\cdot\nabla F_\phi + \frac{n_\phi F_r}{r} + \frac{n_\phi F_\theta}{r}\cot\theta\right)\mathbf{a}_\phi \,, \end{aligned} \tag{4.10}$$

where the directional derivatives of F_r, F_θ and F_ϕ are the same as for a scalar field.

As the radial direction has a special status, it is convenient to introduce the horizontal (or, properly speaking, tangential) component of the vector $\mathbf{F}$:

$$\mathbf{F}_{\mathrm{h}} = F_\theta\mathbf{a}_\theta + F_\phi\mathbf{a}_\phi \,, \tag{4.11}$$

and similarly the horizontal components of the gradient, divergence and Laplacian as

$$\nabla_{\mathrm{h}} V = \frac{1}{r}\frac{\partial V}{\partial \theta}\mathbf{a}_\theta + \frac{1}{r\sin\theta}\frac{\partial V}{\partial \phi}\mathbf{a}_\phi \,, \tag{4.12}$$

$$\nabla_{\mathrm{h}}\cdot\mathbf{F} = \frac{1}{r\sin\theta}\frac{\partial}{\partial \theta}(\sin\theta F_\theta) + \frac{1}{r\sin\theta}\frac{\partial F_\phi}{\partial \phi} \,, \tag{4.13}$$

and

$$\nabla_{\mathrm{h}}^2 V = \frac{1}{r^2\sin\theta}\frac{\partial}{\partial \theta}(\sin\theta\frac{\partial V}{\partial \theta}) + \frac{1}{r^2\sin^2\theta}\frac{\partial^2 V}{\partial \phi^2} \,. \tag{4.14}$$

4.2 The Oscillation Equations

4.2.1 Separation of variables

The displacement $\boldsymbol{\delta}\mathbf{r}$ is separated into radial and horizontal components as

$$\boldsymbol{\delta}\mathbf{r} = \xi_r \mathbf{a}_r + \boldsymbol{\xi}_{\rm h} \ . \tag{4.15}$$

The horizontal component of the equations of motion, (3.43), is

$$\rho_0 \frac{\partial^2 \boldsymbol{\xi}_{\rm h}}{\partial t^2} = -\nabla_{\rm h} p' - \rho_0 \nabla_{\rm h} \Phi' \ . \tag{4.16}$$

As the horizontal gradient of equilibrium quantities is zero, the horizontal divergence of equation (4.16) gives

$$\rho_0 \frac{\partial^2}{\partial t^2} \nabla_{\rm h} \cdot \boldsymbol{\xi}_{\rm h} = -\nabla_{\rm h}^2 p' - \rho_0 \nabla_{\rm h}^2 \Phi' \ . \tag{4.17}$$

The equation of continuity, (3.41), can be written as

$$\rho' = -\frac{1}{r^2}\frac{\partial}{\partial r}(\rho_0 r^2 \xi_r) - \rho_0 \nabla_{\rm h} \cdot \boldsymbol{\xi}_{\rm h} \ . \tag{4.18}$$

This can be used to eliminate $\nabla_{\rm h} \cdot \boldsymbol{\xi}_{\rm h}$ from equation (4.17), which becomes

$$-\frac{\partial^2}{\partial t^2}\left[\rho' + \frac{1}{r^2}\frac{\partial}{\partial r}(r^2 \rho_0 \xi_r)\right] = -\nabla_{\rm h}^2 p' - \rho_0 \nabla_{\rm h}^2 \Phi' \ . \tag{4.19}$$

The radial component of equation (3.43) is

$$\rho_0 \frac{\partial^2 \xi_r}{\partial t^2} = -\frac{\partial p'}{\partial r} - \rho' g_0 - \rho_0 \frac{\partial \Phi'}{\partial r} \ . \tag{4.20}$$

Finally, Poisson's equation (3.44) may be written as

$$\frac{1}{r^2}\frac{\partial}{\partial r}\left(r^2 \frac{\partial \Phi'}{\partial r}\right) + \nabla_{\rm h}^2 \Phi' = 4\pi G \rho' \ . \tag{4.21}$$

It should be noticed that in equations (4.19) – (4.21) derivatives with respect to the angular variables θ and ϕ only appear in the combination $\nabla_{\rm h}^2$.

We now have to consider the energy equation (3.47), together with equation (3.48) for the heat gain. The result clearly depends on the form assumed for the flux $\mathbf{F}$. However, if the flux can be expressed in terms of a gradient of a scalar, as in the diffusion approximation [equation (3.22)], the energy equation also only contains derivatives with respect to θ and ϕ in $\nabla_{\rm h}^2$.

Exercise 4.1:

Show this.

We may now address the separation of the angular variables. The object is to factor out the variation of the perturbations with θ and ϕ as a function $f(\theta, \phi)$. From the form

of the equations this is clearly possible, if f is an eigenfunction of the horizontal Laplace operator,

$$\nabla_{\rm h}^2 f = -\frac{1}{r^2}\Lambda f \ , \tag{4.22}$$

where Λ is a constant. That $1/r^2$ has to appear is obvious from equation (4.14); the choice of sign is motivated later. Writing it out in full, equation (4.22) becomes

$$\frac{1}{\sin\theta}\frac{\partial}{\partial\theta}\left(\sin\theta\frac{\partial f}{\partial\theta}\right) + \frac{1}{\sin^2\theta}\frac{\partial^2 f}{\partial\phi^2} = -\Lambda\, f \ . \tag{4.23}$$

As the coefficients in this equation are independent of ϕ, the solution can be further separated, as

$$f(\theta,\phi) = f_1(\theta) f_2(\phi) \ . \tag{4.24}$$

It follows from equation (4.23) that f_2 satisfies an equation of the form

$$\frac{{\rm d}^2 f_2}{{\rm d}\phi^2} = \alpha f_2 \ , \tag{4.25}$$

where α is another constant; this has the solution $f_2 = \exp(\pm\alpha^{1/2}\phi)$. However, the solution has to be continuous and hence periodic, *i.e.*, $f_2(0) = f_2(2\pi)$. Consequently we must demand that $\alpha^{1/2} = im$, where m is an integer.

When used in equation (4.23), this gives the following differential equation for f_1:

$$\frac{\rm d}{{\rm d}x}\left[(1-x^2)\frac{{\rm d}f_1}{{\rm d}x}\right] + \left(\Lambda - \frac{m^2}{1-x^2}\right) f_1 = 0 \ , \tag{4.26}$$

where $x = \cos\theta$. It can be shown that this equation has a regular solution only when

$$\Lambda = l(l+1) \ , \tag{4.27}$$

where l is a non-negative integer and

$$|m| \le l \ . \tag{4.28}$$

The regular solution is

$$f_1(\theta) = P_l^m(\cos\theta) \ , \tag{4.29}$$

where P_l^m is the Legendre function. By including an appropriate scaling factor we may finally write

$$f(\theta,\phi) = (-1)^m c_{lm} P_l^m(\cos\theta)\exp(im\phi) \equiv Y_l^m(\theta,\phi) \ , \tag{4.30}$$

where Y_l^m is a spherical harmonic; here c_{lm} is a normalization constant given by equation (2.2), such that the integral of $|Y_l^m|^2$ over the unit sphere is 1. Y_l^m is characterized by its *degree* l and its azimuthal order m; the properties of spherical harmonics were discussed in more detail in Section 2.1 (see also Appendix A). From equations (4.22) and (4.27) we also have that

$$\nabla_{\rm h}^2 f = -\frac{l(l+1)}{r^2} f \ . \tag{4.31}$$

The dependent variables in equations (4.19) – (4.21) can now be written as

$$\xi_r(r,\theta,\phi,t) = \sqrt{4\pi}\,\tilde{\xi}_r(r) Y_l^m(\theta,\phi)\exp(-i\omega t) \ , \tag{4.32}$$

$$p'(r,\theta,\phi,t) = \sqrt{4\pi}\,\tilde{p}'(r)Y_l^m(\theta,\phi)\exp(-i\omega t)\ , \tag{4.33}$$

etc. Also it follows from equation (3.38) that if the Eulerian perturbations are on the form given in these equations, so are the Lagrangian perturbations. Then the equations contain $Y_l^m(\theta,\phi)\exp(-i\omega t)$ as a common factor. After dividing by it, the following ordinary differential equations for the amplitude functions $\tilde{\xi}_r, \tilde{p}', \cdots$, result:

$$\omega^2\left[\tilde{\rho}' + \frac{1}{r^2}\frac{\mathrm{d}}{\mathrm{d}r}(r^2\rho_0\tilde{\xi}_r)\right] = \frac{l(l+1)}{r^2}(\tilde{p}' + \rho_0\tilde{\Phi}')\ , \tag{4.34}$$

$$-\omega^2\rho_0\tilde{\xi}_r = -\frac{\mathrm{d}\tilde{p}'}{\mathrm{d}r} - \tilde{\rho}'g_0 - \rho_0\frac{\mathrm{d}\tilde{\Phi}'}{\mathrm{d}r}\ , \tag{4.35}$$

$$\frac{1}{r^2}\frac{\mathrm{d}}{\mathrm{d}r}\left(r^2\frac{\mathrm{d}\tilde{\Phi}'}{\mathrm{d}r}\right) - \frac{l(l+1)}{r^2}\tilde{\Phi}' = 4\pi G\tilde{\rho}'\ , \tag{4.36}$$

together with the energy equation

$$\left(\delta\tilde{p} - \frac{\Gamma_{1,0}p_0}{\rho_0}\delta\tilde{\rho}\right) = \rho_0(\Gamma_{3,0}-1)\delta\tilde{q}\ . \tag{4.37}$$

It should be noted that equations (4.34) – (4.37) do not depend on the azimuthal order m. This is a consequence of the assumed spherical symmetry of the equilibrium state, which demands that the results should be independent of the choice of polar axis for the coordinate system. Changing the polar axis would change the spherical harmonics, in such a way that a new spherical harmonic, with given l and m, would be a linear combination over m of the old spherical harmonics with the given value of l (Edmonds 1960). As this change of axis can have no effect on the dynamics of the oscillations, the equations must be independent of m, as found here.

From equation (4.16) the horizontal component of the displacement is given by

$$\boldsymbol{\xi}_\mathrm{h} = \sqrt{4\pi}\,\tilde{\xi}_\mathrm{h}(r)\left(\frac{\partial Y_l^m}{\partial\theta}\mathbf{a}_\theta + \frac{1}{\sin\theta}\frac{\partial Y_l^m}{\partial\phi}\mathbf{a}_\phi\right)\exp(-i\omega t)\ , \tag{4.38}$$

where

$$\tilde{\xi}_\mathrm{h}(r) = \frac{1}{r\omega^2}(\frac{1}{\rho_0}\tilde{p}' + \tilde{\Phi}')\ . \tag{4.39}$$

Thus the (physical) displacement vector can be written as

$$\begin{aligned}\boldsymbol{\delta r} \;=\; & \sqrt{4\pi}\Re\left\{\left[\tilde{\xi}_r(r)Y_l^m(\theta,\phi)\mathbf{a}_r\right.\right. \\ & \left.\left. +\tilde{\xi}_\mathrm{h}(r)\left(\frac{\partial Y_l^m}{\partial\theta}\mathbf{a}_\theta + \frac{1}{\sin\theta}\frac{\partial Y_l^m}{\partial\phi}\mathbf{a}_\phi\right)\right]\exp(-i\omega t)\right\}\ .\end{aligned} \tag{4.40}$$

As noted in Section 4.1 the frequency ω is in general complex. That this is so may be seen from the energy equation (4.37), if the expression (3.48) for the heating rate perturbation is used. Assuming the time dependence given in equations (4.33) for the perturbed quantities, equation (3.48) can be written as

$$\delta q = \frac{i}{\rho_0\omega}\delta(\rho\epsilon - \mathrm{div}\,\mathbf{F})\ . \tag{4.41}$$

Here the perturbations on the right-hand side can be expressed in terms of the perturbations in, say, density and temperature. For instance, since ϵ is a function $\epsilon(\rho, T)$ of density and temperature, we obtain

$$\delta(\rho\epsilon) = \rho\epsilon \left\{ \left[1 + \left(\frac{\partial \ln \epsilon}{\partial \ln \rho} \right)_T \right] \frac{\delta\rho}{\rho} + \left(\frac{\partial \ln \epsilon}{\partial \ln T} \right)_\rho \frac{\delta T}{T} \right\} . \tag{4.42}$$

The expression for $\delta(\mathrm{div}\,\mathbf{F})$ depends on the treatment of the energy transport, discussed in Section 3.1.3. Often the diffusion approximation is adequate; then $\delta(\mathrm{div}\,\mathbf{F})$ may be obtained in a fashion similar to the derivation of equation (4.42) by perturbing equation (3.22), although with considerable effort. Note that this gives rise to a term in the second derivative of δT with respect to r; the same is true if the Eddington approximation [equation (3.24)] is used, whereas the use of Newton's law of cooling [equation (3.23)] gives a direct relation between the heat loss and the local thermodynamic variables, and hence does not increase the order of the equations. However, regardless of the approximation used, substitution of the relevant relations into the energy equation, written in terms of ρ and T, results in an equation which, because of the factor i/ω in the expression for δq, has complex coefficients. Hence the oscillation equations cannot in general have a real solution.

The complex frequency can be expressed as $\omega = \omega_\mathrm{r} + i\eta$, where ω_r and η are real; consequently the dependence of the perturbations on ϕ and t is of the form

$$\cos(m\phi - \omega_\mathrm{r} t + \delta_0) \mathrm{e}^{\eta t} , \tag{4.43}$$

where δ_0 is the initial phase. For $m \neq 0$ this describes a wave traveling around the equator with angular phase speed ω_r/m, whereas for $m = 0$ the perturbation is a standing wave. The period of the perturbation is $\Pi = 2\pi/\omega_\mathrm{r}$. Its amplitude grows or decays exponentially with time, depending on whether the *growth rate* η is positive or negative.

Neglecting η, we may obtain the mean square components of the displacement, when averaged over a spherical surface and time, from equation (4.40). For the radial component the result is

$$\begin{aligned} \delta r_\mathrm{rms}^2 &= \langle |\delta\mathbf{r} \cdot \mathbf{a}_r|^2 \rangle \\ &= \frac{1}{\Pi} \int_0^\Pi \mathrm{d}t \frac{1}{4\pi} \oint \left\{ \sqrt{4\pi} \Re \left[\tilde{\xi}_r(r) Y_l^m(\theta, \phi) \exp(-i\omega t) \right] \right\}^2 \mathrm{d}\Omega \\ &= \frac{1}{2} |\tilde{\xi}_r(r)|^2 , \end{aligned} \tag{4.44}$$

where Ω is solid angle. Similarly, the mean square length of the horizontal component of $\boldsymbol{\delta}\mathbf{r}$ is

$$\delta h_\mathrm{rms}^2 = \langle |\boldsymbol{\xi}_\mathrm{h}|^2 \rangle = 1/2\, l(l+1) |\tilde{\xi}_\mathrm{h}(r)|^2 , \tag{4.45}$$

where $\tilde{\xi}_\mathrm{h}$ is the amplitude function introduced in equation (4.39).

Exercise 4.2:

Verify equations (4.44) and (4.45). Note that the latter is a little tricky: this requires integration by parts and use of the fact that P_l^m satisfies equation (4.23).

The kinetic energy of pulsation is

$$E_{\rm kin} = \frac{1}{2}\int_V |\mathbf{v}|^2 \rho_0 {\rm d}V \ . \tag{4.46}$$

As in equations (4.44) and (4.45) it follows from equation (4.40) that the time-averaged energy is $1/4\,\omega^2\mathcal{E}$, where

$$\mathcal{E} = 4\pi \int_0^R [|\tilde{\xi}_r(r)|^2 + l(l+1)|\tilde{\xi}_{\rm h}(r)|^2]\,\rho_0 r^2 {\rm d}r \ . \tag{4.47}$$

For $m \neq 0$ $E_{\rm kin}$ is independent of t, in accordance with the running-wave nature of the oscillation in this case, whereas for $m = 0$ we have $E_{\rm kin} = \frac{1}{2}\omega^2\mathcal{E}\cos^2(\omega t - \delta_0)$. It is convenient to introduce the dimensionless measure E of $\mathcal{E}$, by

$$E = \frac{4\pi \int_0^R [|\tilde{\xi}_r(r)|^2 + l(l+1)|\tilde{\xi}_{\rm h}(r)|^2]\rho_0 r^2 {\rm d}r}{M\,[|\tilde{\xi}_r(R)|^2 + l(l+1)|\tilde{\xi}_{\rm h}(R)|^2]} = \frac{M_{\rm mode}}{M} \ , \tag{4.48}$$

where M is the total mass of the star, and $M_{\rm mode}$ is the so-called modal mass; thus E provides a measure of the normalized *inertia* of the mode. These quantities are defined such that the time-averaged kinetic energy in the oscillation is

$$1/2 M_{\rm mode} V_{\rm rms}^2 = 1/2 E M V_{\rm rms}^2 \ , \tag{4.49}$$

where $V_{\rm rms}^2$ is the mean, over the stellar surface and time, of the squared total velocity of the mode.

From equation (4.31) it follows that for any perturbation quantity ψ',

$$\nabla_{\rm h}^2 \psi' = -\frac{l(l+1)}{r^2}\psi' \ . \tag{4.50}$$

Thus if the oscillations are regarded locally as plane waves, as in equation (3.53), we may make the identification

$$\frac{l(l+1)}{r^2} = k_{\rm h}^2 \ , \tag{4.51}$$

where $k_{\rm h}$ is the length of the horizontal component of the wave vector, as in equation (3.63); note in particular that $k_{\rm h}$ depends on r.

For completeness, I note that the modes discussed so far (which are the only modes considered in the following), are known as *spheroidal modes*. In addition there is a second class of modes, the *toroidal modes*, which are briefly discussed in Cox (1980), Section 17.3. In a spherically symmetric (and hence nonrotating) star, they have zero frequency and correspond to infinitely slow, purely horizontal motion. In a rotating star they give rise to oscillations whose frequencies are of the order of the rotation frequency.

4.2.2 Radial oscillations

For *radial* oscillations, with $l = 0$, the perturbation in the gravitational field may be eliminated analytically. From Poisson's equation in the form (4.36) we have, by using the equation of continuity (4.18) with zero horizontal part, that

$$\frac{1}{r^2}\frac{\rm d}{{\rm d}r}\left(r^2 \frac{{\rm d}\tilde{\Phi}'}{{\rm d}r}\right) = -\frac{4\pi G}{r^2}\frac{\rm d}{{\rm d}r}(r^2\rho_0\tilde{\xi}_r) \ , \tag{4.52}$$

or, as the gravitational force must be finite at $r = 0$,

$$\frac{\mathrm{d}\tilde{\Phi}'}{\mathrm{d}r} = -4\pi G\rho_0\tilde{\xi}_r \ . \tag{4.53}$$

Furthermore, the term containing $\tilde{\Phi}'$ drops out in equation (4.34).

With these eliminations, the oscillation equations can be reduced to a relatively simple form. We write the energy equation (4.37) as

$$\tilde{\rho}' = \frac{\rho_0}{\Gamma_{1,0}p_0}\tilde{p}' + \rho_0\tilde{\xi}_r\left(\frac{1}{\Gamma_{1,0}p_0}\frac{\mathrm{d}p_0}{\mathrm{d}r} - \frac{1}{\rho_0}\frac{\mathrm{d}\rho_0}{\mathrm{d}r}\right) - \frac{\rho_0^2}{\Gamma_{1,0}p_0}(\Gamma_{3,0}-1)\delta\tilde{q} \ . \tag{4.54}$$

Then equation (4.34) may be written as

$$\frac{\mathrm{d}\tilde{\xi}_r}{\mathrm{d}r} = -\frac{2}{r}\tilde{\xi}_r - \frac{1}{\Gamma_{1,0}p_0}\frac{\mathrm{d}p_0}{\mathrm{d}r}\tilde{\xi}_r - \frac{1}{\Gamma_{1,0}p_0}\tilde{p}' + \frac{\rho_0}{\Gamma_{1,0}p_0}(\Gamma_{3,0}-1)\delta\tilde{q} \ , \tag{4.55}$$

or, introducing $\zeta \equiv \tilde{\xi}_r/r$,

$$\tilde{p}' = -\Gamma_{1,0}p_0 r\left(\frac{\mathrm{d}\zeta}{\mathrm{d}r} + \frac{3}{r}\zeta + \frac{1}{\Gamma_{1,0}p_0}\frac{\mathrm{d}p_0}{\mathrm{d}r}\zeta\right) + \rho_0(\Gamma_{3,0}-1)\delta\tilde{q} \ . \tag{4.56}$$

By substituting equations (4.53), (4.54) and (4.56) into equation (4.35) we obtain, after a little manipulation,

$$\frac{1}{r^3}\frac{\mathrm{d}}{\mathrm{d}r}\left(r^4\Gamma_{1,0}p_0\frac{\mathrm{d}\zeta}{\mathrm{d}r}\right) + \frac{\mathrm{d}}{\mathrm{d}r}[(3\Gamma_{1,0}-4)p_0]\zeta + \rho_0\omega^2 r\zeta = \frac{\mathrm{d}}{\mathrm{d}r}[\rho_0(\Gamma_{3,0}-1)\delta\tilde{q}] \ . \tag{4.57}$$

Exercise 4.3:

Fill in the missing steps in the derivation of equation (4.57).

It is important to note that the apparent simplicity of equation (4.57) hides a great deal of complexity in the heating term on the right-hand side. Nevertheless, this equation is convenient for discussions of the properties of radial oscillations. In these notes, however, I shall mostly consider the general equations for *nonradial* oscillations, where l can take any value.

4.3 Linear, adiabatic oscillations

To simplify the notation, from now on I drop the tilde on the amplitude functions, and the "0" on equilibrium quantities. This should not cause any confusion.

4.3.1 Equations

For adiabatic oscillations, $\delta q = 0$ and equation (4.37) can be written

$$\rho' = \frac{\rho}{\Gamma_1 p} p' + \rho \xi_r \left(\frac{1}{\Gamma_1 p} \frac{\mathrm{d}p}{\mathrm{d}r} - \frac{1}{\rho} \frac{\mathrm{d}\rho}{\mathrm{d}r} \right) . \tag{4.58}$$

This may be used to eliminate ρ' from equations (4.34) – (4.36). From equation (4.34) we obtain

$$\frac{\mathrm{d}\xi_r}{\mathrm{d}r} = -\left(\frac{2}{r} + \frac{1}{\Gamma_1 p} \frac{\mathrm{d}p}{\mathrm{d}r} \right) \xi_r + \frac{1}{\rho} \left[\frac{l(l+1)}{\omega^2 r^2} - \frac{1}{c^2} \right] p' + \frac{l(l+1)}{\omega^2 r^2} \Phi' , \tag{4.59}$$

where we used that $c^2 = \Gamma_1 p/\rho$ is the square of the adiabatic sound speed [*cf.* equation (3.52)]. It is convenient to introduce the characteristic acoustic frequency S_l by

$$S_l^2 = \frac{l(l+1)c^2}{r^2} = k_\mathrm{h}^2 c^2 . \tag{4.60}$$

Then equation (4.59) can be written as

$$\frac{\mathrm{d}\xi_r}{\mathrm{d}r} = -\left(\frac{2}{r} + \frac{1}{\Gamma_1 p} \frac{\mathrm{d}p}{\mathrm{d}r} \right) \xi_r + \frac{1}{\rho c^2} \left(\frac{S_l^2}{\omega^2} - 1 \right) p' + \frac{l(l+1)}{\omega^2 r^2} \Phi' . \tag{4.61}$$

Equation (4.35) gives

$$\frac{\mathrm{d}p'}{\mathrm{d}r} = \rho(\omega^2 - N^2)\xi_r + \frac{1}{\Gamma_1 p} \frac{\mathrm{d}p}{\mathrm{d}r} p' - \rho \frac{\mathrm{d}\Phi'}{\mathrm{d}r} , \tag{4.62}$$

where, as in equation (3.73), N is the buoyancy frequency, given by

$$N^2 = g \left(\frac{1}{\Gamma_1 p} \frac{\mathrm{d}p}{\mathrm{d}r} - \frac{1}{\rho} \frac{\mathrm{d}\rho}{\mathrm{d}r} \right) . \tag{4.63}$$

Finally, equation (4.36) becomes

$$\frac{1}{r^2} \frac{\mathrm{d}}{\mathrm{d}r} \left(r^2 \frac{\mathrm{d}\Phi'}{\mathrm{d}r} \right) = 4\pi G \left(\frac{p'}{c^2} + \frac{\rho \xi_r}{g} N^2 \right) + \frac{l(l+1)}{r^2} \Phi' . \tag{4.64}$$

Equations (4.61), (4.62) and (4.64) constitute a fourth-order system of ordinary differential equations for the four dependent variables ξ_r, p', Φ' and $\mathrm{d}\Phi'/\mathrm{d}r$. Thus it is a complete set of differential equations.

For radial oscillations equations (4.61) and (4.62), after elimination of the terms in Φ' by means of equation (4.53), reduce to a second-order system in ξ_r and p'; an alternative formulation of this set of equations is obtained from equation (4.57), by setting the right-hand side to zero. The reduction to second order is a useful simplification from a computational point of view, and it may be exploited in asymptotic analyses. However, here I shall always treat radial oscillations in the same way as the nonradial case.

It should be noticed that all coefficients in equations (4.61), (4.62) and (4.64) are real. Also, as discussed below, the same is true of the boundary conditions. Since the frequency only appears in the form ω^2, we may expect that the solution is such that ω^2 is real, in which case the eigenfunctions may also be chosen to be real. This may be proved to be true in general. Thus the frequency is either purely real, in which case the motion is an

undamped oscillator, or purely imaginary, so that the motion grows or decays exponentially. From a physical point of view this results from the adiabatic approximation, which ensures that energy cannot be fed into the motion, except from the gravitational field; thus the only possible type of instability is a dynamical instability. I shall almost always consider the oscillatory case, with $\omega^2 > 0$; note, however, that the convective instability discussed briefly in Section 3.3.2 is an example of a dynamical instability.

4.3.2 Boundary conditions

To supplement the four equations in the general case, we need four boundary conditions. These are discussed in considerable detail in Unno *et al.* (1989), Section 18.1, and in Cox (1980), Section 17.6. Here I give only a brief summary.

The centre, $r = 0$ is a regular singular point of the equations. Thus, as is usual in the theory of differential equations, the equations admit both regular and singular solutions at this point. Two of the conditions serve to select the regular solutions. By expanding the equations, it may be shown that near $r = 0$, ξ_r behaves like r^{l-1}, whereas p' and Φ' behave as r^l. In the special case of radial oscillations, however, the coefficient to the leading-order term in ξ_r vanishes, and ξ_r goes as r. Indeed it is obvious from geometrical considerations that for spherically symmetric oscillations, the displacement must vanish at the centre. From the expansions, two relations between the solution near $r = 0$ may be obtained. In particular, it may be shown that for $l > 0$,

$$\xi_r \simeq l\xi_{\rm h} , \qquad \text{for } r \to 0 . \tag{4.65}$$

In the radial case, one of the conditions was implicitly used to obtain equation (4.53), and only one central condition remains.

One surface condition is obtained by demanding continuity of Φ' and its derivative at the surface radius $r = R$. Outside the star the density perturbation vanishes, and Poisson's equation may be solved analytically. The solution vanishing at infinity is

$$\Phi' = A\, r^{-l-1} , \tag{4.66}$$

where A is a constant. Consequently Φ' must satisfy

$$\frac{{\rm d}\Phi'}{{\rm d}r} + \frac{l+1}{r}\,\Phi' = 0 \qquad \text{at } r = R . \tag{4.67}$$

The second condition depends on the treatment of the stellar atmosphere, and may consequently be quite complicated. These complications are discussed further in Chapter 5. For the moment, I note that if the star is assigned a definite boundary at $r = R$, it is physically reasonable to assume that the boundary is free, so that no forces act on it. In this way the star can be considered as an isolated system. This is equivalent to requiring the pressure to be constant at the perturbed surface. Thus as the second surface boundary condition I take that the Lagrangian pressure perturbation vanish, *i.e.*,

$$\delta p = p' + \xi_r \frac{{\rm d}p}{{\rm d}r} = 0 \qquad \text{at } r = R . \tag{4.68}$$

As shown later, a more detailed analysis of the atmospheric behaviour of the oscillations gives a very similar result, except at high frequencies.

From equation (4.68) one can estimate the ratio between the radial and horizontal components of the displacement on the surface. The amplitude of the horizontal displacement is given by equation (4.39). In most cases, however, the perturbation in the gravitational potential is small. Thus we have approximately, from equation (4.68), that

$$\frac{\xi_{\rm h}(R)}{\xi_r(R)} = \frac{g_{\rm s}}{R\omega^2} \equiv \sigma^{-2} \; , \tag{4.69}$$

where $g_{\rm s}$ is the surface gravity, and σ is a dimensionless frequency, defined by

$$\sigma^2 = \frac{R^3}{GM}\omega^2 \; . \tag{4.70}$$

Thus the surface value of $\xi_{\rm h}/\xi_r$, to this approximation, depends only on frequency. The ratio of the *rms* horizontal to vertical displacement [*cf.* equations (4.44) and (4.45)] is

$$\frac{\delta h_{\rm rms}}{\delta r_{\rm rms}} = \frac{\sqrt{l(l+1)}}{\sigma^2} \qquad \text{at } r = R \; . \tag{4.71}$$

For the important case of the solar five-minute oscillations, $\sigma^2 \sim 1000$, and so the motion is predominantly vertical, except at large l.

Chapter 5

Properties of solar and stellar oscillations.

It is straightforward to solve numerically the equations and boundary conditions derived in the previous chapter. Reference may be made to Chapter 6 or, for example, to Unno *et al.* (1989) Section 18.2. However, some care is required to achieve the accuracy needed in the interpretation of the observed frequencies. The numerical techniques are discussed in some detail in Chapter 6.

The equations and boundary conditions have non-trivial solutions only for specific values of the frequency ω, which is therefore an *eigenvalue* of the problem. Each eigenfrequency corresponds to a mode of oscillation; from the computation one obtains also the *eigenfunction*, *i.e.*, the variation of the perturbations ξ_r, p', *etc.* with r. As the equations are homogeneous, the solution is determined only to within a constant factor. Thus the equations do not determine the amplitude of the motion. This is fixed by non-linear effects, or by a possible external forcing that may be responsible for the oscillations. However, the eigenfunctions resulting from the calculation give the *distribution* of the amplitude with position in the star; thus they may be used, *e.g.*, to relate the observable surface amplitude to the amplitude in the interior, or to the total energy in the oscillation.

This chapter first considers the general dependence of oscillation frequencies on the properties of stars, including their mass and radius. Then the properties of stellar oscillations are discussed in terms of a highly simplified, largely physical, asymptotic description, valid in the limit where the radial order of the mode (which is roughly given by the number of nodes in the eigenfunction in the radial direction) is large. The asymptotic description is made mathematically more rigorous and extended in Chapter 7; however, the results obtained here are at least qualitatively valid. Furthermore numerical examples, based on results of oscillation calculations, are given for a model of the present Sun, for models representing δ Scuti stars and for models of η Bootis. They are to a large extent representative for other stars as well. Further results for other types of stars were given by, for example, Unno *et al.* (1989). Section 5.4 discusses the behaviour of adiabatic oscillations in an isothermal atmosphere, which is often an adequate approximation to real stellar atmospheres. Finally, Section 5.5 presents some general properties of the solutions to the oscillation equations, including an analysis of the effects on the frequencies of a small perturbation to the equilibrium model or the physics of the oscillations.

5.1 The dependence of the frequencies on the equilibrium structure

5.1.1 What do frequencies of adiabatic oscillations depend on?

The coefficients in the adiabatic oscillation equations (4.61), (4.62) and (4.64) obviously depend on the structure of the equilibrium model. Indeed, this is the whole basis for using observed frequencies to probe the structure of, say, the Sun. A closer inspection reveals that the coefficients are determined solely by the set of equilibrium variables

$$\rho,\ p,\ \Gamma_1,\ g\ , \tag{5.1}$$

as functions of r. However, the equilibrium model satisfies the stellar structure equations (3.33) and (3.34); in addition it may be assumed to have a given mass and radius, which at least in the case of the Sun are known with high precision.

If $\rho(r)$ is given, $g(r)$ is determined by equation (3.34); and, given g, the equation (3.33) of hydrostatic support may be integrated from the surface to provide $p(r)$ (the surface pressure is known from theoretical or empirical atmospheric models). Thus of the set (5.1) only the two functions $\rho(r)$ and $\Gamma_1(r)$ are independent, and the adiabatic oscillation frequencies are determined solely by these two functions. Conversely, if no other constraints are imposed, the observed frequencies give direct information only about ρ and Γ_1.

One might imagine that Γ_1 could be determined from the equation of state if p and ρ were known. However, to determine the thermodynamic state the chemical composition must be known, and this cannot be assumed, in particular as it varies through the star. In addition, the equation of state under stellar conditions is not known with sufficient accuracy. On the other hand Γ_1 cannot be completely unconstrained, as it must be close to 5/3 in the interior of the star where the gas is almost fully ionized.

To a fair degree of approximation the chemical composition can be specified by a single parameter, such as the abundance Y by mass of helium. In this approximation just three quantities should suffice to specify fully the thermodynamic state. In principle these three quantities could be ρ, p and Γ_1 which, as argued above, should be obtainable from the oscillation observations. If the equation of state were known one should be able to determine any other thermodynamic variable, including Y, from these observed quantities. Outside the ionization zones, being very nearly constant, Γ_1 gives a poor determination of the thermodynamic state; however, it varies sufficiently in the ionization zones to allow a determination of Y, provided that the properties of the equation of state are known with sufficient accuracy. Indeed, procedures for such a determination of the helium abundance of the Sun have been proposed (*e.g.* Däppen & Gough 1984, 1986; Kosovichev *et al.* 1992). As discussed in Section 7.7.3 an apparently quite efficient technique can be obtained on the basis of the asymptotic behaviour of the oscillations in the helium ionization zone.

The preceding discussion was made in terms of the pair (ρ, Γ_1). However, any other independent pair of model variables, related directly to ρ and Γ_1, may be used instead. As will be discussed extensively below, observed oscillations have in many cases (including the Sun) essentially the nature of standing acoustic waves. Their frequencies are largely determined by the behaviour of sound speed c, and hence it would be natural to use c as one of the variables, combined with, *e.g.*, ρ or Γ_1. Also, it is evident that analysis of such oscillations may be used to determine properties of the sound speed; as discussed in Section 7.7.2 below, the observations for the Sun are sufficiently rich that the observed

frequencies may be inverted to obtain an estimate of the sound speed in most of the Sun. It follows from equation (3.56) that this provides a measure of T/μ. However, it is important to note that measurements of adiabatic oscillation frequencies do not by themselves allow a determination of the temperature in a star. Only if the mean molecular weight can be otherwise constrained (*e.g.* by demanding that its variation in the stellar interior results from normal stellar evolution) is it possible to estimate the stellar interior temperature. This limitation is of obvious importance for the use of observed solar oscillation frequencies to throw a light on the apparent deficit of observed solar neutrinos (*e.g.* Christensen-Dalsgaard 1991a).

5.1.2 The dependence of oscillation frequencies on the physics of the stellar interiors

As discussed in texts on stellar evolution (*e.g.* Christensen-Dalsgaard 1993a; Kippenhahn & Weigert 1990) the computation of stellar models depends on assumptions about the physical properties of matter in the stars, in particular the equation of state, the opacity and the rates of nuclear reactions; these aspects of the calculation might be called the *microphysics*. Furthermore, the computations involve a number of simplifying assumptions, often covering much complex physics which might be called the *macrophysics*:

- The treatment of convection is generally approximated through a parametrization of the properties of the uppermost layers of the convection zone. A typical (and commonly used) example is mixing-length theory which depends on the mixing-length parameter α_c; the value of α_c fixes the value s of the specific entropy in the bulk of the convection zone, where the temperature stratification is essentially adiabatic and where s is therefore nearly constant.
- The dynamical effects of convection (the so-called turbulent pressure) is ignored.
- It is assumed that there is no mixing outside convectively unstable regions; also element settling and diffusion are usually ignored.
- Effects of magnetic fields are ignored.

Similarly, the calculations of oscillation frequencies are often done in the adiabatic approximation. Even when nonadiabatic effects are taken into account, their treatment is uncertain, since there is no definite theory for the perturbation to the convective flux, induced by the oscillations. Also, the perturbations to the turbulent pressure are usually neglected.

The goals of the analysis of observed frequencies are evidently to test both the microphysics and the simplifying assumptions. This must be done in such a way that the results are not compromised by the uncertainties mentioned above. A further complication is that a given region of the model in general is affected by several aspects of the microphysics, *e.g.* both the opacity and the equation of state; under these circumstances it may evidently be difficult or impossible to isolate the cause of discrepancies between observations and models.

In the analysis of solar data a very considerable simplification results from the presence of the convection zone, despite the uncertainties in the detailed description of convection. The reason is that, regardless of these uncertainties, there is no doubt that convection in

almost the entire convection zone is a very efficient means of energy transport, requiring only a minute superadiabatic gradient. Thus to a very good approximation the relation between pressure and density is determined by

$$\frac{\mathrm{d}\ln\rho}{\mathrm{d}\ln p} \simeq \frac{1}{\Gamma_1} , \tag{5.2}$$

such that, as mentioned above, the specific entropy s is virtually constant; also, since radiation plays no role for the energy transport, the structure is independent of opacity. The value of s is determined by the structure of the thin region just beneath the surface where the gradient is significantly superadiabatic. It follows that the structure of the bulk of the convection zone is determined just by the value of s, by the composition (which, because of the very efficient mixing can be assumed to be uniform), and by the equation of state. Consequently modes of oscillation that are sensitive just to the structure of the convection zone are ideally suited to test the properties of the equation of state and to determine the solar composition (see also Christensen-Dalsgaard & Däppen 1992). It will be shown in Section 5.2.3 that solar five-minute oscillations of degree higher than about 40 have this property.

It should also be noted that much of the uncertain macrophysics is concentrated very near the surface. This is true of the dynamical effects of convection, since convective velocities are likely to be very small elsewhere, of the details of convective energy transport, and of the effects of the visible magnetic field. Apart from convective overshoot and a hypothetical strong internal magnetic field, the remaining difficulties listed are concerned with the composition profile in the radiative interior of the model. Although the list of problems is not exhaustive, this argument gives some support to the simplified view of solar structure shown in Figure 5.1.

5.1.3 The scaling with mass and radius

It is evident that the oscillation frequencies depend on the total mass and radius of the star. Indeed, it was noted in Chapter 1 that the dynamical time scale t_{dyn} can be regarded as a characteristic period of radial oscillation. It is interesting that a similar estimate can be obtained by regarding the oscillations as standing acoustic waves. Here we expect that the period is approximately given by the sound travel time across the star, *i.e.*,

$$\Pi \sim \frac{R}{\bar{c}} , \tag{5.3}$$

where $\bar{c}$ is a suitable average of the sound speed. Approximating the density by the mean density and using the equation of hydrostatic support we furthermore have the estimates

$$\rho \sim \frac{M}{R^3} , \qquad p \sim \frac{GM^2}{R^4} \tag{5.4}$$

(*e.g.* Christensen-Dalsgaard 1993a). Using these to estimate $\bar{c}$ in equation (5.3) yields

$$\Pi \sim \left(\frac{R^3}{GM}\right)^{1/2} = t_{\mathrm{dyn}} , \tag{5.5}$$

where I neglected Γ_1.

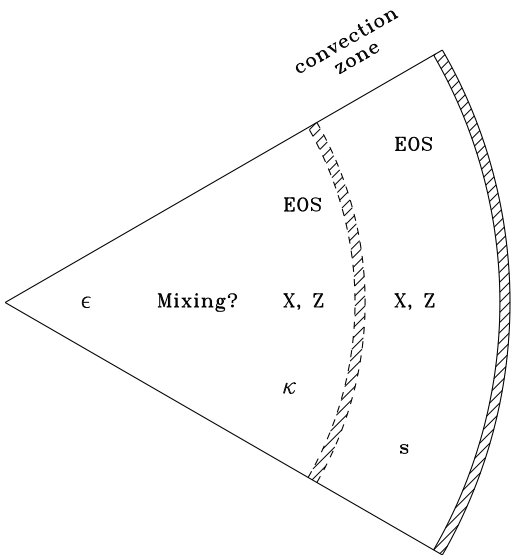

Figure 5.1: Schematic representation of solar structure. The thin hashed area near the surface indicates the region where the physics is uncertain, because of effects of convection, nonadiabaticity, *etc.* At the base of the convection zone, convective overshoot and diffusion introduce additional uncertainty. The structure of the adiabatic part of the convection zone is determined by the equation of state (EOS), and the constant values of specific entropy s, and composition (given by the abundances X and Z of hydrogen and heavy elements). Beneath the convection zone the structure also depends on opacity κ and the energy generation rate ϵ.

This scaling can be brought on a firmer footing. Motivated by the estimates in equation (5.4) I express p and ρ in terms of

$$\hat{p} = \frac{R^4}{GM^2} p \,, \qquad \hat{\rho} = \frac{R^3}{M} \rho \,. \tag{5.6}$$

Also, I measure distance to the centre in terms of $x = r/R$, and the mass inside r in terms of $q = m/M$. Then gravity, sound speed, characteristic acoustic frequency S_l and buoyancy frequency N may be written as

$$\begin{aligned} g &= \frac{GM}{R^2} \hat{g} \,, \quad c = \left(\frac{GM}{R}\right)^{1/2} \hat{c} \,, \\ S_l &= \left(\frac{GM}{R^3}\right)^{1/2} \hat{S}_l \,, \quad N = \left(\frac{GM}{R^3}\right)^{1/2} \hat{N} \,, \end{aligned} \tag{5.7}$$

where

$$\hat{g} = \frac{q}{x^2} \,, \qquad \hat{c}^2 = \frac{\Gamma_1 \hat{p}}{\hat{\rho}} \,, \qquad \hat{S}_l^2 = \frac{l(l+1)\hat{c}^2}{x^2} \,,$$

$$\hat{N}^2 \;=\; \hat{g}\left(\frac{1}{\Gamma_1\hat{p}}\frac{\mathrm{d}\hat{p}}{\mathrm{d}x} - \frac{1}{\hat{\rho}}\frac{\mathrm{d}\hat{\rho}}{\mathrm{d}x}\right) \;. \tag{5.8}$$

Finally, I introduce scaled perturbations $\hat{\xi}_r$, $\hat{p}'$ and $\hat{\Phi}'$ by

$$\xi_r = R\hat{\xi}_r \;, \qquad p' = \frac{GM^2}{R^4}\hat{p}' \;, \qquad \Phi' = \frac{GM}{R}\hat{\Phi}' \;. \tag{5.9}$$

Then the adiabatic oscillation equations (4.61), (4.62) and (4.64), written in terms of $\hat{\xi}_r$, $\hat{p}'$ and $\hat{\Phi}'$ as functions of x, can be expressed solely in terms of $\hat{p}$, $\hat{\rho}$, Γ_1, $\hat{g}$, $\hat{c}$, $\hat{S}_l$ and $\hat{N}$, if ω is replaced by the dimensionless frequency σ, defined by

$$\sigma^2 = \frac{R^3}{GM}\omega^2 \;. \tag{5.10}$$

This evidently corresponds to measuring the period in units of the dynamical time scale.

Exercise 5.1:

Verify the scalings given in equations (5.7) and (5.8) and write down the oscillation equations in the indicated (so-called dimensionless) form.

For models that constitute a so-called *homologous series* (*e.g.* Kippenhahn & Weigert 1990), the functions $q(x)$, $\hat{p}(x)$ and $\hat{\rho}(x)$ are uniquely determined. Thus the dimensionless frequencies σ or, equivalently, the pulsation constants Q defined in equation (2.20), are the same for all models in such a series: in this case the periods scale precisely as $t_{\rm dyn}$. A particular example is the case of polytropic models: for each polytropic index there is a unique set of dimensionless adiabatic oscillation frequencies σ. For more realistic stellar models the scalings are not exactly satisfied and hence σ (or Q) shows some dependence on stellar parameters; however, it is still often the case that the scaling with $t_{\rm dyn}^{-1}$ dominates the variation of the oscillation frequencies. Examples of this are shown below.

5.2 The physical nature of the modes of oscillation

The general oscillation equations appear quite complicated. In particular, analytical solutions can only be obtained in certain, very restricted cases (*cf.* Cox 1980, Section 17.7). While such results offer some insight into the behaviour of the modes, a more fruitful approach is in general to approximate the equations to a point where they can be discussed analytically. This is facilitated by the fact that the observed modes of solar oscillations in the five-minute region generally are of high radial order; the same applies to solar-like oscillations in other stars and to the comparatively long-period oscillations seen in white dwarfs. Thus asymptotic theory is often applicable to an, actually surprisingly high, degree of accuracy.

5.2.1 The Cowling approximation

The general equations are of fourth order. This is a difficulty in asymptotic studies which generally deal with second-order systems. Fortunately the perturbation to the gravitational

potential can often be neglected. To see this we may consider the integral solution in equation (3.45) to Poisson's equation. This can be written in separated form as

$$\Phi'(r) = -\frac{4\pi G}{2l+1}\left[\frac{1}{r^{l+1}}\int_0^r \rho'(r')r'^{l+2}\,\mathrm{d}r' + r^l\int_r^R \frac{\rho'(r')}{r'^{l-1}}\mathrm{d}r'\right] ; \tag{5.11}$$

this is most easily seen by verifying that this solution satisfies the separated Poisson's equation (4.36). From equation (5.11) it follows that $|\Phi'|$ is small compared with ρ' under the following two circumstances:

i) When l is large.

ii) When the radial order $|n|$ is large.

In the former case $(r'/r)^{l+2}$ (which appears in the first integral) is small when $r' < r$, and $(r/r')^{l-1}$ (which appears in the second integral) is small when $r' > r$; in addition Φ' is reduced by the factor $(2l+1)^{-1}$. In the second case Φ' contains integrals over rapidly varying functions of r and is therefore reduced relative to the size of the integrand.

Under these circumstances it appears reasonable to neglect Φ'. This approximation was first studied carefully by Cowling (1941), and is therefore known as the *Cowling approximation*. It reduces the order of the system of equations to two, with a corresponding reduction in the number of boundary conditions.

It must be pointed out that the neglect of Φ' is not quite as obvious as may seem from this discussion. In fact its mathematical justification has not been fully analyzed. As discussed in Section 5.3.1 the properties of the so-called f mode, with no radial zeros, with $l = 1$ are drastically different in the Cowling approximation and for the full equations. Nonetheless, for high-order or high-degree modes the validity of the approximation has been confirmed computationally (*e.g.* Robe 1968; Christensen-Dalsgaard 1991a).

5.2.2 Trapping of the modes

The equations in the Cowling approximation can be written as

$$\frac{\mathrm{d}\xi_r}{\mathrm{d}r} = -\left(\frac{2}{r} - \frac{1}{\Gamma_1}H_p^{-1}\right)\xi_r + \frac{1}{\rho c^2}\left(\frac{S_l^2}{\omega^2} - 1\right)p' , \tag{5.12}$$

$$\frac{\mathrm{d}p'}{\mathrm{d}r} = \rho(\omega^2 - N^2)\xi_r - \frac{1}{\Gamma_1}H_p^{-1}p' , \tag{5.13}$$

where

$$H_p^{-1} = -\frac{\mathrm{d}\ln p}{\mathrm{d}r} ; \tag{5.14}$$

hence H_p is the pressure scale height, *i.e.*, the distance, roughly, over which the pressure changes by a factor e. For oscillations of high radial order, the eigenfunctions vary much more rapidly than the equilibrium quantities; thus, *e.g.*, the left hand side of equation (5.12) is much larger than the first term on the right hand side which contains derivatives of equilibrium quantities. As a first, very rough approximation, I simply neglect these terms, reducing the equations to

$$\frac{\mathrm{d}\xi_r}{\mathrm{d}r} = \frac{1}{\rho c^2}\left(\frac{S_l^2}{\omega^2} - 1\right)p' , \tag{5.15}$$

$$\frac{\mathrm{d}p'}{\mathrm{d}r} = \rho(\omega^2 - N^2)\xi_r . \tag{5.16}$$

These two equations can be combined into a single second-order differential equation for ξ_r; neglecting again derivatives of equilibrium quantities, the result is

$$\frac{\mathrm{d}^2\xi_r}{\mathrm{d}r^2} = \frac{\omega^2}{c^2}\left(1 - \frac{N^2}{\omega^2}\right)\left(\frac{S_l^2}{\omega^2} - 1\right)\xi_r \ . \tag{5.17}$$

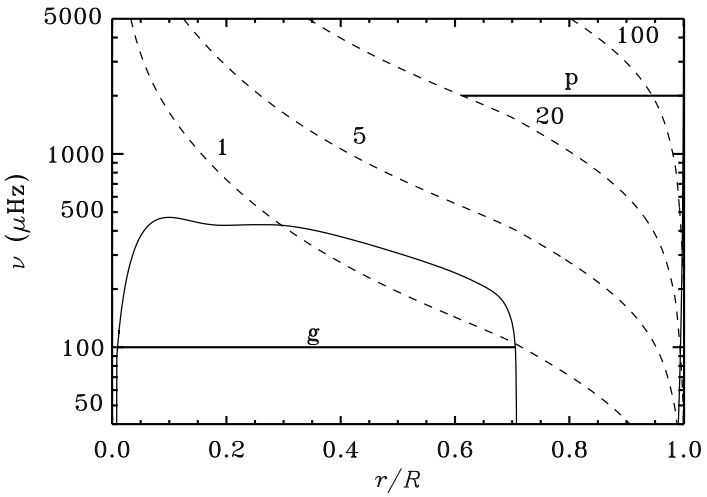

Figure 5.2: Buoyancy frequency N [*cf.* equation (4.63); continuous line] and characteristic acoustic frequency S_l [*cf.* equation (4.60); dashed lines, labelled by the values of l], shown in terms of the corresponding cyclic frequencies, against fractional radius r/R for a model of the present Sun. The heavy horizontal lines indicate the trapping regions for a g mode with frequency $\nu = 100\,\mu$Hz, and for a p mode with degree 20 and $\nu = 2000\,\mu$Hz.

This equation represents the crudest possible approximation to the equations of non-radial oscillations. In fact the assumptions going into the derivations are questionable. In particular, the pressure scale height becomes small near the stellar surface (notice that $H_p = p/(\rho g)$ is proportional to temperature), and so derivatives of pressure and density cannot be neglected. I return to this question in Chapter 7. Similarly, the term in $2/r$ neglected in equation (5.12) is large very near the centre. Nevertheless, the equation is adequate to describe the overall properties of the modes of oscillation, and in fact gives a reasonably accurate determination of their frequencies.

From equation (5.17) it is evident that the characteristic frequencies S_l and N, defined in equations (4.60) and (4.63), play a very important role in determining the behaviour of the oscillations. They are illustrated in Figure 5.2 for a "standard" solar model. S_l tends to infinity as r tends to zero and decreases monotonically towards the surface, due to the decrease in c and the increase in r. As discussed in Section 3.3, N^2 is negative in convection zones (although generally of small absolute value), and positive in convectively stable regions. All normal solar models have a convection zone in the outer about 30 per

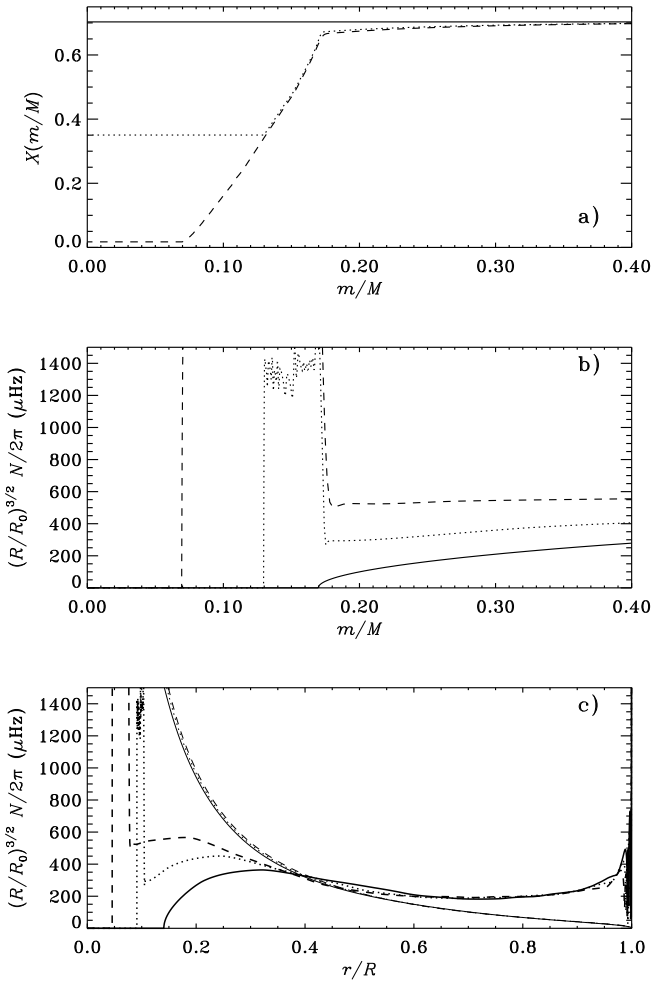

Figure 5.3: (a) Hydrogen content X against mass fraction m/M for three models in a $2.2M_\odot$ evolution sequence. The solid line is for age 0, the dotted line for age 0.47 Gyr and the dashed line for age 0.71 Gyr. Only the inner 40 per cent of the models is shown. (b) Scaled buoyancy frequency, expressed in terms of cyclic frequency, against m/M for the same three models. In the scaling factor, R and R_0 are the radii of the actual and the zero-age main sequence model, respectively. For the model of age 0.71 Gyr, the maximum value of $(R/R_0)^{3/2}N/2\pi$ is 2400 μHz. (c) Scaled buoyancy frequency N (heavy lines) and characteristic acoustic frequency S_l for $l = 2$ (thin lines), for the same three models, plotted against fractional radius r/R.

cent of the radius, whereas the entire interior is stable. The sharp maximum in N very near the centre is associated with the increase towards the centre in the helium abundance in the region where nuclear burning has taken place. Here, effectively, lighter material is

on top of heavier material, which adds to the convective stability and hence increases N. This is most easily seen by using the ideal gas law for a fully ionized gas, equation (3.19) which is approximately valid in the interior of the stars, to rewrite N^2 as

$$N^2 \simeq \frac{g^2\rho}{p}(\nabla_{\rm ad} - \nabla + \nabla_\mu) \; , \tag{5.18}$$

where, following the usual convention,

$$\nabla = \frac{{\rm d}\ln T}{{\rm d}\ln p} \; , \qquad \nabla_{\rm ad} = \left(\frac{\partial \ln T}{\partial \ln p}\right)_{\rm ad} \; , \qquad \nabla_\mu = \frac{{\rm d}\ln \mu}{{\rm d}\ln p} \; . \tag{5.19}$$

In the region of nuclear burning, μ increases with increasing depth and hence increasing pressure, and therefore the term in ∇_μ makes a positive contribution to N^2.

The behaviour of N is rather more extreme in stars with convective cores; this is illustrated in Figure 5.3 for the case of a $2.2M_\odot$ evolution sequence. The convective core is fully mixed and here, therefore, the composition is uniform, with $\nabla_\mu = 0$. However, in stars of this and higher masses the convective core generally shrinks during the evolution, leaving behind a steep gradient in the hydrogen abundance X, as shown in Figure 5.3a. This causes a sharp peak in ∇_μ and hence in N. When plotted as a function of mass fraction m/M, as in panel (b) of Figure 5.3, the location of this peak is essentially fixed although its width increases with the shrinking of the core[1]. However, as illustrated in Figure 5.3c, the location shifts towards smaller radius: this is a consequence of the increase with evolution of the central density and hence the decrease in the radial extent of a region of given mass. This also causes an increase gravity g in this region and hence in N, visible in the figure. In accordance with equation (5.7), the characteristic frequencies have been scaled by $R^{3/2}$ in Figure 5.3: it is evident that S_l, and N in the outer parts of the model, are then largely independent of evolution. Thus the stellar envelope essentially changes homologously, while this is far from the case for the core; it follows that stellar oscillations sensitive to the structure of the core might be expected to show considerable variation with evolution of the dimensionless frequency σ introduced in equation (5.10). This is confirmed by the numerical results shown in Section 5.3.2.

To analyze the behaviour of the oscillations I write equation (5.17) as

$$\frac{{\rm d}^2\xi_r}{{\rm d}r^2} = -K(r)\xi_r \; , \tag{5.20}$$

where

$$K(r) = \frac{\omega^2}{c^2}\left(\frac{N^2}{\omega^2} - 1\right)\left(\frac{S_l^2}{\omega^2} - 1\right) \; . \tag{5.21}$$

The local behaviour of ξ_r depends on the sign of K. Where K is positive, ξ_r is locally an oscillating function of r, and where $K(r)$ is negative the solution is locally an exponentially increasing or decreasing function of r. Indeed, as will be shown in more detail in Chapter 7, in the former case the solution may be written approximately as

$$\xi_r \sim \cos\left(\int K^{1/2}{\rm d}r + \phi\right) \; , \qquad K > 0 \; , \tag{5.22}$$

[1]The erratic variation in N in the chemically inhomogeneous region is caused by small fluctuations, introduced by numerical errors, in $X(m)$.

(ϕ being a phase determined by the boundary conditions) while in the latter case

$$\xi_r \sim \exp\left(\pm \int |K|^{1/2} \mathrm{d}r\right) , \qquad K < 0 . \tag{5.23}$$

Thus according to this description the solution oscillates when

$$\text{o1)} \qquad |\omega| > |N| \qquad \text{and} \qquad |\omega| > S_l , \tag{5.24}$$

or

$$\text{o2)} \qquad |\omega| < |N| \qquad \text{and} \qquad |\omega| < S_l , \tag{5.25}$$

and it is exponential when

$$\text{e1)} \qquad |N| < |\omega| < S_l , \tag{5.26}$$

or

$$\text{e2)} \qquad S_l < |\omega| < |N| . \tag{5.27}$$

These possibilities are discussed graphically in Unno *et al.* (1989), Section 16.

For a given mode of oscillation there may be several regions where the solution oscillates, according to criterion o1) or o2), with intervening regions where it is exponential. However, in general one of these oscillating regions is dominant, with the solution decaying exponentially away from it. The solution is then said to be *trapped* in this region; its frequency is predominantly determined by the structure of the model in the region of trapping. The boundaries of the trapping region are generally at points where $K(r) = 0$; such points are known as *turning points*. From equation (5.22) it follows that within the trapping region the mode oscillates the more rapidly as a function of r, the higher the value of K. Thus, if the order of the mode is roughly characterized by the number of zeros in ${\xi_r}^2$ the order generally increases with increasing K.

From the behaviour of S_l and N shown in Figure 5.2, and the conditions for an oscillating solution, we may expect two classes of modes:

i) Modes with high frequencies satisfying o1), labelled p modes.

ii) Modes with low frequencies satisfying o2), labelled g modes.

These are discussed separately below.

Typical trapping regions, for a p and a g mode in a model of the present Sun, are shown in Figure 5.2. I note also that in evolved stars with convective cores the large values of N at the edge of the core may lead to the condition o2) being satisfied even at quite high frequency. Thus here one might expect that the distinction in frequency between p and g modes becomes less clear. Some consequences of that are illustrated in Section 5.3.2.

5.2.3 p modes

These are trapped between an inner turning point $r = r_\mathrm{t}$ and the surface; the trapping at the surface is in fact not contained in the analysis presented so far, but will be discussed in Section 5.4 and in Chapter 7. The inner turning point is located where $S_l(r_\mathrm{t}) = \omega$, or

$$\frac{c^2(r_\mathrm{t})}{r_\mathrm{t}^2} = \frac{\omega^2}{l(l+1)} . \tag{5.28}$$

[2]The concept of order is defined more precisely in Section 5.3.1.

This condition determines r_t as a function of l and ω.

For p modes, in particular the observed solar modes in the five-minute region, we typically have that $\omega \gg N$. Then K can be approximated by

$$K(r) \simeq \frac{1}{c^2}(\omega^2 - S_l^2) \; . \tag{5.29}$$

In this approximation, therefore, the dynamics of the p modes is solely determined by the variation of the sound speed with r. These modes are standing acoustic waves, with the restoring force being dominated by pressure, and this motivates denoting them p modes. Indeed, equation (5.29) determining the radial behaviour of the modes can be obtained very simply from the dispersion relation (3.55) for a plane sound wave. I write the squared length $|\mathbf{k}|^2$ of the wave vector as the sum of a radial and a horizontal component, *i.e.*,

$$|\mathbf{k}|^2 = k_r^2 + k_h^2 \; . \tag{5.30}$$

Here k_h is determined from l by equation (4.51); thus equation (3.55) becomes

$$\frac{\omega^2}{c^2} = k_r^2 + \frac{l(l+1)}{r^2} \; , \tag{5.31}$$

or

$$k_r^2 = \frac{1}{c^2}(\omega^2 - S_l^2) \; . \tag{5.32}$$

Here, by equation (5.20), k_r^2 must be identified with K, and equation (5.32) is therefore identical to equation (5.29).

The sequence of approximations used to derive equation (5.29) corresponds closely to the approximations made in the analysis of simple sound waves. Thus it is not surprising that the same dispersion relation is recovered. Nevertheless, it is gratifying to see that the full oscillation equations reduce to the correct behaviour in this limit.

The interior reflection of the p modes can be understood very simply in terms of ray theory. A mode can be regarded as a superposition of propagating sound waves. Two such waves are illustrated in Figure 5.4 (additional examples are shown on the cover). As they propagate into the star, the deeper parts of the wave fronts experience a higher sound speed and therefore travel faster. Consequently, the direction of propagation is bent away from the radial direction. This is completely analogous to the refraction experienced by light rays when traveling into a medium with a higher speed of light; mathematically it is expressed by the decrease in the radial component of the wave vector with increasing sound speed shown in equation (5.32). At the reflection point the wave travels horizontally; the condition (5.28) then follows directly from the dispersion relation for sound waves. A complete analysis of p modes in terms of ray theory has been given by Gough (1984, 1986a).

The dependence of the turning point position r_t on mode degree and frequency is of great importance for the interpretation of the observations of the solar 5-minute oscillations. It is illustrated in Figure 5.5, for a normal model of the present Sun. Curves are shown for three different frequencies, spanning the range of the observations. For small l, r_t is very close to the centre, whereas for higher degrees the turning point moves closer to the surface. In particular, I note that for $l \gtrsim 40$ the modes are essentially trapped in the convection zone, which has a depth of about $0.28R$. As discussed in Section 5.1.2, such modes are very well suited for investigations of the properties of the equation of state of stellar matter.

From equation (5.29) it follows that K increases with the frequency. This increases the number of zeros in the eigenfunction, *i.e.*, the mode order. This means, equivalently, that the frequency increases with mode order.

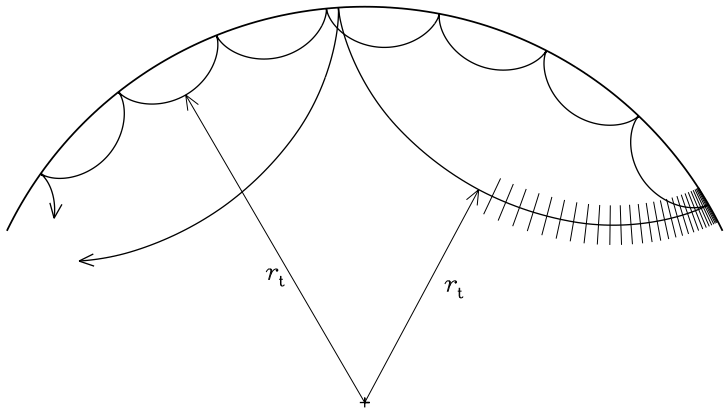

Figure 5.4: Propagation of acoustic waves, corresponding to modes with $l = 30$, $\nu = 3\,\mathrm{mHz}$ (deeply penetrating rays) and $l = 100$, $\nu = 3\,\mathrm{mHz}$ (shallowly penetrating rays). The lines orthogonal to the former path of propagation illustrate the wave fronts.

5.2.4 g modes

Here the turning point positions are determined by the condition $N = \omega$. As seen in Figure 5.2, at low frequencies (where claims have in the past been made for the detection of modes in the Sun; *cf.* Section 2.3) this gives rise to one turning point very near the centre of the Sun, and a second just below the base of the convection zone. At higher frequencies the upper turning point is deeper in the model, and for frequencies close to the maximum in N, the modes are trapped in the deep interior. However, to this approximation the position of the turning points is independent of l.

For high-order g modes typically $\omega^2 \ll S_l^2$, and we may approximate K by

$$K(r) \simeq \frac{1}{\omega^2}(N^2 - \omega^2)\frac{l(l+1)}{r^2} \; ; \tag{5.33}$$

thus in this case the dynamics is dominated by the variation of the buoyancy frequency N with r. Gravity, acting on the density perturbation, provides the dominant restoring force, and this is the reason that the modes are called g modes. The modes are trapped gravity waves. In fact, by arguments similar to those used above for the p modes, one obtains from the dispersion relation (3.74) for gravity waves that the radial component of the wave number is given by

$$k_r^2 = \frac{l(l+1)}{r^2}\left(\frac{N^2}{\omega^2} - 1\right) \; ; \tag{5.34}$$

this is in accordance with the relation for K given in equation (5.33).

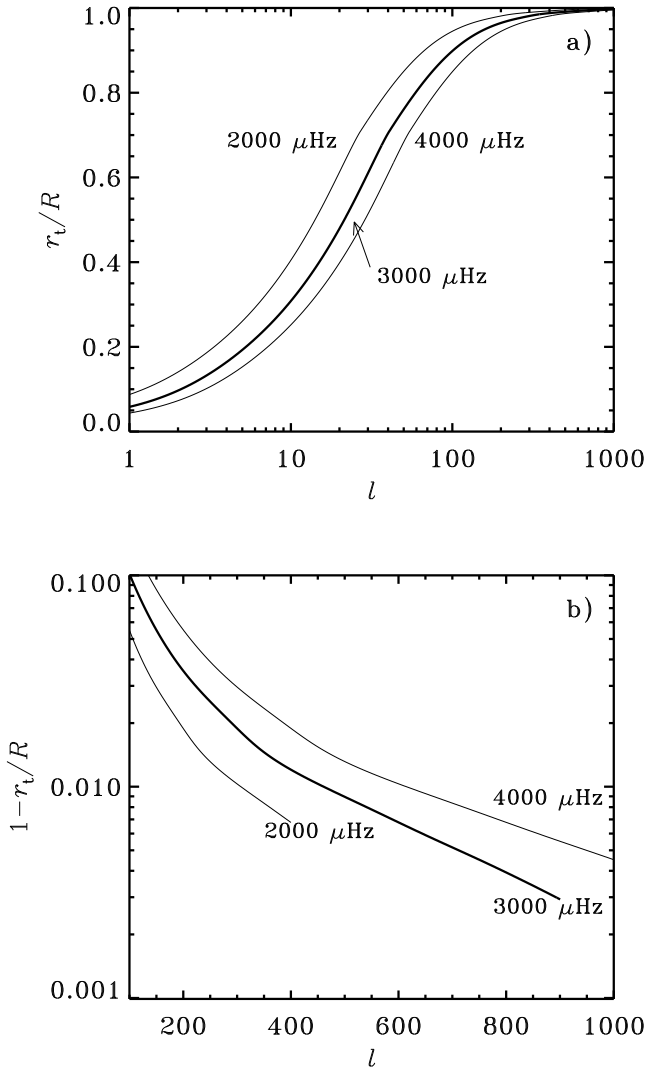

Figure 5.5: The location r_t (a) of the inner turning point, and the depth of penetration $R-r_t$ (b), in units of the solar radius R, for p modes in a standard solar model. The results are shown as functions of degree l, for three typical frequencies.

From equation (5.33) it follows that K increases with decreasing ω. Thus the order of the mode increases with decreasing ω, or, equivalently, ω decreases with increasing order. It may also be noticed that the frequencies of g modes cannot exceed the maximum $N_{\max}$ in the buoyancy frequency in the stellar interior. As shown below (*cf.* Fig. 5.6) one does indeed find an upper limit on numerically computed g-mode frequencies. The approach to this limit as l gets large was analyzed by Christensen-Dalsgaard (1980).

5.3 Some numerical results

To get a feeling for the basic properties of the oscillations, it is useful to consider results of calculations of eigenfrequencies and eigenfunctions. The results presented in this section are largely based on models computed with the code described by Christensen-Dalsgaard (1982). This is similar to other calculations making the traditional assumptions of stellar evolution theory (leading to what is often somewhat misleadingly termed "standard models" in the solar case): the physics of the model (equation of state, energy reactions and opacity) are treated in reasonable, although not full, detail, convection is handled with mixing length theory, and it is assumed that convectively stable regions of the model are not mixed during the evolution. Needless to say the predicted flux of neutrinos for the solar model is substantially higher than the observed value.

5.3.1 Results for the present Sun

For the model of the present Sun, the hydrogen abundance and mixing length were adjusted to obtain a model with the observed solar luminosity and radius at solar age. Figures 5.6 and 5.7 show computed eigenfrequencies for this model, as functions of the degree l. It is convenient to regard l as a continuously varying, real parameter; this is mathematically completely permissible in the separated oscillation equations, although clearly only integral l have physical meaning. Consequently, the curves are shown as continuous, which helps in identifying the modes. The curves are labelled by the radial order which is essentially given by the number of zeros in the radial direction in the eigenfunctions.

It is evident that there are two distinct, but slightly overlapping, groups of modes, with very different behaviour of the frequency as a function of l. The upper set of modes corresponds to the *p modes* discussed in Section 5.2.3, whose dominant restoring force is pressure. The radial order has been indicated on some of the curves; it is evident that the frequencies of these modes increase with order, as mentioned in Section 5.2.3. The modes labelled with order 0, although similar in behaviour to the p modes, are in fact physically distinct; for l greater than about 20 their frequencies are approximately given by the expression (3.84) for a surface gravity wave. They are known as *f modes*. Finally, the lower group of modes corresponds to the *g modes*, discussed in Section 5.2.4, where the dominant restoring force is buoyancy. For these modes the frequencies decrease with increasing number of nodes (*cf.* Section 5.2.4). It is evident that buoyancy demands variation over horizontal surfaces; thus there are no g modes for spherically symmetrical oscillations, *i.e.*, for $l = 0$. Only the g modes of order less than 50 have been shown; in fact, the g-mode spectrum extends to zero frequency at all degrees, although the modes obviously become increasingly crowded with increasing degree. On the other hand the gap between the g and the f modes is real.

It might be noticed that there are apparent crossings of the frequencies, as functions of l, between the f mode and some of the g modes. A closer examination shows that instead the modes make so-called *avoided crossings* where they approach very closely without actually crossing. This phenomenon is well-known from atomic physics; a very clear discussion of the behaviour in the vicinity of an avoided crossing was given by von Neuman & Wigner (1929). Indeed, there is a deep mathematical similarity between the equations of nonradial oscillations and the Schrödinger equation (see Christensen-Dalsgaard 1980, 1981; also, Section 5.5 below).

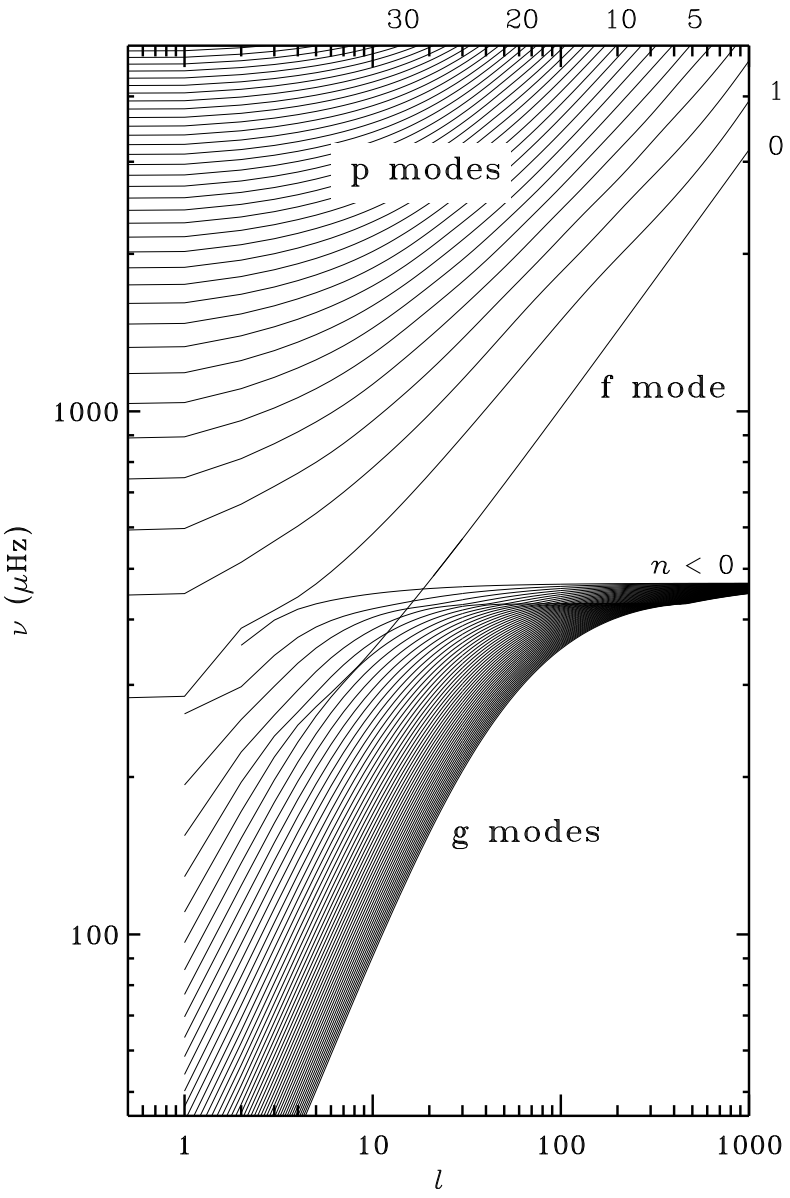

Figure 5.6: Cyclic frequencies $\nu = \omega/2\pi$, as functions of degree l, computed for a normal solar model. Selected values of the radial order n have been indicated.

The precise classification of the modes, *i.e.*, the assignment of radial orders to them, presents some interesting and so far unsolved problems. It appears that at each l it is possible to assign to each mode an integral order n, which ranges from minus to plus infinity, such that, at least for reasonably simple stellar models[3] $|n|$ gives the number of

[3]The definition of a 'simple' model in this context is not straightforward; examples might be zero-age main sequence models or, *e.g.*, polytropes of index between 1.5 and 3.

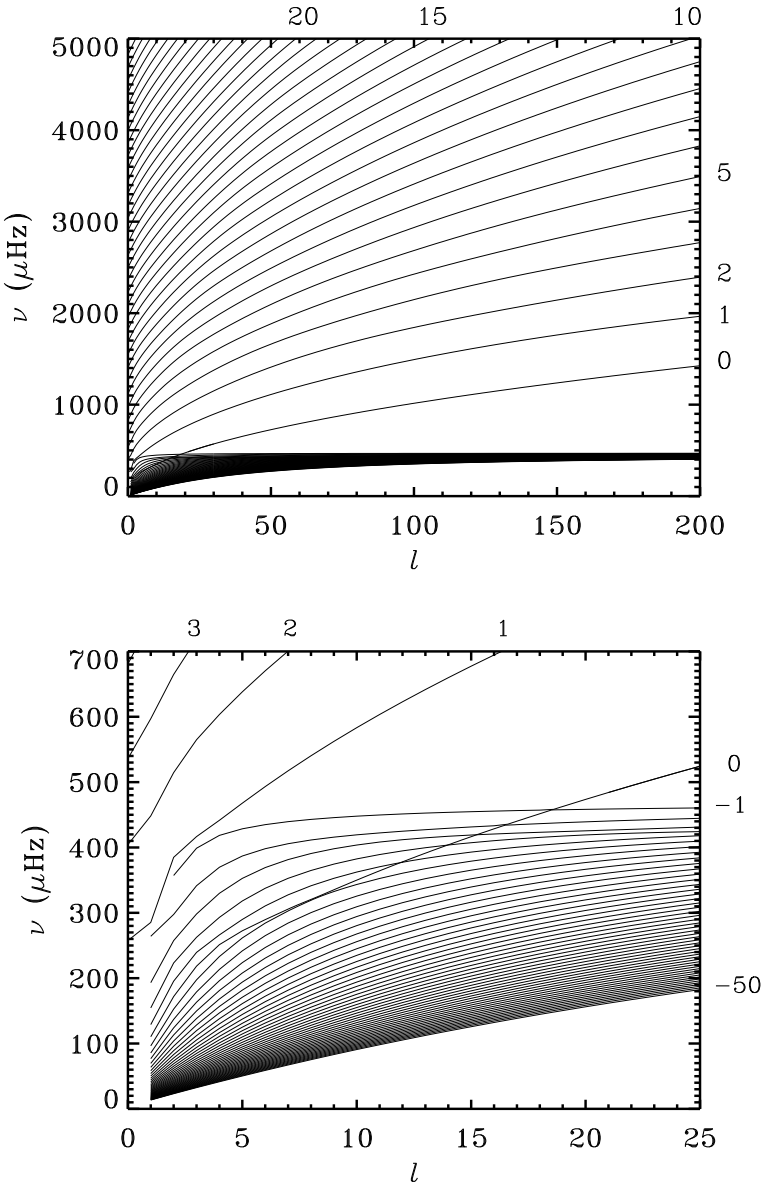

Figure 5.7: Cyclic frequencies $\nu = \omega/2\pi$, as functions of degree l, computed for a normal solar model. Selected values of the radial order n have been indicated.

zeros in ξ_r; the possible zero at $r = 0$ is only counted in the radial case, where $l = 0$. As hinted above, this is arranged such that in simple models $n > 0$ for p modes, $n = 0$ for the f mode and $n < 0$ for g modes. Also, with the single exception of the dipolar f mode discussed below, the frequency is an increasing function of n; this rule is evidently consistent with the fact, mentioned above, that the frequency increases with the number

of radial nodes for p modes and decreases with the number of radial nodes for g modes. It is conventional to denote p, f and g modes of a given degree l_0 as $\mathrm{p}_n(l = l_0)$, $f(l = l_0)$ and $\mathrm{g}_{|n|}(l = l_0)$.

Eckart (1960) proposed a general, and mathematically precise, scheme for the classification of waves in a stratified medium. It was applied by Scuflaire (1974) and Osaki (1975) to the definition of the radial order n for a nonradially pulsating star, on the basis of the behaviour with varying r of the point $(\xi_r(r), p'(r))$ in the so-called phase diagram. Specifically, the order is determined by counting the zeros of ξ_r, assigning a positive value for zeros where the p' axis is crossed in the counter-clockwise direction in the phase diagram, and negative values when the crossing is in the clockwise direction; the former case applies where the mode behaves as a p mode and the latter to g-mode behaviour. It may be shown (Gabriel & Scuflaire 1979; Christensen-Dalsgaard 1980) that in the Cowling approximation this definition has the desirable property of being invariant under a continuous modification of the equilibrium model or a continuous change of l. Also, for simple models or in the limit of high-order modes this definition reduces to the simple counting of radial nodes in the eigenfunction, described above. The Eckart scheme is not generally applicable, however, when solutions of the full equations are considered. One finds, for example, that in models of the present Sun application of this classification procedure to the lowest-order p modes with $l = 1$, computed from the full equations, results in a misidentification of the modes with $n = 1$ and 2; for more evolved models the problem extends to modes of higher order. Guenther (1991) considered an evolution sequence of $1M_\odot$ models extending to the base of the giant branch. In the final model he found it difficult to determine the order of a number of $l = 1$ modes; from his plots of the eigenfunctions it is evident that the origin of the problem is the presence in the solution of a significant slowly varying trend which shifts the radial displacement sufficiently to eliminate several nodes. Problems were also encountered by Lee (1985) for $l = 1$ modes in evolved models of δ Scuti stars, and by Christensen-Dalsgaard & Mullan (1994) for polytropic models of index exceeding 3.3. It is interesting that these difficulties appear to be restricted to $l = 1$, at least for realistic stellar models.

The problem of mode classification may appear somewhat academic, of little interest in analysis of observed frequencies. In fact, it is a severe nuisance when computing modes for a given model, making it very difficult to ensure that all modes have been computed, or to relate the modes to those of another, slightly different model. Thus there is still a need for a reliable classification scheme, valid for a wide range of models. More details on these problems were given by Christensen-Dalsgaard (1991a).

There are a few special cases. For $l = 0$ only modes with $n > 0$ are found; this is in accordance with the fact, mentioned above, that buoyancy can only act in the presence of horizontal variation. Also, for $l = 1$ the mode with $n = 0$ is peculiar in that its frequency is zero; indeed a mode with $l = 1$ and no zero in the radial direction may seem somewhat unphysical, as it displaces the centre of mass of the star. However, the mode corresponds to an infinitely slow, uniform motion of the entire star, without deformation; this must be a solution to the original equations which, if written as an oscillation, has zero frequency (see also Christensen-Dalsgaard 1976).

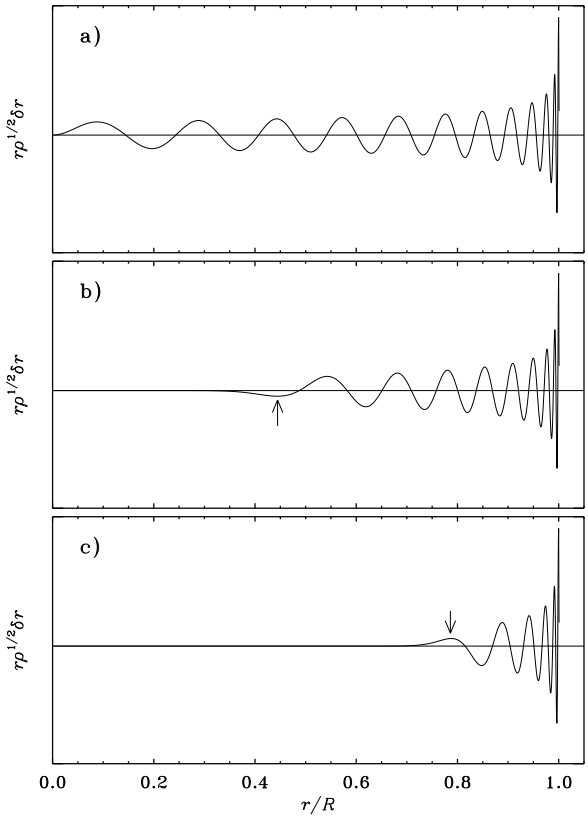

Figure 5.8: Scaled radial displacement eigenfunctions for selected p modes in a normal solar model, with a) $l = 0$, $n = 23$, $\nu = 3310\,\mu$Hz; b) $l = 20$, $n = 17$, $\nu = 3375\,\mu$Hz; c) $l = 60$, $n = 10$, $\nu = 3234\,\mu$Hz. The arrows mark the asymptotic location of the turning points r_t [*cf.* equation (5.28)].

Exercise 5.2:

Verify this statement.

It is interesting that this f mode with $l = 1$ behaves very differently in the Cowling approximation and for the full set of equations. In the Cowling approximation there is a mode with $l = 1$ having no nodes in the radial displacement, intermediate in frequency between the p and the g modes, which must be identified with the f mode. From a physical point of view it can be thought of roughly as an oscillation of the whole star in the gravitational potential defined by the equilibrium model. The connection between this mode and the zero-frequency mode for the full problem can be investigated by making a continuous transition from the Cowling approximation to the full set of equations; this can be accomplished formally by introducing a factor λ on the right-hand side of equation (4.21),

such that $\lambda = 0$ corresponds to the Cowling approximation and $\lambda = 1$ to the full equations (Christensen-Dalsgaard 1978; Christensen-Dalsgaard & Gough 2001). When λ is increased from 0 to 1, the transition from the $l = 1$ f mode in the Cowling approximation to the zero-frequency "mode" in the full case takes place through a sequence of avoided crossings with the g modes, where the frequencies approach very closely without actually crossing. A similar transition occurs for solutions of the full equations, between the f mode with $l = 2$ and the zero-frequency mode with $l = 1$, as l is decreased continuously from 2 to 1 (Aizenman, Smeyers & Weigert 1977; Christensen-Dalsgaard 1978; Christensen-Dalsgaard & Gough 2001).

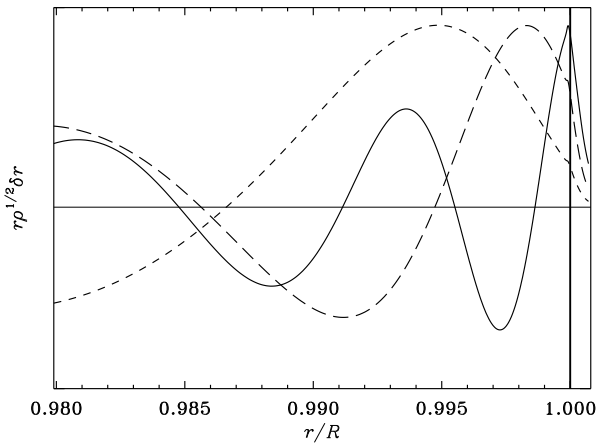

Figure 5.9: Scaled radial displacement eigenfunctions of p modes with $l = 1$, plotted against fractional radius r/R in the outermost parts of a normal solar model. The cases shown are: $\nu = 1612\,\mu$Hz (----------); $\nu = 2293\,\mu$Hz (– – – – – – –); $\nu = 3650\,\mu$Hz (——————).

Figures 5.8 and 5.9 illustrate typical eigenfunctions for p modes. According to equation (4.47) the quantity plotted, *viz.* $r\,\rho^{1/2}\xi_r$, is related to the contribution to the energy density from the radial component of velocity. For the p modes this shows that the energy, at least at low degrees, is distributed throughout most of the star. In particular, the radial modes penetrate essentially to the centre. At higher degree the modes are trapped in the outer part of the model. This is in accordance with the predictions of Section 5.2.3; indeed, the arrows for the modes with $l = 20$ and 60 show the locations of the turning points predicted by equation (5.28). Intuitively, one might expect the sensitivity of the frequency of a mode to the structure of the star to be given roughly by the energy density; thus the frequencies of low-degree p modes should give averages of stellar structure over the entire star. In contrast to the energy, the displacement is strongly peaked towards the surface; this is obvious from Figure 5.8 if it is recalled that the density decreases by about 9 orders of magnitude from the centre to the surface of the Sun. With increasing degree the p modes become confined closer and closer to the surface; however, the behaviour near the surface, at a given frequency, changes little with l.

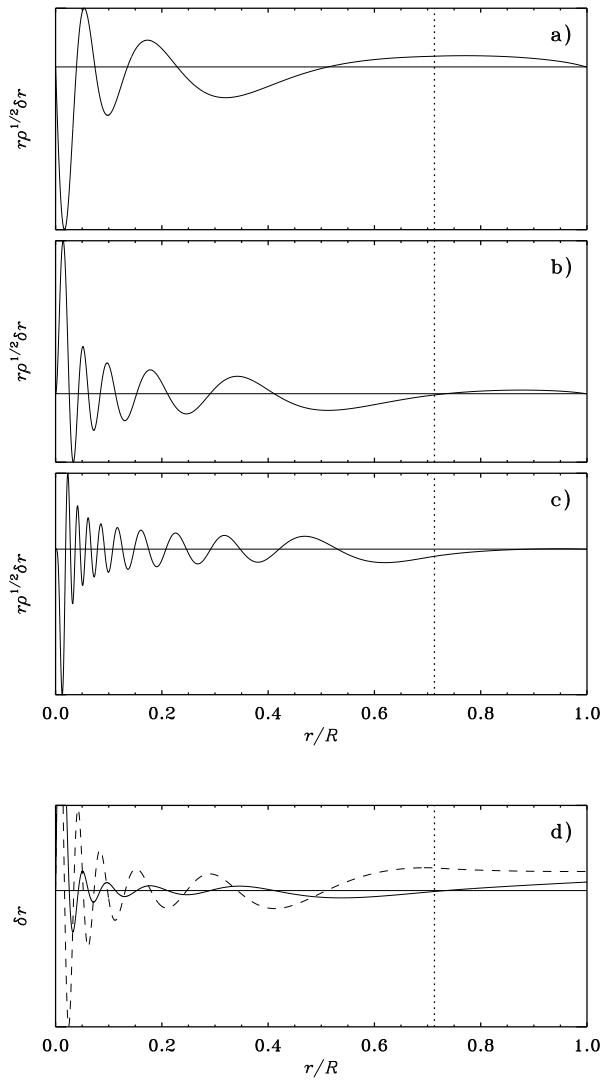

Figure 5.10: Eigenfunctions for selected g modes in a normal solar model. Panels a) to c) show scaled radial displacement eigenfunctions with a) $l = 1$, $n = -5$, $\nu = 110\,\mu$Hz; b) $l = 2$, $n = -10$, $\nu = 103\,\mu$Hz; c) $l = 4$, $n = -19$, $\nu = 100\,\mu$Hz. In panel d) the solid and dashed curves show unscaled radial (ξ_r) and horizontal displacement ($L\xi_{\rm h}$) eigenfunctions, for the $l = 2$, $n = -10$ mode. For clarity, the curve for ξ_r has been truncated: the maximum value is about 2.7 times higher than the largest value shown. The vertical dotted line marks the base of the convective envelope.

Figure 5.9 shows the eigenfunctions in the outer few per cent of the radius of a solar model, for modes of degree $l = 1$ with different frequencies. It is evident that the mode energy decreases in the atmosphere; this can be understood from the discussion in Sec-

tion 5.4, which shows that for an isothermal atmosphere the energy decreases exponentially with height for frequencies below the so-called *acoustical cut-off frequency* which in the solar case corresponds to a cyclic frequency of about 5000 μHz. However, it should be noticed that at frequencies below about 2000 μHz even the photospheric amplitude is substantially smaller than the amplitudes at greater depth. This is related to the reflection of the modes near the surface which is not contained in the simplified discussion in Section 5.2.3; an asymptotic description that includes the surface reflection will be given in Section 7.5.

Figure 5.10 shows eigenfunctions for g modes. These have their largest amplitudes the deep interior of the Sun, with maximum energy very near the centre. At a given frequency the number of radial zeros increases rapidly with l; on the other hand there is little change in the overall distribution of the energy. That the modes extend over essentially the same region of the star is consistent with the fact, mentioned in Section 5.2.4, that for these modes the locations of the turning points depend on frequency but not on degree. It should be noticed in panel (d) that the surface displacement amplitudes for low degree (in this case $l = 2$) remain comparable with the amplitude in much of the interior. Thus, even though the modes are formally evanescent in the convection zone, they retain a potentially observable surface response, providing of course that they are excited in a given star.

We may also consider global properties of the eigenfunctions. Of considerable interest is the inertia parameter E defined in equation (4.48). It is shown for p modes and low-degree g modes in Figure 5.11, as a function of the cyclic frequency $\nu = \omega/2\pi$. Each curve corresponds to a given value of l, with the points for the individual modes being connected by continuous lines. This format for displaying results on the oscillations clearly makes little physical sense, in that non-integer mode orders do not have any meaning; nevertheless it provides a convenient illustration of the dependence of oscillation quantities on frequency and degree. The p-mode results in panel (a) show an obvious marked decrease of the inertia, at fixed surface amplitude, with increasing frequency, as well as a weaker but still substantial decrease with increasing degree. The dependence on degree is a direct result of the variation of the depth of penetration: with increasing degree the lower turning point moves closer to the surface and hence the oscillation involves a smaller part of the star, thus decreasing the inertia. Similarly, the increase with decreasing frequency can be understood from the reflection properties near the surface and is consistent with the eigenfunctions shown in Figure 5.9: since the inertia measure in equation (4.48) is normalized with the surface displacement, the decrease in the value of the eigenfunction at the surface, relative to the interior, leads to an increase in E at low frequency.

The results for low-degree modes, in panel (b) show that at the lowest degrees there is essentially a continuous transition between the p and the g modes, the inertia continuing to rise rapidly with decreasing frequency. At slightly higher degree ($l = 3 - 5$) there is a beginning tendency towards stronger g-mode trapping as the frequency approaches the maximum in N in the deep interior of the model. This trend is strongly accentuated at higher degree, as shown in Figure 5.12. Here the variation is extremely strong, with very large values being reached for high frequencies or high degrees. For such modes a surface amplitude large enough to be observed would correspond to totally unrealistic amplitudes in the interior. This is emphasized also by Figure 5.13 which shows the ratio between the maximum interior, and the surface, radial displacement. The reason for this is the trapping of the modes at high degrees and frequencies near the maximum in the buoyancy frequency N. It is particularly pronounced for modes whose frequencies exceed the secondary maximum in N at 400 μHz. The very low values of E found at selected frequencies for higher

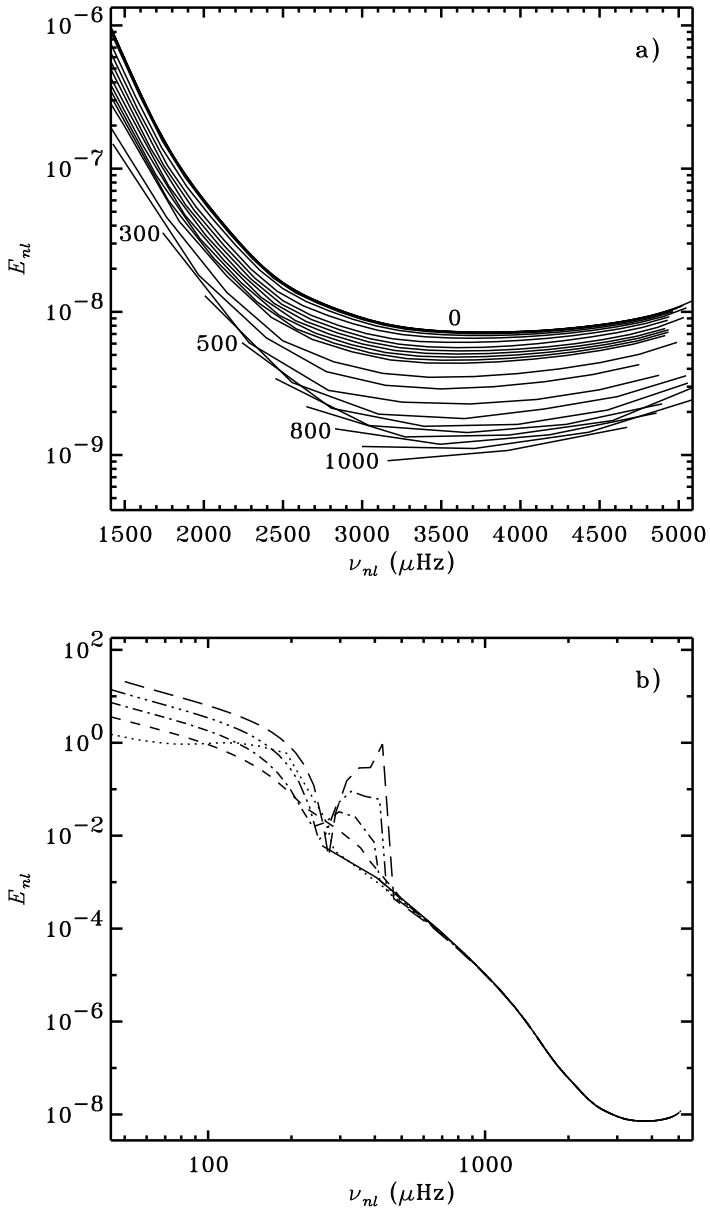

Figure 5.11: The dimensionless inertia E [*cf.* equation (4.48)] for computed modes of oscillation in a normal solar model, plotted against frequency ν for fixed values of the degree l. The inertia has been normalized by the norm of the total displacement at the photospheric level. (a) results for p modes; selected values of l have been indicated. (b) results for low-degree g and p modes, using the following line styles: $l = 0$ (solid), $l = 1$ (dotted), $l = 2$ (short-dashed), $l = 3$ (dot-dashed), $l = 4$ (triple-dot-dashed), and $l = 5$ (long-dashed).

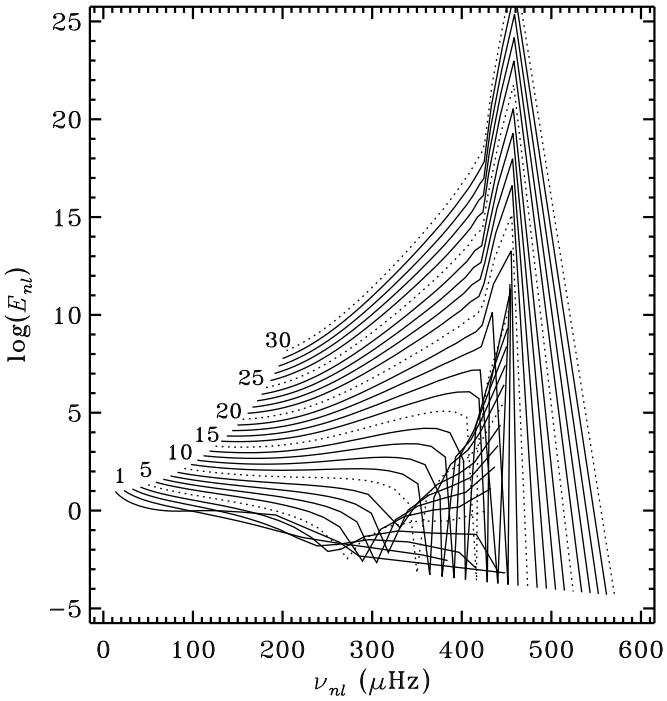

Figure 5.12: The dimensionless inertia E [*cf.* equation (4.48)] for computed f and g modes of oscillation in a normal solar model, plotted against frequency ν for fixed values of the degree l. For clarity, modes of degree 5, 10, 15, 20, 25 and 30 have been shown with dotted lines; in addition, selected values of l are indicated in the figure.

values of l occur where the g modes pass through avoided crossings and take on the character of surface gravity waves; this happens when their frequencies are near the extensions of the f-mode frequencies shown in Figure 5.6. It is interesting that this phenomenon can be traced in inertia to a degree as low as 3. However, in general it is evident that the possibilities for observing g modes, regardless of the excitation mechanisms, must be limited to fairly low values of the degree.

From the preceding discussion, there is obviously a high degree of regularity in the computational results. Also, it is clear that at least some of these properties can be understood in simple terms by considering the asymptotic behaviour of the oscillations; this understanding is of great assistance in the interpretation of the observed modes. This is emphasized by more detailed study of the asymptotic behaviour of the oscillations, which forms an important part of the remainder of these notes.

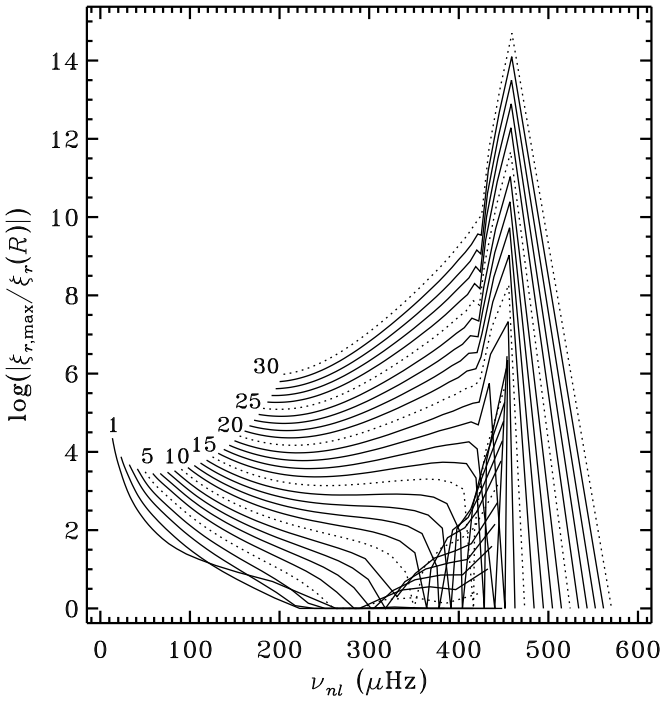

Figure 5.13: The ratio $|\xi_{r,\max}/\xi_r(R)|$ between the maximum and the surface value of the radial component of the displacement for computed f and g modes of oscillation in a normal solar model, plotted against frequency ν for fixed values of the degree l. For clarity, modes of degree 5, 10, 15, 20, 25 and 30 have been shown with dotted lines; in addition, selected values of l are indicated in the figure.

5.3.2 Results for the models with convective cores

To illustrate the effect of a convective core, particularly the maximum in the buoyancy frequency at the edge of the core, Figure 5.14 shows the behaviour of the oscillation frequencies, as functions of stellar age, for a $2.2M_\odot$ evolution sequence. These models may represent δ Scuti stars; characteristic frequencies at a few ages in the sequence were illustrated in Figure 5.3. As in that figure I have applied the scaling according to $t_{\rm dyn}^{-1}$. As a result, the frequencies of largely acoustic modes, including the radial modes, change very little with age. It should be noticed also that except at low order, the acoustic modes exhibit a distinct pattern, with a close pairing of the radial and $l = 2$ modes. Such a pattern of closely-spaced peaks is familiar in solar data (*cf.* Fig. 2.14) and may also have been observed in other cases (*e.g.* Michel *et al.* 1992; see also Fig. 2.23). It will be discussed in more detail, in the light of the asymptotic behaviour of the frequencies, in Section 7.3.

The most striking feature of the computed frequencies, however, is the interaction for $l = 1$ and 2 between the p modes and the g modes. At zero age, there is a clear distinction

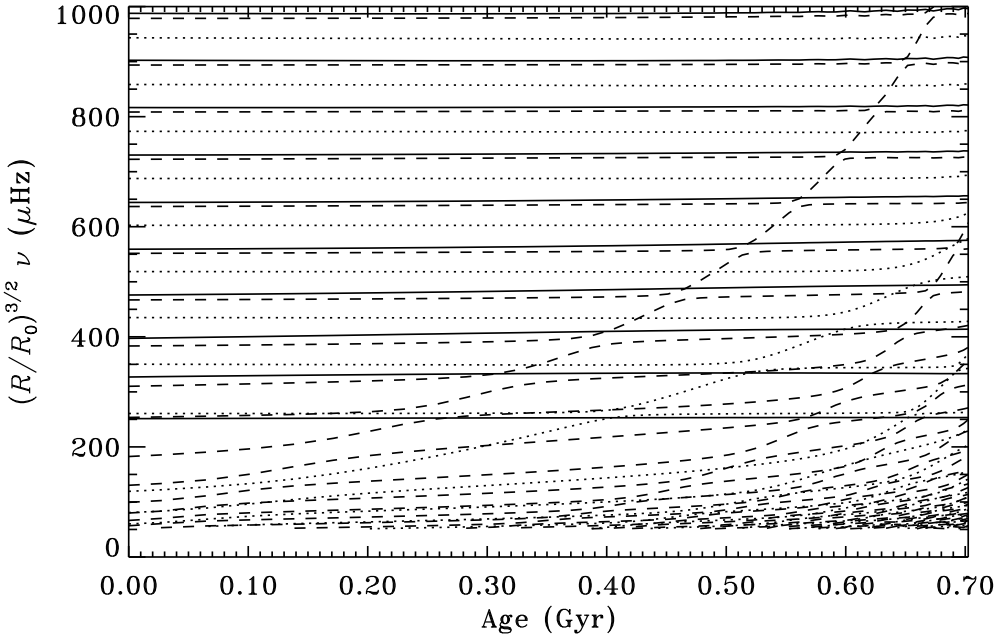

Figure 5.14: Scaled oscillation frequencies, as functions of age, in a $2.2M_\odot$ evolution sequence. Modes of the same radial order have been connected. The solid lines are for radial modes, of degree $l = 0$, the dotted lines are for $l = 1$ and the dashed lines for $l = 2$.

between the p modes, with frequencies exceeding that of the lowest radial mode, and the g modes with frequencies below $200\,\mu$Hz. However, with increasing age the scaled g-mode frequencies increase; this is a consequence of the increase in the scaled buoyancy frequency with age (*cf.* Figure 5.3c) which effectively acts to "pull up" the frequencies of the g modes. As was first found by Osaki (1975), this leads to an interaction between the p and g modes which takes place through a sequence of avoided crossings, similar to those encountered in Figure 5.6. At the avoided crossing the two modes exchange nature, while still maintaining the original labelling. Thus, for example, the $n = 1$ mode for $l = 2$, which at age zero is a purely acoustic mode of frequency $310\,\mu$Hz takes on the nature of a g mode trapped just outside the convective core at the age 0.32 Gyr and again at the age 0.4 Gyr changes back to being predominantly an acoustic mode.

This behaviour is further emphasized by considering the eigenfunctions of these modes; examples of eigenfunctions near the $p_1 - p_2 (l = 2)$ avoided crossing at age 0.4 Gyr are shown in Figure 5.15. Before the avoided crossing, the p_1 mode has a substantial amplitude near the edge of the convective core, and hence to a large extent behaves like a g mode, whereas the p_2 mode is predominantly a p mode, with largest amplitude in the outer parts. At the point of closest approach of the frequencies, at an age of 0.39 Gyr, both modes have a mixed character, with substantial amplitudes in the deep interior and near the

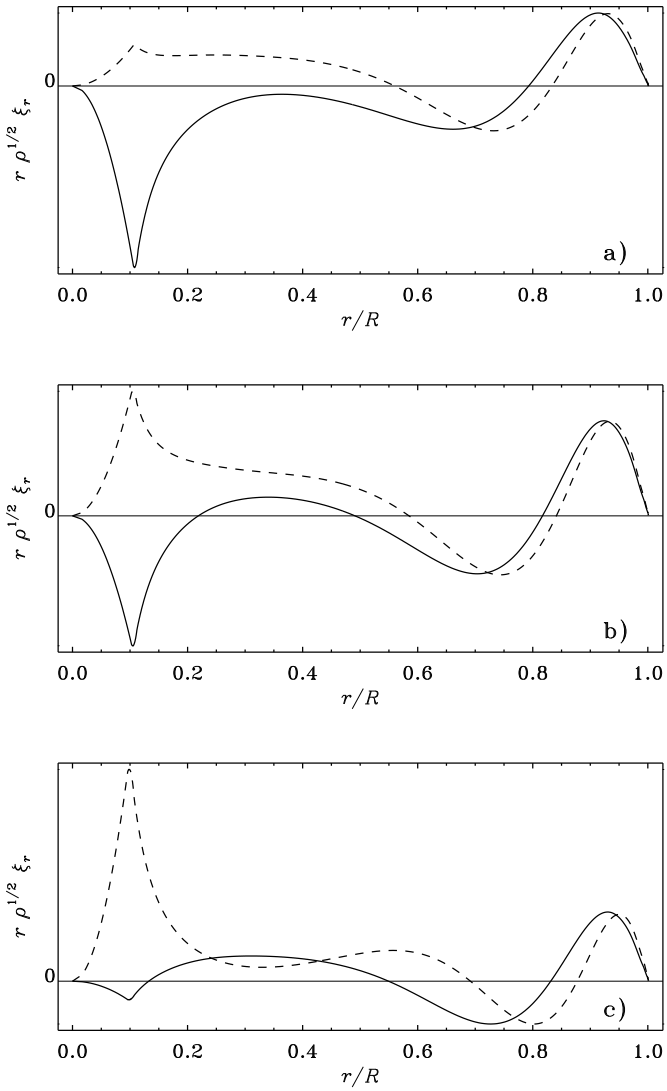

Figure 5.15: Scaled eigenfunctions for the $p_1(l = 2)$ mode (continuous line) and the $p_2(l = 2)$ mode (dashed line) in the vicinity of the avoided crossing near age 0.4 Gyr, $(R/R_0)^{3/2}\nu = 400\,\mu$Hz in Figure 5.14. (a) Age 0.36 Gyr. (b) Age 0.39 Gyr. (c) Age 0.44 Gyr.

surface, whereas after the avoided crossing the p_2 mode looks like a g mode, whereas the p_1 mode largely behaves like a p mode. It should be noted that this behaviour introduces a potential difference between the mathematical classification of the modes and their physical nature: modes with order $n > 0$, which in simple models would be p modes, may take on the character of g modes. Also, it is evident that the presence of the g-like modes in the p-mode spectrum, particularly at late evolutionary stages, complicates the analysis of

observed frequencies. Dziembowski & Królikowska (1990) pointed out that mode selection might be affected by the larger energy of the modes that behave like g modes, thereby restricting the choice of modes in the identification. However, such arguments depend on the mechanisms responsible for exciting the modes and limiting their amplitudes, which are so far incompletely understood. It should also be noted that *if* g-mode like pulsations could in fact be identified, their frequencies would give strong constraints on conditions in the region just outside the stellar core. In fact, Dziembowski & Pamyatnykh (1991) pointed out that measurement of g-mode frequencies might provide a measure of the extent of convective overshoot from the core.

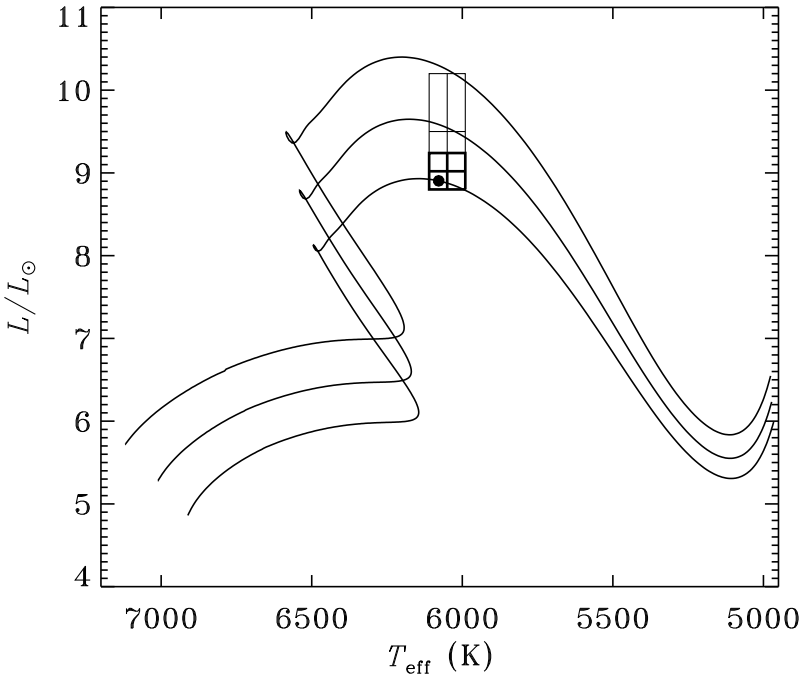

Figure 5.16: Evolutionary tracks in the HR diagram, for models with $Z = 0.03$, $X = 0.7$ and a mixing-length parameter calibrated to obtain the proper solar radius. Models are shown with masses of $1.6M_\odot, 1.63M_\odot$ and $1.66M_\odot$. The thin and bold error boxes indicate the observed location of η Bootis, before and after the *Hipparcos* observations, respectively. The filled circle shows the model identified by Christensen-Dalsgaard *et al.* (1995a) from fits to the observed large frequency separation $\Delta\nu$. (Adapted from Christensen-Dalsgaard *et al.* 1995a).

5.3.3 Results for the subgiant η Bootis

With the continuing contraction of the core after exhaustion of central hydrogen, the buoyancy frequency in the deep stellar interior is increased even further. This brings the frequen-

cies where g-mode-like behaviour can be expected into the frequency range of high-order p modes, which may potentially be excited stochastically by near-surface convection, as seems to be the case in the Sun. An interesting case is the star η Bootis where, as discussed in Section 2.4.1, solar-like oscillations may have been detected by Kjeldsen *et al.* (1995); however, a similar behaviour may have been observed recently in a few other subgiants, including β Hydri. Thus it is of interest to consider the properties of η Bootis in some detail.

The interpretation of the observed frequencies was considered by Christensen-Dalsgaard, Bedding & Kjeldsen (1995a). The star is sufficiently close that its distance is known with reasonable precision; at the time of the analysis, before the publication of the distance determinations from ESA's *Hipparcos* satellite, its luminosity had in this way been determined as $L = (9.5 \pm 0.7)L_\odot$. Also, spectroscopy shows that the effective temperature is $T_{\rm eff} = (6050 \pm 60)\,{\rm K}$ and that the heavy-element abundance is somewhat higher than solar. Figure 5.16 shows the observed location of the star in a Hertzsprung-Russell diagram, together with evolutionary tracks for $Z = 0.03$ and three masses. These identify the star as being in fact past the phase of central hydrogen burning, and with a mass of about $1.6M_\odot$.

Calculation of adiabatic frequencies showed that it is possible to find models in the error box with a $\Delta\nu$ which is consistent with the observed value. This provides an excellent test of the consistency of the frequency observations with the more classical stellar data: $\Delta\nu$ is essentially proportional to the the characteristic dynamical frequency $\omega_{\rm dyn} \equiv (GM/R^3)^{1/2}$ and hence is predominantly determined by the stellar radius; thus it is largely fixed by the location of the star in the HR diagram. The value $\Delta\nu = 40.3\,\mu{\rm Hz}$ inferred from the observations let Christensen-Dalsgaard *et al.* (1995a) to identify the star with the $1.6M_\odot$ model shown with a filled circle in Figure 5.16, just within the pre-*Hipparcos* error box. It is gratifying that the subsequently announced *Hipparcos* results led to $L = (9.0 \pm 0.2)L_\odot$ and hence the smaller error box, also shown in the figure, which was entirely consistent with this inference (Bedding, Kjeldsen & Christensen-Dalsgaard 1998).

To assist the understanding of the behaviour of the oscillations in η Bootis, Figure 5.17 shows the buoyancy frequency and characteristic acoustic frequencies in a model of η Bootis, in units of $\omega_{\rm dyn}$, and compare them with the buoyancy frequency in the present Sun (*cf.* Figure 5.2). The dominant difference between the two models is the very large peak in $\hat{N}$ near the centre of the η Bootis model. This is caused by two effects: during main-sequence evolution the retreating convective core during the phase of central hydrogen burning has left behind a steep gradient in the hydrogen abundance (see also Figure 5.3 and the discussion in Section 5.3.2) leading to a highly stable stratification and hence contributing to a large value of N (*e.g.* Dziembowski & Pamyatnykh 1991); in addition, the increasing central condensation as the core contracts after hydrogen exhaustion drives up the gravitational acceleration in the core, further increasing N. As a result, the maximum value of N exceeds the acoustical cut-off frequency in the stellar atmosphere. Thus *all* trapped acoustic modes may in principle be affected by the buoyancy frequency, taking on g-mode character in the core. In particular, at the frequencies characteristic for the observations of η Bootis, indicated by the horizontal line in Figure 5.17, the modes have extended p-mode regions in the outer parts of the star and a small g-mode region near the centre. The separation between these two regions is quite small for $l = 1$, leading to a substantial coupling between the two types of behaviour; with increasing l, the separation increases rapidly and the coupling becomes small.

The effects of this structure on the oscillations are illustrated in Figure 5.18. The

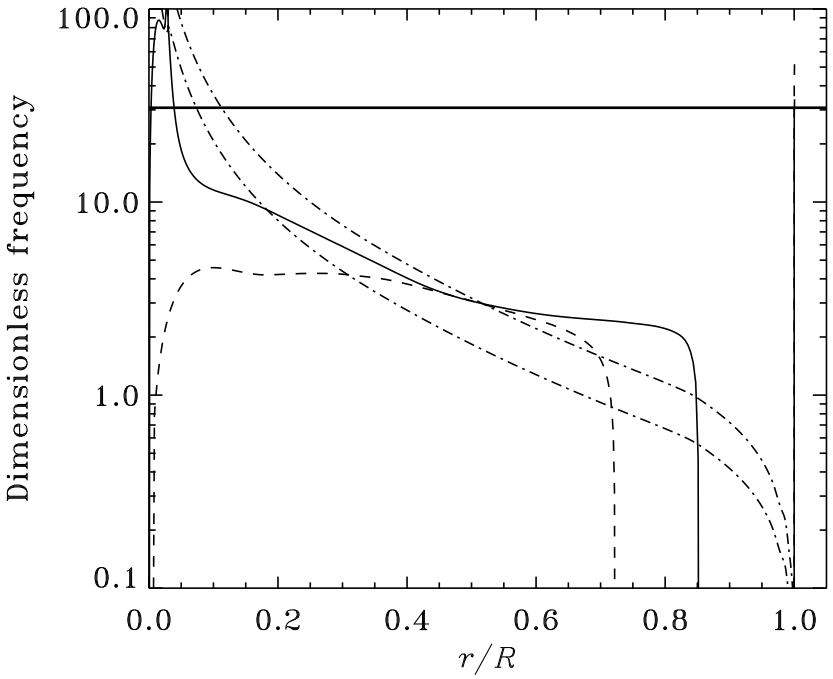

Figure 5.17: Dimensionless buoyancy frequency $\hat{N} \equiv (GM/R^3)^{-1/2}N$ plotted against fractional radius r/R for a model of the present Sun (dashed line) and a model of η Bootis (solid line). The dot-dashed lines show the dimensionless characteristic acoustic frequency $\hat{S}_l = (GM/R^3)^{-1/2}S_l$, where $S_l = cL/r$, for $l = 1$ and 2 in η Bootis. The heavy horizontal line indicates the location of a mode in η Bootis of frequency 850 μHz, typical of the observed frequencies.

frequencies of the radial modes, shown by dashed lines in panel (a), decrease approximately with $\omega_{\rm dyn}$ as a result of the increasing stellar radius. The same general trend is shared by the $l = 1$ modes when they behave like p modes. However, as in the case shown in Figure 5.14 there are additional g-mode branches, with frequencies increasing with age as the maximum value of N increases; as before these interact with the p-mode branches through sequences of avoided crossings. The effect on the mode inertia E normalized at the photospheric amplitude, defined in equation (4.48), is shown in panel (b); for clarity two modes with $l = 1$ have been indicated in both panels by triangles and diamonds, respectively, at the points corresponding to the models in the evolution sequence. Where the $l = 1$ modes behave as p modes, their inertia is very close to that of a radial mode of similar frequency. However, the g-mode behaviour corresponds to an increase in the amplitude in the interior and hence in E. At the avoided crossing there is an interchange of character between the two interacting modes. (It should be noted that the density of models in the sequence is insufficient to resolve fully the variations with age in E, leading to the somewhat irregular behaviour in panel (b); however, the overall variation is clearly visible.)

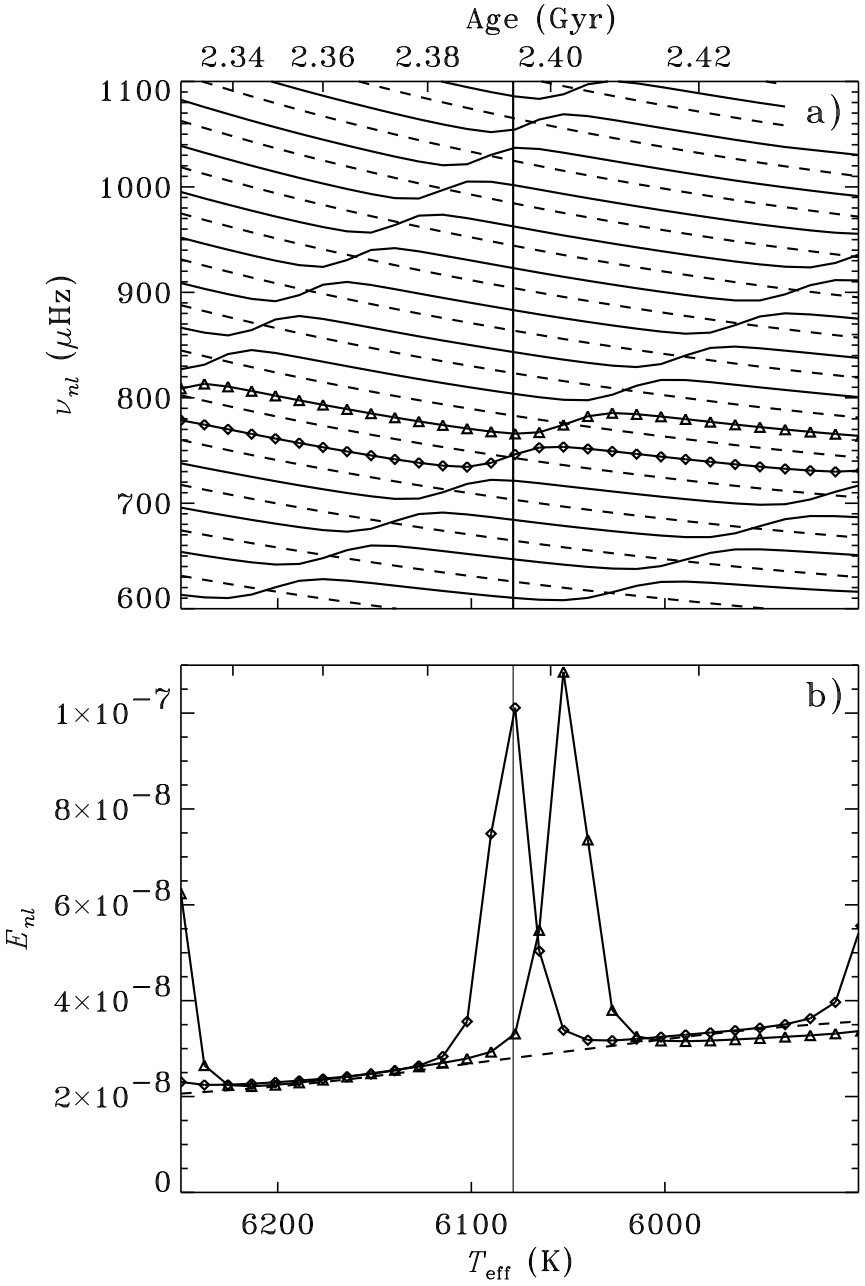

Figure 5.18: (a) Evolution of adiabatic frequencies for model of mass $1.60M_\odot$. The lower abscissa shows the effective temperature $T_{\rm eff}$, the upper abscissa the age of the model in Gyr. The dashed lines correspond to modes of degree $l = 0$, and the solid lines to $l = 1$. The vertical solid line indicates the location of the model whose frequencies are illustrated in Figure 5.20. (Adapted from Christensen-Dalsgaard *et al.* 1995a). (b) The change with age in the normalized mode inertia (*cf.* eq. 4.48). The solid lines show modes with $l = 1$, each model being indicated by triangles or diamonds as in panel (a), whereas the dashed line shows the radial mode with approximately the same frequency.

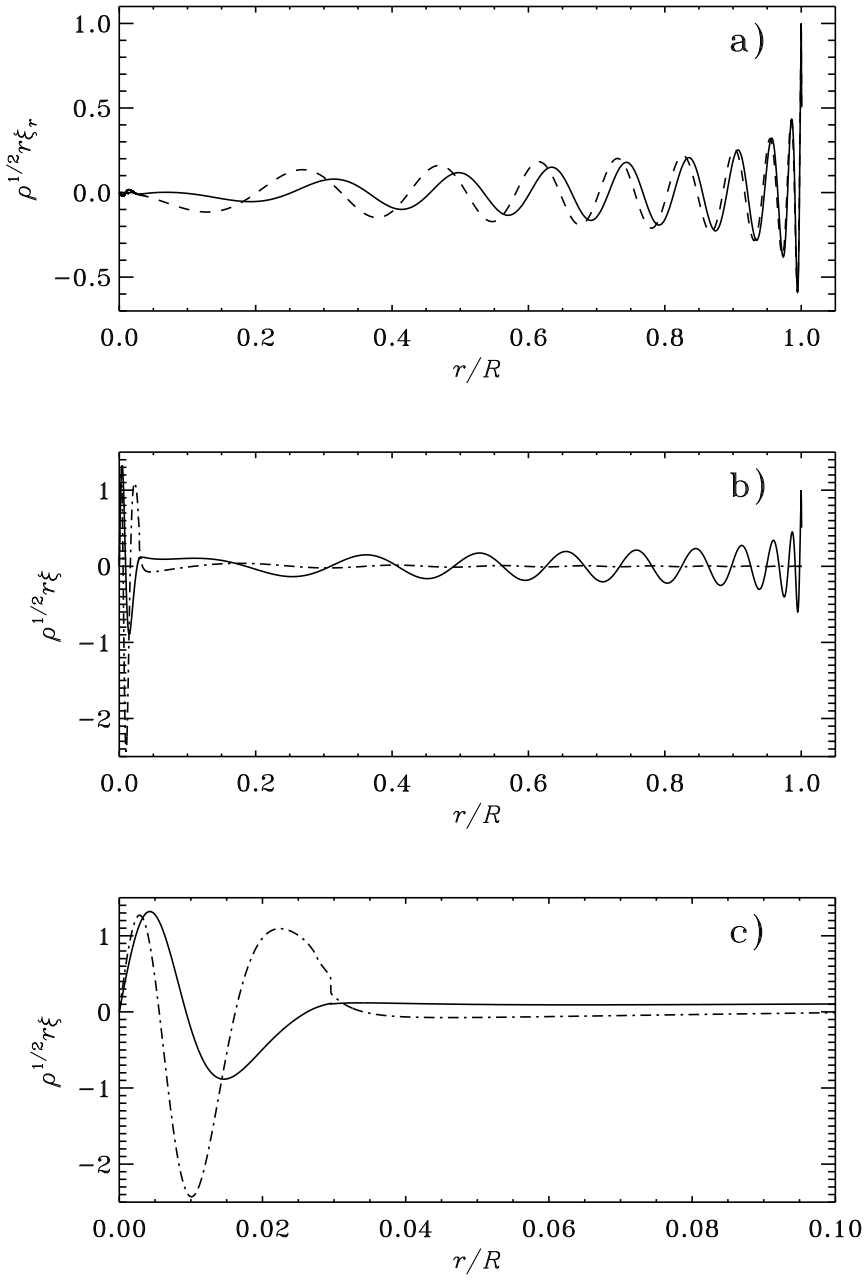

Figure 5.19: Eigenfunctions of selected modes in the model indicated by a vertical line in Figure 5.18. In panel (a) the amplitudes of the vertical displacement are shown for the $l = 1$ mode indicated by triangles (solid line) and the neighbouring radial mode (dashed line). Panels (b) and (c) are for the $l = 1$ mode marked by diamonds: the solid and dot-dashed lines show the amplitudes of the vertical and horizontal displacement, respectively.

The properties of the oscillations are further illustrated by the eigenfunctions shown in Figure 5.19, for the two modes with $l = 1$ undergoing avoided crossing at the vertical line in Figure 5.18 as well as for the neighbouring radial mode. The displacement amplitudes have been weighted by $\rho^{1/2}r$, so that they directly shows the contribution at a given radius to the mode inertia E_{nl} (*cf.* eq. 4.48). The $l = 1$ mode in panel (*a)* is evidently very nearly a pure acoustic mode, with an vertical displacement behaving almost as for the radial mode, apart from the phase shift associated with the difference in frequency. In contrast, the second $l = 1$ mode has very substantial displacement amplitudes in the core, leading to the comparatively large normalized inertia shown in Figure 5.18; this is particularly visible in the enlarged view in Figure 5.19(*c).* It should be noted, however, that the separation between the g-mode and p-mode propagation regions is quite small in this case (see also Figure 5.17), leading to substantial coupling between the two regions and causing the large minimum separation in the avoided crossing and a maximum normalized inertia which is still relatively small, despite the g-mode like behaviour in the core. In contrast, for modes with $l \geq 2$ the separation between the propagation regions is larger and the coupling is much weaker; as a result, a frequency plot corresponding to Figure 5.18(a) shows two sets of frequencies apparently crossing with no avoidance, and the maximum inertia for, for example, $l = 2$ in the frequency region illustrated is around 4×10^{-6}.

The normalized inertia may provide a rough estimate of the likely surface amplitude of the modes, at least if the modes are excited stochastically by convection (*e.g.* Houdek *et al.* 1999; see also Section 10.6): in that case the mode energy is likely to be independent of degree, at fixed frequency. It follows from equation (4.49) that kinetic energy of a mode can be expressed as $1/2A^2ME_{nl}$, where A is the surface amplitude. Assuming that the energy is independent of degree, the amplitude A_{nl} of a mode of degree l, order n and normalized inertia E_{nl} satisfies

$$\frac{A_{nl}}{A_0(\nu_{nl})} \simeq \left[\frac{E_{nl}}{\overline{E}_0(\nu_{nl})}\right]^{-1/2} , \tag{5.35}$$

where $A_0(\nu)$ and $\overline{E}_0(\nu)$ are obtained by interpolating to frequency ν in the results for radial modes. In particular, the modes with strong g-mode character in Figure 5.18 would be expected to have roughly half the surface amplitude of the pure acoustic modes.

The fine structure in the observed and computed frequency spectra can conveniently be compared in an *echelle diagram*, introduced for solar observations in Section 2.3 (*cf.* Figure 2.15). The result for the observed and the model frequencies is shown in Figure 5.20. The open symbols are for a $1.6M_\odot$ model that was chosen to have $\Delta\nu \simeq 40.3\,\mu$Hz; the reference frequency was $\nu_0^{(\mathrm{mod})} = 856\,\mu$Hz. The sizes of the symbols have been scaled by the amplitude ratio A_{nl}/A_0 determined by equation (5.35). The model results for $l = 0$, 2 and 3 clearly reflect the behavior predicted by equation (2.32). In particular, the points for $l = 0$ and 2 run parallel, with a small separation $\delta\nu_0 \simeq 3.3\,\mu$Hz resulting from the last term in that equation. For $l = 1$, equation (2.32) predicts an almost vertical series of points separated by roughly $\Delta\nu/2$ from those for $l = 0$. The model frequencies deviate from this. Comparison with Figure 5.18(a) (where the location of this model is marked by a vertical solid line) indicates that this behavior is associated with the avoided crossings, which change the frequency separation and therefore shift the frequencies relative to the location expected from p-mode asymptotics. As discussed above, even $l = 1$ modes behaving partly like g modes still have sufficiently small normalized inertia E_{nl} that their estimated amplitudes are close to those of the pure p modes. (The figure shows a single exception: a mode at

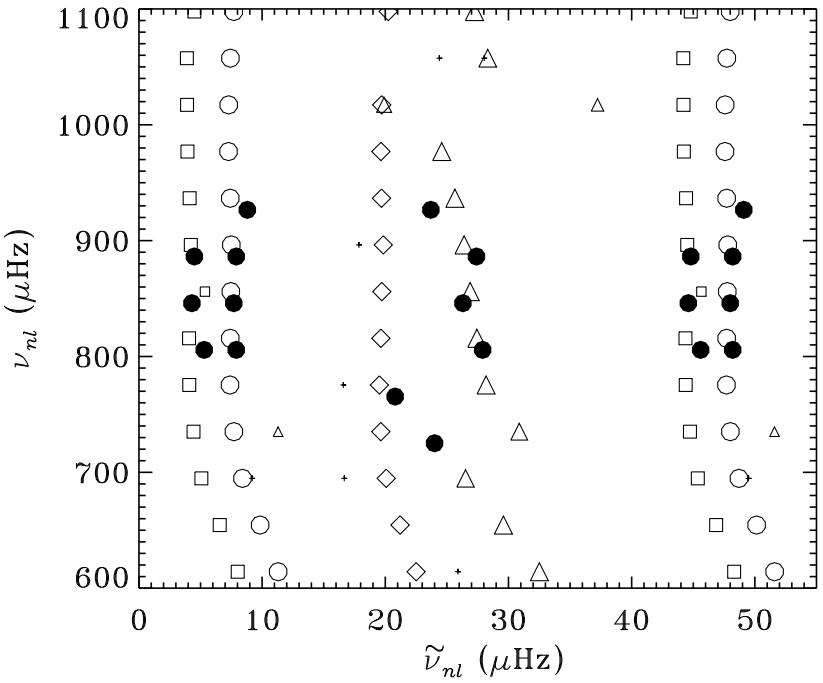

Figure 5.20: Echelle diagram with a frequency separation of $\Delta\nu = 40.3\,\mu$Hz. The open symbols show computed frequencies for a model with $M = 1.60 M_\odot$ and $Z = 0.03$; here the reference frequency was $\nu_0^{(\mathrm{mod})} = 856\,\mu$Hz. Circles are used for modes with $l = 0$, triangles for $l = 1$, squares for $l = 2$ and diamonds for $l = 3$. The size of the symbols indicates the expected relative amplitude of the modes (see text); symbols that would otherwise be too small have been replaced by crosses. The filled circles show observed frequencies from Kjeldsen *et al.* (1995), plotted with the same $\Delta\nu$ but with a reference frequency of $\nu_0^{(\mathrm{obs})} = 846\,\mu$Hz.

730 μHz shifted almost to the $l = 0$ line, with somewhat reduced amplitude.) In contrast, since the g modes of degree 2 and 3 are trapped quite efficiently in the deep interior, their estimated amplitudes are so small as to make the points virtually invisible in Figure 5.20.

The filled circles in Figure 5.20 show the frequencies observed by Kjeldsen *et al.* (1995), again plotted with $\Delta\nu = 40.3\,\mu$Hz, but with the reference frequency $\nu_0^{(\mathrm{obs})} = 846\,\mu$Hz. We can immediately identify modes with degrees $l = 0$ and 2, and the small frequency separation found by Kjeldsen *et al.* ($\delta\nu_0 = (3.1 \pm 0.3)\,\mu$Hz) is in excellent agreement with the model value. The remaining six observed frequencies coincide quite well with $l = 1$ modes in the model and display an irregularity similar to the model frequencies (although differing in detail). This might indicate that the observations of η Bootis show evidence for avoided crossings involving g modes. Note, however, that some of the observed frequencies may arise from modes with $l = 3$.

The interpretation of the observations must clearly be regarded as preliminary, given the uncertainty in extracting individual frequencies in a single-site power spectrum complicated by side lobes. In particular, the indications in the echelle diagram of effects of g-mode trapping is clearly extremely tentative. On the other hand, the close agreement between the observed and computed value of the $l = 0 - 2$ frequency separation is suggestive. The difference of $10\,\mu$Hz in the reference frequency ν_0 required to obtain agreement between the location of the modes in Figure 5.20 is clearly a concern; however, it should be noted that such differences may be induced by errors that are likely present as a result of the simplified treatment of the near-surface layers in the modelling of the star and its oscillations (*cf.* Section 5.1.2). In fact, is of a similar magnitude to the differences observed in comparisons of solar observed and computed frequencies and attributed to errors in the treatment of the superficial layers (see Figure 5.25). Similar effects might be expected for η Bootis (see also Christensen-Dalsgaard *et al.* 1995b).

5.4 Oscillations in stellar atmospheres

In the preceding section I neglected terms of the order of the inverse scale heights in equilibrium quantities. As pointed out, this is invalid near the stellar surface, where the scale heights become small compared with the wavelength of the oscillations. In the present section I discuss these effects in the particularly simple case of an isothermal atmosphere. This has the significant advantage of allowing an analytical solution of the oscillation equations. Furthermore, it is a reasonable approximation to a realistic stellar atmosphere where the temperature variation is substantially slower than the variations in pressure and density. In particular, in the solar case the temperature has a minimum at an optical depth of about 10^{-4}, corresponding to an altitude of about 500 km above the visible surface. An early treatment of this problem was given by Biermann (1947); for a somewhat more recent review, see Schatzman & Souffrin (1967). The extension of the results obtained here to a more general model is discussed in Chapter 7.

I neglect effects of ionization and treat the gas in the atmosphere as ideal, so that the equation of state is given by equation (3.19), where the mean molecular weight μ is taken to be constant. Then equation (3.33) of hydrostatic support gives

$$\frac{\mathrm{d}p}{\mathrm{d}r} = -g\rho = -\frac{p}{H_p} \,, \tag{5.36}$$

where the pressure and density scale heights H_p and H (which are evidently the same in this case) are given by

$$H_p = H = \frac{k_\mathrm{B}T}{g\mu m_\mathrm{u}} \,. \tag{5.37}$$

As the extent of the atmosphere of at least main-sequence stars is much smaller than the stellar radius, g can be taken to be constant. Then H is constant, and the solution to equation (5.36) is

$$p = p_\mathrm{s} \exp\left(-\frac{h}{H}\right) \,. \tag{5.38}$$

Thus, from equation (3.19),

$$\rho = \rho_\mathrm{s} \exp\left(-\frac{h}{H}\right) \,. \tag{5.39}$$

Here I have introduced the altitude $h = r - R$, where R is the photospheric radius (corresponding to the visible surface of the star, *e.g.* defined as the point where the temperature equals the effective temperature), and $p_{\rm s}$ and $\rho_{\rm s}$ are the values of p and ρ at $h = 0$.

We now consider the oscillations. As argued in Section 3.1.4, the motion becomes strongly nonadiabatic in the stellar atmosphere. Nonetheless, for simplicity, I shall here use the adiabatic approximation in the atmosphere. This preserves the most important features of the atmospheric behaviour of the oscillations, at least qualitatively. The study of atmospheric waves and oscillations, with full consideration of effects of radiative transfer, is a very complex and still incompletely developed area (*e.g.* Christensen-Dalsgaard & Frandsen 1983b). It might be noticed that the waves are in fact approximately adiabatic in the upper part of the atmosphere. Here the diffusion approximation (upon which the argument in Section 3.1.4 was based) is totally inadequate, as the gas is optically thin; indeed the density is so low that the gas radiates, and hence loses energy, very inefficiently, and the motion is nearly adiabatic.

I use the Cowling approximation, equations (5.12) and (5.13). Due to the small extent of the atmosphere I neglect the term in $2/r$ (this is consistent with assuming g to be constant, and corresponds to regarding the atmosphere as plane-parallel). Then the equations may be written as

$$\frac{{\rm d}\xi_r}{{\rm d}h} = \frac{1}{\Gamma_1 H}\xi_r - \frac{1}{\Gamma_1 p_{\rm s}}\left(1 - \frac{k_{\rm h}^2 c_{\rm s}^2}{\omega^2}\right)\exp\left(\frac{h}{H}\right)p' \; , \tag{5.40}$$

and

$$\frac{{\rm d}p'}{{\rm d}h} = -\rho_{\rm s}\exp(-\frac{h}{H})(N_{\rm s}^2 - \omega^2)\xi_r - \frac{1}{\Gamma_1 H}p' \; . \tag{5.41}$$

Here the squared sound speed

$$c_{\rm s}^2 = \frac{\Gamma_1 p_{\rm s}}{\rho_{\rm s}} \tag{5.42}$$

and the squared buoyancy frequency

$$N_{\rm s}^2 = \frac{g}{H}\left(1 - \frac{1}{\Gamma_1}\right) \tag{5.43}$$

are constant. In accordance with the plane-parallel approximation I have introduced the horizontal wave number $k_{\rm h}$ instead of the degree l, using equation (4.51). These equations may be combined into a single, second-order equation for ξ_r:

$$\frac{{\rm d}^2\xi_r}{{\rm d}h^2} - \frac{1}{H}\frac{{\rm d}\xi_r}{{\rm d}h} + \frac{1}{H^2}\left[\frac{1}{4}\frac{\omega^2}{\omega_{\rm a}^2} + \frac{k_{\rm h}^2 g H}{\omega^2}\left(1 - \frac{1}{\Gamma_1}\right) - k_{\rm h}^2 H^2\right]\xi_r = 0 \; . \tag{5.44}$$

Here

$$\omega_{\rm a} = \frac{c_{\rm s}}{2H} \tag{5.45}$$

is a characteristic frequency for the atmosphere. In the solar atmosphere H is approximately equal to 120 km, and $\omega_{\rm a}$ is about 0.03 s^{-1}, corresponding to a cyclic frequency of about 5 mHz, or a period of about 3 min.

Exercise 5.3:

Carry through the derivation of equations (5.44) and (5.45). Furthermore, consider the dependence on stellar parameters (M, L and $T_{\rm eff}$) of $\omega_{\rm a}$, measured in units of the characteristic dynamical frequency $(GM/R^3)^{1/2}$ (*cf.* equation 5.10).

Equation (5.44) has constant coefficients, and so the solution can be written down immediately as

$$\xi_r(h) = a_+ \exp\left(\lambda_+ \frac{h}{H}\right) + a_- \exp\left(\lambda_- \frac{h}{H}\right) , \tag{5.46}$$

where

$$\lambda_\pm = \frac{1}{2} \pm \frac{1}{2}\left\{1 - \frac{\omega^2}{\omega_{\rm a}^2} + 4k_{\rm h}^2 H^2 \left[1 - 4\frac{\omega_{\rm a}^2}{\omega^2}\frac{1}{\Gamma_1}\left(1 - \frac{1}{\Gamma_1}\right)\right]\right\}^{1/2} . \tag{5.47}$$

These equations have been the subject of extensive studies in connection with early attempts to interpret observations of solar 5-minute oscillations of high degree (see *e.g.* Stein & Leibacher 1974). From the expression for $\lambda_\pm$ one may qualitatively expect two regimes: one where the frequency is relatively large, $k_{\rm h}$ is relatively small and the first two terms in $\{\cdots\}$ dominate; the second where the frequency is small, $k_{\rm h}$ is large and the last term in $\{\cdots\}$ dominates. These correspond to atmospheric acoustic waves and gravity waves, respectively. From the point of view of global stellar oscillations interest centres on waves with a wavelength much larger than the scale height of the atmosphere. Thus I neglect the last term, reducing equation (5.47) to

$$\lambda_\pm = \frac{1}{2} \pm \frac{1}{2}\left(1 - \frac{\omega^2}{\omega_{\rm a}^2}\right)^{1/2} . \tag{5.48}$$

This is clearly the relation for purely vertical waves.

Equation (5.48) shows the physical meaning of $\omega_{\rm a}$. When $\omega < \omega_{\rm a}$, $\lambda_\pm$ are real, and the motion behaves exponentially in the atmosphere. When $\omega > \omega_{\rm a}$, $\lambda_\pm$ are complex, and the motion corresponds to a wave propagating through the atmosphere. Thus $\omega_{\rm a}$ is the minimum frequency of a propagating wave, and is consequently known as *the acoustical cut-off frequency* (Lamb 1909). The exponential behaviour in the former case provides the upper reflection of p modes, which was absent in the simplified asymptotic analysis of Section 5.3. To study this in more detail, I consider the boundary conditions for an atmosphere of infinite extent. Here the energy density in the motion must be bounded as h tends to infinity. The energy density is proportional to $\rho\xi_r^2$, which for the two solutions behaves as

$$\rho\xi_r^2 \sim \exp(-\frac{h}{H})\exp(2\lambda_\pm \frac{h}{H}) = \exp\left[\pm\left(1 - \frac{\omega^2}{\omega_{\rm a}^2}\right)^{1/2}\frac{h}{H}\right] . \tag{5.49}$$

Therefore only the λ_- solution is acceptable, and here the energy density decreases exponentially. This gives rise to the atmospheric reflection. Thus only modes with frequencies below $\omega_{\rm a}$ are trapped in the stellar interior. At higher frequencies the waves propagate through the atmosphere; oscillations at such frequencies would therefore rapidly lose energy (such waves, generated in the convection zone, may contribute to the heating of the solar chromosphere). In fact, the observed spectrum of oscillations stops at frequencies of about 5 mHz. It should be noticed that $\lambda_- > 0$, so that the displacement *increases* with altitude. This increase can in fact be observed by comparing oscillation amplitudes obtained in spectral lines formed at different levels in the atmosphere.

From this solution we may obtain a more realistic boundary condition, to replace the condition (4.68) discussed earlier. The condition of adiabaticity (4.58) and the continuity equation (3.41) give

$$\frac{\delta p}{p} = \Gamma_1 \frac{\delta\rho}{\rho} = -\Gamma_1 {\rm div}\,\boldsymbol{\delta r} \simeq -\Gamma_1 \frac{{\rm d}\xi_r}{{\rm d}h} = -\Gamma_1 \frac{\lambda_-}{H}\xi_r , \tag{5.50}$$

or

$$p' = \delta p - \xi_r \frac{\mathrm{d}p}{\mathrm{d}h} = \frac{1}{H} p(1 - \Gamma_1 \lambda_-)\xi_r \ , \tag{5.51}$$

where, for simplicity, I neglected the horizontal part of the divergence of $\boldsymbol{\delta}\mathbf{r}$ (this could, quite simply, be included). This provides a boundary condition that may be used in numerical computations, in place of equation (4.68). Typically it is applied at a suitable point, such as the temperature minimum, in the atmosphere of the stellar model.

When ω is small compared with ω_{a}, we can approximate λ_- by

$$\lambda_- \simeq \frac{1}{2}\left[1 - \left(1 - \frac{1}{2}\frac{\omega^2}{\omega_{\mathrm{a}}^2}\right)\right] = \frac{1}{4}\frac{\omega^2}{\omega_{\mathrm{a}}^2} \ . \tag{5.52}$$

Then $\Gamma_1 \lambda_-$ can be neglected in equation (5.51), compared with 1, and we recover the boundary condition in equation (4.68). In this limit the displacement is almost constant throughout the atmosphere. Also, it follows from equation (5.50) that the Lagrangian perturbations to pressure and density, and consequently also to temperature, are small. Physically, this means that the atmosphere is just lifted passively up and down by the oscillation, without changing its structure. Only when the frequency is quite close to the acoustical cut-off frequency does the oscillation have a dynamical effect on the atmosphere.

In reality the Sun, and likely many other stars, is surrounded by a high-temperature corona; in the solar case the temperature exceeds 10^6 K. Here the scale heights are large, and the acoustical cut-off frequency correspondingly small. A typical temperature of 1.6×10^6 K, corresponds to $\omega_{\mathrm{a}} \simeq 0.001\,\mathrm{s}^{-1}$. This is below the frequencies of the modes observed in the solar 5-minute region, and these are therefore propagating in the corona. This atmospheric structure may be approximated by representing it by two isothermal layers, corresponding to the inner atmosphere and the corona, respectively. In the corona the two solutions obtained from equation (5.48) are waves propagating outwards into, and inwards from, the corona. Of these only the former solution is physically realistic (unless one assumes that there is a source of waves in the outer corona!). It may be written, as a function of altitude and time, as

$$\delta r(h,t) = A\rho^{-1/2} \exp[i(k_r h - \omega t)] \ , \tag{5.53}$$

where the radial wave number is

$$k_r = H^{-1}\left(\frac{\omega^2}{\omega_{\mathrm{a}}^2} - 1\right)^{1/2} \ . \tag{5.54}$$

This solution may also be used to obtain a boundary condition on numerical solutions of the oscillation equations in the inner atmosphere, by requiring that the displacement and the pressure perturbation be continuous at the interface between the atmosphere and the corona. I shall not write down this condition in detail. Note, however, that as the solution (5.53) is complex, the relation obtained between ξ_r and p' has complex coefficients. Thus the solution and the eigenfrequency are no longer purely real. Physically, the propagating wave in the corona carries away energy from the oscillation, which is therefore damped, even in the adiabatic approximation. This damping gives rise to an imaginary part in the eigenfrequency, which corresponds to an exponential decay of the solution with time.

To estimate the importance of these effects we return to the solution (5.46), in the inner atmosphere. Because of the effect of the corona both terms must now be included. By

matching to equation (5.53) it may be shown that the two terms are roughly of the same order of magnitude at the interface, where $h = h_c$, say. At the altitude h the ratio between the terms is therefore, roughly,

$$\left|\frac{a_+ \exp(\lambda_+ h/H)}{a_- \exp(\lambda_- h/H)}\right| \sim \left|\frac{\exp[\lambda_+(h-h_c)/H]}{\exp[\lambda_-(h-h_c)/H]}\right| = \exp\left[-\frac{h_c - h}{H}\left(1 - \frac{\omega^2}{\omega_a^2}\right)^{1/2}\right] . \tag{5.55}$$

The base of the corona is approximately at $h_c = 2000$ km. Thus $h_c/H \sim 16$, and the ratio in equation (5.55) is *very* small in the lower part of the atmosphere, unless ω is close to ω_a. Therefore in general it is an excellent approximation to neglect the term in a_+. By the same argument, perturbations to the structure of the atmosphere, or the physics of the oscillations, at the temperature minimum, say, or higher, have little effect on the solution in the deep atmosphere; hence they barely perturb the solution in the interior of the star or the eigenfrequencies. This is fortunate; for the upper solar atmosphere is highly inhomogeneous, and contains magnetic fields of strength sufficient to modify the properties of the oscillations. In addition, the modes may get non-linear at sufficient altitudes, which also affects their propagation. Even so, the assumption of a pure exponentially decaying solution is probably adequate in the inner atmosphere. This has been confirmed by numerical calculations.

The large decrease in the oscillation energy from the lower atmosphere to the base of the corona also limits the importance of the loss of energy in the form of propagating waves in the corona. Detailed, nonadiabatic calculations generally show that this only makes a small contribution to the damping of the modes, except at very high frequencies. The dominant source of damping is heat loss due to the radiative or convective flux in the upper convection zone and the lower atmosphere.

5.5 The functional analysis of adiabatic oscillations

A great deal of insight into the properties of adiabatic oscillations can be obtained by regarding the equations as an eigenvalue problem in a Hilbert space (Eisenfeld 1969; Dyson & Schutz 1979; Christensen-Dalsgaard 1981). Here I consider two different, but very closely related, formulations: one based on the unseparated oscillation equations, valid for general perturbations and a second obtained after separation of the oscillation equations in terms of spherical harmonics.

5.5.1 The oscillation equations as linear eigenvalue problems in a Hilbert space

To obtain the general form, I go back to the perturbed equations of motion, equation (3.43). After separation of the time dependence on the form (4.3) this can be written as

$$\omega^2 \boldsymbol{\delta r} = \mathcal{F}(\boldsymbol{\delta r}) , \tag{5.56}$$

where

$$\mathcal{F}(\boldsymbol{\delta r}) = \frac{1}{\rho_0}\nabla p' - \mathbf{g}' - \frac{\rho'}{\rho_0}\mathbf{g}_0 . \tag{5.57}$$

Here the perturbation quantities denote the amplitudes, after the separation of the time dependence. As indicated, $\mathcal{F}$ is a linear functional of $\boldsymbol{\delta r}$. To see this, note that from the continuity equation (3.41) ρ' is a linear functional of $\boldsymbol{\delta r}$; so, therefore, is the gravitational potential perturbation Φ' as given by equation (3.45). In the adiabatic case p' is obtained from ρ' and $\boldsymbol{\delta r}$ as in equation (3.50); this defines the adiabatic operator $\mathcal{F}_{\rm a}$. The nonadiabatic case is more complicated, but here also it is possible to obtain p' as a linear functional of $\boldsymbol{\delta r}$ (see Christensen-Dalsgaard 1981).

To cast the problems in terms of functional analysis, I introduce a space $\mathcal{H}$ of vector functions of position in the star, with suitable regularity properties, and define an inner product on $\mathcal{H}$ by

$$< \boldsymbol{\xi}, \boldsymbol{\eta} >= \int_V \rho_0 \boldsymbol{\xi}^* \cdot \boldsymbol{\eta} \, {\rm d}V \ , \tag{5.58}$$

for $\boldsymbol{\xi}, \boldsymbol{\eta}$ in $\mathcal{H}$; here "*" denotes the complex conjugate. I also introduce the domain $\mathcal{D}(\mathcal{F})$ of the operator $\mathcal{F}$ as those vectors in $\mathcal{H}$ such that the boundary condition (4.68) is satisfied. The central result of this section is now that, as shown by Lynden-Bell & Ostriker (1967), the operator $\mathcal{F}_{\rm a}$ corresponding to equation (5.57) for adiabatic oscillations is symmetric, in the sense that

$$< \boldsymbol{\xi}, \mathcal{F}_{\rm a}(\boldsymbol{\eta}) >=< \mathcal{F}_{\rm a}(\boldsymbol{\xi}), \boldsymbol{\eta} > , \qquad \text{for } \boldsymbol{\xi}, \boldsymbol{\eta} \in \mathcal{D}(\mathcal{F}) \ . \tag{5.59}$$

The formulation in terms of the spatially separated variables proceeds in a very similar manner. The separated oscillation equations (4.20) and (4.19) may be written

$$\frac{1}{\rho}\frac{{\rm d}p'}{{\rm d}r} + \frac{\rho'}{\rho}g + \frac{{\rm d}\Phi'}{{\rm d}r} \ = \ \omega^2 \xi_r \ , \tag{5.60}$$

$$\frac{1}{r}\left(\frac{p'}{\rho} + \Phi'\right) \ = \ \omega^2 \xi_{\rm h} \ . \tag{5.61}$$

As before, the quantities on the left-hand side can be obtained in terms of ξ_r and $\xi_{\rm h}$; in particular, Φ' is found from ρ' from the separated integral solution to Poisson's equation given in equation (5.11). I introduce the subspace $\mathcal{H}_l$ of the space of pairs of quadratically integrable functions on the interval $[0, R]$, with vectors

$$\xi \equiv (\xi_r, \xi_{\rm h}) \in \mathcal{H}_l \ . \tag{5.62}$$

Then equations (5.60) and (5.61) can be written as

$$\mathcal{F}_l(\xi) = \omega^2 \xi \ , \tag{5.63}$$

defining the operator $\mathcal{F}_l$ corresponding to the separated oscillation equations. Assuming again the adiabatic relation for p' one obtains the linear operator $\mathcal{F}_{{\rm a},l}$ for adiabatic oscillations in $\mathcal{H}_l$. The boundary conditions on ξ_r and $\xi_{\rm h}$ can be imposed by restricting the part of $\mathcal{H}_l$ where $\mathcal{F}_{{\rm a},l}$ is defined. Thus I define the domain of $\mathcal{F}_{{\rm a},l}$ by

$$\mathcal{D}(\mathcal{F}_{{\rm a},l}) = \{(\xi_r, \xi_{\rm h}) | \xi_r - l\xi_{\rm h} \to 0 \quad \text{for} \quad r \to 0 \ \wedge \ \delta p(R) = 0\} \ ; \tag{5.64}$$

the boundary conditions on Φ' are satisfied automatically by the integral expression (5.11). The inner product on $\mathcal{H}_l$ is defined by

$$< \xi, \eta >_l \equiv 4\pi \int_0^R [\xi_r^*(r)\eta_r(r) + L^2 \xi_{\rm h}^*(r)\eta_{\rm h}(r)] r^2 \rho {\rm d}r \ , \tag{5.65}$$

for two vectors $\xi = (\xi_r, \xi_{\rm h})$ and $\eta = (\eta_r, \eta_{\rm h})$ in $\mathcal{H}_l$. Again one may show, using the explicit expression, that the operator $\mathcal{F}_{{\rm a},l}$ is symmetric, *i.e.*,

$$< \mathcal{F}_{{\rm a},l}(\xi), \eta >_l = < \xi, \mathcal{F}_{{\rm a},l}(\eta) >_l \qquad \text{for all} \quad \xi, \eta \in \mathcal{D}(\mathcal{F}_{{\rm a},l}) \ . \tag{5.66}$$

From equations (5.59) and (5.66) follow immediately a number of useful properties of $\mathcal{F}_{\rm a}$ and $\mathcal{F}_{{\rm a},l}$. For simplicity I generally present them in terms of $\mathcal{F}_{\rm a}$; precisely analogous relations are obviously valid for $\mathcal{F}_{{\rm a},l}$. The simplest result is that the squared eigenfrequencies are real. This may be demonstrated by introducing the functional Σ on $\mathcal{D}(\mathcal{F})$ by

$$\Sigma(\boldsymbol{\xi}) = \frac{< \boldsymbol{\xi}, \mathcal{F}_{\rm a}(\boldsymbol{\xi}) >}{< \boldsymbol{\xi}, \boldsymbol{\xi} >} \ ; \tag{5.67}$$

it follows from equation (5.59) that $\Sigma(\boldsymbol{\xi})$ is real. If ω_0^2 is an eigenvalue of the problem with eigenvector $\boldsymbol{\xi}_0$, *i.e.*,

$$\mathcal{F}_{\rm a}(\boldsymbol{\xi}_0) = \omega_0^2 \boldsymbol{\xi}_0 \ , \tag{5.68}$$

then

$$\Sigma(\boldsymbol{\xi}_0) = \omega_0^2 \ , \tag{5.69}$$

and hence ω_0^2 is real. Since the coefficients in equations (4.61), (4.62) and (4.64) are then real, it follows that we may also choose the eigenfunctions to be real at all r.

As is well known, a second property of a symmetric operator is that eigenvectors corresponding to different eigenvalues are orthogonal. Thus if

$$\mathcal{F}_{\rm a}(\boldsymbol{\xi}_1) = \omega_1^2 \boldsymbol{\xi}_1; \qquad \mathcal{F}_{\rm a}(\boldsymbol{\xi}_2) = \omega_2^2 \boldsymbol{\xi}_2; \qquad \omega_1^2 \neq \omega_2^2 \ , \tag{5.70}$$

then

$$< \boldsymbol{\xi}_1, \boldsymbol{\xi}_2 > = 0 \ . \tag{5.71}$$

A very important result concerns the effect of a small perturbation to the oscillation equations. This perturbation could result from a small change to the equilibrium model, from the inclusion of nonadiabatic effects (Christensen-Dalsgaard 1981) or, as discussed in Chapter 8, from the inclusion of the effect of large-scale velocity fields in the model. I characterize the perturbation by a change $\delta\mathcal{F}$ in the operator defining the oscillation equations. If $\boldsymbol{\delta r}_0$ and ω_0 are solutions to the adiabatic oscillation equations,

$$\omega_0^2 \boldsymbol{\delta r}_0 = \mathcal{F}_{\rm a}(\boldsymbol{\delta r}_0) \ , \tag{5.72}$$

the change in ω^2 caused by the perturbation $\delta\mathcal{F}$ can be obtained from first order perturbation analysis (*e.g.* Schiff 1949) as

$$\delta\omega^2 \simeq \frac{< \boldsymbol{\delta r}_0, \delta\mathcal{F}(\boldsymbol{\delta r}_0) >}{< \boldsymbol{\delta r}_0, \boldsymbol{\delta r}_0 >} \ . \tag{5.73}$$

Thus the frequency change can be computed from the unperturbed eigenvector. Similarly, if $\delta\mathcal{F}_l$ is a perturbation to the operator $\mathcal{F}_l$ defining the separated oscillation equations, and ω_0^2, ξ_0 is a solution to the unperturbed problem,

$$\mathcal{F}_{{\rm a},l}(\xi_0) = \omega_0^2 \xi_0 \ , \tag{5.74}$$

then the frequency change can be obtained from

$$\delta\omega^2 \simeq \frac{< \xi_0, \delta\mathcal{F}_l(\xi_0) >_l}{< \xi_0, \xi_0 >_l} \ . \tag{5.75}$$

Some further consequences of this relation are discussed in Section 5.5.3.

Exercise 5.4:

To prove equation (5.73), let $\mathcal{F} = \mathcal{F}_\mathrm{a} + \delta\mathcal{F}$, $\omega^2 = \omega_0^2 + \delta\omega^2$, and $\boldsymbol{\delta r} = \boldsymbol{\delta r}_0 + \delta(\boldsymbol{\delta r})$, such that $\mathcal{F}(\boldsymbol{\delta r}) = \omega^2 \boldsymbol{\delta r}$. Neglect quadratic terms in the perturbations, and use the symmetry of $\mathcal{F}_\mathrm{a}$ (equation 5.59) to eliminate the terms in the perturbation $\delta(\boldsymbol{\delta r})$ to the eigenfunction.

5.5.2 The variational principle

From the symmetry of the operator of adiabatic oscillations it follows that ω^2 satisfies a variational principle (*cf.* Chandrasekhar 1964). Indeed, it is easy to show from equation (5.59) that if $\delta\boldsymbol{\xi} \in \mathcal{H}$ is a small change to the eigenvector, then

$$\Sigma(\boldsymbol{\xi}_0 + \delta\boldsymbol{\xi}) = \omega_0^2 + \mathcal{O}(\|\delta\boldsymbol{\xi}\|^2) \ , \tag{5.76}$$

where $\|\cdots\|$ is the norm corresponding to $< \cdots, \cdots >$. Thus Σ is stationary at the eigenfrequencies. From a physical point of view this reflects Hamilton's principle for the system consisting of the pulsating star. It is conservative, because of the assumption of adiabaticity, and isolated because of the boundary condition (4.68).

It is evident that the variational property, and equivalently the symmetry of the operators $\mathcal{F}$ and $\mathcal{F}_l$, are not valid for nonadiabatic oscillations, where energy is not conserved. Also it depends on the choice of boundary conditions that isolate the system, such as the vanishing of the Lagrangian pressure perturbation. If a different condition is used, such as the match to a solution in an isothermal atmosphere discussed in Section 5.4, the variational property is no longer guaranteed. However, regardless of the boundary condition it is possible to write down expressions analogous to equation (5.69), but possibly containing surface terms; if the effects of the surface properties on the oscillations are small, these expressions may be expected to be approximately variational. In fact it follows from the equations of linear adiabatic oscillations that for any radius r^*

$$\begin{aligned}
\omega^2 \int_0^{r^*} \rho \left(\xi_r^2 + L^2\xi_\mathrm{h}^2\right) r^2 \mathrm{d}r &= \int_0^{r^*} \left(\Gamma_1 p D_1^2 + 2\frac{\mathrm{d}p}{\mathrm{d}r}\,\xi_r D_1 + \frac{1}{\rho}\,\frac{\mathrm{d}\rho}{\mathrm{d}r}\,\frac{\mathrm{d}p}{\mathrm{d}r}\,\xi_r^2\right) r^2 \mathrm{d}r \\
&- \frac{8\pi G}{2l\,+\,1} \int_0^{r^*} r^{-(l-1)} D_2(r) \int_0^r r'^{l+2} D_2(r') \mathrm{d}r' \mathrm{d}r + p'(r^*)\xi_r(r^*) r^{*2} \\
&+ \frac{4\pi G}{2l\,+\,1} \left\{ 2\rho(r^*)\xi_r(r^*) r^{*-(l-1)} \int_0^{r^*} D_2(r) r^{l+2}\,\mathrm{d}r - \left[\rho(r^*)\xi_r(r^*)\right]^2 r^{*3} \right\} \ ;
\end{aligned} \tag{5.77}$$

here

$$\begin{aligned}
D_1 &= \frac{1}{r^2}\frac{\mathrm{d}}{\mathrm{d}r}(r^2\xi_r) - \frac{l(l+1)}{r}\xi_\mathrm{h}, \\
D_2 &= \frac{1}{r^2}\frac{\mathrm{d}}{\mathrm{d}r}(r^2\rho\xi_r) - \frac{l(l+1)}{r}\rho\xi_\mathrm{h}
\end{aligned} \tag{5.78}$$

are the amplitudes of div($\boldsymbol{\delta r}$) and div($\rho\boldsymbol{\delta r}$) respectively. For radial oscillations equation (5.77) may be considerably simplified, to give

$$\omega^2 \int_0^{r^*} \xi_r^2 \rho r^2 \mathrm{d}r = \int_0^{r^*} \left\{ \Gamma_1 p\, r^4 \left[\frac{\mathrm{d}}{\mathrm{d}r} \left(\frac{\xi_r}{r} \right) \right]^2 - r\xi_r^2 \frac{\mathrm{d}}{\mathrm{d}r}[(3\Gamma_1 - 4)p] \right\} \mathrm{d}r + r^* \left[3\Gamma_1 p(r^*)\xi_r(r^*) + r^* \delta p(r^*) \right] \xi_r(r^*) \; . \tag{5.79}$$

These equations are valid at any r^*. If the surface radius is chosen for r^*, and the surface terms are neglected, they reduce to the expression defined symbolically in equation (5.69). In fact, the surface terms are in general relatively small, and even the complete expressions are approximately variational. As discussed by Christensen-Dalsgaard, Gough & Morgan (1979) and J. Christensen-Dalsgaard (1982), they may be utilized in the computation of accurate oscillation frequencies (see also Section 6.6).

5.5.3 Effects on frequencies of a change in the model

As an example of the use of equation (5.75), I discuss in more detail the interpretation of changes in the frequencies caused by changes in the equilibrium model. Consider a mode (n, l), with eigenvector $\xi_{nl} = (\xi_{r,nl}, \xi_{\mathrm{h},nl}) \in \mathcal{H}_l$; without loss of generality I may assume that $\xi_{r,nl}(r)$ and $\xi_{\mathrm{h},nl}(r)$ are real. The relative frequency change caused by the perturbation $\delta\mathcal{F}_l$ is then, according to equation (5.75)

$$\frac{\delta\omega_{nl}}{\omega_{nl}} = \frac{1}{2}\frac{\delta\omega_{nl}^2}{\omega_{nl}^2} = \frac{< \xi_{nl}, \delta\mathcal{F}_l(\xi_{nl}) >_l}{2\omega_{nl}^2 < \xi_{nl}, \xi_{nl} >_l} \; . \tag{5.80}$$

Here the denominator is proportional $\omega_{nl}^2 E_{nl}$, where E_{nl} was defined in equation (4.48). Also, I represent $\delta\mathcal{F}_l$ on component form as

$$\delta\mathcal{F}_l(\xi_{nl}) = (\phi_r[\xi_{nl}], \phi_{\mathrm{h}}[\xi_{nl}]) \; , \tag{5.81}$$

where $\phi_r[\xi_{nl}](r)$ and $\phi_{\mathrm{h}}[\xi_{nl}](r)$ are functions of r. Then we can write equation (5.80) as

$$E_{nl}\frac{\delta\omega_{nl}}{\omega_{nl}} = I_{nl} \; , \tag{5.82}$$

where

$$I_{nl} = \frac{2\pi \int_0^R \left[\xi_{r,nl}(r)\phi_r[\xi_{nl}](r) + L^2 \xi_{h,nl}(r)\phi_{\mathrm{h}}[\xi_{nl}](r) \right] \rho r^2 \mathrm{d}r}{M\omega_{nl}^2 [\xi_r^2(R) + l(l+1)\xi_{\mathrm{h}}^2(R)]} \; . \tag{5.83}$$

Thus I_{nl} gives the integrated effect of the perturbation, normalized to the total surface displacement.

Equations (5.82) and (5.83) provide a linear relation between the change in the model and the change in the frequency. These expressions are somewhat formal. However, it follows from the discussion in Section 5.1 that the changes in the coefficients of the oscillation equations, and hence the changes $\phi_r[\xi_{nl}](r)$ and $\phi_{\mathrm{h}}[\xi_{nl}](r)$ in the components of $\delta\mathcal{F}_l$, can be expressed in terms of changes in two suitably chosen model variables, for example density and sound speed. For simplicity, I assume that the change in the model occurs without a change in its radius (this would in general be the case for models of the Sun, where the radius is known with high accuracy) and let $\delta_r\rho$ and $\delta_r c^2$ denote the changes, between the

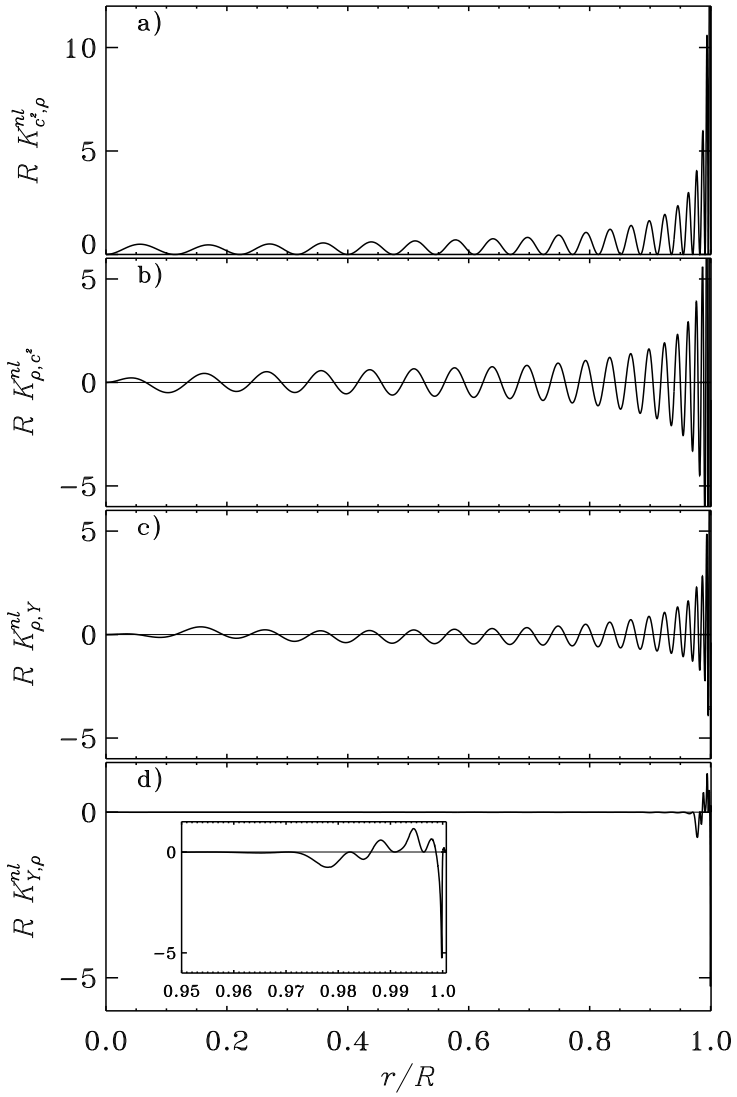

Figure 5.21: Kernels for an $l = 0$, $n = 21$ mode (with frequency $\nu = 3.04\,\mathrm{mHz}$) of a model of the present Sun. Panels (a) and (b) show $RK^{nl}_{c^2,\rho}$ and RK^{nl}_{ρ,c^2}. The $K^{nl}_{c^2,\rho}$ is positive everywhere, while the kernel K^{nl}_{ρ,c^2} takes on both positive and negative values. Panels (c) and (d) similarly show the kernels $RK^{nl}_{\rho,Y}$ and $RK^{nl}_{Y,\rho}$ for the same mode; the insert in panel (d) shows the detailed behaviour of $RK^{nl}_{Y,\rho}$ in the hydrogen and helium ionization zones.

equilibrium models, in ρ and c^2 at fixed r[4]. Then, after some manipulation, equation (5.82) can be written as

$$\frac{\delta\omega_{nl}}{\omega_{nl}} = \int_0^R \left[K^{nl}_{c^2,\rho}(r) \frac{\delta_r c^2}{c^2}(r) + K^{nl}_{\rho,c^2}(r) \frac{\delta_r \rho}{\rho}(r) \right] \mathrm{d}r \tag{5.84}$$

(*e.g.* Gough & Thompson 1991), where the kernels $K^{nl}_{c^2,\rho}$ and K^{nl}_{ρ,c^2} are computed from the eigenfunctions. Examples of such kernels are shown in Figure 5.21.

As discussed in Section 5.1.1, other pairs of "mechanical" variables may be used instead of (c^2, ρ); the transformation between these pairs can be accomplished by means of the equation of hydrostatic support and mass, expressed in terms of the model changes, and suitable integrations by part. If it is also assumed that the equation of state is known, further transformation is possible. An important example is provided by the relation $c^2 = \Gamma_1 p/\rho$, where Γ_1 can be obtained as a function $\Gamma_1(p, \rho, Y, Z)$ of pressure, density and chemical composition as specified by the abundances Y and Z by mass of helium and heavy elements. This yields[5]

$$\begin{aligned} \frac{\delta_r c^2}{c^2} &= \left[\left(\frac{\partial \ln \Gamma_1}{\partial \ln p} \right)_{\rho,Y,Z} + 1 \right] \frac{\delta_r p}{p} + \left[\left(\frac{\partial \ln \Gamma_1}{\partial \ln \rho} \right)_{p,Y,Z} - 1 \right] \frac{\delta_r \rho}{\rho} \\ &\quad + \left(\frac{\partial \ln \Gamma_1}{\partial Y} \right)_{p,\rho,Z} \delta_r Y + \left(\frac{\partial \ln \Gamma_1}{\partial Z} \right)_{p,\rho,Y} \delta_r Z \, . \end{aligned} \tag{5.85}$$

By substituting this into equation (5.84), and eliminating $\delta_r p$ by means of the perturbed equation of hydrostatic support, $\delta\omega_{nl}/\omega_{nl}$ can be expressed in terms of $\delta_r\rho/\rho$, $\delta_r Y$ and $\delta_r Z$. Since the surface heavy-element abundance may be obtained from spectroscopic observations it is reasonable to assume Z to be known; neglecting therefore the term in $\delta_r Z$, we finally obtain

$$\frac{\delta\omega_{nl}}{\omega_{nl}} = \int_0^R \left[K^{nl}_{\rho,Y}(r) \frac{\delta_r \rho}{\rho}(r) + K^{nl}_{Y,\rho}(r) \delta_r Y(r) \right] \mathrm{d}r \, . \tag{5.86}$$

Examples of these kernels are shown in Figure 5.21, panels (c) and (d). In particular, it should be noticed that $K^{nl}_{Y,\rho}$ is significantly different from zero only in the hydrogen and helium ionization zones. As discussed in Section 9.2 this substantially facilitates the determination of $\delta_r\rho/\rho$ through inverse analysis.

5.5.4 Effects of near-surface changes

I now assume that $\delta\mathcal{F}_l$ in equation (5.81) is localized near the stellar surface, in the sense that

$$\phi_r[\xi](r) \simeq 0 \, , \qquad \phi_\mathrm{h}[\xi](r) \simeq 0 \quad \text{for} \quad R - r > \epsilon \, , \tag{5.87}$$

for some small ϵ. For modes extending substantially more deeply than the region of the perturbation, *i.e.*, with $R - r_\mathrm{t} \gg \epsilon$, the eigenfunctions are nearly independent of l at fixed frequency in that region (see also Figure 5.8 and the associated discussion). Hence I_{nl}

[4]These *model changes* should not be confused with the Lagrangian perturbations associated with the oscillations, introduced in Chapters 3 and 4.

[5]As noted by Basu & Christensen-Dalsgaard (1997) one may in addition include a contribution from the intrinsic difference $(\delta\Gamma_1)_\mathrm{int}$ between the model and the true Γ_1, at fixed thermodynamic conditions and composition.

depends little on l at fixed ω. To get a more convenient representation of this property, I introduce

$$Q_{nl} = \frac{E_{nl}}{\overline{E}_0(\omega_{nl})} \,, \tag{5.88}$$

where $\overline{E}_l(\omega)$ is obtained by interpolating to ω in E_{nl} at fixed l. Then

$$Q_{nl}\delta\omega_{nl} \tag{5.89}$$

is independent of l, at fixed ω, for modes such that $R - r_{\rm t} \gg \epsilon$. Conversely, if $Q_{nl}\delta\omega_{nl}$ is independent of l at fixed ω for a given set of modes, then $\delta\mathcal{F}_l$ is probably largely localized outside $r = \max(r_{\rm t})$ over the set of modes considered.

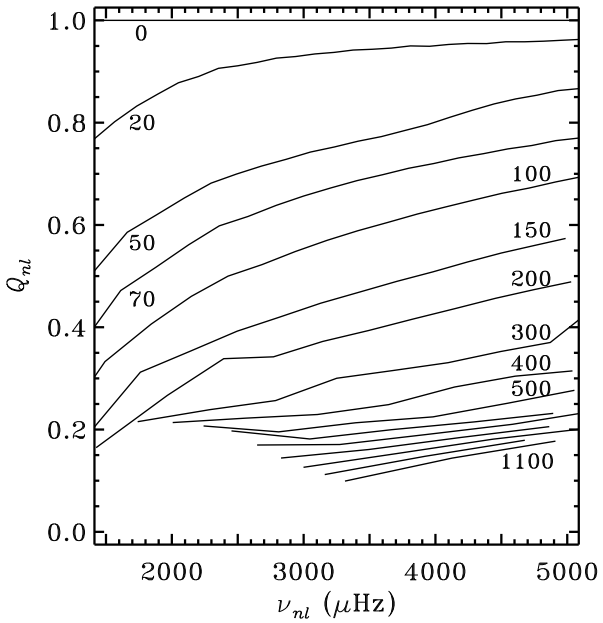

Figure 5.22: The inertia ratio Q_{nl}, defined in equation (5.88), against frequency ν, for f and p modes in a normal solar model. Each curve corresponds to a given degree l, selected values of which are indicated.

Q_{nl} has been plotted in Figure 5.22, for selected values of l. Its variation with l is largely determined by the change in the penetration depth. Modes with higher degree penetrate less deeply and hence have a smaller inertia at given surface displacement. As a consequence of this their frequencies are more susceptible to changes in the model.

An important example concerns the uncertainties in the physics of the model and the oscillations in the near-surface region, discussed in Section 5.1.2 and indicated schematically in Figure 5.1. These are confined to a very thin region, and hence, according to the discussion following equation (5.89), we may expect that their effects on the frequencies, when scaled with Q_{nl}, are largely independent of degree at a given frequency. As discussed

below, and in more detail in Sections 7.7 and 9.2, this can be used to eliminate the effects of the uncertainties in the analysis of observed frequencies.

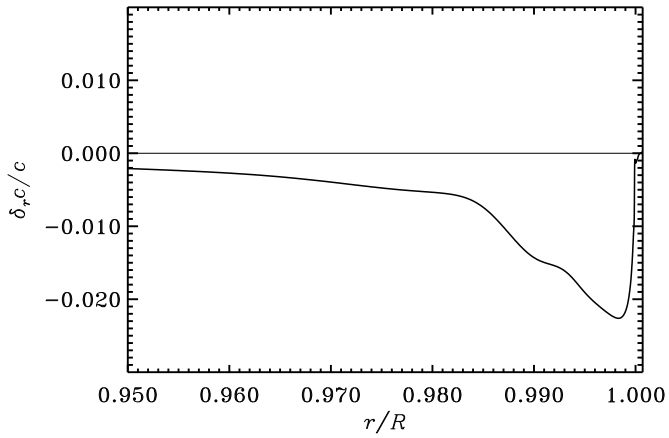

Figure 5.23: Relative sound-speed difference $\delta_r c/c$ between a model with modified surface opacity and a normal model, in the sense (modified model) – (normal model).

To illustrate this behaviour, we may analyze model changes localized very near the solar surface. Specifically, I consider a solar model where the opacity has been artificially increased by a factor of 2 at temperatures below about 10^5 K; this is compared with a normal model of the present Sun. In both models the mixing-length parameter and composition have been adjusted so as to obtain a model with solar radius and luminosity; the effect of this is that the interior of the model is virtually the same. The opacity has no effect in the bulk of the convection zone where energy transport is totally dominated by convection; hence the change in the model is largely confined to the atmosphere and the uppermost parts of the convection zone. Figure 5.23 shows the sound-speed difference $\delta_r c^2$ between the modified and the normal model.

The unscaled differences between frequencies of the two models are shown in Figure 5.24a. It is evident that the differences show a very systematic increase in magnitude with increasing degree. As shown by Figure 5.24b this is entirely suppressed by scaling the differences by Q_{nl}. Indeed, the differences now seem to decrease with increasing l. This is predominantly due to the fact that at the largest values of l the modes can no longer be assumed to be independent, near the surface, of degree at fixed frequency (for an asymptotic description of this behaviour, see for example Gough & Vorontsov 1995). A small additional contribution comes from the fact that the modes only penetrate partly, to a degree-dependent extent, into the region where the sound speed has been modified.

It might also be noted that the frequency differences are very small at low frequency. This is related to the fact that low-frequency modes have very small amplitudes in the surface region (*cf.* Figure 5.9). However, a proper understanding of this feature requires a more careful analysis (see Christensen-Dalsgaard & Thompson 1997).

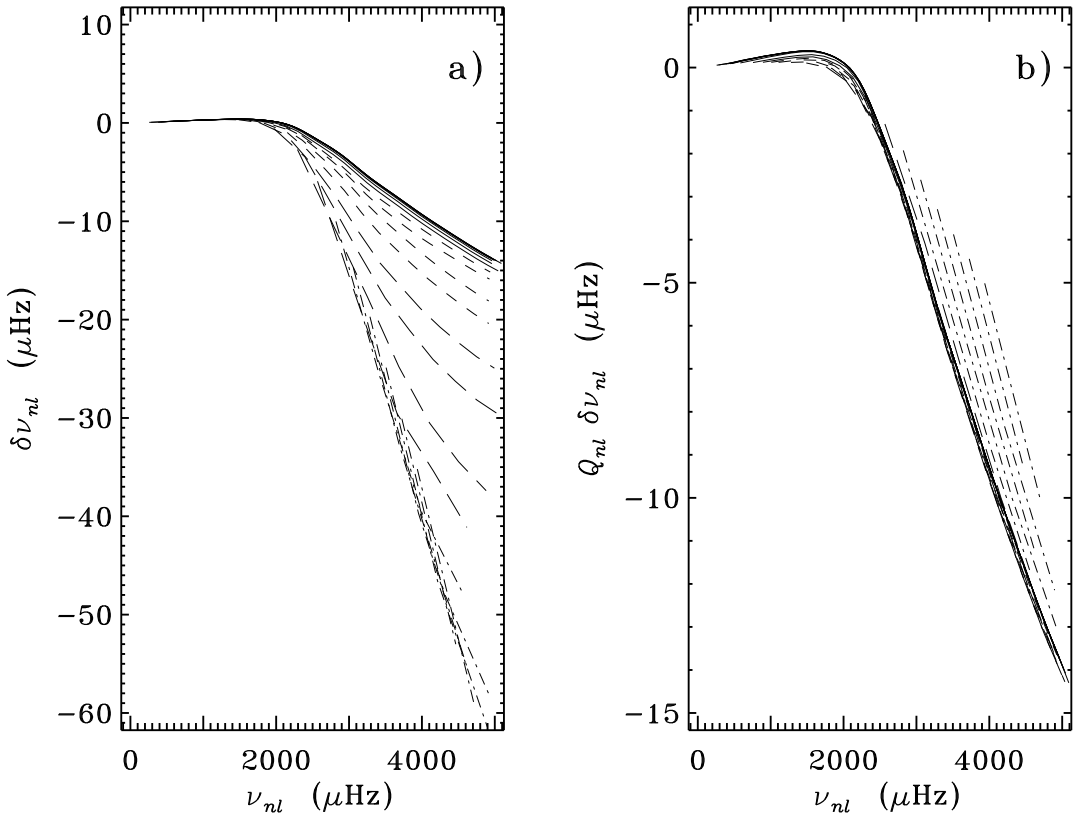

Figure 5.24: Frequency differences between a model with modified surface opacity and a normal model, in the sense (modified model) – (normal model). Panel (a) shows the raw differences. In panel (b) the differences have been scaled by Q_{nl}, in accordance with equation (5.89). Points corresponding to a given degree have been connected, according to the following line styles: $l = 0, 1, 2, 3, 4, 5, 10, 20, 30$ (solid); $l = 40, 50, 70, 100$ (short-dashed); $l = 150, 200, 300, 400$ (long-dashed); $l = 600, 700, 800, 900, 1000, 1100$ (dot-dashed).

A rather similar behaviour is obtained for the observed frequencies, as shown in Figure 5.25. The unscaled differences (panel a) show a strong dependence on l, which is largely (but not completely) suppressed by scaling. This strongly suggests that most of the errors in the model are located very near the surface. I note that this is precisely the region where, according to the arguments in Section 5.1.2, many of the uncertainties in the physics of the model and the oscillations are located. Thus it is not surprising that we obtain an effect on the frequencies of this nature. As discussed in Section 9.2 it is possible to suppress the effect, precisely because of its systematic dependence on frequency. However, I note also in

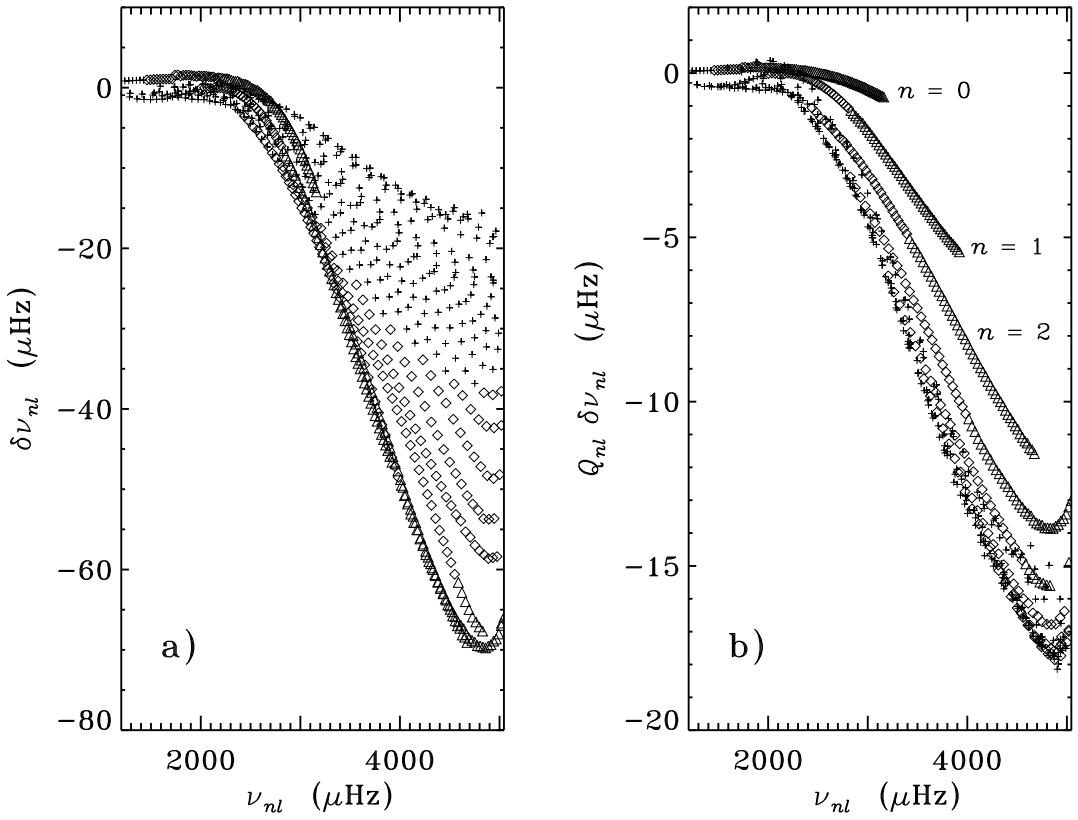

Figure 5.25: Frequency differences between observed data and frequencies of a solar model, in the sense (observations) – (model). The observed frequencies were obtained from the MDI experiment on the SOHO spacecraft (Rhodes *et al.* 1997, 1998), whereas the model frequencies are for Model S of Christensen-Dalsgaard *et al.* (1996). Crosses indicate modes with $l \leq 200$, diamonds are modes with $200 < l \leq 500$ and triangles are modes with $500 < l$. Panel (a) shows the raw differences. In panel (b) the differences have been scaled by Q_{nl}, in accordance with equation (5.89). Here ridges corresponding to low radial orders n are evident; the lowest values have been indicated in the figure.

Figure 5.25b that there is a significant dependence of the differences on degree; this must be associated with errors in the model in deeper layers. I return to the origin of these differences in Section 7.7.2.

For the highest-degree modes the figure shows a clear 'pealing-off' into ridges for each value of the radial order n. Here the upper turning point is so close to the surface that the assumptions of nearly vertical propagation, and degree-independent eigenfunctions, break down. A similar behaviour was noted in Figure 5.24 for differences between model

frequencies. Also, I note that the f modes (with $n = 0$) represent a special case. As discussed in Section 7.5.1, these essentially have the character of surface gravity waves, with frequencies given approximately by equation (3.84); in particular, computed frequencies of normal solar models are essentially independent of the details of the structure of the model (see also Gough 1993; Chitre, Christensen-Dalsgaard & Thompson 1998). Thus the error in the f-mode frequencies evident in Figure 5.25b must arise from effects other than differences between the hydrostatic structure of the Sun and the model. A likely cause are dynamical interactions between the modes and the turbulent motion in the solar convection zone (Murawski, Duvall & Kosovichev 1998; Mędrek, Murawski & Roberts, 1999). However, the details of such mechanisms, and in particular their effects on the p-mode frequencies, are still rather uncertain.

The probable presence of near-surface errors in the model must be taken into account when relating differences between observed and computed frequencies to the corresponding differences between the structure of the star and the model. Specifically, consider the determination of corrections $\delta_r c^2$ and $\delta_r \rho$ to a stellar model, from the differences $\delta\omega_{nl} = \omega_{nl}^{(\mathrm{obs})} - \omega_{nl}$ between observed frequencies $\omega_{nl}^{(\mathrm{obs})}$ and model frequencies ω_{nl}: here we expect differences between the star and the model both in the internal structure, characterized by (c^2, ρ), and in the near-surface layers. In addition, the observed frequencies are unavoidably affected by errors. From the analysis above we therefore expect that equation (5.84) must be replaced by

$$\begin{aligned} \frac{\delta\omega_{nl}}{\omega_{nl}} &= \int_0^R \left[K^{nl}_{c^2,\rho}(r) \frac{\delta_r c^2}{c^2}(r) + K^{nl}_{\rho,c^2}(r) \frac{\delta_r \rho}{\rho}(r) \right] \mathrm{d}r \\ &\quad + Q_{nl}^{-1} \mathcal{G}(\omega_{nl}) + \epsilon_{nl} \ , \end{aligned} \tag{5.90}$$

where the function $\mathcal{G}(\omega)$ accounts for the effect of the near-surface uncertainties, and ϵ_{nl} are the relative observational errors in the frequencies. The term in $\mathcal{G}$ must then be determined as part of the analysis of the frequency differences, or suppressed by means of suitable filtering of the data. As discussed above, for high-degree modes the scaled frequency effects of the near-surface problems can no longer be regarded as purely a function of frequency; a representation which takes this into account has been developed by Di Mauro *et al.* (2002).

Chapter 6

Numerical techniques

The differential equations (4.61), (4.62) and (4.64), in combination with boundary conditions such as equations (4.65) – (4.68), constitute a two point boundary value problem. Non-trivial solutions to the problem can be obtained only at selected values of the frequency ω, which is therefore an eigenvalue of the problem. Problems of this nature are extremely common in theoretical physics, and hence there exists a variety of techniques for solving them. Nevertheless, the computation of solar adiabatic oscillations possesses special features, which merit discussion. In particular, we typically need to determine a large number of frequencies very accurately, to match the volume and precision of the observed data.

Specific numerical techniques are discussed in considerable detail by, for example, Unno *et al.* (1989) and Cox (1980). Here I concentrate more on general properties of the solution method. The choice of techniques and examples is unavoidably biased by my personal experience, but should at least give an impression of what can be achieved, and how to achieve it.

I note that a self-contained package for computing stellar adiabatic oscillations, with documentation and further notes on the numerical techniques, is available on the WWW at `http://astro.phys.au.dk/~jcd/adipack.n/`.

6.1 Difference equations

The numerical problem can be formulated generally as that of solving

$$\frac{\mathrm{d}y_i}{\mathrm{d}x} = \sum_{j=1}^{I} a_{ij}(x) y_j(x) \;, \qquad \text{for} \quad i = 1, \ldots, I \;, \tag{6.1}$$

with suitable boundary conditions at $x = x_1$ and x_2, say. Here the order I of the system is four for the full nonradial case, and two for radial oscillations or nonradial oscillations in the Cowling approximation.

To handle these equations numerically, I introduce a mesh $x_1 = x^{(1)} < x^{(2)} < \ldots < x^{(N_{\mathrm{me}})} = x_2$ in x, where N_{me} is the total number of mesh points. Similarly I introduce $y_i^{(n)} \equiv y_i(x^{(n)})$, and $a_{ij}^{(n)} \equiv a_{ij}(x^{(n)})$. A commonly used, very simple representation of the differential equations is in terms of *second-order centred differences*, where the differential

equations are replaced by the difference equations

$$\frac{y_i^{(n+1)} - y_i^{(n)}}{x^{(n+1)} - x^{(n)}} = \frac{1}{2} \sum_{j=1}^{I} \left[a_{ij}^{(n)} y_j^{(n)} + a_{ij}^{(n+1)} y_j^{(n+1)} \right], \qquad i = 1, \ldots, I \; . \tag{6.2}$$

These equations allow the solution at $x = x^{(n+1)}$ to be determined from the solution at $x = x^{(n)}$.

More elaborate and accurate difference schemes (*e.g.* Press *et al.* 1986; Cash & Moore 1980), can be set up which allow the rapid variation in high-order eigenfunctions to be represented with adequate accuracy on a relatively modest number of meshpoints. Alternatively one may approximate the differential equations on each mesh interval $(x^{(n)}, x^{(n+1)})$ by a set of equations with constant coefficients, given by

$$\frac{\mathrm{d}\eta_i^{(n)}}{\mathrm{d}x} = \sum_{j=1}^{I} \overline{a}_{ij}^{(n)} \eta_j^{(n)}(x), \quad \text{for} \quad i = 1, \ldots, I \; , \tag{6.3}$$

where $\overline{a}_{ij}^{(n)} \equiv \frac{1}{2}(a_{ij}^{(n)} + a_{ij}^{(n+1)})$ (Gabriel & Noels 1976). These equations may be solved analytically on the mesh intervals, and the complete solution is obtained by continuous matching at the mesh points. This technique clearly permits the computation of modes of arbitrarily high order. I have considered its use only for systems of order two, *i.e.*, for radial oscillations or non-radial oscillations in the Cowling approximation.

6.2 Shooting techniques

Perhaps the conceptually simplest technique for handling a boundary value problem is the shooting technique. For simplicity, I consider first the case of a second-order system, such as results from making the Cowling approximation. Then there is one boundary condition, namely equation (4.65), at the centre, and one condition, equation (4.68), at the surface. For any value of ω the equations may be integrated numerically, imposing the central boundary condition on ξ_r and ξ_h, and the quantity

$$\Delta(\omega) \equiv \left(p' + \frac{\mathrm{d}p}{\mathrm{d}r} \xi_r \right) \Big|_{r=R} \tag{6.4}$$

may be evaluated. The eigenfrequencies are obviously the zeros of $\Delta(\omega)$. A convenient method of locating them is to evaluate $\Delta(\omega)$ at a sequence of points $\omega_1, \omega_2, \ldots$; once an interval has been found where Δ changes sign the zero can be found, for instance, by applying the secant method. An attractive feature of the method is precisely this ability to search automatically for all modes in a given frequency range, particularly when it is combined with a method for determining the order of a given mode, so that a check can be made that no modes have been skipped.

A slight elaboration of this basic technique is required to make it computationally efficient. Due to the rapid decrease of temperature near the solar surface, the equations are almost singular there. Far from the eigenfrequencies the solution therefore generally increases rapidly towards the surface; this translates into a dramatic variation of Δ with ω, which complicates the determination of the zeros. To avoid this problem, one may compute solutions $(\xi_r^{(\mathrm{i})}, \xi_\mathrm{h}^{(\mathrm{i})})$ and $(\xi_r^{(\mathrm{s})}, \xi_\mathrm{h}^{(\mathrm{s})})$ satisfying the inner and the surface boundary conditions,

respectively. A continuous match of the interior and exterior solutions requires the existence of non-zero constants $C^{(\mathrm{i})}$ and $C^{(\mathrm{s})}$ such that

$$\begin{aligned} C^{(\mathrm{i})}\xi_r^{(\mathrm{i})}(r_\mathrm{f}) &= C^{(\mathrm{s})}\xi_r^{(\mathrm{s})}(r_\mathrm{f}) \\ C^{(\mathrm{i})}\xi_\mathrm{h}^{(\mathrm{i})}(r_\mathrm{f}) &= C^{(\mathrm{s})}\xi_\mathrm{h}^{(\mathrm{s})}(r_\mathrm{f}) \ , \end{aligned} \tag{6.5}$$

where r_f is an appropriately chosen fitting point. This set of equations has a solution only if the determinant

$$\Delta_\mathrm{f}(\omega) = \xi_r^{(\mathrm{i})}(r_\mathrm{f})\xi_\mathrm{h}^{(\mathrm{s})}(r_\mathrm{f}) - \xi_\mathrm{h}^{(\mathrm{i})}(r_\mathrm{f})\xi_r^{(\mathrm{s})}(r_\mathrm{f}) \tag{6.6}$$

vanishes. Hence the eigenfrequencies are determined as the zeros of Δ_f, as before.

The choice of fitting point should be guided by the expected behaviour of the eigenfunction, in such a way that the integration of the differential equations proceeds in a stable fashion. Thus, for instance, when solving for a strongly trapped g mode of high degree, r_f should be near the maximum in the buoyancy frequency where the mode is trapped; in this way the integration from both the centre and the surface is in the direction where the solution increases. Similarly, when integrating for a p mode of high degree, r_f should be in the oscillatory region near the surface.

The solution of the full fourth-order problem proceeds in a very similar fashion. Here there are two linearly independent solutions that satisfy the boundary conditions at the centre, and two linearly independent solutions that satisfy the conditions at the surface. The condition that these two sets of solutions match continuously at a point r_f leads to a set of equations whose solution requires the vanishing of a 4×4 determinant. It should be noted, however, that problems arise when the effect of the perturbation in the gravitational potential is small. In this case, although the two separate solutions from *e.g.* the centre are formally linearly independent, they are in practice very close to being linearly dependent, and the zeros of Δ_f are therefore ill-determined. This is no major concern in practice, since under these circumstances the Cowling approximation is in general adequate. However, as discussed below the problem may be avoided through the use of some variant of the relaxation technique.

6.3 Relaxation techniques

The relaxation technique considers the set of difference equations, such as equations (6.2), together with the homogeneous boundary conditions and a normalization condition, as a set of equations for the unknown quantities $\{y_i^{(n)}; i = 1, \ldots, I;\ n = 1, \ldots, N_\mathrm{me}; \omega\}$. Due to the appearance of the eigenfrequency, the equations are non-linear in the unknowns. They are solved by linearizing around an assumed initial trial solution, and the solution is obtained by iteration. This technique is equivalent to what is commonly known as the Henyey technique in computations of stellar evolution (Henyey, Forbes & Gould 1964; see also Baker, Moore & Spiegel 1971; Kippenhahn & Weigert 1990).

A disadvantage of this technique is that it requires a reasonably accurate trial solution, both for the eigenfrequency and the eigenfunction, if the iteration is to converge to the desired mode. Also it is not immediately possible to search a given part of the spectrum. These problems may be avoided by dropping one of the boundary conditions, and regarding ω as given (*e.g.* Castor 1971; Osaki & Hansen 1973). The difference equations are then a linear set of equations for the $\{y_i^{(n)}\}$ which may be solved directly. Given the solution, the remaining boundary condition, now regarded as a function of ω, is solved to obtain the

eigenfrequencies. Thus in this form the relaxation technique retains the advantages of the shooting method, in that a region of the spectrum can be scanned. Once a sufficiently close approximation to the solution has been found, the rate of convergence can be increased by switching to simultaneous iteration for the eigenfrequency and eigenfunction.

As for the shooting technique, the straight determination of the eigenfrequency through root-seeking on one of the boundary conditions is rather ill-behaved. This problem may be avoided by imposing all boundary conditions, but permitting for general ω a discontinuity in one component of the eigenfunction at a suitable interior fitting point $r_{\rm f}$. The eigenfrequencies are then determined by requiring that the discontinuity vanish. I have found that this technique allows stable solution of the full set of equations for all relevant degrees and frequencies.

6.4 Formulation as a matrix eigenvalue problem

As discussed in Section 5.5 the equations of adiabatic oscillation, written as in equations (5.60) and (5.61), constitute a linear eigenvalue problem in function space. If the operator on the right hand side is discretized, the result is a linear discrete eigenvalue problem. By solving this, one obtains (approximations to) the eigenvalues and eigenfunctions of the continuous problem.

A method of this nature (but generalized to the non-adiabatic case) was used by Keeley (1977) for radial oscillations. Knölker & Stix (1983) used it for adiabatic non-radial oscillations in the Cowling approximation. In these cases, the operator describing the left hand side of the oscillation equations is a pure differential operator; hence its discrete representation only couples the solution at a few neighbouring meshpoints and results in an eigenvalue problem where the matrix is banded, with only a few off-diagonal elements. Consequently, efficient techniques exist for the determination of the eigenvalues. In contrast, in the full non-radial problem the terms in Φ' couple all parts of the model [see also equation (5.11)]; then the corresponding matrix is full, although for large l it is diagonally dominated, due to the factors $(r'/r)^{l+1}$ and $(r/r')^l$ occurring respectively in the first and second term on the right hand side of equation (5.11). In this case it is not evident that sufficiently fast algorithms exist for the determination of the matrix eigenvalues to make the technique competitive with the shooting or relaxation techniques. No attempt has apparently been made to apply it to this problem.

The matrix eigenvalue problem can also be derived directly from the variational principle as expressed in equation (5.77), by means of the so-called Rayleigh-Ritz method (*e.g.* Strang & Fix 1973). To do so the eigenfunction is expanded on a set of suitable basis functions, and the expansion coefficients are determined by imposing the condition that the expression (5.77) be stationary. Although this method has proven useful in atomic physics (*e.g.* B. L. Christensen-Dalsgaard 1982), the effects of the gravitational potential once again lead to a full matrix in the resulting eigenvalue problem.

I finally note that Pesnell (1990) has developed an efficient algorithm, based on the method of Castor (1971), for computing nonradial oscillations both in the adiabatic and the nonadiabatic case. This involves formulating the oscillation equations as a generalized linear algebraic eigenvalue problem; in contrast to the techniques discussed above, Poisson's equation is left on differential form, and hence the resulting matrices are sparse. Cox *et al.* (1989) applied this method to the computation of solar oscillations.

6.5 Richardson extrapolation

The difference scheme (6.2), which is used by at least some versions of the shooting, relaxation and matrix eigenvalue techniques, is of second order. Consequently the truncation errors in the eigenfrequency and eigenfunction scale as $N_{\rm me}^{-2}$. If $\omega(\frac{1}{2}N_{\rm me})$ and $\omega(N_{\rm me})$ are the eigenfrequencies obtained from solutions with $\frac{1}{2}N_{\rm me}$ and $N_{\rm me}$ meshpoints, the leading order error term therefore cancels in

$$\omega^{(\rm Ri)} \equiv 1/3[4\omega(N_{\rm me}) - \omega(1/2N_{\rm me})] \; . \tag{6.7}$$

The evaluation of $\omega^{(\rm Ri)}$, known as *Richardson extrapolation*, was used by Shibahashi & Osaki (1981) to compute frequencies of solar oscillation. This provides an estimate of the eigenfrequency that is substantially more accurate than $\omega(N_{\rm me})$, although of course at some added computational expense.

6.6 Variational frequencies

The variational property discussed in Section 5.5.2 can be used to obtain an estimate of the oscillation frequency which is at least formally more accurate than the frequency obtained as an eigenvalue of the solution of the oscillation equations (Christensen-Dalsgaard, Gough & Morgan 1979; J. Christensen-Dalsgaard 1982). It follows from equation (5.76) that if the computed eigenfunction is substituted into the functional $\Sigma(\xi)$, the result agrees with the squared eigenfrequency to within an error that is quadratic in the error in the eigenfunction. If the latter error goes as $N_{\rm me}^{-2}$, the error in $\Sigma(\xi)$ would be expected to vary as $N_{\rm me}^{-4}$; this assumes that the evaluation of $\Sigma(\xi)$, for given ξ, is sufficiently accurate.

For realistic solar models the complete expressions (5.77) or (5.79) must be used, including the surface terms. However, since these terms are in general relatively small, the variational property is still approximately satisfied. Hence the expressions may be used to provide estimates of the frequency which are less sensitive to numerical error than the eigenfrequency. On the other hand, it should be noted that the variational property, and the analysis leading to equations (5.77) and (5.79), assume that the solar model satisfies the equations of hydrostatic equilibrium and the mass equation exactly. When the model is itself the result of a numerical solution of the equations of stellar structure this is evidently not the case; then, even if they were to be evaluated with infinitely high precision for the given model, the variational frequency and the eigenfrequency would not agree. The discrepancy provides an estimate of the effect on the frequencies of the inconsistencies in the model. Examples of this were discussed by Christensen-Dalsgaard & Berthomieu (1991).

6.7 The determination of the mesh

Computational efficiency demands that the distribution of mesh points be chosen appropriately. It is immediately obvious from the eigenfunctions (*cf.* Figures 5.8 and 5.10 that a mesh uniform in r is far from optimal; also the distribution of points should clearly be different for p and for g modes.

Procedures exist that determine the optimal mesh as part of the numerical solution of a set of differential equations (Gough, Spiegel & Toomre 1975). In the present case, however, the requirements on the mesh are essentially driven by the behaviour of the modes of high

radial order, whose eigenfunctions are given, with considerable precision, by the asymptotic expression (5.22). Thus to have a roughly constant number of meshpoints between the nodes in the eigenfunction, the mesh should be approximately uniformly spaced in terms of the integral in this equation.

To define a flexible method for setting up the mesh I have adopted a simplified version of the procedure developed by Gough *et al.* (1975). Thus I introduce a variable z, with a range from 0 to 1, such that the mesh is uniform in z, and determined by

$$\frac{\mathrm{d}z}{\mathrm{d}r} = \lambda H(r) \; ; \tag{6.8}$$

here λ is a normalization constant, relating the ranges of z and r, and the function H determines the properties of the mesh. Given H, z is obtained as

$$z(r) = \lambda \int_0^r H(r')\mathrm{d}r' \; , \tag{6.9}$$

with

$$\lambda = \left(\int_0^R H(r)\mathrm{d}r \right)^{-1} \; . \tag{6.10}$$

The mesh $\{r^{(n)}, n = 1, \ldots, N_{\mathrm{me}}\}$ is finally determined by solving the equations

$$z(r^{(n)}) = \frac{n-1}{N_{\mathrm{me}}-1} \; , \tag{6.11}$$

by interpolating in the computed $z(r)$.

The choice of the function H must be guided by the asymptotic behaviour of the modes, as described by the function K in equation (5.22). Specifically, I have used

$$H(r)^2 = R^{-2} + c_1 \frac{\omega_{\mathrm{g}}^2}{c^2} + c_2 \frac{|N|^2}{\omega_{\mathrm{g}}^2 r^2} + c_3 \left(\frac{\mathrm{d}\ln p}{\mathrm{d}r} \right)^2 \; , \tag{6.12}$$

where $\omega_{\mathrm{g}}^2 \equiv GM/R^3 = t_{\mathrm{dyn}}^{-2}$ is a characteristic squared frequency. Here the term in c_1 results from noting that in the limit of an extreme p mode $K \propto c^{-2}$ [*cf.* equation (5.29)], whereas the term in c_2 similarly corresponds to the extreme g-mode case, where $K \propto N^2/r^2$ [*cf.* equation (5.33)]. The term in c_3 provides extra meshpoints near the surface, where the reflection of the p modes takes place. Finally the constant term ensures a reasonable resolution of regions where the other terms are small.

Table 6.1

	c_1	c_2	c_3
p-mode mesh	10.	0.01	0.015
g-mode mesh	0.025	0.1	0.0001

Table 6.1: Parameters in equation (6.12) for determination of meshes suitable for computing p and g modes in a model of the present Sun.

The parameters in this expression can be determined by testing the numerical accuracy of the computed frequencies (*e.g.* Christensen-Dalsgaard & Berthomieu 1991). For normal solar models reasonable choices, based on a fairly extensive (but far from exhaustive) set of calculations, are given in Table 6.1. In the p-mode case the mesh is predominantly determined by the variation of sound speed, with the term in N giving a significant contribution near the centre and the term in $\mathrm{d}\ln p/\mathrm{d}r$ contributing very near the surface. The g-mode mesh is dominated by the term in N in most of the radiative interior, whereas in the convection zone, where $|N|$ is generally small, the constant term dominates; the term in $\mathrm{d}\ln p/\mathrm{d}r$ is again important in the surface layers.

Chapter 7

Asymptotic theory of stellar oscillations

In Chapter 5 I discussed in a qualitative way how different modes of oscillation are trapped in different regions of the Sun. However, the simplified analysis presented there can, with a little additional effort, be made more precise and does in fact provide quite accurate quantitative information about the oscillations.

The second-order differential equation (5.17) derived in the previous chapter cannot be used to discuss the eigenfunctions. Thus in Section 7.1 I derive a more accurate second-order differential equation for ξ_r. In Section 7.2 the asymptotic solution of such equations by means of the JWKB method is briefly discussed, with little emphasis on mathematical rigour; the results are used to obtain asymptotic expressions for the eigenfrequencies and eigenfunctions. They are used in Sections 7.3 and 7.4 to discuss p and g modes. This approximation, however, is invalid near the surface, and furthermore suffers from critical points in the stellar interior where it formally breaks down. In Section 7.5 I discuss an asymptotic formulation derived by D. O. Gough (*cf.* Deubner & Gough 1984) that does not suffer from these problems; in particular, it incorporates the atmospheric behaviour of the oscillations analyzed in Section 5.4. On the other hand, it uses a dependent variable with a less obvious physical meaning. This method gives a unified asymptotic treatment of the oscillations throughout the Sun, although still under certain simplifying assumptions. A similar, but even more complete, treatment was developed by Gough (1993), although this appears so far not to have been substantially applied to numerical calculations.

One of the most important results of the asymptotic analysis is the so-called *Duvall relation*, which was first discovered by Duvall (1982) from analysis of observed frequencies of solar oscillation. A rough justification for the relation is given in Section 7.3, and a more rigorous derivation is presented in Section 7.5. It is shown that frequencies of p modes approximately satisfy

$$\int_{r_\mathrm{t}}^{R} \left(1 - \frac{L^2c^2}{\omega^2 r^2}\right)^{1/2} \frac{\mathrm{d}r}{c} = \frac{[n + \alpha(\omega)]\pi}{\omega} \,. \tag{7.1}$$

This is evidently a very special dependence of the frequencies on n and l. As discussed in Section 7.7, this relation gives considerable insight into the dependence of the frequencies on the sound speed, and it provides the basis for approximate, but quite accurate, methods for inferring the solar internal sound speed on the basis of observed frequencies.

7.1 A second-order differential equation for ξ_r

To obtain this equation I go back to the two equations (5.12) and (5.13) in the Cowling approximation. By differentiating equation (5.12) and eliminating $\mathrm{d}p'/\mathrm{d}r$ using equation (5.13) we obtain

$$\begin{aligned}\frac{\mathrm{d}^2\xi_r}{\mathrm{d}r^2} &= -\left(\frac{2}{r}-\frac{1}{\Gamma_1}H_p^{-1}\right)\frac{\mathrm{d}\xi_r}{\mathrm{d}r}-\left[-\frac{2}{r^2}-\frac{\mathrm{d}}{\mathrm{d}r}\left(\frac{1}{\Gamma_1}H_p^{-1}\right)\right]\xi_r \\ &\quad +\frac{1}{\rho c^2}\left(\frac{S_l^2}{\omega^2}-1\right)\left\{\rho(\omega^2-N^2)\xi_r-\frac{1}{\Gamma_1}H_p^{-1}p'\right. \\ &\quad \left.+\left[\frac{\mathrm{d}}{\mathrm{d}r}\ln\left|\frac{1}{\rho c^2}\left(\frac{S_l^2}{\omega^2}-1\right)\right|\right]p'\right\}\ . \end{aligned} \tag{7.2}$$

Here p' may be expressed in terms of ξ_r and its derivative by means of equation (5.12). The result is

$$\begin{aligned}\frac{\mathrm{d}^2\xi_r}{\mathrm{d}r^2} &= -\left(\frac{2}{r}-\frac{1}{\Gamma_1}H_p^{-1}\right)\frac{\mathrm{d}\xi_r}{\mathrm{d}r} \\ &\quad +\left[-\frac{1}{\Gamma_1}H_p^{-1}+\frac{\mathrm{d}}{\mathrm{d}r}\ln\left|\frac{1}{\rho c^2}\left(\frac{S_l^2}{\omega^2}-1\right)\right|\right]\frac{\mathrm{d}\xi_r}{\mathrm{d}r} \\ &\quad +[-K(r)+\tilde{h}(r)]\xi_r\ , \end{aligned} \tag{7.3}$$

where K is still given by equation (5.21). All other terms in ξ_r are lumped together in $\tilde{h}$; these contain derivatives of equilibrium quantities, and so may be assumed to be negligible compared with K (except, as usual, near the surface). Equation (7.3) may also be written as

$$\frac{\mathrm{d}^2\xi_r}{\mathrm{d}r^2}-\frac{\mathrm{d}\ln f}{\mathrm{d}r}\frac{\mathrm{d}\xi_r}{\mathrm{d}r}+[K(r)-\tilde{h}(r)]\xi_r=0\ , \tag{7.4}$$

where

$$f(r)=\frac{1}{\rho r^2c^2}\left|\frac{S_l^2}{\omega^2}-1\right|\ . \tag{7.5}$$

It should be noticed that the principal difference between equation (7.4) and equation (5.20) derived previously is the presence of a term in $\mathrm{d}\xi_r/\mathrm{d}r$. This occurs because I have now not neglected the term in ξ_r on the right-hand side of equation (5.12), and the corresponding term in p' in equation (5.13). These terms cannot be neglected if ξ_r is rapidly varying, as assumed.

It is convenient to work with an equation without a first derivative, on the form of equation (5.20). I introduce $\hat{\xi}_r$ by

$$\xi_r(r)=f(r)^{1/2}\hat{\xi}_r(r)\ ; \tag{7.6}$$

$\hat{\xi}_r$ satisfies

$$\frac{\mathrm{d}^2\hat{\xi}_r}{\mathrm{d}r^2}+[K(r)-h(r)]\hat{\xi}_r=0\ , \tag{7.7}$$

where

$$h(r)=\tilde{h}(r)-\frac{1}{2}\frac{\mathrm{d}^2\ln f}{\mathrm{d}r^2}+\frac{1}{4}\left(\frac{\mathrm{d}\ln f}{\mathrm{d}r}\right)^2\ . \tag{7.8}$$

Here h, like $\tilde{h}$, is generally small compared with K. When it is neglected asymptotically, equation (7.7) is identical to equation (5.20), apart from the change of the dependent variable. In particular, the trapping properties of the modes, as inferred from this analysis, are the same as obtained previously.

It is obvious that the derivation of equation (7.7) fails near points where $\omega^2 = S_l^2$, and where consequently f has a singular logarithmic derivative. These are the turning points of p modes. This problem can be avoided by deriving instead a second-order differential equation for p' (see Unno *et al.* 1989, Chapter 16); but, hardly surprisingly, this equation has problems at the turning points for the g modes. It is possible to develop a coherent asymptotic theory by suitably combined use of these two equations; a more convenient approach, however, is to use a second-order equation that is valid throughout the model. I return to this in Section 7.5, but base the initial asymptotic analysis on the somewhat simpler equation (7.7).

7.2 The JWKB analysis

To analyze equation (7.7) asymptotically I use the JWKB method (for Jeffreys, Wentzel, Kramers and Brillouin; in fact the method seems to have been first used by Liouville). It is widely used in quantum mechanics (see *e.g.* Schiff 1949, Section 34), and is also described in Unno *et al.* (1989), Chapter 16. It is possible to provide a firm mathematical foundation for the method; knowing that this is so, it is enough here to sketch how it works, without worrying too much about its convergence properties.

The assumption is that the solution varies rapidly compared with equilibrium quantities, *i.e.*, compared with $K(r)$. Thus I write it as

$$\hat{\xi}_r(r) = a(r) \exp[i\Psi(r)] \; , \tag{7.9}$$

where Ψ is rapidly varying, so that the local radial wave number

$$k_r = \frac{\mathrm{d}\Psi}{\mathrm{d}r} \tag{7.10}$$

is large; $a(r)$ is a slowly varying amplitude function. Formally, it is always possible to write the solution in this form. If equation (7.9) is substituted into equation (7.7), neglecting h, one obtains

$$\left(\frac{\mathrm{d}^2 a}{\mathrm{d}r^2} + 2ik_r \frac{\mathrm{d}a}{\mathrm{d}r} + ia \frac{\mathrm{d}k_r}{\mathrm{d}r} - k_r^2 a \right) \exp(i\Psi) = -K(r) a(r) \exp(i\Psi) \; . \tag{7.11}$$

On the left-hand side the dominant term is the one containing k_r^2; to ensure that this term cancels with the right-hand side, k_r must be chosen as

$$k_r(r) = K(r)^{1/2} \; . \tag{7.12}$$

The next-order terms are those in k_r which must cancel. Thus

$$\frac{1}{a}\frac{\mathrm{d}a}{\mathrm{d}r} = -\frac{1}{2}\frac{1}{k_r}\frac{\mathrm{d}k_r}{\mathrm{d}r} \; , \tag{7.13}$$

or, apart from a constant factor,

$$a(r) = |k_r|^{-1/2} = |K(r)|^{-1/4} \; . \tag{7.14}$$

This leaves in equation (7.11) only a term in the second derivative of a. The asymptotic approximation consists of neglecting this term, which by the assumption is small compared with $k_r^2 a$. Then the approximate solution is completely specified by equations (7.12) and (7.14). Since the solution may be chosen to be real, it can be written as

$$\hat{\xi}_r(r) = A\,|K(r)|^{-1/4} \cos\left(\int_{r_0}^{r} K(r')^{1/2}\mathrm{d}r' + \phi\right) , \qquad \text{for} \quad K(r) > 0 , \tag{7.15}$$

or

$$\begin{aligned}\hat{\xi}_r(r) \;=\; & |K(r)|^{-1/4}\left[A_+ \exp\left(\int_{r_0}^{r} |K(r')|^{1/2}\mathrm{d}r'\right) + A_- \exp\left(-\int_{r_0}^{r} |K(r')|^{1/2}\mathrm{d}r'\right)\right] \\ & \text{for} \quad K(r) < 0 ,\end{aligned} \tag{7.16}$$

for some suitable r_0. Here A and ϕ, or A_+ and A_-, are real constants which must be determined from the boundary conditions.

Notice that this solution has the property of being locally exponential where $K < 0$. Thus it is in accordance with the discussion in Section 5.2. On the other hand, it breaks down at the zeros of K; formally this may be seen from the fact that there a, as obtained in equation (7.12), is singular, and its second derivative cannot be neglected in equation (7.11). Thus we need to make a special analysis of the points where $K = 0$. In particular, this is required to connect the solution in the exponential and oscillatory regions, and hence apply the boundary conditions.

I consider a turning point r_1 such that $K(r) < 0$ for $r < r_1$ and $K(r) > 0$ for $r > r_1$. If r_1 is a simple zero for K, close to r_1 we have approximately that

$$K(r) \simeq K_1(r - r_1) , \tag{7.17}$$

where $K_1 > 0$ is a constant. I introduce the new independent variable x by

$$x = K_1^{1/3}(r - r_1) ; \tag{7.18}$$

then the equation for $\hat{\xi}_r$ can be approximated by

$$\frac{\mathrm{d}^2\hat{\xi}_r}{\mathrm{d}x^2} = -x\hat{\xi}_r , \tag{7.19}$$

with the solution

$$\hat{\xi}_r(r) = C_1 \mathrm{Ai}\,(-x) + C_2 \mathrm{Bi}\,(-x) , \tag{7.20}$$

where C_1 and C_2 are constants, and Ai and Bi are the Airy functions (*e.g.* Abramowitz & Stegun 1964).

To be definite, I consider a solution that is trapped in the oscillatory region outside r_1, and hence we need to choose the constants C_1 and C_2 such as to select the solution that decreases exponentially as r decreases beneath r_1. When $x < 0$, and $|x|$ is large, $\mathrm{Ai}\,(-x)$ and $\mathrm{Bi}\,(-x)$ have the following asymptotic behaviour:

$$\begin{aligned}\mathrm{Ai}\,(-x) \;&\simeq\; \frac{1}{2\sqrt{\pi}}\,|x|^{-1/4} \exp\left(-\frac{2}{3}|x|^{3/2}\right) , \\ \mathrm{Bi}\,(-x) \;&\simeq\; \frac{1}{\sqrt{\pi}}\,|x|^{-1/4} \exp\left(\frac{2}{3}|x|^{3/2}\right) .\end{aligned} \tag{7.21}$$

Thus we must require that $C_2 = 0$, and the solution satisfying the boundary condition for $r < r_1$ is therefore

$$\hat{\xi}_r(r) = C_1 \mathrm{Ai}\,(-x)\ . \tag{7.22}$$

We can use this solution to determine the phase ϕ in equation (7.15). For large positive x the asymptotic expansion of $\mathrm{Ai}\,(-x)$ is

$$\mathrm{Ai}\,(-x) \simeq \frac{1}{\sqrt{\pi}}|x|^{-1/4}\cos\left(\frac{2}{3}x^{3/2} - \frac{\pi}{4}\right)\ . \tag{7.23}$$

This must agree with what is obtained from equation (7.15), assuming that there is a region where both this equation and the approximation in equation (7.23) are valid. From the expansion of K in equation (7.17) we obtain

$$\Psi = \int_{r_1}^{r} K(r')^{1/2}\mathrm{d}r' + \phi = \frac{2}{3}x^{3/2} + \phi\ , \tag{7.24}$$

so that equation (7.15) gives

$$\hat{\xi}_r \simeq A K_1^{-1/6} x^{-1/4}\cos\left(\frac{2}{3}x^{3/2} + \phi\right)\ . \tag{7.25}$$

This agrees with equation (7.23) if

$$\phi = -\frac{\pi}{4}\ . \tag{7.26}$$

Sufficiently far from the turning point r_1 the JWKB solution satisfying the boundary conditions at $r = r_1$ is thus

$$\hat{\xi}_r(r) = A_1|K(r)|^{-1/4}\cos\left(\int_{r_1}^{r} K(r')^{1/2}\mathrm{d}r' - \frac{\pi}{4}\right)\ . \tag{7.27}$$

Similarly, if there is an outer turning point at $r = r_2$, so that $K(r) > 0$ for $r < r_2$ and $K(r) < 0$ for $r > r_2$, one finds that the asymptotic solution that is exponentially decaying for $r > r_2$ is

$$\hat{\xi}_r(r) = A_2|K(r)|^{-1/4}\cos\left(\int_{r}^{r_2} K(r')^{1/2}\mathrm{d}r' - \frac{\pi}{4}\right)\ . \tag{7.28}$$

Exercise 7.1:

Verify this.

To obtain the full solution we must match the two separate solutions smoothly at a suitable point between r_1 and r_2, $r = r_{\mathrm{f}}$, say. I define

$$\begin{aligned}\Psi_1 \ &\equiv\ \Psi_1(r_{\mathrm{f}}) = \int_{r_1}^{r_{\mathrm{f}}} K(r)^{1/2}\mathrm{d}r - \frac{\pi}{4}\ ,\\ \Psi_2 \ &\equiv\ \Psi_2(r_{\mathrm{f}}) = \int_{r_{\mathrm{f}}}^{r_2} K(r)^{1/2}\mathrm{d}r - \frac{\pi}{4}\ .\end{aligned} \tag{7.29}$$

Then the conditions that both $\hat{\xi}_r$ and its first derivative be continuous at $r = r_\mathrm{f}$ give

$$\begin{aligned} A_1 K(r_\mathrm{f})^{-1/4} \cos\Psi_1 &= A_2 K(r_\mathrm{f})^{-1/4} \cos\Psi_2 \ , \\ -A_1 K(r_\mathrm{f})^{-1/4} \sin\Psi_1 &= A_2 K(r_\mathrm{f})^{-1/4} \sin\Psi_2 \ . \end{aligned} \tag{7.30}$$

Notice that in the derivative I have neglected terms coming from the differentiation of K; these are small compared with the term included. These linear equations for A_1, A_2 only have a non-trivial solution if their determinant vanishes. This leads to

$$\sin\Psi_1 \cos\Psi_2 + \cos\Psi_1 \sin\Psi_2 = \sin(\Psi_1 + \Psi_2) = 0 \ , \tag{7.31}$$

or

$$\Psi_1 + \Psi_2 = (n-1)\pi \ , \tag{7.32}$$

where n is an integer. Thus

$$\int_{r_1}^{r_2} K(r)^{1/2} \mathrm{d}r = (n - \frac{1}{2})\pi, \qquad n = 1, 2, \ldots \ . \tag{7.33}$$

Here K depends on the frequency ω; thus equation (7.33) implicitly determines the frequencies of the modes trapped between r_1 and r_2. In addition, we find that $A_1 = A_2$.

We can also find the asymptotic behaviour of the eigenfunctions. From the definition of $\hat{\xi}_r$, equations (7.5) and (7.6), it follows from equation (7.27) that for $r_1 < r < r_2$

$$\begin{aligned} \xi_r(r) &= \tilde{A} \rho^{-1/2} r^{-1} c^{-1} \left| \frac{S_l^2}{\omega^2} - 1 \right|^{1/2} |K(r)|^{-1/4} \cos\left(\int_{r_1}^{r} K(r')^{1/2} \mathrm{d}r' - \frac{\pi}{4} \right) \\ &= A \rho^{-1/2} r^{-1} c^{-1/2} \left| \frac{S_l^2/\omega^2 - 1}{N^2/\omega^2 - 1} \right|^{1/4} \cos\left(\int_{r_1}^{r} K(r')^{1/2} \mathrm{d}r' - \frac{\pi}{4} \right) \ , \end{aligned} \tag{7.34}$$

where $A = \tilde{A}\, \omega^{-1/2}$. This expression is clearly valid only at some distance from the turning points, where the asymptotic approximation (7.23) can be used. Thus the apparently singular behaviour in $|\cdots|$ causes no problems.

Notice that in equation (7.34) $c^{-1/2}$ (which is proportional to $T^{-1/4}$) and $|\cdots|^{1/4}$ vary relatively little through the region where the modes are trapped. Thus the variation of ξ_r through the Sun is dominated by $\rho^{-1/2} r^{-1}$. This is the reason why I plotted the eigenfunction in terms of $\rho^{1/2} r \xi_r(r)$ in Figures 5.8 and 5.10.

We can also find the solution in the exponential regions, by using the asymptotic expansion for Ai in equation (7.21). The results are, for the solution corresponding to equation (7.34) in the trapping region

$$\begin{aligned} \xi_r(r) &\simeq \frac{1}{2} A \rho^{-1/2} r^{-1} c^{-1/2} \left| \frac{S_l^2/\omega^2 - 1}{N^2/\omega^2 - 1} \right|^{1/4} \exp\left(- \int_{r}^{r_1} \left| K(r') \right|^{1/2} \mathrm{d}r' \right) \\ &\qquad \text{for } r < r_1 \ , \end{aligned} \tag{7.35}$$

and

$$\begin{aligned} \xi_r(r) &\simeq \frac{1}{2} A \rho^{-1/2} r^{-1} c^{-1/2} \left| \frac{S_l^2/\omega^2 - 1}{N^2/\omega^2 - 1} \right|^{1/4} \exp\left(- \int_{r_2}^{r} \left| K(r') \right|^{1/2} \mathrm{d}r' \right) \\ &\qquad \text{for } r > r_2 \ . \end{aligned} \tag{7.36}$$

7.3 Asymptotic theory for p modes

For high frequencies we may, as in Section 5.2, approximate K by

$$K(r) \simeq \frac{1}{c^2}(\omega^2 - S_l^2) \; . \tag{7.37}$$

As discussed previously the theory, as formulated so far, does not provide reflection at the surface. Mathematically, this is expressed by the lack of a turning point near the surface. Also, the formulation fails near the point where $\omega = S_l$ where the neglected term $h(r)$ in (7.8) is singular. Thus equation (7.33) for the eigenfrequencies cannot immediately be used. It is shown in Section 7.5 below that a proper treatment of the surface and the lower turning point leads to an asymptotic behaviour similar to that discussed above; however, the effective phase shift in the equation corresponding to (7.33) is different. Thus the frequencies for the p modes approximately satisfy

$$\int_{r_\mathrm{t}}^{R} (\omega^2 - S_l^2)^{1/2} \frac{\mathrm{d}r}{c} = (n + \alpha)\pi \; , \tag{7.38}$$

where α is a new phase constant, which contains the contribution 1/4 from the inner turning point, and an, as yet unidentified, contribution from the outer turning point. It is convenient to write this equation as

$$\int_{r_\mathrm{t}}^{R} \left(1 - \frac{L^2}{\omega^2}\frac{c^2}{r^2}\right)^{1/2} \frac{\mathrm{d}r}{c} = \frac{(n + \alpha)\pi}{\omega} \; , \tag{7.39}$$

where $L^2 = l(l+1)$. Notice that the left-hand side of this equation is a function of $w = \omega/L$ [it follows from equation (5.28) that r_t is determined by ω/L]; thus equation (7.39) can be written as

$$\frac{\pi(n + \alpha)}{\omega} = F\left(\frac{\omega}{L}\right) \; , \tag{7.40}$$

where

$$F(w) = \int_{r_\mathrm{t}}^{R} \left(1 - \frac{c^2}{r^2 w^2}\right)^{1/2} \frac{\mathrm{d}r}{c} \; . \tag{7.41}$$

The observed and computed frequencies in fact satisfy relations like equation (7.40) quite closely; this was first noticed by Duvall (1982) for the observed frequencies. An example is illustrated in Figure 7.1.

When the function $F(w)$ is known from observations, equation (7.41) can be inverted to determine $c(r)$. I return to this in Section 7.7.

It is instructive to consider a special case of this equation, which is furthermore a reasonable approximation to the Sun. The solar convection zone is approximately adiabatically stratified, so that

$$\frac{\mathrm{d}\ln p}{\mathrm{d}r} = \Gamma_1 \frac{\mathrm{d}\ln \rho}{\mathrm{d}r} \; ; \tag{7.42}$$

here I assume Γ_1 to be constant (this is evidently not true in the ionization zones of H and He, but they only occupy the outer few per cent of the Sun). We may also assume that g is constant. Finally I take as boundary conditions on the equilibrium structure that $p = \rho = 0$ at $r = R$. With these assumptions the sound speed is given by

$$c^2 = \frac{g}{\mu_\mathrm{p}}(R - r) \; , \tag{7.43}$$

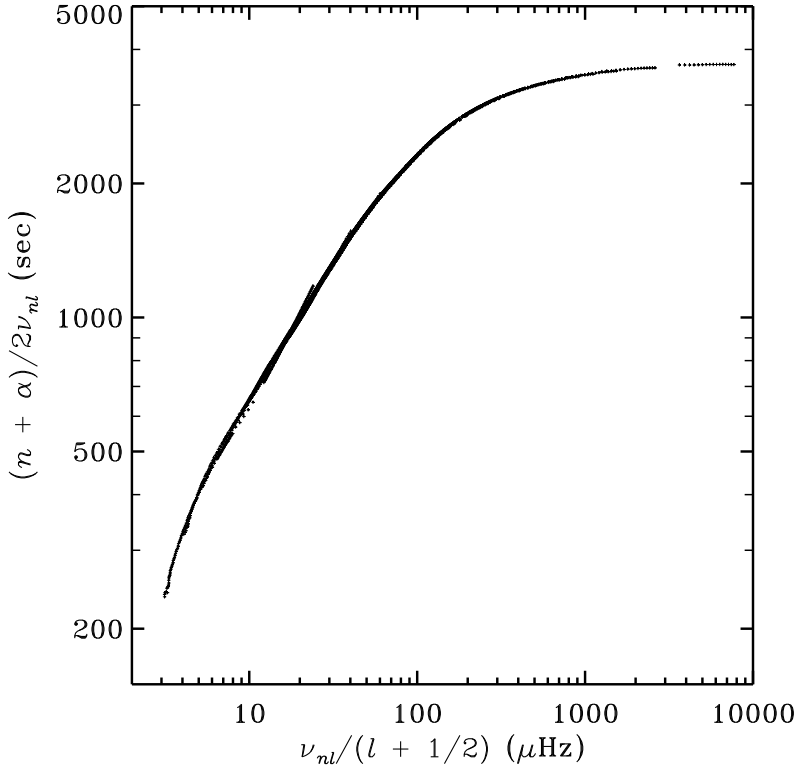

Figure 7.1: Observed frequencies of solar oscillation, plotted according to equation (7.40). The constant value of α, 1.45, was determined such as to minimize the spread in the relation (7.40). (Adapted from Christensen-Dalsgaard *et al.* 1985.)

where $\mu_{\rm p} = 1/(\Gamma_1 - 1)$ is an effective polytropic index of the region considered. I also treat the layer as plane parallel, so that r can be replaced by R in the integral in equation (7.41). Then the integral may easily be evaluated, to yield

$$F(w) = \frac{\pi}{2}\, w\, \frac{\mu_{\rm p} R}{g}\ . \tag{7.44}$$

Exercise 7.2:

Derive equations (7.43) and (7.44).

Thus the dispersion relation (7.40) gives

$$\omega^2 = \frac{2}{\mu_{\rm p}}\frac{g}{R}(n+\alpha)L\ . \tag{7.45}$$

In particular, ω is proportional to $L^{1/2}$. This property is approximately satisfied by the computed (and observed) frequencies at high degree (*cf.* Figure 5.6). Indeed, equation (7.45) might be expected to be approximately valid for modes whose degree is so high that they are entirely trapped within the convection zone.

For modes of low degree, r_t is very close to the centre (see Figure 5.5). In equation (7.39), therefore, the second term in the bracket on the left-hand side is much smaller than unity over most of the range of integration. To exploit this, I consider the difference

$$\begin{aligned} I &= \int_0^R \frac{\mathrm{d}r}{c} - \int_{r_t}^R \left(1 - \frac{c^2}{w^2 r^2}\right)^{1/2} \frac{\mathrm{d}r}{c} \\ &= \int_0^{r_t} \frac{\mathrm{d}r}{c} + \int_{r_t}^R \left[1 - \left(1 - \frac{c^2}{w^2 r^2}\right)^{1/2}\right] \frac{\mathrm{d}r}{c} \\ &\equiv I_1 + I_2 \ , \end{aligned} \tag{7.46}$$

where $w = \omega/L$. Notice that c is almost constant near the centre (it may be shown that the first derivative of c is zero at $r = 0$). Thus I take c to be constant in the first integral, and obtain

$$I_1 = \frac{r_t}{c(0)} \simeq \frac{L}{\omega} = \frac{1}{w} \ , \tag{7.47}$$

by using equation (5.28). In the second integral the integrand is only substantially different from zero for r close to r_t, which was assumed to be small. Thus here I also approximate c by its value at $r = 0$. Furthermore, the upper limit of integration may be replaced by ∞. Then we obtain

$$I_2 = \frac{1}{w} \int_0^1 \left[1 - \left(1 - u^2\right)^{1/2}\right] \frac{\mathrm{d}u}{u^2} = \frac{1}{w} \left(\frac{\pi}{2} - 1\right) \ . \tag{7.48}$$

Thus, finally,

$$I = \frac{1}{w} \frac{\pi}{2} \ , \tag{7.49}$$

and equation (7.39) may be approximated by

$$\int_0^R \frac{\mathrm{d}r}{c} - \frac{L}{\omega} \frac{\pi}{2} = \frac{(n + \alpha)\pi}{\omega} \ , \tag{7.50}$$

or

$$\omega = \frac{(n + L/2 + \alpha)\pi}{\displaystyle\int_0^R \frac{\mathrm{d}r}{c}} \ . \tag{7.51}$$

The derivation of equation (7.51) clearly lacks rigour. However, it may be shown from a more careful asymptotic analysis of the central region (*e.g.* Vandakurov 1967; Tassoul 1980) that the result is correct to leading order, except that L should be replaced by $l + 1/2$. Equation (7.51) may also be written as

$$\nu_{nl} = \frac{\omega_{nl}}{2\pi} \simeq (n + \frac{l}{2} + \frac{1}{4} + \alpha)\Delta\nu \ , \tag{7.52}$$

where

$$\Delta\nu = \left[2 \int_0^R \frac{\mathrm{d}r}{c}\right]^{-1} \tag{7.53}$$

is the inverse of twice the sound travel time between the centre and the surface. This equation predicts a uniform spacing $\Delta\nu$ in n of the frequencies of low-degree modes. Also, modes with the same value of $n + l/2$ should be almost degenerate,

$$\nu_{nl} \simeq \nu_{n-1\,l+2} \; . \tag{7.54}$$

This frequency pattern has been observed for the solar five-minute modes of low degree (*cf.* Chapter 2), and may be used in the search for stellar oscillations of solar type. In fact, as shown in Figure 5.14 it is visible even down to very low radial order for computed frequencies of models near the zero-age main sequence.

The *deviations* from the simple relation (7.52) have considerable diagnostic potential. The expansion of equation (7.39), leading to equation (7.51), can be extended to take into account the variation of c in the core (Gough 1986a); alternatively it is possible to take the JWKB analysis of the oscillation equations to higher order (Tassoul 1980). The result may be written as

$$\nu_{nl} \simeq (n + \frac{l}{2} + \frac{1}{4} + \alpha)\Delta\nu - (AL^2 - \delta)\frac{\Delta\nu^2}{\nu_{nl}} \; , \tag{7.55}$$

where

$$A = \frac{1}{4\pi^2\Delta\nu}\left[\frac{c(R)}{R} - \int_0^R \frac{\mathrm{d}c}{\mathrm{d}r}\frac{\mathrm{d}r}{r}\right] \; . \tag{7.56}$$

Hence

$$\delta\nu_{nl} \equiv \nu_{nl} - \nu_{n-1\,l+2} \simeq -(4l+6)\frac{\Delta\nu}{4\pi^2\nu_{nl}}\int_0^R \frac{\mathrm{d}c}{\mathrm{d}r}\frac{\mathrm{d}r}{r} \; , \tag{7.57}$$

where I neglected the term in the surface sound speed $c(R)$. It is often convenient to represent observed or computed frequencies in terms of a limited set of parameters associated with the asymptotic description of the modes. This may be accomplished by fitting the asymptotic expression to the frequencies. By carrying out a polynomial fit in the quantity $x - x_0$, where $x = n + l/2$ and x_0 is a suitable reference value (Scherrer *et al.* 1983, Christensen-Dalsgaard 1988b) one obtains the average over n of $\delta\nu_{nl}$ as

$$\langle\delta\nu_{nl}\rangle_n \simeq (4l+6)D_0 \; , \tag{7.58}$$

where

$$D_0 \simeq -\frac{1}{4\pi^2 x_0}\int_0^R \frac{\mathrm{d}c}{\mathrm{d}r}\frac{\mathrm{d}r}{r} \; . \tag{7.59}$$

Thus $\delta\nu_{nl}$ is predominantly determined by conditions in the stellar core. Physically, this may be understood from the fact that only near the centre is k_h comparable with k_r. Elsewhere the wave vector is almost vertical, and the dynamics of the oscillations is largely independent of their horizontal structure, *i.e.*, of l; therefore at given frequency the contributions of these layers to the frequency are nearly the same, and hence almost cancel in the difference in equation (7.57).

It should be noted that the accuracy of expressions (7.58) and (7.59) is questionable; they appear to agree fortuitously with frequencies computed for models of the present Sun, whereas they are less successful for models of different ages or masses (Christensen-Dalsgaard 1991a). However, the form of the dependence of $\langle\delta\nu_{nl}\rangle_n$ on l shown in equation (7.58), as well as the argument that this quantity is most sensitive to conditions in stellar cores, probably have a broader range of validity. As a star evolves, the hydrogen abundance

in the core decreases and hence the mean molecular weight increases. For an approximately ideal gas, the sound speed may be obtained from

$$c^2 \simeq \frac{\Gamma_1 k_{\rm B} T}{\mu m_{\rm u}} \; ; \tag{7.60}$$

since the central temperature varies little during hydrogen burning, due to the strong temperature sensitivity of the nuclear reaction rates, the main effect on the sound speed in the core comes from the change in the mean molecular weight μ. Consequently c decreases as the star evolves, the decrease being most rapid at the centre where hydrogen burning is fastest. As a result, c develops a local minimum at the centre, and $\mathrm{d}c/\mathrm{d}r$ is positive in the core. This region gives a negative contribution to D_0 (*cf.* eq. 7.57), of increasing magnitude with increasing age, and hence D_0 decreases with increasing age (see also Christensen-Dalsgaard 1991a). Hence D_0, which can in principle be observed, is a measure of the evolutionary state of the star. On the other hand, the overall frequency separation $\Delta\nu$, defined in equation (7.53), approximately scales as the inverse of the dynamical time scale which, for main-sequence stars, is largely determined by the mass.

These considerations motivate presenting the average frequency separations in a $(\Delta\nu_0, D_0)$ diagram, as illustrated in Figure 7.2; this is analogous to the ordinary Hertzsprung-Russell diagram. As shown in panel (b) (note the different scales) most of the variation in $\Delta\nu_0$ is in fact related to $t_{\rm dyn}$, such that $\Delta\nu_0$ scales as $M^{1/2}/R^{3/2}$. It is evident from Figure 7.2 that on the assumption that the other parameters of the star (such as composition) are known, a measurement of $\Delta\nu$ and D_0 may allow determination of the mass and evolutionary state of the star (Christensen-Dalsgaard 1984b; Ulrich 1986, 1988; Christensen-Dalsgaard 1988b). On the other hand, Gough (1987) analyzed the sensitivity of this result to the other stellar parameters, and found that the uncertainty in the knowledge of the heavy element abundance, in particular, had a severe effect on the determination of the mass and age. As an example of such sensitivity, Figure 7.2(c) shows the consequences of an increase of the hydrogen abundance by 0.03. A careful analysis of the information content in measured frequency separations, when combined with more traditional measurements of stellar properties, was given by Brown *et al.* (1994).

The eigenfunctions of p modes can be found from equation (7.34). It is convenient to use equation (7.38) to get

$$\int_{r_{\rm t}}^{r} K(r')^{1/2} \mathrm{d}r' = -\int_{r}^{R} K(r')^{1/2} \mathrm{d}r' + (n+\alpha)\pi \; , \tag{7.61}$$

so that we obtain

$$\xi_r(r) \simeq \tag{7.62}$$
$$A\rho^{-1/2} c^{-1/2} r^{-1} \left| 1 - \frac{S_l^2}{\omega^2} \right|^{1/4} \cos\left[\omega \int_r^R \left(1 - \frac{S_l^2}{\omega^2} \right)^{1/2} \frac{\mathrm{d}r'}{c} - (-1/4 + \alpha)\pi \right] \; ,$$

where I have again neglected N^2/ω^2. However, the derivation neglects the fact that the present simple asymptotic description breaks down near the lower turning point. As shown in Section 7.5, a more appropriate treatment gives essentially the same result, except that the term $-1/4$ in equation (7.62) must be replaced by $1/4$. Also, to simplify this expression further I note that S_l^2 decreases quite rapidly with increasing r. Near $r = r_{\rm t}$, ω^2 and S_l^2 are

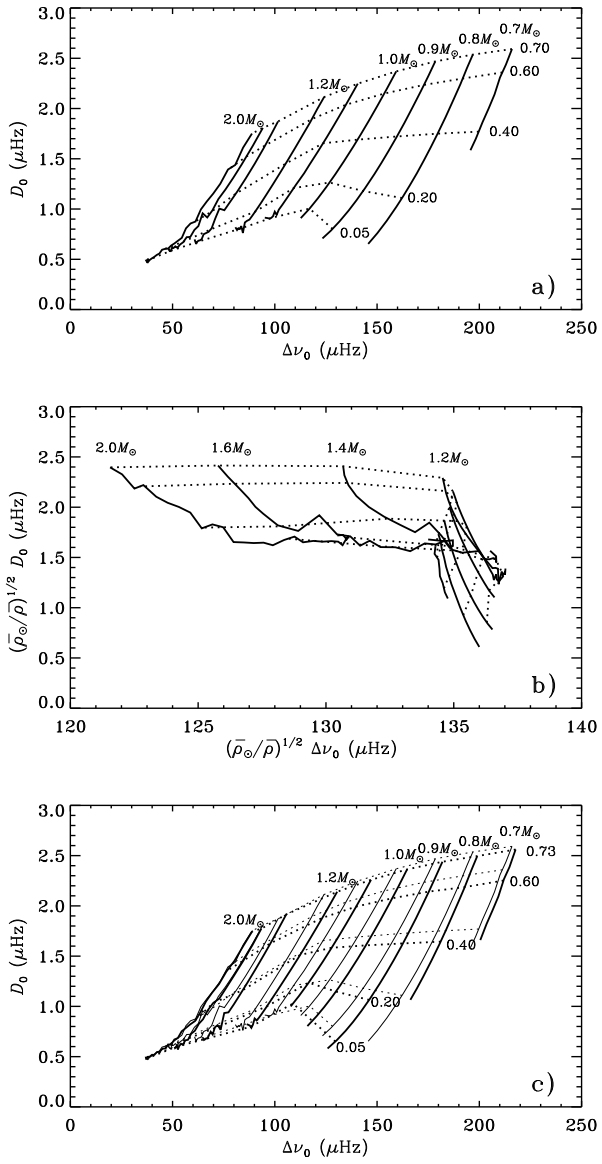

Figure 7.2: Evolution tracks (————) and curves of constant central hydrogen abundance (·····) in $(\Delta\nu_0, D_0)$ diagrams. Here $\Delta\nu_0$ is the average separation between modes of the same degree and adjacent radial order, and D_0 is related to the small separation between ν_{nl} and $\nu_{n-1\,l+2}$ (*cf.* eq. 7.58). The stellar masses, in solar units, and the values of the central hydrogen abundance, are indicated. In panel (b), the frequency separations have been scaled by $(\overline{\rho})^{-1/2}$ ($\overline{\rho} \propto M/R^3$ being the mean density), to take out the variation with $t_{\rm dyn}^{-1}$. Panel (c) shows the effect of increasing the hydrogen abundance by 0.03 (heavy lines), relative to the case presented in panel (a) (shown here with thin lines). (From Christensen-Dalsgaard 1993b.)

comparable, but at some distance from the turning point we can assume that $S_l^2/\omega^2 \ll 1$. Here, therefore

$$\xi_r(r) \simeq A\rho^{-1/2}c^{-1/2}r^{-1}\cos\left[\omega\int_r^R \frac{\mathrm{d}r'}{c} - (1/4+\alpha)\pi\right] . \tag{7.63}$$

To this approximation the eigenfunction is independent of l. Oscillations with the same frequency but different l therefore have approximately the same eigenfunctions near the surface, if they are normalized to the same surface value. This was also seen in Figure 5.8. This property is important for the interpretation of the observed frequencies. It may be understood physically in the following way: near the surface the vertical wavelength is much shorter than the horizontal wavelength (*i.e.*, $k_r \gg k_\mathrm{h}$); the tangential component of the displacement therefore has essentially no influence on the dynamics of the oscillation, which is consequently independent of l.

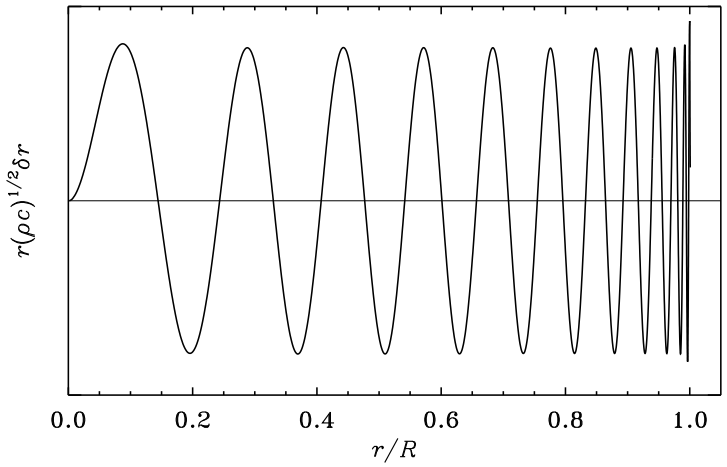

Figure 7.3: Scaled eigenfunction for radial p mode of order $n = 23$ and frequency $\nu = 3310\,\mu$Hz in a normal solar model (the same mode as was shown in Figure 5.8a). According to the asymptotic equation (7.63) the quantity plotted should oscillate between fixed limits in the region where the mode is trapped.

From equation (7.63) one should expect that $c^{1/2}\rho^{1/2}r\,\xi_r(r)$ behaves like a cosine function with a non-uniform argument. This is confirmed to high accuracy by Figure 7.3. Thus equation (7.63) in fact gives a reasonable description of the eigenfunctions of high-order p modes in the region where they are trapped.

7.4 Asymptotic theory for g modes

For these in general $\omega^2 \ll S_l^2$, and I approximate K by

$$K(r) \simeq \frac{l(l+1)}{r^2} \left(\frac{N^2}{\omega^2} - 1 \right) . \tag{7.64}$$

Typically a mode is trapped between two zeros r_1 and r_2 of K, and equation (7.33) is immediately valid. Thus the frequencies are determined by

$$\int_{r_1}^{r_2} L \left(\frac{N^2}{\omega^2} - 1 \right)^{1/2} \frac{\mathrm{d}r}{r} = (n - 1/2)\pi , \tag{7.65}$$

or

$$\int_{r_1}^{r_2} \left(\frac{N^2}{\omega^2} - 1 \right)^{1/2} \frac{\mathrm{d}r}{r} = \frac{(n - 1/2)\pi}{L} . \tag{7.66}$$

Here the left-hand side is solely a function of ω, so that equation (7.66) can be written, in analogy with equation (7.40), as

$$\frac{n - 1/2}{L} = G(\omega) , \tag{7.67}$$

where

$$G(\omega) = \frac{1}{\pi} \int_{r_1}^{r_2} \left(\frac{N^2}{\omega^2} - 1 \right)^{1/2} \frac{\mathrm{d}r}{r} . \tag{7.68}$$

I have here implicitly assumed that N has a single maximum, so that there is a single, well-defined trapping region at each frequency. In many stellar models, including some models of the Sun, there may be several maxima in N, and this may give rise to, at least mathematically, interesting phenomena. Roughly speaking, to each maximum there corresponds asymptotically a separate spectrum of g modes; where modes corresponding to different regions happen to have nearly the same frequencies, the modes may interact in "avoided crossings" (*e.g.* Christensen-Dalsgaard, Dziembowski & Gough 1980).

In the model illustrated in Figure 5.2 N has a weak secondary maximum near $r/R = 0.35$, and at a frequency of about $410\,\mu$Hz; this is in fact faintly reflected in the behaviour of the frequencies shown in Figure 5.6, where there is an accumulation of modes at this frequency, for $l > 15$. I neglect this local maximum and assume that N has a single maximum, $N_{\max}$, in the interior of the Sun; from equation (7.68) it then follows that

$$G(\omega) \to 0 \qquad \text{for } \omega \to N_{\max} . \tag{7.69}$$

Consequently

$$\omega \to N_{\max} \qquad \text{for } L \to \infty . \tag{7.70}$$

This behaviour is clearly visible in Figures 5.6 and 5.7.

For high-order, low-degree g modes ω is much smaller than N over most of the interval $[r_1, r_2]$. This suggests that a similar approximation to the one leading to equation (7.51) should be possible. In fact, the integral may be expanded near the centre, in much the same way as the integral in equation (7.39), by using the fact that $N \sim r$ near $r = 0$. However, the expansion near the upper turning point can apparently not be done in a similarly

simple fashion, and in any case the result does not quite have the correct dependence on l. A proper asymptotic analysis (Tassoul 1980) shows that the frequencies of low-degree, high-order g modes are given by

$$\omega = \frac{L \int_{r_1}^{r_2} N \frac{\mathrm{d}r}{r}}{\pi(n + l/2 + \alpha_\mathrm{g})} , \tag{7.71}$$

where α_g is a phase constant. Thus in this case the *periods* are asymptotically equally spaced in the order of the mode. The spacing decreases with increasing l, as is also obvious from Figure 5.6.

The analysis was carried to the next asymptotic order by Tassoul (1980). Ellis (1988), Provost & Berthomieu (1986) and Gabriel (1986) compared the resulting expressions with numerically computed frequencies for polytropic or solar models.

In the trapping region the eigenfunction is given by equation (7.34). We may assume that $\omega^2 \ll S_l^2$, and so obtain

$$\begin{aligned} \xi_r(r) &\simeq A\rho^{-1/2} r^{-1} c^{-1/2} \left(\frac{S_l}{\omega}\right)^{1/2} \left|\frac{N^2}{\omega^2} - 1\right|^{-1/4} \cos\left[L \int_{r_1}^{r} \left(\frac{N^2}{\omega^2} - 1\right)^{1/2} \frac{\mathrm{d}r'}{r'} - \frac{\pi}{4}\right] \\ &= A \left(\frac{L}{\omega}\right)^{1/2} \rho^{-1/2} r^{-3/2} \left|\frac{N^2}{\omega^2} - 1\right|^{-1/4} \cos\left[L \int_{r_1}^{r} \left(\frac{N^2}{\omega^2} - 1\right)^{1/2} \frac{\mathrm{d}r'}{r'} - \frac{\pi}{4}\right] . \end{aligned} \tag{7.72}$$

Except close to the turning points r_1, r_2 we may assume that $N^2/\omega^2 \gg 1$ (note, from Figure 5.2, that N increases very rapidly from 0 at the centre and at the base of the convection zone). Here, therefore,

$$\xi_r(r) \simeq A L^{1/2} \rho^{-1/2} r^{-3/2} N^{-1/2} \cos\left[L \int_{r_1}^{r} \left(\frac{N^2}{\omega^2} - 1\right)^{1/2} \frac{\mathrm{d}r'}{r'} - \frac{\pi}{4}\right] . \tag{7.73}$$

Hence we expect that $\rho^{1/2} r^{3/2} N^{1/2} \xi_r$ behaves like a distorted cosine function. This is confirmed by Figure 7.4. Thus equation (7.73), as the corresponding equation for the p modes, gives a fairly accurate description of the eigenfunction in the trapping region.

Outside the trapping region the eigenfunction locally decays exponentially; this is also described by saying that the mode is *evanescent*. In particular, g modes are always evanescent in convection zones. From Figure 5.2 it follows that in the solar case this evanescent region is essentially restricted to the convection zone for $\nu < 200\,\mu$Hz. At higher frequencies the evanescent region extends more deeply, and for frequencies near the maximum in N the mode is oscillatory only in a narrow region around $x = 0.1$. Thus one would expect such modes to be very efficiently trapped. To study the trapping I use the asymptotic expression (7.36). In the convection zone we can assume that $N = 0$; and for low-frequency (and high-degree) modes I neglect ω^2/S_l^2 compared with 1. Then $K \simeq -L^2/r^2$, and the variation in ξ_r through the convection zone may be approximated by

$$\begin{aligned} \xi_r(r) &\simeq \frac{1}{2} \left(\frac{L}{\omega}\right)^{1/2} \rho^{-1/2} r^{-3/2} \exp\left(-L \int_{r_2}^{r} \frac{\mathrm{d}r'}{r'}\right) \\ &= \frac{1}{2} \left(\frac{L}{\omega}\right)^{1/2} {r_2}^L \rho^{-1/2} r^{-(3/2+L)} . \end{aligned} \tag{7.74}$$

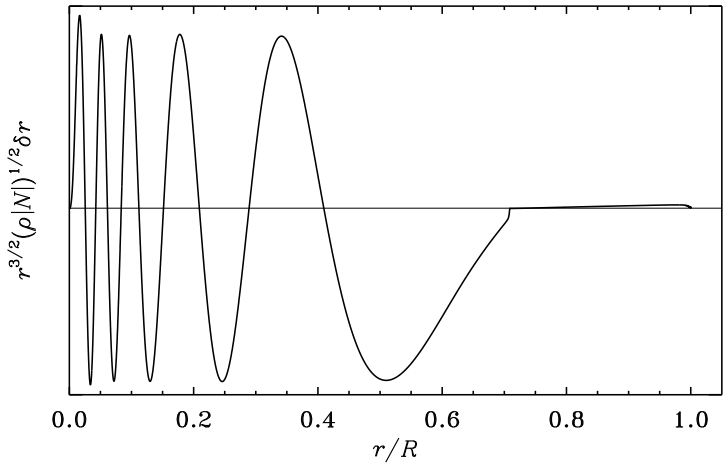

Figure 7.4: Scaled eigenfunction for high-order g mode of degree 2, radial order $n = -10$ and frequency $\nu = 104\,\mu$Hz in a normal solar model (the same mode as was shown in Figure 5.10b). According to the asymptotic equation (7.73) the quantity plotted should oscillate between fixed limits in the region where the mode is trapped.

Thus the density decrease with increasing radius causes an increase in the amplitude, but this is compensated for by the power law decrease represented by r^{-L} (note that this is the global manifestation of the locally exponential behaviour in the evanescent region). To get an idea about the relative importance of these two effects I note that the radius $r_{\rm b}$ at the base of the solar convection zone is about 0.7 R, whereas the ratio between the surface density and the density at the base of the convection zone is about 10^{-6}. Thus we obtain

$$\xi_r(r_{\rm b})/\xi_r(R) \sim 10^{-3}(0.7)^{-(3/2+L)} \sim 10^{-2.8+0.15L} \,. \tag{7.75}$$

This approximation, however, assumed the validity of the asymptotic expression (7.36) right up to the surface. This is not true, as the assumptions underlying the analysis break down close to the surface where the pressure scale height becomes small. It appears that these effects dominate unless l is quite large. An attempt at analyzing this, based on the more complete asymptotic theory to be described in the following section, is provided in Section 7.6.2.

This analysis roughly describes the trapping of low-frequency modes. At higher frequencies the deepening of the evanescent region must also be taken into account, and the asymptotic analysis becomes rather complicated. Reference may be made, however, to the numerical results presented in Figures 5.12 and 5.13. At low frequencies the increase in the interior amplitude with degree, at fixed frequency, is roughly in accordance with the asymptotic discussion given above. The steep increase with increasing frequency at $\nu > 400\,\mu$Hz is related to the faint local maximum in N at that frequency, which was discussed above (*cf.* Figure 5.2); modes with higher frequency suddenly get trapped much deeper in the

Sun, and their maximum amplitudes consequently rise very rapidly. For comparison one might note that a mode with a velocity amplitude of $1\,\mathrm{m\,sec}^{-1}$ and a period of 1 hour has a relative surface displacement amplitude of about 10^{-6}. Thus modes with an amplitude ratio of more than 10^6 are not likely to be seen. Clearly there is little hope of observing g modes of degree greater than 20.

A more careful analysis than presented here would probably allow an understanding of many of the features shown in Figures 5.12 and 5.13. This would be interesting but has, as far as I know, not been undertaken so far.

7.5 A general asymptotic expression

An approximate asymptotic description of the oscillations has been derived by Gough (see Deubner & Gough 1984), on the basis of earlier work by Lamb (1932). This does not assume that the pressure and density scale heights are much larger than the wavelength; but it assumes that the oscillations vary much more rapidly than r and g, so that the problem is locally one of oscillations of a plane-parallel layer under constant gravity. Also, as usual, the perturbation in the gravitational potential is neglected. Then the governing equations are equations (5.12) and (5.13), but without the term in $2/r$ in the former. When manipulating the equations, I neglect derivatives of r and g, but keep derivatives of the thermodynamic quantities. I note that Gough (1993) generalized this treatment to include also sphericity and varying gravity, although at the expense of obtaining considerably more complicated expressions.

7.5.1 Derivation of the asymptotic expression

The trick of the analysis is to write the equations in terms of

$$\chi = \mathrm{div}\,\boldsymbol{\delta r}\ . \tag{7.76}$$

By using the equation of continuity and the condition of adiabaticity we may also write χ as

$$\chi = -\frac{1}{\Gamma_1}\left(\frac{p'}{p} - \frac{\rho g}{p}\xi_r\right)\ . \tag{7.77}$$

The oscillation equations can be written as

$$\frac{\mathrm{d}\xi_r}{\mathrm{d}r} = \chi + \frac{1}{\rho}\frac{k_\mathrm{h}^2}{\omega^2}p'\ , \tag{7.78}$$

and

$$\frac{\mathrm{d}p'}{\mathrm{d}r} = \rho\left(\omega^2 + g\frac{\mathrm{d}\ln\rho}{\mathrm{d}r}\right)\xi_r + g\rho\chi\ . \tag{7.79}$$

In keeping with the plane-parallel approximation I have expressed l by k_h, given by equation (4.51), and I assume k_h to be constant.

By multiplying equation (7.77) by $\Gamma_1 p$ and differentiating we obtain, on using equations (7.78) and (7.79)

$$\frac{\mathrm{d}\Gamma_1}{\mathrm{d}r}p\chi - \Gamma_1 g\rho\chi + \Gamma_1 p\frac{\mathrm{d}\chi}{\mathrm{d}r} = -\rho\omega^2\xi_r + \frac{gk_\mathrm{h}^2}{\omega^2}p'\ . \tag{7.80}$$

This equation, together with equation (7.77), can be used to express ξ_r in terms of χ and its first derivative. The result is

$$\rho\left(g-\frac{\omega^4}{gk_{\rm h}^2}\right)\xi_r=\Gamma_1\left[p\chi+\frac{\omega^2}{gk_{\rm h}^2}\left(p\frac{{\rm d}\chi}{{\rm d}r}-g\rho\chi+p\frac{{\rm d}\ln\Gamma_1}{{\rm d}r}\chi\right)\right]\ . \tag{7.81}$$

Finally, by differentiating equation (7.80) and using equations (7.78), (7.79) and (7.81) to eliminate ξ_r, p' and their derivatives, we obtain the following second-order differential equation for χ:

$$\begin{aligned}&\frac{{\rm d}^2\chi}{{\rm d}r^2}+\left(\frac{2}{c^2}\frac{{\rm d}c^2}{{\rm d}r}+\frac{1}{\rho}\frac{{\rm d}\rho}{{\rm d}r}\right)\frac{{\rm d}\chi}{{\rm d}r}\\&+\left[\frac{1}{\Gamma_1}\frac{{\rm d}^2\Gamma_1}{{\rm d}r^2}-\frac{2}{\Gamma_1}\frac{{\rm d}\Gamma_1}{{\rm d}r}\frac{g\rho}{p}+k_{\rm h}^2\left(\frac{N^2}{\omega^2}-1\right)-\frac{1}{\rho}\frac{{\rm d}\rho}{{\rm d}r}\frac{1}{\Gamma_1}\frac{{\rm d}\Gamma_1}{{\rm d}r}+\frac{\rho\omega^2}{\Gamma_1 p}\right]\chi=0\ .\end{aligned} \tag{7.82}$$

Here I have introduced the adiabatic sound speed c from equation (3.52) and the buoyancy frequency N from equation (3.73).

The differential equation for χ contains no interior singular points. However, it is clear from equation (7.81) that the case where the coefficient of ξ_r vanishes is in some sense singular. This occurs when

$$\omega^2=gk_{\rm h}\ . \tag{7.83}$$

It is easy to show that then the solution for χ to equation (7.81) grows exponentially towards the interior; as this is clearly unacceptable, χ must be zero. Then equation (7.77) gives

$$p'=g\rho\xi_r\ , \tag{7.84}$$

and equation (7.78) has the solution

$$\xi_r=a\exp(k_{\rm h}r)\ , \tag{7.85}$$

where a is an arbitrary constant. It is easy to show that the resulting p' satisfies equation (7.79). Thus this is one possible solution to the plane-parallel oscillation equations. It should be noticed that equation (7.83) agrees with equation (3.84) for the frequency of a surface gravity wave. Thus the mode we have found must be identified with a surface gravity wave; and we have shown that its frequency is independent of the structure of the model below the surface, if sphericity is neglected. This result was first obtained by Gough. It is obvious from Figure 5.6 that the mode can be followed to degrees well below 10, although here the correction to the frequency given by equation (7.83) becomes significant.

To analyze equation (7.82) it is convenient to eliminate the term in ${\rm d}\chi/{\rm d}r$. Thus I introduce X by

$$X=c^2\rho^{1/2}\chi\ . \tag{7.86}$$

After considerable manipulation one then finds that X satisfies the differential equation

$$\frac{{\rm d}^2X}{{\rm d}r^2}+\left[k_{\rm h}^2\left(\frac{N^2}{\omega^2}-1\right)+\frac{\omega^2}{c^2}-\frac{1}{2}\frac{\rm d}{{\rm d}r}(H^{-1})-\frac{1}{4}H^{-2}\right]X=0\ , \tag{7.87}$$

where I have introduced the density scale height H by

$$H^{-1}=-\frac{{\rm d}\ln\rho}{{\rm d}r}\ . \tag{7.88}$$

Finally, I define a characteristic frequency ω_c by

$$\omega_c^2 = \frac{c^2}{4H^2}\left(1 - 2\frac{\mathrm{d}H}{\mathrm{d}r}\right) , \tag{7.89}$$

and use equation (4.60) for the acoustic frequency S_l, to obtain

$$\frac{\mathrm{d}^2X}{\mathrm{d}r^2} + \frac{1}{c^2}\left[S_l^2\left(\frac{N^2}{\omega^2} - 1\right) + \omega^2 - \omega_c^2\right]X = 0 . \tag{7.90}$$

This is the final second-order differential equation. Considering that the only approximations made in deriving it are the constancy of g and the neglect of the derivatives of r, it is remarkably simple.

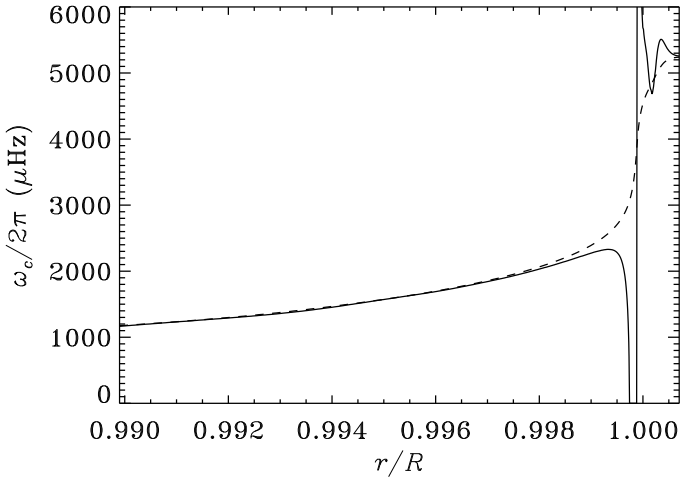

Figure 7.5: The acoustical cut-off frequency ω_c defined in equation (7.89) (solid line), and the approximation ω_a appropriate to an isothermal region [*cf.* equation (5.45); dashed line] in the outermost parts of a normal model of the present Sun.

It might be noticed that equation (7.90) can also be derived from a careful analysis of the propagation of waves in stellar interiors. This has been carried out by Gough (1986a).

Notice that if H is constant (as was assumed in Section 5.4), equation (7.89) for ω_c reduces to the frequency ω_a defined in equation (5.45). Thus ω_c, as introduced here, generalizes the acoustical cut-off frequency defined for the isothermal atmosphere. Figure 7.5 shows ω_c and ω_a in the outer parts of a normal solar model; they are in fact quite similar, except in a thin region very near the top of the convection zone, where the rapid variation in the superadiabatic gradient causes large excursions in ω_c.

Near the surface S_l^2 is small, and the coefficient of X in equation (7.90) is dominated by the last two terms; hence X is exponential when $\omega^2 < \omega_c^2$. This provides the trapping

of the modes at the surface. In the interior ω_c^2 (which roughly varies as g^2/T) is generally small, below about $600\,\mu$Hz in models of the present Sun.

We may write equation (7.90) as

$$\frac{\mathrm{d}^2X}{\mathrm{d}r^2} + K(r)X = 0\,, \tag{7.91}$$

where

$$\begin{aligned} K(r) &= \frac{\omega^2}{c^2}\left[1 - \frac{\omega_c^2}{\omega^2} - \frac{S_l^2}{\omega^2}\left(1 - \frac{N^2}{\omega^2}\right)\right] \\ &\equiv \frac{\omega^2}{c^2}\left(1 - \frac{\omega_{l,+}^2}{\omega^2}\right)\left(1 - \frac{\omega_{l,-}^2}{\omega^2}\right)\,, \end{aligned} \tag{7.92}$$

defining the characteristic frequencies $\omega_{l,+}$ and $\omega_{l,-}$. They are plotted in Figure 7.6, in a model of the present Sun. Equation (7.92) shows that the trapping of the modes is determined by the value of the frequency, relative to behaviour of $\omega_{l,+}$ and $\omega_{l,-}$. In the interior of the Sun, particularly for large l,

$$\omega_{l,+} \simeq S_l\,; \qquad \omega_{l,-} \simeq N\,. \tag{7.93}$$

Thus here we recover the conditions for trapping discussed in Section 5.2.2. This was indeed to be expected, as the assumptions entering the present formulation provide a natural transition from the previously discussed simplified asymptotic treatment to the atmospheric behaviour of the oscillations. On the other hand, near the surface where $S_l/\omega \ll 1$

$$\omega_{l,+} \simeq \omega_c\,, \tag{7.94}$$

while $\omega_{l,-}$ is small. Thus the trapping near the surface is controlled by the behaviour of $\omega_{l,+}$. As shown in Figure 7.6 trapping extends in frequency up to about 5.3 mHz, although the spike in $\omega_{l,+}$ just beneath the photosphere provides some partial reflection at even higher frequency. Also, modes with frequency $\nu \gtrsim 2\,$mHz propagate essentially to the photosphere, while modes of lower frequency are reflected at some depth in the convection zone. This behaviour is visible in the eigenfunctions shown in Figure 5.9; also it is largely responsible for the transition of the mode energy normalized with the surface displacement, shown in Figure 5.11, from steep decrease to near constancy with increasing frequency.

7.5.2 The Duvall law for p-mode frequencies

We may apply the JWKB analysis discussed in Section 7.2 to equation (7.90). Thus the asymptotic expression (7.33) for the frequency gives

$$\omega \int_{r_1}^{r_2} \left[1 - \frac{\omega_c^2}{\omega^2} - \frac{S_l^2}{\omega^2}\left(1 - \frac{N^2}{\omega^2}\right)\right]^{1/2} \frac{\mathrm{d}r}{c} \simeq \pi(n - 1/2)\,, \tag{7.95}$$

where r_1 and r_2 are adjacent zeros of K such that $K > 0$ between them.

This expression is now also formally valid for p modes. Given the rapid variation of $\omega_{l,+}$ near the surface its practical validity might be questioned. Christensen-Dalsgaard (1984c) evaluated the left-hand side of equation (7.95), substituting computed eigenfrequencies

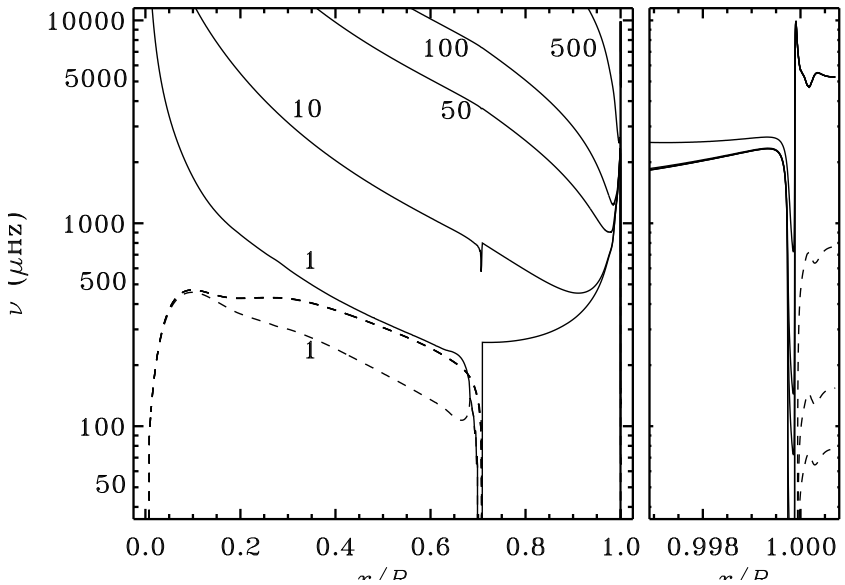

Figure 7.6: Characteristic frequencies $\omega_{l,+}/(2\pi)$ (continuous curves) and $\omega_{l,-}/(2\pi)$ (dashed curves) for a model of the present Sun (*cf.* eq. 7.92). The curves are labelled with the degree l. The right-hand panel shows the outermost parts of the model on an expanded horizontal scale. The figure may be compared with the simple characteristic frequencies plotted in Figure 5.2.

for ω, and found that the deviations from the asymptotic relation were relatively modest; however, substantially better agreement is obtained if $\omega_{\rm c}$ is replaced by the simple expression for an isothermal atmosphere, given in equation (5.45).

Equation (7.95) may be used to justify the approximate relation (7.38) for the frequencies of acoustic modes, with $\alpha = \alpha(\omega)$ being a function of frequency (see also Deubner & Gough 1984). Here I present an argument derived by Christensen-Dalsgaard & Pérez Hernández (1992). Assuming that the term in N^2 can be neglected, I write equation (7.95) as

$$\frac{\pi(n-1/2)}{\omega} \simeq F\left(\frac{\omega}{L}\right) - \frac{1}{\omega}(I_1+I_2+I_3)\;, \tag{7.96}$$

where

$$F(w) = \int_{r_{\rm t}}^{R} \left(1-\frac{c^2}{w^2r^2}\right)^{1/2} \frac{{\rm d}r}{c}\;, \tag{7.97}$$

and the dimensionless integrals $I_1 - I_3$ are defined by

$$I_1 \;=\; \omega\int_{r_2}^{R}\left(1-\frac{S_l^2}{\omega^2}\right)^{1/2}\frac{{\rm d}r}{c}\;, \tag{7.98}$$

$$I_2 \;=\; \omega\int_{r_1}^{r_2}\left[\left(1-\frac{S_l^2}{\omega^2}\right)^{1/2} - \left(1-\frac{\omega_{\rm c}^2}{\omega^2}-\frac{S_l^2}{\omega^2}\right)^{1/2}\right]\frac{{\rm d}r}{c}\;, \tag{7.99}$$

$$I_3 \;=\; \omega \int_{r_\mathrm{t}}^{r_1} \left(1 - \frac{S_l^2}{\omega^2}\right)^{1/2} \frac{\mathrm{d}r}{c} \; . \tag{7.100}$$

I assume that $\omega_\mathrm{c}^2 > 0$ in the vicinity of the lower turning point, so that $r_\mathrm{t} < r_1$ [where r_t is given by equation (5.28)]; also I have assumed that $R > r_2$ for all modes of interest.

To show that equation (7.39) is approximately valid, with α being a function of ω, we must show that $I_1 + I_2 + I_3$ is predominantly a function of frequency. In so doing I make the assumptions:

- $S_l^2/\omega^2 \ll 1$ at the upper turning point.
- $\omega_\mathrm{c}^2/\omega^2 \ll 1$ at the lower turning point.

Near the upper turning point we may then neglect the term in S_l^2/ω^2, and hence the position of the turning point is approximately given by $r_2 \simeq R_\mathrm{t}$, where R_t is defined by $\omega = \omega_\mathrm{c}(R_\mathrm{t})$. Thus r_2 is a function of frequency alone; the same is therefore obviously true for I_1. I_3 is small; in fact, by expanding S_l^2 in the vicinity of r_t, neglecting the variation in ω_c and c, it is straightforward to show that

$$I_3 \simeq \frac{1}{3}\left(\frac{\omega_{\mathrm{c,t}}}{\omega}\right)^3 \omega \frac{H_{\mathrm{c,t}}}{c_\mathrm{t}} \sim \left(\frac{\omega_{\mathrm{c,t}}}{\omega}\right)^2 \; , \tag{7.101}$$

where $\omega_{\mathrm{c,t}}$, c_t and $H_{\mathrm{c,t}}$ are the values of ω_c, c and the sound-speed scale height at r_t. Thus, although I_3 depends on r_t and hence on ω/L, the term is $\mathcal{O}((\omega_\mathrm{c}/\omega)^2)$ and hence negligible.

This leaves I_2 to be dealt with. To investigate its dependence on l and ω I rewrite it as

$$I_2 = \frac{1}{\omega}\int_{r_1}^{r_2} \frac{\omega_\mathrm{c}^2}{\left(1 - \dfrac{S_l^2}{\omega^2}\right)^{1/2} + \left(1 - \dfrac{\omega_\mathrm{c}^2}{\omega^2} - \dfrac{S_l^2}{\omega^2}\right)^{1/2}} \frac{\mathrm{d}r}{c} \; . \tag{7.102}$$

Since ω_c^2/c decreases quite rapidly with increasing depth (*cf.* Figure 7.5), this integral is dominated by the region near the upper turning point r_2. It is true that the integrand is nearly singular, with an integrable singularity, at $r = r_1$; but the contribution from that is essentially $\mathcal{O}(\omega_{\mathrm{c,t}}^2/\omega^2)$ and is therefore small. Near r_2, S_l^2/ω^2 is negligible; thus we can approximate I_2 as

$$I_2 \simeq \frac{1}{\omega}\int_{r_1}^{r_2} \frac{\omega_\mathrm{c}^2}{1 + \left(1 - \dfrac{\omega_\mathrm{c}^2}{\omega^2}\right)^{1/2}} \frac{\mathrm{d}r}{c}, \tag{7.103}$$

which is obviously a function of frequency alone.

It follows that equation (7.96) may finally be written as

$$\int_{r_\mathrm{t}}^{R} \left(1 - \frac{L^2c^2}{\omega^2 r^2}\right)^{1/2} \frac{\mathrm{d}r}{c} = \frac{[n + \alpha(\omega)]\pi}{\omega} \; , \tag{7.104}$$

with

$$\alpha \simeq \alpha(\omega) = \frac{1}{\pi}(I_1 + I_2) - 1/2 \; . \tag{7.105}$$

This argument is evidently valid in general for stellar models where ω_c^2/c decreases sufficiently rapidly with increasing depth.

It is instructive to consider the analysis for the special case where the outer layers of the star can be approximated by an adiabatically stratified, plane-parallel layer; also I neglect the variation of Γ_1. Then we obtain equation (7.43) for c, and furthermore

$$\omega_c^2 = \frac{g\mu_p}{4(R-r)}\left(1+\frac{2}{\mu_p}\right) , \tag{7.106}$$

where $\mu_p = 1/(\Gamma_1 - 1)$ is the effective polytropic index of the layer. Finally N is zero. From equation (7.106) ω_c is small except near the surface, and so it is reasonable to neglect it in most of the region where the p mode is trapped (notice, however, that this becomes questionable for high l, where the trapping region is confined very close to the surface). To approximate equation (7.95) I use a trick similar to that employed to derive equation (7.51). Thus I write equation (7.95) as

$$\begin{aligned}\frac{\pi(n-1/2)}{\omega} &= \int_{r_1}^{R}\left(1-\frac{S_l^2}{\omega^2}\right)^{1/2}\frac{\mathrm{d}r}{c} - \int_{r_2}^{R}\left(1-\frac{S_l^2}{\omega^2}\right)^{1/2}\frac{\mathrm{d}r}{c} \\ &- \int_{r_1}^{r_2}\left[\left(1-\frac{S_l^2}{\omega^2}\right)^{1/2} - \left(1-\frac{\omega_c^2}{\omega^2}-\frac{S_l^2}{\omega^2}\right)^{1/2}\right]\frac{\mathrm{d}r}{c} .\end{aligned} \tag{7.107}$$

Here, approximately, r_2 is given by $\omega_c(r_2) = \omega$, and is therefore close to the surface. Furthermore, the dominant contribution to the third integral in question (7.107) comes from the region near r_2. In the last two integrals I therefore use the approximations (7.43) and (7.106) for c and ω_c; furthermore I neglect the variation of r in S_l. These integrals may then, with a little effort, be evaluated analytically. The result is

$$\frac{\pi(n-\frac{1}{2})}{\omega} = \int_{r_1}^{R}\left(1-\frac{S_l^2}{\omega^2}\right)^{1/2}\frac{\mathrm{d}r}{c} - \frac{1}{2}[\mu_p(\mu_p+2)]^{1/2}\frac{\pi}{\omega} . \tag{7.108}$$

This may also be written as equation (7.39), with

$$\alpha = 1/2[\mu_p(\mu_p+2)]^{1/2} - 1/2 . \tag{7.109}$$

Thus in this case α is a constant which is related to the effective polytropic index of the surface layers.

Exercise 7.3:

Derive equation (7.108).

If the entire layer is polytropic, with equation (7.43) and (7.106) everywhere valid, equation (7.90) may be solved analytically (*e.g.* Christensen-Dalsgaard 1980). The condition that the solution decreases exponentially at great depths determines the eigenfrequencies as

$$\omega^2 = \frac{2}{\mu_p}\left(n+\frac{\mu_p}{2}\right)L\frac{g}{R} . \tag{7.110}$$

This is in accordance with equation (7.45) obtained asymptotically, but with a different α,

$$\alpha = \frac{\mu_{\rm p}}{2} \; . \tag{7.111}$$

It is easy to show that the difference between this exact α and the asymptotic approximation in equation (7.109) is small; it tends to zero for large $\mu_{\rm p}$.

A minor point in these relations concerns the definition of L (which also enters into $S_l = cL/r$). In the analysis I have so far taken $L = \sqrt{l(l+1)}$. In fact, it may be shown from a more careful analysis of the asymptotic behaviour of the oscillation equations near the centre that a more appropriate choice would have been $L_0 = l + 1/2$ (note, however, that $L = L_0 + \mathcal{O}(l^{-1})$ and that even for $l = 1$ they are very similar). In the rest of this chapter I shall replace L by L_0 and, for convenience, suppress the subscript '0'. [Note that this was also used in the formulation of equation (7.52).]

7.6 Asymptotic properties of eigenfunctions

An initial discussion of p- and g-mode eigenfunctions was presented above, based on the simplified asymptotic description (*cf.* eqs 7.63 and 7.73). It was noted that the presence of singularities in the asymptotic equations caused problems in these approximations, particularly for the phase of the p-mode eigenfunction. Such problems are avoided in the formulation developed in Section 7.5. That formulation, on the other hand, was derived under the assumption that derivatives of r and g could be neglected. Thus, as is indeed found from numerical applications, a straightforward derivation of eigenfunctions from asymptotic analysis of (7.90) leads to amplitude functions deviating from the correct variation by low powers of r or g.

As already mentioned, a more complete asymptotic description which does not suffer from this approximation was developed by Gough (1993). In a formal sense it is quite similar to the formulation presented here, although with considerably more complicated expressions for the characteristic frequencies and eigenfunction scalings. It is likely that an asymptotic analysis based on these equations would yield the correct behaviour; however, such an analysis has apparently not been published, and will not be attempted here. Instead I shall apply a pragmatic, although certainly not rigorous, approach. The analysis in Sections 7.3 and 7.4 is correct, to leading order, away from the singular points. Consequently, we can expect that the variation of the amplitude functions in equations (7.63) and (7.73) are correct in these regions. I shall assume that this is the case and obtain the relevant powers of r and/or g in the analysis of equation (7.90) such that the final p- and g-mode expressions have the correct behaviour [the dependence with c and ρ is included fully in the derivation of equation (7.90) and is therefore correctly included]. What is gained by using equation (7.90) is therefore principally the correct treatment of the phases at the turning points.

7.6.1 Asymptotic properties of the p-mode eigenfunctions

I neglect the term in N^2 in equation (7.90), and assume that there is a region outside $r_{\rm t}$ where $\omega_{\rm c}^2$ can be neglected. In that region, except near $r_{\rm t}$, JWKB analysis of equation (7.90) leads to the following approximate solution for X:

$$X(r) \simeq A_X c^{1/2} r^{-1} \left(1 - \frac{L^2c^2}{\omega^2 r^2}\right)^{-1/4} \cos\left[\omega \int_{r_{\rm t}}^{r} \left(1 - \frac{L^2c^2}{\omega^2 r'^2}\right)^{1/2} \frac{{\rm d}r'}{c} - \frac{\pi}{4}\right] , \tag{7.112}$$

where the constant A_X is determined by the boundary conditions; the factor r^{-1} does not follow from the analysis but was, as discussed above, introduced to obtain the correct final amplitude function. An expression for ξ_r can be derived from the general equation (7.81). I neglect the derivative of Γ_1 and write the equation as

$$\rho g \left(1 - \frac{\omega^4}{\omega_{\rm f}^4}\right) \xi_r \simeq \Gamma_1 p \left[\chi + \frac{\omega^2}{g k_{\rm h}^2} \left(\frac{{\rm d}\chi}{{\rm d}r} - \frac{\Gamma_1 g}{c^2}\chi\right)\right] , \tag{7.113}$$

where $\omega_{\rm f}^2 = g k_{\rm h}$ is the squared f-mode frequency. For high-order p modes we can assume that $\omega \gg \omega_{\rm f}$. On the right-hand side we need to estimate the term in ${\rm d}\chi/{\rm d}r$, compared with the terms in χ. To do so, when differentiating here and in the following I assume that the eigenfunction varies on a scale short compared with scale heights of equilibrium quantities and only differentiate through the argument of cos in equation (7.112). It follows that the amplitude of ${\rm d}\chi/{\rm d}r$ is, to leading order, ω/c times the amplitude of χ. Consequently, the magnitudes of the coefficients to χ in the three terms in the square bracket on the right-hand side of equation (7.113) are

$$1 , \qquad \frac{\omega^3}{g c k_{\rm h}^2} , \qquad \frac{\omega^2}{k_{\rm h}^2}\frac{\Gamma_1}{c^2} . \tag{7.114}$$

To estimate the magnitude of the second component I write it as

$$\frac{\omega^2}{c^2 k_{\rm h}^2}\frac{\omega c}{g} = \frac{\omega^2}{S_l^2}\frac{\omega c}{g} . \tag{7.115}$$

In the first factor $\omega > S_l$ in regions of p-mode trapping. The second factor may be estimated from equation (5.18), neglecting ∇_μ, by writing it as

$$N^2 \simeq \frac{\Gamma_1 g^2}{c^2}(\nabla_{\rm ad} - \nabla) ; \tag{7.116}$$

thus $\omega c/g \sim (\nabla_{\rm ad} - \nabla)^{1/2}\omega/N \gg 1$ for typical p modes, at least in radiative regions where $\nabla_{\rm ad} - \nabla$ is of order unity. (Near the surface, in convective regions where this estimate is not valid, it is typically the case that $\omega^2 \gg S_l^2$.) It follows that the second component in the set (7.114) is typically much greater than unity. The ratio between the second and third components is

$$\frac{\Gamma_1 g}{\omega c} \simeq \frac{\Gamma_2^{1/2} N}{(\nabla_{\rm ad} - \nabla)^{1/2}\omega} , \tag{7.117}$$

which is again typically much smaller than unity.

Using these estimates, it follows from equations (7.113) and (7.112) that

$$\begin{aligned} \xi_r &\simeq -\frac{c^2}{\omega^2}\frac{{\rm d}\chi}{{\rm d}r} \simeq -\rho^{-1/2}\omega^{-2}\frac{{\rm d}X}{{\rm d}r} \\ &\simeq -A_X \omega^{-1}(\rho c)^{-1/2} r^{-1} \left(1 - \frac{L^2 c^2}{\omega^2 r^2}\right)^{1/4} \cos\left[\omega \int_{r_{\rm t}}^r \left(1 - \frac{L^2 c^2}{\omega^2 r'^2}\right)^{1/2} \frac{{\rm d}r'}{c} + \frac{\pi}{4}\right] . \end{aligned} \tag{7.118}$$

By using equation (7.104) this equation may be written as

$$\begin{aligned} &\xi_r(r) \simeq \\ &A\,(\rho c)^{-1/2} r^{-1} \left(1 - \frac{L^2 c^2}{\omega^2 r^2}\right)^{1/4} \cos\left[\omega \int_r^R \left(1 - \frac{L^2 c^2}{\omega^2 r'^2}\right)^{1/2} \frac{{\rm d}r'}{c} - (\alpha + 1/4)\pi\right] , \end{aligned} \tag{7.119}$$

where A is a new constant; this corresponds to equation (7.63).

To find the horizontal displacement I note that in equation (5.12) the first term on the right-hand side can be neglected compared with the left-hand side, so that

$$\frac{\mathrm{d}\xi_r}{\mathrm{d}r} \simeq \frac{1}{\rho c^2}\left(\frac{S_l^2}{\omega^2}-1\right)p' \simeq -\frac{r\omega^2}{c^2}\left(1-\frac{S_l^2}{\omega^2}\right)\xi_\mathrm{h}\ , \tag{7.120}$$

using equation (4.39). Thus

$$\xi_\mathrm{h}(r) \simeq -\frac{c^2}{r\omega^2}\left(1-\frac{S_l^2}{\omega^2}\right)^{-1}\frac{\mathrm{d}\xi_r}{\mathrm{d}r} \simeq \tag{7.121}$$

$$-A\,\rho^{-1/2}c^{1/2}r^{-2}\omega^{-1}\left(1-\frac{L^2c^2}{\omega^2r^2}\right)^{-1/4}\sin\left[\omega\int_r^R\left(1-\frac{L^2c^2}{\omega^2r'^2}\right)^{1/2}\frac{\mathrm{d}r'}{c}-(\alpha+1/4)\pi\right]\ .$$

It may be noted that the ratio between the amplitudes of the root-mean-square lengths of the horizontal and vertical components of the displacement is

$$\left|\frac{L\xi_\mathrm{h}}{\xi_r}\right| \sim \frac{Lc}{r\omega}\left(1-\frac{L^2c^2}{\omega^2r^2}\right)^{-1/2} = \frac{S_l}{\omega}\left(1-\frac{S_l^2}{\omega^2}\right)^{-1/2} \tag{7.122}$$

(*cf.* eq. 4.45); thus well above the lower turning point, where $\omega \gg S_l$, the oscillation is predominantly vertical.

From these expressions, we can finally find the asymptotic form of the energy integral $\mathcal{E}$ (*cf.* eq. 4.47), replacing $\sin^2$ and $\cos^2$ by the average value 1/2:

$$\begin{aligned}\mathcal{E} &\simeq 2\pi A^2\int_{r_\mathrm{t}}^R\left[c^{-1}\left(1-\frac{L^2c^2}{\omega^2r^2}\right)^{1/2}+\frac{L^2c}{\omega^2r^2}\left(1-\frac{L^2c^2}{\omega^2r^2}\right)^{-1/2}\right]\mathrm{d}r \\ &\simeq 2\pi A^2\int_{r_\mathrm{t}}^R\left(1-\frac{L^2c^2}{\omega^2r^2}\right)^{-1/2}\frac{\mathrm{d}r}{c}\ .\end{aligned} \tag{7.123}$$

7.6.2 Asymptotic properties of the g-mode eigenfunctions

We consider the region where a g mode is trapped, and assume that $\omega^2 \ll S_l^2, N^2$. Then

$$K \simeq k_\mathrm{h}^2\left(\frac{N^2}{\omega^2}-1\right)\ . \tag{7.124}$$

In the corresponding JWKB expression for the eigenfunction, comparison with equation (7.72) will show that the extra factor $gr^{-3/2}$ must be included. Thus we obtain

$$X(r) \simeq Agr^{-3/2}\left(\frac{N^2}{\omega^2}-1\right)^{-1/4}\cos\left[\int_{r_1}^r k_\mathrm{h}\left(\frac{N^2}{\omega^2}-1\right)^{1/2}\mathrm{d}r'-\frac{\pi}{4}\right]\ , \tag{7.125}$$

where $k_\mathrm{h}^{-1/2}$ was assumed to be constant and was absorbed in the amplitude A. To determine ξ_r we use again equation (7.113). On the left-hand side we can assume that $\omega \ll \omega_\mathrm{f}$. On the right-hand side, according to equation (7.125) the amplitude of $\mathrm{d}\chi/\mathrm{d}r$ is now, to

leading order, $k_{\rm h}N/\omega$ times the amplitude of χ. Thus the magnitudes of the three terms on the right-hand side of equation (7.113) scale as

$$1\ , \qquad \frac{\omega N}{g k_{\rm h}}\ , \qquad \frac{\omega^2 \Gamma_1}{k_{\rm h}^2 c^2}\ . \tag{7.126}$$

Here, using equation (7.116), the second component is

$$\frac{\omega N}{g k_{\rm h}} \simeq \frac{\omega}{c k_{\rm h}} (\nabla_{\rm ad} - \nabla)^{1/2} \simeq \frac{\omega}{S_l} (\nabla_{\rm ad} - \nabla)^{1/2} \ll 1\ , \tag{7.127}$$

and the third component is

$$\frac{\omega^2 \Gamma_1}{k_{\rm h}^2 c^2} = \Gamma_1 \frac{\omega^2}{S_l^2} \ll 1\ . \tag{7.128}$$

Thus the dominant term is the first. The result finally is

$$\begin{aligned} \xi_r &\simeq \frac{c^2}{g}\chi = \rho^{-1/2} g^{-1} X \\ &\simeq A \rho^{-1/2} r^{-3/2} \left(\frac{N^2}{\omega^2} - 1\right)^{-1/4} \cos\left[\int_{r_1}^r \frac{L}{r}\left(\frac{N^2}{\omega^2} - 1\right)^{1/2} {\rm d}r' - \frac{\pi}{4}\right]\ . \end{aligned} \tag{7.129}$$

To find the horizontal displacement we again use equation (7.120), now approximated by

$$\frac{{\rm d}\xi_r}{{\rm d}r} \simeq \frac{L^2}{r}\xi_{\rm h}\ . \tag{7.130}$$

Thus we obtain

$$\begin{aligned} \xi_{\rm h} &\simeq \frac{r}{L^2}\frac{{\rm d}\xi_r}{{\rm d}r} \\ &\simeq -A \rho^{-1/2} L^{-1} r^{-3/2} \left(\frac{N^2}{\omega^2} - 1\right)^{1/4} \sin\left[\int_{r_1}^r \frac{L}{r}\left(\frac{N^2}{\omega^2} - 1\right)^{1/2} {\rm d}r' - \frac{\pi}{4}\right]\ . \end{aligned} \tag{7.131}$$

Here the ratio between the amplitudes of the root-mean-square lengths of the horizontal and vertical components of the displacement is therefore

$$\left|\frac{L\xi_{\rm h}}{\xi_r}\right| \sim \left(\frac{N^2}{\omega^2} - 1\right)^{1/2}\ , \tag{7.132}$$

demonstrating that the oscillation is predominantly in the horizontal direction.

We may attempt to use equation (7.90) to describe the properties of g modes in an outer convection zone, *e.g.* in the solar case, to correct for the approximations discussed in connection with equation (7.75). We assume that $N^2 \simeq 0$ and $\omega^2 \ll \omega_{\rm c}^2$, so that equation (7.90) is approximated by

$$\frac{{\rm d}^2 X}{{\rm d}r^2} = \left(\frac{L^2}{r^2} + \frac{\omega_{\rm c}^2}{c^2}\right) X = \left[\frac{L^2}{r^2} + \frac{1}{4H^2}\left(1 - 2\frac{{\rm d}H}{{\rm d}r}\right)\right] X = 0\ , \tag{7.133}$$

using equation (7.89). Compared with the equation leading to equation (7.74), this differs by the inclusion of the term in $\omega_{\rm c}^2$; since the density scale height H is much smaller than

the stellar radius near the surface, there this term dominates over L^2/r^2, unless L is very large.

It is possible to carry the analysis somewhat further if we approximate the convection zone by a plane-parallel adiabatically stratified layer, and neglect the variation in Γ_1; this approximation was also used in Sections 7.3 and 7.5.2 to analyze various aspects of the Duvall law. Then $\rho = \rho_0 z^{\mu_\mathrm{p}}$, where $z = R - r$ is the depth and, as before, $\mu_\mathrm{p} = 1/(\Gamma_1 - 1)$ is the effective polytropic index. Also, we have equations (7.43) and (7.106) for c and ω_c; we write the relevant equations as

$$c^2 = \frac{g}{\mu_\mathrm{p}} z \; , \qquad \omega_\mathrm{c}^2 = \frac{g\mu_\mathrm{p}}{4z}\left(1 + \frac{2}{\mu_\mathrm{p}}\right) \; , \qquad H^{-1} = \frac{\mu_\mathrm{p}}{z} \; . \tag{7.134}$$

It follows that equation (7.133) can be written as

$$\frac{\mathrm{d}^2 X}{\mathrm{d}z^2} - \left[\frac{L^2}{R^2} + \frac{1}{4z^2}\mu_\mathrm{p}(\mu_\mathrm{p} + 2)\right] X = 0 \; , \tag{7.135}$$

where, in accordance with the assumption of a plane-parallel layer, I replaced r by R in the first term. A solution can be found to this equation in terms of modified Bessell functions. However, here I assume that L is not very large, so that the term in z^{-2} dominates. Then the regular solution to equation (7.135) is

$$X \simeq X_0 z^{1+\mu_\mathrm{p}/2} \; , \tag{7.136}$$

where X_0 is a constant. It follows from equation (7.86) that $\chi \simeq \chi_0$ is approximately constant. To determine ξ_r we use again equation (7.113), with $\omega \ll \omega_\mathrm{f}$. Obviously the term in $\mathrm{d}\chi/\mathrm{d}r$ can be neglected; however, since formally $c^2 \to 0$ at the surface both terms in χ must be included. The result is that

$$\xi_r \simeq \frac{1}{g}\left(c^2 - \frac{\Gamma_1 r^2 \omega^2}{L^2}\right)\chi_0 \; . \tag{7.137}$$

Neglecting c^2 at the surface, this shows that χ_0 is related to $\xi_r(R)$ by

$$\chi_0 \simeq -\frac{L^2 g}{\Gamma_1 R^2 \omega^2}\xi_r(R) \; . \tag{7.138}$$

Also, it follows that equation (7.75) is replaced by

$$\xi_r(r_\mathrm{b})/\xi_r(R) \simeq -\frac{r_\mathrm{b}^2}{R^2}\frac{L^2 c(r_\mathrm{b})^2}{\omega^2 R^2}\left[\frac{1}{\Gamma_1} - \frac{\omega^2}{S_l(r_\mathrm{b})^2}\right] = -\frac{r_\mathrm{b}^4}{R^4}\frac{S_l(r_\mathrm{b})^2}{\omega^2}\left[\frac{1}{\Gamma_1} - \frac{\omega^2}{S_l(r_\mathrm{b})^2}\right] \; , \tag{7.139}$$

where I neglected the variation in mass, and typically $\omega^2/S_l(r_\mathrm{b})^2 \ll 1$. I have found that numerical results, for modes of degree $l \leq 5$, in a model of the present Sun are in reasonable agreement with this relation.

To estimate the horizontal component of the displacement I again use equation (5.12) where, however, the term in ξ_r can no longer be neglected. Since we consider an adiabatically stratified convection zone, $\Gamma^{-1}H_p^{-1} = H^{-1}$, and hence equation (5.12) can be approximated by

$$\frac{\mathrm{d}\xi_r}{\mathrm{d}r} - H^{-1}\xi_r = \frac{r\omega^2}{c^2}\left(\frac{S_l^2}{\omega^2} - 1\right)\xi_\mathrm{h} \; . \tag{7.140}$$

When differentiating ξ_r, as given by equation (7.137), we neglect derivatives of g and r; using also equations (7.134) we obtain

$$\frac{\mathrm{d}\xi_r}{\mathrm{d}r} - H^{-1}\xi_r = -\left(1 + \frac{1}{\mu_\mathrm{p}} - \frac{\Gamma_1 r^2\omega^2\mu_\mathrm{p}}{L^2 gz}\right)\chi_0 = -\Gamma_1\left(1 - \frac{\omega^2}{S_l^2}\right)\chi_0 \; ; \tag{7.141}$$

Thus equation (7.140) gives, using also equation (7.138), that

$$\xi_\mathrm{h} \simeq -\frac{\Gamma_1 c^2}{rS_l^2}\chi_0 \simeq \frac{g}{r\omega^2}\xi_r(R) \simeq \sigma^{-2}\xi(R) \tag{7.142}$$

is approximately constant in the convection zone. It should also be noticed that this result, reassuringly, is consistent with the surface condition given in equation (4.69).

It would be interesting to match this behaviour in the convection zone to the region of trapping in the interior, to obtain the asymptotic behaviour of the mode energy. However, I have so far not been able to carry this analysis through to a result which resembles the numerical behaviour.

7.7 Analysis of the Duvall law

It was shown in Section 7.5.2, on the basis of the asymptotic theory of p modes, that such modes satisfy the *Duvall law*: we can find a function $\alpha(\omega)$ of frequency such that the quantity $[n + \alpha(\omega)]/\omega$ depends principally on frequency ω and degree l only in the combination $w \equiv \omega/L$, *i.e.*,

$$\frac{(n+\alpha)\pi}{\omega} = F\left(\frac{\omega}{L}\right) \; . \tag{7.143}$$

Here the function $F(\omega/L)$ is related to the adiabatic sound speed $c(r)$ by

$$F(w) = \int_{\ln r_\mathrm{t}(w)}^{\ln R} \left(1 - \frac{a^2}{w^2}\right)^{1/2} a^{-1}\mathrm{d}\ln r \; , \tag{7.144}$$

where $a = c/r$. Also, the function $\alpha(\omega)$ is primarily determined by conditions near the stellar surface. As illustrated in Figure 7.1 the observed frequencies of solar oscillation satisfy a relation of the form given in equation (7.143) quite accurately. This suggests that these relations are useful tools for analysing solar oscillation frequencies. It should be noted, however, that they are only approximately valid. In fact, a much more precise fit to the observed frequencies can be obtained by including additional terms (*e.g.* Gough & Vorontsov 1995) which take into account the effect of the perturbation in the gravitational potential (significant at low degree) and the dependence of the modes on degree near the upper turning point (important at high degree).

In this section I illustrate some properties of the Duvall law by applying it to frequencies computed for solar models, as well as to observed frequencies. The results are based on computations by Christensen-Dalsgaard, Proffitt & Thompson (1993) who considered both normal solar models and models which included effects of diffusion and gravitational settling of helium; recent opacity tables (Iglesias, Rogers & Wilson 1992) and a reasonable approximation to the equation of state were used. Thus the results illustrate both how well modern solar models fit the observed frequencies and the sensitivity of such analyses to relatively subtle features of the model calculations, such as gravitational settling.

7.7.1 The differential form of the Duvall law

A very powerful relation can be obtained by considering the effect on equation (7.104) of small changes to the equilibrium structure. I consider two cases (two solar models or a solar model and the Sun) with the same surface radius, labelled with the superscripts $^{(1)}$ and $^{(2)}$, and introduce the differences $\delta\omega_{nl} = \omega_{nl}^{(2)} - \omega_{nl}^{(1)}$, $\delta_r c(r) = c^{(2)}(r) - c^{(1)}(r)$ and $\delta\alpha(\omega) = \alpha^{(2)}(\omega) - \alpha^{(1)}(\omega)$. By substituting $c^{(2)}(r) = c^{(1)}(r) + \delta_r c(r)$ and $\alpha^{(2)}(\omega) = \alpha^{(1)}(\omega) + \delta\alpha(\omega)$ into equation (7.104), retaining only terms linear in $\delta_r c$, $\delta\alpha$ and $\delta\omega$, one obtains

$$S_{nl}\frac{\delta\omega_{nl}}{\omega_{nl}} \simeq \int_{r_t}^{R}\left(1 - \frac{c^2L^2}{\omega_{nl}^2 r^2}\right)^{-1/2}\frac{\delta_r c}{c}\frac{\mathrm{d}r}{c} + \pi\frac{\delta\alpha(\omega_{nl})}{\omega_{nl}} , \tag{7.145}$$

where

$$S_{nl} = \int_{r_t}^{R}\left(1 - \frac{L^2c^2}{r^2\omega_{nl}^2}\right)^{-1/2}\frac{\mathrm{d}r}{c} - \pi\frac{\mathrm{d}\alpha}{\mathrm{d}\omega} , \tag{7.146}$$

and I have suppressed the superscript $^{(1)}$. This relation was first obtained by Christensen-Dalsgaard, Gough & Pérez Hernández (1988).

Exercise 7.4:

Derive equation (7.145). If initially you obtain a different result, you may be in good company: so did the referee of Christensen-Dalsgaard *et al.* (1988).

Equation (7.145) may be written as

$$S_{nl}\frac{\delta\omega_{nl}}{\omega_{nl}} \simeq \mathcal{H}_1\left(\frac{\omega_{nl}}{L}\right) + \mathcal{H}_2(\omega_{nl}) , \tag{7.147}$$

where

$$\mathcal{H}_1(w) = \int_{r_t}^{R}\left(1 - \frac{c^2}{r^2w^2}\right)^{-1/2}\frac{\delta_r c}{c}\frac{\mathrm{d}r}{c} , \tag{7.148}$$

and

$$\mathcal{H}_2(\omega) = \frac{\pi}{\omega}\delta\alpha(\omega) . \tag{7.149}$$

Some properties of this equation were discussed by Christensen-Dalsgaard, Gough & Pérez Hernández (1988) and by Christensen-Dalsgaard *et al.* (1989). As pointed out in the latter paper, $\mathcal{H}_1(\omega/L)$ and $\mathcal{H}_2(\omega)$ can be obtained separately, to within a constant, by means of a double-spline fit of the expression (7.147) to p-mode frequency differences. The dependence of $\mathcal{H}_1$ on ω/L is determined by the sound-speed difference throughout the star, whereas $\mathcal{H}_2(\omega)$ depends on differences in the upper layers of the models.

There is a close analogy between equation (7.147) and the 'exact' equation (5.90). From equations (7.123) and (7.146) it follows that S_{nl}, apart from the term in the derivative of α, is proportional to the energy integral $\mathcal{E}$. Thus one finds that the scaling Q_{nl} in equation (5.90) is essentially asymptotically equal to S_{nl}/S_0, where $S_0 = \lim_{w\to 0} S(w)$ (Christensen-Dalsgaard 1991b); one may show that $S_0 = \tau_0$ where

$$\tau_0 = \int_0^R \frac{\mathrm{d}r}{c} \tag{7.150}$$

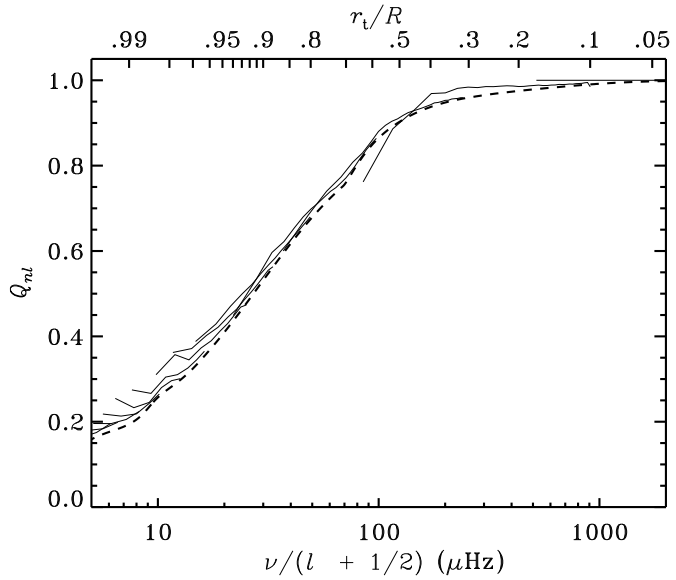

Figure 7.7: The solid lines show the inertia ratio Q_{nl}, defined in equation (5.88), against $\nu/(l+1/2)$ in a normal solar model, each curve corresponding to a given degree l. The upper abscissa shows the turning-point radius r_t, related to $\nu/(l+1/2)$ through equation (5.28). The heavy dashed curve shows the asymptotic scaling $\tilde{S}_{nl}/\tau_0$, where $\tilde{S}_{nl}$ is defined as in equation (7.146) but neglecting the term in $\mathrm{d}\alpha/\mathrm{d}\omega$.

is the acoustical radius of the star. The close correspondence between Q_{nl} and S_{nl}/τ_0 is illustrated in Figure 7.7. Furthermore, the term $\mathcal{G}(\omega)$ in equation (5.90) to some extent corresponds to the term $\mathcal{H}_2(\omega)$ in equation (7.147), in that both terms contain contributions from the uncertain regions very near the stellar surface. However, as discussed in Section 7.7.3 below $\mathcal{H}_2$ may also be used to gain information about somewhat deeper regions.

Since c/r decreases quite rapidly with increasing r, $(Lc/r\omega)^2 \ll 1$ except near the turning point r_t; hence as a rough approximation $1 - L^2c^2/r^2\omega^2$ may be replaced by 1 in the integrals in equations (7.145) and (7.146). If furthermore the terms in $\delta\alpha$ and $\mathrm{d}\alpha/\mathrm{d}\omega$ can be neglected, the result is the very simple relation between the changes in sound speed and frequency:

$$\frac{\delta\omega}{\omega} \simeq \frac{\displaystyle\int_{r_t}^{R} \frac{\delta_r c}{c}\frac{\mathrm{d}r}{c}}{\displaystyle\int_{r_t}^{R} \frac{\mathrm{d}r}{c}} \,. \tag{7.151}$$

This shows that the change in sound speed in a region of the Sun affects the frequency

with a weight determined by the time spent by the mode, regarded as a superposition of traveling waves, in that region. Thus changes near the surface, where the sound speed is low, have relatively large effects on the frequencies. Although this expression is only a rough approximation, it is a useful guide in attempts to interpret frequency differences between models, or between observed and computed frequencies.

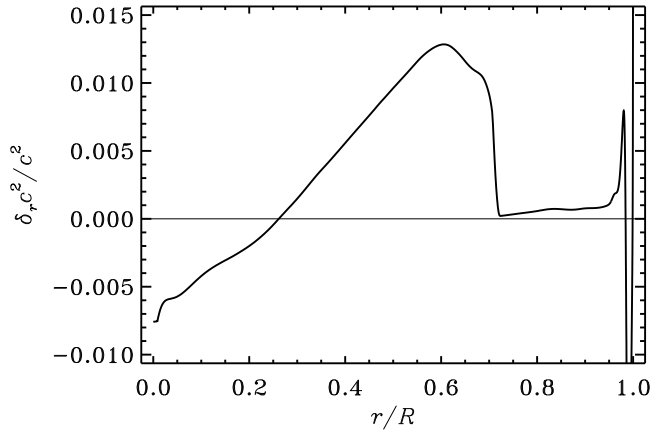

Figure 7.8: Fractional difference in sound speed between a model of the present Sun with diffusion and a normal model, without diffusion. From Christensen-Dalsgaard, Proffitt & Thompson (1993).

To illustrate the behaviour of the separation in equation (7.147) I consider differences between two models of Christensen-Dalsgaard *et al.* (1993): a model with diffusion and settling and a normal solar model. Figure 7.8 shows the sound-speed difference between these models. It is dominated by the fact that the convection zone is slightly deeper in the model with diffusion: since the temperature and sound-speed gradients are steeper in the convection zone than in the radiative region below, there is a region where the sound speed increases more rapidly with depth in the diffusive model, and this leads to the behaviour seen in the figure. Furthermore, due to settling of helium out of the convection zone the hydrogen abundance X_e in the convective envelope is higher by about 0.03 in the diffusive model, compared with the normal model. This causes differences in Γ_1, and hence in the sound speed, in the ionization zones of hydrogen and helium.

Figure 7.9a shows scaled frequency differences, at selected values of l, between these two models, plotted against ν/L (with $L = l + 1/2$; see above). I have normalized the scaling by S_0, such that it tends to unity at low degree; hence the scaled frequency differences correspond in magnitude to the differences for low-degree modes. The upper abscissa shows the location of the lower turning point, which is related to ω/L through equation (5.28). The general behaviour of the frequency differences reflects the asymptotic expression (7.147). The dependence of $S\delta\nu/\nu$ on ν/L can be understood from the sound-speed difference shown in Figure 7.8: for $\nu/L \lesssim 100\,\mu$Hz the modes are entirely trapped in the convection zone, and the frequency difference is dominated by the term $\mathcal{H}_2(\nu)$ arising from differences near

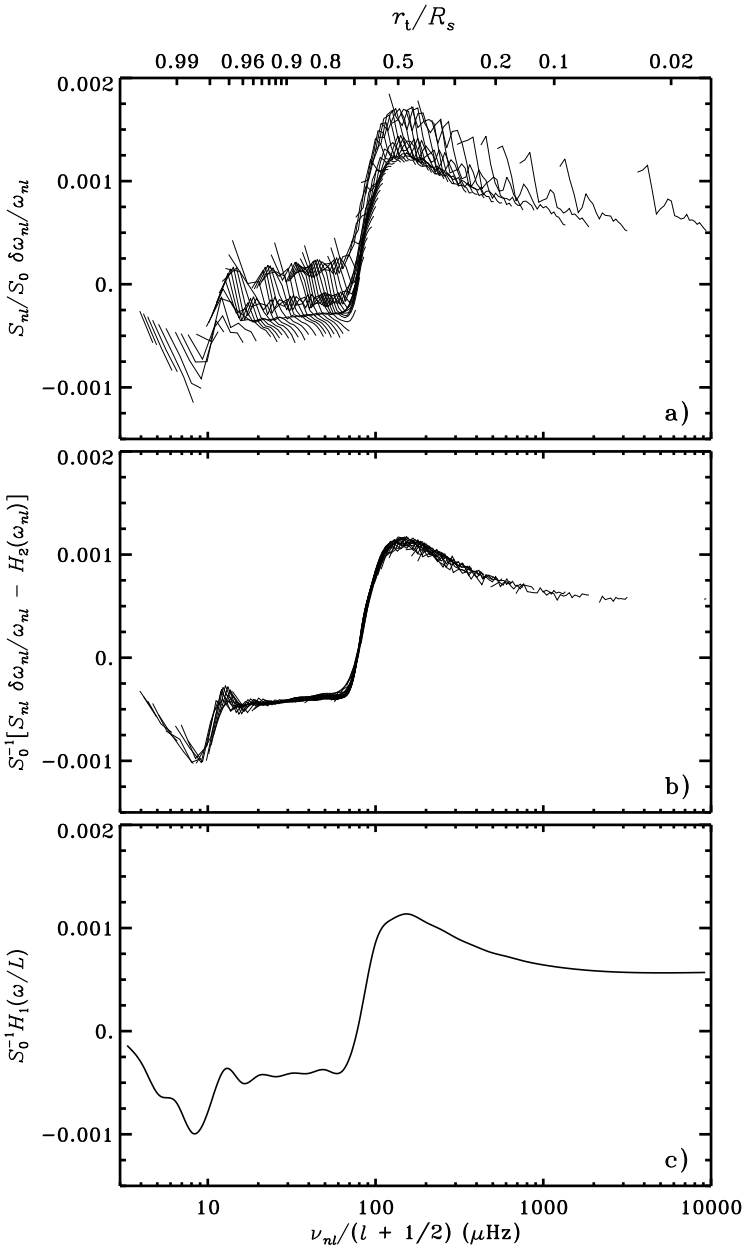

Figure 7.9: Scaled frequency differences corresponding to the model differences shown in Figure 7.8, plotted against $\nu/(l + 1/2)$. The upper abscissa shows the location of the lower turning point, which is related to $\nu/(l+1/2)$ through equation (5.28). In panels (a) and (b) points corresponding to fixed l have been connected. (a) Original scaled frequency differences. (b) Scaled differences, after subtraction of the function $\mathcal{H}_2(\omega)$ obtained from the spline fit. (c) The fitted function $\mathcal{H}_1(\omega/L)$.

the surface, particularly the difference in X_e. In contrast, modes with $\nu/L > 100\,\mu$Hz sense the substantial positive $\delta_r c$ just beneath the convection zone, and hence display a positive frequency difference; the transition occurs quite abruptly as the modes begin to penetrate beyond the convection zone.

This qualitative description suggests that the frequency differences may be analyzed in detail in terms of equation (7.147). To do so, I have determined the functions $\mathcal{H}_1$ and $\mathcal{H}_2$ by means of the spline fit of Christensen-Dalsgaard *et al.* (1989), where details about the fitting method may be found. Briefly, the procedure is to approximate $\mathcal{H}_1(\omega/L)$ and $\mathcal{H}_2(\omega)$ by splines, the coefficients of which are determined through a least-squares fit to the scaled frequency differences. The knots of the splines in $w \equiv \omega/L$ are distributed uniformly in $\log w$ over the range considered, whereas the knots for the ω-splines are uniform in ω. I used 28 knots in w and 20 knots in ω. [As a technical point, I note that in the separation in equation (7.147) $\mathcal{H}_1$ and $\mathcal{H}_2$ are evidently each only determined up to a constant term; hence in the following, when comparing $\mathcal{H}_2$ for different cases, we are permitted to shift $\mathcal{H}_2$ by a constant.]

Figure 7.9b shows the result of subtracting the function $\mathcal{H}_2(\omega)$ so obtained from the scaled frequency differences. It is evident that what remains is in fact very nearly a function of ω/L alone, directly reflecting the behaviour of $\delta_r c/c$, as discussed above. The function $\mathcal{H}_1(w)$ obtained from the fit is shown in Figure 7.9c. Similarly, Figure 7.10a shows the residual scaled frequency differences after subtraction of the term in $\mathcal{H}_1(\omega/L)$; these are clearly predominantly functions of frequency, although with some scatter. The fitted function $\mathcal{H}_2(\omega)$ is shown in Figure 7.10b.

The same analysis can obviously be applied to differences between observed frequencies and those of suitable reference models. To illustrate the power of helioseismic analysis to investigate even quite subtle features in the Sun, I consider two such reference models: one which does not include effects of settling and diffusion, and a second where settling and diffusion of helium and heavy elements are taken into account. Further details of the models were given by Christensen-Dalsgaard (1996b). The computed frequencies are compared with a set of observed data, combining modes with $l \leq 3$ from the BiSON network (Elsworth *et al.* 1994) with data for $l \geq 4$ from Libbrecht, Woodard & Kaufman (1990).

Figure 7.11a shows scaled differences between the observations and the model without diffusion and settling. It is evident already from this raw difference plot that in this case the term in $\mathcal{H}_2$ plays an important rôle. That should not be a surprise: as mentioned in Section 5.1.2 there are substantial uncertainties in the treatment of the near-surface layers and these are expected to produce effects that, when scaled, are mainly functions of frequency (see also Section 5.5.3). However, there is also evidence for a contribution from $\mathcal{H}_1$. This becomes clear if the spline fit is carried out and the contribution from $\mathcal{H}_2$ is subtracted from the scaled differences. The result is shown in Figure 7.11b, while the fitted $\mathcal{H}_1$ is shown in Figure 7.11c. There is again a sharp step corresponding in position to $r_t \simeq 0.7R$, *i.e.*, the base of the convection zone. As discussed in connection with the model comparison this may be taken as evidence that the convection zone in the Sun is somewhat deeper than in the model.

Corresponding results for the model including settling and diffusion are shown in Figure 7.12. In the original scaled differences shown in panel (a) it is difficult to discern any trend beyond the very obvious effect of the near-surface errors. Nonetheless, after carrying out the spline fit the residuals in panel (b) show a very definite dependence on ν/L, indicating remaining problems in the interior of the model. This is also clear from panel (c), which

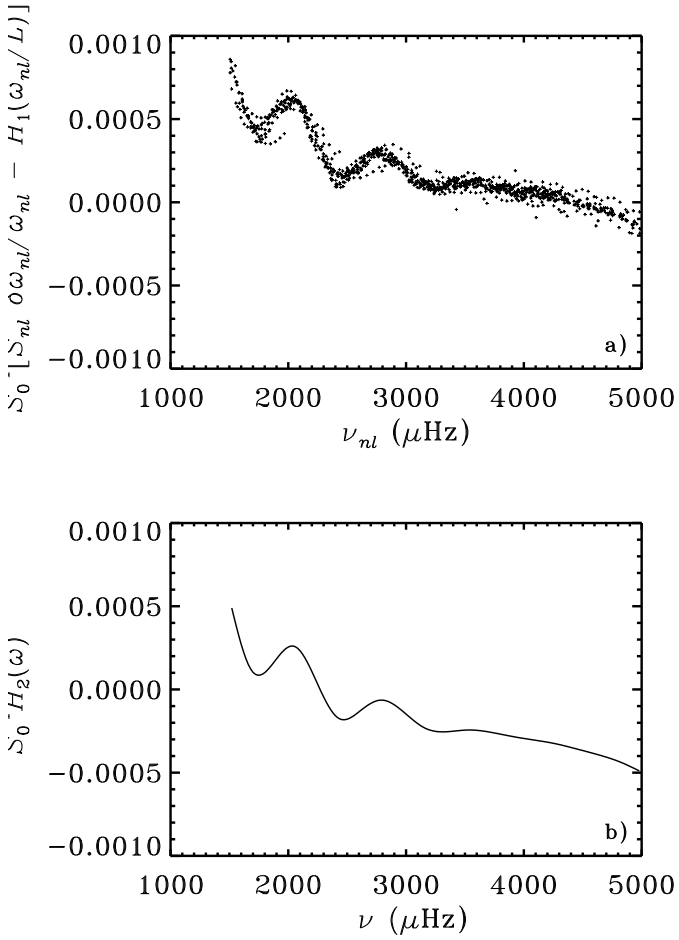

Figure 7.10: The frequency-dependent part of the scaled frequency differences corresponding to the model differences shown in Figure 7.8. (a) Scaled differences after subtraction of the function $\mathcal{H}_1(\omega/L)$ resulting from the spline fit. (b) The fitted function $\mathcal{H}_2(\omega)$.

shows the fitted function $\mathcal{H}_1$; here there is evidently a step at a turning-point location corresponding approximately to the base of the convection zone. Nevertheless, it is evident even from this simple analysis that the inclusion of diffusion and settling very substantially improves the agreement between the model and the Sun.

It is evident that there is considerably more scatter in Figure 7.11b than in the corresponding Figure 7.9b. This is due to observational errors, both random and systematic. In particular, it may be noticed that there is an apparent break at around $\nu/L \simeq 15\,\mu$Hz. In fact, the observed frequencies were obtained from two separate sets of observations, the merge taking place at $l = 400$; it has later been found that there were slight systematic errors in the high-degree set. This difficulty is clearly reflected in the fitted $\mathcal{H}_1(\omega/L)$ in Figure 7.11c. Furthermore, there appear to be problems at low degree, corresponding to

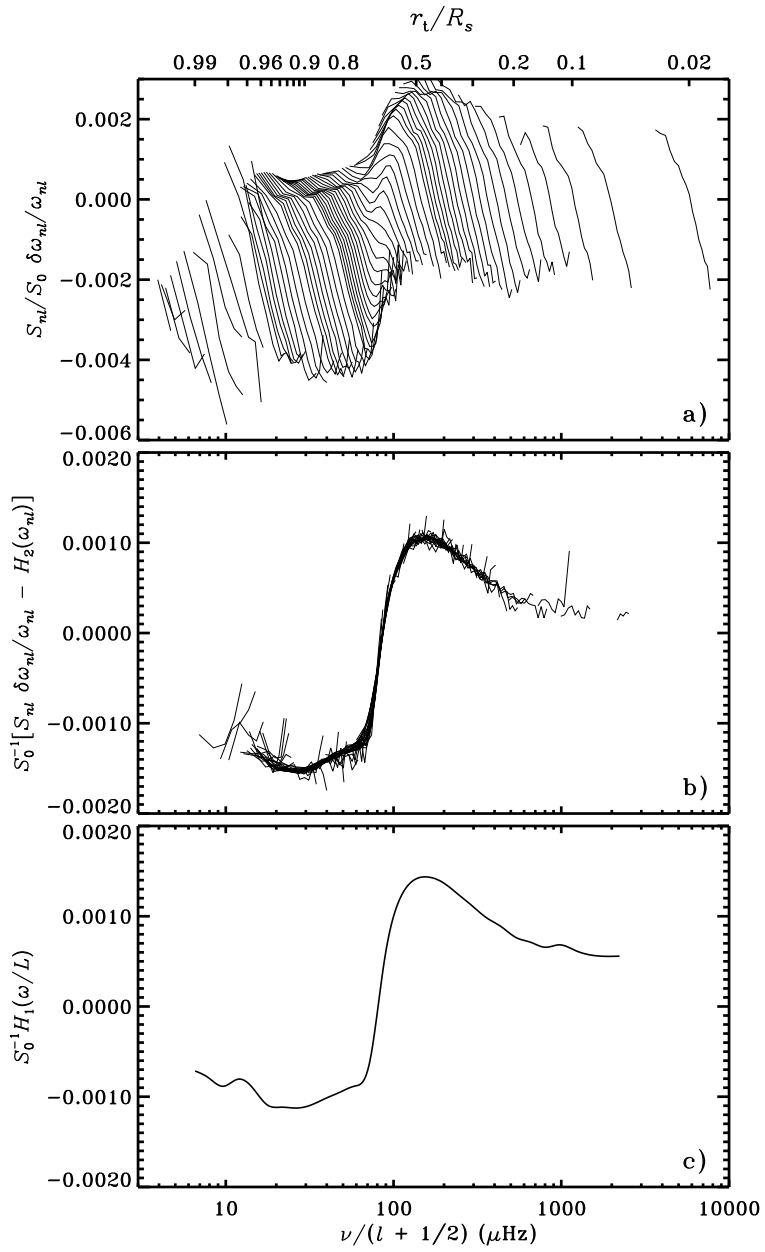

Figure 7.11: Scaled frequency differences between observed frequencies (see text) and a solar model neglecting settling and diffusion, in the sense (observations) – (model), plotted against $\nu/(l+1/2)$. The upper abscissa shows the location of the lower turning point, which is related to $\nu/(l+1/2)$ through equation (5.28). In panels (a) and (b) points corresponding to fixed l have been connected. (a) Original asymptotically scaled frequency differences. (b) Scaled differences, after subtraction of the function $\mathcal{H}_2(\omega)$ obtained from the spline fit. (c) The fitted function $\mathcal{H}_1(\omega/L)$.

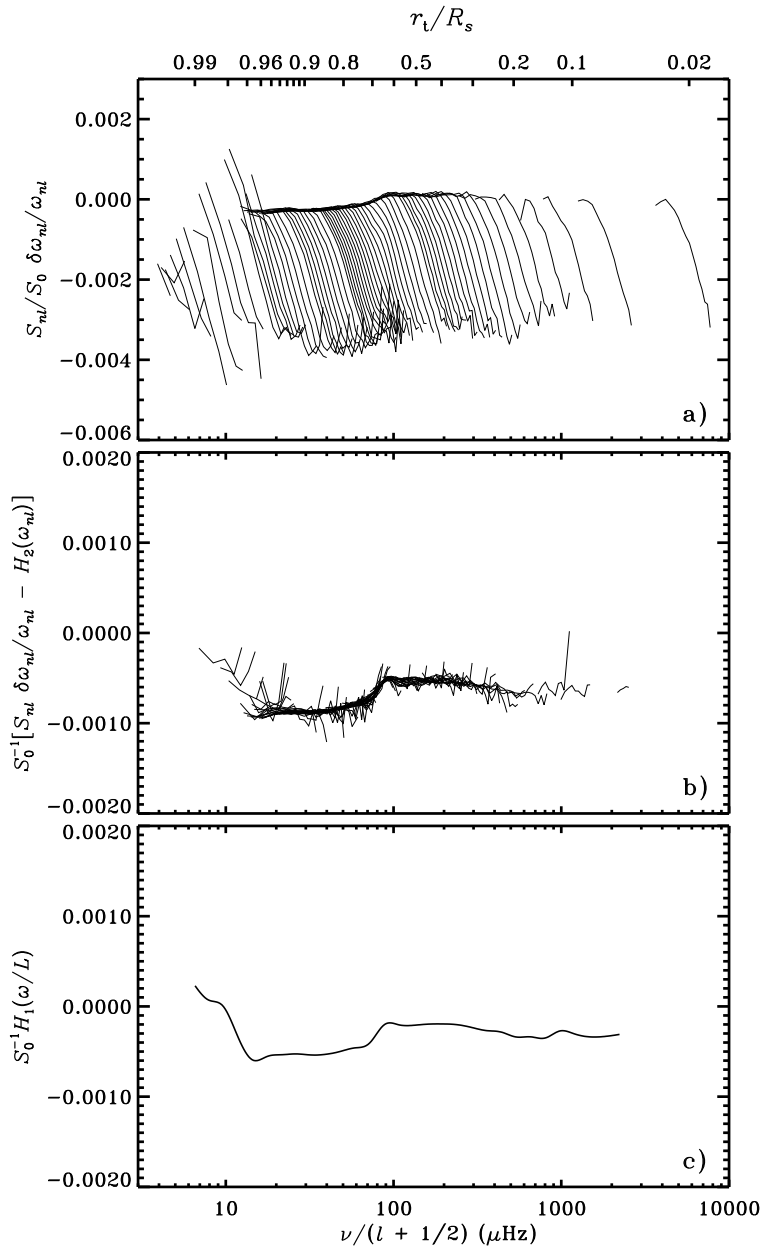

Figure 7.12: Scaled frequency differences between observed frequencies (see text) and a solar model including settling and diffusion, in the sense (observations) – (model), plotted against $\nu/(l + 1/2)$. See caption to Figure 7.11.

the highest values of ν/L.

The residual after subtraction of the fitted $\mathcal{H}_1$ from the scaled differences, and the fitted $\mathcal{H}_2$, are shown in Figure 7.13. In panel (a) are shown the residuals for the model neglecting diffusion and settling. As before, these are indeed predominantly a function of frequency.

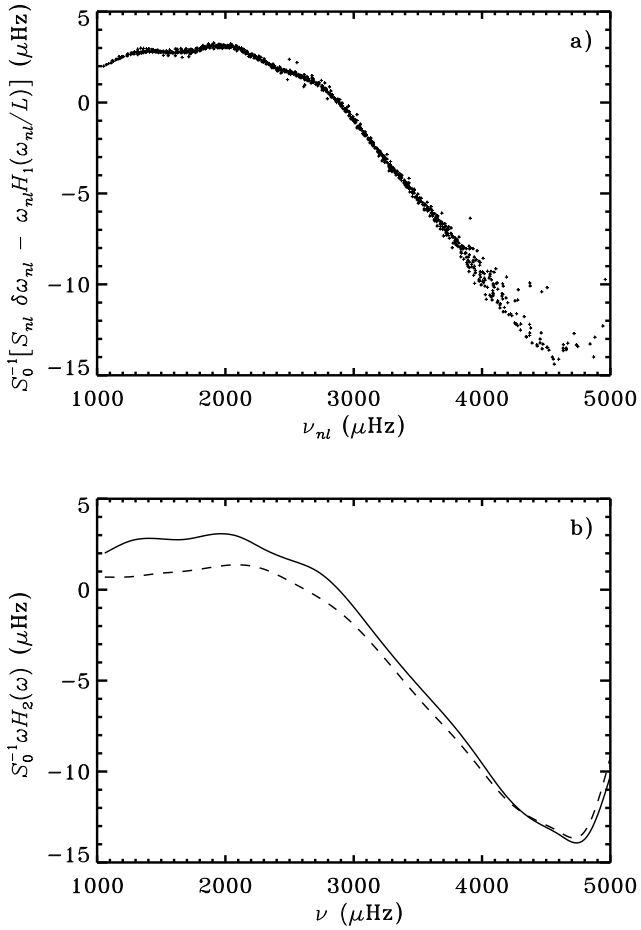

Figure 7.13: The frequency-dependent part of the scaled frequency differences between observations and models. (a) Scaled differences, shown in Figure 7.11a, after subtraction of the function $\mathcal{H}_1(\omega/L)$ resulting from the spline fit. (b) The solid line shows the fitted function $\mathcal{H}_2(\omega)$ for this data set, while the dashed line shows the corresponding fitted function obtained from the differences in Figure 7.12a.

They are dominated by a slowly varying trend which, as argued in Section 7.7.3 below reflects errors in the near-surface region of the model. However, there is also a weak but clearly noticeable oscillatory signal. As discussed in Section 7.7.3 this probably reflects a difference between the Sun and the model in the hydrogen abundance in the convective envelope. This oscillatory behaviour is also very evident in the fitted $\mathcal{H}_2(\omega)$, shown as a solid line in panel (b). In contrast, $\mathcal{H}_2(\omega)$ for the model with settling and diffusion, shown as a dashed line, gives very little evidence for such oscillations, indicating that the envelope hydrogen abundance for this model is quite similar to that of the Sun.

7.7.2 Inversion of the Duvall law

The function $F(w)$ in equation (7.143) can be determined from the observations (*cf.* Figure 7.1). Given F, equation (7.144) is an integral equation of the Abel type, and can be inverted analytically to obtain the sound speed implicitly, thus:

$$r = R \exp\left[-\frac{2}{\pi}\int_{a_s}^{a}\left(w^{-2}-a^{-2}\right)^{-1/2}\frac{\mathrm{d}F}{\mathrm{d}w}\mathrm{d}w\right] \tag{7.152}$$

(Gough 1984). This relation was used by Christensen-Dalsgaard *et al.* (1985) to infer the sound speed in the solar interior. The properties of this inversion technique were discussed in considerable detail by Gough (1986b).

Exercise 7.5:

Confirm that equation (7.152) is a solution to equation (7.144). This is most simply done by substituting equation (7.144) into equation (7.152).

The asymptotic description leading to equation (7.152) clearly suffers from systematic errors. It has been found, for example, that for the most deeply penetrating modes of low degree the perturbation to the gravitational potential has a substantial effect on the functions $F(\omega/L)$ obtained by fitting the relation (7.143) to computed or observed frequencies; this may cause problems for the inversion in the solar core. Also, for modes trapped near the surface the behaviour near the upper turning point depends on the degree; this introduces what is effectively an l-dependent term in α. It is possible to generalize equation (7.143) to take such effects into account and hence obtain a substantially more precise inversion (*e.g.* Vorontsov & Shibahashi 1991).

Alternatively, it appears that the systematic errors cancel to some extent when differences are taken between inversions of different sets of frequencies. Christensen-Dalsgaard *et al.* (1985) made use of this by considering differences between inversions done for the solar data and for frequencies for a reference model. A more systematic approach follows from the separation of scaled frequency differences in equation (7.147). Here the function $\mathcal{H}_1(\omega/L)$ is related to the sound-speed difference between the models, or between the Sun and the model, through equation (7.148). As shown by Christensen-Dalsgaard, Gough & Thompson (1989), given a determination of $\mathcal{H}_1$, that equation is an integral equation for $\delta_r c/c$, with the solution

$$\frac{\delta_r c}{c} = -\frac{2a}{\pi}\frac{\mathrm{d}}{\mathrm{d}\ln r}\int_{a_s}^{a}(a^2-w^2)^{-1/2}\mathcal{H}_1(w)\mathrm{d}w\,, \tag{7.153}$$

where $a_s = a(R)$. [It should be noticed that the right-hand side of equation (7.148) is the same functional of w as that which arises in the asymptotic expression for the linear frequency splitting due to latitudinally-independent rotation at a rate $\Omega(r)$, with $\delta_r c/c$ instead of Ω (Gough 1984). Thus it can be inverted in the same way.]

Christensen-Dalsgaard *et al.* (1989) carried out a careful test of the differential method, as applied to several different pairs of models. Also, Christensen-Dalsgaard, Gough & Thompson (1988) used the method to invert differences between observed frequencies and frequencies computed for a solar model. Here I illustrate its properties by applying it to the

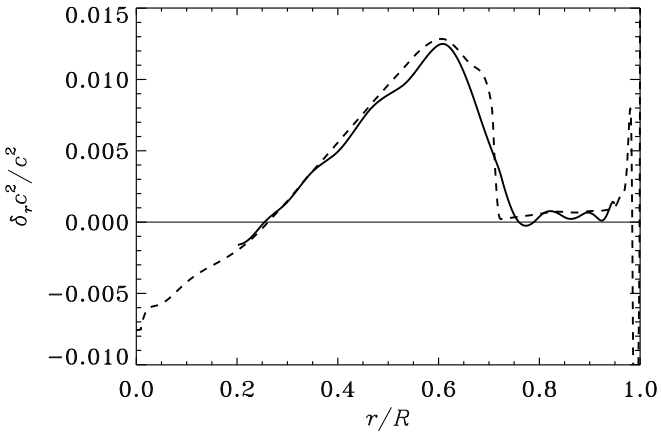

Figure 7.14: The solid line shows the difference in squared sound speed $\delta_r c^2/c^2$ inferred by applying equation (7.153) to the function $\mathcal{H}_1(\omega/L)$ shown in Figure 7.9c. For comparison, the dashed line shows the true difference between the two models. Adapted from Christensen-Dalsgaard, Proffitt & Thompson (1993).

model pair shown in Figure 7.8 and to differences between solar and computed frequencies such as those shown in Figures 7.11 and 7.12.

Figure 7.14 shows the $\delta_r c^2/c^2$ inferred from the scaled frequency differences in Figure 7.9 between the diffusive and the normal solar model, by applying equation (7.153) to the fitted function $\mathcal{H}_1(\omega/L)$ shown in Figure 7.9c. For comparison, the figure also shows the true sound-speed difference, previously plotted in Figure 7.8. It is evident that the inversion reproduces the main features of the true $\delta_r c^2/c^2$ with considerable precision. One noticeable difference is that the transition at the base of the convection zone is less sharp: as discussed in Section 9.1 it is a general property of inverse analyses that they smooth the properties of the true structure. However, otherwise the inferred and the true $\delta_r c^2/c^2$ are quite close over the entire range, $0.2R < r < 0.95R$, where the solution is plotted. At smaller and larger radii the systematic errors associated with the asymptotic representation increasingly affect the results; hence here the solution has not been obtained.

From the frequency differences illustrated in Figures 7.11 and 7.12 we may now infer the error in the sound speed in the solar models. Figure 7.15 shows the results of evaluating $\delta_r c/c$ by applying equation (7.153) to the $\mathcal{H}_1(\omega/L)$ shown in Figures 7.11c and 7.12c. The sound-speed differences are small, corresponding to errors in T/μ in the models of generally less than 2 per cent. Nonetheless, the differences are clearly highly systematic. It is interesting that the relatively subtle, and often neglected, effect of gravitational settling leads to a substantial improvement in the agreement between the model and the observations, largely by increasing the depth of the convection zone in the model. This is a striking illustration of the power of helioseismology to probe the details of the solar interior. However, it should also be pointed out that modest modifications in the opacity, well within the

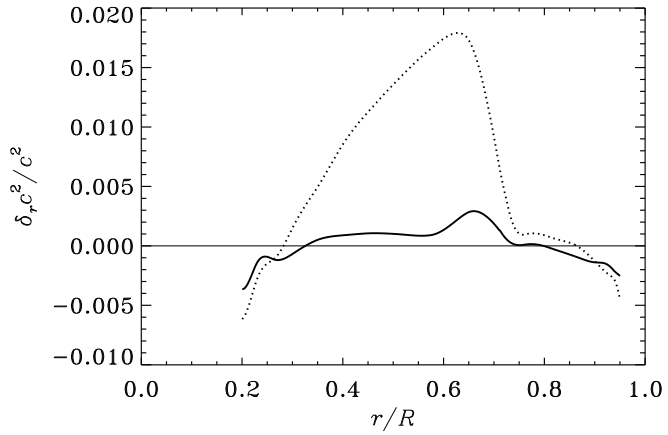

Figure 7.15: The dotted line shows the difference in squared sound speed $\delta_r c^2/c^2$ between the Sun and a solar model without diffusion and settling, inferred by applying equation (7.153) to the function $\mathcal{H}_1(\omega/L)$ shown in Figure 7.11c, corresponding to differences between observed and model frequencies. The solid line shows the corresponding $\delta_r c^2/c^2$ between the Sun and a model including diffusion and gravitational settling, obtained from $\mathcal{H}_1(\omega/L)$ in Figure 7.12c.

precision of current opacity tables, might introduce changes in the sound speed of similar magnitude. The separation of opacity uncertainties from effects of diffusion and settling is a major challenge, which will undoubtedly require better physical understanding of the processes involved.

The cause of the dominant difference between the Sun and the nondiffusive model is probably that the depth of the convection zone in the model is too small. In fact, the model with diffusion has a slightly deeper convection zone. From a more careful analysis of such results of inversions it is possible to obtain an estimate of the convection-zone depth $d_{\rm b}$ which is largely independent of other uncertainties in the model. In this way Christensen-Dalsgaard, Gough & Thompson (1991) found that $d_{\rm b} = (0.713 \pm 0.003)\, R$.

It should finally be mentioned that several other techniques have been developed to invert the Duvall law (7.143) (Brodsky & Vorontsov 1987, 1988a; Shibahashi 1988; Shibahashi & Sekii 1989). Gough & Thompson (1991) have made a comparison of these different techniques. The results suggest that, at least for the cases considered, the differential technique described here is superior. Nonasymptotic inversion of similar data sets will be discussed in Section 9.2.

7.7.3 The phase-function difference $\mathcal{H}_2(\omega)$

The function $\mathcal{H}_2(\omega)$ is predominantly determined by the region near the stellar surface. Christensen-Dalsgaard & Pérez Hernández (1992) analyzed the relation of $\mathcal{H}_2(\omega)$ to the differences in sound speed and Γ_1 in the outer parts of the Sun: differences localized very

near the surface give rise to a component of $\mathcal{H}_2$ that varies slowly with ω, whereas differences at somewhat greater depth introduce an oscillatory variation with ω in $\mathcal{H}_2$, the "frequency" of which increases with the depth of the difference. This is in fact a general property of frequency differences caused by sharply localized modifications to stellar structure (*e.g.* Thompson 1988; Vorontsov 1988; Gough 1990), and reflects the variation with frequency in the phase of the eigenfunction at the location of the modification. At the surface the behaviour of the eigenfunction changes slowly with frequency, whereas at greater depth a change in frequency causes the eigenfunction to "sweep through" the point where the model was changed, causing a rapid variation in the frequency change. In the case of the variation of $\mathcal{H}_2$ with ω, Christensen-Dalsgaard & Pérez Hernández (1991) found several cases where the relatively sharp change in Γ_1 in the second helium ionization zone caused an oscillatory behaviour of $\mathcal{H}_2(\omega)$. Similar variations in the basic phase function $\alpha(\omega)$ were analyzed, for example, by Brodsky & Vorontsov (1988b, 1989) and Baturin & Mironova (1990). Vorontsov, Baturin & Pamyatnykh (1992) showed how the phase could be separated in a quantitative fashion into components varying slowly and rapidly with frequency. This type of analysis provides a powerful diagnostic of the properties of the ionization zones of hydrogen and helium, of great interest both for the analysis of the equation of state and for attempts to determine the helium abundance of the solar convection zone.

It is very convenient to express $\mathcal{H}_2(\omega)$ in terms of differences between two models, or the Sun and a model, in a form analogous to equation (5.90). Christensen-Dalsgaard & Pérez Hernández (1992) showed that $\alpha(\omega)$, and hence $\mathcal{H}_2(\omega)$, can be determined directly from the model structure, without computing full modes of oscillation. In this way they were able to find kernels relating $\mathcal{H}_2$ to the model changes. The kernels turn out to be particularly simple if the model changes are expressed in terms of c and the (isothermal) acoustical cut-off frequency

$$\omega_{\mathrm{a}} = \frac{c}{2H_p} = \frac{\Gamma_1 g}{2c} \tag{7.154}$$

(*cf.* eq. 5.45). Thus I express $\mathcal{H}_2$ as

$$\mathcal{H}_2(\omega) = \int_{r_0}^{R} \left[K_c(r;\omega)\frac{\delta_r c}{c} + K_{\omega_{\mathrm{a}}}(r;\omega)\frac{\delta_r \omega_{\mathrm{a}}}{\omega_{\mathrm{a}}} \right] \mathrm{d}r + \mathcal{G}_2(\omega) \;, \tag{7.155}$$

where r_0 is a point suitably deep in the convection zone. Here, as in equation (5.90), the term $\mathcal{G}_2(\omega)$ contains the contributions from the differences (or errors) in the physics of the oscillations: as argued in Section 5.5.3 such errors are likely to be confined very close to the stellar surface and hence probably depend on frequency alone, when properly scaled.

The kernel K_c varies slowly with position and frequency, and hence give little interesting contribution to $\mathcal{H}_2$. On the other hand, the kernels $K_{\omega_{\mathrm{a}}}$ have a very distinct behaviour. This is illustrated in Figure 7.16, both as a function of r (at fixed frequency) and as a function of frequency (at fixed r). The r-dependence is qualitatively similar to the behaviour of the scaled eigenfunctions shown in Figure 5.8: the kernels oscillate within an envelope which varies as $c(r)^{-1}$. The frequency dependence clearly illustrates the behaviour discussed above in a qualitative manner: at the surface the kernels vary slowly with frequency (the erratic variations at the lowest frequencies are due to numerical errors), and the variation with frequency becomes increasingly rapid with increasing depth. In fact, as shown by Christensen-Dalsgaard & Pérez Hernández (1992) the kernels may be approximated by

$$K_{\omega_{\mathrm{a}}}(r;\omega) \simeq -\frac{1}{c(r)} \cos[2\omega(\tau(r) - \tau')] \;, \tag{7.156}$$

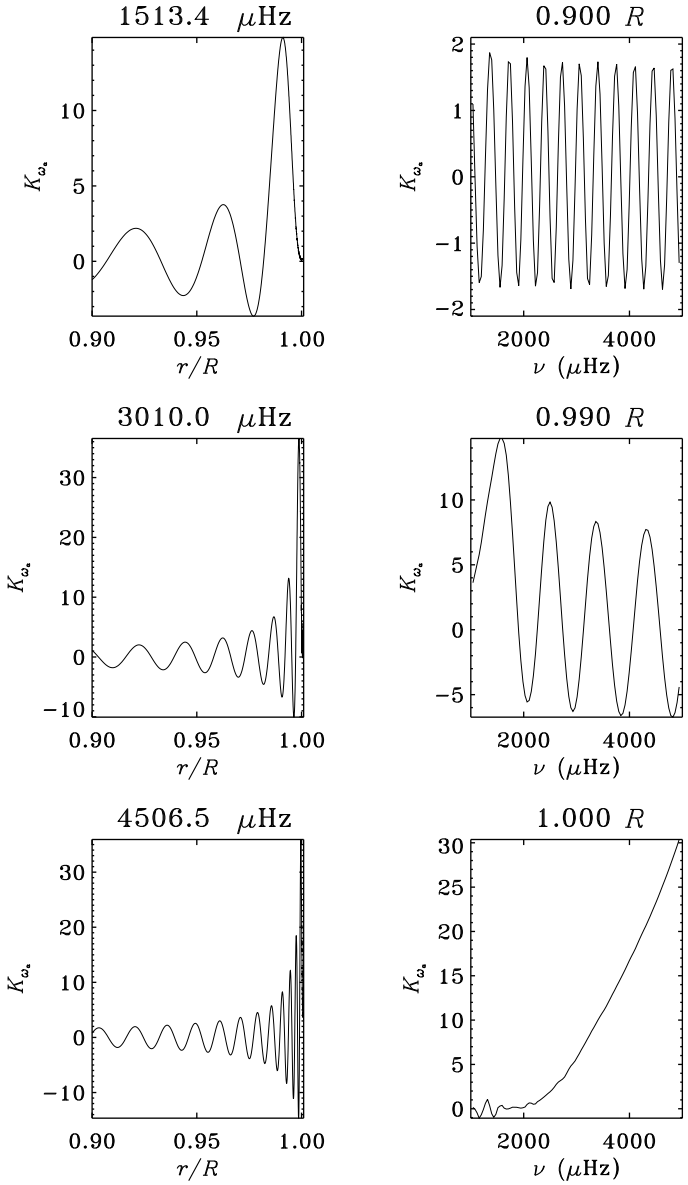

Figure 7.16: The kernels $K_{\omega_a}(r;\omega)$ relating changes in ω_a to $\mathcal{H}_2(\omega)$ (*cf.* eq. 7.155). The left-hand column shows the kernels as functions of r at the frequencies indicated, whereas the right-hand column shows the kernels against frequency, at the radii indicated.

where

$$\tau(r) = \int_r^R \frac{\mathrm{d}r}{c} \tag{7.157}$$

is the acoustical depth, *i.e.*, the sound travel time between the point considered and the surface; also, τ' is roughly a constant. It is evident that according to equation (7.156) K_{ω_a}

is an oscillatory function of ω, oscillating increasingly rapidly with increasing τ and hence increasing depth.

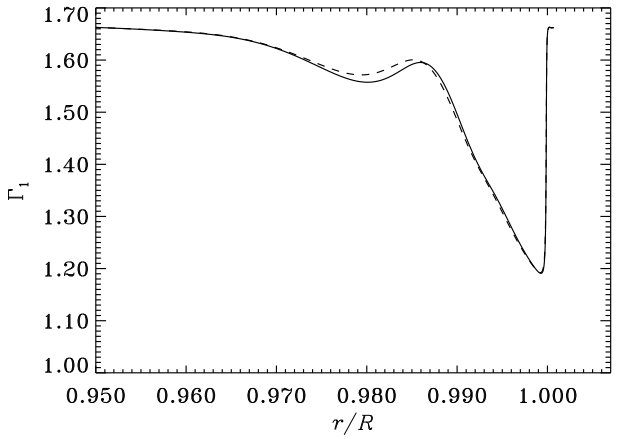

Figure 7.17: The adiabatic exponent Γ_1 in a normal solar model (solid curve) and in a model with helium diffusion and settling (dashed curve).

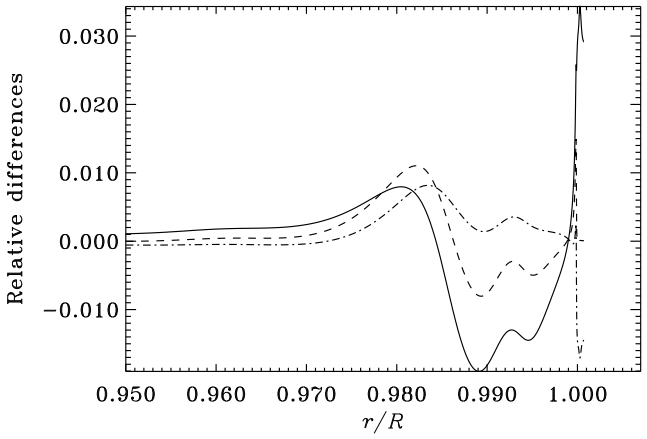

Figure 7.18: Fractional differences between a model of the present Sun with diffusion and a normal model, without diffusion. The solid curve shows $\delta_r c^2/c^2$, the dashed curve $\delta_r \Gamma_1/\Gamma_1$ and the dot-dashed curve $\delta_r \omega_a/\omega_a$ (*cf.* eq. 7.154).

According to equation (7.155) the variation of K_{ω_a} with ω at a certain r corresponds to the $\mathcal{H}_2(\omega)$ arising from a localized change in ω_a at that position. Hence a sharp feature in $\delta_r \omega_a$ at some point $r = r^*$ will give rise to an oscillatory contribution to $\mathcal{H}_2(\omega)$ with a

'frequency' which, from equation (7.156), is approximately $2\tau(r^*)$. Such contributions are in fact clearly visible both in Figure 7.10b, corresponding to the difference between two models differing in the envelope helium abundance, and in Figure 7.13b for the differences between the Sun and a model. The 'frequency' of the variation corresponds to a depth of roughly $0.02R$, *i.e.*, the region of the second ionization of helium.

To understand the origin of this feature I first consider the behaviour of Γ_1. In regions of no or full ionization it is very close to 5/3. However, ionization causes a decrease of Γ_1 below this value; as illustrated in Figure 7.17, there is a major dip in Γ_1 in the overlapping regions of hydrogen and first helium ionization and a smaller, secondary dip in the region of second helium ionization. It is evident that the depth of the second dip must depend on the helium abundance. The effect is clearly visible by comparing the solid curve in Figure 7.17, for the normal nondiffusive model with an envelope helium abundance $Y_\mathrm{e} = 0.28$, with the dashed curve for the model with diffusion and settling, where Y_e has been reduced to 0.25. These effects are also evident in the differences between the two models, shown in Figure 7.18 (the sound-speed difference was also shown in Figure 7.8, but for the whole model). In particular, there is a fairly sharp feature in $\delta_r\omega_\mathrm{a}$ at $r \simeq 0.985R$, which is responsible for the oscillatory contribution to $\mathcal{H}_2(\omega)$ noted in Figure 7.10b.

These results suggest that $\mathcal{H}_2$ may provide useful information about the properties of the upper parts of the convection zone, including the solar envelope helium abundance which is otherwise quite uncertain. In fact, it was noted in Section 5.1.2 that the structure of the adiabatic part of the convection zone is determined by the composition, in particular the value of Y_e, as well as the specific entropy s which is essentially constant; in addition, the equation of state must be known. Indeed, the $\mathcal{H}_2(\omega)$ which results from the differences between the observed and the computed frequencies (*cf.* Figure 7.13b) shows oscillations which are superficially quite similar to those resulting from the difference in Y_e, although overlayed by a substantial slowly varying trend. As shown by Figure 7.16, this slowly varying component approximately corresponds to the contributions that may arise from differences in the outermost parts of the model. More generally, the uncertain physics in the layers immediately below the photosphere and in the solar atmosphere may be expected to give rise to a similar behaviour, as indicated by the function $\mathcal{G}_2(\omega)$ in equation (7.155). This complicates the interpretation of the $\mathcal{H}_2(\omega)$ determined from the observed frequencies. It was shown by Pérez Hernández & Christensen-Dalsgaard (1994a) that the slowly varying part of $\mathcal{H}_2$ can be suppressed in a consistent way through filtering. Furthermore, Pérez Hernández & Christensen-Dalsgaard (1994b) made a fit of the resulting filtered $\mathcal{H}_2$ to models differing in Y_e and s, as well as the surface properties; in this way they inferred that $Y_\mathrm{e} = 0.243 \pm 0.002$. It might be noted that this is quite close to the value obtained in the model with helium settling and diffusion.

The results of such fits, or more generally of any attempt to measure Y_e from analysis of solar oscillation frequencies, depend critically on the equation of state. Indeed, all such methods utilize the variation of Γ_1 in the ionization zones; this variation evidently depends on the details of the ionization processes and hence on the thermodynamic properties of the plasma. In fact, Pérez Hernández & Christensen-Dalsgaard (1994b) found that the quality of the fit depended quite sensitively on the assumed equation of state, giving strong preference for one formulation over another, even though both were comparatively sophisticated. This indicates that it may be possible to get some separate information about the composition and the thermodynamic properties of matter in the solar convection zone. However, it is evident that one might conceive of errors in the equation of state with an effect similar

to that corresponding to a change in the helium abundance. Such effects evidently cannot be separated on the basis of an analysis of the oscillation frequencies.

I finally note that the function $\alpha(\omega)$ also enters into the asymptotic behaviour of low-degree modes (*cf.* eq. 7.55); this is visible in the curvature, essentially similar for the different degrees, in the echelle diagram of low-degree solar observations in Figure 2.15. This suggests that it may be possible to obtain information about the near-surface regions, similar to what can be determined from $\mathcal{H}_2(\omega)$, by analyzing observations of stellar oscillations where only modes of degree less than three are generally visible. Brodsky & Vorontsov (1988a) presented a method to determine a function closely related to $\alpha(\omega)$ on the basis of low-degree data alone. This was applied to models of main-sequence stars by Pérez Hernández & Christensen-Dalsgaard (1993), who found a characteristic dependence on the stellar parameters. Further analyses of the effects on the frequencies or frequency separations of the detailed properties of the helium ionization zones were carried out by Monteiro & Thompson (1998) and Miglio *et al.* (2003). A demonstration of the practical utility of this type of analysis, given realistic observational errors and other uncertainties, requires more extensive investigations, however.

Chapter 8

Rotation and stellar oscillations

I have so far assumed that there are no velocity fields in the equilibrium model. This is manifestly false for an object like the Sun which is rotating; in particular, the observed surface rotation depends on latitude, thus implying the presence of velocity fields. In addition, other large-scale velocity fields, such as those caused by convection, could have an effect on the modes. Hence we must investigate such effects. Apart from their intrinsic interest, the principal purpose of such studies is obviously to be able to probe the velocity fields from the observed properties of the oscillations.

It is straightforward to see, from a purely geometrical argument, that rotation might affect the observed frequencies. Assume the angular velocity Ω to be uniform, and consider an oscillation with a frequency ω_0, independent of m, in the frame rotating with the star. I introduce a coordinate system in this frame, with coordinates (r', θ', ϕ') which are related to the coordinates (r, θ, ϕ) in an inertial frame through

$$(r', \theta', \phi') = (r, \theta, \phi - \Omega t) \; . \tag{8.1}$$

It follows from equation (4.40) that, in the rotating frame, the perturbations depend on ϕ' and t as $\cos(m\phi' - \omega_0 t)$; hence, the dependence in the inertial frame is $\cos(m\phi - \omega_m t)$, where

$$\omega_m = \omega_0 + m\Omega \; . \tag{8.2}$$

Thus an observer in the inertial frame finds that the frequency is split uniformly according to m.

This description is obviously incomplete. Even in the case of uniform rotation, the effects of the Coriolis force must be taken into account in the rotating frame, causing a contribution to the frequency splitting (Cowling and Newing 1949; Ledoux 1949). Furthermore, in general the angular velocity is a function $\Omega(r, \theta)$ of position. Nevertheless, as shown below, the effect of the Coriolis force is often small and equation (8.2) is approximately correct if Ω is replaced by a suitable average of the position-dependent angular velocity.

To arrive at an expression valid for any rotation law it is convenient to consider first the even more general case of an arbitrary stationary velocity field in the star.

8.1 The effect of large-scale velocities on the oscillation frequencies

We need to reconsider the derivation of the perturbation equations, including the effects of a velocity field. I shall assume that the equilibrium structure is stationary, so that all local time derivatives vanish. Even with this assumption the determination of the equilibrium structure is a non-trivial problem, due to the distortion caused by the velocity fields (*e.g.* due to centrifugal effects in a rotating star). However, here I assume that the velocity $\mathbf{v}_0$ in the equilibrium state is sufficiently slow that terms quadratic in $\mathbf{v}_0$ can be neglected. The equation of continuity (3.6) gives, because of the assumed stationarity

$$\mathrm{div}\,(\rho_0\mathbf{v}_0) = 0\ . \tag{8.3}$$

Also, because of the neglect of terms of order $|\mathbf{v}|^2$, the equations of motion (3.9) reduce to

$$0 = -\nabla p_0 + \rho_0\mathbf{g}_0\ . \tag{8.4}$$

As usual I have replaced the body force per unit mass $\mathbf{f}$ by the gravitational acceleration $\mathbf{g}$. Thus equation (3.30) of hydrostatic support is unchanged. In the solar case, the ratio between the neglected centrifugal force and surface gravity is of order 2×10^{-5} and so the error in equation (8.4) is in fact small.

The perturbation analysis also requires some care. It was treated in considerable detail by Lynden-Bell & Ostriker (1967), and is discussed in Cox (1980), Chapter 5. Here I just present a few of the main features.

The velocity at a given point in space can be written as

$$\mathbf{v} = \mathbf{v}_0 + \mathbf{v}'\ , \tag{8.5}$$

where $\mathbf{v}'$ is the Eulerian velocity perturbation. The displacement $\boldsymbol{\delta}\mathbf{r}$ must be determined relative to the moving equilibrium fluid; it is related to the velocity perturbation by

$$\frac{\mathrm{d}\boldsymbol{\delta}\mathbf{r}}{\mathrm{d}t} = \boldsymbol{\delta}\mathbf{v} = \mathbf{v}' + (\boldsymbol{\delta}\mathbf{r}\cdot\nabla)\mathbf{v}_0\ . \tag{8.6}$$

Here $\boldsymbol{\delta}\mathbf{v}$ is the Lagrangian velocity perturbation and, as in Section 3.1, $\mathrm{d}/\mathrm{d}t$ is the material time derivative,

$$\frac{\mathrm{d}\boldsymbol{\delta}\mathbf{r}}{\mathrm{d}t} = \frac{\partial\boldsymbol{\delta}\mathbf{r}}{\partial t} + (\mathbf{v}_0\cdot\nabla)\boldsymbol{\delta}\mathbf{r}\ ; \tag{8.7}$$

in contrast to the zero-velocity case, the local and the material time derivatives of perturbations are now different.

The perturbed continuity equation may be written as

$$\begin{aligned} 0 &= \frac{\partial\rho'}{\partial t} + \mathrm{div}\,(\rho'\mathbf{v}_0 + \rho_0\mathbf{v}') \\ &= \frac{\partial}{\partial t}[\rho' + \mathrm{div}\,(\rho_0\boldsymbol{\delta}\mathbf{r})] + \mathrm{div}\,\{\rho'\mathbf{v}_0 + \rho_0[(\mathbf{v}_0\cdot\nabla)\boldsymbol{\delta}\mathbf{r} - (\boldsymbol{\delta}\mathbf{r}\cdot\nabla)\mathbf{v}_0]\}\ , \end{aligned} \tag{8.8}$$

on using equations (8.6) and (8.7). After some manipulation, using equation (8.3), this may be reduced to

$$\frac{\partial A}{\partial t} + \mathrm{div}\,(A\mathbf{v}_0) = 0\ , \tag{8.9}$$

where

$$A = \rho' + \mathrm{div}\,(\rho_0 \boldsymbol{\delta r}) \ . \tag{8.10}$$

This may also, by using again equation (8.3), be written as

$$\rho_0 \frac{\mathrm{d}}{\mathrm{d}t}\left(\frac{A}{\rho_0}\right) = 0 \ , \tag{8.11}$$

from which we conclude that $A = 0$, *i.e.*, that equation (3.41) is valid in this case also.

To obtain the perturbed momentum equation I use equation (3.8); from the fact that Lagrangian perturbation and material time derivative commute,

$$\frac{\mathrm{d}}{\mathrm{d}t}(\delta\psi) = \delta\left(\frac{\mathrm{d}\psi}{\mathrm{d}t}\right) \tag{8.12}$$

for any quantity ψ, we then obtain

$$\rho_0 \frac{\mathrm{d}\boldsymbol{\delta v}}{\mathrm{d}t} = \delta(-\nabla p + \rho \mathbf{g}) = -\nabla p' + \rho_0 \mathbf{g}' + \rho' \mathbf{g}_0 \ , \tag{8.13}$$

by using equation (8.4). Alternatively this may be written, from equation (8.6), as

$$\rho_0 \frac{\mathrm{d}^2 \boldsymbol{\delta r}}{\mathrm{d}t^2} = -\nabla p' + \rho_0 \mathbf{g}' + \rho' \mathbf{g}_0 \ , \tag{8.14}$$

or, by using equation (8.7) and neglecting the term quadratic in $\mathbf{v}_0$,

$$\rho_0 \frac{\partial^2 \boldsymbol{\delta r}}{\partial t^2} + 2\rho_0 (\mathbf{v}_0 \cdot \nabla)\left(\frac{\partial \boldsymbol{\delta r}}{\partial t}\right) = -\nabla p' + \rho_0 \mathbf{g}' + \rho' \mathbf{g}_0 \ , \tag{8.15}$$

which replaces equation (3.43). Finally, from the commutativity in equation (8.12), one finds that the perturbed energy equation (3.46) is still valid. Thus to this level of accuracy, the only change in the perturbation equations is the inclusion of the term in the first time derivative of $\boldsymbol{\delta r}$ in equation (8.15)

As the equilibrium structure is independent of time, we may still separate the time dependence as $\exp(-i\omega t)$. Using, for simplicity, the same symbols for the amplitude functions in this separation, we obtain from the equations of motion

$$-\omega^2 \rho_0 \boldsymbol{\delta r} - 2i\omega\rho_0 (\mathbf{v}_0 \cdot \nabla)\boldsymbol{\delta r} = -\nabla\, p' + \rho_0 \mathbf{g}' + \rho' \mathbf{g}_0 \ . \tag{8.16}$$

Here the term in $\mathbf{v}_0$ is a small perturbation. Thus we can investigate its effect by means of perturbation analysis, as discussed in Section 5.5. Following equations (5.56) and (5.57) I write equation (8.16) as

$$\omega^2 \boldsymbol{\delta r} = \mathcal{F}(\boldsymbol{\delta r}) + \delta\mathcal{F}(\boldsymbol{\delta r}) \ , \tag{8.17}$$

where

$$\delta\mathcal{F}(\boldsymbol{\delta r}) = -2i\omega (\mathbf{v}_0 \cdot \nabla)\boldsymbol{\delta r} \ . \tag{8.18}$$

It now follows from equation (5.73) and the definition of the inner product that the change in ω caused by the velocity field is, to first order,

$$\delta\omega = -i \frac{\int_V \rho_0 \boldsymbol{\delta r}^* \cdot (\mathbf{v}_0 \cdot \nabla)\boldsymbol{\delta r}\, \mathrm{d}V}{\int_V \rho_0 |\boldsymbol{\delta r}|^2\, \mathrm{d}V} \ . \tag{8.19}$$

8.2 The effect of pure rotation

Now $\mathbf{v}_0$ is taken to correspond to a pure rotation, with angular velocity $\Omega = \Omega(r, \theta)$ that may depend on r and θ. I assume that the entire star is rotating around a common axis and choose this as the axis of the spherical polar coordinate system. Then

$$\mathbf{v}_0 = \Omega r \sin\theta \, \mathbf{a}_\phi = \mathbf{\Omega} \times \mathbf{r} \; , \tag{8.20}$$

where I have introduced the rotation vector

$$\mathbf{\Omega} = \Omega(\cos\theta \, \mathbf{a}_r - \sin\theta \, \mathbf{a}_\theta) \; . \tag{8.21}$$

We must now evaluate equation (8.19) for a normal mode of oscillation, and hence we have to consider the derivative in the direction of $\mathbf{v}_0$. From equation (4.30) the perturbations depend on ϕ as $\exp(im\phi)$; thus for a scalar quantity a

$$(\mathbf{v}_0 \cdot \nabla) a = \Omega r \sin\theta \frac{1}{r \sin\theta} \frac{\partial a}{\partial \phi} = im\Omega \, a \; . \tag{8.22}$$

For a vector $\mathbf{F}$ I use equation (4.10), and note that the directional derivatives of the coordinates of $\mathbf{F}$ can be found by using equation (8.22). The result is

$$(\mathbf{v}_0 \cdot \nabla)\mathbf{F} = im\Omega\mathbf{F} + \Omega[-F_\phi \sin\theta \, \mathbf{a}_r - F_\phi \cos\theta \, \mathbf{a}_\theta + (F_r \sin\theta + F_\theta \cos\theta) \, \mathbf{a}_\phi] \; . \tag{8.23}$$

This can also be written as

$$(\mathbf{v}_0 \cdot \nabla)\mathbf{F} = im\Omega\mathbf{F} + \mathbf{\Omega} \times \mathbf{F} \; . \tag{8.24}$$

Thus equation (8.16) becomes

$$-\omega^2 \rho_0 \boldsymbol{\delta}\mathbf{r} + 2m\omega\Omega\rho_0 \boldsymbol{\delta}\mathbf{r} - 2i\omega\rho_0 \mathbf{\Omega} \times \boldsymbol{\delta}\mathbf{r} = -\nabla p' + \rho_0 \mathbf{g}' + \rho' \mathbf{g}_0 \; . \tag{8.25}$$

In the case of a uniform rotation rate Ω this equation may be obtained much more simply. Here we may transform to a coordinate system rotating with the star, with coordinates $(r', \theta', \phi') = (r, \theta, \phi - \Omega t)$. In this system the dependence of the perturbations on ϕ' and t is as

$$\cos(m\phi' + m\Omega t - \omega t) = \cos(m\phi' - \omega' t) \; , \tag{8.26}$$

where $\omega' \equiv \omega - m\Omega$ (see also the simple analysis in the introduction to this chapter). To write down the equations of motion in the rotating system I note that here there is no term in the equilibrium velocity; however, we must add the term $-2\rho_0 \mathbf{\Omega} \times \boldsymbol{\delta}\mathbf{v}$ from the Coriolis force on the right-hand side. Using that to the required order of precision the velocity perturbation is $\boldsymbol{\delta}\mathbf{v} = -i\omega\boldsymbol{\delta}\mathbf{r}$, the result is

$$-\omega'^2 \rho_0 \boldsymbol{\delta}\mathbf{r} = -\nabla p' + \rho_0 \mathbf{g}' + \rho' \mathbf{g}_0 + 2i\omega\rho_0 \mathbf{\Omega} \times \boldsymbol{\delta}\mathbf{r} \; . \tag{8.27}$$

But this agrees with equation (8.25), if a term in Ω^2 is neglected.

In the general case of non-uniform rotation it might be argued that this relation would hold locally at any given point in the fluid, thus resulting again in equation (8.25). However, it is not clear (to me, at least) whether this is a consistent derivation of that relation, or whether it results from fortuitous cancellation of terms coming from the variation of Ω. In

any case it allows a simple interpretation of the two terms in Ω in equation (8.25): the first term comes from the coordinate rotation, or equivalently from the advection of the rotating star relative to an observer in an inertial frame, and the second term comes from the Coriolis force.

We must now calculate the integral. By substituting $\boldsymbol{\delta}\mathbf{r}$, given by the complex form of equation (4.40), for $\mathbf{F}$ in equation (8.23) we obtain

$$\begin{aligned}(\mathbf{v}_0\cdot\nabla)\boldsymbol{\delta}\mathbf{r} &= im\Omega\,\boldsymbol{\delta}\mathbf{r} \\ &\quad +\sqrt{4\pi}\Omega\left[-\xi_{\rm h}\frac{\partial Y_l^m}{\partial\phi}\mathbf{a}_r-\xi_{\rm h}\frac{\cos\theta}{\sin\theta}\frac{\partial Y_l^m}{\partial\phi}\mathbf{a}_\theta+\left(\xi_r\sin\theta\,Y_l^m+\xi_{\rm h}\cos\theta\frac{\partial Y_l^m}{\partial\theta}\right)\mathbf{a}_\phi\right]\,.\end{aligned} \tag{8.28}$$

Thus

$$\begin{aligned}\tilde{R} &\equiv \int_V \rho_0\boldsymbol{\delta}\mathbf{r}^*\cdot(\mathbf{v}_0\cdot\nabla)\boldsymbol{\delta}\mathbf{r}\,{\rm d}V \\ &= im\int_V\rho_0\Omega|\boldsymbol{\delta}\mathbf{r}|^2\,{\rm d}V+4\pi\int_V\rho_0\Omega\left[-{\xi_r}^*(Y_l^m)^*\xi_{\rm h}\frac{\partial Y_l^m}{\partial\phi}-|\xi_{\rm h}|^2\left(\frac{\partial Y_l^m}{\partial\theta}\right)^*\frac{\partial Y_l^m}{\partial\phi}\frac{\cos\theta}{\sin\theta}\right. \\ &\quad \left.+\xi_{\rm h}^*\xi_r\left(\frac{\partial Y_l^m}{\partial\phi}\right)^*Y_l^m+|\xi_{\rm h}|^2\left(\frac{\partial Y_l^m}{\partial\phi}\right)^*\frac{\partial Y_l^m}{\partial\theta}\frac{\cos\theta}{\sin\theta}\right]{\rm d}V\,.\end{aligned} \tag{8.29}$$

Here Y_l^m is always multiplied by its complex conjugate, so that the ϕ-dependence cancels. Hence the integration over ϕ is trivial. It should be noticed also that all terms in the second integral in equation (8.29) contain the ϕ-derivative of Y_l^m or its complex conjugate, which is proportional to im. Thus $\tilde{R}$ contains im as a factor, and can be written, using equation (4.30), as

$$\tilde{R} = im\,8\pi^2c_{lm}^2R_{nlm}\,, \tag{8.30}$$

where

$$\begin{aligned}R_{nlm} &= \int_0^\pi\sin\theta{\rm d}\theta\int_0^R\left\{|\xi_r(r)|^2P_l^m(\cos\theta)^2\right. \\ &\quad +|\xi_{\rm h}(r)|^2\left[\left(\frac{{\rm d}P_l^m}{{\rm d}\theta}\right)^2+\frac{m^2}{\sin^2\theta}P_l^m(\cos\theta)^2\right] \\ &\quad -P_l^m(\cos\theta)^2\left[{\xi_r}^*(r)\xi_{\rm h}(r)+\xi_r(r)\xi_{\rm h}^*(r)\right] \\ &\quad \left.-2P_l^m(\cos\theta)\frac{{\rm d}P_l^m}{{\rm d}\theta}\frac{\cos\theta}{\sin\theta}|\xi_{\rm h}(r)|^2\right\}\Omega(r,\theta)\rho_0(r)r^2{\rm d}r\,.\end{aligned} \tag{8.31}$$

Similarly, the denominator in equation (8.19) can be written as

$$\tilde{I}\equiv\int_V\rho_0|\boldsymbol{\delta}\mathbf{r}|^2{\rm d}V = 8\pi^2c_{lm}^2I_{nlm}\,, \tag{8.32}$$

where

$$\begin{aligned}I_{nlm} &= \int_0^\pi\sin\theta{\rm d}\theta\int_0^R\left\{|\xi_r(r)|^2P_l^m(\cos\theta)^2\right. \\ &\quad \left.+|\xi_{\rm h}(r)|^2\left[\left(\frac{{\rm d}P_l^m}{{\rm d}\theta}\right)^2+\frac{m^2}{\sin^2\theta}P_l^m(\cos\theta)^2\right]\right\}\rho_0(r)r^2{\rm d}r \\ &= \frac{2}{2l+1}\frac{(l+|m|)!}{(l-|m|)!}\int_0^R\left[|\xi_r|^2+l(l+1)|\xi_{\rm h}|^2\right]\rho_0(r)r^2{\rm d}r\end{aligned} \tag{8.33}$$

[compare with equation (4.47)]. From equations (8.19), (8.30) and (8.32) we finally obtain the *rotational splitting*, *i.e.*, the perturbation in the frequencies caused by rotation, as

$$\delta\omega_{nlm} = m\frac{R_{nlm}}{I_{nlm}} \, . \tag{8.34}$$

This may obviously be written on the form

$$\delta\omega_{nlm} = m\int_0^R \int_0^\pi K_{nlm}(r,\theta)\Omega(r,\theta) r \mathrm{d}r\mathrm{d}\theta \, , \tag{8.35}$$

where the *kernel* K_{nlm} is defined by equations (8.31) and (8.33).

From equations (8.31) and (8.33), as well as the symmetry property of the Legendre function with respect to m (eq. A.8), it follows that R_{nlm}/I_{nlm} is an even function of m and hence that $\delta\omega_{nlm}$ is an odd function of m,

$$\delta\omega_{nl\,-m} = -\delta\omega_{nlm} \, . \tag{8.36}$$

Also, since $P_l^m(x)$ is either symmetrical or antisymmetrical around $x = 0$, the factor multiplying $\Omega(r,\theta)$ in equation (8.31) is symmetrical around the equator, $\theta = \pi/2$; thus

$$K_{nlm}(r,\pi-\theta) = K_{nlm}(r,\theta) \, . \tag{8.37}$$

This has the important consequence that the rotational frequency splitting is sensitive only to the part of Ω that is symmetrical around the equator.

Exercise 8.1:

Confirm the symmetry properties in equations (8.36) and (8.37).

The rotational splitting for a uniformly rotating star was first obtained by Cowling & Newing (1949) and Ledoux (1949). The general case, as presented here, was considered by Hansen, Cox & van Horn (1977) and Gough (1981).

8.3 Splitting for spherically symmetric rotation

To proceed we must make an explicit assumption about the variation of Ω with θ. For simplicity I shall assume first that Ω is independent of θ. In fact, as mentioned earlier, the solar surface rotation depends on θ; however, the assumption of θ-independent rotation can be regarded as the first term in an expansion of Ω, say, in terms of powers of $\cos\theta$. In this case the integrals over θ in equation (8.31) only involve Legendre functions and may be evaluated analytically. Two of the terms require a little care. One contains

$$\begin{aligned}\int_0^\pi P_l^m(\cos\theta)\frac{\mathrm{d}P_l^m}{\mathrm{d}\theta}\frac{\cos\theta}{\sin\theta}\sin\theta\mathrm{d}\theta &= -\int_{-1}^1 P_l^m(x)\frac{\mathrm{d}P_l^m}{\mathrm{d}x}x\mathrm{d}x \\ &= -\frac{1}{2}xP_l^m(x)^2\Big|_{-1}^1 + \frac{1}{2}\int_{-1}^1 P_l^m(x)^2\mathrm{d}x \, ,\end{aligned} \tag{8.38}$$

and here the integrated term vanishes, as $P_l^m(x)$ is either symmetrical or anti-symmetrical in $x = \cos\theta$. The other non-trivial integral, which was already encountered in the evaluation of I_{nlm}, is

$$\begin{aligned}
&\int_0^\pi \left[\left(\frac{\mathrm{d}P_l^m}{\mathrm{d}\theta} \right)^2 + \frac{m^2}{\sin^2\theta} P_l^m(\cos\theta)^2 \right] \sin\theta \mathrm{d}\theta \\
&= -\int_0^\pi P_l^m(\cos\theta) \left[\frac{\mathrm{d}}{\mathrm{d}\theta} \left(\sin\theta \frac{\mathrm{d}P_l^m}{\mathrm{d}\theta} \right) - \frac{m^2}{\sin\theta} P_l^m(\cos\theta) \right] \mathrm{d}\theta \\
&= L^2 \int_{-1}^1 P_l^m(x)^2 \mathrm{d}x \ ,
\end{aligned} \tag{8.39}$$

by using that P_l^m satisfies equation (4.26). As usual, I have introduced $L^2 \equiv l(l+1)$. For adiabatic oscillations we can take ξ_r and ξ_h to be real. Thus, from equation (8.31), (8.33) and (8.34), we finally obtain for the rotational splitting

$$\delta\omega_{nlm} = m \frac{\int_0^R \Omega(r) \left({\xi_r}^2 + L^2\xi_\mathrm{h}^2 - 2\xi_r\xi_\mathrm{h} - \xi_\mathrm{h}^2 \right) r^2 \rho \mathrm{d}r}{\int_0^R \left({\xi_r}^2 + L^2\xi_\mathrm{h}^2 \right) r^2 \rho \mathrm{d}r} \ , \tag{8.40}$$

where I have dropped the subscript "0" on ρ. It should be noticed that the integrands in equation (8.40) are given solely in terms of ξ_r, ξ_h and l, and therefore are independent of m. Hence in the case of spherically symmetric rotation the rotational splitting is proportional to m.

It is convenient to write equation (8.40) as

$$\delta\omega_{nlm} = m\beta_{nl} \int_0^R K_{nl}(r)\Omega(r)\mathrm{d}r \ , \tag{8.41}$$

where

$$K_{nl} = \frac{\left({\xi_r}^2 + L^2\xi_\mathrm{h}^2 - 2\xi_r\xi_\mathrm{h} - \xi_\mathrm{h}^2 \right) r^2 \rho}{\int_0^R \left({\xi_r}^2 + L^2\xi_\mathrm{h}^2 - 2\xi_r\xi_\mathrm{h} - \xi_\mathrm{h}^2 \right) r^2 \rho \mathrm{d}r} \ , \tag{8.42}$$

and

$$\beta_{nl} = \frac{\int_0^R \left({\xi_r}^2 + L^2\xi_\mathrm{h}^2 - 2\xi_r\xi_\mathrm{h} - \xi_\mathrm{h}^2 \right) r^2 \rho \mathrm{d}r}{\int_0^R \left({\xi_r}^2 + L^2\xi_\mathrm{h}^2 \right) r^2 \rho \mathrm{d}r} \ . \tag{8.43}$$

By using this definition we ensure that the *rotational kernel* K_{nl} is unimodular, *i.e.*,

$$\int_0^R K_{nl}(r)\mathrm{d}r = 1 \ . \tag{8.44}$$

Hence for uniform rotation, where $\Omega = \Omega_\mathrm{s}$ is constant,

$$\delta\omega_{nlm} = m\beta_{nl}\Omega_\mathrm{s} \ . \tag{8.45}$$

In this case the effect of rotation is completely given by the constant β_{nl}. For high-order or high-degree p modes the terms in ${\xi_r}^2$ and $L^2\xi_\mathrm{h}^2$ dominate; as shown in Figure 8.1, β_{nl} is then close to one. Thus the rotational splitting between adjacent m-values is given approximately by the rotation rate. Physically, the neglected terms in equation (8.43) arise

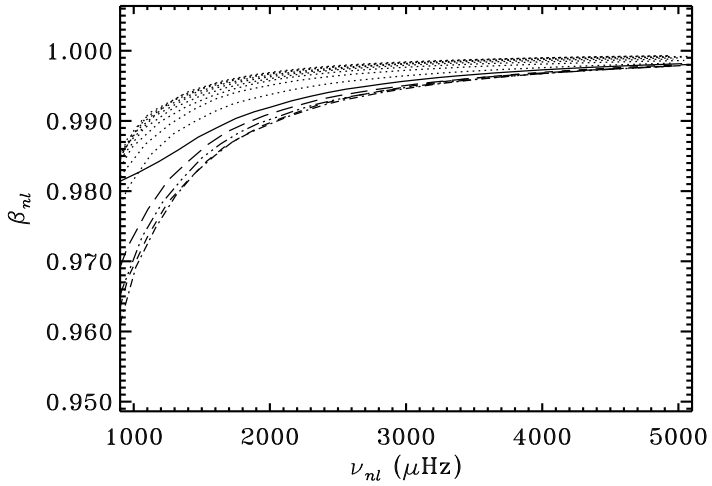

Figure 8.1: Coefficients β_{nl} for acoustic modes in a normal solar model. Points corresponding to fixed l have been connected, according to the following line styles: $l = 1$: ————; $l = 2$: ----------; $l = 3$: —·—·—; $l = 4$: —···—···—; $l = 5$: – – – – – – –; $l = 10, 15, \ldots, 50$: ····· (with β_{nl} increasing with l).

from the Coriolis force; thus rotational splitting for p modes is dominated by advection. For high-order g modes, on the other hand, we can neglect the terms containing ξ_r, so that

$$\beta_{nl} \simeq 1 - \frac{1}{L^2} \; . \tag{8.46}$$

In particular, the splitting of high-order g modes of degree 1 is only *half* the rotation rate.

Returning to the case where Ω depends on r, it should be noted that the integral in equation (8.41) provides a weighted average of $\Omega(r)$. For high-order p modes we can use the asymptotic behaviour of the eigenfunctions to obtain

$$\delta\omega_{nlm} \simeq m \frac{\displaystyle\int_{r_\mathrm{t}}^{R} \left(1 - \frac{L^2c^2}{r^2\omega_{nl}^2}\right)^{-1/2} \Omega(r) \, \frac{\mathrm{d}r}{c}}{\displaystyle\int_{r_\mathrm{t}}^{R} \left(1 - \frac{L^2c^2}{r^2\omega_{nl}^2}\right)^{-1/2} \frac{\mathrm{d}r}{c}} \simeq m \, \frac{\displaystyle\int_{r_\mathrm{t}}^{R} \Omega(r) \, \frac{\mathrm{d}r}{c}}{\displaystyle\int_{r_\mathrm{t}}^{R} \frac{\mathrm{d}r}{c}} \; , \tag{8.47}$$

where in the last equality I crudely approximated $(1 - L^2c^2/r^2\omega^2)$ by 1. Note that the last equality corresponds to neglecting the terms in ξ_h in equation (8.42) and using that, according to equation (7.34), $\xi_r \sim (\rho c)^{-1/2} r^{-1}$ outside the turning point; in this approximation we obtain the intuitively appealing result that the rotational splitting is an average of the rotation rate, weighted by the sound travel time in the radial direction. The first, more accurate expression can also be obtained from ray theory (Gough 1984). In fact, it is straightforward to show that the weight given to $\Omega(r)$ is simply the sound-travel time,

corresponding to the radial distance $\mathrm{d}r$, along a ray; this evidently becomes infinite at the lower turning point. It should be noted that the first part of equation (8.47) may also be written as

$$S_{nl}\delta\omega_{nlm} \simeq m \int_{r_\mathrm{t}}^{R} \left(1 - \frac{c^2 L^2}{\omega_{nl}^2 r^2}\right)^{-1/2} \Omega(r) \frac{\mathrm{d}r}{c} \,, \tag{8.48}$$

in complete analogy with equation (7.145) for the frequency change resulting from a change in the sound speed; here I neglected the term $\pi \mathrm{d}\alpha/\mathrm{d}\omega$ in equation (7.146) which in general is small.

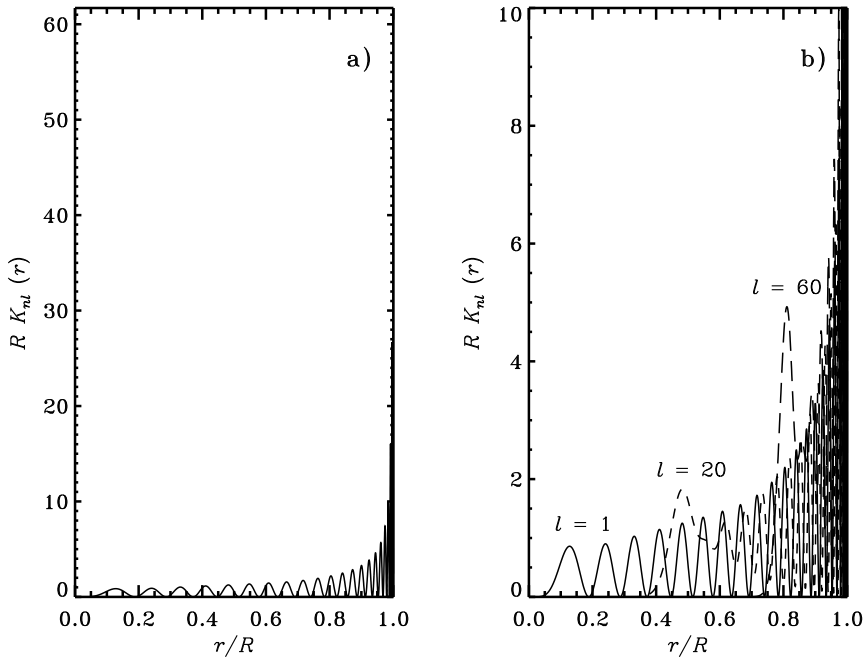

Figure 8.2: Kernels K_{nl} for the frequency splitting caused by spherically symmetric rotation (*cf.* eq. 8.42). In a) is plotted $RK_{nl}(r)$ for a mode with $l = 1$, $n = 22$ and $\nu = 3239\,\mu$Hz. The maximum value of $RK_{nl}(r)$ is 62. In b) is shown the same mode, on an expanded vertical scale, (——————) together with the modes $l = 20$, $n = 17$, $\nu = 3375\,\mu$Hz (- - - - - - - - - - - -), and $l = 60$, $n = 10$, $\nu = 3234\,\mu$Hz (– – – – – – –). Notice that the kernels almost vanish inside the turning-point radius r_t, and that there is an accumulation just outside the turning point.

Figure 8.2 shows a few kernels for the case of spherically symmetric rotation, for high-order p modes. The strong increase towards the solar surface, which is also implicit in equation (8.47), is evident. Also, the kernels clearly get very small beneath the turning point, but are locally enhanced just above it. This effect arises from the term in ξ_h in equation (8.42); physically it corresponds to the fact that the waves travel approximately

horizontally in this region, and hence spend a relatively long time there, as also indicated by the integrable singularity at $r = r_\mathrm{t}$ in equation (8.47).

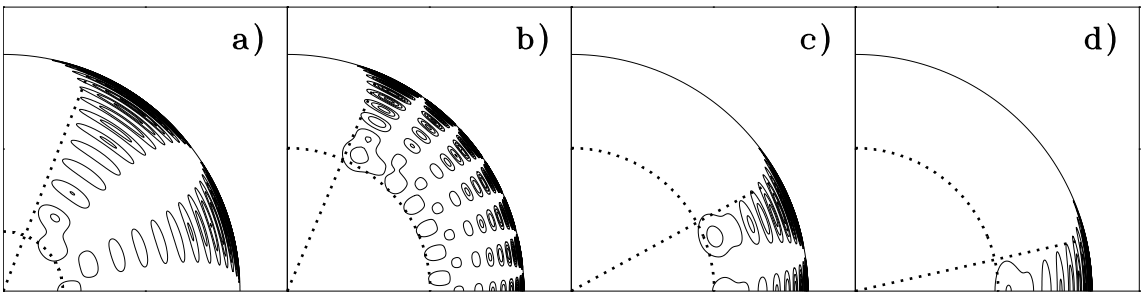

Figure 8.3: Contour plots of rotational kernels K_{nlm} in a solar quadrant. The modes all have frequencies near 2 mHz; the following pairs of (l, m) are included: a) $(5, 2)$; b) $(20, 8)$; c) $(20, 17)$; and d) $(20, 20)$. The dotted circles mark the locations of the lower radial turning point r_t and the dotted lines show the latitudinal turning points, at co-latitude Θ, defined by $\sin\Theta = m/L$.

8.4 General rotation laws

In the general case, where Ω depends on both r and θ, the rotational splitting may be computed from equations (8.31), (8.33) and (8.34), by evaluating the two-dimensional integral in equation (8.31). This integral is in general m-dependent, and so the splitting is no longer a linear function of m. Selected examples of the resulting kernels $K_{nlm}(r, \theta)$ (*cf.* eq. 8.35) are illustrated in Figure 8.3.

To illustrate the properties of the splitting, it is instructive to rewrite equation (8.31) for R_{nlm}, using integration by parts:

$$\begin{aligned} R_{nlm} \;=\; \int_0^\pi \mathrm{d}\theta \int_0^R P_l^m(\cos\theta)^2 \left\{ \left[{\xi_r}^2 + (L^2-1)\xi_\mathrm{h}^2 - 2\xi_r\xi_\mathrm{h} \right] \sin\theta\, \Omega(r,\theta) \right. \\ \left. + \xi_\mathrm{h}^2 \left(\frac{3}{2}\cos\theta\, \frac{\partial\Omega}{\partial\theta} + \frac{1}{2}\sin\theta\, \frac{\partial^2\Omega}{\partial\theta^2} \right) \right\} r^2\rho\, \mathrm{d}r \end{aligned} \tag{8.49}$$

(Cuypers 1980). I consider again the case of high-order p modes; here the terms in ${\xi_r}^2$ and $L^2\xi_\mathrm{h}^2$ dominate, and consequently

$$\delta\omega_{nlm} \simeq m\, \frac{\int_0^\pi \sin\theta\, [P_l^m(\cos\theta)]^2 \int_0^R \Omega(r,\theta)[\xi_r(r)^2 + L^2\xi_\mathrm{h}(r)^2] r^2\rho\, \mathrm{d}r\mathrm{d}\theta}{\int_0^\pi \sin\theta\, \left[P_l^m(\cos\theta)\right]^2 \mathrm{d}\theta \int_0^R [\xi_r(r)^2 + L^2\xi_\mathrm{h}(r)^2] r^2\rho\, \mathrm{d}r}\,. \tag{8.50}$$

Hence, the splitting is simply an average of the angular velocity $\Omega(r, \theta)$, weighted by $r^2\rho[\xi_r(r)^2 + L^2\xi_\mathrm{h}(r)^2]P_l^m(\cos\theta)^2$. Approximating the eigenfunction as in the derivation of equation (8.47) and using, furthermore, an asymptotic approximation to P_l^m, this may

be written as

$$\delta\omega_{nlm} \simeq \tag{8.51}$$
$$m \frac{\displaystyle\int_{-\cos\Theta}^{\cos\Theta} \left(\cos^2\Theta - \cos^2\theta\right)^{-1/2} \int_{r_t}^{R} \left(1 - \frac{L^2c^2}{r^2\omega^2}\right)^{-1/2} \Omega(r,\theta)\,\frac{\mathrm{d}r}{c}\,\mathrm{d}(\cos\theta)}{\displaystyle\pi \int_{r_t}^{R} \left(1 - \frac{L^2c^2}{r^2\omega^2}\right)^{-1/2} \frac{\mathrm{d}r}{c}} ,$$

where $\Theta = \sin^{-1}(m/L)$ (Gough and Thompson 1990, 1991; Gough 1991). The asymptotic approximation to P_l^m shows that a given spherical harmonic is confined essentially to the latitude band between $\pm\Theta$; within this region P_l^m oscillates as a function of θ, whereas at higher latitudes it decreases exponentially. The variation of the extent of the P_l^m with m/L allows resolution of the latitudinal variation of the angular velocity, in much the same way as the variation of the depth of penetration with ω/L allows resolution of the variation with radius. In particular, with increasing l the sectoral modes (with $l = |m|$) get increasingly confined towards the equator (see also Figure 2.1). Thus, the rotational splitting of sectoral modes provides a measure of the solar equatorial angular velocity.

Exercise 8.2:

Confirm the statements about the oscillatory properties of the spherical harmonics, by analyzing equation (4.26) satisfied by the Legendre function.

To study the splitting without making the asymptotic approximation, it is convenient to consider a parameterized representation of $\Omega(r,\theta)$. To illustrate the principle, we may consider an expansion on the form

$$\Omega(r,\theta) = \sum_{s=0}^{s_{\max}} \Omega_s(r) \cos^{2s}\theta \ . \tag{8.52}$$

Then the integrals over θ can be evaluated analytically, in much the same way as the derivation of equation (8.40), and the rotational splitting becomes (see also Cuypers 1980)

$$\delta\omega_{nlm} = m \sum_{s=0}^{s_{\max}} \int_0^R K_{nlms}(r)\Omega_s(r)\mathrm{d}r \ . \tag{8.53}$$

Here

$$\begin{aligned} K_{nlms}(r) \ = \ & \rho r^2 I_{nl}^{-1} \left\{ \left[(\xi_r - \xi_\mathrm{h})^2 + (L^2 - 2s^2 - 3s - 2)\xi_\mathrm{h}^2 \right] Q_{lms} \right. \\ & \left. + s(2s-1)\xi_\mathrm{h}^2 Q_{lms-1} \right\} \ , \end{aligned} \tag{8.54}$$

where

$$I_{nl} = \int_0^R \rho r^2 \left({\xi_r}^2 + L^2\xi_\mathrm{h}^2 \right) \mathrm{d}r \ , \tag{8.55}$$

and

$$Q_{lms} = \frac{2l+1}{2} \frac{(l-|m|)!}{(l+|m|)!} \int_{-1}^{1} x^{2s} [P_l^m(x)]^2 \mathrm{d}x \ . \tag{8.56}$$

For spherically symmetric rotation, $\Omega_s = 0$ for $s > 0$. Since $Q_{lm0} = 1$, the kernel $K_{nlm0}(r) = \beta_{nl} K_{nl}(r)$ is independent of m, and the splitting is uniform in m. Thus we recover the results of Section 8.3.

The factor Q_{lms} is a polynomial in m^2 of degree s; thus, in accordance with equation (8.36), $\delta\omega_{nlm}$ is a polynomial of odd powers of m. Up to $s = 2$ explicit expressions for the Q_{lms} are

$$Q_{lm1} = \frac{2L^2 - 2m^2 - 1}{4L^2 - 3} \, , \tag{8.57}$$

and

$$Q_{lm2} = R^m_{l+1} \left(R^m_{l+2} + R^m_{l+1} + R^m_l \right) + R^m_l \left(R^m_{l+1} + R^m_l + R^m_{l-1} \right) \, , \tag{8.58}$$

where

$$R^m_l = \frac{l^2 - m^2}{4l^2 - 1} \, . \tag{8.59}$$

Hence equation (8.53) leads to an expansion of the rotational splitting in odd powers of m, with expansion coefficients that are related to the expansion functions $\Omega_s(r)$. As discussed by Brown *et al.* (1989), this forms the basis for an inversion to determine the Ω_s, and hence to estimate the rotation rate as a function of r and θ.

The choice of expansion

$$\Omega(r, \theta) = \sum_{s=0}^{s_{\max}} \Omega_s(r) \psi_{2s}(\cos\theta) \, , \tag{8.60}$$

for $\Omega(r, \theta)$, and of the expansion for $\delta\omega_{nlm}$, are clearly not unique. In particular, it was pointed out by Ritzwoller & Lavely (1991) that a more suitable expansion of the rotational splitting could be obtained in terms of Clebsch-Gordon coefficients. This is equivalent to the odd terms in the expansion (2.43) of the m-dependence of the frequencies in terms of the polynomials $\mathcal{P}^{(l)}_j(m)$. Choosing also expansion functions for the rotation rate $\Omega(r, \theta)$ as

$$\psi_{2s}(\cos\theta) = -(\sin\theta)^{-1} P^1_{2s+1}(\cos\theta) \tag{8.61}$$

(*e.g.* Ritzwoller & Lavely 1991; Pijpers 1997), the relations decouple such that each expansion coefficient for the splitting is related to a single expansion function for the angular velocity:

$$2\pi a_{2s+1}(n, l) = \int_0^R K^s_{nls}(r) \Omega_s(r) \mathrm{d}r \tag{8.62}$$

(see also Schou *et al.* 1998). This forms a convenient basis for the so-called 1.5-dimensional inversions for $\Omega(r, \theta)$ (*cf.* Section 9.1.2).

It should be noted that, in general, averaging or expansion of the observed frequencies may involve loss of information; for the purpose of inversion it is, in principle, preferable to work directly in terms of the observed frequencies. In fact, as mentioned in Chapter 9 a direct inversion of the frequency splittings $\delta\omega_{nlm}$ for individual m, in terms of a discretized representation of $\Omega(r, \theta)$ on a grid in r and θ, is now computationally feasible (see also Schou, Christensen-Dalsgaard & Thompson 1994). On the other hand, by suitably combining the frequencies before inversion, the computational effort required may be greatly reduced. Furthermore, it is often the case that the quality of the observations does not allow a complete determination of the individual frequencies; in that case inversion has to be based on expansions such as the one given in equation (2.43).

Chapter 9

Helioseismic inversion

The expression (8.41) for the splitting caused by spherically symmetric rotation is a particularly simple example of the relation between the observable properties of the oscillation frequencies, and the properties of the solar interior which we wish to determine. The determination of $\Omega(r)$ from the $\delta\omega_{nlm}$ constitutes the simplest example of an *inverse problem*. In particular, there is a linear relation between the observables and the property of the solar interior. In contrast, the oscillation frequencies depend in a non-linear fashion on the structure of the Sun, as specified by for example $\rho(r)$ and $c(r)$ (*cf.* Section 5.1). However, by assuming that the real solar structure can be obtained from the structure of a given reference model by applying small corrections, the differences in frequency between the observations and the reference model can be obtained from a linear perturbation analysis of the oscillation equations, resulting, once more, in a linear relation between the frequency differences and the corrections to the model; this was discussed in some detail in Section 5.5.3 (see eq. 5.84). Thus the linear inverse problem forms the basis for much of the inverse theory for solar oscillations.

Inverse problems have a vast literature, covering their application in, for example, geophysics and radiation theory (*e.g.* Parker 1977; Craig & Brown 1986; Deepak 1977; Tarantola 1987). The application to the solar inverse problem was discussed by Gough (1985), and Christensen-Dalsgaard, Schou & Thompson (1990) made a systematic comparison of different inversion techniques, as applied to the problem of spherically symmetric rotation. The following discussion is to a large extent based on their results.

9.1 Inversion of the rotational splitting

Given the simplicity of the rotational-splitting inverse problem, it serves as a very useful prototype of more general inversions. Furthermore, a determination of the solar internal rotation is of great intrinsic interest. For these reasons, in this section I consider rotational inversion in some detail.

9.1.1 One-dimensional rotational inversion

I first consider the inversion for a spherically symmetric rotation rate $\Omega(r)$. Thus the data are

$$\Delta_i = \int_0^R K_i(r)\Omega(r)\mathrm{d}r + \epsilon_i \ , \qquad i = 1, \ldots, M \ , \tag{9.1}$$

where, for notational simplicity, I represent the pair (n, l) by the single index i; M is the number of modes in the data set considered. Δ_i is the scaled rotational splitting $m^{-1}\beta_{nl}^{-1}\delta\omega_{nlm}$, the kernels K_i having been normalized as in equation (8.44), and ϵ_i is the observational error in Δ_i. The goal of the inversion is to determine an approximation $\bar{\Omega}(r_0)$ to the true angular velocity, as a function of position r_0 in the Sun; obviously this is only possible for those parts of the Sun about which the oscillations provide data. In most cases considered so far, the inversion is carried out through linear operations on the data. Hence $\bar{\Omega}$ is linearly related to the data: for each r_0 there exists a set of *inversion coefficients* $c_i(r_0)$ such that

$$\bar{\Omega}(r_0) = \sum_i c_i(r_0)\Delta_i \ . \tag{9.2}$$

It follows from equation (9.1) that this may be written as

$$\bar{\Omega}(r_0) = \int_0^R \mathcal{K}(r_0, r)\Omega(r)\mathrm{d}r \ , \tag{9.3}$$

where the *averaging kernel* $\mathcal{K}(r_0, r)$ is given by

$$\mathcal{K}(r_0, r) = \sum_i c_i(r_0)K_i(r) \ . \tag{9.4}$$

The inversion coefficients and averaging kernels clearly depend on the choice of inversion method, and of possible parameters that enter into the method; indeed, the inversion may be thought of as a way to determine coefficients and averaging kernels such as to obtain as much information about the angular velocity as possible. As discussed below, the determination of the coefficients must take into account the estimated errors in the data. On the other hand, once the method and parameters have been chosen, the coefficients and averaging kernels are independent of the data values. Hence they can be used to make a data-independent comparison of different inversion methods; this was the approach taken by Christensen-Dalsgaard *et al.* (1990).

The averaging kernels provide an indication of the resolution of the inversion; it is clearly desirable to achieve averaging kernels that are sharply peaked around $r = r_0$, and with small amplitude far away from that point. As a quantitative measure of resolution it is common to use a width of $\mathcal{K}(r_0, r)$ obtained as the distance between the quartile points, defined such that one quarter of the area of $\mathcal{K}(r_0, r)$, regarded as function of r, lies below the lower, and one quarter of the area above the upper, quartile point. The inversion coefficients give information about the propagation of errors from the data to the solution $\bar{\Omega}(r_0)$. If the standard error on Δ_i is $\sigma(\Delta_i)$, the standard error in the result of the inversion is given by

$$\sigma[\bar{\Omega}(r_0)]^2 = \sum_i c_i(r_0)^2\sigma(\Delta_i)^2 \ . \tag{9.5}$$

(The generalization to a non-diagonal covariance matrix is fairly obvious.) In particular, if (somewhat unrealistically) $\sigma(\Delta_i) = \sigma$ is assumed to be the same for all the observed modes

$$\sigma[\bar{\Omega}(r_0)] = \Lambda(r_0)\sigma \ , \tag{9.6}$$

where I introduced the *error magnification*

$$\Lambda(r_0) = \left[\sum_i c_i(r_0)^2\right]^{1/2} . \tag{9.7}$$

The optimization of the inversion techniques is often based on a trade-off between width of the averaging kernels and error or error magnification magnification (*cf.* Figure 9.2 below).

A procedure which is based explicitly on the determination of the inversion coefficients is the technique of *optimally localized averages*, developed by Backus and Gilbert (1970); this has been used extensively for helioseismic inversion. The goal is to choose the coefficients $c_i(r_0)$ such as to make $\mathcal{K}(r_0, r)$ approximate as far as possible a delta function $\delta(r - r_0)$ centred on r_0; then $\bar{\Omega}(r_0)$ provides an approximation to $\Omega(r_0)$. This is achieved by determining the coefficients $c(r_0)$ such as to minimize

$$\int_0^R (r - r_0)^2 \mathcal{K}(r_0, r)^2 \mathrm{d}r + \mu \sum_{ij} E_{ij} c_i c_j , \tag{9.8}$$

subject to the constraint

$$\int_0^R \mathcal{K}(r_0, r)\mathrm{d}r = 1 ; \tag{9.9}$$

here E_{ij} is the covariance matrix of the data. This is equivalent to solving the set of linear equations

$$\sum_j W_{ij} c_j = b , \tag{9.10}$$

and

$$\sum_j c_j = 1 , \tag{9.11}$$

where b is a Lagrange multiplier. Here

$$W_{ij} = S_{ij} + \mu E_{ij} , \tag{9.12}$$

where

$$S_{ij} = \int_0^R (r - r_0)^2 K_i(r) K_j(r) \mathrm{d}r . \tag{9.13}$$

Furthermore, μ is a parameter which, as discussed below, must be adjusted to optimize the result.

The effect of the minimization is most easily understood for $\mu = 0$. Minimizing equation (9.8) subject to equation (9.9) ensures that $\mathcal{K}(r_0, r)$ is large close to r_0, where the weight function $(r - r_0)^2$ is small, and small elsewhere. This is precisely the required "delta-ness" of the combined kernel. However, with no further constraints, the optimization of the combined kernel may result in numerically large coefficients of opposite sign. Hence, the variance in $\bar{\Omega}$, which can be estimated as

$$\sigma^2(\bar{\Omega}) = \sum_{ij} E_{ij} c_i c_j , \tag{9.14}$$

would be large. The effect of the second term in equation (9.8), when $\mu > 0$, is to restrict $\sigma^2(\bar{\Omega})$. The size of μ determines the relative importance of the localization and the size of

the variance in the result. Hence, μ must be determined to ensure a trade-off between the localization and the error, measured by the width of $\mathcal{K}(r_0, r)$ and $\Lambda(r_0)$, respectively; μ is generally known as *the trade-off parameter*.

The principal difficulty of this method is computational expense: at each target radius r_0 it involves the solution of a set of linear equations whose order is the number of data points. Jeffrey (1988) proposed an alternative version where the coefficients were determined by minimizing the difference between $\mathcal{K}(r_0, r)$ and the delta function $\delta(r - r_0)$. This is computationally more efficient, in that only one matrix inversion is required, but results in averaging kernels with somewhat undesirable properties.

More recently Pijpers & Thompson (1992, 1994) have developed this method further, by matching $\mathcal{K}(r_0, r)$ instead to a prescribed *target function* $\mathcal{T}(r_0, r)$ which more closely matches the behaviour that can be achieved with the given mode set. They dubbed this the *SOLA* technique (for Subtractive Optimally Localized Averaging), to distinguish it from the *MOLA* technique (for Multiplicative Optimally Localized Averaging) discussed above. Specifically, the coefficients $c_i(r_0)$ are determined by minimizing

$$\int_0^R [\mathcal{K}(r_0, r) - \mathcal{T}(r_0, r)]^2 \, \mathrm{d}r + \mu \sum_{ij} E_{ij} c_i c_j \ , \tag{9.15}$$

where again μ is a tradeoff parameter. In addition, the width of $\mathcal{T}(r_0, r)$ functions as a parameter, in most cases depending on r_0, of the method. As before, the inclusion of the last term in equation (9.15) serves to limit the error in the solution. The minimization leads to the following system of linear equations for the $c_i(r_0)$:

$$\sum_j (K_{ij} + \mu E_{ij}) c_j(r_0) = T_i(r_0) \ ; \tag{9.16}$$

here

$$K_{ij} = \int_0^R K_i(r) K_j(r) \mathrm{d}r \ , \tag{9.17}$$

and

$$T_i(r_0) = \int_0^R \mathcal{T}(r_0, r) K_i(r) \mathrm{d}r \ . \tag{9.18}$$

In equation (9.16) the coefficient matrix on the left-hand side is independent of r_0. Thus it can be inverted or, more efficiently, suitably factored, once and for all; after this the determination of the coefficients at each target point r_0 is virtually free. Compared with the MOLA technique the computational effort is therefore reduced by roughly a factor given by the number of target locations. An additional advantage of the technique is the ability to choose the target function such as to tailor the averaging kernels to have specific properties. In addition to the usual trade-off parameter μ controlling the weight given to the errors, the method obviously depends on parameters controlling the properties of the target functions $\mathcal{T}(r_0, r)$. These are often taken to be of gaussian shape; it was argued by Thompson (1993) that the radial resolution, for inversion of acoustic modes, is proportional to the sound speed c, and hence the width of $\mathcal{T}(r_0, r)$ is generally taken to be proportional to $c(r_0)$, the constant of proportionality serving as a parameter characterizing the targets.

A second commonly used technique is the regularized least-squares, or Tikhonov, method (see, for example, Craig and Brown 1986). Here the solution $\bar{\Omega}(r)$ is parameterized, often as a piecewise constant function on a grid $r_0 < r_1 < \ldots < r_N$, with $\bar{\Omega}(r) = \Omega_j$ on the

interval $[r_{j-1}, r_j]$; the parameters Ω_j are determined through a least-squares fit to the data. In general, this least-squares procedure needs to be regularized to obtain a smooth solution. This is achieved by including in the minimization a term which restricts the square of $\bar{\Omega}$, or the square of its first or second derivative. Thus, for example one may minimize

$$\sum_i \left[\int_0^R K_i(r)\bar{\Omega}(r)\mathrm{d}r - \Delta_i \right]^2 + \mu^2 \int_0^R \left(\frac{\mathrm{d}^2\bar{\Omega}}{\mathrm{d}r^2} \right)^2 \mathrm{d}r \ , \tag{9.19}$$

where in the last term a suitable discretized approximation to $\mathrm{d}^2\bar{\Omega}/\mathrm{d}r^2$, in terms of the Ω_j, is used. The minimization of equation (9.19) clearly leads to a set of linear equations for $\bar{\Omega}_j$, defining the solution; however, it is still the case that the procedure can be formulated as in equation (9.2) and hence leads to the determination of inversion coefficients and averaging kernels. By restricting the second derivative the last term in equation (9.19) suppresses rapid oscillations in the solution, and hence ensures that it is smooth; the weight μ^2 given to this term serves as a trade-off parameter, determining the balance between resolution and error for this method.

The asymptotic expression (8.48) for the frequency splitting provides the basis for a final example of an inversion method in widespread use. The right-hand side of that equation is a function $\mathcal{H}(\omega/L)$ which is in principle determined by the observed splittings after scaling with S. Given $\mathcal{H}(w)$, the angular velocity can be obtained from

$$\Omega(r) = -\frac{2a}{\pi} \frac{\mathrm{d}}{\mathrm{d}\ln r} \int_{a_s}^a (a^2 - w^2)^{-1/2} \mathcal{H}(w)\mathrm{d}w \ , \tag{9.20}$$

where $a = c/r$ and $a_s = a(R)$. This is entirely equivalent to equation (7.153) determining the sound-speed difference from the function $\mathcal{H}_1(\omega/L)$ fitted to the scaled frequency differences. In practice, since the asymptotic expressions are not exact, the scaled splittings are not precisely functions of ω/L. Hence, an approximation to $\mathcal{H}(\omega/L)$ is obtained by making a least-squares fit to $S\Delta\omega_{nl}$ of a function of that form, for example by representing it as a spline over a suitably chosen set of knots. The number of knots determines the resolution achieved in representing $\mathcal{H}(w)$ and hence in the inferred solution $\bar{\Omega}(r)$; therefore, in this case the number of knots serves as trade-off parameter. Again, the processes of carrying out the spline fit to the scaled data and evaluating the integral in equation (9.20) are linear, and hence the method allows the evaluation of inversion coefficients and averaging kernels (see Christensen-Dalsgaard *et al.* 1990 for details).

An illustration of the use of these methods is provided by the results obtained by Christensen-Dalsgaard *et al.* (1990). They considered a set consisting of about 830 modes at selected degrees between 1 and 200, and frequencies between 2000 and 4000 μHz; for simplicity, the standard errors were assumed to be the same for all modes. Figure 9.1 shows examples of averaging kernels $\mathcal{K}(r_0, r)$ for the MOLA, regularized least-squares and asymptotic methods. The trade-off parameters were chosen such that the error magnification at $r_0 = 0.5R$ was close to 1 in all three cases. It should be realized that the kernels entering into the combination are of the form shown in Figure 8.2. Thus, a very large degree of cancellation has been achieved of the dominant contribution from near the surface. Nevertheless, it is obvious that the averaging kernels are only approximate realizations of delta functions; structure on a scale smaller than roughly $0.05R$ is not resolved.

This limitation is inherent in any inversion method. Indeed, it is evident that from a finite set of data one can never completely resolve the function $\Omega(r)$. To obtain a definite

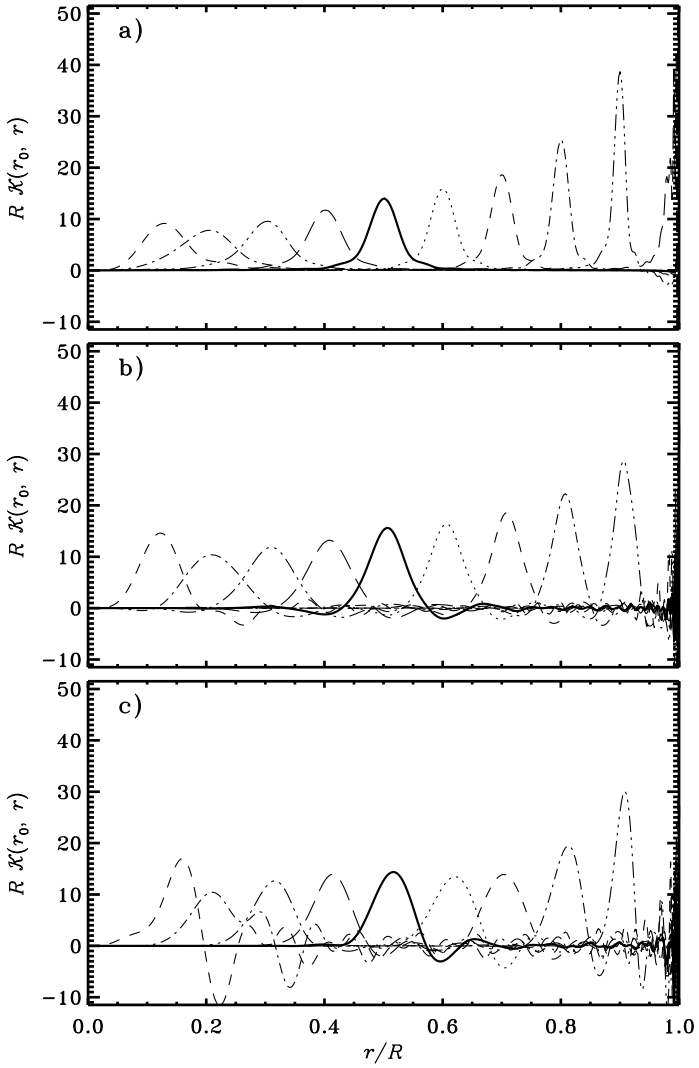

Figure 9.1: Averaging kernels $\mathcal{K}(r_0, r)$ at selected radii ($r_0/R = 0.1, 0.2, \ldots, 1.0$) for inversion by means of the MOLA technique (panel a), the Tikhonov inversion with second-derivative smoothing (panel b) and asymptotic inversion (panel c). The parameters in each inversion method have been chosen to obtain approximately the same error magnification for $r_0 = 0.5R$. In each case, the kernel at $r_0 = 0.5R$ is shown as a bolder curve. From Christensen-Dalsgaard *et al.* (1990).

solution additional constraints must be invoked. The constraints used here essentially demand that the solution be smooth. This is ensured in the method of optimally localized kernels by representing the solution by smooth averaging kernels whose shape is determined by the minimization in equation (9.8). For the Tikhonov method smoothness is explicitly

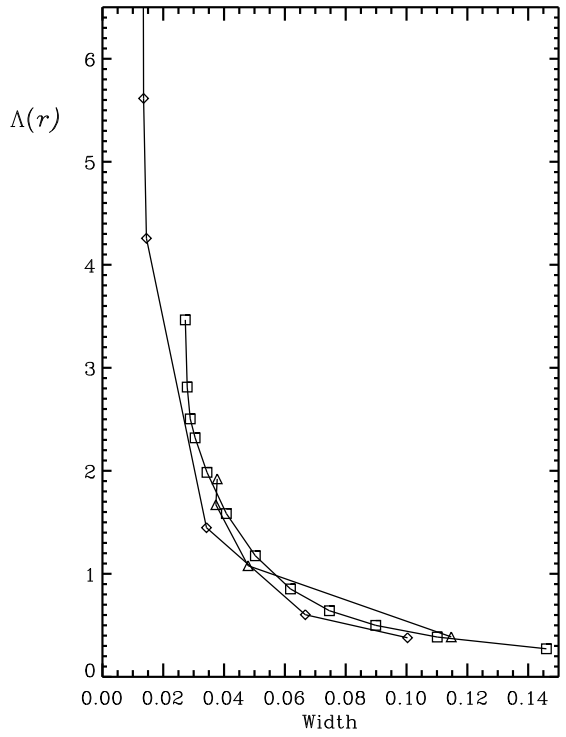

Figure 9.2: The trade-off between error magnification $\Lambda(r_0)$ (*cf.* eq. 9.7) and width (defined as distance between quartile points), for inversion at $r_0 = 0.5R$. Results are shown for the MOLA technique (▫), Tikhonov inversion (◇) and asymptotic inversion (△), in each case varying the relevant trade-off parameter over a wide range. From Christensen-Dalsgaard *et al.* (1990).

demanded by constraining the second derivative of the solution, whereas in the case of the asymptotic technique the constraints lie partly in using the asymptotic description, which in itself assumes that the solution varies on a scale larger than the wavelength of the modes, partly in the spline fit to the scaled data.

All methods contain trade-off parameters which determine the relative weight given to the demands of resolution on the one hand, and smoothness or minimizing errors on the other. To illustrate this balance, it is common to consider trade-off diagrams, where a measure of error is plotted against a measure of the width of the averaging kernels. An example is shown in Figure 9.2. The similarity, in terms of such global measures, between the three conceptually rather different methods is quite striking.

It is also of interest to consider in detail the way in which the different methods utilize the data, as expressed in terms of the inversion coefficients. In the case of the asymptotic technique it may be shown that these depend on ω/L alone; hence for the purpose of comparison it is sensible to plot the coefficients as a function of ω/L in all cases. In Figure 9.3 the coefficients for the optimally localized averages and the Tikhonov inversions are compared with those obtained with the asymptotic technique, for $r_0 = 0.5R$. It is evident that

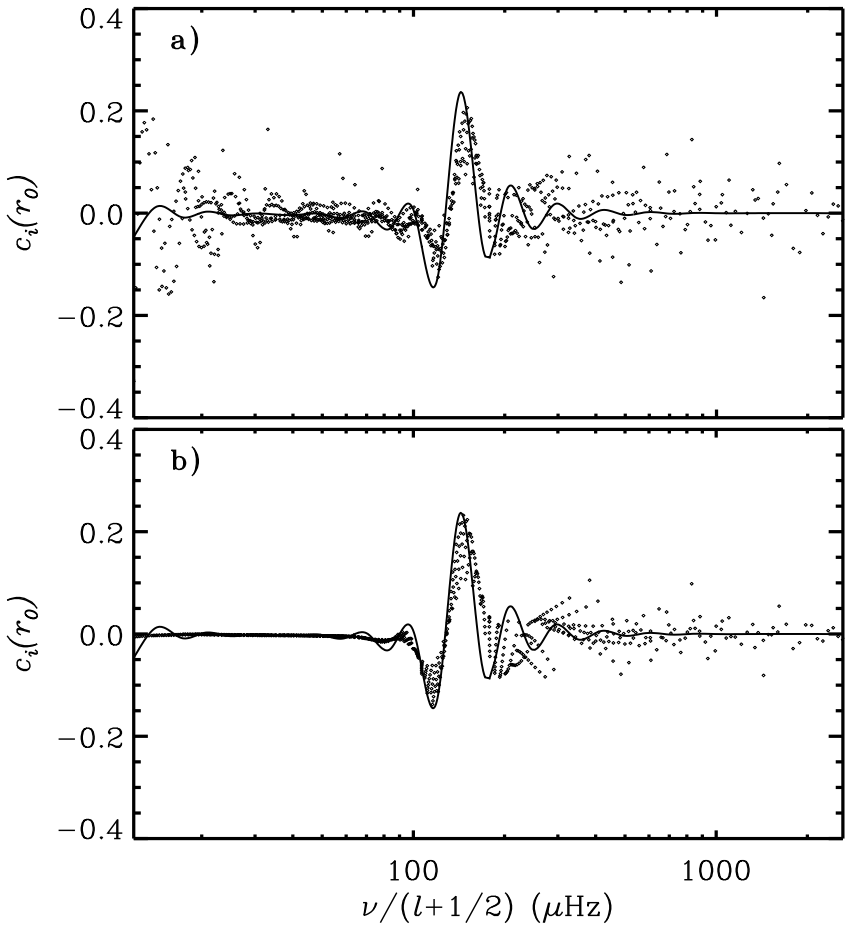

Figure 9.3: Inversion coefficients $c_i(r_0)$ for the inversions illustrated in Figure 9.1, at $r_0 = 0.5R$; they have been plotted against $\nu/(l+1/2)$ which, according to equation (5.28), measures the depth of penetration of the modes. The continuous line in both panels shows coefficients for the asymptotic method which are functions of $\nu/(l + 1/2)$. Panel (a) gives the coefficients obtained with the MOLA technique, whereas panel (b) shows coefficients for Tikhonov inversion. From Christensen-Dalsgaard *et al.* (1990).

the overall behaviour of the coefficients is quite similar in all three cases; in particular, the modes dominating the inversion are those whose turning point r_t is in the vicinity of the target radius r_0. At a more subtle level, there are significant differences. In particular, unlike the Tikhonov case, inversion by optimally localized averages makes substantial use of modes of high degree. It may be shown that these are used essentially only to improve the averaging kernels near the surface; in fact, as can be seen in Figure 9.1 the $\mathcal{K}(r_0, r)$

for Tikhonov inversion have quite substantial amplitude at very short wavelength near the surface, whereas such structure is entirely suppressed by the minimization in equation (9.8) for the optimally localized averages. Christensen-Dalsgaard, Hansen & Thompson (1993) found that considerable insight into such details of the behaviour of the inversion methods can be obtained by analyzing the Tikhonov case by means of the so-called Generalized Singular Value Decomposition; this provides a natural basis for expressing the inverse problem which can then be used to study the properties of other inversion methods.

Graphs such as Figure 9.2 are very useful for the choice of the trade-off parameter; however, it is evident that this choice depends critically on the particular application, including the errors in the data. The question of how to fix the trade-off parameter, or indeed even how to choose the inversion method, has given rise to a great deal of debate, occasionally of an almost philosophical (or, dare one say, religious) nature. It has been suggested that inversion methods should be chosen which aim at fitting the data; this makes the method of optimally localized averages, whose goal is instead to design the averaging kernels, less attractive. Also, a great deal of emphasis has been placed on techniques for objectively determining the trade-off parameters, based on the errors in the data and possibly the properties of the solution. In contrast, the approach taken in helioseismology has to a large extent been pragmatic: in fact, it can be argued that since no method, or choice of trade-off, can provide the exact solution given the necessarily incomplete data, the most important aspect of the inversion is to be able to interpret the result and its significance. In this respect, the averaging kernels which graphically illustrate the resolution, and the inversion coefficients which allow evaluation of effects of errors in the data, are clearly very useful. By choosing different inversion methods, and different values of the trade-off parameters, considering in each case the properties of the resulting inversion, one can hope to obtain a more complete impression of the underlying solution. In this process prior knowledge, or prejudices, about the solution clearly play a significant role; these should ideally be formulated in a well-defined statistical sense, but probably often are not.

9.1.2 Two-dimensional rotational inversion

So far, I have considered inversion for a function that depends on r alone. It is evidently desirable, however, to carry out inversion for more general properties which are functions both of r and θ. Here I concentrate on the case of determining the angular velocity $\Omega(r,\theta)$; it should be noticed, however, that another interesting inverse problem concerns the departure of the structure from spherical symmetry caused, for example, by a latitude dependence of the energy transport in the convection zone.

As is evident from Chapter 8, the latitude dependence of rotation is reflected in the dependence of the frequencies on azimuthal order m. Thus in general individual frequencies ω_{nlm} have to be analyzed. This greatly increases the amount of data to be considered, compared with the simple case discussed in Section 9.1.1, and computational efficiency becomes a crucial consideration. However, it is still generally the case that the inferred angular velocity $\bar{\Omega}(r_0,\theta_0)$ at some location (r_0,θ_0) is linearly related to the data; as discussed by Schou *et al.* (1992) this allows the introduction of inversion coefficients and generalized averaging kernels $\mathcal{K}(r_0,\theta_0,r,\theta)$ defined such that $\bar{\Omega}(r_0,\theta_0)$ is related to the true angular velocity $\Omega(r,\theta)$ through

$$\bar{\Omega}(r_0,\theta_0) = \int_0^\pi \int_0^R \mathcal{K}(r_0,\theta_0,r,\theta)\Omega(r,\theta)\, r\mathrm{d}r\mathrm{d}\theta \ . \tag{9.21}$$

The form of the inverse problem evidently depends on the representation of the data. The general problem has the form

$$\omega_{nlm} - \omega_{nl0} = \delta\omega_{nlm} = m \int_0^R \int_0^\pi K_{nlm}(r,\theta)\Omega(r,\theta) r \mathrm{d}r\mathrm{d}\theta \tag{9.22}$$

(*cf.* eq. 8.35). However, it is often the case that the data do not allow determination of individual frequencies ω_{nlm}. In that case, it is customary to make fits of the general form shown in equation (2.43), *i.e.*,

$$\omega_{nlm} = \omega_{nl0} + 2\pi \sum_{j=1}^{j_{\max}} a_j(n,l)\, \mathcal{P}_j^{(l)}(m) \;, \tag{9.23}$$

where $\mathcal{P}_j^{(l)}$ is a polynomial of degree j. Since the fitting procedure is in general linear, the *a coefficients* $a_j(n,l)$ are linearly related to the frequency splittings,

$$2\pi a_j(n,l) = \sum_m \gamma_j(l,m)(\omega_{nlm} - \omega_{nl0}) \;, \tag{9.24}$$

for some coefficients $\gamma_j(l,m)$. It immediately follows from equations (8.35) and (8.36) that rotation gives rise to odd a coefficients, related to $\Omega(r,\theta)$ by

$$2\pi a_{2j+1}(n,l) = \int_0^R \int_0^\pi K_{nlj}^{(a)}(r,\theta)\Omega(r,\theta) r \mathrm{d}r\mathrm{d}\theta \;, \tag{9.25}$$

where the kernels $K_{nlj}^{(a)}$ can be determined in a straightforward manner from the kernels $K_{nlm}(r,\theta)$.

As discussed in Section 8.4 it may also be convenient to expand the dependence of $\Omega(r,\theta)$ on θ on the form

$$\Omega(r,\theta) = \sum_{s=0}^{s_{\max}} \Omega_s(r) \psi_{2s}^{(1)}(\cos\theta) \;, \tag{9.26}$$

where $\psi_{2s}^{(1)}(x)$ is a polynomial in x^2 of degree s. [Note that, as discussed at the end of Section 8.2, the rotational splitting is sensitive only to the component of Ω that is symmetrical around the equator; thus only even powers of $\cos\theta$ enter into the expansion (9.26).] Based on the expansions given in equations (9.23) and (9.26), the inverse problem can be formulated as the determination of the expansion functions $\Omega_s(r)$ through a series of one-dimensional inversions of the a coefficients $a_j(n,l)$ (see, for example, Korzennik *et al.* 1988; Brown *et al.* 1989; Thompson 1990). Such procedures are often called 1.5-dimensional (or 1.5D) inversions. By chosing the polynomials $\mathcal{P}_j^{(l)}$ as defined after equation (2.43) (Ritzwoller & Lavely 1991; Schou, Christensen-Dalsgaard & Thompson 1994) and the corresponding expansion of Ω (*cf.* eq. 8.61), the relations between the a coefficients and the expansion functions of Ω simplify to

$$2\pi a_{2s+1}(n,l) = \int_0^R K_{nls}^s(r)\Omega_s(r)\mathrm{d}r \;, \tag{9.27}$$

so that the separate 1-dimensional inversions can be carried out independently.

The 1.5-dimensional techniques very considerably reduce the computational efforts required for the inversion. However, the expansion of Ω evidently imposes a rather special

structure on the solution, unless a large number of terms is included. An alternative is to perform direct two-dimensional inversions, based either on equations (9.22) or equations (9.25). Even given the large amount of data (as many as 200 000 individual frequencies ω_{nlm}, or of order 50 000 a coefficients $a_j(n,l)$), this can be handled by means of a straightforward regularized least-squares technique (*e.g.* Sekii 1991; Schou 1991; Schou, Christensen-Dalsgaard & Thompson 1992, 1994). Here the inferred $\bar{\Omega}(r,\theta)$ is represented on a suitable grid (r_p,θ_q) in r and θ, $p=1,\ldots,n_r$, $q=1,\ldots,n_\theta$, by expansion coefficients Ω_{pq}. These expansion coefficients can be determined through a regularized least-squares fitting technique, analogous to the one described in equation (9.19). Assuming that splittings $\delta\omega_{nlm}$ for individual models are available, related to $\Omega(r,\theta)$ by equation (9.22), the solution is determined by minimizing

$$\sum_{nlm}\left(\frac{\int_{r,\theta}K_{nlm}\bar{\Omega}r\mathrm{d}r\mathrm{d}\theta-\delta\omega_{nlm}}{\sigma_{nlm}}\right)^2 \qquad (9.28)$$
$$+\mu_r\int_{r,\theta}f_r(r,\theta)\left(\frac{\partial^2\bar{\Omega}}{\partial r^2}\right)^2\mathrm{d}\theta\mathrm{d}r+\mu_\theta\int_{r,\theta}f_\theta(r,\theta)\left(\frac{\partial^2\bar{\Omega}}{\partial\theta^2}\right)^2\mathrm{d}\theta\mathrm{d}r\ ;$$

here σ_{nlm} is the standard deviation for the observed splitting $\delta\omega_{nlm}$. The last two terms serve to regularize the solution, as before, and depend on the weight functions f_r and f_θ and the trade-off parameters μ_r and μ_θ. Instead of $\delta\omega_{nlm}$, expansion coefficients a_{2j+1} with the corresponding kernels may evidently also be used. As in the 1-dimensional case, the trade-off parameters must be determined such as to ensure a balance between resolution and error. However, here one must also balance the resolution in the radial and latitude directions (*e.g.* Schou *et al.* 1994).

To illustrate the resolution properties of the inversions we may consider the averaging kernels which, as discussed above, can be defined both for inversions assuming an expansion of Ω in powers of $\cos\theta$ and for the full 2-dimensional techniques. Examples of such kernels are shown in Figure 9.4, both for an inversion using expansions of the splittings and Ω and for a full, two-dimensional inversion. In the former case, only a_1, a_3 and a_5 were included and the latitude information is consequently relatively limited; hence the kernels have a substantial extent in latitude. A particularly striking feature is the fact that the attempt to determine the angular velocity close to the pole results in what contains aspects of extrapolation from lower latitudes: indeed, it is obvious that the rotation of the region very near the pole has little effect on the frequency splittings and hence cannot be determined from the inversion. The inversion based on individual splittings provides substantially better resolution in latitude, as might have been anticipated. Within the convection zone it is possible to determine the rotation over a region extending only a few per cent of the solar radius in both radial and latitude directions, for realistic sets of observed frequency splittings.

The MOLA and SOLA techniques, discussed in Section 9.1.1, may obviously also be generalized to the two-dimensional case, in principle. They offer considerable advantages in terms of the ability to control the resolution, and possibly other properties of the averaging kernels. However, a naive implementation would involve a prohibitive computational effort, since this requires inversion of matrices whose order is given by the number of data values. Fortunately, by utilizing the special properties of the kernels, very substantial improvements of computational efficiency can be achieved. One class of techniques, the so-called $\mathbb{R}^1\otimes\mathbb{R}^1$

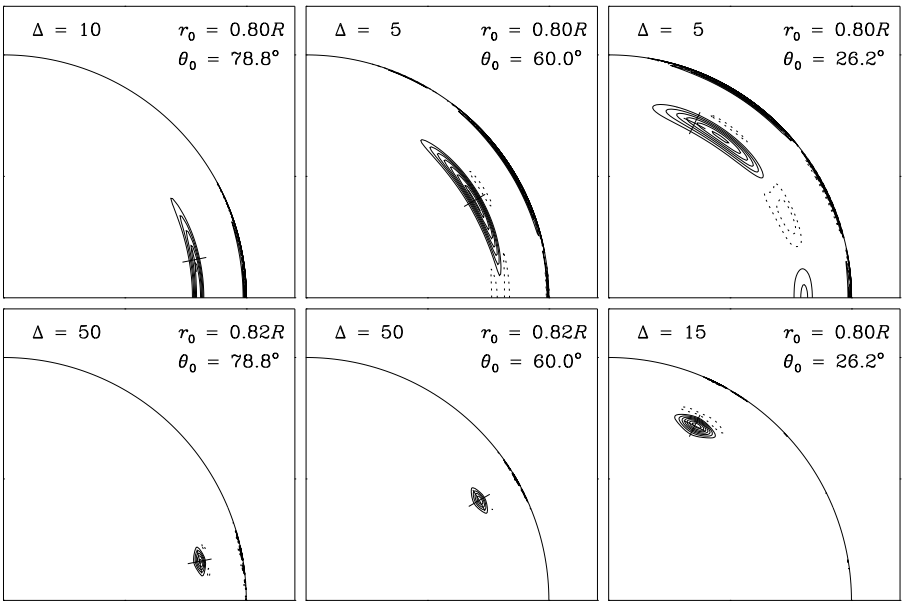

Figure 9.4: Contour plots of two-dimensional averaging kernels $R^{-2}\mathcal{K}(r_0, \theta_0, r, \theta)$ [*cf.* equation (9.21)]. Results are shown at a target radii near $r_0 = 0.8R$ and three different target co-latitudes, as indicated. The plots are in the (r, θ) plane, with the polar axis towards the top of the page. Positive contours are indicated by solid lines, negative contours by dashed lines; Δ is the value of the separation between contour levels. The cross shows the target location (r_0, θ_0). The top row shows kernels for an inversion based on just a_1, a_3 and a_5 and using a corresponding expansion of Ω. The bottom row shows results for a full two-dimensional regularized least-squares inversion, for a mode set aiming at representing the results of 1 year's observations with high spatial resolution. Adapted from Schou *et al.* (1994).

methods, uses explicitly the fact that the kernels can be written as

$$K_{nlm}(r, \theta) = F_{1\,nl}(r) G_{1\,lm}(\theta) + F_{2\,nl}(r) G_{2\,lm}(\theta) \tag{9.29}$$

[*cf.* equations (8.31), (8.34) and (8.35)], where the first term generally dominates; a similar expression applies in the case of kernels for a coefficients (*e.g.* Pijpers 1997). It was pointed out by Sekii (1993) and Pijpers & Thompson (1996) that as a result the inversion can essentially be separated into distinct, and computationally more manageable, inversions in r and θ.

Larsen & Hansen (1997) showed that the linear equations [equations (9.16) – (9.18)] arising in the SOLA technique can be solved efficiently by using explicitly the discretized representation of the kernels. By using also the structure given by equation (9.29), Larsen (1997) has developed an iterative technique which allows two-dimensional SOLA inversion

to be carried out with fairly modest means (see also Larsen *et al.* 1998). These efficient techniques have been applied to the very extensive and accurate data obtained with the GONG and SOHO projects.

Further details on the implementation of rotational inversion, and tests of the various techniques, were provided by Schou *et al.* (1998).

9.2 Inversion for solar structure

In its most general form, the dependence of the oscillation frequencies on solar structure may be expressed as

$$\omega_{nl} = \mathcal{F}_{nl}[\rho(r), c^2(r), \ldots] \; , \tag{9.30}$$

where, as indicated, other properties beyond the "mechanical" structure as characterized by ρ and c^2 may affect the frequencies. This equation is often approximated by the corresponding equation for the adiabatic frequencies, *i.e.*,

$$\omega_{nl}^{\rm ad} = \mathcal{F}_{nl}^{\rm ad}[\rho(r), c(r)] \; , \tag{9.31}$$

where the functional $\mathcal{F}_{nl}^{\rm ad}$ is determined through the solution of the equations of adiabatic oscillation. The inverse problem for solar structure then consists of inferring properties of the structure by "solving" equation (9.30) or (9.31), given a set of observed frequencies $\{\omega_{nl}^{\rm (obs)}\}$.

A difficulty in this process is that the frequencies depend on solar structure in a complicated, nonlinear way. As is common for nonlinear equations, the analysis proceeds through linearisation around an initial reference model. Let $(\rho_0(r), c_0(r))$ correspond to the reference model, which has adiabatic oscillation frequencies $\omega_{nl}^{(0)}$. We seek to determine corrections $\delta_r\rho(r) = \rho(r) - \rho_0(r)$ and $\delta_r c^2(r) = c^2(r) - c_0^2(r)$ to match the differences $\omega_{nl}^{\rm (obs)} - \omega_{nl}^{(0)}$ between the observed frequencies and those of the reference model. As discussed in Sections 5.5.3 and 5.5.4, linearization of equation (9.30), assuming $\delta_r\rho$ and $\delta_r c^2$ to be small, leads to

$$\begin{aligned} \frac{\delta\omega_{nl}}{\omega_{nl}} \; &= \; \int_0^R \left[K_{c^2,\rho}^{nl}(r) \frac{\delta_r c^2}{c^2}(r) + K_{\rho,c^2}^{nl}(r) \frac{\delta_r\rho}{\rho}(r) \right] {\rm d}r \\ &\quad + Q_{nl}^{-1} \mathcal{G}(\omega_{nl}) + \epsilon_{nl} \; , \end{aligned} \tag{9.32}$$

where the kernels $K_{c^2,\rho}^{nl}$ and K_{ρ,c^2}^{nl} are determined from the eigenfunctions in the reference model (see also Section 5.5.3). In equation (9.32) I included a contribution from the uncertainties in the near-surface region, expressed by the term in $\mathcal{G}$; this may be assumed to contain the difference between the "true" function $\mathcal{F}_{nl}$ in equation (9.30) and the adiabatic approximation $\mathcal{F}_{nl}^{\rm ad}$ in equation (9.31). Furthermore, I explicitly included the observational errors ϵ_{nl}. An additional constraint on $\delta_r\rho$ is that the mass of the Sun and the reference model be the same, *i.e.*,

$$4\pi \int_0^R \frac{\delta_r\rho(r)}{\rho(r)} \rho(r) r^2 {\rm d}r = 0 \; . \tag{9.33}$$

In this way the original nonlinear inverse problem is reduced to a linear problem, which may be analyzed by means of techniques similar to those discussed in Section 9.1.1.

Unlike the rotational case, the linearized inverse problem given by equation (9.32) involves three unknown functions: $\delta_r\rho(r)$, $\delta_r c^2(r)$ and $\mathcal{G}(\omega)$. These may, after suitable

parametrization, be determined through least-squares fitting with appropriate regularization (*e.g.* Dziembowski, Pamyatnykh, & Sienkiewicz 1990). Alternatively, some form of optimally localized averages may be used, by forming a linear combination of equations (9.32),

$$\begin{aligned}\sum_i c_i(r_0)\frac{\delta\omega_i}{\omega_i} &= \sum_i c_i(r_0)\int_0^R K^i_{c^2,\rho}(r)\frac{\delta_r c^2}{c^2}(r)\mathrm{d}r \\ &+ \sum_i c_i(r_0)\int_0^R K^i_{\rho,c^2}(r)\frac{\delta_r\rho}{\rho}(r)\mathrm{d}r \\ &+ \sum_i c_i(r_0)Q_i^{-1}\mathcal{G}(\omega_i) + \sum_i c_i(r_0)\epsilon_i \ ,\end{aligned} \tag{9.34}$$

where, as in Section 9.1.1, i labels the modes. If the goal is to determine the correction to $c^2(r_0)$, the coefficients $c_i(r_0)$ must be chosen such that the first term on the right-hand side of equation (9.34) provides an average of $\delta_r c^2/c^2$ localized near $r = r_0$, while minimizing the effect of the remaining terms.

A natural generalization of the SOLA technique is to obtain the coefficients $c_i(r_0)$ through minimization of

$$\int_0^R \left[\mathcal{K}_{c^2,\rho}(r_0,r) - \mathcal{T}(r_0,r)\right]^2 \mathrm{d}r + \beta\int_0^R \mathcal{C}_{\rho,c^2}(r_0,r)^2\mathrm{d}r + \mu\sum_{ij} E_{ij}c_i(r_0)c_j(r_0) \ , \tag{9.35}$$

where

$$\mathcal{K}_{c^2,\rho}(r_0,r) = \sum_i c_i(r_0)K^i_{c^2,\rho}(r) \tag{9.36}$$

is the averaging kernel; the *cross term*

$$\mathcal{C}_{\rho,c^2}(r_0,r) = \sum_i c_i(r_0)K^i_{\rho,c^2}(r) \tag{9.37}$$

measures the influence of the contribution from $\delta_r\rho$ on the inferred $\delta_r c^2$, and E_{ij} is the covariance matrix, as before. The constraint (9.33) is incorporated by adding a fictitious data point, with zero data and zero error, and with zero sound-speed kernel and a density kernel given by ρr^2. The term in $\mathcal{G}(\omega)$, where $\mathcal{G}$ is assumed to be a slowly varying function of frequency, may be suppressed by restricting the combinations of the data to those that are insensitive to a contribution of this form (Däppen *et al.* 1991; Kosovichev *et al.* 1992). Specifically, the coefficients may be constrained to satisfy

$$\sum_i c_i(r_0)Q_i^{-1}\psi_\lambda(\omega_i) = 0 \ , \lambda = 0,\ldots,\Lambda \ , \tag{9.38}$$

for a suitably chosen set of functions ψ_λ. It was shown by Basu *et al.* (1996a) that an equivalent, but potentially more flexible, suppression of the near-surface terms may be based on the filtering technique considered by Pérez Hernández & Christensen-Dalsgaard (1994a).

The SOLA inversion is characterized by the trade-off parameters β and μ controlling the influence of the cross term and the errors, respectively, by the parameters determining the target function $\mathcal{T}(r_0,r)$ and by the number Λ of terms included in the suppression

of the surface effects. The considerations involved in the choice of these parameters were discussed by Rabello-Soares, Basu & Christensen-Dalsgaard (1999a).

The form of the surface term in equation (9.32) assumed that the local properties of the eigenfunctions in the near-surface region are independent of degree; this is what led to the function $\mathcal{G}$ being just dependent on frequency. From an asymptotic point of view this corresponds to assuming that the rays characterizing the modes are nearly vertical in this region. For modes of high degree this approximation no longer holds. Brodsky & Vorontsov (1993) showed how the asymptotic relation (7.1) should be modified in this case, by introducing l-dependent terms in the phase function α. The introduction of the corresponding terms in structure inversion by means of the SOLA or MOLA techniques, generalizing the constraints in equations (9.38), was discussed by Di Mauro *et al.* (2002); they also applied the techniques to preliminary observed frequencies of high-degree modes, obtained by Rhodes *et al.* (1998) from analysis of observations from the SOI/MDI instrument on the SOHO spacecraft.

Although the inversion has been discussed in terms of the pair (c^2, ρ), other sets of variables characterizing the equilibrium structure of the Sun may be used (see also Section 5.1.1). In particular, as discussed in Section 5.5.3, the frequency changes can be expressed in terms of changes $\delta_r\rho$ and $\delta_r Y$ in density and helium abundance, if the equation of state (and the heavy-element abundance) are assumed to be known. Another equivalent, and commonly used, pair is (u, Y), where $u = p/\rho$ is the squared isothermal sound speed. From the point of view of inversion, these pairs have the substantial advantage that the kernels corresponding to $\delta_r Y$ are relatively small and essentially confined to the ionization zones of hydrogen and helium. Thus in the minimization corresponding to equation (9.35), it is comparatively easy to suppress the cross term $\mathcal{C}_{\rho,Y}(r_0, r)$. Furthermore, inversion can be carried out to determine the difference $\delta_r Y$ between the solar and model helium abundance (*e.g.* Kosovichev *et al.* 1992). It should be noted, however, that differences between the solar and model equations of state may introduce systematic errors in the results of such inversions. Basu & Christensen-Dalsgaard (1997) showed how the differences in equation of state might be taken explicitly into account in the inversion, albeit at the expense of an increase in the error in the solution; they also pointed out that the inversion might be carried out to determine the intrinsic difference in Γ_1 between the solar and model equations of state, *i.e.*, the difference at fixed p, ρ and composition.

I finally note that asymptotic inversion techniques to determine the solar internal sound speed were discussed in Section 7.7.2; in particular, it is possible to estimate the sound speed directly from the data, without the use of linearization. Such techniques were originally developed in geophysics (see Brodsky & Levshin 1979); their application to the helioseismic problem was first considered by Gough (1984). In these techniques, the uncertainties associated with the near-surface region are contained in the function $\alpha(\omega)$ or, for the differential technique, in the function $\mathcal{H}_2(\omega)$ (*cf.* Section 7.7.3).

9.3 Some results of helioseismic inversion

To illustrate the power of current helioseismic analysis, it is instructive to present a few selected results of the application of helioseismic inversion; results of the use of the differential asymptotic technique were already shown in Figure 7.13. I first consider inversion to determine solar structure. As discussed in Section 5.1, this is carried out to determine

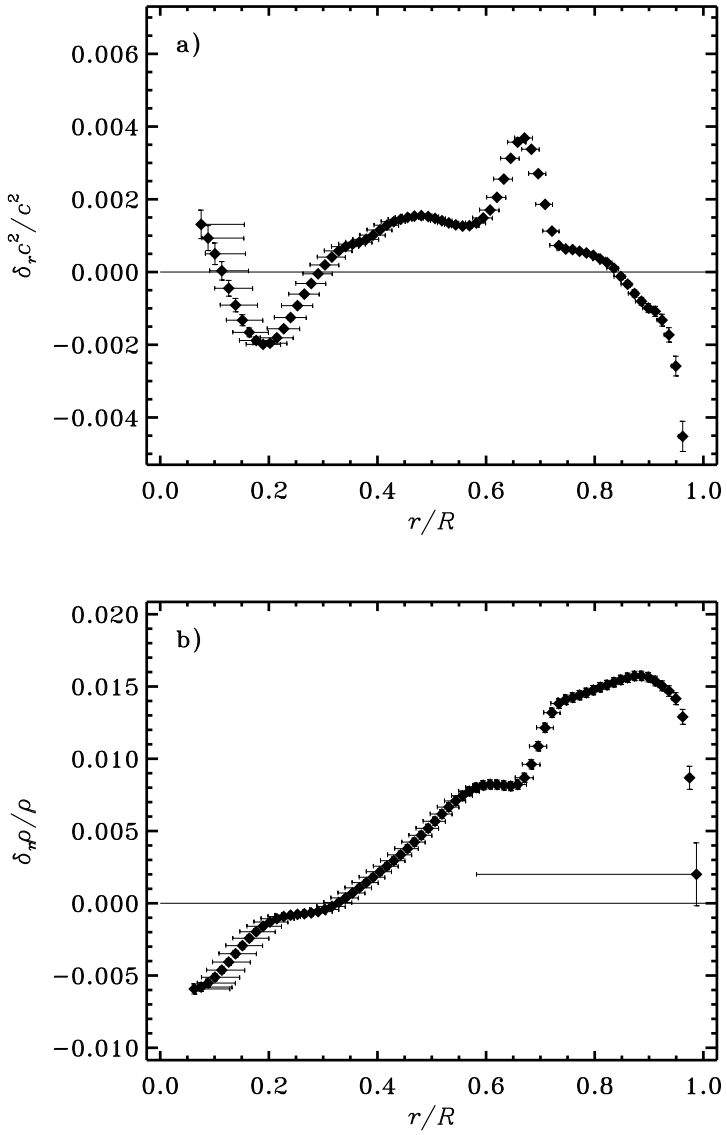

Figure 9.5: Corrections to a reference solar model, obtained by inverting differences between the observed frequencies and the frequencies of the model. Panel a) shows corrections to the squared sound speed c^2, and panel b) shows corrections to ρ. The vertical bars indicate the errors in the results, based on the errors in the observed frequencies, whereas the horizontal bars provide a measure of the resolution in the inversion (from Basu *et al.* 1996b).

corrections to an assumed initial reference model. An example is provided by the results of Basu *et al.* (1996b), based on observations by the LOWL instrument, developed at the High Altitude Observatory (Tomczyk *et al.* 1995). The inversions were carried out in terms of corrections $\delta_r c^2$ and $\delta_r \rho$. In the former case the variable pair (c^2, ρ) was used, while the

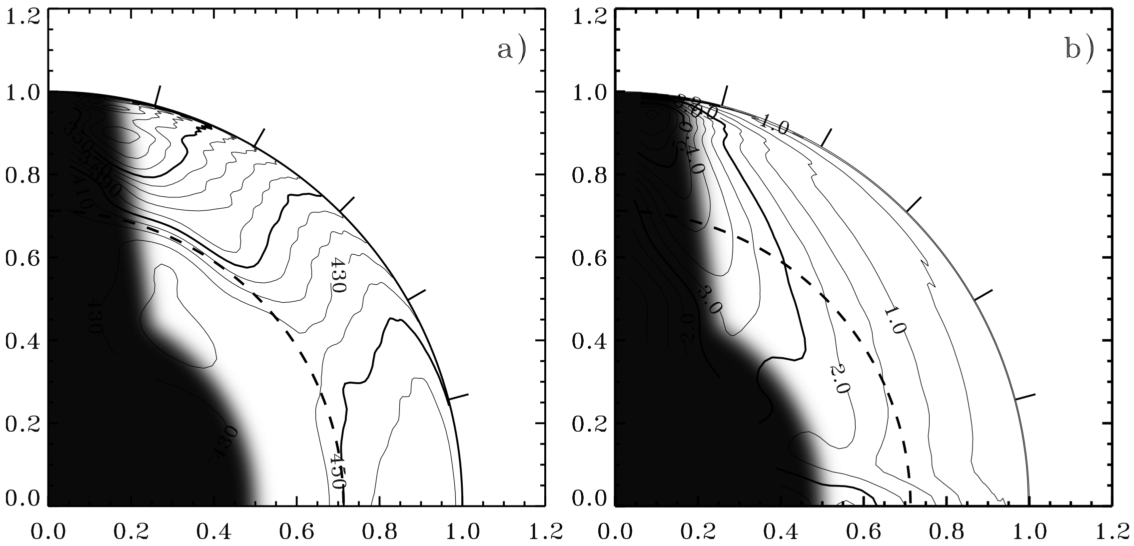

Figure 9.6: Inferred rotation rate $\Omega/2\pi$ (panel a) and the associated error (panel b) in a quadrant of the Sun, obtained by means of SOLA inversion of 144 days of MDI data. The equator is at the horizontal axis and the pole is at the vertical axis, both axes being labelled by fractional radius. Some contours are labelled in nHz, and, for clarity, selected contours are shown as bold. The dashed circle is at the base of the convection zone and the tick marks at the edge of the outer circle are at latitudes 15°, 30°, 45°, 60°, and 75°. The shaded area indicates the region in the Sun where no reliable inference can be made with the present data. (Adapted from Schou *et al.*, 1998.)

density inversion used the pair (ρ, Y); as discussed in Section 5.5.3 it is therefore sensitive to possible errors in the equation of state. As reference was used a model typical of recent normal solar models, computed with little *a priori* attempt to match the observations. The model included settling of helium and heavy elements, and used equation of state and opacity tables from Livermore. The inversion for the corrections was performed by means of the SOLA method discussed in Section 9.2. The results are shown in Figure 9.5; there are evidently systematic differences between the Sun and the model but these are generally fairly small. It is probable that the sharp bump in $\delta_r c^2/c^2$ at $r/R \simeq 0.65$ is a result of weak mixing just beneath the convection zone, which partly offsets the sharp gradient in the hydrogen abundance established by helium settling in this region. Similarly, the negative $\delta_r c^2/c^2$ at the edge of the core could result from partial mixing of the central region. One cannot exclude, however, that errors in the opacity may play a significant role. Nonetheless, it is remarkable that models computed without direct reference to the observations, but based solely on our knowledge of the physics of the solar interior, are so successful in reproducing the structure as inferred from the helioseismic analysis.

To illustrate the determination of the solar internal angular velocity, I present results obtained by Schou *et al.* (1998) from analysis of early data from the MDI instrument on

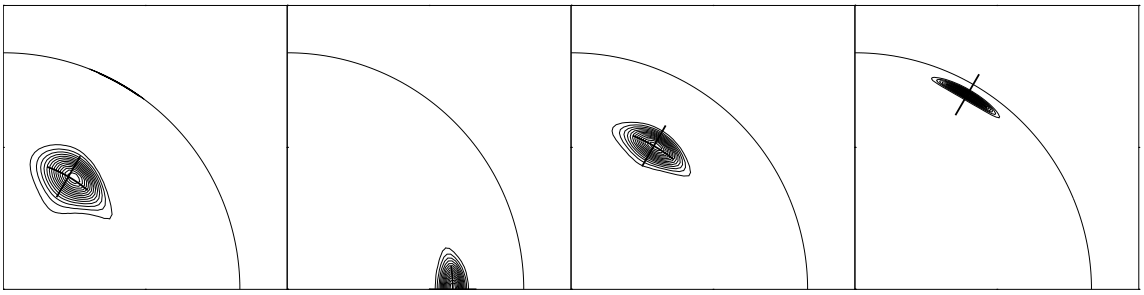

Figure 9.7: Averaging kernels for the SOLA inversion shown in Figure 9.6, targeted at the following radii and latitudes in the Sun: $0.55R$, 60°; 0.7, 0°; 0.7, 60°; $0.95R$, 60°. The corresponding locations are indicated with crosses. (Adapted from Schou et al. 1998.)

the SOHO spacecraft. The inversion was carried out as a fully two-dimensional SOLA inversion of a coefficients, extending to a_{35}, to determine $\bar{\Omega}(r_0, \theta_0)$. The resulting $\bar{\Omega}$ and the estimated errors are presented in Figure 9.6, as contour plots. Strikingly, the error in a substantial part of the Sun is less than 2 nHz. To illustrate the resolution, Figure 9.7 shows selected averaging kernels. Further details of the solution are visible in Figure 9.8, which shows cuts at fixed latitudes, as functions of distance to the centre; here, in addition to the SOLA results, solutions obtained from a two-dimensional regularized least-squares inversion have been included.

There is a striking change in the behaviour of rotation near the base of the convection zone, at a depth of about 28 per cent of the solar radius (as inferred helioseismically; *e.g.* Christensen-Dalsgaard, Gough & Thompson 1991); this is marked by the heavy dashed circle in Figure 9.6 and the heavy dashed line in Figure 9.8. Within the convection zone the variation with latitude in the rotation rate is quite similar to the behaviour observed directly on the surface; in particular, the values at the outermost points in the solution are essentially in agreement with the surface values. (It should be noted that the inversion does not impose continuity with the surface angular velocity.) Near the base of the convection zone there is a transition such that the angular velocity in the radiative interior is roughly independent of latitude, at a value intermediate between the surface equatorial and polar values, but substantially closer to the former. This transition region is known as the *tachocline* (Spiegel & Zahn 1992) and likely plays an important role in the generation of the solar magnetic field and the origin of the solar magnetic cycle. The apparent width of the tachocline in Figure 9.8 in part reflects the finite resolution of the inversion, as determined by the radial extent of the averaging kernels. This must be taken into account in estimating the true width of the tachocline. Charbonneau *et al.* (1999) applied several analysis techniques to LOWL data; they obtained a tachocline width, defined in terms of a representation of the transition by an error function, of $(0.039 \pm 0.013)\,R$ and an equatorial central radius $r_c = (0.693 \pm 0.002)\,R$, essentially placing the transition beneath the convection zone.

Although the overall features of rotation, as presented above, have been found using several different data sets and analysis methods, it should be mentioned that there are problems at the level of finer details, particularly at higher latitudes. These have become

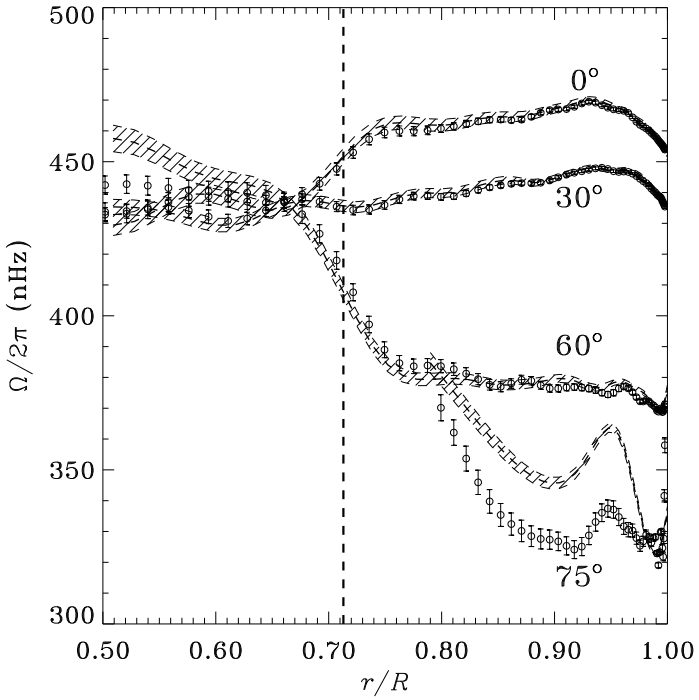

Figure 9.8: Inferred rotation rate $\Omega/2\pi$ as a function of radius at the latitudes indicated, obtained from inversion of 144 days of MDI data. The circles with 1-σ error bars show results of a SOLA inversion, while the dashed lines with 1-σ error band were obtained with regularized least-squares inversion. The heavy vertical dashed line marks the base of the convection zone. (Adapted from Schou *et al.*, 1998.)

apparent in comparisons between results based on data from the GONG and SOI/MDI projects, in both cases analyzed with the procedures used by both projects (*e.g.* Schou *et al.*, 2002). Also, as illustrated by the comparison of the SOLA and least-squares results in Figure 9.8, different inversion methods may give different results at high latitude. Clearly, the underlying causes for these various differences, and how to correct for them, need to be identified.

The data used in the inversions presented in Figures 9.6 and 9.8 did not permit inference of the rotation rate very near the centre. However, analysis of low-degree splittings from the BiSON network provided a tantalizing hint that the core rotation might be *below* the general rotation rate of the radiative interior (Elsworth *et al.* 1995). Chaplin *et al.* (1999) carried out a more detailed analysis of a combination of LOWL and BiSON frequencies, using a version of the MOLA technique especially designed to localize the averaging kernels to the solar core. The results are shown in Figure 9.9. They are consistent with constant rotation of the radiative interior, although with a possible suggestion of a down-turn in the core; analysis of the averaging kernels showed that constraining the measure of rotation to the inner 20 % of the solar radius was only possible at the expense of very substantial

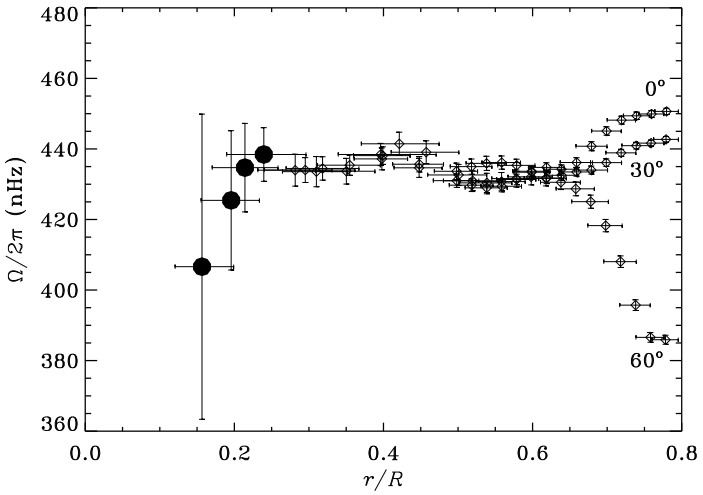

Figure 9.9: The inferred rotation as a function of fractional radius inside the Sun at three solar latitudes: the equator, 30° and 60°; the vertical axis shows the rotation frequency in nHz. The vertical error bars indicate the statistical uncertainty on the rotation rate (±1 standard deviation), whereas the horizontal bars provide a measure of the radial resolution of the inversion. Note that the result becomes much more uncertain in the deep interior, where furthermore the different latitudes cannot be separated. The observations used to infer the rotation were from the LOWL instrument and the BiSON network. (From Chaplin *et al.* 1999.)

errors in the inferred rotation rate.

A more detailed discussion of recent results of helioseismology, with extensive references, was presented by Christensen-Dalsgaard (2002).

Chapter 10

Excitation and damping of the oscillations

So far I have almost exclusively considered adiabatic oscillations, and therefore have been unable to investigate the stability or instability of the modes. Such questions are of obvious interest, however. Here I consider some simple aspects of mode excitation, including properties of the nonadiabatic problem. A major goal is to get a feel for the conditions under which a mode may be *self-excited*, *i.e.*, with a positive growth rate. Also, in cases where all modes are damped, they may still be driven to observable amplitudes by stochastic forcing from near-surface convection; this seems, for example, to be the case for solar oscillations.

10.1 A perturbation expression for the damping rate

In the present section I derive an expression which allows an estimate of the growth or damping rate on the basis of the adiabatic eigenfunction. The procedure is to use the perturbation expression in equation (5.73) which was derived from the oscillation equations written as a linear eigenvalue problem in equation (5.56). Now, however, I take the perturbation $\delta\mathcal{F}$ to be the departure from adiabatic oscillations in the momentum equation. From the perturbed energy equation, equations (3.47) and (3.48) it follows that

$$\begin{aligned} \frac{p'}{p} &= \Gamma_1\frac{\rho'}{\rho} + \xi_r\left(\frac{\mathrm{d}\ln p}{\mathrm{d}r} - \Gamma_1\frac{\mathrm{d}\ln\rho}{\mathrm{d}r}\right) + \frac{i}{\omega}\frac{\Gamma_3-1}{p}(\rho\epsilon - \operatorname{div}\mathbf{F})' \\ &= \frac{p'_{\rm ad}}{p} + \frac{i}{\omega}\frac{\Gamma_3-1}{p}(\rho\epsilon - \operatorname{div}\mathbf{F})' \,, \end{aligned} \tag{10.1}$$

where I dropped the subscript "0" on equilibrium quantities, and assumed a time dependence as $\exp(-i\omega t)$. Here

$$p'_{\rm ad} = p\,\Gamma_1\frac{\rho'}{\rho} + \xi_r p\left(\frac{\mathrm{d}\ln p}{\mathrm{d}r} - \Gamma_1\frac{\mathrm{d}\ln\rho}{\mathrm{d}r}\right) \tag{10.2}$$

is the pressure perturbation corresponding to adiabatic oscillations. It follows that the perturbed momentum equation (3.43) can be written, after separation of the time dependence, as

$$-\rho\omega^2\boldsymbol{\delta}\mathbf{r} = -\nabla p'_{\rm ad} + \rho\,\mathbf{g}' + \rho'\mathbf{g} - \frac{i}{\omega}\nabla[(\Gamma_3-1)(\rho\epsilon - \operatorname{div}\mathbf{F})'] \,. \tag{10.3}$$

This is of the form considered in equation (5.56):

$$\omega^2 \boldsymbol{\delta r} = \mathcal{F}_{\rm ad}(\boldsymbol{\delta r}) + \delta\mathcal{F}(\boldsymbol{\delta r}) \; , \tag{10.4}$$

with

$$\mathcal{F}_{\rm ad}(\boldsymbol{\delta r}) = \frac{1}{\rho}\nabla p'_{\rm ad} - \mathbf{g}' - \frac{\rho'}{\rho}\mathbf{g} \; , \tag{10.5}$$

and

$$\delta\mathcal{F}(\boldsymbol{\delta r}) = \frac{i}{\omega\rho}\nabla[(\Gamma_3 - 1)(\rho\epsilon - \mathrm{div}\,\mathbf{F})'] \; . \tag{10.6}$$

As argued in Section 5.5, $\mathcal{F}_{\rm ad}$ is in fact a linear operator on $\boldsymbol{\delta r}$. It may be shown that the same is true for $\delta\mathcal{F}$.

Exercise 10.1:

Show that $\delta\mathcal{F}$ may be obtained as a linear operator on $\boldsymbol{\delta r}$, assuming the diffusion approximation, equation (3.22). Note that since $\delta\mathcal{F}$ is assumed to be a small perturbation, it may be derived assuming that $\delta\rho$, δp and δT are related adiabatically.

The effects on the frequency of departures from adiabaticity can now immediately be obtained from the perturbation expression (5.73) as

$$\delta\omega^2 = \frac{i}{\omega}\frac{\int_V \boldsymbol{\delta r}^* \cdot \nabla[(\Gamma_3 - 1)(\rho\epsilon - \mathrm{div}\,\mathbf{F})']\mathrm{d}V}{\int_V \rho|\boldsymbol{\delta r}|^2\mathrm{d}V} \; . \tag{10.7}$$

The integral in the numerator can be rewritten as

$$\int_V \mathrm{div}\,[\boldsymbol{\delta r}^*(\Gamma_3 - 1)(\rho\epsilon - \mathrm{div}\,\mathbf{F})']\mathrm{d}V - \int_V \mathrm{div}\,(\boldsymbol{\delta r}^*)(\Gamma_3 - 1)(\rho\epsilon - \mathrm{div}\,\mathbf{F})'\mathrm{d}V \; ; \tag{10.8}$$

the first integral can be transformed, by using Gauss's theorem (3.3), into an integral over the stellar surface which can be neglected, whereas in the second integral we use the continuity equation (3.42). The result is, finally, that the frequency change caused by non-adiabaticity is

$$\delta\omega = \frac{i}{2\omega^2}\frac{\int_V \frac{\delta\rho^*}{\rho}(\Gamma_3 - 1)(\rho\epsilon - \mathrm{div}\,\mathbf{F})'\mathrm{d}V}{\int_V \rho|\boldsymbol{\delta r}|^2\mathrm{d}V} \; . \tag{10.9}$$

This is the desired expression. It should be noted that this expression is valid also in the full nonadiabatic case, if the nonadiabatic eigenfunctions are used.

10.1.1 The quasi-adiabatic approximation

To evaluate the integral in the numerator in equation (10.9) we need an expression for $(\rho\epsilon - \mathrm{div}\,\mathbf{F})'$. Using that $\epsilon = \epsilon(\rho, T)$ (I neglect a possible Eulerian perturbation in the composition) it is easy to see that

$$(\rho\epsilon)' = \rho\epsilon\left[\epsilon_T\frac{T'}{T} + (\epsilon_\rho + 1)\frac{\rho'}{\rho}\right] \; , \tag{10.10}$$

where

$$\epsilon_T = \left(\frac{\partial \ln \epsilon}{\partial \ln T}\right)_\rho , \qquad \epsilon_\rho = \left(\frac{\partial \ln \epsilon}{\partial \ln \rho}\right)_T . \tag{10.11}$$

Similarly, the perturbation in the flux can be evaluated from the diffusion approximation, equation (3.22), and in particular assuming that there are no other contributions (such as convection) to the heat transport. The result is

$$\mathbf{F}' = \left[(3-\kappa_T)\frac{T'}{T} - (1+\kappa_\rho)\frac{\rho'}{\rho}\right] F_{\rm r}\mathbf{a}_r - \frac{4a\tilde{c}T^3}{3\kappa\rho}\nabla T' , \tag{10.12}$$

where

$$\kappa_T = \left(\frac{\partial \ln \kappa}{\partial \ln T}\right)_\rho , \qquad \kappa_\rho = \left(\frac{\partial \ln \kappa}{\partial \ln \rho}\right)_T , \tag{10.13}$$

and $F_{\rm r}$ is the equilibrium radiative flux (which is of course in the radial direction). The underlying assumption in the perturbation treatment leading to equation (5.73) and hence (10.9) is that $\delta\mathcal{F}$ should be evaluated for the *adiabatic* eigenfunction. Regardless of the assumption of adiabaticity we may obtain ρ' from the equation of continuity as

$$\frac{\delta\rho}{\rho} = -\mathrm{div}\,(\boldsymbol{\delta}\mathbf{r}), \qquad \rho' = \delta\rho - \xi_r\frac{\mathrm{d}\rho}{\mathrm{d}r} . \tag{10.14}$$

From adiabaticity it follows that the temperature perturbation can be computed from

$$\frac{\delta T}{T} = (\Gamma_3 - 1)\frac{\delta\rho}{\rho}, \qquad T' = \delta T - \xi_r\frac{\mathrm{d}T}{\mathrm{d}r} . \tag{10.15}$$

Hence, given $\boldsymbol{\delta}\mathbf{r}$, ρ' and T' can be computed, and then $(\rho\epsilon - \mathrm{div}\,\mathbf{F})'$ can be obtained from equations (10.10) and (10.12). Since this approximation to the damping rate can be obtained from the adiabatic eigenfunction, it is known as the *quasi-adiabatic* approximation. As the adiabatic eigenfunctions may be chosen to be real, the integrals in equation (10.9) are real, and hence $\delta\omega$ is purely imaginary. Thus it represents a pure damping or excitation, with no effect on the (real) oscillation frequency.

It should be noted that the approximation is not without problems. The perturbation approach is based on the assumption that the perturbation is small. This is true in most of the star, but not very near the surface where nonadiabatic effects become strong. Here nonadiabaticity has a substantial effect on the eigenfunction, and hence an evaluation of the integral in equation (10.9) based on the adiabatic eigenfunctions is questionable. Nonetheless, we may hope that the quasi-adiabatic approximation at least gives an indication of the stability properties of the mode. A separate problem, which would equally affect a full nonadiabatic treatment, is the neglect of convective contributions to the heat flux. This introduces a major uncertainty in the calculation of the stability of modes in cool stars with extensive outer convection zones. Indeed, it was shown by Baker & Gough (1979) that the transition to stability at the cool side of the Cepheid instability strip most likely is the result of the increased importance of convection. Houdek (2000) made a more detailed analysis, based on a sophisticated mixing-length model of the interaction between convection and pulsations, and similarly showed that convection caused the return to stability at the cool side of the instability region for δ Scuti variables.

10.1.2 A simple example: perturbations in the energy generation rate

To illustrate some simple properties of equation (10.9) I consider the case where the nonadiabaticity is dominated by the energy generation. Here it is convenient to work purely in terms of Lagrangian perturbations, by noting that

$$(\rho\epsilon - \mathrm{div}\,\mathbf{F})' = \delta(\rho\epsilon - \mathrm{div}\,\mathbf{F}) \;, \tag{10.16}$$

since the equilibrium model is assumed to be in thermal equilibrium. Also, it is obvious that $\delta(\rho\epsilon)$ can be obtained from an expression analogous to equation (10.10). Neglecting the term in $\mathbf{F}$ and using equation (10.15) we find

$$\delta\omega = \frac{i}{2\omega^2} \frac{\int_V \left|\frac{\delta\rho}{\rho}\right|^2 (\Gamma_3 - 1)[\epsilon_\rho + 1 + (\Gamma_3 - 1)\epsilon_T]\rho\epsilon \mathrm{d}V}{\int_V \rho|\boldsymbol{\delta}\mathbf{r}|^2 \mathrm{d}V} \;. \tag{10.17}$$

Since ϵ_T and ϵ_ρ are positive, and $\Gamma_3 \simeq 5/3$, it is obvious that the integrals in equation (10.17) are positive. With the assumed time dependence as $\exp(-i\omega t)$ this corresponds to a growth in the oscillation amplitude, *i.e.*, to instability of the mode.

The physical nature of this instability is very simple and closely related to the operation of a normal heat energy: at compression the gas is hotter than normal and this, together with the increased density, causes an increase in the release of energy; this increases the tendency of the gas to expand back towards equilibrium; at expansion the gas is cooler and less dense and hence the energy production is low; this similarly increases the tendency of collapse towards the equilibrium; both effects increase the oscillation amplitude. This mechanism is closely analogous to the operation of a normal car engine where energy is also released (through the ignition of the air–fuel mixture) at the point of maximum compression.

For acoustic modes, which have large amplitudes in the outer part of the star, the damping and excitation are normally dominated by the effects of the flux. This is more complicated and will be discussed in Section 10.2. However, the destabilization through nuclear reactions may play an important role for g modes in several cases; this includes the Sun which becomes unstable towards a few low-order g modes in relatively early phases of its evolution (see, for example, Christensen-Dalsgaard, Dilke & Gough 1974).

10.1.3 Radiative damping of acoustic modes

I now consider the effects on high-order or high-degree acoustic modes and hence neglect the effect of nuclear reactions. As in Problem 2.2(vi) (*cf.* Appendix C) I assume that the flux perturbation is dominated by the term in $\nabla T'$ in equation (10.12), to obtain

$$(\mathrm{div}\,\mathbf{F})' = \frac{4a\check{c}T^4}{3\kappa\rho}|\mathbf{k}|^2\frac{T'}{T} = \omega^2\frac{4a\check{c}T^4}{3\kappa\rho c^2}\frac{T'}{T} \;, \tag{10.18}$$

where in the last equality I used the dispersion relation for plane sound waves. Here T'/T can be obtained from the adiabatic relation (10.15) where, in accordance with the treatment of plane sound waves, I neglect derivatives of equilibrium quantities. Hence

$$\frac{T'}{T} = \frac{\delta T}{T} = (\Gamma_3 - 1)\frac{\delta\rho}{\rho} \;; \tag{10.19}$$

As a result equation (10.9) for the damping rate becomes

$$\delta\omega = -\frac{i}{2}\frac{\int_V (\Gamma_3 - 1)^2 \left|\frac{\delta\rho}{\rho}\right|^2 \frac{4a\tilde{c}T^4}{3\kappa\rho c^2}\mathrm{d}V}{\int_V \rho|\boldsymbol{\delta}\mathbf{r}|^2\mathrm{d}V} \ . \tag{10.20}$$

It is evident from equation (10.20) that $\delta\omega$ is negative, *i.e.*, the mode is damped. This is again obvious from physical considerations: the effect of the term in the temperature gradient is to increase the heat flux from regions that are compressed and heated, and to decrease it from regions that are expanded; hence effectively there is heat loss at compression and heat gain at expansion, and this works to dampen the oscillation. It should be pointed out here that the opacity fluctuations, acting through the first term in equation (10.12), may counteract that: if opacity is increased at compression the flux of radiation going out through the star is preferentially absorbed at compression, hence heating the gas and contributing to the excitation of the oscillation. This mechanism, the so-called *Eddington valve*, is responsible for the pulsations of the stars in the instability strip.

To compare with the asymptotic expression derived below it is instructive to write equation (10.20) in terms of $\boldsymbol{\delta}\mathbf{r}$; from the continuity equation we have, still assuming a plane sound wave and using the dispersion relation, that

$$\left|\frac{\delta\rho}{\rho}\right| = |\mathrm{div}\,\boldsymbol{\delta}\mathbf{r}| = |\mathbf{k}||\boldsymbol{\delta}\mathbf{r}| = \frac{\omega}{c}|\boldsymbol{\delta}\mathbf{r}| \ . \tag{10.21}$$

Hence we obtain

$$\frac{\delta\omega}{\omega} = -\frac{i\omega}{2}\frac{\int_V \frac{(\gamma-1)^2}{\gamma^2}\frac{4a\tilde{c}T^4}{3\kappa p^2}|\boldsymbol{\delta}\mathbf{r}|^2\rho\mathrm{d}V}{\int_V \rho|\boldsymbol{\delta}\mathbf{r}|^2\mathrm{d}V} \ , \tag{10.22}$$

by using $c^2 = \gamma p/\rho$; for simplicity I assume that $\Gamma_3 = \Gamma_1 = \gamma$.

It is of some interest to consider also the damping from the asymptotic point of view. I start from the modified dispersion relation derived in Problem 2.2

$$\omega^2 = c^2|\mathbf{k}|^2\phi_\mathrm{F} \ , \tag{10.23}$$

where

$$\phi_\mathrm{F} = \frac{1 + \dfrac{i}{\omega\gamma\tau_\mathrm{F}}}{1 + \dfrac{i}{\omega\tau_\mathrm{F}}} \ , \qquad \tau_\mathrm{F} = \frac{3\kappa\rho p}{4a\tilde{c}(\gamma-1)T^4|\mathbf{k}|^2} = \frac{3\kappa\gamma p^2}{4a\tilde{c}(\gamma-1)T^4\omega^2} \ . \tag{10.24}$$

If nonadiabatic effects are weak, *i.e.*, $\omega\tau_\mathrm{F} \gg 1$, we can write equation (10.23) as

$$\omega^2 = c^2|\mathbf{k}|^2 - c^2|\mathbf{k}|^2(1-\phi_\mathrm{F}) \simeq c^2|\mathbf{k}|^2 - i\omega_\mathrm{ad}\frac{\gamma-1}{\gamma\tau_\mathrm{F}} \ , \tag{10.25}$$

where ω_ad is the frequency in the adiabatic case. Equation (10.25) is a perturbed version of the sound-wave dispersion relation, of the form considered in Appendix B. Hence the effect of the damping on the frequencies can be obtained from equations (B.6) and (B.7) as

$$S\frac{\delta\omega}{\omega} \simeq -\frac{i}{2\omega}\int_{r_\mathrm{t}}^R \left(1 - \frac{L^2c^2}{\omega^2r^2}\right)^{-1/2}\frac{\gamma-1}{\gamma\tau_\mathrm{F}}\frac{\mathrm{d}r}{c} \ , \tag{10.26}$$

where

$$S = \int_{r_t}^{R} \left(1 - \frac{L^2 c^2}{\omega^2 r^2}\right)^{-1/2} \frac{\mathrm{d}r}{c} - \pi \frac{\mathrm{d}\alpha}{\mathrm{d}\omega} \; . \tag{10.27}$$

By substituting the expression for τ_{F} we finally obtain

$$S\frac{\delta\omega}{\omega} \simeq -\frac{i\omega}{2} \int_{r_t}^{R} \frac{(\gamma-1)^2}{\gamma^2} \frac{4a\tilde{c}T^4}{3\kappa p^2} \left(1 - \frac{L^2 c^2}{\omega^2 r^2}\right)^{-1/2} \frac{\mathrm{d}r}{c} \; . \tag{10.28}$$

This equation essentially corresponds to equation (10.22) if we note that asymptotically $\rho|\boldsymbol{\delta}\mathbf{r}|^2 \mathrm{d}V$ can be identified with $c^{-1}(1 - L^2c^2/\omega^2r^2)^{-1/2}\mathrm{d}r$, to within a constant factor.

10.2 The condition for instability

The arguments presented in this section were originally derived by J. P. Cox. They provide insight into the reason why unstable stars tend to be found in well-defined regions of the HR diagram, particularly the Cepheid instability strip, and are presented here essentially in the form given by Cox (1967, 1974).

Expressing the frequency in terms of real and imaginary parts as $\omega = \omega_{\mathrm{r}} + i\eta$, equation (10.9) can be written approximately as

$$\eta \simeq \frac{C_{\mathrm{r}}}{2\omega_{\mathrm{r}}^2 I} \; , \tag{10.29}$$

where

$$C_{\mathrm{r}} = \mathrm{Re}\left[\int_V \frac{\delta\rho^*}{\rho}(\Gamma_3 - 1)(\rho\epsilon - \mathrm{div}\,\mathbf{F})' \mathrm{d}V\right] \; , \tag{10.30}$$

and

$$I = \int_V \rho|\boldsymbol{\delta}\mathbf{r}|^2 \mathrm{d}V \; . \tag{10.31}$$

Clearly the question of stability or instability depends on the sign of C_{r}: if $C_{\mathrm{r}} > 0$ the mode is unstable, whereas if $C_{\mathrm{r}} < 0$ the mode is stable.

I consider just the outer parts of the star, where the nuclear energy generation can be neglected. The analysis is restricted to radial oscillations; however, as we know that the behaviour of the modes is largely independent of degree near the surface the results are likely to be at least qualitatively valid for nonradial oscillations as well. Also, I neglect convection. Finally I assume that the oscillations are either quasi-adiabatic or strongly nonadiabatic. In the former region all perturbation quantities can be taken to be real; the strongly nonadiabatic situation is discussed below. Then we can approximate C_{r} by

$$C_{\mathrm{r}} \simeq -L \int_M \frac{\delta\rho}{\rho}(\Gamma_3 - 1) \frac{\mathrm{d}}{\mathrm{d}m}\left(\frac{\delta L}{L}\right) \mathrm{d}m \; . \tag{10.32}$$

I now assume that $\delta\rho > 0$ everywhere in the region of interest. This would in general hold for the fundamental mode. However, even for higher-order modes the dominant excitation and damping generally take place so close to the surface that $\delta\rho$ has constant sign in this region. It now follows from equation (10.32) that the contribution of a given layer to the damping or excitation depends on the rate of change of δL: if δL increases towards the surface, the layer gives a negative contribution to C_{r} and hence contributes to the damping,

whereas if δL decreases towards the surface, the layer contributes to the excitation. This is entirely consistent with the simple heat-engine argument given in Section 10.1.2, if we notice that we are considering the situation at positive $\delta\rho$, *i.e.*, at compression: if δL increases outwards, more energy leaves the layer at the top than flows in at the bottom; hence there is a net energy loss from the layer at compression, which acts to damp the motion. The reverse is true, of course, if δL decreases towards the surface: then energy is dammed up at compression, and the motion is excited. Clearly, the behaviour of the mode depends on the global effect as determined by the integral in equation (10.32).

We now need to consider the behaviour of the luminosity perturbation in more detail. It is given by an expression corresponding to equation (10.12) for the perturbation in the flux. The radiative luminosity may be expressed as

$$L = -\frac{4a\tilde{c}}{3\kappa} 16\pi^2 r^4 T^4 \frac{\mathrm{d}\ln T}{\mathrm{d}m} \; ; \tag{10.33}$$

hence, expressing the equation in terms of the Lagrangian luminosity perturbation,

$$\frac{\delta L}{L} = 4\frac{\delta r}{r} + (4-\kappa_T)\frac{\delta T}{T} - \kappa_\rho \frac{\delta\rho}{\rho} - \left(\frac{\mathrm{d}\ln T}{\mathrm{d}m}\right)^{-1} \frac{\mathrm{d}}{\mathrm{d}m}\left(\frac{\delta T}{T}\right) \; . \tag{10.34}$$

For low-order modes one can probably neglect the term in the $\mathrm{d}(\delta T/T)/\mathrm{d}m$, as well as a term in the displacement. Thus we obtain

$$\frac{\delta L}{L} \simeq (4-\kappa_T)\frac{\delta T}{T} - \kappa_\rho \frac{\delta\rho}{\rho} \; . \tag{10.35}$$

In the region where the oscillations are nearly adiabatic, $\delta T/T \simeq (\Gamma_3 - 1)\delta\rho/\rho$, and hence

$$\frac{\delta L}{L} \simeq \left(\frac{\delta L}{L}\right)_{\mathrm{a}} = \left[(4-\kappa_T)(\Gamma_3 - 1) - \kappa_\rho\right]\frac{\delta\rho}{\rho} \; . \tag{10.36}$$

In most of the star, κ_ρ is close to unity, κ_T is negative (as, for example, for Kramers opacity) and $\Gamma_3 \simeq 5/3$. Also, $\delta\rho/\rho$ generally increases outwards. Hence it follows from equation (10.36) that in most cases δL increases towards the surface, so that the tendency is towards stability. This is quite reassuring: after all most stars do not show obvious variability, suggesting that special circumstances are required to excite modes to large amplitudes.

In fact, it is clear that there are two circumstances that may give rise to a decrease in $(\delta L)_{\mathrm{a}}$: a strong decrease in Γ_3 or a strong increase in κ_T. Both effects are likely to occur in ionization zones of abundant elements. As an example, Figure 10.1 shows $\Gamma_3 - 1$ in the ionization zone of He in a stellar envelope model (see also Figure 7.15 for the qualitatively very similar behaviour of Γ_1 in the Sun). This occurs because the degree of ionization increases at compression, absorbing the energy that would otherwise have gone towards increasing the temperature and hence reducing the temperature increase. Similarly, although perhaps less obvious, there is a tendency for ionization zones to be associated with 'bumps' in κ_T: it should be noted that since what matters in equations (10.32) and (10.36) is effectively the second derivative of opacity even quite minor features in the opacity can lead to substantial contributions to the excitation, provided that they are confined to a narrow temperature interval. These two mechanisms are generally known as the γ- and κ-mechanisms for mode excitation.

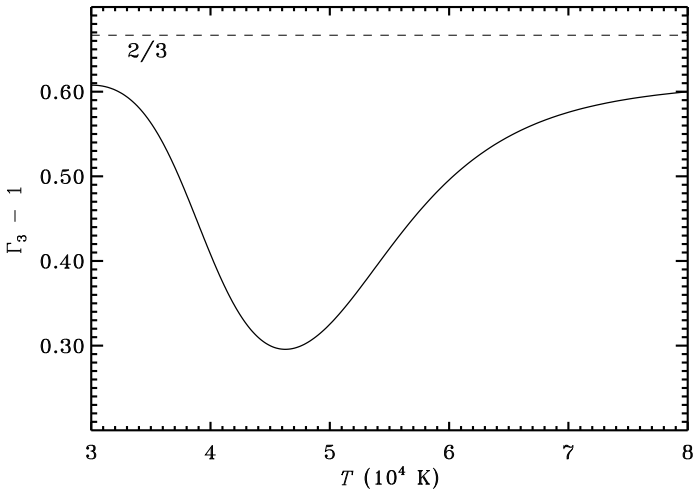

Figure 10.1: $\Gamma_3 - 1$ against temperature in the region of He^+ ionization in an equilibrium model of a stellar envelope.

The description given so far suffers from two problems. First, it is clearly only the lower part of the Γ_3-decrease that will contribute to driving; the upper part similarly contributes to damping, and since $\delta\rho/\rho$ is assumed to increase outwards the damping part is likely to dominate. A similar remark can be made about effects of opacity bumps. Secondly, the argument depends on the quasi-adiabatic approximation, in that the adiabatic relation was used to derive equation (10.35) for δL. The great beauty of Cox's analysis is that it is precisely the transition to nonadiabaticity which is decisive for the occurrence of instability of a star.

To make plausible the transition from adiabaticity to nonadiabaticity I use an argument very similar to the one presented in Section 3.1.4. I write the perturbed energy equation, neglecting the term in ϵ, as

$$\frac{\mathrm{d}}{\mathrm{d}t}\left(\frac{\delta T}{T}\right) - (\Gamma_3 - 1)\frac{\mathrm{d}}{\mathrm{d}t}\left(\frac{\delta\rho}{\rho}\right) \simeq -\frac{L}{4\pi\rho r^2 c_V T}\frac{\mathrm{d}}{\mathrm{d}r}\left(\frac{\delta L}{L}\right) \ . \tag{10.37}$$

This can also be written, approximately, as

$$\Delta\left(\frac{\delta L}{L}\right) \sim \Psi\left[\frac{\delta T}{T} - (\Gamma_3 - 1)\frac{\delta\rho}{\rho}\right] \ , \tag{10.38}$$

where

$$\Psi = \frac{\langle c_V T\rangle \Delta m}{\Pi L} \ . \tag{10.39}$$

Here $\Delta(\delta L/L)$ is the change in $\delta L/L$ between the surface and the point considered, Δm is the mass outside this point, and $\langle c_V T\rangle$ is a suitable average over this region; also Π is the pulsation period. Thus Ψ has a very simple physical meaning: it is the ratio between the thermal energy stored in the layer outside the point considered and the energy radiated by the star in a pulsation period.

Now equation (10.38) can be understood in simple physical terms. Very near the surface $\Psi \ll 1$: the energy content in the stellar matter is so small that it cannot appreciably affect the luminosity perturbation; thus the luminosity perturbation is *frozen in*, *i.e.*, constant. This is clearly the strongly nonadiabatic limit. Conversely, at great depth $\Psi \gg 1$: the energy content is so large that the flow of energy over a pulsation period has no effect on the energy content; this corresponds to the almost adiabatic case. Thus the transition from adiabatic to nonadiabatic oscillations occurs in the *transition region*, where

$$\frac{\langle c_V T \rangle_{\rm TR} (\Delta m)_{\rm TR}}{\Pi L} \sim 1 \; . \tag{10.40}$$

The question of stability or instability is now decided by the relative location of the transition region and the relevant ionization zone. It has been shown by Cox that the Cepheid instability strip is controlled by the ionization of He^+; thus in the following I consider only this zone. Also, to understand the location of the instability strip it is convenient to think in terms of varying the radius, and hence the effective temperature, at fixed luminosity.

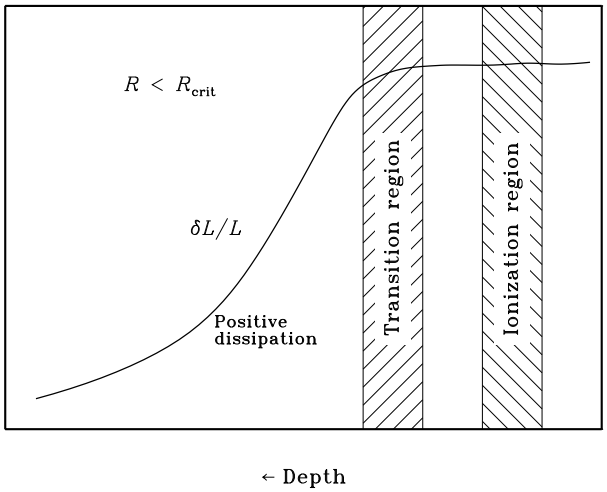

Figure 10.2: $\delta L/L$ at instant of minimum stellar radius and hence maximum compression against depth below the surface (schematic) for a star with $R < R_{\rm crit}$ (see text for explanation of symbols). Only the He^+ ionization zone is shown (after Cox 1967).

Consider first a star of small radius and hence large effective temperature. Here the He^+ ionization zone lies close to the surface, *i.e.*, very likely above the transition region (*cf.* Figure 10.2). Below the transition region $\delta L/L$ follows the adiabatic behaviour and hence increases outwards; this contributes to the damping. Above the transition region δL is approximately constant, and there is no contribution to the excitation and damping. Thus the net effect is that $C_{\rm r} < 0$, *i.e.*, the star is stable.

Now increase the radius, and hence reduce $T_{\rm eff}$, sufficiently that the transition region coincides with the He^+ ionization zone. As illustrated in Figure 10.3, at this critical radius

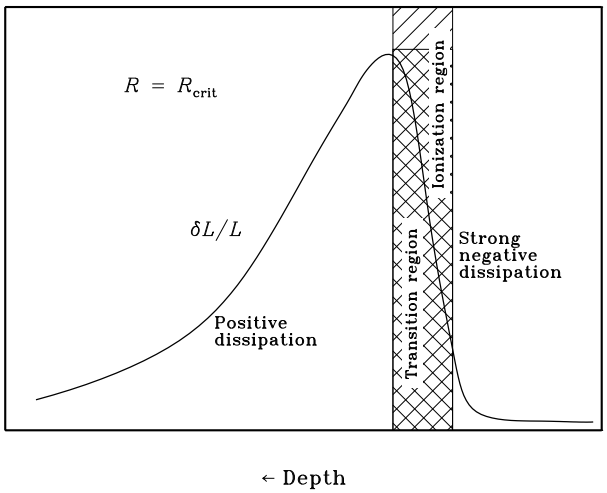

Figure 10.3: $\delta L/L$ at instant of minimum stellar radius and hence maximum compression against depth below the surface (schematic) for a star with $R = R_{\rm crit}$ (see text for explanation of symbols). Only the He^+ ionization zone is shown (after Cox 1967).

$R_{\rm crit}$ the situation changes dramatically. We still get damping in the interior of the star; however, the lower part of the ionization zone now contributes strongly to the excitation, and the corresponding damping in the upper part of the ionization zone is absent because the luminosity perturbation is frozen in here. Thus in this case there is chance for instability. This is precisely what happens: the point where $R = R_{\rm crit}$ corresponds to the location of the instability strip.

Finally, at even larger radius and lower $T_{\rm eff}$ the entire ionization zone lies in the quasi-adiabatic region and hence it makes both positive and negative contributions to the excitation. As argued above, the general increase towards the surface of $\delta\rho/\rho$ makes it plausible that the net effect is damping of the modes. In fact, computations show that it is difficult to reproduce the lower (so-called red) edge of the instability strip unless effects of perturbations in the convective flux are taken into account.

This argument may be more quantitative, to determine the approximate location of the instability strip. In fact, it is not difficult to obtain a relation that determines the slope of the strip (see Problem 6.2 in Appendix C). It was arguments of this kind which first led Cox to identify the He^+ ionization as being mainly responsible for the Cepheid instability.

The location of the transition region, as given in equation (10.40), depends on the period of oscillation. I have so far argued for the behaviour of a single mode (although the changing radius would also tend to increase the period and hence push the transition region deeper). However, it should be noted that higher-order modes would tend to have transition regions closer to the surface. It follows that they should become unstable at higher effective temperatures. This is indeed confirmed by more detailed stability calculations.

The arguments as given here refer specifically to the Cepheid instability strip. However,

very similar arguments can be applied to other driving mechanisms, at least in fairly hot stars where convection can be neglected. Thus any suitable feature that may cause a substantial dip in $(\delta L/L)_{\rm a}$ might be expected to give rise to an instability region. It has been found, through improvements in the treatment of iron line contributions, that there is a bump in the opacities near temperatures of 2×10^5 K which can account for the β Cephei and other B star pulsations in this way (*e.g.* Moskalik & Dziembowski 1992); before these improvements the origin of B-star pulsations was a major mystery. A similar mechanism is responsible for the excitation of g modes in at least some pulsating white dwarfs (*e.g.* Winget *et al.* 1982).

10.3 Stochastic excitation of oscillations

Nonadiabatic calculations taking convection into account generally find that modes in stars on the cool side of the instability strip are stable. In particular, this is the case for the modes observed in the Sun (*e.g.* Balmforth 1992a). Thus the presence of oscillations in the Sun and other cool stars requires other excitation mechanisms. In these stars the convective motion near the surface likely reaches speeds close to that of sound. Such turbulent motion with near-sonic speed is an efficient source of acoustic radiation, and it is likely that this 'noise' excites the normal modes of the star, to the observed amplitude.

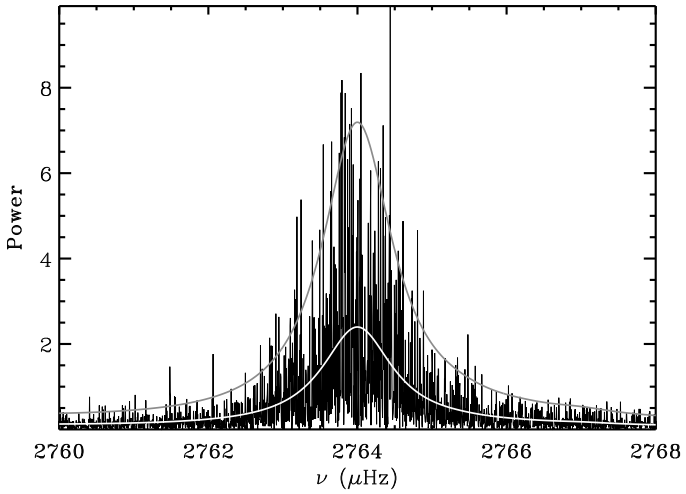

Figure 10.4: Observed spectrum, from Doppler observations with the BiSON network, of a single radial mode of solar oscillations. The smooth curve shows the fitted Lorentzian profile, multiplied by three for clarity. (See Chaplin *et al.* 2002.)

Since the excitation is caused by a very large number of convective elements, the driving is essentially random. The problem of a damped oscillator driven by random forcing was considered by Batchelor (1956), and the analysis is discussed in Problem 6.1 in Appendix C. The outcome is that the average power spectrum resulting for a mode of frequency ω_0, and

damping rate η, is approximately

$$\langle P(\omega)\rangle \simeq \frac{1}{4\omega_0^2}\frac{\langle P_f(\omega)\rangle}{(\omega-\omega_0)^2+\eta^2}\ , \tag{10.41}$$

where $\langle P_f(\omega)\rangle$ is the average power spectrum of the forcing function. If the forcing spectrum is a slowly varying functions of frequency, the result is therefore a Lorentzian spectrum, with a width determined by the linear damping rate of the mode.

If a single realization, rather than the average, of the spectrum is considered, as is generally the case for observations of stellar oscillations, the result is a random function with a Lorentzian envelope. An example is shown in Figure 10.4, based on observations of solar oscillations with the BiSON network. Such Lorentzian profiles are often assumed in the fits carried out to determine the frequency and other properties of the modes. It should be noticed, however, that the observed profiles show definite asymmetries and hence cannot be strictly represented by Lorentzian profiles. This behaviour can be understood from the detailed properties of the excitation, in particular the fact that the dominant contributions to the forcing arise from a relatively thin region (*e.g.*, Duvall *et al.* 1993; Gabriel 1993, 2000; Roxburgh & Vorontsov 1995; Abrams & Kumar 1996; Nigam & Kosovichev 1998; Rast & Bogdan 1998; Rosenthal 1998). Neglecting this effect in the fitting causes systematic errors in the inferred frequencies; however, it appears that these are of a form similar to the effects of the near-surface errors [*i.e.*, the term $Q_{nl}^{-1}\mathcal{G}(\omega_{nl})$ in equation (9.32)], and hence have no effect on the results of structure inversion (*e.g.* Rabello-Soares *et al.* 1999b; Basu *et al.* 2000). Observational determination of the asymmetry does, however, provide constraints on the properties of subsurface convection (Chaplin & Appourchaux 1999; Kumar & Basu 1999; Nigam & Kosovichev 1999).

As a result of the stochastic nature of the excitation, the observed amplitude of a mode varies over time. The statistical properties of this variation were discussed by Kumar, Franklin & Goldreich (1988) and Chang & Gough (1998). If the modes are observed over a time short compared with the damping time, the energy distribution is exponential,

$$p(E)\mathrm{d}E = \langle E\rangle^{-1}\exp(-E/\langle E\rangle)\mathrm{d}E\ , \tag{10.42}$$

where $\langle E\rangle$ is the average energy, and the energy E is proportional to the squared amplitude.

It is straightforward, and instructive, to simulate such stochastically excited, damped, oscillations. An example of such a simulation, for a long-period variable, is illustrated in Figure 10.5. It is evident that the amplitude varies strongly and in an irregular fashion, and hence at any given time there is a significant probability that any given mode may be invisible; this must be kept in mind in the interpretation of such pulsating stars. Panel b) shows the distribution of mode energy, obtained by analyzing the time series in 1-year segments. Here N is the total number of segments, and n is a scaled binned number of realizations,

$$n = \frac{\Delta n(E)}{\exp(\Delta E/2\langle E\rangle)-\exp(-\Delta E/2\langle E\rangle)}\ , \tag{10.43}$$

where $\Delta n(E)$ is the number of realizations in the interval $[E-\Delta E/2, E+\Delta E/2]$. It may be shown that n/N behaves like $\exp(-E/\langle E\rangle)$ (*cf.* Chang & Gough 1998); as is clear from Figure 10.5b the simulated data do indeed have this property. Very interestingly, the observed distribution of solar oscillation amplitudes satisfies this relation quite closely (*e.g.* Chaplin *et al.* 1997). An example, based on BiSON data, is shown in Figure 10.6.

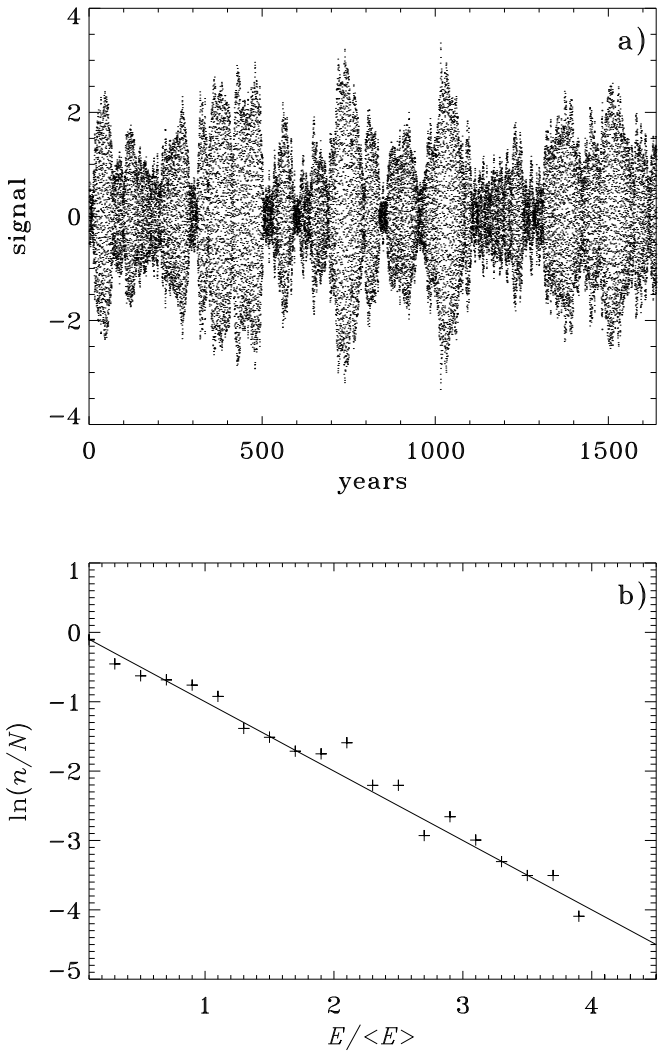

Figure 10.5: Artificial time series for an oscillation with a period of 82 days, a damping time of 60 years and a sampling-time interval of 20 days. The top panel shows the computed time series which, as indicated, covers about 1600 years. In the bottom panel the points show the binned, normalized distribution of mode power, in units of the mean power; the line corresponds to the expected exponential distribution in equation (10.42) (see text). (From Christensen-Dalsgaard *et al.* 2001.)

Exercise 10.2:

Verify this property of the distribution, as described by equation (10.43).

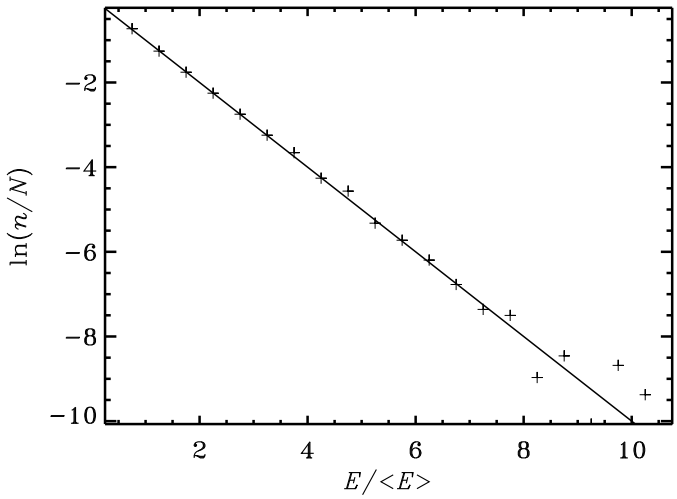

Figure 10.6: Binned, normalized distribution of observed solar mode power, in units of mean power; this is based on 3368 individual samples, each containing 14 modes, of BiSON observations. The line corresponds to the expected exponential distribution in equation (10.42). (See Chaplin *et al.* 1997.)

The distribution function in equation (10.42) also defines the relation between the average $\langle A \rangle$ and the standard deviation $\sigma(A)$ of the amplitude:

$$\sigma(A) = \left(\frac{4}{\pi} - 1 \right)^{1/2} \langle A \rangle \simeq 0.52 \langle A \rangle \; . \tag{10.44}$$

It was noticed by Christensen-Dalsgaard, Kjeldsen & Mattei (2001) that observed amplitudes of semiregular variables on the red-giant branch approximately followed this relation, suggesting that their variability may have a cause similar to the solar oscillations.

As indicated by equation (10.41) this excitation mechanism results in a definite prediction of the oscillation amplitude, given a model for the power in the stochastic forcing. This can be evaluated from models of convection, such as the mixing-length description. A rough estimate was made by Christensen-Dalsgaard & Frandsen (1983a); following Goldreich & Keeley (1977) they assumed equipartition between the energy in a single mode of oscillation and the energy of a convective eddy with a time scale corresponding to the period of the mode. The results were analyzed by Kjeldsen & Bedding (1995) who found, as already discussed in Section 2.4.1, that the amplitudes scaled as L/M (*cf.* eq. 2.44). A more careful calculation was carried out by Houdek *et al.* (1999), who determined the damping or excitation rates of radial modes, using a nonlocal mixing-length description of the interaction between convection and pulsation; for the stable modes they estimated the stochastically excited amplitudes, from the computed damping rates and a mixing-length calculation of the energy input to the modes from convection. The results are summarized in Figure 10.7. It should also be noted that computations by Stein & Nordlund (2001) of the energy input from convection to the oscillations, based on detailed hydrodynamical

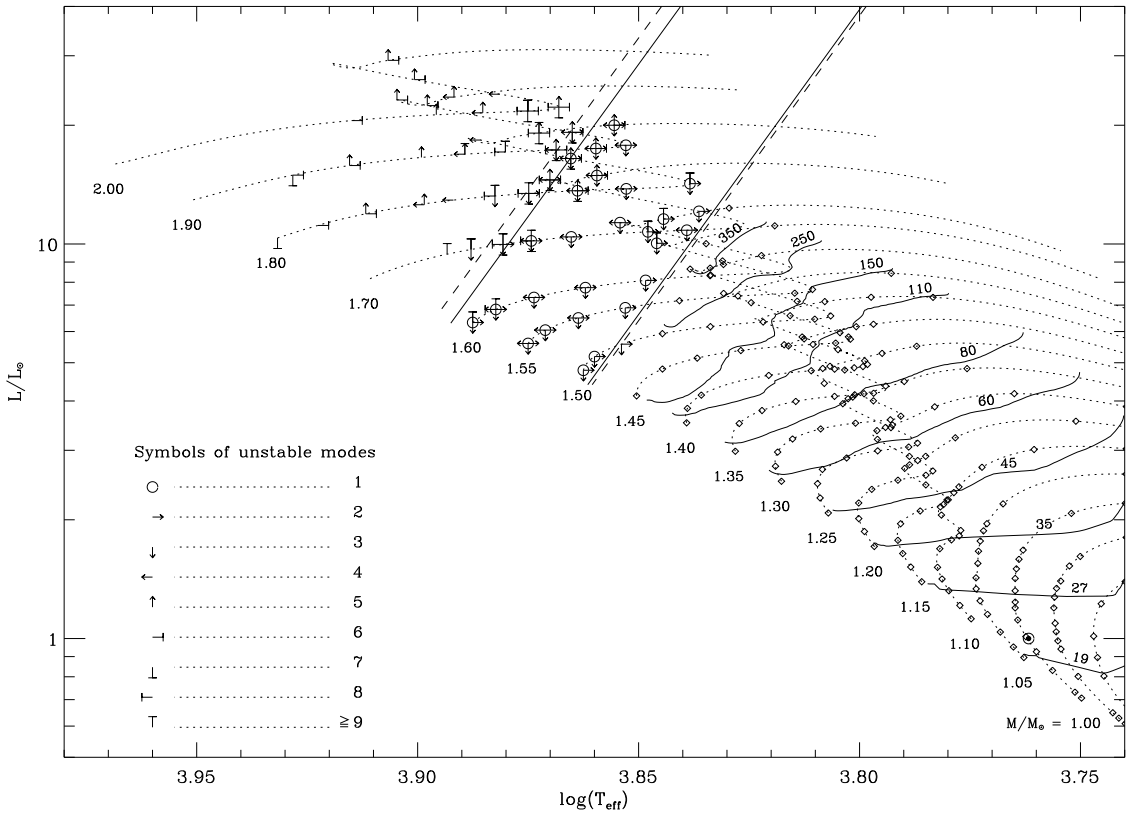

Figure 10.7: Unstable modes and mean velocity amplitudes of stochastically excited modes, for radial oscillations. Evolution tracks, at the masses indicated, are shown with dotted curves, some models being marked with diamonds. Selected models with unstable modes are indicated by the symbols, as listed in the figure; note that, as argued in Section 10.2, the higher-order modes tend to be excited in models with higher effective temperature. The solid and dashed straight lines indicate the instability strips of the $n = 1$ and 2 modes, respectively. The contours to the right of the instability strip show computed velocity amplitudes, averaged over frequency; the values of the amplitudes, in $\mathrm{cm\,s^{-1}}$, are given. For the Sun, indicated by $\odot$, the predicted mean amplitude is $20\,\mathrm{cm\,s^{-1}}$. (From Houdek *et al.* 1999.)

simulations, have yielded results in general agreement with the observed properties of solar oscillations.

The stochastic mechanism is expected to result in the excitation of all modes in a broad range of frequencies, with amplitudes reflecting the presumed slow frequency dependence of the forcing function. This property is indeed observed in the Sun and in the few cases where solar-like oscillations have been observed in other stars (see Section 2.4.1). It greatly simplifies the identification of the modes, compared with oscillations excited through radi-

ative instability. In the latter case the mechanisms determining the final amplitude, and hence the selection of modes which reach an observable level, are unknown and apparently lead to detectability, with current techniques, of only a fairly small subset of the unstable modes.

References

Abramowitz, M. & Stegun, I. A., 1964. *Handbook of Mathematical Functions*, NBS Applied Mathematics Series No. 55, NBS, Washington, D.C.

Abrams, D. & Kumar, P., 1996. [Asymmetries of solar p-mode line profiles]. *Astrophys. J.*, **472**, 882 – 890.

Aizenman, M., Smeyers, P. & Weigert, A., 1977. [Avoided crossing of modes of non-radial stellar oscillations]. *Astron. Astrophys.*, **58**, 41 – 46.

Andreasen, G. K. & Petersen, J. O., 1987. [Cepheids in the Magellanic Clouds. I. Fourier decomposition of LMC Cepheid light curves]. *Astron. Astrophys.*, **180**, 129 – 144.

Appourchaux, T., Fröhlich, C., Andersen, B., Berthomieu, G., Chaplin, W. J., Elsworth, Y., Finsterle, W., Gough, D. O., Isaak, G. R., Kosovichev, A. G., Provost, J., Scherrer, P. H., Sekii, T. & Toutain, T., 2000. [Observational upper limits to low-degree solar g-modes]. *Astrophys. J.*, **538**, 401 – 414.

Bachmann, K. T., Duvall, T. L., Harvey, J. W. & Hill, F., 1995. [Measurement of high-degree solar oscillation frequencies]. *Astrophys. J.*, **443**, 837 – 842.

Backus, G. & Gilbert, F., 1970. [Uniqueness in the inversion of inaccurate gross Earth data]. *Phil. Trans. R. Soc. London, Ser. A*, **266**, 123 – 192.

Baker, N. H. & Gough. D. O., 1979. [Pulsations of model RR Lyrae stars]. *Astrophys. J.*, **234**, 232 – 244.

Baker, N. H., Moore, D. W. & Spiegel, E. A., 1971. [Aperiodic behaviour of a non-linear oscillator]. *Q. Jl. Mech. appl. Math.*, **24**, 391 – 422.

Balmforth, N. J., 1992a. [Solar pulsational stability. I: Pulsation-mode thermodynamics]. *Mon. Not. R. astr. Soc.*, **255**, 603 – 631.

Balmforth, N. J., 1992b. [Solar pulsational stability. III: Acoustical excitation by turbulent convection]. *Mon. Not. R. astr. Soc.*, **255**, 639 – 649.

Barban, C., Michel, E., Martic, M., Schmitt, J., Lebrun, J. C., Baglin, A. & Bertaux, J. L., 1999. [Solar-like oscillations of Procyon A: stellar models and time series simulations versus observations]. *Astron. Astrophys.*, **350**, 617 – 625.

Barban, C., Michel, E., Martic, M., Schmitt, J., Lebrun, J. C., Baglin, A. & Bertaux, J. L., 1999. [Solar-like oscillations of Procyon A: stellar models and time series simulations versus observations]. *Astron. Astrophys.*, **350**, 617 – 625.

Basu, S. & Christensen-Dalsgaard, J., 1997. [Equation of state and helioseismic inversions]. *Astron. Astrophys.*, **322**, L5 – L8.

Basu, S., Thompson, M. J., Christensen-Dalsgaard, J. & Pérez Hernández, F. 1996a. [Filtering out near-surface uncertainties from helioseismic inversion]. *Mon. Not. R. astr. Soc.*, **280**, 651 – 660.

Basu, S., Christensen-Dalsgaard, J., Schou, J., Thompson, M. J. & Tomczyk, S., 1996b. [Solar structure as revealed by LOWL data]. *Proc. Conf. on "Windows on the Sun's interior", Bombay, Oct. 1995; Bull. Astron. Soc. India*, **24**, 147 – 150.

Basu, S., Chaplin, W. J., Christensen-Dalsgaard, J., Elsworth, Y., Isaak, G. R., New, R., Schou, J., Thompson, M. J. & Tomczyk, S., 1997. [Solar internal sound speed as inferred from combined BiSON and LOWL oscillation frequencies]. *Mon. Not. R. astr. Soc.*, **292**, 243 – 251.

Basu, S., Turck-Chièze, S., Berthomieu, G., Brun, A. S., Corbard, T., Gonczi, G., Christensen-Dalsgaard, J., Provost, J., Thiery, S., Gabriel, A. H. & Boumier, P., 2000. [Structure of the solar core: Effect of asymmetry of peak profiles]. *Astrophys. J.*, **535**, 1078 – 1084.

Batchelor, G. K., 1956. *The theory of homogeneous turbulence.* Cambridge University Press.

Batchelor, G. K., 1967. *An Introduction to Fluid Mechanics*, Cambridge University Press.

Baturin, V. A. & Mironova, I. V., 1990. [On the possibility of determining helium abundance from helioseismological data]. *Pis'ma Astron. Zh.*, **16**, 253 – 259 (English translation: *Sov. Astron. Lett.*, **16**, 108 – 111).

Bedding, T. R., 2003. [Solar-like oscillations in semiregular variables]. In *Asteroseismology across the HR diagram*, eds M. J. Thompson, M. S. Cunha & M. J. P. F. G. Monteiro, Kluwer Academic Publishers, Dordrecht, *Astrophys. Space Sci.*, 61 – 64.

Bedding, T. R. & Kjeldsen, H., 1995. [More on solar-like oscillations in η Boo]. In *IAU Colloquium 155: Astrophysical Applications of Stellar Pulsation*, *A.S.P. Conf. Ser.*, eds Stobie, R.S., & Whitelock, P.A., San Francisco, **83**, 109 – 110.

Bedding, T. R., Butler, R. P., Kjeldsen, H., Baldry, I. K., O'Toole, S. J., Tinney, C. G., Marcey, G. W., Kienzle, F. & Carrier, F., 2001. [Evidence for solar-like oscillations in beta Hydri]. *Astrophys. J.*, **549**, L105 – L108.

Bedding, T. R., Butler, R. P., Kjeldsen, H., Baldry, I. K., O'Toole, S. J., Tinney, C. G., Marcey, G. W., Kienzle, F. & Carrier, F., 2001. [Evidence for solar-like oscillations in beta Hydri]. *Astrophys. J.*, **549**, L105 – L108.

Bedding, T. R., Kjeldsen, H. & Christensen-Dalsgaard, J., 1998. [Hipparcos parallaxes for η Boo and κ^2 Boo: two successes for asteroseismology]. In *Proc. Tenth Cambridge Workshop on Cool Stars, Stellar Systems and the Sun*, ASP Conf. Proc. vol. 154, eds Donahue, R. A. & Bookbinder, J. A., ASP, San Francisco, p. 741.

Bertello, L., Varadi, F., Ulrich, R. K., Henney, C. J., Kosovichev, A. G., García, R. A. & Turck-Chièze, S., 2000. [Identification of solar acoustic modes of low angular degree and low radial order]. *Astrophys. J.*, **537**, L143 – L146.

Biermann, L., 1947. [Über die Ursache der chromosphärischen Turbulenz und des UV-Exzesses der Sonnenstrahlung]. *Z. Astrophys.*, **25**, 161 – 177.

Billères, M., Fontaine, G., Brassard, P., Charpinet, S., Liebert, J., Saffer, R. A. & Vauclair, G., 1997. [Discovery of p-mode instabilities in the hot subdwarf B star PG 1047+003]. *Astrophys. J.*, **487**, L81 – L84.

Blackman, R. B. & Tukey, J. W., 1959. *The Measurement of Power Spectra*, Dover, New York.

Bouchy, F. & Carrier, F., 2001. [P-mode observations on α Cen A]. *Astron. Astrophys.*, **374**, L5 – L8.

Bracewell, R. N., 1978. *The Fourier Transform and its Applications*, 2. ed., McGraw-Hill, New York.

Bradley, P. A. & Winget, D. E., 1994. [An asteroseismological determination of the structure of the DBV white dwarf GD 358]. *Astrophys. J.*, **430**, 850 – 857.

Brassard, P., Fontaine, G., Billères, M., Charpinet, S., Liebert, J. & Saffer, R. A., 2001. [Discovery and asteroseismological analysis of the pulsating sdB star PG 0014+067]. *Astrophys. J.*, **563**, 1013 – 1030.

Breger, M., 1995a. [Asteroseismology of delta Scuti stars: review]. In *Proc. GONG'94: Helio- and Astero-seismology from Earth and Space*, eds Ulrich, R. K., Rhodes Jr, E. J. & Däppen, W., Astronomical Society of the Pacific Conference Series, San Francisco, **76**, 596 – 605.

Breger, M., 1995b. [Astrophysical applications of delta Scuti stars]. In *Proc. IAU Colloq. 155: Astrophysical Applications of Stellar Pulsation*, eds Stobie, R. S. & Whitelock, P. A., ASP Conf. Ser., **83**, 70 – 79.

Breger, M. & Montgomery, M. H. (eds), 2000. *Delta Scuti and related stars*, ASP Conference Series, **210**, San Francisco.

Breger, M., Handler, G., Garrido, R., Audard, N., Zima, W., Paparó, M., Beichbuchner, F., Zhi-ping, L., Shi-yang, J., Zong-li, L., Ai-ying, Z., Pikall, H., Stankov, A., Guzik, J. A., Sperl, M., Krzesinski, J., Ogloza, W., Pajdosz, G., Zola, S., Thomassen, T., Solheim, J.-E., Serkowitsch, E., Reegen, P., Rumpf, T., Schmalwieser, A. & Montgomery, M. H., 1999. [30+ frequencies for the δ Scuti variable 4 Canum Venaticorum: results of the 1996 multisite campaign]. *Astron. Astrophys.*, **349**, 225 – 235.

Breger, M., Martin, B., Garrido, R., Shi-yang, Jiang, Zhi-ping, Li, Hube, D. P., Stich, J.,Ostermann, W., Paparo, M., 1993b. [EP Cancri: a nonradially pulsating δ Scuti star in the Praesepe cluster]. *Astron. Astrophys.*, **281**, 90 – 94.

Breger, M., Stich, J., Garrido, R., Martin, B., Shi-yang, Jiang, Zhi-ping, Li, Hube, D. P., Ostermann, W., Paparo, M., Schreck, M., 1993a. [Nonradial pulsation of the δ Scuti star BU Cancri in the Praesepe cluster]. *Astron. Astrophys.*, **271**, 482 – 486.

Breger, M., Zima, W., Handler, G., Poretti, E., Shobbrook, R. R., Nitta, A., Prouton, O. R., Garrido, R., Rodriguez, E., Thomassen, T., 1998. [The δ Scuti star FG Vir. III. The 1995 multisite campaign and the detection of 24 pulsation frequencies]. *Astron. Astrophys.*, **331**, 271 – 279.

Brodsky, M. A. & Levshin, A., 1979. [An asymptotic approach to the inversion of free oscillation data]. *Geophys. J. R. astr. Soc.*, **58**, 631 – 654.

Brodsky, M. A. & Vorontsov, S. V., 1987. [An asymptotic technique for solving the inverse problem of helioseismology]. *Pis'ma Astron. Zh.*, **13**, 438 – 443 (English translation: *Sov. Astron. Lett.*, **13**, 179 – 181).

Brodsky, M. A. & Vorontsov, S. V., 1988a. [On the technique of the inversion of helioseismological data]. *Proc. IAU Symposium No 123, Advances in helio- and asteroseismology*, p. 137 – 140, eds Christensen-Dalsgaard, J. & Frandsen, S., Reidel, Dordrecht.

Brodsky, M. A. & Vorontsov, S. V., 1988b. [Helioseismological inverse problem: diagnostics of the structure of the lower solar atmosphere]. *Seismology of the Sun & Sun-like Stars*, p. 487 – 491, eds Domingo, V. & Rolfe, E. J., ESA SP-286.

Brodsky, M. A. & Vorontsov, S. V., 1989. [The inverse problem of helioseismology: probing the structure of the lower solar atmosphere]. *Pis'ma Astron. Zh.*, **15**, 61 – 69 (English translation: *Sov. Astron. Lett.*, **15**, 27 – 30).

Brodsky, M. A. & Vorontsov, S. V., 1993. [Asymptotic theory of intermediate- and high-degree solar acoustic oscillations]. *Astrophys. J.*, **409**, 455 – 464.

Brown, T. M. & Christensen-Dalsgaard, J., 1990. [A technique for estimating complicated power spectra from time series with gaps]. *Astrophys. J.*, **349**, 667 – 674.

Brown, T. M. & Morrow, C. A. 1987. [Depth and latitude dependence of solar rotation]. *Astrophys. J.*, **314**, L21 - L26.

Brown, T. M., Christensen-Dalsgaard, J., Dziembowski, W. A., Goode, P., Gough, D. O. & Morrow, C. A., 1989. [Inferring the Sun's internal angular velocity from observed p-mode frequency splittings]. *Astrophys. J.*, **343**, 526 – 546.

Brown, T. M., Christensen-Dalsgaard, J., Mihalas, B. & Gilliland, R. L., 1994. [The effectiveness of oscillation frequencies in constraining stellar model parameters]. *Astrophys. J.*, **427**, 1013 – 1034.

Brown, T. M., Gilliland, R. L., Noyes, R. W. & Ramsey, L. W., 1991. [Detection of possible p-mode oscillations of Procyon]. *Astrophys. J.*, **368**, 599 – 609.

Brown, T. M., Kennelly, E. J., Korzennik, S. G., Nisenson, P., Noyes, R. W. & Horner, S. D., 1997. [A radial velocity search for p-mode pulsations in η Bootis]. *Astrophys. J.*, **475**, 322 – 327.

Buzasi, D., 2000. [Platforms of opportunity: asteroseismology by piggyback]. In *Stellar Clusters and Associations: Convection, Rotation and Dynamos*, eds R. Pallavicini, G. Micela & S. Sciortino, ASP Conf. Ser., **198**, San Francisco, p. 557 – 560.

Buzasi, D., Catanzarite, J., Laher, R., Conrow, T., Shupe, D., Gautier III, T. N., Kreidl, T. & Everett, D., 2000. [The detection of multimodal oscillations on α Ursae Majoris]. *Astrophys. J.*, **532**, L133 – L136.

Cash, J. R. & Moore, D. R., 1980. [A high order method for the numerical solution of two-point boundary value problems]. *BIT*, **20**, 44 – 52.

Castor, J. I., 1971. [On the Calculation of Linear, Nonadiabatic Pulsations of Stellar Models]. *Astrophys. J.*, **166**, 109 – 129.

Chandrasekhar, S., 1964. [A general Variational Principle Governing the Radial and the Non-radial Oscillations of Gaseous Masses]. *Astrophys. J.*, **139**, 664 – 674.

Chang, H.-Y. & Gough, D. O., 1998. [On the power distribution of solar p modes]. *Solar Phys.*, **181**, 251 – 263.

Chang, H.-Y. & Gough, D. O., 1998. [On the power distribution of solar p modes]. *Solar Phys.*, **181**, 251 – 263.

Chaplin, W. J. & Appourchaux, T., 1999. [Depth of excitation and reversal of asymmetry of low-ℓ solar p modes: a complementary analysis of BiSON and VIRGO/SPM data]. *Mon. Not. R. astr. Soc.*, **309**, 761 – 768.

Chaplin, W. J., Christensen-Dalsgaard, J., Elsworth, Y., Howe, R., Isaak, G. R., Larsen, R. M., New, R., Schou, J., Thompson, M. J. & Tomczyk, S., 1999. [Rotation of the solar core from BiSON and LOWL frequency observations]. *Mon. Not. R. astr. Soc.*, **308**, 405 – 414.

Chaplin, W. J., Elsworth, Y., Howe, R., Isaak, G. R., McLeod, C. P., Miller, B. A., van der Raay, H. B., Wheeler, S. J. & New, R., 1996. [BiSON performance]. *Solar Phys.*, **168**, 1 – 18.

Chaplin, W. J., Elsworth, Y., Howe, R., Isaak, G. R., McLeod, C. P., Miller, B. A. & New, R., 1997. [The observation and simulation of stochastically excited solar p modes]. *Mon. Not. R. astr. Soc.*, **287**, 51 – 56.

Chaplin, W. J., Elsworth, Y., Isaak, G. R., Marchenkov, K. I., Miller, B. A., New, R., Pinter, B. & Appourchaux, T., 2002. [Peak finding at low signal-to-noise: low-ℓ solar

acoustic eigenmodes at $n \leq 9$ from the analysis of BiSON data]. *Mon. Not. R. astr. Soc.*, **336**, 979 – 991.

Chaplin, W. J., Elsworth, Y., Isaak, G. R., Marchenkov, K. I., Miller, B. A. & New, R., 2001a. [Changes to low-ℓ solar p-mode frequencies over the solar cycle: correlations on different time-scales]. *Mon. Not. R. astr. Soc.*, **322**, 22 – 30.

Chaplin, W. J., Elsworth, Y., Isaak, G. R., Marchenkov, K. I., Miller, B. A. & New, R., 2001b. [Rigid rotation of the solar core? On the reliable extraction of low-ℓ rotational p-mode splittings from full-disc observations of the Sun]. *Mon. Not. R. astr. Soc.*, **327**, 1127 – 1136.

Chaplin, W. J., Elsworth, Y., Isaak, G. R., McLeod, C. P., Miller, B. A. & New, R., 1998. [An analysis of solar p-mode frequencies extracted from BiSON data: 1991–1996]. *Mon. Not. R. astr. Soc.*, **300**, 1077 – 1090.

Chaplin, W. J., Elsworth, Y., Isaak, G. R., Miller, B. A. & New, R., 1999. [Skew-symmetric solar p modes in low-ℓ BiSON data]. *Mon. Not. R. astr. Soc.*, **308**, 424 – 430.

Charbonneau, P., Christensen-Dalsgaard, J., Henning, R., Larsen, R. M., Schou, J., Thompson, M. J. & Tomczyk, S., 1999. [Helioseismic constraints on the structure of the solar tachocline]. *Astrophys. J.*, **527**, 445 – 460.

Charpinet, S., Fontaine, G., Brassard, P. & Dorman, B., 1996. [The potential of asteroseismology for hot, subdwarf B stars: a new class of pulsating stars?]. *Astrophys. J.*, **471**, L103 – L106.

Charpinet, S., Fontaine, G., Brassard, P., Chayer, P., Rogers, F., Iglesias, C. A & Dorman, B., 1997. [A driving mechanism for the newly-discovered class of pulsating subdwarf B stars]. *Astrophys. J.*, **483**, L123 – L126.

Chitre, S. M., Christensen-Dalsgaard, J. & Thompson, M. J., 1998. [Diagnostic potential of the solar f modes]. In *Structure and dynamics of the interior of the Sun and Sun-like stars; Proc. SOHO 6/GONG 98 Workshop*, eds S.G. Korzennik & A. Wilson, ESA SP-418, ESA Publications Division, Noordwijk, The Netherlands, p. 141 – 145.

Christensen-Dalsgaard, B. L., 1982. [On the use of the finite-element method with Lagrange multipliers in scattering theory]. *J. Phys. A*, **15**, 2711 – 2722.

Christensen-Dalsgaard, J., 1976. [On isolated stars in non-radial oscillation]. *Mon. Not. R. astr. Soc.*, **174**, 87 – 89.

Christensen-Dalsgaard, J., 1978. [Solar oscillations]. *PhD Dissertation*, University of Cambridge.

Christensen-Dalsgaard, J., 1980. [On adiabatic non-radial oscillations with moderate or large l]. *Mon. Not. R. astr. Soc.*, **190**, 765 – 791.

Christensen-Dalsgaard, J., 1981. [The effect of non-adiabaticity on avoided crossings of non-radial stellar oscillations]. *Mon. Not. R. astr. Soc.*, **194**, 229 – 250.

Christensen-Dalsgaard, J., 1982. [On solar models and their periods of oscillation]. *Mon. Not. R. astr. Soc.*, **199**, 735 – 761.

Christensen-Dalsgaard, J., 1984a. [Optimized response functions for two-dimensional observations of solar oscillations]. *Proceedings of Conference on Solar Seismology from Space*, p. 219, eds Ulrich, R. K., Harvey, J., Rhodes, E. J. & Toomre, J., NASA, JPL Publ. 84-84.

Christensen-Dalsgaard, J., 1984b. [What will asteroseismology teach us?]. *Space Research Prospects in Stellar Activity and Variability*, p. 11 – 45, ed. Praderie, F., Paris Observatory Press.

Christensen-Dalsgaard, J., 1984c. [Solar oscillations]. *Theoretical Problems in Stellar Stability and Oscillations*, p. 155 – 207, Institut d'Astrophysique, Liège.

Christensen-Dalsgaard, J., 1987. [Helio- and asteroseismology: Basic techniques and inverse problems]. *Methodes mathematiques pour l'astrophysique*, p. 479 – 524, eds Auvergne, M. & Baglin, A., (Société Française des Spécialiste d'Astronomie, Paris).

Christensen-Dalsgaard, J., 1988a. [Study of solar structure based on p-mode helioseismology]. *Seismology of the Sun & Sun-like Stars*, p. 431 – 450, eds Domingo, V. & Rolfe, E. J., ESA SP-286.

Christensen-Dalsgaard, J., 1988b. [A Hertzsprung-Russell diagram for stellar oscillations]. *Proc. IAU Symposium No 123, Advances in helio- and asteroseismology*, p. 295 – 298, eds Christensen-Dalsgaard, J. & Frandsen, S., Reidel, Dordrecht.

Christensen-Dalsgaard, J., 1991a. [Some aspects of the theory of solar oscillations]. *Geophys. Astrophys. Fluid Dynamics*, **62**, 123 – 152.

Christensen-Dalsgaard, J., 1991b. [Solar oscillations and the physics of the solar interior]. In *Challenges to theories of the structure of moderate-mass stars*, *Lecture Notes in Physics*, vol. **388**, p. 11 – 36, eds Gough, D. O. & Toomre, J., Springer, Heidelberg.

Christensen-Dalsgaard, J., 1993a. *Lecture Notes on Stellar Structure and Evolution (3. ed)*, D.f.I. Print, Aarhus.

Christensen-Dalsgaard, J., 1993b. [On the asteroseismic HR diagram]. In *Proc. GONG 1992: Seismic investigation of the Sun and stars*, ed. Brown, T. M., Astronomical Society of the Pacific Conference Series, San Francisco, **42**, 347 – 350.

Christensen-Dalsgaard, J., 1996a. [Testing a solar model: the forward problem]. In *Proc. VI IAC Winter School "The structure of the Sun"*, ed. T. Roca Cortes, Cambridge University Press, 47 – 139.

Christensen-Dalsgaard, J., 1996b. [Helioseismology, solar models and solar neutrinos]. In *Proc. Workshop on Theoretical and Phenomenological Aspects of Underground Physics (TAUP'95)*, ed. Fatas, M., *Nucl. Phys. B, Suppl.*, **48**, 325 – 334.

Christensen-Dalsgaard, J., 2002. [Helioseismology]. *Rev. Mod. Phys.*, **74**, 1073 – 1129.

Christensen-Dalsgaard, J. & Berthomieu, G., 1991. [Theory of solar oscillations]. In *Solar interior and atmosphere*, p. 401 – 478, eds Cox, A. N., Livingston, W. C. & Matthews, M., Space Science Series, University of Arizona Press.

Christensen-Dalsgaard, J. & Däppen, W., 1992. [Solar oscillations and the equation of state]. *Astron. Astrophys. Rev.*, **4**, 267 – 361.

Christensen-Dalsgaard, J. & Frandsen, S., 1983a. [Stellar 5 min oscillations]. *Solar Phys.*, **82**, 469 – 486.

Christensen-Dalsgaard, J. & Frandsen, S., 1983b. [Radiative transfer and solar oscillations]. *Solar Phys.*, **82**, 165 – 204.

Christensen-Dalsgaard, J. & Gough, D. O., 1982. [On the interpretation of five-minute oscillations in solar spectrum line shifts]. *Mon. Not. R. astr. Soc.*, **198**, 141 – 171.

Christensen-Dalsgaard, J. & Gough, D. O., 2001. [On the dipolar f mode of stellar oscillation]. *Mon. Not. R. astr. Soc.*, **326**, 1115 – 1121.

Christensen-Dalsgaard, J. & Mullan, D. J., 1994. [Accurate frequencies of polytropic models]. *Mon. Not. R. astr. Soc.*, **270**, 921 – 935.

Christensen-Dalsgaard, J. & Pérez Hernández, F., 1992. [Phase-function differences for stellar acoustic oscillations – I. Theory]. *Mon. Not. R. astr. Soc.*, **257**, 62 – 88.

Christensen-Dalsgaard, J. & Schou, J., 1988. [Differential rotation in the solar interior]. *Seismology of the Sun & Sun-like Stars*, p. 149 – 153, eds Domingo, V. & Rolfe, E. J.,

ESA SP-286.

Christensen-Dalsgaard, J. & Thompson, M. J., 1997. [On solar p-mode frequency shifts caused by near-surface model changes]. *Mon. Not. R. astr. Soc.*, **284**, 527 – 540.

Christensen-Dalsgaard, J., Bedding, T. R. & Kjeldsen, H., 1995a. [Modelling solar-like oscillations in η Bootis]. *Astrophys. J.*, **443**, L29 – L32.

Christensen-Dalsgaard, J., Bedding, T. R., Houdek, G., Kjeldsen, H., Rosenthal, C., Trampedach, R., Monteiro, M. J. P. F. G. & Nordlund, Å., 1995b. [Near-surface effects in modelling oscillations of η Boo]. In *Proc. IAU Colloq. 155: Astrophysical Applications of Stellar Pulsation*, eds Stobie, R. S. & Whitelock, P. A., ASP Conf. Ser., **83**, 447 – 448.

Christensen-Dalsgaard, J., Däppen, W., Ajukov, S. V., Anderson, E. R., Antia, H. M., Basu, S., Baturin, V. A., Berthomieu, G., Chaboyer, B., Chitre, S. M., Cox, A. N., Demarque, P., Donatowicz, J., Dziembowski, W. A., Gabriel, M., Gough, D. O., Guenther, D. B., Guzik, J. A., Harvey, J. W., Hill, F., Houdek, G., Iglesias, C. A., Kosovichev, A. G., Leibacher, J. W., Morel, P., Proffitt, C. R., Provost, J., Reiter, J., Rhodes Jr., E. J., Rogers, F. J., Roxburgh, I. W., Thompson, M. J., Ulrich, R. K., 1996. [The current state of solar modeling]. *Science*, **272**, 1286 – 1292.

Christensen-Dalsgaard, J., Duvall, T. L., Gough, D. O., Harvey, J. W. & Rhodes, E. J., 1985. [Speed of sound in the solar interior]. *Nature*, **315**, 378 – 382.

Christensen-Dalsgaard, J., Dziembowski, W. & Gough, D. O., 1980. [How deep is the solar convection zone?]. *Lecture Notes in Physics*, **125**, p. 313 – 341, eds Dziembowski, W. & Hill, H. A., Springer, Heidelberg.

Christensen-Dalsgaard, J., Gough, D. O. & Morgan, J. G., 1979. [Dirty solar models]. *Astron. Astrophys.*, **73**, 121 – 128.

Christensen-Dalsgaard, J., Gough, D. O. & Thompson, M. J., 1988. [Determination of the solar internal sound speed by means of a differential asymptotic inversion]. *Seismology of the Sun & Sun-like Stars*, p. 493 – 497, eds V. Domingo & E. J. Rolfe, ESA SP-286, Noordwijk, Holland.

Christensen-Dalsgaard, J., Gough, D. O. & Thompson, M. J., 1989. [Differential asymptotic sound-speed inversions]. *Mon. Not. R. astr. Soc.*, **238**, 481 – 502.

Christensen-Dalsgaard, J., Gough, D. O. & Thompson, M. J., 1991. [The depth of the solar convection zone]. *Astrophys. J.*, **378**, 413 – 437.

Christensen-Dalsgaard, J., Gough, D. O. & Toomre, J., 1985. [Seismology of the Sun]. *Science*, **229**, 923 – 931.

Christensen-Dalsgaard, J., Gough, D. O. & Pérez Hernández, F., 1988. [Stellar disharmony]. *Mon. Not. R. astr. Soc.*, **235**, 875 – 880.

Christensen-Dalsgaard, J., Hansen, P. C. & Thompson, M. J., 1993. [Generalized singular value decomposition analysis of helioseismic inversions]. *Mon. Not. R. astr. Soc.*, **264**, 541 – 564.

Christensen-Dalsgaard, J., Kjeldsen, H. & Mattei, J. A., 2001. [Solar-like oscillations of semiregular variables]. *Astrophys. J.*, **562**, L141 – L144.

Christensen-Dalsgaard, J., Proffitt, C. R. & Thompson, M. J., 1993. [Effects of diffusion on solar models and their oscillation frequencies]. *Astrophys. J.*, **403**, L75 – L78.

Christensen-Dalsgaard, J., Schou, J. & Thompson, M. J., 1990. [A comparison of methods for inverting helioseismic data]. *Mon. Not. R. astr. Soc.*, **242**, 353 – 369.

Claverie, A., Isaak, G. R., McLeod, C. P., van der Raay, H. B., Pallé, P. L. & Roca Cortes, T., 1984. [Continuous observation of solar oscillations from two suitably spaced ground

stations]. *Mem. Soc. Astron. Ital.*, **55**, 63 – 66.

Costa, J. E. S., Kepler, S. O. & Winget, D. E., 1999. [Direct measurement of a secular pulsation period change in the pulsating hot pre-white dwarf PG 1159–035]. *Astrophys. J.*, **522**, 973 – 982.

Cowling, T. G., 1941. [The non-radial oscillations of polytropic stars]. *Mon. Not. R. astr. Soc.*, **101**, 367 – 375.

Cowling, T. G. & Newing, R. A., 1949. [The oscillations of a rotating star]. *Astrophys. J.*, **109**, 149 – 158.

Cox, A. N., Guzik, J. A. & Kidman, R. B., 1989. [Oscillations of solar models with internal element diffusion]. *Astrophys. J.*, **342**, 1187 – 1206.

Cox, J. P., 1967. In *Aerodynamic Phenomena in Stellar Atmospheres*, IAU Symp. No 28, p. 3, Academic Press, London.

Cox, J. P., 1974. [Pulsating stars]. *Rep. Prog. Phys.*, **37**, 563 – 698.

Cox, J. P., 1980. *Theory of Stellar Pulsation*, Princeton University Press.

Cox, J. P. & Giuli, R. T., 1968. *Principles of Stellar Structure*, Gordon & Breach, New York.

Cox, J. P. & Whitney, C., 1958. [Stellar pulsation. IV. A semitheoretical period-luminosity relation for classical Cepheids]. *Astrophys. J.*, **127**, 561 – 572.

Craig, I. J. D. & Brown, J. C., 1986. *Inverse problems in astronomy: a guide to inversion strategies for remotely sensed data*, Adam Hilger, Bristol.

Cuypers, J. 1980. [On the calculation of the frequency splitting of adiabatic nonradial stellar oscillations by slow differential rotation]. *Astron. Astrophys.*, **89**, 207 – 208.

Däppen, W. & Gough, D. O., 1984. [On the determination of the helium abundance of the solar convection zone]. *Theoretical Problems in Stellar Stability and Oscillations*, p. 264 – 269 (Institut d'Astrophysique, Liège).

Däppen, W. & Gough, D. O., 1986. [Progress report on helium abundance determination]. *Seismology of the Sun and the distant Stars*, p. 275 – 280, ed. Gough, D. O., Reidel, Dordrecht.

Däppen, W., Gough, D. O., Kosovichev, A. G. & Thompson, M. J., 1991. [A new inversion for the hydrostatic stratification of the Sun]. In *Challenges to theories of the structure of moderate-mass stars*, *Lecture Notes in Physics*, vol. **388**, p. 111 – 120, eds Gough, D. O. & Toomre, J., Springer, Heidelberg.

Deepak, A., 1977. *Inversion Methods in Atmospheric Remote Sounding*, Academic, New York.

Deubner, F.-L. & Gough, D. O., 1984. [Helioseismology: Oscillations as a diagnostic of the solar interior]. *Ann. Rev. Astron. Astrophys.* **22**, 593 – 619.

Di Mauro, M. P., Christensen-Dalsgaard, J., Rabello-Soares, M. C. & Basu, S., 2002. [Inferences on the solar envelope with high-degree modes]. *Astron. Astrophys.*, **384**, 666 – 677.

Domingo, V., Fleck, B. & Poland, A. I., 1995. [The SOHO mission: an overview]. *Solar Phys.*, **162**, 1 – 37.

Duvall, T. L., 1982. [A dispersion law for solar oscillations]. *Nature*, **300**, 242 – 243.

Duvall, T. L. & Harvey, J. W., 1983. [Observations of solar oscillations of low and intermediate degree]. *Nature*, **302**, 24 – 27.

Duvall, T. L., Dziembowski, W. A., Goode, P. R., Gough, D. O., Harvey, J. W. & Leibacher, J. W., 1984. [The internal rotation of the Sun]. *Nature*, **310**, 22 – 25.

Duvall, T. L., Harvey, J. W., Jefferies, S. M. & Pomerantz, M. A., 1991. [Measurements of high-frequency solar oscillation modes]. *Astrophys. J.*, **373**, 308 – 316.

Duvall, T. L., Jefferies, S. M., Harvey, J. W., Osaki, Y. & Pomerantz, M. A., 1993. [Asymmetries of solar oscillation line profiles]. *Astrophys. J.*, **410**, 829 – 836.

Dyson, J. & Schutz, B. F., 1979. [Perturbations and stability of rotating stars. I. Completeness of normal modes]. *Proc. Roy. Soc. London*, **A368**, 389 – 410.

Dziembowski, W. A. & Pamyatnykh, A. A., 1991. [A potential asteroseismological test for convective overshooting theories]. *Astron. Astrophys.*, **248**, L11 – L14.

Dziembowski, W. A., Gough, D. O., Houdek, G. & Sienkiewicz, R., 2001. [Oscillations of α UMa and other red giants]. *Mon. Not. R. astr. Soc.*, **328**, 601 – 610.

Dziembowski, W. A., Pamyatnykh, A. A. & Sienkiewicz, R., 1990. [Solar model from the helioseismology and the neutrino flux problem]. *Mon. Not. R. astr. Soc.*, **244**, 542 – 550.

Dziembowski, W. & Królikowska, M., 1990. [On the mechanism of mode selection in δ Scuti stars]. *Acta Astron.*, **40**, 19 – 26.

Eckart, C., 1960. *Hydrodynamics of Oceans and Atmospheres*, Pergamon Press.

Eddington, A. S., 1926. *The Internal Constitution of the Stars*, Cambridge University Press.

Edmonds, A. R., 1960. *Angular Momentum in Quantum Mechanics*, 2. Edition, Princeton University Press, Princeton, N. J.

Edmonds, P. D. & Gilliland, R. L., 1996. [K giants in 47 Tucanae: detection of a new class of variable stars]. *Astrophys. J.*, **464**, L157 – L160.

Eggen, O. J., 1957a. [Population type I, short-period variable stars in the Hertzsprung gap]. *Astron. J.*, **62**, 14 (Abstract).

Eggen, O. J., 1957b. [Distribution of the nearer bright stars in the color-luminosity array]. *Astron. J.*, **62**, 45 – 55.

Eisenfeld, J., 1969. [A completeness theorem for an integro-differential operator]. *J. Math. Anal. Applic.*, **26**, 357 – 375.

Ellis, A. N., 1988. [Inversion of asymptotic gravity-mode frequencies and its application to the Sun]. *Proc. IAU Symposium No 123, Advances in helio- and asteroseismology*, p. 147 – 150, eds Christensen-Dalsgaard, J. & Frandsen, S., Reidel, Dordrecht.

Elsworth, Y., Howe, R., Isaak, G. R., McLeod, C. P. & New, R., 1990. [Evidence from solar seismology against non-standard solar-core models]. *Nature*, **347**, 536 – 539.

Elsworth, Y., Howe, R., Isaak, G. R., McLeod, C. P., Miller, B. A., New, R., Wheeler, S. J. & Gough, D. O., 1995. [Slow rotation of the Sun's interior]. *Nature*, **376**, 669 – 672.

Elsworth, Y., Howe, R., Isaak, G. R., McLeod, C. P., Miller, B. A., Wheeler, S. J. & New, R., 1995. [Fine spacing of the $l = 0$, $l = 2$ acoustic eigenmodes and the solar neutrino problem: particle physics and cosmological implications]. In *Proc. GONG'94: Helio- and Astero-seismology from Earth and Space*, eds Ulrich, R. K., Rhodes Jr, E. J. & Däppen, W., Astronomical Society of the Pacific Conference Series, vol. 76, San Francisco, **76**, 51 – 54.

Emden, R., 1907. *Gaskugelen* (Teubner, Leibzig und Berlin).

Fossat, E., 1991. [The IRIS network for full disk helioseismology: Present status of the programme]. *Solar Phys.*, **133**, 1 – 12.

Frandsen, S., Carrier, F., Aerts, C., Stello, D., Maas, T., Burnet, M., Bruntt, H., Teixeira, T. C., de Medeiros, J. R., Bouchy, F., Kjeldsen, H., Pijpers, F. & Christensen-Dalsgaard, J., 2002. [Detection of solar-like oscillations in the G7 giant star ξ Hya].

Astron. Astrophys., **394**, L5 – L8.

Fröhlich, C., Crommelynck, D. A., Wehrli, C., Anklin, M., Dewitte, S., Fichot, A., Finsterle, W., Jiménez, A., Chevalier, A. & Roth, H., 1997. [In-flight performance of the VIRGO solar irradiance instrument on SOHO]. *Solar Phys.*, **175**, 267 – 286.

Fröhlich, C., Romero, J., Roth, H., Wehrli, C., Andersen, B. N., Appourchaux, T., Domingo, V., Telljohann, U., Berthomieu, G., Delache, P., Provost, J., Toutain, T., Crommelynck, D. A., Chevalier, A., Fichot, A., Däppen, W., Gough, D., Hoeksema, T., Jiménez, A., Gómez, M. F., Herreros, J. M., Roca Cortés, T., Jones, A. R., Pap, J. M. & Willson, R. C., 1995. [VIRGO: Experiment for helioseismology and solar irradiance monitoring]. *Solar Phys.*, **162**, 101 – 128.

Gabriel, A. H., Charra, J., Grec, G., Robillot, J.-M., Roca Cortés, T., Turck-Chièze, S., Ulrich, R., Basu, S., Baudin, F., Bertello, L., Boumier, P., Charra, M., Christensen-Dalsgaard, J., Decaudin, M., Dzitko, H., Foglizzo, T., Fossat, E., García, R. A., Herreros, J. M., Lazrek, M., Pallé, P. L., Pétrou, N., Renaud, C. & Régulo, C., 1997. [Performance and early results from the GOLF instrument flown on the SOHO mission]. *Solar Phys.*, **175**, 207 – 226.

Gabriel, A. H., Grec, G., Charra, J., Robillot, J.-M., Roca Cortés, T., Turck-Chièze, S., Bocchia, R., Boumier, P., Cantin, M., Cespédes, E., Cougrand, B., Crétolle, J., Damé, L., Decaudin, M., Delache, P., Denis, N., Duc, R., Dzitko, H., Fossat, E., Fourmond, J.-J., García, R. A., Gough, D., Grivel, C., Herreros, J. M., Lagardère, H., Moalic, J.-P., Pallé, P. L., Pétrou, N., Sanchez, M., Ulrich, R. & van der Raay, H. B., 1995. [Global oscillations at low frequency from the SOHO mission (GOLF)]. *Solar Phys.*, **162**, 61 – 99.

Gabriel, M., 1986. [Solar g modes: a method to find the depth of the convection zone]. *Seismology of the Sun and the distant Stars*, p. 177 – 186, ed. Gough, D. O., Reidel, Dordrecht.

Gabriel, M., 1993. [On the location of the excitation of solar p-modes]. *Astron. Astrophys.*, **274**, 935 – 939.

Gabriel, M., 2000. [Linear interaction between pulsations and convection, scattering and line profiles of solar p-modes]. *Astron. Astrophys.*, **353**, 399 – 408.

Gabriel, M. & Noels, A., 1976. [Stability of a 30 $M_\odot$ star towards g^+ modes of high spherical harmonic values]. *Astron. Astrophys.*, **53**, 149 – 157.

Gabriel, M. & Scuflaire, R., 1979. [Properties of non-radial stellar oscillations]. *Acta Astron.*, **29**, 135 – 149.

Gilliland, R. L., Brown, T. M., Kjeldsen, H., McCarthy, J. K., Peri, M. L., Belmonte, J. A., Vidal, I., Cram, L, E., Palmer, J., Frandsen, S., Parthasarathy, M., Petro, L., Schneider, H., Stetson, P. B. & Weiss, W. W., 1993. [A search for solar-like oscillations in the stars of M67 with CCD ensemble photometry on a network of 4 m telescopes]. *Astron. J.*, **106**, 2441 – 2476.

Goldreich, P. & Keeley, D. A., 1977. [Solar seismology. II. The stochastic excitation of the solar p-modes by turbulent convection]. *Astrophys. J.*, **212**, 243 – 251.

Gough, D. O., 1981. [A new measure of the solar rotation]. *Mon. Not. R. astr. Soc.*, **196**, 731 – 745.

Gough, D. O., 1984. [On the rotation of the Sun]. *Phil. Trans. R. Soc. London, Ser. A*, **313**, 27 – 38.

Gough, D. O., 1985. [Inverting helioseismic data]. *Solar Phys.*, **100**, 65 – 99.

Gough, D. O., 1986a. [EBK quantization of stellar waves]. *Hydrodynamic and magnetohydrodynamic problems in the Sun and stars*, ed. Osaki, Y., University of Tokyo Press, p. 117 – 143.

Gough, D. O., 1986b. [Asymptotic sound-speed inversions]. *Seismology of the Sun and the distant Stars*, p. 125 – 140, ed. Gough, D. O., Reidel, Dordrecht.

Gough, D. O., 1987. [Seismological measurement of stellar ages]. *Nature*, **326**, 257 – 259.

Gough, D. O., 1990. [Comments on helioseismic inference]. *Progress of seismology of the sun and stars*, *Lecture Notes in Physics*, vol. **367**, 283 – 318, eds Osaki, Y. & Shibahashi, H., Springer, Berlin.

Gough, D. O., 1993. [Course 7. Linear adiabatic stellar pulsation]. In *Astrophysical fluid dynamics, Les Houches Session XLVII*, eds Zahn, J.-P. & Zinn-Justin, J., Elsevier, Amsterdam, 399 – 560.

Gough, D. O. & Thompson, M. J., 1990. [The effect of rotation and a buried magnetic field on stellar oscillations]. *Mon. Not. R. astr. Soc.*, **242**, 25 – 55.

Gough, D. O. & Thompson, M. J., 1991. [The inversion problem]. In *Solar interior and atmosphere*, eds Cox, A. N., Livingston, W. C. & Matthews, M., p. 519 – 561, Space Science Series, University of Arizona Press.

Gough, D. O. & Toomre, J., 1991. [Seismic observations of the solar interior]. *Ann. Rev. Astron. Astrophys.*, **29**, 627 – 685.

Gough, D. O. & Vorontsov, S. V., 1995. [Seismology of the solar envelope: measuring the acoustic phase shift generated in the outer layers]. *Mon. Not. R. astr. Soc.*, **273**, 573 – 582.

Gough, D. O., Leibacher, J. W., Scherrer, P. H. & Toomre, J., 1996. [Perspectives in helioseismology]. *Science*, **272**, 1281 – 1283.

Gough, D. O., Spiegel, E. A. & Toomre, J., 1975. [Highly stretched meshes as functionals of solutions]. *Lecture Notes in Physics*, **35**, 191 – 196, ed. Richtmyer, R. D., Springer, Heidelberg.

Grec, G., Fossat, E. & Pomerantz, M., 1980. [Solar oscillations: full disk observations from the geographic South Pole]. *Nature*, **288**, 541 – 544.

Grec, G., Fossat, E. & Pomerantz, M., 1983. [Full-disk observations of solar oscillations from the geographic South Pole: latest results]. *Solar Phys.*, **82**, 55 – 66.

Guenther, D. B., 1991. [The p-mode oscillation spectra of an evolving $1M_\odot$ sun-like star]. *Astrophys. J.*, **375**, 352 – 365.

Guenther, D. B. & Demarque, P., 2000. [α Centauri AB]. *Astrophys. J.*, **531**, 503 – 520.

Guenther, D. B., Demarque, P., Buzasi, D., Catanzarite, J., Laher, R., Conrow, T. & Kreidl, T., 2000. [Evolutionary model and oscillation frequencies for α Ursae Majoris: a comparison with observations]. *Astrophys. J.*, **530**, L45 – L48.

Handler, G., Arentoft, T., Shobbrook, R. R., Wood, M. A., Crause, L. A., Crake, P., Podmore, F., Habanyama, A., Oswalt, T., Birch, P. V., Lowe, G., Sterken, C., Meintjes, P., Brink, J., Claver, C. F., Medupe, R., Guzik, J. A., Beach, T. E., Martinez, P., Leibowitz, E. M., Ibbetson, P. A., Smith, T., Ashoka, B. N., Raj, N. E., Kurtz, D. W., Balona, L. A., O'Donoghue, D., Costa, J. E. S. & Breger, M., 2000. [Delta Scuti Network observations of XX Pyx: detection of 22 pulsation modes and of short-term amplitude and frequency variations]. *Mon. Not. R. astr. Soc.*, **318**, 511 – 525.

Hansen, C. J., Cox, J. P. & van Horn, H. M., 1977. [The effects of differential rotation on the splitting of nonradial modes of stellar oscillation]. *Astrophys. J.*, **217**, 151 – 159.

Harvey, J. W., Hill, F., Hubbard, R. P., Kennedy, J. R., Leibacher, J. W., Pintar, J. A., Gilman, P. A., Noyes, R. W., Title, A. M., Toomre, J., Ulrich, R. K., Bhatnagar, A., Kennewell, J. A., Marquette, W., Partrón, J., Saá, O. & Yasukawa, E., 1996. [The Global Oscillation Network Group (GONG) project]. *Science*, **272**, 1284 – 1286.

Harvey, J. W., Kennedy, J. R. & Leibacher, J. W., 1987. [GONG: to see inside our Sun]. *Sky and Telescope*, **74**, 470 – 476.

Henyey, L. G., Forbes, J. E. & Gould, N. L., 1964. [A new method of automatic computation of stellar evolution]. *Astrophys. J.*, **139**, 306 – 317.

Hernández, M. M., Pérez Hernández, F., Michel, E., Belmonte, J. A., Goupil, M. J. & Lebreton, Y., 1998. [Seismology of δ Scuti stars in the Praesepe cluster. II. Identification of radial modes and their associated stellar parameters]. *Astron. Astrophys.*, **338**, 511 – 520.

Hill, F., 1990. [Networks for helioseismic observation]. *Proc. IAU Colloquium No 121, Inside the Sun*, p. 265 – 278, eds Berthomieu G. & Cribier M., Kluwer, Dordrecht.

Hill, F. & Newkirk, G., 1985. [On the expected performance of a solar oscillation network]. *Solar Phys.*, **95**, 201 – 219.

Hill, F., Gough, D. O., Merryfield, W. J. & Toomre, J., 1991. [Simulation of effects of atmospheric seeing on the observation of high-degree solar oscillations]. *Astrophys. J.*, **369**, 237 – 246.

Houdek, G., 2000. [Convective effects on p-mode stability in Delta Scuti stars]. In *Delta Scuti and related stars*, eds M. Breger & M. H. Montgomery, ASP Conference Series, **210**, San Francisco, p. 454 – 463.

Houdek, G., Balmforth, N. J., Christensen-Dalsgaard, J. & Gough, D. O., 1999. [Amplitudes of stochastically excited oscillations in main-sequence stars]. *Astron. Astrophys.*, **351**, 582 – 596.

Innis, J. L., Isaak, G. R., Brazier, R. I., Belmonte, J. A., Palle, P. L., Roca Cortes, T. & Jones, A. R., 1988. [High precision velocity observations of Arcturus using the 7699 Å line of potassium]. *Seismology of the Sun & Sun-like Stars*, p. 569 – 573, eds Domingo, V. & Rolfe, E. J., ESA SP-286, ESA Publications Division, Noordwijk, The Netherlands.

Jackson, J. D., 1975. *Classical Electrodynamics*, 2. ed., Wiley, New York.

Jeffery, C. S. & Pollacco, D., 2000. [Radial velocities of pulsating subdwarf B stars: KPD 2109+4401 and PB 8783]. *Mon. Not. R. astr. Soc.*, **318**, 974 – 982.

Jeffrey, W., 1988. [Inversion of helioseismic data]. *Astrophys. J.*, **327**, 987 – 992.

Kawaler, S. D., 1995. [Probing the extraordinary ends of ordinary stars: white dwarf seismology with the Whole Earth Telescope]. In *Proc. IAU Colloq. 155: Astrophysical Applications of Stellar Pulsation*, eds Stobie, R. S. & Whitelock, P. A., ASP Conf. Ser., **83**, 81 – 90.

Keeley, D. A., 1977. [Linear stability analysis of stellar models by the inverse iteration method]. *Astrophys. J.*, **211**, 926 – 933.

Kepler, S. O., Winget, D. E., Nather, R. E., Bradley, P. A., Grauer, A. D., Fontaine, G., Bergeron, P., Vauclair, G., Claver, C. F., Marar, T. M. K., Seetha, S., Ashoka, B. N., Mazeh, T., Leibowitz, E., Dolez, N., Chevreton, M., Barstow, M. A., Clemens, J. C., Kleinman, S. J., Sansom, A. E., Tweedy, R. W., Kanaan, A., Hine, B. P., Provencal, J. L., Wesemael, F., Wood, M. A., Brassard, P., Solheim, J. E. & Emanuelsen, P.-I., 1991. [A detection of the evolutionary time scale of the DA white dwarf G117–B15A with the Whole Earth Telescope]. *Astrophys. J.*, **378**, L45 – L48.

Kilkenny, D., Koen, C., O'Donoghue, D. & Stobie, R. S., 1997. [A new class of rapidly pulsating stars – I. EC 14026 – 2647, the class prototype]. *Mon. Not. R. astr. Soc.*, **285**, 640 – 644.

Kilkenny, D., Koen, C., O'Donoghue, D., van Wyk, F., Larson, K. A., Shobbrook, R., Sullivan, D. J., Burleigh, M., Dobbie, P. D. & Kawaler, S. D., 1999. [The EC 14026 stars – X. A multi-site campaign on the sdBV star PG 1605+072]. *Mon. Not. R. astr. Soc.*, **303**, 525 – 534.

Kippenhahn, R. & Weigert, A., 1990. *Stellar structure and evolution*, Springer-Verlag, Berlin.

Kjeldsen, H. & Bedding, T. R., 1995. [Amplitudes of stellar oscillations: the implications for asteroseismology]. *Astron. Astrophys.*, **293**, 87 – 106.

Kjeldsen, H., Bedding, T. R., Frandsen, S. & Dall, T. H., 1999. [A search for solar-like oscillations and granulation in α Cen A]. *Mon. Not. R. astr. Soc.*, **303**, 579 – 587.

Kjeldsen, H., Bedding, T. R., Viskum, M. & Frandsen, S., 1995. [Solarlike oscillations in η Boo]. *Astron. J.*, **109**, 1313 – 1319.

Knölker, M. & Stix, M., 1983. [A convenient method to obtain stellar eigenfrequencies]. *Solar Phys.*, **82**, 331 – 341.

Korzennik, S. G., Cacciani, A., Rhodes, E. J., Tomczyk, S. & Ulrich, R. K., 1988. [Inversion of the solar rotation rate versus depth and latitude]. *Seismology of the Sun & Sun-like Stars*, p. 117 – 124, eds Domingo, V. & Rolfe, E. J., ESA SP-286.

Kosovichev, A. G., Christensen-Dalsgaard, J., Däppen, W., Dziembowski, W. A., Gough, D. O. & Thompson, M. J., 1992. [Sources of uncertainty in direct seismological measurements of the solar helium abundance]. *Mon. Not. R. astr. Soc.*, **259**, 536 – 558.

Kumar, P. & Basu, S., 1999. [Line asymmetry of solar p-modes: Properties of acoustic sources]. *Astrophys. J.*, **519**, 396 – 399.

Kumar, P., Franklin, J. & Goldreich, P., 1988. [Distribution function for the time-averaged energies of stochastically excited solar p-modes]. *Astrophys. J.*, **328**, 879 – 887.

Kumar, P., Franklin, J. & Goldreich, P., 1988. [Distribution function for the time-averaged energies of stochastically excited solar p-modes]. *Astrophys. J.*, **328**, 879 – 887.

Lamb, H., 1909. [On the theory of waves propagated vertically in the atmosphere]. *Proc. London Math. Soc.*, **7**, 122 – 141.

Lamb, H., 1932. *Hydrodynamics*, 6th ed., Cambridge University Press.

Landau, L. D. & Lifshitz, E. M., 1959. *Fluid Mechanics*, Pergamon, Oxford.

Larsen, R. M., 1997. [Iterative algorithms for two-dimensional helioseismic inversion]. In B.H. Jacobsen (ed.), Proc. Interdisciplinary Inversion Workshop 5, Aarhus University, p. 123 – 137.

Larsen, R. M. & Hansen, P. C., 1997. [Efficient implementation of the SOLA mollifier method]. *Astron. Astrophys. Suppl.*, **121**, 587 – 598.

Larsen, R. M., Christensen-Dalsgaard, J., Kosovichev, A. G. & Schou, J., 1998. [Improved SOLA inversions of MDI data]. In *Structure and dynamics of the interior of the Sun and Sun-like stars; Proc. SOHO 6/GONG 98 Workshop*, eds S.G. Korzennik & A. Wilson, ESA SP-418, ESA Publications Division, Noordwijk, The Netherlands, p. 813 – 818.

Lazrek, M., Baudin, F., Bertello, L., Boumier, P., Charra, J., Fierry-Fraillon, D., Fossat, E., Gabriel, A. H., García, R. A., Gelly, B., Gouiffes, C., Grec, G., Pallé, P. L., Pérez Hernández, F., Régulo, C., Renaud, C., Robillot, J.-M., Roca-Cortés, T., Turck-Chièze,

S. & Ulrich, R. K., 1997. [First results on p modes from GOLF experiment]. *Solar Phys.*, **175**, 227 – 246.

Ledoux, P., 1949. [Contributions à l'Étude de la Structure Interne des Étoiles et de leur Stabilité]. *Mem. Soc. R. Sci. Liège, 4th ser.*, **9**, 3 – 294. ([Chapitre V: Stabilité dynamique et pulsations d'étoiles gazeuses animées d'un mouvement de rotation uniforme]. p. 263 – 294).

Ledoux, P. & Walraven, T., 1958. [Variable stars]. *Handbuch der Physik*, vol. 51, chapter IV p. 353 – 604 (Springer-Verlag).

Lee, U., 1985. [Stability of the Delta Scuti stars against nonradial oscillations with low degree l]. *Publ. Astron. Soc. Japan*, **37**, 279 – 291.

Leibacher, J. W., Noyes, R. W., Toomre, J. & Ulrich, R. K., 1985. [Helioseismology]. *Scientific American*, **253**, (September) p. 34 – 43 (US p. 48 – 57).

Libbrecht, K. G., 1988. [Solar and stellar seismology]. *Space Sci. Rev.*, **47**, 275 – 301.

Libbrecht, K. G., 1989. [Solar p-mode frequency splittings]. *Astrophys. J.*, **336**, 1092 – 1097.

Libbrecht, K. G. & Woodard, M. F., 1990. [Solar-cycle effects on solar oscillation frequencies]. *Nature*, **345**, 779 – 782.

Libbrecht, K. G., Popp, B. D., Kaufman, J. M. & Penn, M. J., 1986. [The excitation and damping of solar oscillations]. *Nature*, **323**, 235 – 238.

Libbrecht, K. G., Woodard, M. F. & Kaufman, J. M., 1990. [Frequencies of solar oscillation]. *Astrophys. J. Suppl.*, **74**, 1129 – 1149.

Loumos, G. L. & Deeming, T. J., 1978. [Spurious results from Fourier analysis of data with closely spaced frequencies]. *Astrophys. Space Sci.*,

Lynden-Bell, D. & Ostriker, j. P., 1967. [On the stability of differentially rotating bodies]. *Mon. Not. R. astr. Soc.*, **136**, 293 – 310.

Martić, M., Schmitt, J., Lebrun, J.-C., Barban, C., Connes, P., Bouchy, F., Michel, E., Baglin, A., Appourchaux, T. & Bertaux, J.-L., 1999. [Evidence for global pressure oscillations on Procyon]. *Astron. Astrophys.*, **351**, 993 – 1002.

Mattei, J. A., Foster, G., Hurwitz, L. A., Malatesta, K. H., Willson, L. A. & Mennissier, M.-O., 1997. [Classification of red variables]. In *Proc. ESA Symposium: Hipparcos – Venice '97*, eds B. Battrick, M. A. C. Perryman, P. L. Bernacca, K. S. O'Flaherty, ESA SP-402, p. 269 – 274.

McGraw, J. T. & Robinson, E. L., 1976. [High-speed photometry of luminosity-variable DA dwarfs: R808, GD99, and G117-B15a]. *Astrophys. J.*, **205**, L155 – L158.

Merline, W. J., 1998. [Evidence for solar-like oscillations in Arcturus]. In *A Half-Century of Stellar Pulsation Interpretation: A Tribute to Arthur N. Cox*, eds Bradley, P. A. & Guzik, J. A., ASP Conf. Ser., **135**, 208 – 212.

Metcalfe, T. S., Winget, D. E. & Charbonneau, P., 2001. [Preliminary constraints on $^{12}C(\alpha,\gamma)^16O$ from white dwarf seismology]. *Astrophys. J.*, **557**, 1021 – 1027.

Michel, E. & Baglin, A., 1991. [STEPHI – seismology of δ Scuti stars from multi-site photometry campaigns]. *Adv. Space Res.*, **vol. 11, No. 4**, 167 – 170.

Michel, E., Belmonte, J. A., Alvarez, M., Jiang, S. Y., Chevreton, M., Auvergne, M., Goupil, M. J., Baglin, A., Mangeney, A., Roca Cortés, T., Liu, Y. Y., Fu, J. N., Dolez, N., 1992. [Multi-periodicity of the δ Scuti star GX Pegasi. Second photometry campaign of the STEPHI network]. *Astron. Astrophys.*, **255**, 139 – 148.

Miglio, A., Christensen-Dalsgaard, J., Di Mauro, M. P., Monteiro, M. J. P. F. G. & Thompson, M. J., 2003. [Seismic analysis of the helium ionization zones in low- and moderate-

mass stars]. In *Asteroseismology across the HR diagram*, eds M. J. Thompson, M. S. Cunha & M. J. P. F. G. Monteiro, Kluwer Academic Publishers, Dordrecht, in the press.

Mihalas, D. & Mihalas, B. W., 1984. *Foundations of Radiation Hydrodynamics*, Oxford University Press.

Monteiro, M. J. P. F. G. & Thompson, M. J., 1998. [On the seismic signature of the HeII ionization zone in stellar envelopes]. In *Proc. IAU Symp. 185: New eyes to see inside the Sun and stars*, eds Deubner, F.-L., Christensen-Dalsgaard, J. & Kurtz, D. W., Kluwer, Dordrecht, p. 317 – 318.

Monteiro, M. J. P. F. G., Christensen-Dalsgaard, J. & Thompson, M. J., 1994. [Seismic study of overshoot at the base of the solar convective envelope]. *Astron. Astrophys.*, **283**, 247 – 262.

Morel, P., Provost, J., Lebreton, Y., Thévenin, F. & Berthomieu, G., 2000. [Calibrations of α Cen A & B]. *Astron. Astrophys.*, **363**, 675 – 691.

Moskalik, P. & Dziembowski, W. A., 1992. [New opacities and the origin of the β Cephei pulsation]. *Astron. Astrophys.*, **256**, L5 – L8.

Murawski, K., Duvall, T. L., & Kosovichev, A. G., 1998. [Damping and frequency shift of the solar f-mode due to the interaction with turbulent convection]. In *Structure and dynamics of the interior of the Sun and Sun-like stars; Proc. SOHO 6/GONG 98 Workshop*, eds S.G. Korzennik & A. Wilson, ESA SP-418, ESA Publications Division, Noordwijk, The Netherlands, p. 825 – 828.

Mędrek, M., Murawski, K. & Roberts, B., 1999. [Damping and frequency reduction of the f-mode due to turbulent motion in the solar convection zone]. *Astron. Astrophys.*, **349**, 312 – 316.

Nigam, R. & Kosovichev, A. G., 1998. [Measuring the Sun's eigenfrequencies from velocity and intensity helioseismic spectra: asymmetrical line profile-fitting formula]. *Astrophys. J.*, **505**, L51 – L54.

Nigam, R. & Kosovichev, A. G., 1999. [Source of solar acoustic modes]. *Astrophys. J.*, **514**, L53 – L56.

Nordlund, Å. & Stein, R. F., 1989. [Simulating magnetoconvection]. *Solar and stellar granulation,* Proc. NATO ARW, Capri, June 21 – 25, p. 453 – 470, eds Rutten, R. J. & Severino, G., Kluwer, Dordrecht.

O'Brien, M. S. & Kawaler, S. D., 2000. [The predicted signature of neutrino emission in observations of pulsating pre-white dwarfs]. *Astrophys. J.*, **539**, 372 – 378.

O'Brien, M. S., Vauclair, G., Kawaler, S. D., Watson, T. K., Winget, D. E., Nather, R. E., Montgomery, M., Nitta, A., Kleinman, S. J., Sullivan, D. J., Jiang, X. J., Marar, T. M. K., Seetha, S., Ashoka, B. N., Bhattacharya, J., Leibowitz, E. M., Hemar, S., Ibbetson, P., Warner, B., van Zyl, L., Moskalik, P., Zola, S., Pajdosz, G., Krzesinski, J., Dolez, N., Chevreton, M., Solheim, J.-E., Thomassen, T., Kepler, S. O., Giovannini, O., Provencal, J. L., Wood, M. A. & Clemens, J. C., 1998. [Asteroseismology of a Star Cooled by Neutrino Emission: The Pulsating Pre–White Dwarf PG 0122+200]. *Astrophys. J.*, **495**, 458 – 467.

O'Donoghue, D., Koen, C., Kilkenny, D., Stobie, R. S. & Lynas-Gray, A. E., 1999. [The EC14026 stars: sdB pulsators]. In *Proceedings of the 11th European White Dwarf Workshop*, eds J.-E. Solheim & E. Meištas, p. 149 – 157, Astronomical Society of the Pacific Conference Series, Vol. 169, San Francisco, 1999.

O'Toole, S. J., Bedding, T. R., Kjeldsen, H., Teixeira, T. C., Roberts, G., van Wyk, F.,

Kilkenny, D., D'Cruz, N. & Baldry, I. K., 2000. [Time series spectroscopy of pulsating subdwarf B stars: PG 1605+072]. *Astrophys. J.*, **537**, L53 – L56.

Osaki, Y., 1975. [Nonradial oscillations of a 10 solar mass star in the main-sequence stage]. *Publ. Astron. Soc. Japan*, **27**, 237 – 258.

Osaki, Y. & Hansen, C. J., 1973. [Nonradial oscillations of cooling white dwarfs]. *Astrophys. J.*, **185**, 277 – 292.

Parker, R. L., 1977. [Understanding inverse theory]. *Ann. Rev. Earth Planet. Sci.*, **5**, 35 – 64.

Pérez Hernández, F. & Christensen-Dalsgaard, J., 1993. [The phase function for solar-like stars]. In *Proc. GONG 1992: Seismic investigation of the Sun and stars*, ed. Brown, T. M., Astronomical Society of the Pacific Conference Series, San Francisco, **42**, 343 – 346.

Pérez Hernández, F. & Christensen-Dalsgaard, J., 1994a. [The phase function for stellar acoustic oscillations. II. Effects of filtering]. *Mon. Not. R. astr. Soc.*, **267**, 111 – 124.

Pérez Hernández, F. & Christensen-Dalsgaard, J., 1994b. [The phase function for stellar acoustic oscillations. III. The solar case]. *Mon. Not. R. astr. Soc.*, **269**, 475 – 492.

Pesnell, W. D., 1990. [Nonradial, nonadiabatic stellar pulsations]. *Astrophys. J.*, **363**, 227 – 233.

Petersen, J. O., 1973. [Masses of double mode Cepheid variables determined by analysis of period ratios]. *Astron. Astrophys.*, **27**, 89 – 93.

Petersen, J. O., 1974. [Effects upon period ratios of Cepheid models from artificial changes in opacity and mean molecular weight]. *Astron. Astrophys.*, **34**, 309 – 311.

Petersen, J. O., 1975. [On Epstein's weighting function and pulsation constants of Cepheid models]. *Mém. Soc. R. Sci. Liège, 6th ser.*, **8**, 299 – 305.

Petersen, J. O., 1978. [Masses of double mode Cepheid variables based on observed periods]. *Astron. Astrophys.*, **62**, 205 – 215.

Pijpers, F. P., 1997. [Solar rotation inversions and the relationship between a-coefficients and mode splittings]. *Astron. Astrophys.*, **326**, 1235 – 1240.

Pijpers, F. P. & Thompson, M. J., 1992. [Faster formulations of the optimally localized averages method for helioseismic inversion]. *Astron. Astrophys.*, **262**, L33 – L36.

Pijpers, F. P. & Thompson, M. J., 1994. [The SOLA method for helioseismic inversion]. *Astron. Astrophys.*, **281**, 231 – 240.

Pijpers, F. P. & Thompson, M. J., 1996. [A modified $\mathbb{R}^1 \otimes \mathbb{R}^1$ method for helioseismic inversions]. *Mon. Not. R. astr. Soc.*, **279**, 498 – 510.

Press, W. H., Flannery, B. P., Teukolsky, S. A. & Vetterling, W. T., 1986. *Numerical Recipes*, Cambridge University Press.

Provost, J. & Berthomieu, G., 1986. [Asymptotic properties of low degree solar gravity modes]. *Astron. Astrophys.*, **165**, 218 – 226.

Rabello-Soares, M. C., Basu, S. & Christensen-Dalsgaard, J., 1999a. [On the choice of parameters in solar structure inversion]. *Mon. Not. R. astr. Soc.*, **309**, 35 – 47.

Rabello-Soares, M. C., Christensen-Dalsgaard, J., Rosenthal, C. S. & Thompson, M. J., 1999b. [Effects of line asymmetries on the determination of solar internal structure]. *Astron. Astrophys.*, **350**, 672 – 679.

Rast, M. P. & Bogdan, T. J., 1998. [On the asymmetry of solar acoustic line profiles]. *Astrophys. J.*, **496**, 527 – 537.

Reitz, J. R., Milford, F. J., & Christy, R. W. 1979. *Foundations of Electromagnetic Theory*, 3. ed., Addison-Wesley, Reading, Massachusetts.

Rhodes, E. J., Kosovichev, A. G., Schou, J., Scherrer, P. H. & Reiter, J., 1997. [Measurements of frequencies of solar oscillations from the MDI medium-l program]. *Solar Phys.*, **175**, 287 – 310.

Rhodes, Jr, E. J., Reiter, J., Kosovichev, A. G., Schou, J. & Scherrer, P. H., 1998. [Initial SOI/MDI high-degree frequencies and frequency splittings]. In *Structure and dynamics of the interior of the Sun and Sun-like stars; Proc. SOHO 6/GONG 98 Workshop*, eds S.G. Korzennik & A. Wilson, ESA SP-418, ESA Publications Division, Noordwijk, The Netherlands, p. 73 – 82.

Rhodes, Jr, E. J., Reiter, J., Kosovichev, A. G., Schou, J. & Scherrer, P. H., 1998. [Initial SOI/MDI high-degree frequencies and frequency splittings]. In *Structure and dynamics of the interior of the Sun and Sun-like stars; Proc. SOHO 6/GONG 98 Workshop*, eds S.G. Korzennik & A. Wilson, ESA SP-418, ESA Publications Division, Noordwijk, The Netherlands, p. 73 – 82.

Ritzwoller, M. H. & Lavely, E. M., 1991. [A unified approach to the helioseismic forward and inverse problems of differential rotation]. *Astrophys. J.*, **369**, 557 – 566.

Robe, H., 1968. [Les oscillations non radiales des polytropes]. *Ann. d'Astrophys.*, **31**, 475 – 482.

Rosenthal, C. S., 1998. [Peaks and throughs in helioseismology: the power spectrum of solar oscillations]. *Astrophys. J.*, **508**, 864 – 875.

Roxburgh, I. W. & Vorontsov, S. V., 1995. [An asymptotic description of solar acoustic oscillations with an elementary excitation source]. *Mon. Not. R. astr. Soc.*, **272**, 850 – 858.

Schatzman, E. & Souffrin, P., 1967. [Waves in the solar atmosphere]. *Ann. Rev. Astron. Astrophys.*, **5**, 67 – 84.

Scherrer, P. H., Bogart, R. S., Bush, R. I., Hoeksema, J. T., Kosovichev, A. G., Schou, J., Rosenberg, W., Springer, L., Tarbell, T. D., Title, A., Wolfson, C. J., Zayer, I., and the MDI engineering team, 1995. [The Solar Oscillation Investigation – Michelson Doppler Imager]. *Solar Phys.*, **162**, 129 – 188.

Scherrer, P. H., Wilcox, J. M., Christensen-Dalsgaard, J. & Gough, D. O., 1983. [Detection of solar five-minute oscillations of low degree]. *Solar Phys.*, **82**, 75 – 87.

Schiff, L. I., 1949. *Quantum Mechanics*, McGraw Hill, New York.

Schou, J., 1991. [On the 2-dimensional rotational inversion problem]. In *Challenges to theories of the structure of moderate-mass stars*, *Lecture Notes in Physics*, vol. **388**, p. 93 – 100, eds Gough, D. O. & Toomre, J., Springer, Heidelberg.

Schou, J., 1992. *On the analysis of helioseismic data*, PhD Dissertation, Aarhus University.

Schou, J., 1998. [How low can we get: the quest for ever lower frequencies]. In *Structure and dynamics of the interior of the Sun and Sun-like stars; Proc. SOHO 6/GONG 98 Workshop*, eds S.G. Korzennik & A. Wilson, ESA SP-418, ESA Publications Division, Noordwijk, The Netherlands, p. 341 – 344.

Schou, J., 1999. [Migration of zonal flows detected using Michelson Doppler Imager f-mode frequency splittings]. *Astrophys. J.*, **523**, L181 – L184.

Schou, J. & Buzasi, D. L., 2001. [Observations of p-modes in α Cen]. In *Helio- and Asteroseismology at the Dawn of the Millennium: Proc. SOHO 10 / GONG 2000 Workshop*, ESA SP-464, ESA Publications Division, Noordwijk, The Netherlands, 391 – 394.

Schou, J., Antia, H. M., Basu, S., Bogart, R. S., Bush, R. I., Chitre, S. M., Christensen-Dalsgaard, J., Di Mauro, M. P., Dziembowski, W. A., Eff-Darwich, A., Gough, D.

O., Haber, D. A., Hoeksema, J. T., Howe, R., Korzennik, S. G., Kosovichev, A. G., Larsen, R. M., Pijpers, F. P., Scherrer, P. H., Sekii, T., Tarbell, T. D., Title, A. M., Thompson, M. J., Toomre, J., 1998. [Helioseismic studies of differential rotation in the solar envelope by the Solar Oscillations Investigation using the Michelson Doppler Imager]. *Astrophys. J.*, **505**, 390 – 417.

Schou, J., Christensen-Dalsgaard, J. & Thompson, M. J., 1992. [The resolving power of current helioseismic inversions for the Sun's internal rotation]. *Astrophys. J.*, **385**, L59 – L62.

Schou, J., Christensen-Dalsgaard, J. & Thompson, M. J., 1994. [On comparing helioseismic two-dimensional inversion methods]. *Astrophys. J.*, **433**, 389 – 416.

Schou, J., Howe, R., Basu, S., Christensen-Dalsgaard, J., Corbard, T., Hill, F., Larsen, R. M., Rabello-Soares, M. C. & Thompson, M. J., 2002. [A comparison of solar p-mode parameters from the Michelson Doppler Imager and the Global Oscillation Network Group: splitting coefficients and rotation inversions]. *Astrophys. J.*, **567**, 1234 – 1249.

Scuflaire, R., 1974. [The non radial oscillations of condensed polytropes]. *Astron. Astrophys.*, **36**, 107 – 111.

Sekii, T., 1991. [Two-dimensional inversion for solar internal rotation]. *Publ. Astron. Soc. Japan*, **43**, 381 – 411.

Sekii, T., 1993. [A new strategy for 2D inversion for solar rotation]. *Mon. Not. R. astr. Soc.*, **264**, 1018 – 1024.

Shapley, H., 1914. [On the nature and cause of Cepheid variation]. *Astrophys. J.*, **40**, 448 – 465.

Shibahashi H., 1988. [Inverse problem: acoustical potential vs acoustic length]. *Proc. IAU Symposium No 123, Advances in helio- and asteroseismology*, p. 133 – 136, eds Christensen-Dalsgaard, J. & Frandsen, S., Reidel, Dordrecht.

Shibahashi, H. & Osaki, Y., 1981. [Theoretical eigenfrequencies of solar oscillations of low harmonic degree l in five-minute range]. *Publ. Astron. Soc. Japan*, **33**, 713 – 719.

Shibahashi, H. & Sekii, T., 1988. [Sound velocity distribution in the Sun inferred from asymptotic inversion of p-mode spectra]. *Seismology of the Sun & Sun-like Stars*, p. 471 – 480, eds Domingo, V. & Rolfe, E. J., ESA SP-286.

Smith, P. H., McMillan, R. S. & Merline, W. J., 1987. [Evidence for periodic radial velocity variations in Arcturus]. *Astrophys. J.*, **317**, L79 – L84.

Spiegel, E. A. & Zahn, J.-P., 1992. [The solar tachocline]. *Astron. Astrophys.*, **265**, 106 – 114.

Stein, R. F. & Leibacher, J., 1974. [Waves in the solar atmosphere]. *Ann. Rev. Astron. Astrophys.*, **12**, 407 – 435.

Stein, R. F. & Nordlund, Å., 2001. [Solar oscillations and convection: II. Excitation of radial oscillations]. *Astrophys. J.*, **546**, 585 – 603.

Stein, R. F., Nordlund, Å. & Kuhn, J. R., 1989. [Convection and waves]. *Solar and stellar granulation, Proc. NATO ARW, Capri, June 21 – 25*, p. 381 – 399, eds Rutten, R. J. & Severino, G., Kluwer, Dordrecht, Holland.

Strang, G. & Fix, G. J., 1973. *An analysis of the finite element method*, Prentice-Hall.

Sørensen, J. M., 1988. [Measurements of oscillation parameters from synthetic time series]. *Seismology of the Sun & Sun-like Stars*, p. 41 – 45, eds Domingo, V. & Rolfe, E. J., ESA SP-286.

Tarantola, A., 1987. *Inverse Problem Theory*, Elsevier, Amsterdam.

Tassoul, M., 1980. [Asymptotic approximations for stellar nonradial pulsations]. *Astrophys. J. Suppl.*, **43**, 469 – 490.

Teixeira, T. C., Christensen-Dalsgaard, J., Carrier, F., Aerts, C., Frandsen, S., Stello, D., Maas, T., Burnet, M., Bruntt, H., de Medeiros, J. R., Bouchy, F., Kjeldsen, H. & Pijpers, F., 2003. [Giant vibrations in the dip]. In *Asteroseismology across the HR diagram*, eds M. J. Thompson, M. S. Cunha & M. J. P. F. G. Monteiro, Kluwer Academic Publishers, Dordrecht, *Astrophys. Space Sci.*, 233 – 236.

Thompson, M. J., 1988. [Evidence for a thin perturbative layer near the base of the solar convection zone]. *Seismology of the Sun & Sun-like Stars*, p. 321 – 324, eds Domingo, V. & Rolfe, E. J., ESA SP-286.

Thompson, M. J., 1990. [A new inversion of solar rotational splitting data]. *Solar Phys.*, **125**, 1 – 12.

Thompson, M. J., 1993. [Seismic investigation of the Sun's internal structure and rotation]. In *Proc. GONG 1992: Seismic investigation of the Sun and stars*, ed. Brown, T. M., Astronomical Society of the Pacific Conference Series, San Francisco, **42**, 141 – 154.

Tomczyk, S., Schou, J. & Thompson, M. J., 1996. [Low-degree frequency splitting measurements and the rotation of the solar core]. *Proc. Conf. on "Windows on the Sun's interior", Bombay, Oct. 1995; Bull. Astron. Soc. India*, **24**, 245 – 250.

Tomczyk, S., Streander, K., Card, G., Elmore, D., Hull, H. & Cacciani, A., 1995. [An instrument to observe low-degree solar oscillations]. *Solar Phys.*, **159**, 1 – 21.

Toutain, T. & Fröhlich, C., 1992. [Characteristics of solar p-modes: Results from the IPHIR experiment]. *Astron. Astrophys.*, **257**, 287 – 297.

Ulrich, R. K., 1986. [Determination of stellar ages from asteroseismology]. *Astrophys. J.*, **306**, L37 - L40.

Ulrich, R. K., 1988. [Can stellar mass be measured by asteroseismology?]. *Proc. IAU Symposium No 123, Advances in helio- and asteroseismology*, p. 299 – 302, eds Christensen-Dalsgaard, J. & Frandsen, S., Reidel, Dordrecht.

Unno, W. & Spiegel, E. A., 1966. [The Eddington approximation in the radiative heat equation]. *Publ. Astron. Soc. Japan*, **18**, 85 – 95.

Unno, W., Osaki, Y., Ando, H. & Shibahashi, H., 1989. *Nonradial Oscillations of Stars (2nd edition)* (University of Tokyo Press).

Vandakurov, Yu. V., 1967. [On the frequency distribution of stellar oscillations]. *Astron. Zh.*, **44**, 786 – 797 (English translation: *Soviet Astronomy AJ*, **11**, 630 – 638).

Vorontsov, S. V., 1988. [A search of the effects of magnetic field in the solar five-minute oscillations]. *Proc. IAU Symposium No 123, Advances in helio- and asteroseismology*, p. 151 – 154, eds Christensen-Dalsgaard, J. & Frandsen, S., Reidel, Dordrecht.

Vorontsov, S. V. & Shibahashi, H., 1990. [Second-order asymptotic inversions of the sound speed inside the Sun]. *Progress of seismology of the sun and stars*, *Lecture Notes in Physics*, vol. **367**, 326 – 328, eds Osaki, Y. & Shibahashi, H., Springer, Berlin.

Vorontsov, S. V., Baturin, V. A. & Pamyatnykh, A. A., 1992. [Seismology of the solar envelope: towards the calibration of the equation of state]. *Mon. Not. R. astr. Soc.*, **257**, 32 – 46.

Whittaker, E. T. & Watson, G. N., 1927. *A course of modern analysis*, Cambridge University Press.

Winget, D. E., 1988. [Seismological investigations of compact stars]. *Proc. IAU Symposium No 123, Advances in helio- and asteroseismology*, p. 305 – 324, eds Christensen-Dalsgaard, J. & Frandsen, S., Reidel, Dordrecht.

Winget, D. E., 1993. [The Whole Earth Telescope]. In *Proc. GONG 1992: Seismic investigation of the Sun and stars*, ed. Brown, T. M., Astronomical Society of the Pacific Conference Series, San Francisco, **42**, 331 – 342.

Winget, D. E., Kepler, S. O., Kanaan, A., Montgomery, M. H. & Giovannini, O., 1997. [An empirical test of the theory of crystallization in stellar interiors]. *Astrophys. J.*, **487**, L191 – L194.

Winget, D. E., Kepler, S. O., Robinson, E. L., Nather, R. E., O'Donoghue, D., 1985. [A measurement of secular evolution in the pre-white dwarf star PG 1159-035]. *Astrophys. J.*, **292**, 606 – 613.

Winget, D. E., Nather, R. E., Clemens, J. C., Provencal, J. L., Kleinman, S. J., Bradley, P. A., Claver, C. F., Dixson, J. S., Montgomery, M. H., Hansen, C. J., Hine, B. P., Birch, P., Candy, M., Marar, T. M. K., Seetha, S., Ashoka, B. N., Leibowitz, E. M., O'Donoghue, D., Warner, B., Buckley, D. A. H., Tripe, P., Vauclair, G., Dolez, N., Chevreton, M., Serre, T., Garrido, R., Kepler, S. O., Kanaan, A., Augusteijn, T., Wood, M. A., Bergeron, P. & Grauer, A. D., 1994. [Whole Earth telescope observations of the DBV white dwarf GD 358]. *Astrophys. J.*, **430**, 839 – 849.

Winget, D. E., Van Horn, H. M., Tassoul, M., Hansen, C. J., Fontaine, G. & Carroll, B. W., 1982. [Hydrogen-driving and the blue edge of compositionally stratified ZZ Ceti star models]. *Astrophys. J.*, **252**, L65 – L68.

Wood, M. A., 1992. [Constraints on the age and evolution of the Galaxy from the white dwarf luminosity function]. *Astrophys. J.*, **386**, 539 – 561.

Woodard, M. F., Korzennik, S. G., Rabello-Soares, M. C., Kumar, P., Tarbell, T. D. & Acton, S., 2001. [Energy distribution of solar oscillation modes inferred from space-based measurements]. *Astrophys. J.*, **548**, L103 – L106.

Zhevakin, S. A., 1953. [K Teorii Cefeid. I][1] (in Russian). *Astron. Zh.*, **30**, 161 – 179.

von Neuman, J. & Wigner, E., 1929. [Über merkwürdige diskrete Eigenwerte. Über das Verhalten von Eigenwerten bei adiabatischen Prozessen]. *Phys. Z.*, **30**, 467 – 470.

[1] On the theory of Cepheids. I.

Appendix A

Useful properties of Legendre functions

The following expressions are mainly taken from Abramowitz & Stegun (1964) and Whittaker & Watson (1927).

Differential equation:

$$(1-x^2)\frac{\mathrm{d}^2 P_l^m}{\mathrm{d}x^2} - 2x\frac{\mathrm{d}P_l^m}{\mathrm{d}x} + \left[l(l+1) - \frac{m^2}{1-x^2}\right] P_l^m = 0 \tag{A.1}$$

$$\frac{\mathrm{d}}{\mathrm{d}x}\left[(1-x^2)\frac{\mathrm{d}P_l^m}{\mathrm{d}x}\right] + \left[l(l+1) - \frac{m^2}{1-x^2}\right] P_l^m = 0 \tag{A.2}$$

Legendre Polynomials: $P_l(x) = P_l^0(x)$. Explicit expressions for the first few cases:

$$\begin{aligned} P_0(x) &= 1 \\ P_1(x) &= x \\ P_1^1(x) &= -(1-x^2)^{1/2} \\ P_2(x) &= 1/2(3x^2-1) \end{aligned} \tag{A.3}$$

General expressions, for $m > 0$:

$$P_l(x) = \frac{1}{2^l l!}\frac{\mathrm{d}^l (x^2-1)^l}{\mathrm{d}x^l} \tag{A.4}$$

$$P_l^m(x) = (-1)^m (1-x^2)^{m/2}\frac{\mathrm{d}^m P_l(x)}{\mathrm{d}x^m} \tag{A.5}$$

$$P_m^m(x) = (-1)^m \frac{(2m)!2^{-m}}{m!}(1-x^2)^{m/2} \tag{A.6}$$

Note that equation (A.4) shows that $P_l(x)$ is a polynomial of degree l. Also, equation (A.6) shows that

$$P_m^m(\cos\theta) = (-1)^m \frac{(2m)!2^{-m}}{m!}\sin^m\theta \tag{A.7}$$

Expression for negative azimuthal order:

$$P_l^{-m}(\cos\theta) = \frac{(l-m)!}{(l+m)!} P_l^m(\cos\theta)\ . \tag{A.8}$$

Recursion relations:

$$\begin{aligned}
(l-m+1)P_{l+1}^m(x) &= (2l+1)xP_l^m(x) - (l+m)P_{l-1}^m(x) && \text{(A.9)}\\
(1-x^2)\frac{\mathrm{d}P_l^m}{\mathrm{d}x} &= lxP_l^m(x) - (l+m)P_{l-1}^m(x) && \text{(A.10)}\\
x\frac{\mathrm{d}P_l}{\mathrm{d}x} - \frac{\mathrm{d}P_{l-1}}{\mathrm{d}x} &= lP_l(x) && \text{(A.11)}
\end{aligned}$$

Integrals:

$$\int_{-1}^{1} P_l^m(x)P_{l'}^m(x)\mathrm{d}x = \delta_{ll'}\frac{(n+m)!}{(l+1/2)(l-m)!} \tag{A.12}$$

Asymptotic expansion, for $m \geq 0$, large l:

$$P_l^m(\cos\theta) = \frac{\Gamma(l+m+1)}{\Gamma(l+3/2)}(\frac{\pi}{2}\sin\theta)^{-1/2}\cos\left[(l+\frac{1}{2})\theta - \frac{\pi}{4} + \frac{m\pi}{2}\right] + \mathcal{O}(l^{-1}) \tag{A.13}$$

Appendix B

Effects of a perturbation on acoustic-mode frequencies

In several of the Problems we consider the effect on the frequencies of acoustic modes, as described by the asymptotics leading to the Duvall law, of various modifications (such as the perturbation in the gravitational potential, changes in the sound speed and rotation). These results all reflect a more general expression, which is derived here.

I start from the dispersion relation for a plane sound wave, with the addition of some perturbation $\delta_r a(r)$ which, as indicated, is assumed to be a function of r alone:

$$\omega^2 = c^2|\mathbf{k}|^2 + \delta_r a(r) \tag{B.1}$$

(*cf.* eq. 3.55), where for simplicity I dropped "0" on equilibrium quantities. I now use that $|\mathbf{k}|^2 = k_r^2 + k_{\rm h}^2$, where $k_{\rm h}^2$ is given by equation (4.51). Therefore, k_r is given by

$$\begin{aligned} k_r &= \left(\frac{\omega^2}{c^2} - \frac{L^2}{r^2} - \frac{1}{c^2}\delta_r a\right)^{1/2} \\ &\simeq \frac{\omega}{c}\left[\left(1 - \frac{L^2c^2}{\omega^2 r^2}\right)^{1/2} - \frac{1}{2\omega^2}\left(1 - \frac{L^2c^2}{\omega^2 r^2}\right)^{-1/2}\delta_r a\right] , \end{aligned} \tag{B.2}$$

where in the last equality I assumed that $\delta_r a$ was small. The condition that we have a standing wave can be expressed as

$$\int_{r_{\rm t}}^{R} k_r {\rm d}r = (n+\alpha)\pi , \tag{B.3}$$

where, as usual, α takes into account the phase change at the surface. By substituting equation (B.2) we obtain

$$\frac{(n+\alpha)\pi}{\omega} \simeq \int_{r_{\rm t}}^{R}\left(1 - \frac{L^2c^2}{\omega^2 r^2}\right)^{1/2}\frac{{\rm d}r}{c} - \frac{1}{2\omega^2}\int_{r_{\rm t}}^{R}\left(1 - \frac{L^2c^2}{\omega^2 r^2}\right)^{-1/2}\delta_r a\frac{{\rm d}r}{c} . \tag{B.4}$$

If we neglect the term in $\delta_r a$ we obviously obtain the usual Duvall law, equation (7.1). Hence equation (B.4) shows the effect of the perturbation on the Duvall law.

We can now find the effect on the oscillation frequencies of the perturbation. I assume that the result is to change the frequency from ω to $\omega + \delta\omega$. Also it should be recalled that $\alpha = \alpha(\omega)$ in general depends on ω. By multiplying equation (B.4) by ω and perturbing it we obtain

$$\pi \frac{\mathrm{d}\alpha}{\mathrm{d}\omega}\delta\omega = \delta\omega \int_{r_\mathrm{t}}^{R} \left(1 - \frac{L^2c^2}{\omega^2 r^2}\right)^{1/2} \frac{\mathrm{d}r}{c} + \omega \int_{r_\mathrm{t}}^{R} \left(1 - \frac{L^2c^2}{\omega^2 r^2}\right)^{-1/2} \frac{L^2c^2}{\omega^2 r^2} \frac{\delta\omega}{\omega} \frac{\mathrm{d}r}{c}$$
$$- \frac{1}{2\omega} \int_{r_\mathrm{t}}^{R} \left(1 - \frac{L^2c^2}{\omega^2 r^2}\right)^{-1/2} \delta_r a \frac{\mathrm{d}r}{c} \,. \tag{B.5}$$

From this we finally obtain

$$S\frac{\delta\omega}{\omega} \simeq \frac{1}{2\omega^2} \int_{r_\mathrm{t}}^{R} \left(1 - \frac{L^2c^2}{\omega^2 r^2}\right)^{-1/2} \delta_r a \frac{\mathrm{d}r}{c} \,, \tag{B.6}$$

where

$$S = \int_{r_\mathrm{t}}^{R} \left(1 - \frac{L^2c^2}{\omega^2 r^2}\right)^{-1/2} \frac{\mathrm{d}r}{c} - \pi \frac{\mathrm{d}\alpha}{\mathrm{d}\omega} \,. \tag{B.7}$$

This is the desired general expression.

It should be noticed that equation (B.6) has a very simple physical interpretation: Apart from the (generally small) term in $\mathrm{d}\alpha/\mathrm{d}\omega$ in S, the equation shows that the change in ω^2 is just a weighted average of $\delta_r a$, with the weight function

$$\mathcal{W}(r) = \frac{1}{c} \left(1 - \frac{L^2c^2}{\omega^2 r^2}\right)^{-1/2} \,. \tag{B.8}$$

However, it is easily seen that $\mathcal{W}(r)\mathrm{d}r$ is just the sound travel time, corresponding to the radial distance $\mathrm{d}r$, along the ray describing the mode. Hence the weight in the average simply gives the time that the mode, regarded as a superposition of plane waves, spends in a given region of the star.

Example I. Effect of a change in sound speed: If the sound speed is changed from c to $c + \delta_r c$, the dispersion relation for sound waves can be written

$$\omega^2 = c^2|\mathbf{k}|^2 + 2c\delta_r c|\mathbf{k}|^2 = c^2|\mathbf{k}|^2 + 2\omega^2 \frac{\delta_r c}{c} \,. \tag{B.9}$$

Hence here $\delta_r a = 2\omega^2 \delta_r c/c$. Consequently, the frequency change is given by

$$S\frac{\delta\omega}{\omega} \simeq \int_{r_\mathrm{t}}^{R} \left(1 - \frac{L^2c^2}{\omega^2 r^2}\right)^{-1/2} \frac{\delta_r c}{c} \frac{\mathrm{d}r}{c} \,. \tag{B.10}$$

It should be noted that in general a change to the model would result also in an intrinsic change $\delta\alpha$ in α. As a result, the general asymptotic expression for the frequency change [which can be obtained by including explicitly a term in the change in α when deriving equation (B.5) from equation (B.4)] is

$$S\frac{\delta\omega}{\omega} \simeq \int_{r_\mathrm{t}}^{R} \left(1 - \frac{L^2c^2}{\omega^2 r^2}\right)^{-1/2} \frac{\delta_r c}{c} \frac{\mathrm{d}r}{c} + \pi \frac{\delta\alpha}{\omega} \,. \tag{B.11}$$

Thus we recover equation (7.145).

Example II. Effect of rotation: As discussed in Chapter 8 the dominant effect of rotation is purely geometrical. In a system rotating with the star, the dispersion relation is as usual $\omega_0^2 = c^2|\mathbf{k}|^2$; from equation (8.2) the dispersion relation in the inertial system is therefore, to lowest order in Ω,

$$\omega^2 = c^2|\mathbf{k}|^2 + 2m\omega\Omega \ , \tag{B.12}$$

where I assume that the rotation rate Ω depends on r alone. Hence here $\delta_r a(r) = 2m\omega\Omega(r)$, and we obtain the perturbation in the frequency caused by rotation as

$$S\delta\omega \simeq m \int_{r_t}^{R} \left(1 - \frac{L^2c^2}{\omega^2 r^2}\right)^{-1/2} \Omega(r) \frac{\mathrm{d}r}{c} \ . \tag{B.13}$$

Appendix C

Problems

The following problems have been used in courses on stellar pulsations in Aarhus. They originally appeared on the weekly problem sheets (Ugesedler), but are collected here for convenience and more general use. In a few cases reference is made to programming and plotting with IDL. Obviously any other convenient graphics package may be used instead.

The problems are collected in sections corresponding approximately to the sections of the main text, although the numbering has not been maintained.

C.1 Analysis of oscillation data

Problem 1.1:

Discrete Fourier transform. Observationally, the data are typically given at discrete times t_n. Hence the continuous Fourier transform considered in Section 2.2 is not immediately relevant. Here we consider the simple case where the data are uniformly spaced in time,

$$t_n = n\Delta t \ , \qquad n = 0, \ldots, N-1 \tag{C.1}$$

(this can in fact often be arranged). Then we define the discrete Fourier transform as

$$\hat{v}(\omega_j) = \frac{1}{N} \sum_{n=0}^{N-1} v(t_n) \exp(i\omega_j t_n) \ , \tag{C.2}$$

given at the discrete frequencies ω_j. For the moment we do not specify ω_j.

i) Find the discrete transform of the simple harmonic oscillator given in equation (2.19). Sketch the power $|\hat{v}(\omega_j)|^2$. Compare with the continuous transform.

A very efficient procedure for computing the discrete transform is the *Fast Fourier Transform* (FFT). This requires that the number of data points is a power 2^μ of 2, and provides the transform only at the frequencies

$$\omega_j = \frac{2\pi}{N\Delta t} j = \frac{2\pi}{T} j \ , \qquad j = 0, \ldots, N \ , \tag{C.3}$$

where $T = N\Delta t$ is the total duration of the observing run. For more details about the FFT, see also *Numerical Recipes* (Press *et al.* 1986).

ii) Sketch the power resulting from a FFT of the time string given by the harmonic oscillator in equation (2.19); for simplicity take the frequency ω_0 of the oscillator to be $2\pi j_0/(N\Delta t)$ for some integer j_0. Note that very little of the sinc function structure in the continuous transform is preserved.

Normally, the number of data points will evidently not be an integral power of 2. In that case, the data are extended by zeros up to a total number $N_1 = 2^\mu > N$.

iii) Consider the effect on the FFT of the simple harmonic oscillator of extending the data by zeros in this way. Show how this can be used to resolve the structure of the peak of the power spectrum (note that we do not need to take the smallest possible power of 2).

Note: In manipulating the Fourier transforms, it is useful to recall that

$$\cos x = \frac{1}{2}(e^{ix} + e^{-ix}) \; ;$$
$$\sum_{n=0}^{N} x^n = \frac{1 - x^{N+1}}{1 - x} \; . \tag{C.4}$$

Problem 1.2:

Multiperiodic harmonic oscillations. (This requires access to a computer with graphics facilities. Here reference is made to the graphics and data analysis package IDL, which is a very convenient tool for this type of exercise).
Consider a time string consisting of a sum of harmonic oscillators,

$$v(t) = \sum_{k=0}^{K} a_k \cos(\omega_k t - \delta_k) \; . \tag{C.5}$$

Take the amplitudes a_k and the phases δ_k to be uniformly distributed random numbers, between 0 and 1, and 0 and 2π, respectively. Also choose suitably "random" frequencies ω_k.

i) Plot $v(t)$ for a total time T that is substantially larger than the longest period $2\pi/\omega_k$, for several different numbers K of individual oscillations. Note how the appearance of the time string becomes increasingly "chaotic" as K is increased.

ii) Plot the power spectra of the time strings found under i), using IDL's FFT routine. Consider the extent to which the individual frequencies can be separated. How does this depend on the number of modes or the total duration of the time string?

A typical observed time string of solar oscillations (corresponding, for example, to observations made in light integrated over the solar surface) contains of order 50 modes. Clearly, separating them is no trivial task.

Problem 1.3:

A non-harmonic oscillator. A simple model of a large-amplitude pulsating star (*e.g.* a Cepheid) is provided by the following function

$$v(t) = a_0 \sin[\omega t + \alpha \sin(\omega t)] \; . \tag{C.6}$$

i) Show that $v(t)$ is periodic, with the period $\Pi = 2\pi/\omega$.

ii) Sketch (or get IDL to plot) $v(t)$ for $\omega = 1$, $a_0 = 1$, $\alpha = 0.5$.

iii) For small α, find a simple expression for $v(t)$ by expanding it in powers of α, including the term of order α^2. (If this is too hard, consider just the term of order α). Try to guess what the expansion to higher orders in α will look like, qualitatively.

iv) Use IDL to find the Fourier transform and power spectrum of $v(t)$ for some typical cases. Compare with the expansion obtained in iii).

Problem 1.4:

A double-mode non-harmonic oscillator. In Problem 1.3 we considered a simple model of a large-amplitude pulsating star, with the signal $v(t) = a_0 \sin[\omega t + \alpha \sin(\omega t)]$; the effect of the term in α is roughly to give a distortion to the phase which depends on the instantaneous amplitude of the oscillation. This distortion may result from non-linear effects near the surface of the star affecting what is essentially a harmonic oscillation in the stellar interior.

We can generalize this concept to multiperiodic oscillators. For simplicity, we consider a double-mode star, and assume that the signal can be written as

$$\begin{aligned} v(t) &= a_1 \sin[\omega_1 t + \alpha a_1 \sin(\omega_1 t) + \alpha a_2 \sin(\omega_2 t)] \\ &+ a_2 \sin[\omega_2 t + \beta a_1 \sin(\omega_1 t) + \beta a_2 \sin(\omega_2 t)] \; . \end{aligned} \tag{C.7}$$

i) For small α and β, expand $v(t)$ in terms of harmonic functions. Include enough terms to get a feel for what the form of a general term might be.

ii) Use IDL to plot the time series and the power spectrum for typical cases. (It may be a good idea to use a logarithmic scale for the power, suitably truncated, to show the presence of weak peaks.) Compare with the expansion in i).

iii) What would happen if the star were pulsating in several modes?

Problem 1.5:

Spatial analysis of oscillation observations. As mentioned briefly in Section 2.1, the analysis of observations of solar oscillations essentially proceeds by multiplying the observed Doppler velocity field $v(\theta, \phi, t)$ by different spherical harmonics $Y_{l_0}^{m_0}(\theta, \phi)$ and integrating over the area A of the solar disk that is observed. The result is a function $v_{l_0 m_0}(t)$ of time that predominantly contains contributions from modes with $l = l_0$, $m = m_0$. Had the integration been over the entire Sun, the orthogonality of the spherical harmonics would have given complete isolation of these modes. However, since we can only see part of the Sun other modes leak in and complicate the analysis.

To illustrate these effects, we take out the ϕ-dependent part of the analysis, by considering an oscillation of the form

$$v(t) = V_0 \cos(m\phi - \omega t) \; . \tag{C.8}$$

This signal is observed over the interval in longitude from $\phi = -\phi_c$ to $\phi = \phi_c$ (we take $\phi = 0$ to correspond to the centre of the disk). The analysis results in an average over the interval:

$$v_{m_0}(t) = \frac{1}{2\phi_c} \int_{-\phi_c}^{\phi_c} v(t) \cos(m_0 \phi) \mathrm{d}\phi \; . \tag{C.9}$$

i) Write $v_{m_0}(t)$ as

$$v_{m_0}(t) = S_{m_0 m} V_0 \cos(\omega t) \tag{C.10}$$

and find an expression for the *spatial response function* $S_{m_0 m}$. Have we seen something similar before?

ii) What happens in the limits of very small ϕ_c; or $\phi_c = \pi$? What does the latter case correspond to?

iii) Plot $S_{m_0 m}$ for some typical cases.

Note that this behaviour is in fact very similar to the behaviour of the corresponding response functions $S_{l_0 m_0 l m}$ for the real observations. In fact, the calculation carried out here is essentially the ϕ-part of the full integral over the observed area on the solar disk.

Problem 1.6:

Spatial response functions. We consider observations of solar oscillations through an aperture of radius d, in units of the radius of the solar disk, and centred on the disk.

i) Show that the velocity response function, defined in analogy with equation (2.7), is given by

$$S_l^{(v)}(d) = \frac{2\sqrt{2l+1}}{d^2} \int_{x_1}^1 P_l(x) x^2 \mathrm{d}x \ , \tag{C.11}$$

where $x_1 = \sqrt{1-d^2}$.

ii) Using the explicit expressions and recursion relations for $P_l(x)$ in Appendix A, calculate $S_l^{(v)}(d)$ for $d = 1$ and $d = 0.5$, and for as many l-values as you can be bothered to consider. What is the effect of restricting the aperture?

iii) A more intelligent way to compute the responses can be obtained by deriving recursion relations for the functions

$$\mathcal{P}_l^k(x) = \int x^k \frac{\mathrm{d}P_l}{\mathrm{d}x} \mathrm{d}x \ , \qquad \mathcal{Q}_l^k(x) = \int x^k P_l(x) \mathrm{d}x \ , \tag{C.12}$$

based on the recursion relations for P_l and its derivative, as well as a little integration by parts. Try to see whether you can find a way of doing that, and make a more extensive computation for the cases considered in ii). It may help to look in Christensen-Dalsgaard & Gough (1982).

C.2 A little hydrodynamics

Problem 2.1:

Waves at a density discontinuity. In Section 3.3.3 a relation is derived for gravity waves on a free surface. It is interesting also to consider gravity waves at an interface where the density jumps discontinuously. Examples are waves in a glass with oil on top of water, or waves at the interface between a helium-rich core and a hydrogen-rich envelope.

- Consider a system consisting of an infinite layer of density ρ_1 on top of an infinite layer of density ρ_2, with $\rho_1 < \rho_2$. The assumptions are otherwise as in Section 3.3.3. By requiring that the vertical displacement and the pressure are continuous at the perturbed interface between the layers, show that the oscillation frequencies are given by

$$\omega^2 = \frac{\rho_2 - \rho_1}{\rho_2 + \rho_1} g_0 k \ . \tag{C.13}$$

Does this make sense in the limits $\rho_1 \to 0$ and $\rho_1 \to \rho_2$?

Problem 2.2:

Damping of simple sound waves. To illustrate the effects of non-adiabaticity, we consider the radiative damping of the simple sound waves discussed in Section 3.3.1.

Except where otherwise noted, the assumptions are the same as in that section.

At low density, we use Newton's law of cooling, equation (3.23), for the radiative cooling. Also, we assume the ideal gas law, so that in particular $\Gamma_1 = \Gamma_2 = \Gamma_3 = \gamma = 5/3$, and that there is no nuclear energy generation. Finally, we consider a perturbation in the form of a plane wave, as in equation (3.53).

i) Assume that the opacity κ is constant (*i.e.*, independent of ρ and T). Show that the relation between p' and ρ', on complex form, can be written

$$\frac{p'}{p_0} = \gamma_{\rm N} \frac{\rho'}{\rho_0} \ , \tag{C.14}$$

where

$$\gamma_{\rm N} = \gamma \phi_{\rm N} \ , \qquad \phi_{\rm N} = \frac{1 + \dfrac{3i}{4\gamma\omega\tau_{\rm N}}}{1 + \dfrac{i}{\omega\tau_{\rm N}}} \ , \tag{C.15}$$

and

$$\tau_{\rm N} = \frac{p_0}{4a\tilde{c}\kappa_0\rho_0(\gamma - 1)T_0^4} \tag{C.16}$$

is a characteristic time scale for cooling by Newton's law.

ii) Show that the dispersion relation for a plane sound wave is

$$\omega^2 = c_0^2 |\mathbf{k}|^2 \phi_{\rm N} \ , \tag{C.17}$$

where $c_0 = (\gamma p_0/\rho_0)^{1/2}$ is the adiabatic sound speed.

iii) Consider a wave where the wave number $\mathbf{k}$ is real. Show that the imaginary part of ω is negative and that therefore the wave is damped, *i.e.*, that the amplitude decreases with time. What is the physical explanation for the damping? (You may assume that the damping is weak, so that $\mathrm{Re}(\omega) \gg \mathrm{Im}(\omega)$.)

iv) As a more realistic case, assume that the opacity depends on ρ and T, such that $\kappa \propto \rho^a T^b$ where a and b are positive (this corresponds to conditions in stellar atmospheres where the opacity is dominated by H^- absorption). Find the expression for $\gamma_{\rm N}$ in this case, and verify that the wave is damped in this case also. What is the effect of the opacity variation on the magnitude of the damping rate?

v) Discuss the behaviour of the dispersion relation in the limits $\tau_{\rm N} \to \infty$ and $\tau_{\rm N} \to 0$. Consider also the behaviour corresponding to $\rho \to 0$ at fixed T (corresponding to conditions high in a stellar atmosphere).

We now consider the limit of high density, where the diffusion approximation, equation (3.22), can be used for the radiative flux. We still assume that equilibrium quantities are constant and consider a plane wave.

vi) Show that the perturbation in the radiative cooling rate is given by

$$(\mathrm{div}\,\mathbf{F})' = \frac{4a\tilde{c}T_0^4}{3\kappa_0\rho_0}|\mathbf{k}|^2\frac{T'}{T_0} \tag{C.18}$$

(remember that we assume that $\nabla T_0 = 0$).

vii) Hence show that equations (C.14) and (C.17) are still valid, if γ_N and ϕ_N are replaced by γ_F and ϕ_F, where

$$\gamma_\mathrm{F} = \gamma\phi_\mathrm{F}\ , \qquad \phi_\mathrm{F} = \frac{1+\dfrac{i}{\gamma\omega\tau_\mathrm{F}}}{1+\dfrac{i}{\omega\tau_\mathrm{F}}}\ , \qquad \tau_\mathrm{F} = \frac{3\kappa_0\rho_0 p_0}{4a\tilde{c}(\gamma-1)T_0^4|\mathbf{k}|^2}\ . \tag{C.19}$$

Compare this expression for the time scale τ_F for radiative diffusion with the estimate given in Section 3.1.4.

viii) Show that this also results in damping of a sound wave. Discuss the physics of the damping.

Finally, we consider the effects of nuclear energy generation on the waves. We assume that the energy generation rate $\epsilon \propto \rho T^n$, and that radiative effects can be neglected.

ix) Show that in this case the relation between p' and ρ' can be written

$$\frac{p'}{p_0} = \gamma_\epsilon\frac{\rho'}{\rho_0}\ , \tag{C.20}$$

where

$$\gamma_\epsilon = \gamma\phi_\epsilon\ , \qquad \phi_\epsilon = \frac{1-\dfrac{i(n-2)}{n\gamma\omega\tau_\epsilon}}{1-\dfrac{i}{\omega\tau_\epsilon}}\ , \tag{C.21}$$

and

$$\tau_\epsilon = \frac{p_0}{n\rho_0\epsilon_0(\gamma-1)} \tag{C.22}$$

is a characteristic time scale for nuclear heating.

x) Show that this leads to excitation of the sound wave, such that its amplitude grows with time. Discuss the physics of the excitation.

xi) Discuss qualitatively the case where both nuclear energy generation and radiative damping, in the diffusion approximation, are taken into account. For which waves might the overall effect be an excitation?

Problem 2.3:

Dispersion relation for sound waves in a gravitating fluid. We consider acoustic waves in a homogeneous system, as in Section 3.3.1, but include the effect of self-gravity on the wave. Hence in the equation of motion, the term $\rho_0 \nabla \Phi'$ should be included on the right-hand side, but we continue to neglect the equilibrium gravitational acceleration.

i) Show that equation (3.51) should be replaced by

$$\frac{\partial^2 \rho'}{\partial t^2} = c_0^2 \nabla^2 \rho' + 4\pi G \rho_0 \rho' \ . \tag{C.23}$$

ii) We assume a plane-wave solution, on the form given in equation (3.53). Show that the dispersion relation is

$$\omega^2 = c_0^2 \left|\mathbf{k}\right|^2 - 4\pi G \rho_0 \ . \tag{C.24}$$

iii) When the frequency ω obtained from equation (C.24) is imaginary, the perturbation either grows or decays exponentially with time. Show that this occurs when the wavelength λ of the wave satisfies $\lambda > \lambda_{\rm crit}$ and find $\lambda_{\rm crit}$. Compare with equation (10.4) of *Lecture Notes on Stellar Structure and Evolution*.

C.3 Properties of solar and stellar oscillations

Problem 3.1:

Rays of sound waves. Ray theory is a very powerful tool for understanding the propagation of waves in a medium where conditions vary slowly. It is entirely analogous to the study of the propagation of light rays. An important example is its use to describe the properties of acoustic oscillations in the Sun. We consider an acoustic wave that propagates in the $(x - z)$ plane where the sound speed c depends on z but not x. The wave is described by a wave vector $\mathbf{k} = (k_x, k_z)$ and has a given frequency ω; one may think of it as being excited with a fixed frequency at some point in the region. Clearly, ω and $\mathbf{k}$ satisfy the dispersion relation (3.55). The $x-$component k_x of $\mathbf{k}$ is fixed, whereas the $z-$component k_z depends on z.

i) Show from equation (3.55) that

$$k_z = \left(\frac{\omega^2}{k_x^2 c^2} - 1 \right)^{1/2} k_x \ . \tag{C.25}$$

The propagation of the ray is parallel to the wave vector. Hence we can describe the position (x, z) of a point on the ray by the equations

$$\begin{aligned} \frac{\mathrm{d}x}{\mathrm{d}s} &= k_x \\ \frac{\mathrm{d}z}{\mathrm{d}s} &= k_z \ , \end{aligned} \tag{C.26}$$

where s is a suitably chosen measure of position along the ray. From these equations we obtain

$$\frac{\mathrm{d}x}{\mathrm{d}z} = \frac{k_x}{k_z} \ , \tag{C.27}$$

which determines the shape of the ray.

ii) Let z measure depth beneath some surface, and assume that $c(z)^2$ increases linearly with z,

$$c(z)^2 = c_0^2 + Az \ , \tag{C.28}$$

where c_0 and A are constants (this corresponds approximately to conditions near a stellar surface). Try to sketch, qualitatively, the behaviour of the ray.

iii) Find the solution to the equation for the ray.

iv) What happens at a horizontal interface where c jumps from a value c_1 to a value c_2? Have you seen anything like that before?

Problem 3.2:

Trapping of g modes. We consider g modes trapped near a maximum in the buoyancy frequency, corresponding to the steep gradient in composition outside a convective core. Specifically, we make the following assumptions:

- $S_l/\omega \gg 1$.
- N^2 is only non-zero in a narrow interval $[r_1, r_2]$:

$$N^2 = \begin{cases} 0 & \text{for } r < r_1 \\ N_{\mathrm{m}}^2 & \text{for } r_1 \le r \le r_2 \\ 0 & \text{for } r_2 < r \ . \end{cases} \tag{C.29}$$

- The region considered is so thin that we can make the plane-parallel assumption, replacing $l(l+1)/r^2$ by $k_{\rm h}^2$ which we take to be constant.
- The oscillations are described by the simplified equations (5.20) and (5.21).

i) Show under these assumptions that ξ_r approximately satisfies

$$\frac{{\rm d}^2\xi_r}{{\rm d}r^2} = -k_{\rm h}^2 \left(\frac{N^2}{\omega^2} - 1 \right) \xi_r \ . \tag{C.30}$$

ii) Show that the solution to equation (C.30), corresponding to modes trapped in the region considered, have the form

$$\xi_r(r) = \begin{cases} A \exp[k_{\rm h}(r - r_1)] & \text{for } r < r_1 \\ B_1 \cos[\beta k_{\rm h}(r - r_1)] + B_2 \sin[\beta k_{\rm h}(r - r_1)] & \text{for } r_1 \le r \le r_2 \\ C \exp[-k_{\rm h}(r - r_2)] & \text{for } r_2 < r \ , \end{cases} \tag{C.31}$$

where

$$\beta^2 = \left(\frac{N_{\rm m}^2}{\omega^2} - 1 \right) \ . \tag{C.32}$$

iii) The solution must satisfy continuity of ξ_r and ${\rm d}\xi_r/{\rm d}r$. Show that this leads to the following relation which implicitly determines ω:

$$\tan(\beta\Delta) = \frac{2\beta}{\beta^2 - 1} \ , \tag{C.33}$$

where $\Delta = k_{\rm h}(r_2 - r_1)$.

iv) Sketch the left-hand side and the right-hand side of equation (C.33) as a function of β and argue that the equation has an infinite number of solutions β_n, corresponding to the frequencies ω_n, $n = 1, 2, \ldots$.

v) Assume Δ to be very large. Show that the lowest-order modes satisfy

$$\beta\Delta \simeq n\pi \ , \tag{C.34}$$

and hence

$$\omega^2 \simeq \frac{N_{\rm m}^2}{1 + (n\pi/\Delta)^2} \ . \tag{C.35}$$

vi) Sketch (or plot) the solution $\xi_r(r)$ in this approximation for the first few values of n.

vii) Does equation (C.35) look familiar? (Hint: Relate $r_2 - r_1$ to the vertical wavelength, and hence the vertical wavenumber k_r, of the mode.)

viii) Consider the opposite extreme of very high-order modes. Show that $\omega_n \to 0$ for $n \to \infty$, and that consequently the frequencies are still given by equation (C.35). Show also that the periods Π_n of pulsation may be approximated by

$$\Pi_n \simeq \Pi_0 n \ , \qquad \Pi_0 = \frac{2\pi^2}{N_{\rm m}\Delta} \ . \tag{C.36}$$

Thus the periods increase linearly with n.

ix) Try to solve the dispersion relation (C.33) numerically, to obtain $\omega_n/N_{\rm m}$ as a function of Δ, and make plots of the corresponding eigenfunctions.

Problem 3.3:

A simple example of avoided crossings. Avoided crossings play a major role in understanding the properties of spectra of stellar oscillations. Here we analyze a very simple physical system that exhibits this behaviour.

Consider two coupled oscillators, with a time dependence described by $y_1(t)$ and $y_2(t)$, and satisfying the differential equations

$$\begin{aligned} \frac{{\rm d}^2 y_1}{{\rm d}t^2} &= -\omega_1(\lambda)^2 y_1 + \alpha y_2 \\ \frac{{\rm d}^2 y_2}{{\rm d}t^2} &= -\omega_2(\lambda)^2 y_2 + \alpha y_1 \ . \end{aligned} \tag{C.37}$$

Here α is a coupling parameter, which we assume to be constant. In the absence of coupling (*i.e.*, for $\alpha = 0$) the oscillators have frequencies ω_1 and ω_2 which, as indicated, depend on a parameter λ. We assume that at $\lambda = \lambda_0$ the two uncoupled oscillators cross, *i.e.*, $\omega_1(\lambda_0) = \omega_2(\lambda_0)$

i) Show that the system in equation (C.37) has solutions of the form

$$\left\{ \begin{array}{c} y_1(t) \\ y_2(t) \end{array} \right\} = \left\{ \begin{array}{c} c_1 \\ c_2 \end{array} \right\} \exp(-i\omega t) \ , \tag{C.38}$$

where the frequencies are given by

$$\omega_\pm^2 = \frac{1}{2}(\omega_1^2 + \omega_2^2) \pm \frac{1}{2}\left[(\omega_1^2 - \omega_2^2)^2 + 4\alpha^2\right]^{1/2} \ . \tag{C.39}$$

ii) Discuss the behaviour of $\omega_\pm$, as functions of λ, far from λ_0 (in the sense that $|\omega_1^2(\lambda) - \omega_2^2(\lambda)| \gg \alpha$) and at $\lambda = \lambda_0$.

To analyze the behaviour of the system in more detail and find the coefficients, we simplify the expressions by assuming that $\omega_1^2 = 1$, $\omega_2^2 = \lambda$.

iii) Make a plot of $\omega_\pm^2(\lambda)$. Show that the two solutions are the two branches of a hyperbola.

iv) Find the coefficients $\{c_1^{(\pm)}(\lambda), c_2^{(\pm)}(\lambda)\}$, normalized such that $(c_1^{(\pm)})^2 + (c_2^{(\pm)})^2 = 1$. What is their behaviour far from the avoided crossing? And at the point of closest approach of the frequencies? Make a plot of the coefficients.

Problem 3.4:

A perturbation treatment of avoided crossings. As shown by von Neuman & Wigner (1929) it is possible to describe the behaviour of the eigenfrequencies near an avoided crossing by a simple extension of the usual first-order perturbation analysis. This Problem reproduces von Neuman & Wigner's analysis.

We consider the eigenvalue problem

$$\mathcal{F}\xi = \sigma\xi \; . \tag{C.40}$$

Here we express the operator $\mathcal{F}$ as

$$\mathcal{F} = \mathcal{F}_0 + \lambda\,\delta\mathcal{F} \; , \tag{C.41}$$

where $\lambda\,\delta\mathcal{F}$ is a small perturbation. (We use the real parameter λ to vary the perturbation; $\delta\mathcal{F}$ is a fixed operator.) We assume that both $\mathcal{F}_0$ and $\delta\mathcal{F}$ are symmetric operators. The eigenvalues and eigenvectors for the unperturbed operator $\mathcal{F}_0$ are given by

$$\mathcal{F}_0\xi_i^{(0)} = \sigma_i^{(0)}\xi_i^{(0)} \; , \qquad i = 1, 2, \ldots \; . \tag{C.42}$$

Here the $\xi_i^{(i)}$ are taken to be normalized, $\|\xi_i^{(i)}\|^2 = \; < \xi_i^{(i)}, \xi_i^{(i)} > \; = 1$. We assume that $\sigma_1^{(0)}$ and $\sigma_2^{(0)}$ are very close together and neglect the remaining eigenvalues and eigenvectors in the following.

We let $\sigma(\lambda)$ be the eigenvalue of the perturbed operator, and assume that the corresponding eigenvector $\xi(\lambda)$ can be expressed as

$$\xi(\lambda) = c_1(\lambda)\xi_1^{(0)} + c_2(\lambda)\xi_2^{(0)} \; . \tag{C.43}$$

i) By substituting equation (C.43) into equation (C.40), and taking the scalar product of the resulting equation with $\xi_1^{(0)}$ and $\xi_2^{(0)}$, show that the eigenvalues are

$$\begin{aligned} \sigma_\pm(\lambda) \; = \; & \frac{1}{2}\left[\sigma_1^{(0)} + \sigma_2^{(0)} + \lambda(< \delta\mathcal{F} >_{11} + < \delta\mathcal{F} >_{22})\right] \\ & \pm\frac{1}{2}\left\{\left[\sigma_1^{(0)} - \sigma_2^{(0)} + \lambda(< \delta\mathcal{F} >_{11} - < \delta\mathcal{F} >_{22})\right]^2 + 4\lambda^2|< \delta\mathcal{F} >_{12}|^2\right\}^{1/2} \; , \end{aligned} \tag{C.44}$$

where

$$< \delta\mathcal{F} >_{ij} = < \xi_i^{(0)}, \delta\mathcal{F}\xi_j^{(0)} > \; , \qquad i, j = 1, 2 \; . \tag{C.45}$$

ii) Sketch the behaviour of the eigenvalues. Show that the minimum separation between $\sigma_+(\lambda)$ and $\sigma_-(\lambda)$ is

$$\Delta\sigma_{\min} = \Delta\sigma_0\frac{2|< \delta\mathcal{F} >_{12}|}{[(< \delta\mathcal{F} >_{11} - < \delta\mathcal{F} >_{22})^2 + 4|< \delta\mathcal{F} >_{12}|^2]^{1/2}} \; , \tag{C.46}$$

where $\Delta\sigma_0 = \sigma_2^{(0)} - \sigma_1^{(0)}$, and occurs at

$$\lambda = \lambda_{\min} = \frac{\Delta\sigma_0(< \delta\mathcal{F} >_{11} - < \delta\mathcal{F} >_{22})}{(< \delta\mathcal{F} >_{11} - < \delta\mathcal{F} >_{22})^2 + 4| < \delta\mathcal{F} >_{12} |^2} \ . \tag{C.47}$$

iii) Compare this solution with the eigenfrequencies obtained in Problem 3.3.

iv) Show that if the coupling term $< \delta\mathcal{F} >_{12}$ is zero, equation (C.44) reduces to the usual expression for the change in the eigenvalue induced by a perturbation, equation (5.73).

v) Discuss the behaviour of the coefficients $c_{1,2}^{(\pm)}(\lambda)$ associated with the eigenvalues $\sigma_\pm(\lambda)$ in the limit where $|\Delta\sigma_{\min}/\Delta\sigma_0| \ll 1$.

Note that if the coupling term $< \delta\mathcal{F} >_{12}$ vanishes, the avoided crossing is replaced by a true crossing of the eigenvalues. It may be shown that this is the case for the eigenvalue problem in equation (5.56) if we consider two eigenfunctions $\boldsymbol{\xi}_1^{(0)}$ and $\boldsymbol{\xi}_2^{(0)}$ with different values of the degree l. This is the reason why the curves for $l = 0$ and $l = 1$, for instance, cross in Figure 5.14.

Problem 3.5:

The perturbation of the stellar surface. The displacement given in equation (4.40) shows how each part of the star is moved by the oscillation. We take $t = 0$.

i) Consider the behaviour in the equatorial plane. Sketch or plot the perturbed surface for $(l, m) = (0, 0), (1, 1), (2, 2)$ using the expressions in the notes on the Legendre functions. Consider different values of the ratio $\xi_{\rm h}/\xi_r$.

ii) Repeat i), but in the plane passing through the pole, at $\phi = 0$.

C.4 Asymptotic theory of stellar oscillations

Problem 4.1:

A simple derivation of the Duvall law. Equation (7.39) can be justified rather more simply than by going through the full JWKB analysis (even though the arguments are essentially equivalent). We start from the dispersion relation for a plane sound wave, neglecting self-gravity (equation 3.55):

$$\omega^2 = c_0^2 |\mathbf{k}|^2 \ , \tag{C.48}$$

and write $|\mathbf{k}|^2 = k_r^2 + k_{\rm h}^2$. For a wave corresponding to a mode of oscillation, $k_{\rm h}$ is given by equation (4.51).

i) Dropping subscripts "0" on equilibrium quantities, show that

$$k_r^2 = \frac{\omega^2}{c^2} - \frac{L^2}{r^2} \ , \tag{C.49}$$

where $L^2 = l(l+1)$.

ii) Argue that the condition for a standing wave (*i.e.*, a mode of oscillation) is roughly that

$$\int_{r_t}^{R} k_r \mathrm{d}r = n\pi \ . \tag{C.50}$$

A more careful analysis shows that n in equation (C.49) should be replaced by $n + \alpha$, where α takes care of the behaviour near the lower turning point r_t and the surface.

iii) Use equation (C.50), modified in this way, and equation (C.49) to derive equation (7.39).

Problem 4.2:

The effect of the gravitational potential perturbation on p-mode frequencies. By combining the results of Problems 2.3 and 4.1, we can estimate the error made in the Cowling approximation.

i) Repeat the analysis in Problem 4.1, but using the dispersion relation (C.24) (*cf.* Problem 2.3) for a gravitating fluid, to obtain the following modified form of equation (7.39):

$$\omega \int_{r_t'}^{R} \left(1 - \frac{L^2c^2}{\omega^2 r^2} + \frac{4\pi G\rho}{\omega^2}\right)^{1/2} \frac{\mathrm{d}r}{c} \simeq \pi(n+\alpha) \ . \tag{C.51}$$

ii) The last term in the bracket in equation (C.51) arises from the effect of the perturbation in the gravitational potential. Since this term is generally small, we can expand the bracket. Show that the result may be written as

$$\frac{\pi(n+\alpha)}{\omega} \simeq \int_{r_t}^{R} \left(1 - \frac{L^2c^2}{\omega^2 r^2}\right)^{1/2} \frac{\mathrm{d}r}{c} + \frac{2\pi G}{\omega^2} \int_{r_t}^{R} \rho \left(1 - \frac{L^2c^2}{\omega^2 r^2}\right)^{-1/2} \frac{\mathrm{d}r}{c} \ , \tag{C.52}$$

with the usual definition of r_t.

We note that, as r_t is a function of ω/L, equation (C.52) may be written as

$$\frac{\pi(n+\alpha)}{\omega} = F\left(\frac{\omega}{L}\right) + \frac{1}{\omega^2} F_\Phi\left(\frac{\omega}{L}\right) \ , \tag{C.53}$$

where the functions $F(w)$ and $F_\Phi(w)$ are defined by equation (C.52). This is a generalization of equation (7.40).

From equation (C.52) we can derive an approximate expression for the difference $\delta\omega^{(\Phi)} = \omega^{(F)} - \omega^{(C)}$ between the frequency $\omega^{(F)}$ obtained taking the perturbation in the gravitational potential into account, and the frequency $\omega^{(C)}$ obtained in the Cowling approximation.

iii) Show by expanding equation (C.52) in $\delta\omega^{(\Phi)}$, including only the linear term, and neglecting a small term arising from the frequency-dependence of α, that

$$\delta\omega^{(\Phi)} \simeq -\frac{1}{\omega}\frac{2\pi G\int_{r_\mathrm{t}}^{R}\rho\left(1-\dfrac{L^2c^2}{\omega^2r^2}\right)^{-1/2}\dfrac{\mathrm{d}r}{c}}{\displaystyle\int_{r_\mathrm{t}}^{R}\left(1-\frac{L^2c^2}{\omega^2r^2}\right)^{-1/2}\frac{\mathrm{d}r}{c}} \; . \tag{C.54}$$

Thus the frequency change induced by the gravitational potential perturbation depends on an average of the density structure of the equilibrium model, over the region where the mode is trapped.

Problem 4.3:

Effects of a change to the model. We assume that the oscillation frequencies are given by the Duvall law, equation (7.104), where $\alpha = \alpha(\omega)$ is a function of frequency. Consider the case where the structure of the equilibrium model is changed (keeping the surface radius R fixed) such that $c(r)$ is replaced by $c(r) + \delta_r c(r)$, and $\alpha(\omega)$ is replaced by $\alpha(\omega) + \delta\alpha(\omega)$ (note that δ as used here should not be confused with the use of δ elsewhere to denote the Lagrangian perturbation). As a result of these changes, the eigenfrequency ω_{nl} is changed to $\omega_{nl} + \delta\omega_{nl}$.

i) Show that $\delta\omega_{nl}$ is given by

$$S_{nl}\,\frac{\delta\omega_{nl}}{\omega_{nl}} \simeq \int_{r_t}^{R}\left(1-\frac{L^2c^2}{r^2\omega_{nl}^2}\right)^{-1/2}\frac{\delta_r c}{c}\frac{\mathrm{d}r}{c} + \pi\frac{\delta\alpha}{\omega_{nl}} \; , \tag{C.55}$$

where

$$S_{nl} = \int_{r_t}^{R}\left(1-\frac{L^2c^2}{r^2\omega_{nl}^2}\right)^{-1/2}\frac{\mathrm{d}r}{c} - \pi\frac{\mathrm{d}\alpha}{\mathrm{d}\omega} \; . \tag{C.56}$$

ii) Sketch the behaviour of the weight function

$$\mathcal{W} = \frac{1}{c}\left(1-\frac{L^2c^2}{r^2\omega_{nl}^2}\right)^{-1/2} \tag{C.57}$$

for a typical increase of the sound speed with depth (you may, for example, assume that c^2 increases roughly linearly with depth). What is the effect of the singularity at $r = r_t$?

iii) Discuss the physical interpretation of $\mathcal{W}$ (try to think in terms of travel time for sound waves).

iv) Having made it through this derivation, go back and reconsider Problem 4.2 on the effect of the perturbation in the gravitational potential on the oscillation frequencies.

Problem 4.4:

The effect of discontinuities on oscillation frequencies. Sharp features in the stellar model introduce characteristic oscillations in the frequencies as a function of mode order. An example was encountered in Section 7.7.3 where we discussed the effect on the phase function $\mathcal{H}_2(\omega)$ of the rapid variation in Γ_1 in the second helium ionization zone. Another important example is the effect of the boundaries of convective regions. Here we discuss the effects of such features in a very simple way. The analysis is based on Appendix B of Monteiro, Christensen-Dalsgaard & Thompson (1994; but see the end of this problem for a correction to that paper). We assume that the oscillations are described by equation (7.90).

i) At the base of a convective envelope the temperature gradient $\nabla \equiv \mathrm{d}\ln T/\mathrm{d}\ln p$ goes from being adiabatic in the convection zone to being radiative below it. The transition occurs very abruptly, in such a way that ∇ is continuous but its gradient $\mathrm{d}\nabla/\mathrm{d}r$ is essentially discontinuous (see also *Lecture Notes on Stellar Structure and Evolution*, Fig. 6.3a). Argue that as a result ω_c^2 in equation (7.90) is discontinuous, whereas the other terms are continuous.

ii) Certain simplified models of convective overshoot predict that ∇ is discontinuous at the edge of the convective region. Argue that in this case ω_c^2 has a δ-function singularity at the convection-zone boundary.

The results of i) and ii) suggests that we consider an equation of the form

$$\frac{\mathrm{d}^2Y}{\mathrm{d}x^2} + [\omega^2 - V^2(x)]Y(x) = 0 \; , \tag{C.58}$$

on the interval $[0, x_t]$, where the "potential" $V(x)$ has either a discontinuity or a δ-function behaviour at some location in $[0, x_t]$. The eigenfrequencies ω are determined by imposing the boundary conditions

$$Y(0) = Y(x_t) = 0 \; . \tag{C.59}$$

iii) As a reference case we consider the potential being constant everywhere, $V = V_{\rm a}$, say. Show that the corresponding eigenfrequencies satisfy the following dispersion relation

$$\omega_0^2 - V_{\rm a}^2 = \left(\frac{n\pi}{x_{\rm t}}\right)^2 , \tag{C.60}$$

n being an integer corresponding to the $(number\,of\,zeros + 1)$ of the eigenfunction.

iv) To illustrate the effects of a discontinuity we consider the following modified potential:

$$V_1(x) = \begin{cases} V_{\rm b} & \text{for } 0 \le x < \alpha_1 x_{\rm t} \\ V_{\rm a} & \text{for } \alpha_1 x_{\rm t} \le x < x_{\rm t} \ . \end{cases} \tag{C.61}$$

Show that Y and $\mathrm{d}Y/\mathrm{d}x$ are everywhere continuous. Hence, imposing the same boundary conditions as before, show that ω satisfies the dispersion relation

$$\tan(\Lambda_{\rm b}\alpha_1 x_{\rm t}) = -\frac{\Lambda_{\rm b}}{\Lambda_{\rm a}} \tan[\Lambda_{\rm a}(1-\alpha_1)x_{\rm t}] , \tag{C.62}$$

where

$$\Lambda_{\rm a} = \left(\omega^2 - V_{\rm a}^2\right)^{1/2} , \qquad \Lambda_{\rm b} = \left(\omega^2 - V_{\rm b}^2\right)^{1/2} . \tag{C.63}$$

v) To study the effect of a δ-function singularity, consider the following modified potential:

$$V_2^2(x) = V_{\rm a}^2 + A_\delta \delta(x - \alpha_2 x_{\rm t}) . \tag{C.64}$$

Show that $Y(x)$ is still everywhere continuous, whereas $\mathrm{d}Y/\mathrm{d}x$ satisfies the following jump condition at $x = \alpha_2 x_{\rm t}$:

$$\left.\frac{\mathrm{d}Y}{\mathrm{d}x}\right|_{\alpha_2 x_{\rm t}+} - \left.\frac{\mathrm{d}Y}{\mathrm{d}x}\right|_{\alpha_2 x_{\rm t}-} = A_\delta Y(\alpha_2 x_{\rm t}) . \tag{C.65}$$

(Hint: integrate the differential equation (C.58) across the $x = \alpha_2 x_{\rm t}$.) Hence derive the following dispersion relation for ω:

$$\tan(\Lambda_{\rm a}\alpha_2 x_{\rm t}) = -\frac{\tan[\Lambda_{\rm a}(1-\alpha_2)x_{\rm t}]}{1 + A_\delta \Lambda_{\rm a}^{-1} \tan[\Lambda_{\rm a}(1-\alpha_2)x_{\rm t}]} . \tag{C.66}$$

We now consider the discontinuity or the singularity as small perturbations on a high-order mode. Specifically, we assume that $\omega_0 \gg V_{\rm a}$; also, writing $\omega = \omega_0 + \delta\omega$, and $\delta V^2 = V_{\rm a}^2 - V_{\rm b}^2$, we assume that $|\delta\omega| \ll \omega_0$, $|\delta V^2| \ll V_{\rm a}^2$, and that $|A_\delta| \ll V_{\rm a}$.

vi) Show, by expanding equation (C.62) in terms of the small quantities, that in the case of a discontinuity the frequency change has a periodic component which is approximately given by

$$\delta\omega_{\rm p1} \sim \frac{\delta V^2}{4 x_{\rm t} \omega_0^2} \sin(2\Lambda_{\rm a}\alpha_1 x_{\rm t}) . \tag{C.67}$$

vii) Show, by expanding equation (C.66) in terms of the small quantities, that in the case of a δ-function singularity the frequency change has a periodic component which is approximately given by

$$\delta\omega_{\rm p2} \sim \frac{A_\delta}{2x_{\rm t}\omega_0}\,\cos(2\Lambda_{\rm a}\alpha_2 x_{\rm t})\ . \tag{C.68}$$

Note that in both cases the analysis predicts a frequency perturbation which oscillates as a function of the unperturbed frequency ω_0. With the assumption that $\omega_0 \gg V_{\rm a}$ the "frequency" of this oscillation is approximately $2\omega_0\alpha_i x_{\rm t}$; hence it measures the location of the discontinuity or singularity. The two cases differ in the frequency dependence of the amplitude of the oscillation (ω_0^{-2} for a discontinuity, ω_0^{-1} for a singularity) and in the phase of the oscillation. This in principle allows a determination of the nature of the sharp feature. As discussed by Monteiro *et al.* an analysis of this nature allows testing for the presence of overshoot below the solar convection zone.

viii) (Optional) Some stars have growing convective cores during parts of the core hydrogen burning phase. Argue that this leads to a discontinuity in density. Try to carry out a similar analysis for this case.

Erratum to Monteiro et al. (1994): As found by a student in the course on Stellar Pulsations in 2012 there is a misprint in equation (B13). The correct equation is

$$\tan[\Lambda_a(\alpha_2\tau_t)] = -\frac{\tan[\Lambda_a(\tau_t-\alpha_2\tau_t)]}{1+A_\delta(\omega^2-V_a^2)^{-1/2}\tan[\Lambda_a(\tau_t-\alpha_2\tau_t)]}$$

C.5 Rotation and stellar oscillations

Problem 5.1:

Asymptotic description of rotational splitting. We can derive the asymptotic expression for the rotational splitting of p-mode frequencies very simply from the plane-wave treatment in Section 3.3.1. We neglect the Coriolis force, so that the only change in the equation of motion is the addition of the term $-2m\omega\Omega\rho_0\boldsymbol{\delta}\mathbf{r}$ on the right-hand side (*cf.* eq. 8.25). This is treated as a perturbation to the Duvall relation, equation (7.1), in much the same way as the analysis of the effect of the perturbation in the gravitational potential in Problem 4.2.

i) Show that the dispersion relation for plane sound waves is changed to

$$\omega^2 = c^2|\mathbf{k}|^2 + 2m\omega\Omega\ . \tag{C.69}$$

ii) We assume that the rotation rate $\Omega = \Omega(r)$ is a function of r alone, and that it is small. Show that the modified Duvall relation can be written

$$\pi \frac{n+\alpha}{\omega} = \int_{r_t}^{R} \left(1 - \frac{L^2c^2}{\omega^2 r^2}\right)^{1/2} \frac{\mathrm{d}r}{c} - \frac{m}{\omega} \int_{r_t}^{R} \left(1 - \frac{L^2c^2}{\omega^2 r^2}\right)^{-1/2} \Omega(r) \frac{\mathrm{d}r}{c} \,. \quad \text{(C.70)}$$

iii) Hence show that the effect of rotation is to produce a frequency shift $\delta\omega$ given by

$$S\,\delta\omega \simeq m \int_{r_t}^{R} \left(1 - \frac{L^2c^2}{r^2\omega^2}\right)^{-1/2} \Omega(r) \frac{\mathrm{d}r}{c} \,, \quad \text{(C.71)}$$

where

$$S = \int_{r_t}^{R} \left(1 - \frac{L^2c^2}{r^2\omega^2}\right)^{-1/2} \frac{\mathrm{d}r}{c} - \pi \frac{\mathrm{d}\alpha}{\mathrm{d}\omega} \,. \quad \text{(C.72)}$$

Does this look familiar?

Problem 5.2:

Asymptotic inversion of rotational splitting. Given the result of Problem 5.1, and the treatment of the asymptotic sound-speed inversion in Section 7.7.2, find a method for inverting observed rotational splittings to determine the rotation rate $\Omega(r)$, assuming it to be a function of r alone.

C.6 Excitation and damping of stellar oscillations

Problem 6.1:

Stochastic excitation of oscillations. It is generally believed that the observed modes of solar oscillation are damped. This has been indicated by a number of calculations, although there have been reports to the contrary also. If the modes are in fact stable, their most likely cause is the turbulent convection near the solar surface. In the uppermost part of the convection zone the velocity of the convective elements gets close to the sound speed. Such elements are quite efficient at emitting acoustic noise, and the noise excites the normal modes of the system. Essentially similar processes are responsible for the generation of the notes of wind instruments, including an organ.

In this Problem we do not go into the physical details of this excitation process, but instead concentrate on one aspect: its stochastic nature. The excitation of each mode is caused by the effect of a very large number of essentially uncorrelated convective elements. Consequently, the effective excitation force is a random function of time. Here we model the process through the behaviour of a damped harmonic oscillator that is

excited by a random forcing. It may in fact be shown that this is a reasonable model for the nonlinear interaction between convection and the mode. We do not aim at a mathematically rigorous treatment of stochastic differential equations, but rather at getting a feel for the properties of the solution.

As a preparation, we first consider a simple damped oscillator, with no forcing.

i) Consider an oscillator with amplitude $A(t)$ which satisfies the differential equation

$$\frac{\mathrm{d}^2A}{\mathrm{d}t^2} + 2\eta\frac{\mathrm{d}A}{\mathrm{d}t} + \omega_0^2 A = 0 \ , \tag{C.73}$$

with initial condition $A(0) = A_0$ and $\mathrm{d}A/\mathrm{d}t = 0$ at $t = 0$. Find the solution for $t > 0$ and show that for $\eta > 0$ it corresponds to a damped oscillation. You may assume that $|\eta| \ll \omega_0$.

ii) Find the Fourier transform of the solution from i), observed from $t = 0$ to $t \to \infty$, and the corresponding power spectrum [see also equation (2.38)]. This spectrum is known as a *Lorentz profile*.

We now consider an oscillator forced by a random function $f(t)$ and hence satisfying the equation

$$\frac{\mathrm{d}^2A}{\mathrm{d}t^2} + 2\eta\frac{\mathrm{d}A}{\mathrm{d}t} + \omega_0^2 A = f(t) \ . \tag{C.74}$$

This equation is most easily dealt with in terms of its Fourier transform. We introduce the Fourier transforms $\tilde{A}(\omega)$ and $\tilde{f}(\omega)$ by

$$\tilde{A}(\omega) = \int A(t)e^{i\omega t}\mathrm{d}t \ , \qquad \tilde{f}(\omega) = \int f(t)e^{i\omega t}\mathrm{d}t \ , \tag{C.75}$$

where we do not attempt to specify the limits of integration precisely.

iii) Show, by suitable use of integration by parts and neglecting the resulting boundary terms, that $\tilde{A}$ satisfies

$$-\omega^2\tilde{A} - 2i\eta\omega\tilde{A} + \omega_0^2\tilde{A} = \tilde{f} \ . \tag{C.76}$$

iv) Show from equation (C.76) that the power spectrum of the oscillator is given by

$$P(\omega) = |\tilde{A}(\omega)|^2 = \frac{|\tilde{f}(\omega)|^2}{(\omega_0^2 - \omega^2)^2 + 4\eta^2\omega^2} \ . \tag{C.77}$$

Equation (C.77) describes the solution resulting from a particular realization of the forcing. It is more interesting to consider an average over several such realizations (obtained either by repeated observation of the same mode or by averaging data for several similar modes). Furthermore, since the damping rate is generally very small compared with the oscillation frequency, we are mainly interested in the behaviour close to $\omega = \omega_0$.

v) Show that for $|\omega - \omega_0| \ll \omega_0$ the average power of the oscillation, as a function of frequency, is given by

$$\langle P(\omega) \rangle \simeq \frac{1}{4\omega_0^2} \frac{\langle P_f(\omega) \rangle}{(\omega - \omega_0)^2 + \eta^2} \, , \tag{C.78}$$

where $\langle P_f(\omega) \rangle$ is the average power of the forcing function.

Since $\langle P_f(\omega) \rangle$ is often a slowly varying function of frequency, the frequency-dependence of $\langle P(\omega) \rangle$ is dominated by the denominator in equation (C.78). This behaviour is exactly the same as the profile for the unforced damped oscillator in ii). Hence we obtain the remarkable result that the spectrum of a stochastically forced damped oscillator is Lorentzian, with a width determined by the linear damping rate η. Consequently, under the assumption of stochastic excitation one can make a meaningful comparison between computed damping rates and observed line widths. In the solar case rather detailed calculations by Balmforth (1992b), including a relatively sophisticated treatment of convection and radiation, have in fact resulted in good agreement with the observations. However, a more careful analysis of the statistical properties of the observed oscillations is required to confirm that this is indeed the correct model for the excitation of the solar modes. As discussed in Section 10.3, the observed amplitude distribution is in fact in accord with expectations. Based on such models of excitation, predictions have been carried out of amplitudes of similar oscillations in other stars, of obvious significance for attempts to detect such oscillations. In the longer run, we may hope to be able to probe properties of convection in different stars through observations of their oscillation amplitudes.

Finally it should be remarked that numerical simulations of such stochastically excited oscillators are both relatively straightforward and very instructive.

Problem 6.2:

The location of the instability strip in the HR diagram. We have found that instability requires coincidence of the He^+ ionization zone and the transition from adiabatic to nonadiabatic oscillations. Here we analyse this condition in more detail.

We consider the outer layers of a star. The mass of the layer is Δm, and its thickness is Δr; we assume that $\Delta m \ll M$ and $\Delta r \ll R$, where M and R are the mass and radius of the star. The pressure on the stellar surface is assumed to be zero.

i) Show from the equation of hydrostatic support that the pressure at the base of the layer is

$$p_1 = \frac{GM\Delta m}{4\pi R^4} \, , \tag{C.79}$$

where G is the gravitational constant.

We assume that energy transport is through radiation, and that the opacity is given by the Kramers expression, which we write on the form

$$\kappa = \tilde{\kappa}_0 p T^{-4.5} \, , \tag{C.80}$$

where $\tilde{\kappa}_0$ is a constant, and T is temperature.

ii) Show from the equations of hydrostatic support and radiative energy transport that the temperature T_1 at the base of the layer satisfies

$$p_1 \simeq K \left(\frac{M}{L}\right)^{1/2} T_1^{4.25} , \tag{C.81}$$

where L is the luminosity of the star and K is a constant.

In equation (10.40), it was argued that the transition from adiabaticity to nonadiabaticity occurs at a depth $(\Delta r)_{\rm TR}$ such that

$$\frac{\langle c_V T\rangle_{\rm TR}(\Delta m)_{\rm TR}}{L\Pi} \sim 1 , \tag{C.82}$$

where $\langle c_V T\rangle_{\rm TR}$ is an average of $c_V T$ over the region outside the transition point, $(\Delta m)_{\rm TR}$ is the mass of that region and Π is the pulsation period. The condition for instability is that $(T_1)_{\rm TR} \simeq T_{\rm ion}$, where $(T_1)_{\rm TR}$ is the temperature at the transition point and $T_{\rm ion} \simeq 4 \times 10^4\,{\rm K}$ is the temperature where He^+ ionizes.

We write the pulsation period as

$$\Pi = \Pi_0 \frac{R^{3/2}}{M^{1/2}} , \tag{C.83}$$

where Π_0 is a constant, and approximate $\langle c_V T\rangle_{\rm TR}$ by $c_V (T_1)_{\rm TR}$, where c_V is assumed to be constant.

iii) Show, using equations (C.79) and (C.81) – (C.83), that the instability condition leads to the following relation between L and R:

$$L \propto R^{5/3} . \tag{C.84}$$

iv) Show that equation (C.84) can be expressed as

$$L \propto T_{\rm eff}^{-\nu} , \tag{C.85}$$

and find the exponent ν.